UNIVERSITY OF CALIFORNIA, SAN DIEGO

Semiconducting polymers for stretchable, ultra-flexible, and mechanically robust organic photovoltaics

A Dissertation submitted in partial satisfaction of the requirements for the degree of Doctor of Philosophy

in

Chemical Engineering

by

Suchol Savagatrup

Committee in charge:

Professor Darren Lipomi, Chair
Professor Renkun Chen
Professor Nathan Gianneschi
Professor Jan Talbot
Professor Liangfang Zhang

2016

This Dissertation of Suchol Savagatrup is approved, and it is acceptable in quality and form for publication on microfilm and electronically:

Chair

University of California, San Diego

2016

DEDICATION

To my mentors, friends, and family. I could not have gone this far without you.

TABLE OF CONTENTS

LIST OF FIGURES

LIST OF TABLES

ACKNOWLEDGEMENTS

I find it difficult to express how fortunate I am to have been a part of the Lipomi Group. It has been a great honor to call such a tremendous group of people my family, and such an amazing laboratory my home. I feel compelled to be as comprehensive as possible while expressing my sincere gratitude to the many individuals who have contributed to a culture of close collaboration, unconditional support, and unlimited inspiration. All of you have so many admirable characteristics that I have tried to emulate, and without each and every one of you, I would not have reached this far.

First, I would like to thank the original members of the Lipomi Group who welcomed me into the lab. Adam Printz was my main scientific partner; many of my projects would have met an early end without his help. His tireless attitude toward developing new methods and experiments to solve fundamental problems has always been refreshing. I truly appreciated and missed his back up—when he left for Stanford—on enforcing the absolute best standard of cleanliness and safety in the lab. Despite our short overlap, I will always appreciate Dan Burke and the lively lab culture that he started. His open and candid communication definitely set the tone for cultivating a close-knit group. In addition, his unique advice and perspective on navigating graduate school have helped me through trying times. Timothy O'Connor's unbounded cheerfulness, enthusiasm, creativity, and optimism have motivated me to become a more positive person. I have never met someone who cares so deeply for his friends and the community to which he belongs. Our conversations on the philosophy of science and technology have been eye-opening. Aliaksandr Zaretski is the true example of perseverance and ambition. It would be

extremely unwise to bet against his inevitable success. I hope some of his natural charisma and jovial personality have rubbed off on me.

Throughout my four years in the lab, Daniel Rodriquez has played a crucial role in many of my projects. I certainly do not take his tenacious work ethic and dependability, as well as his friendship, for granted. Similarly, I thank Sam Root, who has always been a source of interesting insights and discussions on polymer physics and classical chemical engineering. During the last two years while he occupied the seat behind mine, I have learned something new from him every day. Brandon Marin's enthusiasm toward teaching and mentorship have been extremely inspirational, and I would like to thank him for his help while I was preparing for my oral prequalification exam. Specifically, our intense and comprehensive practice talks gave me the confidence I needed. Both Bérenger Roth and Fumitaka Sugiyama, who occupied the seat next to mine at different times, have been the sources of stimulating collaborations. I would also like to thank Julian Ramirez who has always been willing to take on new tasks to improve the lab. In addition, none of the work I have presented here would have been completed without the tremendous dedication by Aditya Makaram, Esther Chan, Eduardo Valle, Nathaniel de los Santos, and Jason Kim. I wish nothing but success for their futures.

In addition to my labmates, I would like to thank several others who have helped me throughout my graduate career. Thanks to Professor Renkun Chen, Professor Nathan Gianneschi, Professor Jan Talbot, and Professor Liangfang Zhang for serving on my Senate and Defense committees. I would also like to thank Professor Richard Herz and Professor Kalyanasundaram Seshadri, who along with Professor Jan Talbot proctored my prequalification exam. I would not have started at UC San Diego without the encouraging

words from Professor Shirley Meng, and for that I will always be grateful. Her students, JaeWook Shin and Ziying Wang, helped me tremendously when I started graduate school. Dana Jimenez has been the absolute best person for academic guidance. From the time I arrived at UC San Diego through the end of my graduate career, I always appreciated her positive and welcoming personality. I will miss her ability to instantly fix all of my problems.

Darren Lipomi has been more than the best advisor I have ever had. He is passionate, intense, and ambitious in the pursuit for knowledge. More importantly, he leads by example. Darren's dedication to shape me into the best version of myself and to inspire me to chase after my dreams is unmatched. His ability to create such a positive, inviting, and inspirational environment for his group is not a skill many people have. His group is a part of his family, and he clearly believes that his purpose is to put his students in the best possible positions for their future careers. He has not only provided me with invaluable guidance throughout the years at UC San Diego, but has believed in me and has helped me grow both professionally and personally. Darren, I cannot express my gratitude enough for you and what you have done for me.

Finally, I would like to thank my friends and family. I greatly appreciate the support structure provided by my close friends—Greg Landau, Charles Dhong, Brian Lu, Krzys Brozek, Darren Kurt, Yolanda Luk, and Katie Wynn—throughout my undergraduate and graduate careers. All of whom have helped and encouraged me to always push forward. Lastly, my mother and father, Chantima and Amarin, and my aunt and uncle, Amara and Johnny, have made many sacrifices to help me reach this point. I am truly grateful for their constant and continued support.

I also include the following acknowledgements below as required by the University of California, San Diego.

Chapter 1, in full, is a reprint of the material as it appears in *Chemistry of Materials*, 2014, 26, 3028 – 3041. American Chemical Society, 2014. **Suchol Savagatrup**, Adam D. Printz, Timothy F. O'Connor, Aliaksandr V. Zaretski, and Darren J. Lipomi. The dissertation author was the primary investigator and author of this paper.

Chapter 2, in full, is a reprint of the material as it appears in *Energy & Environmental Science*, 2015, 8, 55 – 80. Royal Society of Chemistry, 2015. **Suchol Savagatrup**, Adam D. Printz, Timothy F. O'Connor, Aliaksandr V. Zaretski, Daniel Rodriquez, Eric J. Sawyer, Kirtana M. Rajan, Raziel I. Acosta, Samuel E. Root, and Darren J. Lipomi. The dissertation author was the primary investigator and author of this paper.

Chapter 3, in full, is a reprint of the material as it appears in *Advanced Functional Materials*, 2014, 24, 1169 – 1181. Wiley-VCH Verlag GmbH & Co. KGaA, 2014. **Suchol Savagatrup**, Aditya S. Makaram, Daniel J. Burke, and Darren J. Lipomi. The dissertation author was the primary investigator and author of this paper.

Chapter 4, in full, is a reprint of the material as it appears in *Macromolecules*, 2014, 47, 1981 – 1992. American Chemical Society, 2014. **Suchol Savagatrup**,[†] Adam D. Printz,[†] Daniel Rodriquez, and Darren J. Lipomi. ([†] Equal contribution). The dissertation author was the primary investigator and author of this paper.

Chapter 5, in full, is a reprint of the material as it appears in *Synthetic Metals*, 2015, 203, 208 – 214. Elsevier B.V., 2015. **Suchol Savagatrup**,[†] Adam D. Printz,[†] Haosheng Wu, Kirtana Rajan, Eric J. Sawyer, Aliaksandr V. Zaretski, Christopher J. Bettinger, and

Darren J. Lipomi († Equal contribution). The dissertation author was the primary investigator and author of this paper.

Chapter 6, in full, is a reprint of the material as it appears in *Chemistry of Materials*, 2015, 27, 3902 – 3911. American Chemical Society, 2015. **Suchol Savagatrup**, Daniel Rodriquez, Adam D. Printz, Alexander B. Sieval, Jan C. Hummelen, and Darren J. Lipomi. The dissertation author was the primary investigator and author of this paper.

Chapter 7, in full, is a reprint of the material as it appears in *Advanced Functional Materials*, 2015, 25, 427 – 436. Wiley-VCH Verlag GmbH & Co. KGaA, 2015. **Suchol Savagatrup**, Esther Chan, Sandro M. Renteria-Garcia, Adam D. Printz, Aliaksandr V. Zaretski, Timothy F. O'Connor, Daniel Rodriquez, Eduardo Valle, and Darren J. Lipomi. The dissertation author was the primary investigator and author of this paper.

Chapter 8, in full, is a reprint of the material as it appears in *RSC Advances*, 2014, 4, 13635 – 13643. The Royal Society of Chemistry, 2014. Adam D. Printz,† **Suchol Savagatrup**,† Daniel J. Burke, Trevor N. Purdy, and Darren J. Lipomi. († Equal contribution). The dissertation author was the primary investigator and author of this paper.

Chapter 9, in full, is a reprint of the material as it appears in *Chemistry of Materials*, 2016, 28, 2363 – 2373. American Chemical Society, 2016. Bérenger Roth,† **Suchol Savagatrup**,† Nathaniel De Los Santos, Ole Hagemann, Jon E. Carlé, Martin Helgesen, Francesco Livi, Eva Bundgaard, Roar R. Søndergaard, Frederik C. Krebs, and Darren J. Lipomi († Equal contribution). The dissertation author was the primary investigator and author of this paper.

Chapter 10, in part is currently being prepared for submission for publication of the material by **Suchol Savagatrup**, Xikang Zhao, Esther Chan, Jianguo Mei, and Darren J. Lipomi. The dissertation author was the primary investigator and author of this materials.

Chapter 11, in part is currently being prepared for submission for publication of the material by **Suchol Savagatrup**, Adam D. Printz, Timothy F. O'Connor, Insik Kim, and Darren J. Lipomi. The dissertation author was the primary investigator and author of this materials.

VITA

2012	Bachelor of Science in Chemical Engineering, University of California, Berkeley
2015	Teaching Assistant, Department of NanoEngineering, University of California, San Diego
2015	Master of Science in Chemical Engineering, University of California, San Diego
2012–2016	Graduate Researcher, University of California, San Diego
2016	Doctor of Philosophy in Chemical Engineering, University of California, San Diego

PUBLICATIONS

D. Rodriquez, **S. Savagatrup**, E. Valle, C. Proctor, C. McDowell, G. Bazan, T.-Q. Nguyen, D. J. Lipomi. "Mechanical Properties of Solution-Processed Small-Molecule Semiconductor Films" *ACS Applied Materials & Interfaces*, 2016, 8, 11649.

S. E. Root, **S. Savagatrup**, C. J. Pais, G. Arya, D. J. Lipomi. "Predicting the Mechanical Properties of Organic Semiconductors using Coarse-Grained Molecular Dynamics Simulations" *Macromolecules*, 2016, 49, 2886.

A. D. Printz, A. S.-C. Chiang, **S. Savagatrup**, D. J. Lipomi. "Fatigue in Organic Semiconductors: Spectroscopic Evolution of Microstructure due to Cyclic Loading in Poly(3-Heptylthiophene)" *Synthetic Metals*, 2016, 217, 144.

B. Roth, [†] **S. Savagatrup**, [†] N. De Los Santos, O. Hagemann, J. E. Carle, M. Helgesen, F. Livi, E. Bundgaard, R. R. Sondergaard, F. C. Krebs, D. J. Lipomi. "Mechanical Properties of a Library of Low-Bandgap Polymers" *Chemistry of Materials*, 2016, 28, 2363. ([†] Equal contribution)

T. F. O'Connor, **S. Savagatrup**, D. J. Lipomi. "Soft Power: Stretchable and Ultra-flexible Energy Sources for Wearable and Implantable Devices." Invited for: Stretchable Bioelectronics for Medical Devices and Systems. J. A. Rogers, D.-H. Kim, and R. Ghaffari, Editors. Springer, 2016.

A. D. Printz, A. V. Zaretski, **S. Savagatrup**, A. S.-C. Chiang, D. J. Lipomi. "Yield Point of Semiconducting Polymer films on Stretchable Substrates Determined by Onset of Buckling." *ACS Applied Materials & Interfaces*, 2015, 7, 23257.

T. F. O'Connor, A. V. Zaretski, **S. Savagatrup**, A. D. Printz, C. D. Wilkes, M. I. Diaz, E. J. Sawyer, D. J. Lipomi. "Wearable Organic Solar Cells with High Cyclic Bending Stability: Materials Selection Criteria." *Solar Energy Materials & Solar Cells*, 2015, 144, 438.

S. Savagatrup, D. Rodriquez, A. D. Printz, A. B. Sieval, J. C. Hummelen, and D. J. Lipomi. "[70]PCBM and Incompletely Separated Grades of Methanofullerenes Produce Bulk Heterojunctions with Increased Robustness for Ultra-Flexible and Stretchable Electronics." *Chemistry of Materials*, 2015, 27, 3902.

S. Savagatrup, † A. D. Printz, † H. Wu, K. M. Rajan, E. J. Sawyer, A. V. Zaretski, C. J. Bettinger, and D. J. Lipomi. "Viability of Stretchable Poly(3-Heptylthiophene) (P3HpT) for Organic Solar Cells and Field-Effect Transistors." *Synthetic Metals*, 2015, 203, 208. († Equal contribution)

A. D. Printz, **S. Savagatrup**, D. Rodriquez, and D. J. Lipomi. "Role of Molecular Mixing on the Stiffness of Polymer:Fullerene Bulk Heterojunction Films." *Solar Energy Materials & Solar Cells*, 2015, 134, 64.

A. V. Zaretski, H. Moetazedi, C. Kong, E. J. Sawyer, **S. Savagatrup**, E. Valle, T. F. O'Connor, A. D. Printz, and D. J. Lipomi. "Metal-Assisted Exfoliation (MAE): Green, Roll-to-Roll Compatible Method for Transferring Graphene to Flexible Substrates." *Nanotechnology*, 2015, 26, 4.

S. Savagatrup, E. Chan, S. M. Renteria-Garcia, A. D. Printz, A. V. Zaretski, T. F. O'Connor, D. Rodriquez, E. Valle, and D. J. Lipomi. "Plasticization of PEDOT:PSS by Common Additives for Mechanically Robust Devices and Wearable Sensors." *Advanced Functional Materials*, 2015, 25, 427.

S. Savagatrup, A. D. Printz, T. F. O'Connor, A. V. Zaretski, D. Rodriquez, E. J. Sawyer, K. M. Rajan, R. I. Acosta, S. E. Root, and D. J. Lipomi. "Mechanical Degradation and Stability of Organic Solar Cells: Molecular and Microstructural Determinants." *Energy and Environmental Science*, 2015, 8, 55.

E. J. Sawyer, **S. Savagatrup**, T. F. O'Connor, A. S. Makaram, D. J. Burke, A. V. Zaretski, A. D. Printz, and D. J. Lipomi. "Toward Intrinsically Stretchable Organic Semiconductors: Mechanical Properties of High-Performance Conjugated Polymers." *Proc. SPIE*, 2014, 9185, 991850U-1.

S. Savagatrup, A. D. Printz, T. F. O'Connor, A. V. Zaretski, and D. J. Lipomi. "Molecularly Stretchable Electronics." *Chemistry of Materials*, 2014, 26, 3028.

S. Savagatrup,[†] A. D. Printz,[†] D. Rodriquez, and D. J. Lipomi. "Best of Both Worlds: Conjugated Polymers Exhibiting Good Photovoltaic Properties and High Tensile Elasticity." *Macromolecules,* 2014, 47, 1981. ([†] Equal contribution)

A. D. Printz,[†] **S. Savagatrup,**[†] D. J. Burke, T. Purdy, and D. J. Lipomi. "Increased Elasticity of a Low-Bandgap Conjugated Copolymer by Random Segmentation for Mechanically Robust Solar Cells." *RSC Advances,* 2014, 4, 13635. ([†] Equal contribution)

T. F. O'Connor, A. V. Zaretski, B. A. Shiravi, **S. Savagatrup**, A. D. Printz, M. I. Diaz, and D. J. Lipomi. "Stretching and Conformal Bonding of Organic Solar Cells to Hemispherical Surfaces." *Energy and Environmental Science*, 2014, 7, 370.

S. Savagatrup, A. S. Makaram, D. J. Burke, and D. J. Lipomi. "Mechanical Properties of Conjugated Polymers and Polymer-Fullerene Composites as a Function of Molecular Structure." *Advanced Functional Materials,* 2014, 24, 1169.

A. Kusoglu, **S. Savagatrup**, K. T. Clark, and A. Z. Weber. "Role of Mechanical Factors in Controlling the Structure-Function Relationship of PFSA Ionomers." *Macromolecules,* 2012, 45, 7467.

ABSTRACT OF THE DISSERTATION

Semiconducting polymers for stretchable, ultra-flexible, and mechanically robust organic photovoltaics

by

Suchol Savagatrup

Doctor of Philosophy in Chemical Engineering

University of California, San Diego, 2016

Professor Darren J. Lipomi, Chair

The original vision of organic electronics comprises the use of organic conductors and semiconductors specifically designed to accommodate large strains to enable highly deformable and mechanically robust devices for organic photovoltaics, biosensors, and electronic skins. However, mechanical properties of organic materials are often

overlooked; as a result, many of these materials are unable to accommodate the mechanical stresses required for their intended applications. Thus, it is important to understand the parameters that govern mechanical properties of these materials. Chapter 1 provides an introduction to the characteristics, applications, and fabrications of stretchable electronics. The idea of intrinsically stretchable electronics comprising molecularly designs of semiconducting polymers is outlined. Chapter 2 focuses on the mechanical degradation and stability of organic solar cells. The key highlights are the importance of mechanical properties and mechanical effects on the viability of organic solar cells during manufacture and in operational environment. Chapter 3 and Appendix A investigate the effects of the length of the alkyl side chains in poly(3-alkylthiophenes) on the deformability of the pure polymer films and their blends with fullerenes. Chapter 4, 5, and Appendix B provide studies on the inherent competition between good photovoltaic performance and mechanical compliance; a critical length of the alkyl side chains on the poly(3-alkylthiophene) allows for co-optimization of both photovoltaic and mechanical properties. In Chapter 6 and Appendix C, the effect of incompletely separated grades of electron acceptors on the mechanical deformability of organic solar cells is investigated in an effort to simultaneously improve the mechanical robustness of the organic solar cells and reduce the energy of production. Chapter 7 describes the plasticization of the common transparent electrode using common processing additives. Chapter 8, 9, and 10 investigate the mechanical properties of low-bandgap polymers as the function of the molecular structure and solid-state packing. Chapter 11 introduces a novel experimental method, photovoltaic mapping (PVMAP), which combines the use of non-damaging electrode and gradients in processing parameter to spatially map the photovoltaic properties of organic solar cells.

Chapter 1

Molecularly stretchable electronics

Suchol Savagatrup, Adam D. Printz, Timothy F. O'Connor, Aliaksandr V. Zaretski, and Darren J. Lipomi

Department of NanoEngineering, University of California, San Diego

9500 Gilman Drive, Mail Code 0448, La Jolla, CA 92093-0448

Abstract

This Perspective describes electronic materials whose molecular structure permits extreme deformation without the loss of electronic function. This approach—"molecularly stretchable" electronics—is complementary to the highly successful approaches enabled by stretchable composite materials. We begin by identifying three general types of stretchable electronic materials: (1) random composites of rigid structures sitting atop or dispersed in an elastic matrix, (2) deterministic composites of patterned serpentine, wavy, or fractal structures on stretchable substrates, and (3) molecular materials—non-composite conductors and semiconductors—that accommodate strain intrinsically by the rational design of their chemical structures. We then identify a short-term and a long-term goal of intrinsically stretchable organic electronics: the short-term goal is improving the mechanical stability of devices for which commercialization seems inevitable; the long-term goal is enablement of electronic devices in which every component is highly elastic, tough, ductile, or some combination thereof. Finally, we describe our and others' attempts to identify the molecular and microstructural determinants of the mechanical properties of organic semiconductors, along with applications of especially deformable materials in stretchable and mechanically robust devices. Our principal conclusion is that while the field of plastic electronics has achieved impressive gains in the last several years in terms of electronic performance, all semiconducting polymers are not equally "plastic" in the sense of "deformable," and thus materials tested on glass substrates may fail in the real world and may not be amenable to stretchable—or even modestly flexible—systems. The goal of this Perspective is to draw attention to the ways in which organic conductors and

semiconductors specifically designed to accommodate large strains can enable highly deformable devices, which embody the original vision of organic electronics.

1.1. Electronics in the 21st century

1.1.1. Plastic electronics

Advances in two branches of materials science in the twentieth century left virtually no aspect of modern life untouched: plastics and semiconductors. It is little wonder that the advent of the hybrid technology, plastic electronics, in the form of conducting and semiconducting polymers—for which Heeger, MacDiarmid, and Shirakawa were awarded the Nobel Prize in Chemistry in 2000—excited researchers in fields as diverse as condensed matter physics and biomedical engineering.[1] Early work focused on improving the conductivity of polyacetylene[2,3] and unsubstituted polymers of aromatic compounds.[4] This period was also characterized by an interest in the bulk properties familiar to polymer scientists, namely mechanical and thermal properties, and processability.[2-6] The early 1990s, however, saw the discovery of the polymer solar cell[7-9] and light-emitting device,[10] and substantial development of the polymer field-effect transistor.[11-13] Research in the area turned toward improving the performance of these devices, while bulk properties became less prominent. As work on devices began in earnest, researchers have attained electronic figures of merit that might have been difficult to predict a decade ago.[14,15] Among other achievements, organic semiconductor devices have been prepared with charge-carrier mobilities well over 10 $cm^2\ V^{-1}\ s^{-1}$,[14] and efficiencies of organic solar cells have surpassed ten percent.[16]

Investigating organic semiconductors and devices with the goal of improving the electronic figures of merit however, has left important aspects such as mechanical compliance behind. The names "plastic electronics" and "flexible electronics" are virtually synonymous with organic and polymer electronics,[17-19] but the descriptors mask the wide variety of mechanical properties possessed by organic conductors and semiconductors.[20] Evaporated films of pentacene[20] and drawn fibers of polyacetylene,[1] for example, have tensile moduli >10 GPa, while polyaniline films can have moduli around 10 MPa (though these films were likely plasticized by residual solvent).[20] The mechanical properties of semiconducting polymers with common structural characteristics, such as polythiophenes, vary with a strong dependence on factors such as the length of the alkyl side chain.[21,22] We previously found large differences in elasticity and ductility between polythiophenes whose structures differed by a single carbon atom on the alkyl side chain.[22] We measured a tensile modulus of 1.15 GPa for poly(3-hexylthiophene) (P3HT, **Figure 1.1**) and 90 MPa for poly(3-heptylthiophene) (P3HpT), and the stiffer material was also significantly more brittle.[21,22] The transparent conductive polymer PEDOT:PSS also exhibits a large dependence of mechanical compliance on the presence of common additives (e.g., surfactants and secondary dopants),[23,24] and the modulus and ductility of polymer:fullerene composites for organic solar cells are strongly dependent on the identity of the polymer[21,22,25,26] and the conditions used to cast the thin films.[27] In the design of new organic electronic materials, however, mechanical properties are generally not considered, but almost certainly occupy a range of values that is relevant to the stability of devices in the solid state.

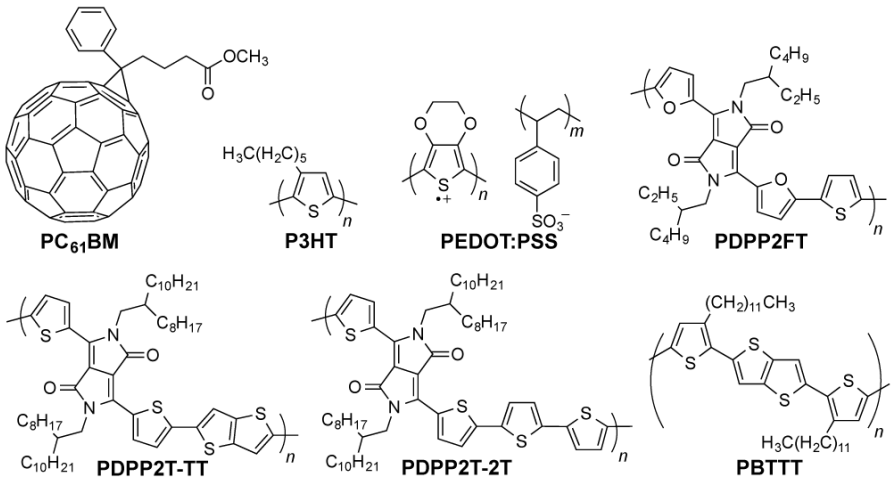

Figure 1.1. Chemical structures of conjugated polymers discussed in the text.

There are at least two reasons to increase the priority of mechanical compliance in research on organic semiconductors. The first reason is to improve the mechanical stability of flexible organic devices that now seem destined for commercialization.[28-31] Nominally flexible devices, especially those for portable outdoor use, will be subjected to bending, tensile, and shear stresses produced by roll-to-roll fabrication, manipulation, thermal expansion and contraction, and the forces produced by wind, rain, and snow.[28] Even small forces will produce large strains if the devices are fabricated on ultra-thin substrates,[19,32] which are required to obtain significant reductions in cost[32] and embodied energy[33] possible with organic devices. Encapsulating these devices in glass will surrender essentially all of the advantages that define the field. The second reason to understand and improve the intrinsic mechanical properties of organic semiconductors is for the burgeoning field of stretchable electronics.[34-39] That is, electronic materials and devices designed for form factors inaccessible to conventional metals and semiconductors on stiff, planar substrates.[36] These applications include consumer devices and textiles,[40] systems for energy conversion and storage,[28,38,41,42] and biomedicine, such as implantable sensors,[43,44]

artificial retinas,[45,46] artificial skin for prostheses,[19,47-50] and sensors for soft robotics.[51,52] Compared to inorganic semiconductors, an ability that remains mostly unique to organics is facile chemical functionalization,[53,54] which can tune the bandgaps of individual semiconductors for multijunction solar cells,[55,56] provide chemoselectivity for chemical and biological sensors,[57] allow electrochromic behavior for all perceptible colors,[58-61] and tailor the mechanical compliance for specific applications in portable displays,[62] solar cells,[21,22,25,26] and biomedical devices.[19,45]

1.1.2. Limitations of conventional semiconductors and devices.

Silicon integrated circuits (ICs) are man-made devices of unmatched sophistication.[63] Technological advancements—e.g., purification of silicon, resolution of photolithography, and design of integrated circuits—combined with enormous economic driving forces have rendered these devices ubiquitous. The scale of investment, performance metrics, and extraordinarily low rate of error present in a silicon IC suggest that achieving the same level of computational sophistication could take decades to accomplish with nanocarbon, nanowires, nanocrystals, and organics.[64] Silicon ICs are, however, relatively expensive, and the contribution of cost and embodied energy of a typical device is dominated by the complexity of the manufacturing phase of its life cycle (it consumes comparatively little energy during the "use phase").[65,66] They are also generally limited to rigid substrates and planar geometries. For applications in chemical and biological sensing, displays, and energy, it may be permissible to sacrifice computational speed and other performance metrics for the sake of another attribute, such as low cost or mechanical compliance.

1.2. Stretchable electronics

1.2.1. Stretchable (not just flexible) systems

Stretchable electronics are both an extension and significant departure from flexible electronics.[36,67-71] Flexible systems are characterized by active materials that can withstand small bending radii by virtue of their thinness (though greater bending strains can be applied if the thin material is itself highly elastic).[19,32,72,73] For thin substrates under bending deformation, the tensile strain imposed on the apex of the bend, ε_{peak}, is equal to the ratio of the thickness of the substrate, d_s, to the diameter of curvature, $2r$, or $\varepsilon_{peak} = d_s/2r$.[72,74] For films whose thickness is small compared to that of the substrate and whose mechanical properties are similar to those of the substrate,[72] it is clear that even very brittle materials (such as crystalline silicon, which fractures at 0.7% strain[74]) can be bent to operationally small values of r, but this ability is, nevertheless, critically dependent on the thinness of the substrate.[32] In one of the most impressive demonstrations of the flexibility of organic semiconductors to date, Kaltenbrunner et al. fabricated an organic solar cell based on a composite of poly(3-hexylthiophene) and [6,6]-phenyl C_{61} butyric acid methyl ester (P3HT:PCBM) on a 1.4-μm polyester foil and achieved bending radii ~35 μm (**Figure 1.2a** and **1.2b**).[32] To render this device stretchable, the authors bonded it to a pre-strained elastomeric substrate. Release of the pre-strain generated wrinkles that accommodated further cycles of strain.[32]

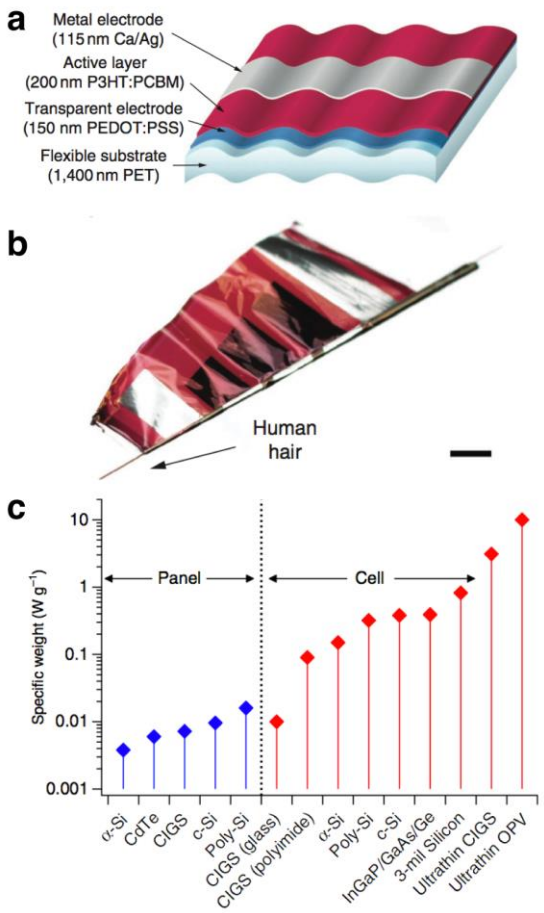

Figure 1.2. Organic solar cells fabricated on ultra-thin polyester substrates. (a) Schematic diagram. (b) Device partially wrapped around a human hair. (c) Power-to-mass ratio for several photovoltaic technologies. This plot highlights the potential cost savings of OPV devices, which are 5–10 times more efficient than the second-most efficient technology per unit mass. Reproduced with permission from ref. [32], copyright 2012 Nature Publishing Group.

The seminal studies that characterized the behavior of metallic and other thin films on compliant substrates for ultra-flexible and stretchable applications were those of Hutchinson and Whitesides;[75,76] Lacour, Suo, and Wagner;[34,77-82] and Lu and Vlassak.[83,84] Rogers and coworkers, in addition to substantially furthering the fundamental thin-film mechanics and the design criteria of the geometries intended to accommodate strain in flexible and stretchable form factors,[35-37,67,85-88] also demonstrated several successful applications, including a hemispherical electronic eye camera,[46,87,89] the first stretchable solar module,[42] electrotactile devices,[90] and conformable devices for in vivo use in brain[43]

and cardiac[44] electrophysiology. Recently, tattoo-like[69] and bioresorbable[91] materials have added significantly to the toolkit of stretchable devices. Someya and coworkers have pioneered the use of stretchable layouts and conductive elastomers to confer stretchability to organic electronics, and have made substantial progress in the areas of electronic skin-like sensors, solar cells, and conformable light-emitting devices.[19,47,70,92-95] These authors and others realized that devices exhibiting only flexibility were limited to bending deformations and cylindrical or conical form factors. In order to enable deformation in response to tensile and compressive stresses, elasticity and ductility—i.e., stretchability—is required.

1.2.2. Methods of making electronics stretchable

Methods of rendering otherwise brittle materials stretchable fall into three broad categories that can be differentiated, with some overlap, on the size scale at which they accommodate strain.[28,88] The first approach, based on *random* compositing (**Figure 1.3a – 1.3c**), depends on percolated pathways for charges. This method is broad and includes intentionally fractured thin films[34,77,78,80-82] and bulk composite materials that contain conductive nanoparticles.[96-99] The second method, based instead on *deterministic* compositing (**Figure 1.3d** and **1.3e**), converts global tensile strains to local bending strains using laterally or topographically patterned thin films.[23,79,88,100,101] These two- or three-dimensionally patterned structures include fishnet[47] or fractal[88] geometries that accommodate strain by out-of-plane twisting.[69] A related technique includes exploiting the micron-scale sinusoidal wrinkles that form on a thin film on an elastic substrate under compressive strain;[102,103] these waves accommodate tensile strains by local

unbending.[35,79,104,105] The third method—the focus of this Perspective—does not in principle rely on composite structures. Rather, the conducting and semiconducting materials accommodate strain by virtue of their molecular structures and morphology in the solid state (**Figure 1.3f** and **1.3g**). The borderline between composite stretchable materials and molecularly stretchable materials is not always distinct. An exemplary case is the loudspeaker reported by the groups of Suo and Whitesides fabricated from a stretchable, transparent, ionic conductive membrane.[106]

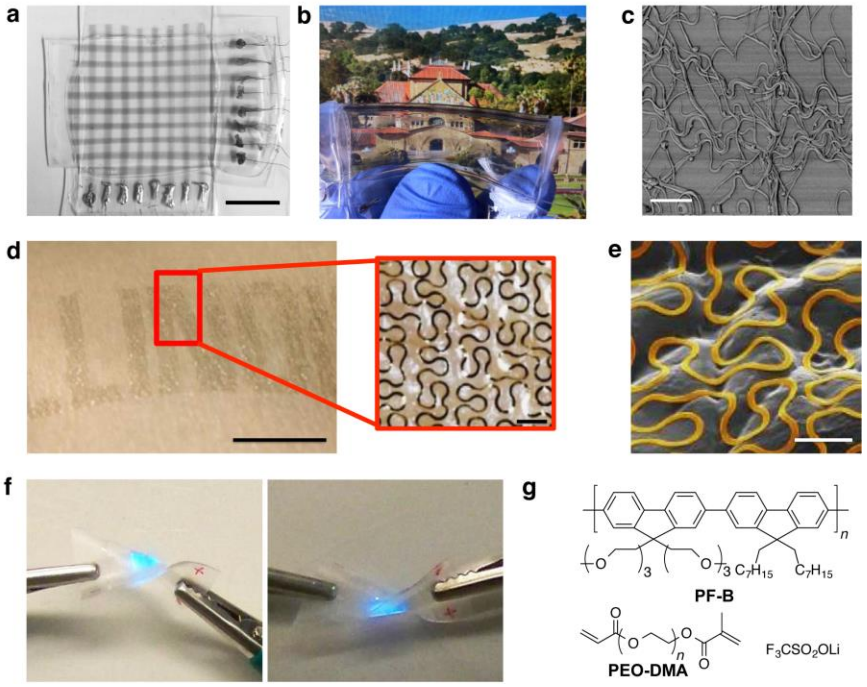

Figure 1.3. Images of representative examples of mechanisms for producing stretchable electronic materials: percolation through random networks (a–c), deterministic patterning of waves and fractals (d, e), and use of elastic molecular materials. (a) High-contrast photograph of a stretchable, transparent pressure sensor based on wavy films of carbon nanotubes embedded in a silicone elastomer (scale bar, 1 cm). (b) Photograph exhibiting extreme flexibility and transparency. (c) Atomic force micrograph, phase contrast, of bundles of buckled carbon nanotubes (scale bar, 600 nm). (d) Photograph of metallic wires in a fractal pattern adhered to skin (scale bar, 1 cm). A blow-up within the region indicated by the red box is shown in the optical micrograph (scale bar, 1 mm) and (e) in the scanning electron micrograph (scale bar, 500 μm). (f) Photographs of an ultra-flexible and stretchable organic light-emitting device fabricated using carbon nanotube-based top and bottom electrodes and an intrinsically stretchable emissive layer based on a stretchable polyfluorene conjugated polymer (PF-B), PEO-DMA, and LiTf (g). (a–c) Reproduce with permission from ref. [107], copyright 2011 Nature Publishing Group. (d, e) Reproduced with permission from ref. [88], copyright 2014 Nature Publishing Group. (f, g) Reproduced with permission from ref. [108], copyright 2014 Wiley-VCH Verlag GmbH & Co. KGaA.

1.2.3. Random composites for stretchable electronics

One method of producing a material that is on the whole stretchable is to start with an intact material—e.g., a film on a stretchable substrate—and stretch it to fracture it deliberately.[78] Many materials naturally form fractured surfaces that nonetheless maintain uninterrupted pathways for conducting charge.[34] This approach has enabled stretchable interconnects as well as devices whose active components require only conductivity, such as capacitive tactile sensors.[77] The mechanism of reversible deformation and evolution of conductivity under cyclic loading has been characterized by Lacour and coworkers for metals.[78] A later study determined that intentional fracture is also an effective strategy for producing stretchable transparent electrodes from the transparent conductor PEDOT:PSS (see **Figure 1.1** for structure) on polydimethylsiloxane (PDMS) substrates.[23] The authors, however, noted that the relationship between strain and conductivity was critically dependent on the method by which the hydrophobic substrate was activated: brittle plasma-oxidized surfaces cracked upon straining and propagated these cracks through the PEDOT:PSS film.[23] These cracks rendered the film non-conductive upon very small strains.[23] Another type of stretchable random composite can be produced from micro- or nanostructures, such as two-dimensional plates or one-dimensional wires, which sit atop or are mixed into an elastomeric matrix. Such materials comprising graphene,[98] conductive nanowires,[108-110] or other conductive particles retain percolated pathways while absorbing strain, presumably by sliding motions of the components[111] or by dynamic reconfiguration—loss and reformation—of electrical connections with strain within or on top of the stretchable matrix.[23,112] In one study, stretchable transparent conductive films of carbon nanotubes were spray-coated on PDMS substrates, stretched, and then relaxed.[107]

The first cycle of stretch-and-release generated buckles whose amplitudes were parallel to the substrate, and which accommodated subsequent cycles of stretching.[107] Films of this type have among the most favorable combinations of elasticity, conductivity, and transparency of any material in the literature, and have been used for transparent, elastic pressure and strain sensors.[107]

1.2.4. Deterministic composites for stretchable electronics

The most successful stretchable electronic devices produced so far have used a deterministic strategy that combines photolithography and soft lithographic printing of metals and semiconductors on elastic substrates,[88] which may or may not bear relief structures to localize strain to specific areas of the device.[42] One method is to exploit the topographic buckles that form when an elastic substrate bearing a relatively rigid film is compressed.[79] This approach has been developed and utilized with extraordinary success by Rogers and coworkers.[35,68,74] While the use of buckled silicon nanomembranes[35] and patterns of metals as interconnects[79] are well known, the method has also been used on semiconducting polymers for the first stretchable organic solar cell,[38] stretchable organic thin-film transistors,[113] and stretchable supercapacitors based on thick buckled films of carbon nanotubes.[104] Another approach is to use serpentine or fractal patterns,[88] which accommodate strain by out-of-plane bending and twisting. This approach has been used in optoelectronic devices, along with epidermal, tattoo-like biosensors,[69] electrotactile fingertip sensors,[90] and biologically resorbable devices.[91] A common element to both random and deterministic compositing is that an elastic substrate provides the restoring force, and that typically the most sensitive components (e.g., the semiconductors) are

located near mechanically neutral planes[90] or on thicker regions of the substrate.[42] Thus, most of the strain is absorbed in the regions containing the conductors, whose function is not generally sensitive to bending strains.

1.2.5. Molecular materials for stretchable electronics

A complementary approach to random and deterministic compositing is to design and use materials that can accommodate strain by virtue of their molecular structure and morphology, as opposed to topology.[21,22,25,26,108,110,114] These intrinsically—or "molecularly"—stretchable materials could simplify patterning (e.g., by printing on elastomeric sheets) and in principle would not require design of relief structures to direct strain away from sensitive semiconducting components. Molecularly stretchable materials based on π-conjugated polymers and small molecules would have additional advantages associated with their organic nature, including low-cost,[115,116] facile manufacturing,[117] and tunability by synthesis.[118] The remainder of this Perspective focuses on work by our group and by other researchers (1) to understand the molecular structural parameters that determine the mechanical properties of organic semiconductors and (2) to apply this knowledge toward the realization of mechanically robust and intrinsically stretchable optoelectronic devices.

1.3. Mechanical properties of organic semiconductors

1.3.1. Plastic electronics

The promise of organic—especially polymeric—conductors and semiconductors is, somewhat obviously, to produce plastic electronic devices. The common perception is

that all organic electronic materials are already highly flexible and elastic. The origin of this notion, we believe, arises from both the small bending radii allowable by the thinness of organic semiconductors, along with the now-synonymous relationship of the words "polymer" and "plastic." While these words are interchangeable in everyday speech, the word plastic implies deformable, and is an adjective that does not describe all π-conjugated polymers to the same extent.[20,21,119] Conjugated polymers exhibit a range of mechanical behavior that depends on the presence of fused or isolated rings in the main chain,[114,119] length and composition of any pendant groups,[21,22] propensity to form crystallites,[27,119] and microstructural order.[26] The work of Heeger, Smith, and Wudl characterized the mechanical properties of early conjugated[2-4] and other comb-like polymers,[5] but the discovery and development of the polymer light-emitting device by Friend,[10] and the discoveries of the bulk heterojunction solar cells by Heeger and Wudl,[7,120] and independently by Friend,[9] combined with the steady increase in performance of the organic thin-film transistor[12,13] in the 1990s, refocused attention from mechanical properties to electronic ones. New polymers with bandgaps that can be dialed in by synthesis,[15,118,121] computational tools that relate charge transport to molecular structure and packing in the solid state,[122] and spectroscopic, micrographic, and synchrotron-based methods of linking morphology to charge-transport characteristics are the subject of an enormously successful literature[123] that has propelled organic devices from laboratory curiosities to modules that can compete with or outmatch other thin-film technologies in several important metrics.[124] In the field of "plastic electronics," the focus on the second word may have come, however, at the expense of the first. There are, we believe, both near-term and long-term goals for increasing the elasticity, toughness, and ductility of organic semiconductors.[21,22,29,30,125-130]

The first, near-term goal, is to enable organic electronic devices—e.g., roll-to-roll fabricated organic solar modules—to survive the rigors of manufacture, transportation, installation, and manipulation in portable applications and environmental forces in utility-scale applications.[131] Indeed, the "Workshop on Key Scientific and Technological Issues for Development of Next-Generation Organic Solar Cells," sponsored by the National Science Foundation and Office of Naval Research in 2012, identified mechanical behavior as an important component of future research:[31]

> Do organic cells fracture cohesively or at interfaces when temperature cycling causes some layers to thermally expand more than others? What has to be done to prevent solar cells from failing mechanically?
>
> –NSF/ONR Workshop Report, September 2012. (Ref. [31])

As a matter of fact, the most popular active material for organic solar cells is a blend of P3HT and a fullerene derivative (PCBM), which fractures at ≤2.5% tensile strain on PDMS substrates.[119] Krebs et al. noted that for portable organic solar modules deployed in rural Africa:[132]

> …mechanical failure mechanisms were dominant during the field test and therefore these would have to be improved significantly before the photochemical stability of the [semiconducting] polymer becomes a problem.
>
> –Krebs et al.[132]

For portable and outdoor applications, it is likely that mechanical degradation is a principal route by which organic solar cells fail. Mechanical routes of degradation include cracking and cohesive failure[29,127,129] of the individual components, and interfacial failure[30,128] (e.g., between the organic semiconductor and the electrodes). Molecular control over the elasticity, ductility, toughness, and surface energy would seem to be a priority for research in organic solar cells, but has received relatively little attention in the body of literature concerned with the stability of devices[133,134] (a notable exception is the work of the

Dauskardt laboratory[29,30,127-129]). Proposed solutions that involve manufacturing and encapsulating devices using thick polymeric or glass layers abandon many of the advantages of organics, not the least of which is the low production energy of conjugated polymers and semiconducting small molecules, and the minute quantities required.[33,116,135] Indeed, the analysis by Anctil et al. has shown that the 130-μm poly(ethylene terephthalate) (PET) substrates and encapsulants most commonly employed for flexible organic solar cells make up around twenty percent of the embodied energy of conventional modules[33] and by extrapolation around forty percent in modules that do not contain ITO. Exploitation of the extraordinarily favorable ratio of power to mass possible with organics[32] cannot proceed using thick substrates and encapsulants, but thin substrates will endure large strains even with relatively small forces. The use of thin substrates and encapsulants is thus contingent on favorable mechanical properties of organic semiconductors. A complete picture of the factors that describe the interplay between mechanical and charge-transport properties of organic semiconductors, however, has yet to emerge.

The second, longer-term goal that drives our interest in intrinsically stretchable electronics is to access form factors that are unavailable to conventional semiconductors. Despite the intuitive notion that applications requiring elasticity, toughness, and ductility appear to be a problem for which organic materials are an ideal fit, devices based on inorganic materials using deterministic composites described in Section 2.4 have overtaken organics in terms of electronic and mechanical performance metrics.[69] There are, however, several compelling reasons to explore molecularly stretchable materials for applications that are complementary to inorganic-elastomeric hybrid systems. Such molecularly stretchable devices could, if necessary, sacrifice state-of-the-art performance for one or

more of the following characteristics for which organics may have advantages: tunability of absorption, emission, and chemical sensitivity by synthesis;[54,118] simplification of fabrication by roll-to-roll printing on planar elastomeric sheets;[117,136] the potential for melt processing and embossing;[137] relaxed standards of purity;[138,139] low embodied energy;[33,116] low cost;[115] extreme thinness and light weight;[32] disposability;[132] self-healing and other forms of response to stimuli;[140] thermally activated charge transport;[141] semitransparency[142] and aesthetic considerations;[136] and the fundamental knowledge that could be created en route to the development of elastomeric materials that are also high-performance semiconductors.

1.3.2. Stretchable conjugated polymers

The effect of stretch aligning on conjugated polymers such as polyacetylene is to increase both conductivity and tensile strength.[1-3] For polymers with alkyl solubilizing groups such as P3HT, stretch aligning has also been shown to increase field-effect charge-carrier mobility along the strained axis.[143,144] The mechanism for increased strength and charge transport is by alignment of chains, a phenomenon that is confirmed by X-ray diffraction and by polarization-dependent absorption.[130,144] Other microstructural changes can occur with strain, as O'Connor and coworkers recently reported a reorientation of crystallites in P3HT films from predominantly edge-on to highly face-on after uniaxial[144] and biaxial[145] stretching. The mechanism for this reorientation has not yet been elucidated, but the effect has important implications for solar cells, in which it may be beneficial to have the axis of π stacking perpendicular to the electrodes[145] (though it may be better still to have the *molecular* axes of the polymers perpendicular to the electrodes[14]).

One of the most successful synthetic attempts to date to produce a tough, stretchable semiconducting polymer was that of Müller et al., who synthesized a P3HT-block-polyethylene copolymer capable of undergoing elongations of 600% (**Figure 1.4a**).[126] Remarkably, this material retained a high value of field-effect mobility even with weight fractions of the insulating component as high as 90%.[126] While the ductility of this material was impressive (**Figure 1.4b)**, elastic semiconductors that do not have such a high weight percentage of an insulating component will be desirable. To this end, we believe an effective strategy would be to understand the structural determinants of the mechanical properties of well-known conjugated polymers, while applying the insights generated toward the synthesis of new materials that exhibit the "best of both worlds"[22]—favorable mechanical and electronic properties.

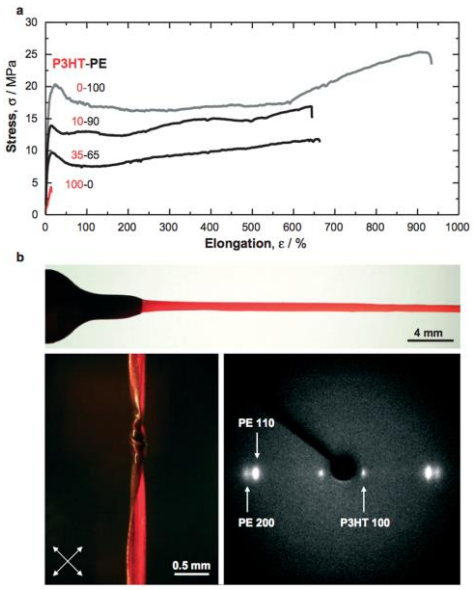

Figure 1.4. Tough, stretchable diblock copolymers of polythiophene and polyethylene. (a) Stress vs. elongation for the block copolymers and for the homopolymers. (b) Images exhibiting the mechanical behavior of the block copolymers, and wide-angle X-ray diffraction pattern of a highly stretch-aligned sample. Reproduced with permission from ref. [126], copyright 2007 Wiley-VCH Verlag GmbH & Co. KGaA.

1.3.3. Mechanical properties of regioregular polythiophene: A case study

We began our investigations by considering the effect of the side chain on the mechanical properties of the poly(3-alkylthiophene)s (P3ATs).[21,22] The P3ATs are probably the most well characterized class of organic electronic materials,[146-148] and the effects of the length of the side chain is their most widely explore aspect.[6,148-153] While the P3ATs have been the subject of numerous studies,[154] the low production energy,[33] ease of derivatization,[147] reports of new benchmarks in efficiency,[155] and research investment suggests that they will continue to be an important part of research, and also of future commercial products.[156] We began by measuring the elasticity and ductility of a series of P3ATs where A = butyl, hexyl, octyl, and dodecyl.[21] We chose this sequence because the length of the side chains that separate butyl, octyl, and dodecyl is a constant four atoms apart, and hexyl because P3HT is the standard material in the literature. We measured the elasticity using the buckling-based metrology,[102] which relates the wavelength of the sinusoidal wrinkles that form when a film is compressed on an elastic substrate to the tensile modulus of the film.[103] This method avoids the difficulties in preparing sub-100-nm, free-standing thin films for tensile testing and effects of the substrate in nanoindentation of ultra thin films.[102] Our results, plotted in **Figure 1.5a**, show a dramatic decrease in tensile modulus with increasing length of the alkyl side chains, with the difference between polymers with hexyl and octyl chains being nearly an order of magnitude. This trend was predicted by a semi-empirical theory reported by Seitz,[157] used for the first time on conjugated polymers by Tahk et al.,[20] and applied to polythiophenes with different alkyl side chains by us.[21] The explanation for the overall trend is familiar in the field of comb-like polymers, where longer alkyl side chains dilute the volume fraction

of load-bearing, main-chain bonds and a concomitant reduction in secondary interactions between the main chains,[5] which are responsible for the high strength of oriented polyacetylenes.

We note that an examination of the early literature reveals a reversal in attitudes regarding the desirability of high mechanical compliance. For polyacetylenes, a tensile modulus >10 GPa was regarded as favorable,[1] while the inclusion of alkyl pendant groups on comb-like polymers was described as paying the "ultimate penalty" for processability (i.e., a substantial lowering of the tensile modulus).[5] If one places value on elasticity and ductility however, as is implied in plastic electronics, the ability to deform without fracture should be maximized. The design of molecularly stretchable electronic materials is tantamount to having charge mobilities and other electronic figures of merit that are as large as possible with tensile moduli that are as low as possible.

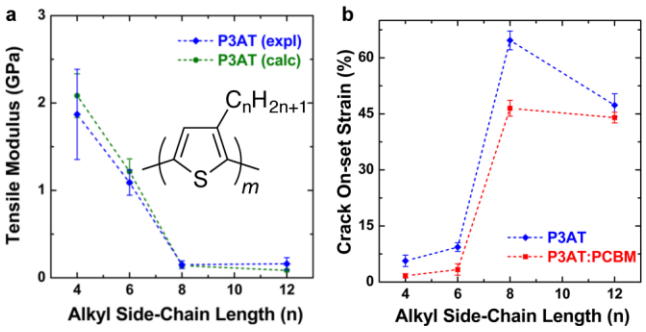

Figure 1.5. Tensile modulus (a) and crack-onset strain (b) as a function of the length of the alkyl side chain for n = 4, 6, 8, and 12. Reproduced with permission from ref. [21], copyright 2014 Wiley-VCH Verlag GmbH & Co. KGaA.

We also discovered a trend in ductility for P3ATs that followed a similar trend to that of the elasticity.[21] In a measurement of crack-onset strain for the same sequence of materials (**Figure 1.5b**), we observed a curious reduction in strain (increase in effective

brittleness) between polythiophenes with octyl and dodecyl side chains, which is unexpected based on the similarity of the tensile moduli. We attributed this effect, however, to reduced adhesion to the substrate.[21] Indeed, surface energy, as manifested in water contact angle, decreased with increasing length of the side chain.[21] Locally delaminated areas experienced large strains, and thus effective brittleness increased with reduced adhesion. The presence of PEDOT:PSS, however, seemed to serve as an adhesion layer for conjugated polymers to stick to PDMS, and increased the crack-onset strain.[25,114] Lu et al. observed the same effect in copper films on polyimide foils with and without chromium adhesion layers.[73,83] Adhesion is thus an important design consideration for devices intended for flexible and stretchable applications.[30]

1.3.4. Stretchable solar cells

To examine the differences in photovoltaic properties between two P3AT:fullerene composites with disparate mechanical properties, we fabricated devices on PDMS substrates and measured the current density vs. voltage (*J*–*V*) characteristics before stretching and at ten percent uniaxial tensile strain.[21] Extensive cracking visible in the P3HT:PCBM film (**Figure 1.6a**) correlated with short circuits (**Figure 1.6c**), whereas the P3DDT:PCBM film, which exhibited completely ductile behavior (**Figure 1.6b**), produced normal photovoltaic plots (**Figure 1.6d**).[21] The resistor-like behavior was probably produced by the liquid eutectic gallium-indium (EGaIn, **Figure 1.6e**) seeping through the cracks and making contact directly with the PEDOT:PSS in the P3HT:PCBM devices. The electrodes, along with the active materials, were strained during these experiments. While uniaxial deformation is important to measure mechanical properties and to characterize the

evolution in photovoltaic properties with strain, resiliency in response to biaxial deformation is more consistent with realistic applications and potential routes of mechanical failure.[25]

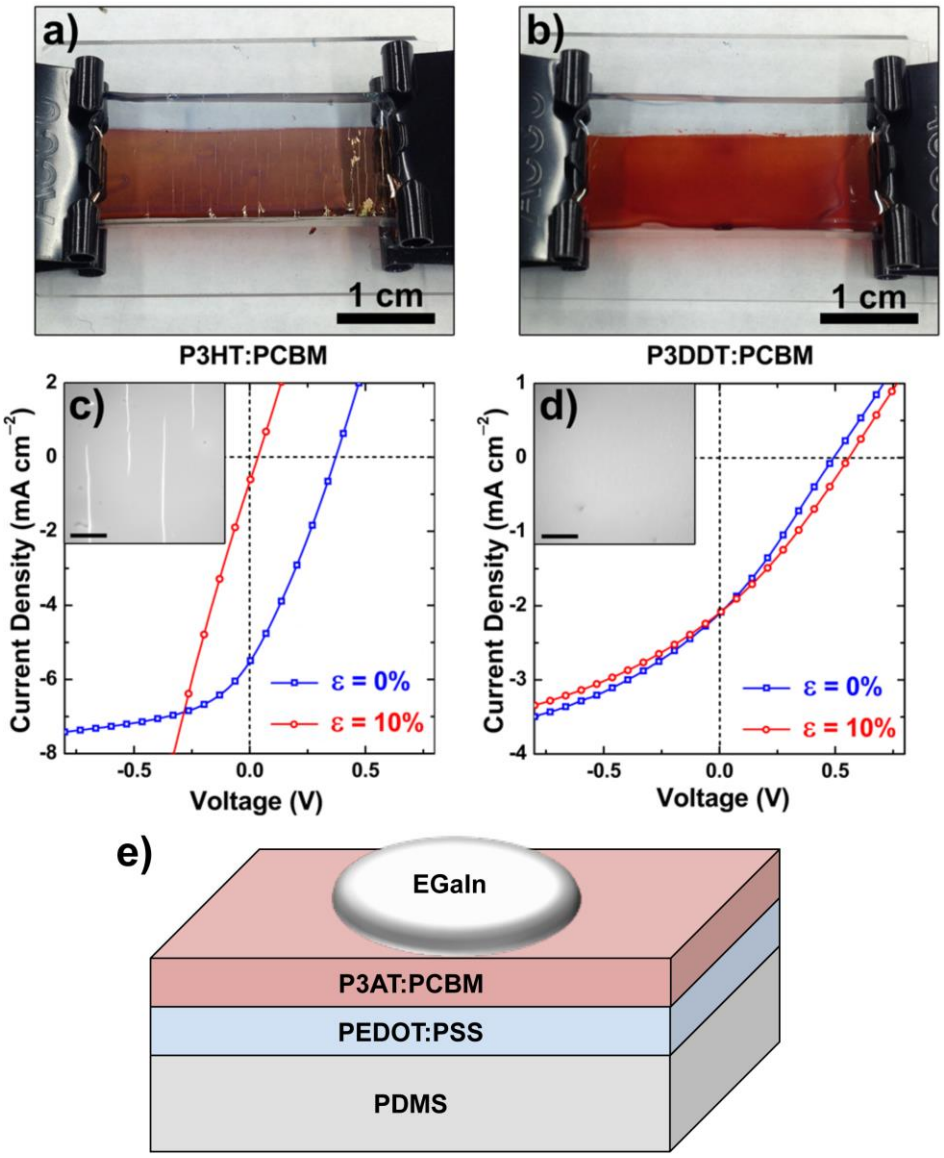

Figure 1.6. Photographs and photovoltaic properties of uniaxially stretched devices based on P3HT:PCBM (a) and P3DDT:PCBM (b). The more brittle active layer based on P3HT exhibits behavior resembling a short circuit (c) while that based on the elastic and ductile P3DDT exhibits a photovoltaic effect in both the equilibrium and strained states (d). The insets are optical micrographs of the device surfaces; the scale bars are 0.5 cm. (e) Schematic diagram of the geometry used to collect the photovoltaic data, in which eutectic gallium-indium (EGaIn) served as the low-work-function electrode. (a-d) Reproduced with permission from ref. [21], copyright 2014 Wiley-VCH Verlag GmbH & Co. KGaA.

1.3.5. Conformal bonding to hemispheres

Conformal bonding of organic electronic devices has long been a goal of the community concerned with plastic electronics. Bonding to 3D surfaces other than conical and cylindrical ones, however, requires biaxial stretchability, not just flexibility. A hemisphere is one of the simplest curvilinear surfaces that requires biaxial stretchability for a device to make conformal, wrinkle-free contact.[25] Our goal was to bond an all-elastomeric solar cell to the convex surface of a glass hemisphere (**Figure 1.7a**).[25] We began by calculating the strain that would be generated by bonding such a cell to a hemisphere with a 16-mm diameter, and determined from a finite-element analysis that the greatest equivalent strain of 24% would occur 4 mm from the apex (**Figure 1.7b**).[25] Based on our previous measurements of elasticity and ductility, we reasoned that P3OT:PCBM films would survive the transfer, but that P3HT:PCBM would not.[25] Visual inspection revealed significant cracking in the more brittle composite, while as predicted, the more elastic composite remained intact.[25] The photovoltaic responses (**Figure 1.7c**) showed similar behavior when the light was shone from the convex (device-incident) or concave (glass-incident) surface, which exhibited similar qualitative features as the device fabricated on planar glass. The P3HT:PCBM device produced plots resembling short circuits.[25] The low short-circuit current density and fill factor of devices based on P3OT (or all alkyl chains $\geq$ octyl) is well known and struck us as unfortunate that the best performing polymer mechanically would be among the worst electronically. This apparent competition between mechanical and electronic properties led us to investigate the interplay of mechanical and electronic behavior more closely.

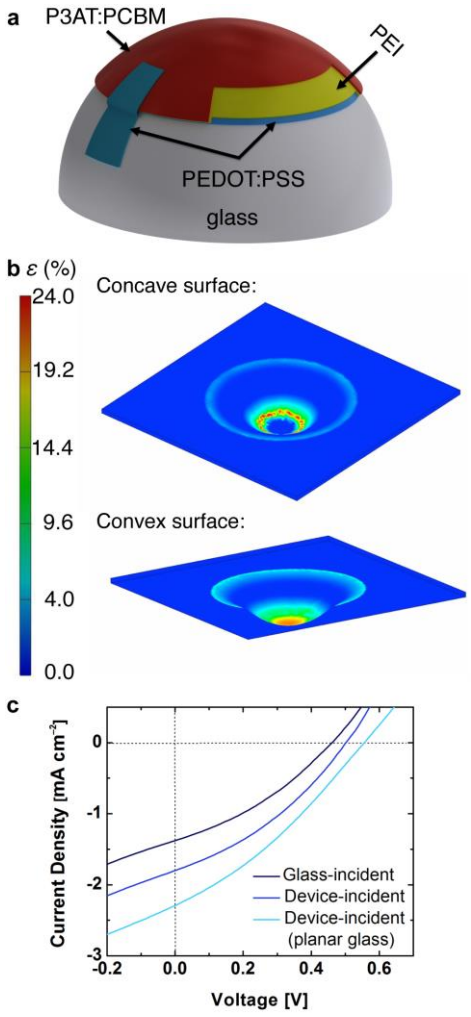

Figure 1.7. Hemispherical solar cells. (a) Schematic diagram of an all-organic "inverted" solar cell on a hemispherical glass substrate. (b) Computational model of the strain produced on the concave and convex surface of the solar cell. (c) Photovoltaic properties of the device when the light was incident on the concave surface (glass-incident), convex surface (device-incident), and on planar glass. Reproduced with permission from ref. [25], copyright 2014 Royal Society of Chemistry.

1.3.6. Trade-off between electronic and mechanical properties

The all-sp^2 hybridization of the carbon atoms in the main chain of a conjugated polymer is responsible for semiconducting behavior, but also produces high stiffness.[157] Furthermore, crystallinity in materials is generally regarded as beneficial for charge transport, but also reduces the compliance of materials within groups having similar

molecular structures.[119] The trend has been observed in polythiophenes, where the copolymer PBTTT (**Figure 1.1**) forms a highly crystalline structure after thermal annealing, which also increases the modulus and the charge-carrier mobility.[119] The O'Connor group has shown that slow evaporation of the solvent when casting P3HT:PCBM active layers produce devices that are not only more efficient, but also stiffer and more brittle than their counterparts produced by fast evaporation.[27] These differences were directly correlated to order in the conjugated polymer film from UV-vis absorption spectra[27] using the weakly interacting H aggregate model proposed by Spano and coworkers.[158] Our measurements, combined with the fact that the trend in field-effect mobility of P3ATs,[159] along with photovoltaic efficiency in polymer:polymer[153] and polymer:fullerene[160] bulk heterojunction solar cells follows the opposite trend as compliance, further supported the notion that mechanical compliance and electronic performance tend to be in competition.[21]

1.3.7. Best of both worlds?

We initially believed that, like transparency and conductivity, compliance and charge mobility (or photovoltaic efficiency) might be properties that were fundamentally incompatible, and that only by compositing would we be able to maximize both properties in a single material. We examined more closely the sharp drop-off in modulus that we observed between P3ATs with hexyl and octyl side chains by preparing films of several "hybrid" materials whose side chains average to seven carbon atoms: a physical blend (P3HT:P3OT), a block copolymer (P3HT-*b*-P3OT), a statistical copolymer (P3HT-*co*-P3OT), and poly(3-heptylthiophene) (P3HpT, whose side chain contains exactly seven

carbon atoms, **Figure 1.8**).[22] The results of our mechanical measurements are shown in **Figure 1.9**, which exhibits three salient features. The first feature is that P3HpT (C_7) has a modulus of a similar order of magnitude as that of P3OT (C_8), P3DT (C_{10}), and P3DDT (C_{12}). The second feature is the modulus of poly(3-pentylthiophene) (P3PT, C_5), which lies on the line connecting P3BT (C_4) and P3HT (C_6). This placement suggests that the low modulus of P3HpT is probably not a consequence of an odd number of carbon atoms in the side chain. The third feature is the relative placement of the other "hybrid" materials. The block copolymer falls on the line connecting P3HT and P3OT—the "synergistic" modulus—while the statistical copolymer and the physical blend lie below this line.[22] We hypothesized that the P3HT and P3OT domains are not cocrystallized in either the block copolymer or the physical blend. We based this hypothesis on the spectroscopic similarity of the block copolymer and the physical blend and the overlap in the spectra of both of these systems to that of a mathematical superposition of the spectra of the pure homopolymers. The lack of cocrystallization suggests that in the block copolymer, compliant domains of P3OT are tethered by rigid domains of P3HT due to covalent connectivity, while no such connectivity exists in the physical blend, whose mechanical properties appear to be dominated by the more compliant P3OT.[22] The statistical copolymer, which could only exhibit one possible form of crystalline packing, had a modulus similar to that of the physical blend.

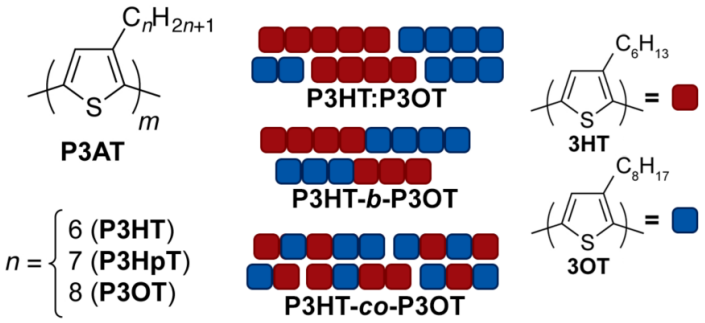

Figure 1.8. Chemical structures of the P3ATs with n = 6–8 and "hybrid" polymers including a physical blend of P3HT and P3OT (P3HT:P3OT), a block copolymer (P3HT-*b*-P3OT), and a statistical copolymer (P3HT-*co*-P3OT). Reproduced with permission from ref. [22], copyright 2014 American Chemical Society.

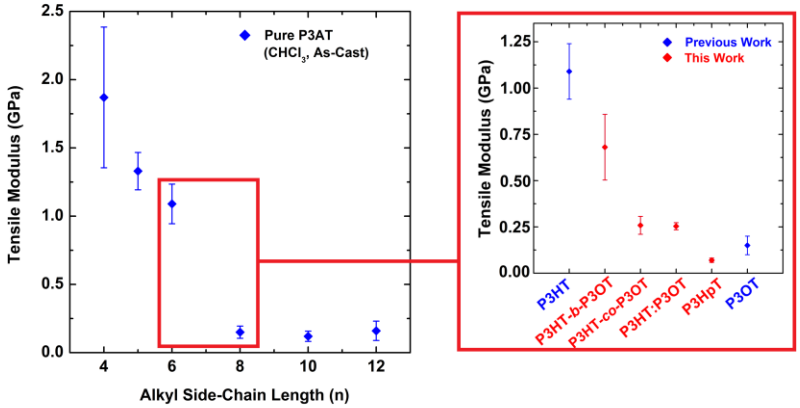

Figure 1.9. Elaborated plot of tensile modulus vs. alkyl side chain length that includes the hybrid materials whose number of carbon atoms in the side chain averages to n = 7. Reproduced with permission from ref. [22], copyright 2014 American Chemical Society.

We also performed a detailed microstructural analysis of the films formed by these polymers of UV-vis spectra in the solid state.[22] According to the weakly interacting H aggregate model, the extent of order is correlated to the relative intensities of absorption of the 0→0 to 0→1 vibronic transitions.[158] Awartani et al. found a direct correlation between the extent of crystallites in the solid state to the mechanical compliance in P3HT:PCBM films.[27] In comparing the physical blend and the block copolymer, we found nearly identical spectroscopically determined order, but a substantially different mechanical response.[22] We also found substantially similar mechanical behavior between the physical

blend and the statistical copolymer, yet different structural order.[22] We did not observe a correlation between thin-film order and mechanical compliance in our samples, probably because of the insensitivity of the UV-vis spectra to spatial distribution and covalent connectivity of the compliant and rigid blocks within the film. The correlation between the crystalline order and the photovoltaic parameters, however, was roughly present in the physical blend, block copolymer, and statistical copolymer. **Figure 1.10** plots the power conversion efficiency of the P3AT:PCBM blend as a function of tensile modulus of the polymer. A pure correlation between efficiency and stiffness would place all data points on a line connecting P3OT in the bottom left quadrant to P3HT in the top right one.[22]

The observation that some of the hybrid materials lie above and to the left of this line—that is, in the "favorable" quadrant—strongly suggests that mechanical and electronic properties need not always be in competition. This notion is exemplified by the presence of P3HpT in the extreme top-left corner, which is simultaneously the most efficient and most elastic material studied. We attribute the uniqueness of P3HpT to its tendency to produce crystallites that are similarly well ordered as those of P3HT, while its glass transition temperature is the first in the series of P3ATs with increasing side-chain length to be extrapolated to be significantly below room temperature (most measurements of T_g of P3HT place it near or just below 25 °C).[161] The electronic absorption spectra and the photovoltaic properties appear thus to be manifestations of the crystalline regions in the film, while the mechanical properties seem to be dominated by the amorphous regions. These observations may underpin design criteria for truly "rubber" semiconductors.[22]

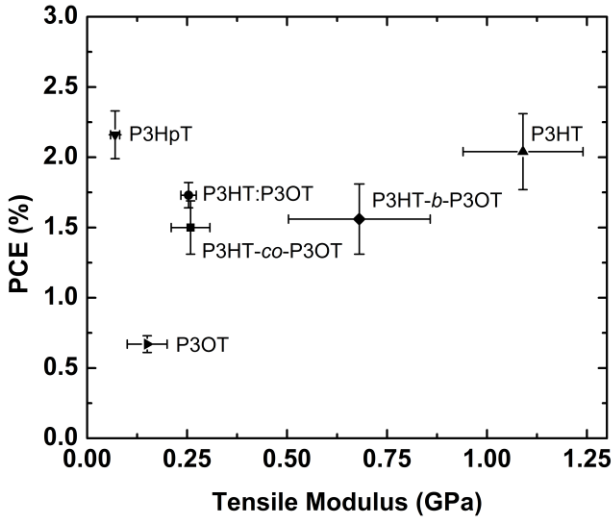

Figure 1.10. Plot of power conversion efficiency (*PCE*) of a P3AT:PCBM vs. tensile modulus of the pure polymer. The position of P3HpT in the upper-left quadrant suggests that photovoltaic performance and mechanical compliance need not be in competition. Reproduced with permission from ref. [22], copyright 2014 American Chemical Society.

1.3.8. Segmented copolymers

While P3ATs will almost certainly have a role in the future of organic electronics, they are not the highest-performing materials in the literature in terms of charge-carrier mobility in OTFTs and efficiency in solar cells.[16,118] Donor-acceptor copolymers comprising alternating units of electron-rich (e.g., thiophene, benzodithiophene) and electron poor (e.g., benzothiadiazole, diketopyrrolopyrrole) heterocycles produce low bandgaps and high mobilities for both holes and electrons.[15] We were inspired by the fact that low-bandgap conjugated polymers can exhibit high mobilities and photovoltaic efficiencies even with high disorder.[162,163] We hypothesized that structural randomness, intentionally introduced by a new type of synthetic strategy based on random segmentation, could produce a material that might have increased elasticity without deleterious effects on the photovoltaic properties.[26]

We began our investigation by considering the structure PDPP2FT (see **Figure 1.1**), which was first reported by the Fréchet group.[164] This material exhibited good electronic performance (*PCE* ~ 5.0%) and a high solubility that is thought to be an effect of the furan units in the main chain.[164] We started by preparing oligomers of PDPP2FT by the Stille polymerization. After a short reaction time (ca. 15 min) in which we observed the first formation of coupled species by color change, we introduced bithiophene (2T) units, which were included randomly in the polymer backbone (**Figure 1.11a**).[26] Analysis by ^{1}H NMR and UV-vis spectroscopy and gel permeation chromatography was consistent with the presence of one 2T unit for approximately every 4.4 DPP units. Spectroscopic and chromatographic evidence suggested that there was little contamination by the homopolymers, PDPP2FT and the poly(terthiophene), PT2T. The segmented sample, PDPP2FT-seg-2T, exhibited substantial broadening of features in the UV-vis spectra, which is consistent with reduced structural order in the solid state (X-ray diffraction studies, which are forthcoming, will be needed to verify this hypothesis). We then made a similar plot of *PCE* vs. tensile modulus of the pure polymer (**Figure 1.11b**). Our hypothesis that it would be possible to increase the elasticity by intentionally randomizing the structure is consistent with the plot, in which the segmented material was both more elastic and similarly efficient to the unsegmented homopolymer, PDPP2FT.[26] This synthetic strategy might also be useful for the preparation of functional copolymers analogous to block copolymers by polycondensation of two types of macromonomers.[165,166] Typical block copolymers are synthesized by living, chain-growth mechanisms, and thus materials that follow step-growth kinetics, as do low-bandgap conjugated polymers, are generally not amenable to block copolymerization.[167] We note that efficiencies of our devices based on

PDPP2FT (≤3%) were lower than those originally reported for this material (~5.0%). We attribute the lower efficiencies of our devices, in part, to our use of stretchable materials for the electrodes (PEDOT:PSS for the anode and EGaIn for the cathode), because of our ultimate interest in systems in which every component is compliant.

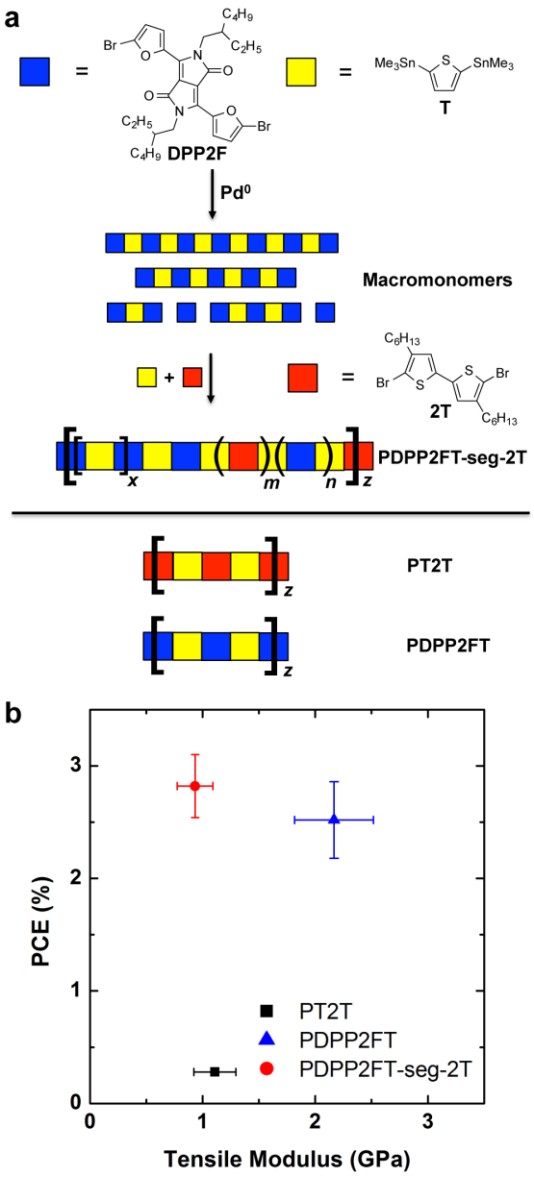

Figure 1.11. Mechanical and photovoltaic properties of segmented polymers. (a) A strategy based on Stille polycondensation reactions produces a randomly segmented, low-bandgap polymer, PDPP2FT-seg-2T. (b) A plot of power conversion efficiency (*PCE*) vs. tensile modulus places this material in the "favorable" quadrant of the plot. Reproduced with permission from ref. [26], copyright 2014 Royal Society of Chemistry.

1.3.9. Intrinsically stretchable light-emitting devices

Our studies and those of others have revealed several structural characteristics that influence the mechanical properties of conjugated polymers, including the length of the alkyl side chain,[21] the presence of fused vs. isolated rings in the main chain,[114] structural randomness,[26] and the ability of the side chains to interdigitate in the crystallites.[119] Another route may be to replace methylene units with oxygen atoms in the side chain that permit a high range of motion.[108] This route can be predicted by a preliminary application of the semi-empirical theory of Seitz to increase the modulus significantly, probably owing to increased configurational entropy of the side chains under strain.[157] The laboratory of Pei and coworkers used a polyfluorene copolymer that incorporated side chains with ethylene oxide units as light emitting devices that maintained their performance up to strains as high as 45 percent (**Figure 1.3f** and **1.3g**).[108] The authors also introduced one of the first stretchable transparent electrodes based on carbon nanotubes embedded in an elastic substrate as both the top and bottom electrodes of this device.[108] Later, the same group produced a stretchable light-emitting device with an active emissive layer comprising a poly(phenylenevinylene) derivative, SuperYellow, and electrodes made of stretchable films of silver nanowires.[110] This approach suggests it is possible to combine stretchable random composites (i.e., silver nanowire films on elastic substrates) with intrinsically stretchable conjugated polymers (**Figure 1.12**). The mechanism of reversible deformation in this system, that is, whether the emissive layer absorbs the strain elastically or plastically, is an open question, as the substrate supplies the restoring force. Furthermore, it is likely that the addition of non-electroactive polymers and ionic species

to the conjugated polymers increased the compliance of the emissive layer, and thus the electroactive polymer may not have absorbed the strain on its own.

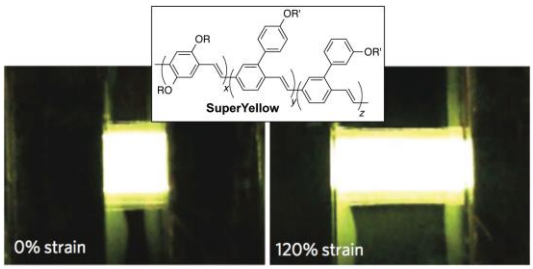

Figure 1.12. Intrinsically stretchable light-emitting devices. A stretchable device uses SuperYellow, a polyphenylenevinylene derivative, as the emissive material. In this device, stretchable films of silver nanowires are used as both the top and bottom electrodes. Reproduced with permission from ref. [110], copyright 2013 Nature Publishing Group.

1.4. Outlook

This Perspective began by describing the value of stretchable electronics, and how the field of plastic—that is, organic—electronics may have fallen behind the significant progress made by stretchable composite systems. The two approaches are, however, complementary, and there are many compelling reasons for pursuing intrinsically stretchable electronic materials and devices whose molecular structures permit truly elastic and plastic behavior. The field of molecularly stretchable electronics is in its infancy, but significant progress on understanding how molecular structure influences the electronic properties has already been made. Such fundamental insights are necessary to develop a predictive framework so that, ideally, a device engineer can specify the mechanical and electronic properties needed for a particular application, and a chemist can synthesize a material that will exhibit these properties. Synthetic techniques will always constrain available structures,[116] but the several methods identified to produce elastic-yet-high-performance materials suggest that there may be many functionally equivalent materials

with different molecular structures. Several general strategies for imparting intrinsic stretchability to semiconducting materials are emerging from work in this area. For example, polymers exhibiting low-T_g amorphous domains but well-ordered crystalline domains (e.g., P3HpT), along with high-mobility polymers with structural randomness to reduce crystalline order (e.g., PDPP2FT-seg-2T), could represent general strategies for producing materials with favorable combinations of mechanical and electronic properties. From the standpoint of integration, molecularly stretchable materials may offer advantages over deterministic composites because most of the engineering takes place at the molecular level, as opposed to at the level of the device (i.e., it is relatively easy to swap out a rigid semiconducting polymer for an elastic one in the context of an existing manufacturing process).

The principal challenge in the field is to obtain a better predictive understanding of the ways in which molecular structure simultaneously influences electronic and mechanical properties. The ability to obtain good electronic properties from highly amorphous films seems to represent a way forward. Another strategy, which involves preparing stretchable nanowire "fabrics" from solution processing[168] or electrospinning,[169] represents a middle ground between composite and molecular approaches to elastic semiconductors. A concerted effort involving a five-way (at least) collaboration between device engineers, materials scientists, synthetic chemists, and theorists specializing in both electronic structure calculations and the mechanical behavior of soft materials will be required to meet the challenges represented by high-performance molecular semiconductors with predictable mechanical properties. There is a significant intellectual draw to multifunctional materials in which the properties are regarded as antithetical. Stretchable

semiconductors join transparent conductors as examples of this class of materials. Another class of multifunctional materials that will be required to commercialize stretchable organic (and some inorganic) devices is stretchable encapsulants against water and oxygen. Significant work will be required to address this challenge, because elastomers generally permit significant diffusion of gases. We hope this Perspective will be successful in identifying the importance, preliminary results, and potential way forward in this technologically and intellectually exciting field.

Acknowledgements

This work was supported by the Air Force Office of Scientific Research (AFOSR) Young Investigator Program, grant number FA9550-13-1-0156. Additional support was provided by laboratory startup funds from the University of California, San Diego. S. S. acknowledges a fellowship from the National Science Foundation Graduate Research Fellowship Program under Grant No. DGE-1144086. A. Z. acknowledges a fellowship from SoCal Clean Energy Technology Acceleration Program from the von Liebig Center at UCSD sponsored by the US Department of Energy.

Chapter 1, in full, is a reprint of the material as it appears in *Chemistry of Materials*, 2014, 26, 3028-3041. American Chemical Society, 2014. Suchol Savagatrup, Adam D. Printz, Timothy F. O'Connor, Aliaksandr V. Zaretski, and Darren J. Lipomi. The dissertation author was the primary investigator and author of this paper.

References

(1) Heeger, A. J. *Angew. Chem., Int. Ed.* **2001**, *40*, 2591.

(2) Cao, Y.; Smith, P. A.; Heeger, A. J. *Synthetic Met.* **1991**, *41-43*, 181.

(3) Cao, Y.; Smith, P.; Heeger, A. J. *Polymer* **1991**, *32*, 1210.

(4) Tokito, S.; Smith, P.; Heeger, A. J. *Synthetic Met.* **1990**, *36*, 183.

(5) Postema, A. R.; Liou, K.; Wudl, F.; Smith, P. *Macromolecules* **1990**, *23*, 1842.

(6) Moulton, J.; Smith, P. *Polymer* **1992**, *33*, 2340.

(7) Yu, G.; Gao, J.; Hummelen, J. C.; Wudl, F.; Heeger, A. J. *Science* **1995**, *270*, 1789.

(8) Yu, G.; Heeger, A. J. *Journal of Applied Physics* **1995**, *78*, 4510.

(9) Halls, J. J. M.; Walsh, C. A.; Greenham, N. C.; Marseglia, E. A.; Friend, R. H.; Moratti, S. C.; Holmes, A. B. *Nature* **1995**, *376*, 498.

(10) Burroughes, J. H.; Bradley, D. D. C.; Brown, A. R.; Marks, R. N.; Mackay, K.; Friend, R. H.; Burns, P. L.; Holmes, A. B. *Nature* **1990**, *347*, 539.

(11) Tsumura, A.; Koezuka, H.; Ando, T. *Appl. Phys. Lett.* **1986**, *49*, 1210.

(12) Bao, Z. N.; Dodabalapur, A.; Lovinger, A. J. *Appl. Phys. Lett.* **1996**, *69*, 4108.

(13) Bao, Z. N.; Lovinger, A. J. *Chem. Mater.* **1999**, *11*, 2607.

(14) Tseng, H. R.; Phan, H.; Luo, C.; Wang, M.; Perez, L. A.; Patel, S. N.; Ying, L.; Kramer, E. J.; Nguyen, T. Q.; Bazan, G. C.; Heeger, A. J. *Adv. Mater.* **2014**, *online*, 10.1002/adma.201305084.

(15) Chen, Z. Y.; Lee, M. J.; Ashraf, R. S.; Gu, Y.; Albert-Seifried, S.; Nielsen, M. M.; Schroeder, B.; Anthopoulos, T. D.; Heeney, M.; McCulloch, I.; Sirringhaus, H. *Adv. Mater.* **2012**, *24*, 647.

(16) Dou, L. T.; You, J. B.; Hong, Z. R.; Xu, Z.; Li, G.; Street, R. A.; Yang, Y. *Adv. Mater.* **2013**, *25*, 6642.

(17) Peet, J.; Heeger, A. J.; Bazan, G. C. *Acc. Chem. Res.* **2009**, *42*, 1700.

(18) Shaheen, S. E.; Brabec, C. J.; Sariciftci, N. S.; Padinger, F.; Fromherz, T.; Hummelen, J. C. *Appl. Phys. Lett.* **2001**, *78*, 841.

(19) Kaltenbrunner, M.; Sekitani, T.; Reeder, J.; Yokota, T.; Kuribara, K.; Tokuhara, T.; Drack, M.; Schwodiauer, R.; Graz, I.; Bauer-Gogonea, S.; Bauer, S.; Someya, T. *Nature* **2013**, *499*, 458.

(20) Tahk, D.; Lee, H. H.; Khang, D. Y. *Macromolecules* **2009**, *42*, 7079.

(21) Savagatrup, S.; Makaram, A. S.; Burke, D. J.; Lipomi, D. J. *Adv. Funct. Mater.* **2014**, *24*, 1169.

(22) Savagatrup, S.; Printz, A. D.; Rodriquez, D.; Lipomi, D. J. *Macromolecules* **2014**, *in press*.

(23) Lipomi, D. J.; Lee, J. A.; Vosgueritchian, M.; Tee, B. C.-K.; Bolander, J. A.; Bao, Z. N. *Chem. Mater.* **2012**, *24*, 373.

(24) Vosgueritchian, M.; Lipomi, D. J.; Bao, Z. N. *Adv. Funct. Mater.* **2012**, *22*, 421.

(25) O'Connor, T. F.; Zaretski, A. V.; Shiravi, B. A.; Savagatrup, S.; Printz, A. D.; Diaz, M. I.; Lipomi, D. J. *Energy Environ. Sci.* **2014**, *7*, 370.

(26) Printz, A. D.; Savagatrup, S.; Burke, D. J.; Purdy, T.; Lipomi, D. J. *RSC Adv.* **2014**, *4*, 13635.

(27) Awartani, O.; Lemanski, B.; Ro, H. W.; Richter, L. J.; DeLongchamp, D. M.; O'Connor, B. T. *Adv. Energy Mater.* **2013**, *3*, 399.

(28) Lipomi, D. J.; Bao, Z. N. *Energ. Environ. Sci.* **2011**, *4*, 3314.

(29) Brand, V.; Bruner, C.; Dauskardt, R. H. *Sol. Energy Mater. Sol. Cells* **2012**, *99*, 182.

(30) Dupont, S. R.; Oliver, M.; Krebs, F. C.; Dauskardt, R. H. *Sol. Energy Mater. Sol. Cells* **2012**, *97*, 171.

(31) Hu, B. *Workshop on Key Scientific and Technological Issues for Development of Next-Generation Organic Solar Cells*, 2012.
http://web.utk.edu/~opvwshop/files/Report.pdf, accessed on 4/18/14.

(32) Kaltenbrunner, M.; White, M. S.; Glowacki, E. D.; Sekitani, T.; Someya, T.; Sariciftci, N. S.; Bauer, S. *Nat. Comm.* **2012**, *3*, 770.

(33) Anctil, A.; Babbitt, C. W.; Raffaelle, R. P.; Landi, B. J. *Prog. Photovolt: Res. Appl.* **2012**, *DOI: 10.1002/pip*.

(34) Lacour, S. P.; Wagner, S.; Huang, Z. Y.; Suo, Z. *Appl. Phys. Lett.* **2003**, *82*, 2404.

(35) Choi, W. M.; Song, J. Z.; Khang, D. Y.; Jiang, H. Q.; Huang, Y. Y.; Rogers, J. A. *Nano Lett.* **2007**, *7*, 1655.

(36) Kim, D. H.; Rogers, J. A. *Adv. Mater.* **2008**, *20*, 4887.

(37) Khang, D. Y.; Rogers, J. A.; Lee, H. H. *Adv. Funct. Mater.* **2009**, *19*, 1526.

(38) Lipomi, D. J.; Tee, B. C.-K.; Vosgueritchian, M.; Bao, Z. N. *Adv. Mater.* **2011**, *23*, 1771.

(39) Wagner, S.; Bauer, S. *MRS Bull.* **2012**, *37*, 207.

(40) Krebs, F. C.; Biancardo, M.; Winther-Jensen, B.; Spanggard, H.; Alstrup, J. *Sol. Energy Mater. Sol. Cells* **2006**, *90*, 1058.

(41) Spurgeon, J. M.; Boettcher, S. W.; Kelzenberg, M. D.; Brunschwig, B. S.; Atwater, H. A.; Lewis, N. S. *Adv. Mater.* **2010**, *22*, 3277.

(42) Lee, J.; Wu, J. A.; Shi, M. X.; Yoon, J.; Park, S. I.; Li, M.; Liu, Z. J.; Huang, Y. G.; Rogers, J. A. *Adv. Mater.* **2011**, *23*, 986.

(43) Kim, D. H.; Viventi, J.; Amsden, J. J.; Xiao, J. L.; Vigeland, L.; Kim, Y. S.; Blanco, J. A.; Panilaitis, B.; Frechette, E. S.; Contreras, D.; Kaplan, D. L.; Omenetto, F. G.; Huang, Y. G.; Hwang, K. C.; Zakin, M. R.; Litt, B.; Rogers, J. A. *Nat. Mater.* **2010**, *9*, 511.

(44) Viventi, J.; Kim, D. H.; Moss, J. D.; Kim, Y. S.; Blanco, J. A.; Annetta, N.; Hicks, A.; Xiao, J. L.; Huang, Y. G.; Callans, D. J.; Rogers, J. A.; Litt, B. *Sci Transl Med* **2010**, *2*.

(45) Ghezzi, D.; Antognazza, M. R.; Maccarone, R.; Bellani, S.; Lanzarini, E.; Martino, N.; Mete, M.; Pertile, G.; Bisti, S.; Lanzani, G.; Benfanati, F. *Nat. Photonics* **2013**, *7*, 400.

(46) Ko, H. C.; Stoykovich, M. P.; Song, J. Z.; Malyarchuk, V.; Choi, W. M.; Yu, C. J.; Geddes, J. B.; Xiao, J. L.; Wang, S. D.; Huang, Y. G.; Rogers, J. A. *Nature* **2008**, *454*, 748.

(47) Someya, T.; Kato, Y.; Sekitani, T.; Iba, S.; Noguchi, Y.; Murase, Y.; Kawaguchi, H.; Sakurai, T. *Proc. Natl. Acad. Sci. USA* **2005**, *102*, 12321.

(48) Sokolov, A. N.; Tee, B. C.-K.; Bettinger, C. J.; Tok, J. B.-H.; Bao, Z. N. *Acc. Chem. Res.* **2011**.

(49) Pan, L. J.; Chortos, A.; Yu, G. H.; Wang, Y. Q.; Isaacson, S.; Allen, R.; Shi, Y.; Dauskardt, R. H.; Bao, Z. N. *Nat. Comm.* **2014**, *5*, 3002.

(50) Benight, S. J.; Wang, C.; Tok, J. B.-H.; Bao, Z. N. *Prog. Polym. Sci.* **2013**, *39*, 1961.

(51) Ilievski, F.; Mazzeo, A. D.; Shepherd, R. F.; Chen, X.; Whitesides, G. M. *Angew. Chem., Int. Ed.* **2011**, *50*, 1890.

(52) Shepherd, R. F.; Ilievski, F.; Choi, W.; Morin, S. A.; Stokes, A. A.; Mazzeo, A. D.; Chen, X.; Wang, M.; Whitesides, G. M. *Proc. Natl. Acad. Sci. USA* **2011**, *108*, 20400.

(53) Fang, L.; Zhou, Y.; Yao, Y. X.; Diao, Y.; Lee, W. Y.; Appleton, A. L.; Allen, R.; Reinspach, J.; Mannsfeld, S. C. B.; Bao, Z. N. *Chem. Mater.* **2013**, *25*, 4874.

(54) Mei, J. G.; Bao, Z. N. *Chem. Mater.* **2014**, *26*, 604.

(55) Dou, L. T.; You, J. B.; Yang, J.; Chen, C. C.; He, Y. J.; Murase, S.; Moriarty, T.; Emery, K.; Li, G.; Yang, Y. *Nat. Photonics* **2012**, *6*, 180.

(56) Andersen, T. R.; Dam, H. F.; Andreasen, B.; Hosel, M.; Madsen, M. V.; Gevorgyan, S. A.; Sondergaard, R. R.; Jorgensen, M.; Krebs, F. C. *Sol. Energy Mater. Sol. Cells* **2014**, *120*, 735.

(57) Roberts, M. E.; Sokolov, A. N.; Bao, Z. N. *J. Mater. Chem.* **2009**, *19*, 3351.

(58) Thompson, B. C.; Kim, Y. G.; McCarley, T. D.; Reynolds, J. R. *J. Am. Chem. Soc* **2006**, *128*, 12714.

(59) Ding, Y.; Invernale, M. A.; Sotzing, G. A. *Acs Applied Materials & Interfaces* **2010**, *2*, 1588.

(60) Jensen, J.; Hosel, M.; Kim, I.; Yu, J. S.; Jo, J. D.; Krebs, F. C. *Adv. Funct. Mater.* **2013**, *24*, 1228.

(61) Jensen, J.; Dyer, A. L.; Shen, D. E.; Krebs, F. C.; Reynolds, J. R. *Adv. Funct. Mater.* **2013**, *23*, 3728.

(62) Yu, Z. B.; Zhang, Q. W.; Li, L.; Chen, Q.; Niu, X. F.; Liu, J.; Pei, Q. B. *Adv. Mater.* **2011**, *23*, 664.

(63) Willson, C. G.; Roman, B. J. *ACS Nano* **2008**, *2*, 1323.

(64) Lipomi, D. J.; Martinez, R. V.; Cademartiri, L.; Whitesides, G. M. "Soft Lithographic Approaches to Nanofabrication" In *Polymer Science, A Comprehensive Reference*, vol. 7; Kumacheva, E.; Russell, T. Eds., Elsevier, 2012. doi:10.1016/B978-0-444-53349-4.00180-1

(65) Williams, E. D.; Ayres, R. U.; Heller, M. *Environ. Sci. Technol.* **2002**, *36*, 5504.

(66) Williams, E. *Environmental Science & Technology* **2004**, *38*, 6166.

(67) Khang, D. Y.; Jiang, H. Q.; Huang, Y.; Rogers, J. A. *Science* **2006**, *311*, 208.

(68) Kim, D. H.; Ahn, J. H.; Choi, W. M.; Kim, H. S.; Kim, T. H.; Song, J. Z.; Huang, Y. G. Y.; Liu, Z. J.; Lu, C.; Rogers, J. A. *Science* **2008**, *320*, 507.

(69) Kim, D. H.; Lu, N. S.; Ma, R.; Kim, Y. S.; Kim, R. H.; Wang, S. D.; Wu, J.; Won, S. M.; Tao, H.; Islam, A.; Yu, K. J.; Kim, T. I.; Chowdhury, R.; Ying, M.; Xu, L. H.; Li, M.; Chung, H. J.; Keum, H.; McCormick, M.; Liu, P.; Zhang, Y. W.; Omenetto, F. G.; Huang, Y.; Coleman, T.; Rogers, J. A. *Science* **2011**, *333*, 838.

(70) Sekitani, T.; Someya, T. *Adv. Mater.* **2010**, *22*, 2228.

(71) Sekitani, T.; Someya, T. *MRS Bull.* **2012**, *37*, 236.

(72) Suo, Z.; Ma, E. Y.; Gleskova, H.; Wagner, S. *Appl. Phys. Lett.* **1999**, *74*, 1177.

(73) Suo, Z. *MRS Bull.* **2012**, *37*, 218.

(74) Baca, A. J.; Ahn, J. H.; Sun, Y. G.; Meitl, M. A.; Menard, E.; Kim, H. S.; Choi, W. M.; Kim, D. H.; Huang, Y.; Rogers, J. A. *Angew. Chem., Int. Ed.* **2008**, *47*, 5524.

(75) Bowden, N.; Brittain, S.; Evans, A. G.; Hutchinson, J. W.; Whitesides, G. M. *Nature* **1998**, *393*, 146.

(76) Bowden, N.; Huck, W. T. S.; Paul, K. E.; Whitesides, G. M. *Appl. Phys. Lett.* **1999**, *75*, 2557.

(77) Cotton, D. P. J.; Graz, I. M.; Lacour, S. P. *IEEE Sens. J.* **2009**, *9*, 2008.

(78) Graz, I. M.; Cotton, D. P. J.; Lacour, S. P. *Appl. Phys. Lett.* **2009**, *98*, 071902.

(79) Jones, J.; Lacour, S. P.; Wagner, S.; Suo, Z. G. *J. Vac. Sci. Technol., A* **2004**, *22*, 1723.

(80) Lacour, S. P.; Jones, J.; Suo, Z.; Wagner, S. *IEEE Electr. Device L.* **2004**, *25*, 179.

(81) Lacour, S. P.; Jones, J.; Wagner, S.; Li, T.; Suo, Z. G. *Proc. IEEE* **2005**, *93*, 1459.

(82) Lacour, S. P.; Chan, D.; Wagner, S.; Li, T.; Suo, Z. *Appl. Phys. Lett.* **2006**, *88*, 204103.

(83) Lu, N. S.; Wang, X.; Suo, Z. G.; Vlassak, J. *Appl. Phys. Lett.* **2007**, *91*, 221909.

(84) Lu, N. S.; Wang, X.; Suo, Z. G.; Vlassak, J. *J. Mater. Res.* **2009**, *24*, 379.

(85) Sun, Y. G.; Choi, W. M.; Jiang, H. Q.; Huang, Y. G. Y.; Rogers, J. A. *Nat. Nanotechnol.* **2006**, *1*, 201.

(86) Khang, D. Y.; Xiao, J. L.; Kocabas, C.; MacLaren, S.; Banks, T.; Jiang, H. Q.; Huang, Y. Y. G.; Rogers, J. A. *Nano Lett.* **2008**, *8*, 124.

(87) Shin, G.; Jung, I.; Malyarchuk, V.; Song, J. Z.; Wang, S. D.; Ko, H. C.; Huang, Y. G.; Ha, J. S.; Rogers, J. A. *Small* **2010**, *6*, 851.

(88) Fan, J. A.; Yeo, W. H.; Su, Y. W.; Hattori, Y.; Lee, W.; Jung, S. Y.; Zhang, Y. H.; Liu, Z. J.; Cheng, H. Y.; Falgout, L.; Bajema, M.; Coleman, T.; Gregoire, D.; Larsen, R. J.; Huang, Y. G.; Rogers, J. A. *Nat. Comm.* **2014**, *5*, 3266.

(89) Jung, I.; Shin, G.; Malyarchuk, V.; Ha, J. S.; Rogers, J. A. *Appl. Phys. Lett.* **2010**, *96*.

(90) Ying, M.; Bonifas, A. P.; Lu, N.; Su, Y. W.; Li, R.; Cheng, H. Y.; Ameen, A.; Huang, Y. G.; Rogers, J. A. *Nanotechnology* **2012**, *23*, 344005.

(91) Hwang, S. W.; Tao, H.; Kim, D. H.; Cheng, H. Y.; Song, J. K.; Rill, E.; Brenckle, M. A.; Panilaitis, B.; Won, S. M.; Kim, Y. S.; Song, Y. M.; Yu, K. J.; Ameen, A.; Li, R.; Su, Y. W.; Yang, M. M.; Kaplan, D. L.; Zakin, M. R.; Slepian, M. J.; Huang, Y. G.; Omenetto, F. G.; Rogers, J. A. *Science* **2012**, *337*, 1640.

(92) Sekitani, T.; Takamiya, M.; Noguchi, Y.; Nakano, S.; Kato, Y.; Sakurai, T.; Someya, T. *Nat. Mater.* **2007**, *6*, 413.

(93) Sekitani, T.; Noguchi, Y.; Hata, K.; Fukushima, T.; Aida, T.; Someya, T. *Science* **2008**, *321*, 1468.

(94) Rogers, J. A.; Someya, T.; Huang, Y. G. *Science* **2010**, *327*, 1603.

(95) Someya, T. *Nat. Mater.* **2010**, *9*, 879.

(96) Chun, K. Y.; Oh, Y.; Rho, J.; Ahn, J. H.; Kim, Y. J.; Choi, H. R.; Baik, S. *Nat. Nanotechnol.* **2010**, *5*, 853.

(97) Yamada, T.; Hayamizu, Y.; Yamamoto, Y.; Yomogida, Y.; Izadi-Jajafabadi, A.; Futaba, D. N.; Hata, K. *Nat. Nanotechnol.* **2011**, *6*, 296.

(98) Kim, K. S.; Zhao, Y.; Jang, H.; Lee, S. Y.; Kim, J. M.; Kim, K. S.; Ahn, J. H.; Kim, P.; Choi, J. Y.; Hong, B. H. *Nature* **2009**, *457*, 706.

(99) Sekitani, T.; Nakajima, H.; Maeda, H.; Fukushima, T.; Aida, T.; Hata, K.; Someya, T. *Nat. Mater.* **2009**, *8*, 494.

(100) Yuan, H. C.; Shin, J. H.; Qin, G. X.; Sun, L.; Bhattacharya, P.; Lagally, M. G.; Celler, G. K.; Ma, Z. Q. *Appl. Phys. Lett.* **2009**, *94*, 013102.

(101) Rogers, J. A.; Lagally, M. G.; Nuzzo, R. G. *Nature* **2011**, *477*, 45.

(102) Stafford, C. M.; Harrison, C.; Beers, K. L.; Karim, A.; Amis, E. J.; Vanlandingham, M. R.; Kim, H. C.; Volksen, W.; Miller, R. D.; Simonyi, E. E. *Nat. Mater.* **2004**, *3*, 545.

(103) Chung, J. Y.; Nolte, A. J.; Stafford, C. M. *Adv. Mater.* **2011**, *23*, 349.

(104) Yu, C. J.; Masarapu, C.; Rong, J. P.; Wei, B. Q.; Jiang, H. Q. *Adv. Mater.* **2009**, *21*, 4793.

(105) Qi, Y.; Kim, J.; Nguyen, T. D.; Lisko, B.; Purohit, P. K.; McAlpine, M. C. *Nano Lett.* **2011**, *11*, 1331.

(106) Keplinger, C.; Sun, J. Y.; Foo, C. C.; Rothemund, P.; Whitesides, G. M.; Suo, Z. *Science* **2013**, *341*, 984.

(107) Lipomi, D. J.; Vosgueritchian, M.; Tee, B. C.-K.; Fox, C. H.; Lee, J. A.; Bao, Z. N. *Nat. Nanotechnol.* **2011**, *6*, 788.

(108) Yu, Z. B.; Niu, X. F.; Liu, Z.; Pei, Q. B. *Adv. Mater.* **2011**, *23*, 3989.

(109) Rathmell, A. R.; Bergin, S. M.; Hua, Y. L.; Li, Z. Y.; Wiley, B. J. *Adv. Mater.* **2010**, *22*, 3558.

(110) Liang, J. J.; Li, L.; Niu, X. F.; Yu, Z. B.; Pei, Q. B. *Nat. Photonics* **2013**, *7*, 817.

(111) Wu, J. H.; Zang, J. F.; Rathmell, A. R.; Zhao, X. H.; Wiley, B. J. *Nano Lett.* **2013**, *13*, 2381.

(112) Tee, B. C.-K.; Wang, C.; Allen, R.; Bao, Z. N. *Nat. Nanotechnol.* **2012**, *7*, 825.

(113) Wu, H. S.; Kustra, S.; Gates, E. M.; Bettinger, C. J. *Org. Electron.* **2013**, *14*, 1636.

(114) Lipomi, D. J.; Chong, H.; Vosgueritchian, M.; Mei, J. G.; Bao, Z. N. *Sol. Energy Mater. Sol. Cells* **2012**, *107*, 355.

(115) Espinosa, N.; Hosel, M.; Angmo, D.; Krebs, F. C. *Energ. Environ. Sci.* **2012**, *5*, 5117.

(116) Burke, D. J.; Lipomi, D. J. *Energ. Environ. Sci.* **2013**, *6*, 2053.

(117) Manceau, M.; Angmo, D.; Jorgensen, M.; Krebs, F. C. *Org. Electron.* **2011**, *12*, 566.

(118) Fachetti, A. *Chem. Mater*. **2011**, *23*, 733.

(119) O'Connor, B.; Chan, E. P.; Chan, C.; Conrad, B. R.; Richter, L. J.; Kline, R. J.; Heeney, M.; McCulloch, I.; Soles, C. L.; DeLongchamp, D. M. *ACS Nano* **2010**, *4*, 7538.

(120) Sariciftci, N. S.; Smilowitz, L.; Heeger, A. J.; Wudl, F. *Science* **1992**, *258*, 1474.

(121) Bronstein, H.; Chen, Z. Y.; Ashraf, R. S.; Zhang, W. M.; Du, J. P.; Durrant, J. R.; Tuladhar, P. S.; Song, K.; Watkins, S. E.; Geerts, Y.; Wienk, M. M.; Janssen, R. A. J.; Anthopoulos, T.; Sirringhaus, H.; Heeney, M.; McCulloch, I. *J. Am. Chem. Soc* **2011**, *133*, 3272.

(122) Giri, G.; Verploegen, E.; Mannsfeld, S. C. B.; Atahan-Evrenk, S.; Kim, D. H.; Lee, S. Y.; Becerril, H. A.; Aspuru-Guzik, A.; Toney, M. F.; Bao, Z. *Nature* **2011**, *480*, 504.

(123) Salleo, A.; Kline, R. J.; DeLongchamp, D. M.; Chabinyc, M. L. *Adv. Mater*. **2010**, *22*, 3812.

(124) Chiechi, R. C.; Hummelen, J. C. *ACS Macro Lett.* **2012**, *1*, 1180.

(125) Bauer, S.; Bauer-Gogonea, S.; Graz, I.; Kaltenbrunner, M.; Keplinger, C.; Schwodiauer, R. *Adv. Mater.* **2014**, *26*, 149.

(126) Muller, C.; Goffri, S.; Breiby, D. W.; Andreasen, J. W.; Chanzy, H. D.; Janssen, R. A. J.; Nielsen, M. M.; Radano, C. P.; Sirringhaus, H.; Smith, P.; Stingelin-Stutzmann, N. *Adv. Funct. Mater*. **2007**, *17*, 2674.

(127) Dupont, S. R.; Novoa, F.; Voroshazi, E.; Dauskardt, R. H. *Adv. Funct. Mater*. **2013**, *24*, 1325.

(128) Dupont, S. R.; Voroshazi, E.; Heremans, P.; Dauskardt, R. H. *Org. Electron.* **2013**, *14*, 1262.

(129) Bruner, C.; Dauskardt, R. H. *Macromolecules* **2014**, *47*, 1117.

(130) Awartani, O.; Kudenov, M. W.; O'Connor, B. T. *Appl. Phys. Lett.* **2014**, *104*, 093306.

(131) Krebs, F. C.; Espinosa, N.; Hosel, M.; Sondergaard, R. R.; Jorgensen, M. *Adv. Mater.* **2014**, *26*, 29.

(132) Krebs, F. C.; Nielsen, T. D.; Fyenbo, J.; Wadstrom, M.; Pedersen, M. S. *Energ. Environ. Sci.* **2010**, *3*, 512.

(133) Jorgensen, M.; Norrman, K.; Gevorgyan, S. A.; Tromholt, T.; Andreasen, B.; Krebs, F. C. *Adv. Mater.* **2011**, *24*, 580.

(134) Reese, M. O.; Gevorgyan, S. A.; Jorgensen, M.; Bundgaard, E.; Kurtz, S. R.; Ginley, D. S.; Olson, D. C.; Lloyd, M. T.; Morvillo, P.; Katz, E. A.; Elshner, A.; Haillant, O.; Currier, T. R.; Shrotriya, V.; Hermenau, M.; Riede, M.; Kirov, K. R.; Trimmel, G.; Rath, T.; Ignanas, O.; Zhang, F. L.; Andersson, M.; Tvingstedt, K.; Lira-Cantu, M.; Laird, D.; McGuiness, C.; Gowrisanker, S.; Pannone, M.; Xiao, M.; Hauch, J.; Steim, R.; DeLongchamp, D. M.; Rosch, R.; Hoppe, H.; Espinosa, N.; Urbina, A.; Yaman-Uzunoglu, G.; Bonekamp, J. B.; van Breemen, A. J. J. M.; Girotto, C.; Voroshazi, E.; Krebs, F. C. *Sol. Energy Mater. Sol. Cells* **2011**, *95*, 1253.

(135) Osedach, T. P.; Andrew, T. L.; Bulovic, V. *Energ. Environ. Sci.* **2013**, *6*, 711.

(136) Amb, C. M.; Craig, M. R.; Koldemir, U.; Subbiah, J.; Choudhyry, K. R.; Gevorgyan, S. A.; Jorgensen, M.; Krebs, F. C.; So, F.; Reynolds, J. R. *ACS Appl. Mater. Interfaces* **2012**, *4*, 1847.

(137) He, X. M.; Gao, F.; Tu, G.; Hasko, D.; Huttner, S.; Steiner, U.; Greenham, N. C.; Friend, R. H.; Huck, W. T. S. *Nano Lett.* **2010**, *10*, 1302.

(138) Sivula, K.; Luscombe, C. K.; Thompson, B. C.; Frechet, J. M. J. *Journal of the American Chemical Society* **2006**, *128*, 13988.

(139) Savagatrup, S.; Rodriquez, D.; Printz, A. D.; Sieval, A.; Hummelen, J. C.; Lipomi, D. J. *in preparation* **2014**.

(140) Herbst, F.; Dohler, D.; Michael, P.; Binder, W. H. *Macromol. Rapid Commun.* **2013**, *24*, 203.

(141) Coropceanu, V.; Cornil, J.; da Silva, D. A.; Olivier, Y.; Silbey, R.; Bredas, J. L. *Chem. Rev.* **2007**, *107*, 926.

(142) Lee, J. Y.; Connor, S. T.; Cui, Y.; Peumans, P. *Nano Lett.* **2010**, *10*, 1276.

(143) Yasuda, T.; Han, L. Y.; Tsutsui, T. *J. Photopolym. Sci. Technol.* **2009**, *22*, 713.

(144) O'Connor, B.; Kline, R. J.; Conrad, B. R.; Richter, L. J.; Gundlach, D.; Toney, M. F.; DeLongchamp, D. M. *Adv. Funct. Mater.* **2011**, *21*, 3697.

(145) Gargi, D.; Kline, R. J.; DeLongchamp, D. M.; Fischer, D. A.; Toney, M. F.; O'Connor, B. T. *J. Phys. Chem. C* **2013**, *117*, 17421.

(146) McCullough, R. D.; Tristramnagle, S.; Williams, S. P.; Lowe, R. D.; Jayaraman, M. *J. Am. Chem. Soc* **1993**, *115*, 4910.

(147) McCullough, R. D. *Adv. Mater.* **1998**, *10*, 93.

(148) Brinkmann, M. *Polym. Phys.* **2011**, *49*, 1218.

(149) Babel, A.; Jenekhe, S. A. *Synthetic Met.* **2005**, *148*, 169.

(150) Ren, G. Q.; Wu, P. T.; Jenekhe, S. A. *ACS Nano* **2011**, *5*, 376.

(151) Chen, S. A.; Ni, J. M. *Macromolecules* **1992**, *25*, 6081.

(152) Causin, V.; Marega, C.; Marigo, A.; Valentini, L.; Kenny, J. M. *Macromolecules* **2005**, *38*, 409.

(153) Friedel, B.; McNeill, C. R.; Greenham, N. C. *Chem. Mater.* **2010**, *22*, 3389.

(154) Jorgensen, M.; Carle, J. E.; Sondergaard, R. R.; Lauritzen, M.; Dagnaes-Hansen, N. A.; Byskov, S. L.; Andersen, T. R.; Larsen-Olsen, T. T.; Bottiger, A. P. L.; Andreasen, B.; Fu, L.; Zuo, L. J.; Liu, Y.; Bundgaard, E.; Zhan, X. W.; Chen, H. Z.; Krebs, F. C. *Sol. Energy Mater. Sol. Cells* **2013**, *119*, 84.

(155) Liao, S. H.; Li, Y. L.; Jen, T. H.; Cheng, Y. S.; Chen, S. A. *J. Am. Chem. Soc* **2012**, *134*, 14271.

(156) Nielsen, T. D.; Cruickshank, C.; Foged, S.; Thorsen, J.; Krebs, F. C. *Sol. Energy Mater. Sol. Cells* **2010**, *94*, 1553.

(157) Seitz, J. T. *J. Appl. Polym. Sci.* **1993**, *49*, 1331.

(158) Clark, J.; Silva, C.; Friend, R. H.; Spano, F. C. *Phys. Rev. Lett.* **2007**, *98*, 206406.

(159) Salammal, S. T.; Mikayelyan, E.; Grigorian, S.; Pietsch, U.; Koenen, N.; Scherf, U.; Kayunkid, N.; Brinkmann, M. *Macromolecules* **2012**, *45*, 5575.

(160) Nguyen, L. H.; Hoppe, H.; Erb, T.; Gunes, S.; Gobsch, G.; Sariciftci, N. S. *Adv. Funct. Mater.* **2007**, *17*, 1071.

(161) Kim, J. Y.; Frisbie, C. D. *J. Phys. Chem. C* **2008**, *112*, 17726.

(162) Pearson, A. J.; Wang, T.; Dunbar, A. D. F.; Yi, H. N.; Watters, D. C.; Coles, D. M.; Staniec, P. A.; Iraqi, A.; Jones, R. A. L.; Lidzey, D. G. *Adv. Funct. Mater.* **2013**, *24*, 659.

(163) Park, S. H.; Roy, A.; Beaupre, S.; Cho, S.; Coates, N.; Moon, J. S.; Moses, D.; Leclerc, M.; Lee, K.; Heeger, A. J. *Nat. Photonics* **2009**, *3*, 297.

(164) Woo, C. H.; Beaujuge, P. M.; Holcombe, T. W.; Lee, O. P.; Fréchet, J. M. J. *J. Am. Chem. Soc.* **2010**, *132*, 15547.

(165) Arriola, D. J.; Carnahan, E. M.; Hustad, P. D.; Kuhlman, R. L.; Wenzel, T. T. *Science* **2006**, *213*, 714.

(166) Zhang, M.; Moore, R. B.; Long, T. E. *J. Polym. Sci. A: Polym. Chem.* **2012**, *50*, 3710.

(167) Ku, S. Y.; Brady, M. A.; Treat, N. D.; Cochran, J. E.; Robb, M. J.; Kramer, E.; Chabinyc, M. L.; Hawker, C. J. *J. Am. Chem. Soc* **2012**, *134*, 16040.

(168) Kim, F. S.; Ren, G. Q.; Jenekhe, S. A. *Chem. Mater.* **2011**, *23*, 682.

(169) Greiner, A.; Wendorff, J. H. *Angew. Chem., Int. Ed.* **2007**, *46*, 5670.

Chapter 2

Mechanical degradation and stability of organic solar cells: molecular and microstructural determinants

Suchol Savagatrup, Adam D. Printz, Timothy F. O'Connor, Aliaksandr V. Zaretski, Daniel Rodriquez, Eric J. Sawyer, Kirtana M. Rajan, Raziel I. Acosta, Samuel E. Root, and Darren J. Lipomi

Department of NanoEngineering, University of California, San Diego

9500 Gilman Drive, Mail Code 0448, La Jolla, CA 92093-0448

Abstract

The mechanical properties of organic semiconductors and the mechanical failure mechanisms of devices play critical roles in the yield of modules in roll-to-roll manufacturing and the operational stability of organic solar cells (OSCs) in portable and outdoor applications. This paper begins by reviewing the mechanical properties—principally stiffness and brittleness—of pure films of organic semiconductors. It identifies several determinants of the mechanical properties including molecular structures, polymorphism, and microstructure and texture. Next, a discussion of the mechanical properties of polymer:fullerene bulk heterojunction blends reveals the strong influence of the size and purity of the fullerenes, the effect of processing additives as plasticizers, and the details of molecular mixing—i.e., the extent of intercalation of fullerene molecules between the side chains of the polymer. Mechanical strain in principle affects the photovoltaic output of devices in several ways, from strain-evolved changes in alignment of chains, degree of crystallinity, and orientation of texture, to debonding, cohesive failure, and cracking, which dominate changes in the high-strain regime. These conclusions highlight the importance of mechanical properties and mechanical effects on the viability of OSCs during manufacture and in operational environments. The review—whose focus is on molecular and microstructural determinants of mechanical properties—concludes by suggesting several potential routes to maximize both mechanical resilience and photovoltaic performance for improving the lifetime of devices in the near term and enabling devices that require extreme deformation (i.e., stretchability and ultra-flexibility) in the future.

2.1. Motivation

Organic solar cells (OSCs) have achieved benchmarks in the research laboratory that may have seemed out of reach only a decade ago: power conversion efficiencies over 10 percent,[1] projected lifetimes of devices on rigid substrates of over years,[2] power-to-mass ratios of 10 W g^{-1},[3] and projected energy payback times on the order of days.[4] These achievements have been realized, in general, by an approach that uses power conversion efficiency (*PCE*) or some other figure of merit to guide the design and selection of materials and parameters for processing. For organic solar cells to reach the performance and robustness needed to provide inexpensive power on the scale of gigawatts or—in a best-case scenario—terawatts,[5] significant work remains to be done to translate the gains in the research laboratory toward the production of modules in a roll-to-roll manner.[6] Krebs and coworkers have suggested an alternative approach in which the requirements for manufacturing inform the design of materials.[7] The minimum requirements for low-cost and green[8, 9] materials to be amenable to manufacturing include stability while printing from solution,[10] in air,[11] at low temperatures, from environmentally benign solvents,[12, 13] without vacuum steps,[14] and with tolerance of inhomogeneities in thickness and morphology that appear in printed films.[7, 15] (Fundamental and theoretical studies designed to understand the mechanism of operation, of course, inform all efforts to improve the efficiencies of devices.[16-19]) One aspect of the design of materials that is seldom considered[20, 21]—but that is critical to the stability and lifetime of thin, flexible, lightweight modules destined for outdoor or portable use—is mechanical stability.[22-24] This attribute is generally excluded from an approach that is centered on efficiency,[7] but is included in one

that is centered on the requirements for manufacturing and viability under conditions in outdoor[25] and portable environments.[26]

It may seem, because thin films of virtually any material are flexible relative to thicker specimens, that organic semiconductors are already sufficiently compliant for flexible applications and for high yield in roll-to-roll manufacturing. An examination of the modest literature on the mechanical properties of organic semiconductors reveals that their responses to mechanical deformation are highly variable[22, 24, 27-33] (see **Figure 2.1** for structures referred to in the text, and **Table 2.1** for a summary of the mechanical properties of pure organic semiconductors and composites). Moreover, good electronic performance—associated with long conjugation lengths and high degrees of crystallinity—seems to correlate with stiffness and brittleness.[24, 28, 33] Some studies, however, have shown that this correlation is not a fundamental trade-off and that it is, in principle, possible to achieve the "best of both worlds" of mechanical and electronic performance.[27, 29, 34-36] Predicting trends in mechanical properties requires an understanding of the ways in which a molecular structure produces a solid-state microstructure,[28] and how structures at both length scales influence the mechanical and electronic properties of a solid material.[24, 27, 33]

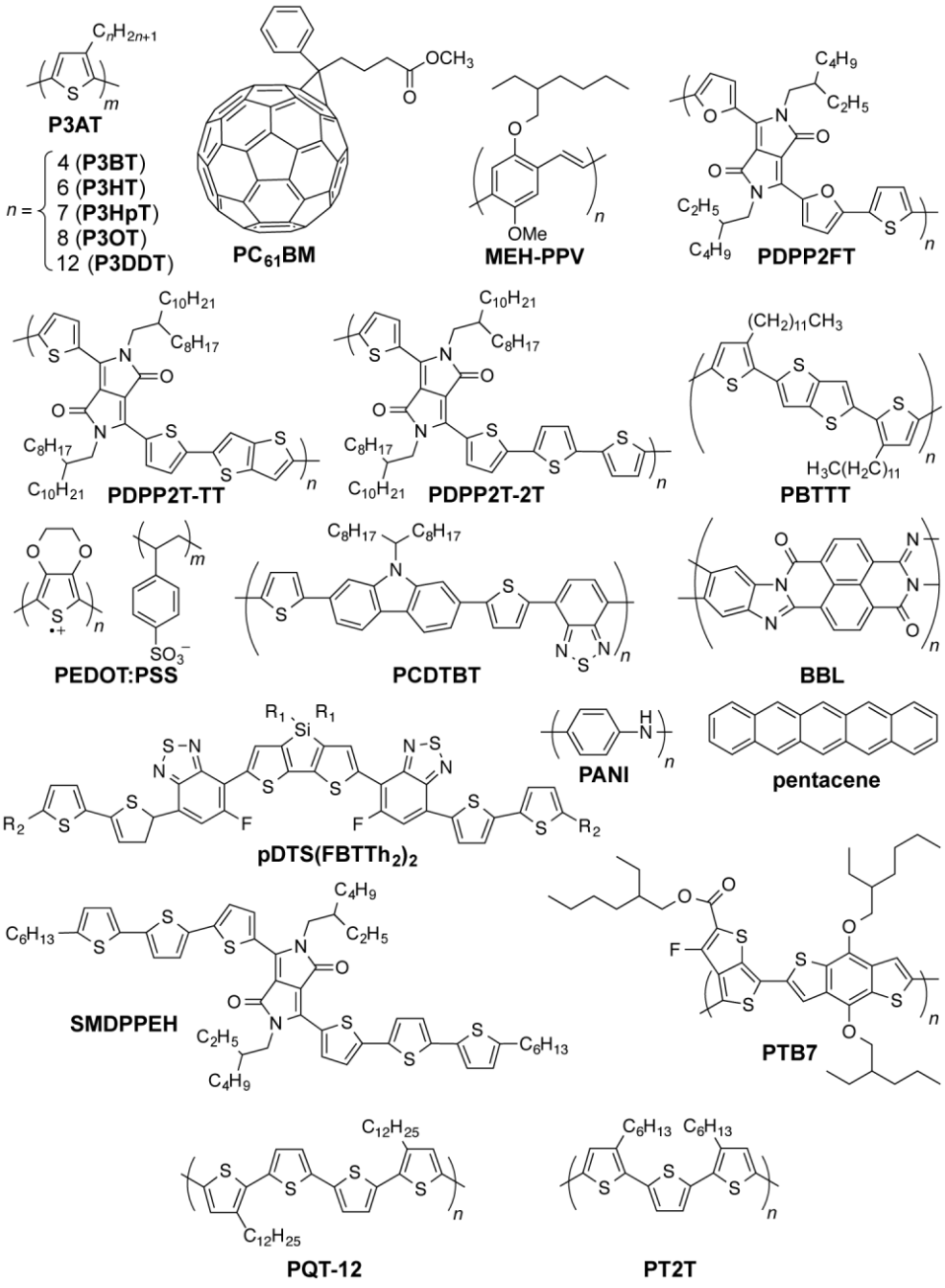

Figure 2.1. Chemical structures of organic conductors and semiconductors discussed in the text.

Table 2.1. Tensile moduli (along with crack-onset strains) of all organic electronic materials measured by the buckling technique.

Materials	Notes	Tensile modulus [GPa]	Crack on-set strain [%]	Reference
P3HT	AC	1.33 ± 0.01		32
		1.3		88
		0.92		31
		0.252 ± 0.06	>150	33
		1.09 ± 0.15	9 ± 1.2	28
		0.22 ± 0.03		24
P3HT:PCBM	Ratio 1:0.8, AC	6.02 ± 0.03		32
	Ratio 1:1, AC	4.3		31
	Ratio 1:1, AC	1.97 ± 0.07		131
	Ratio 1:1, AN	2.75 ± 0.09		131
	Ratio 1:0.5, AC	2.02 ± 0.48	3 ± 1.5	28
	Ratio 1:1, AN (ODCB)	~1.74 to 1.97	~2% to >80%	24
P3HT:Fullerene	$PC_{71}BM$ (90%), AC	0.67 ± 0.07		125
	$PC_{71}BM$ (90%), AN	1.76 ± 0.04		125
	$PC_{71}BM$ (90%), AC	2.72 ± 0.40		125
	$PC_{71}BM$ (90%), AN	3.21 ± 0.06		125
	ICBA (99%), AC	3.27 ± 0.86		125
	ICBA (99%), AN	6.53 ± 1.88		125
P3BT	AC	1.87 ± 0.52	6 ± 1.5	28
P3BT:PCBM	Ratio 1:0.5, AC	5.2 ± 0.61	2 ± 0.6	28
P3PT	AC	1.33 ± 0.14		27
P3HpT	AC	0.07 ± 0.01	58	27
	AN	0.13 ± 0.01		131
P3HpT:PCBM	Ratio 1:1, AC	0.61 ± 0.09		131
	Ratio 1:1, AN	1.46 ± 0.16		131
	Ratio 1:1, AN (ODCB)	1.79 ± 0.35		27
P3OT	AC	0.15 ± 0.05	65 ± 2.5	28
P3OT:PCBM	Ratio 1:0.5, AC	0.52 ± 0.16	47 ± 2.1	28
P3DT	AC	0.12 ± 0.4		27
P3DDT	AC	0.16 ± 0.07	47 ± 3.1	28
P3DDT:PCBM	Ratio 1:0.5, AC	0.47 ± 0.17	44 ± 1.4	28
DPPT-TT	AC	0.99		31
DPPT-TT:PCBM	Ratio 1:1, AC	1.4		31
DPPT-2T	AC	0.74		31
DPPT-2T:PCBM	Ratio 1:1, AC	0.84		31
PT2T	AC	1.11 ± 0.19		29
	AN	1.01 ± 0.27		131
PT2T:PCBM	Ratio 1:2, AC	1.6 ± 0.36		29
	Ratio 1:1, AC	2.0 ± 0.36		131
	Ratio 1:1, AN	2.61 ± 0.39		131
PDPP2FT	AC	2.17 ± 0.35		29
PDPP2FT:PCBM	Ratio 1:2, AC	2.76 ± 0.77		29
MEH:PPV	AC	0.119 ± 0.005		131
	AN	0.023 ± 0.001		131
MEH:PPV:PCBM	AC	3.79 ± 0.07		131
	AN	4.92 ± 0.09		131
PBTTT	AC (ODCB)	0.879 ± 0.243	<2.5	33
	AN (ODCB)	1.8 ± 0.345	<2.5	33
	AC	1.8 ± 0.19		131
	AN	2.9 ± 0.30		131
PBTTT:PCBM	AC	3.76 ± 0.8		131
	AN	4.38 ± 0.68		131
PEDOT:PSS		2.26 ± 0.05		32
	5% DMSO, 10% Zonyl	0.03 ± 0.01		71
	5% DMSO, 1% Zonyl	3.14 ± 0.12		71
	5% DMSO, 0.1% Zonyl	7.49 ± 1.5		71
PANI		0.03		32
Pentacene		16.09		32
PCBM	C60	3.06 ± 0.17		24
	C60	6.2		88

† Ratios are reported in weight ratio. Films with thermal annealing treatments are denoted as annealed (AN), while untreated films are denoted as as-cast (AC). Films are spin-coated from chloroform or otherwise noted.

The range over which mechanical properties vary will have significant consequences for the long-term stability of devices, and will thus influence the selection of materials for particular applications. Annealed films of pure PBTTT and composite films of P3HT:PCBM—the *Drosophila* of organic solar cells—crack at strains <2.5% on polydimethylsiloxane (PDMS) substrates under typical processing conditions.[33] Evaporated films of the molecular semiconductor pentacene (and presumably other van der Waals solids) are likely to be more brittle than are films of P3HT:PCBM.[32] Other researchers have noted the importance of understanding the mechanical failure mechanisms.[21] In the report of a Workshop on Key Scientific and Technological Issues for Development of Next-Generation Organic Solar Cells, sponsored by the US National Science Foundation and the Office of Naval Research, researchers asked, "What has been done to prevent solar cells from failing mechanically?"[37] Moreover, in a well-known paper in which researchers deployed roll-to-roll fabricated, OSC-powered, LED lanterns in rural Zambia, one of the principal conclusions was that "…mechanical failure mechanisms were dominant during the field test and therefore these would have to be improved significantly before the photochemical stability of the [semiconducting] polymer becomes a problem."[26] Mechanical stability is of critical importance not only for portable applications—for which accommodation of strain is an operational requirement[38]—but also for roll-to-roll production, transportation, and for utility-scale applications.[7, 25]

In large-scale solar farms and in portable applications, thin organic solar modules will be subject to a range of stresses due to environmental forces.[25] The pressure of wind and the weight of rain and snow will strain the devices to an extent that depends on the compliance and thermal expansion of the encapsulants and support structures. Robust

encapsulants and support structures will add significant expense to the modules,[39] and it is thus desirable to use active materials that can accommodate at least some strain without the need for expensive, rigid supports. Even the thinnest support structures add significantly to the production costs of thin-film PV modules: Anctil et al. calculated that a 130-μm poly(ethyleneterephthalate) (PET) substrate contributes approximately 10% of the embodied energy (along with a roughly equal amount for the encapsulants) of organic modules made using conventional materials, and nearly double that amount in ITO-free devices.[39] One inevitable mode of mechanical deformation that will occur even in the presence of protective layers is thermal expansion and contraction due to diurnal and seasonal variations in temperature. Materials and devices must thus tolerate the extreme conditions in a given geographical area, as well as exhibit resistance to fatigue in the face of cyclic loading due to modest thermal cycling. It is possible that the surface of a highly absorbing device may reach temperatures of 70 °C in the Southwestern US, and a *range* of as much as 100 °C over the lifetime of a device in the Midwest, if one accounts for inevitable extremes in temperatures. One of the goals of the community interested in the mechanical properties of organic semiconductors is thus to mitigate the effects of thermal expansion and contraction on the lifetime and performance of OSCs.

There are a large number of competing technologies in the field of solar photovoltaics. All of these technologies ostensibly have the same goal: achieving the most favorable cost per watt, amortized over the lifetime of the device, for utility-scale installations.[40] Organic solar cells, however, have several characteristics that would be difficult or impossible to replicate in conventional or other thin-film technologies. These characteristics include: semitransparency[41, 42] and tunable color for aesthetic

considerations,[43] thermally activated charge transport[44] and possibly increased efficiency at elevated temperature, high-speed manufacturing under ambient conditions,[6, 25] extreme thinness and light weight,[3] and the potential to tolerate high strains without loss of function.[30, 31] One strategy to hedge against a winner-take-all outcome (if a non-organic PV technology becomes dominant for utility-scale applications) is to focus on areas in which OSCs could "run away" with part of the PV market.[22] Mechanical compliance is the fundamental attribute that provides the basis for all advantages of OSCs.[45] Physical robustness is a prerequisite for fabricating devices on ultrathin substrates, because small forces can produce strains large enough to crack, delaminate, or plastically deform thin films of semiconducting polymers.[3, 46, 47] Moreover, in some portable,[26] wearable,[38] and implantable[48] applications, extreme mechanical compliance[30] and resistance to mechanical failure is at least as important as photochemical[49] and morphological[21] stability.[50-52]

This article reviews the current state of knowledge of the mechanical failure of organic solar cells. The focus is on the ways in which molecular structure influences the microstructure of conjugated materials in the solid state, and how these parameters combine to dictate mechanical properties. The focus on molecular structure and microstructure reflects the expertise of the authors, and we thus invite readers interested in other important aspects of mechanical stability, such as continuum theories of deformation and fracture, to consult references herein.

2.2. Mechanical properties of organic semiconductors

The factors that ultimately control the mechanical stability of OSCs can be reduced to intermolecular and surface forces present in samples of organic semiconductors and

ancillary materials, and how they influence the properties of thin films (mediated by the conditions of processing). The early literature—in the 1980s and early 1990s—contained several studies of the mechanical properties of some of the first-reported conjugated polymers.[53-57] It is apparent, however, that the discovery of the polymer solar cell by Heeger and Wudl,[58] and independently by Friend,[59] along with the discovery of the organic light-emitting device by Friend,[60] and invention[61] and refinement[62] of the polymer thin-film transistor, shifted the focus from bulk properties—i.e., mechanical properties—familiar to polymer scientists and mechanical engineers, to electronic properties familiar to physicists and electrical engineers. Mechanical properties thus took a back seat to electronic performance, during which time important work was done on improving electronic figures of merit (e.g., power conversion efficiency, *PCE*, in organic solar cells). Much of the success of the field in improving the performance of devices came through the proliferation of the molecular structures accessible by synthetic chemistry.[8, 63-67] Mechanical properties, such as tensile modulus, ductility, fracture toughness, and other parameters of new materials, however, are seldom reported and would be difficult to judge based only on molecular structure. Nevertheless, recent work has attempted to produce some generalities about the ways in which molecular structure and solid-state microstructure influence the mechanical properties of these materials. Far more is known about the mechanical properties of semiconducting polymers than is known about their small-molecule counterparts, and thus Section 2.1 begins with a discussion of the structural determinants of the mechanical properties of pure conjugated polymers.

There is no single figure of merit possessed by an organic semiconductor or composite that will predict the mechanical stability of a whole module: desirable properties

will depend largely on the application and on the properties of other materials in the device. The substrate and encapsulant provide structural support, and if the substrate fails mechanically then the device will most likely fail electronically, so it is not necessary that the organic semiconductors provide structural support (e.g., high tensile strength may be desirable, but not if the film fractures at low strains). In general, the active materials should deform with the substrate. That is, they should have a low modulus and high elastic limit. The strain at which cracks appear in a film on an elastic substrate is often taken as a measure of the ductility of a thin film, but the so-called crack-onset strain is highly dependent on the adhesion between the film and the substrate (poorly adhered films crack at smaller strains than well adhered films of the same modulus).[28] Adhesive[68, 69] and cohesive[23, 52, 70] fracture energies have been proposed to predict the mechanical modes of degradation within the active materials and electrodes in whole modules, and we will return to these figures of merit in more detail in Section 3.2.2. Adhesive energy, however, is sensitive to the order in which layers are deposited,[68, 69] and cohesive energy often depends on thickness.[50] Of all these figures of merit, tensile modulus has the advantages of being easily measured, intrinsic to the material (as opposed to its interaction with a substrate or overlayer), insensitive to thickness for those typically used in devices ($\geq$ 50 nm), and easily relatable (and sometimes predictable) on the basis of chemical structure and microstructure. Additionally, tensile modulus and crack-onset strain (i.e., effective brittleness) are correlated for every system of conjugated polymers in which both quantities are reported in the same paper,[24, 27, 28, 33, 71] and thus a low tensile modulus can be used as a proxy for a favorable response to deformation in mechanically robust applications. Tensile modulus, however, will not predict the mechanical response past the elastic limit,

nor will it predict the elastic limit (though we have observed that low tensile modulus is correlated with high elastic limit in P3ATs).[30]

2.2.1. Mechanical properties of pure organic semiconductors

2.2.1.1. Conjugated polymers

The basic structural motif of a conjugated polymer—the alternating arrangement of single and double bonds along the backbone[72]—gives rise to the band structure, but also restricts conformational freedom of unsubstituted conjugated and other rod-like polymers.[73] These materials are thus typically insoluble and rigid. The rigidity of all-sp^2-hybridized materials originally made conjugated polymers attractive for their mechanical strength,[72] which was demonstrated in aligned films of polyacetylene (modulus of 50 GPa and tensile strength of 0.9 GPa)[54] and other structurally simple polymers.[55] For flexible electronic devices, however, tensile strength is less important than is elasticity and toughness,[50] which contributes to the robustness of thin-film devices. The installation of aliphatic side chains on conjugated main chains renders these materials soluble,[64, 74] and also has the effect of increasing the compliance and ductility.[28, 57] Polymers can, however, have similar molecular structures but adopt different microstructures (e.g., polymorphs,[75, 76] textures,[77-79] and degrees of crystallinity[33]) in the solid state, and highly crystalline samples tend to be stiffer and more brittle than samples of the same material that are amorphous or have low crystallinity.[29, 33, 80] The favorable correlation between crystallinity and charge transport on one hand, and the unfavorable correlation between crystallinity and brittleness on the other, is an example of a recurring theme in which charge transport and mechanical properties tend to be in competition.

2.2.1.2. Experimental determination of the mechanical properties of conjugated polymers

The mechanical properties of conjugated polymers (principally the properties under tensile loading, such as ultimate strength and tensile modulus) have been determined in the past by direct tensile testing[81] and by nanoindentation.[82-84] It is, however, difficult to obtain mechanical data from the geometry that is most relevant to organic optoelectronics—a thin film.[85, 86] Films of organic materials can have thickness-dependent mechanical properties due to unsaturated intermolecular bonds at interfaces (a skin-depth effect)[87] and because of confinement of a plastic zone at the crack tip during decohesion of layers sandwiched between relatively rigid substrates.[50, 52] The mechanical (and adhesive) properties of organic thin films are thus not necessarily reflective of the properties of samples that are macroscopic in every dimension. Organic films with thicknesses ≤100 nm tend to confound measurements by direct tensile testing because (1) it is difficult to produce and manipulate free-standing thin films and (2) thin areas, inclusions, and other defects can concentrate stress and thus dominate the mechanical response. Nanoindentation has produced useful qualitative and relative data, but the accuracy of the mechanical measurements are limited by the convolution of the effect of the substrate, viscoelastic behavior of the polymer, and the uncertainty of the tip size and contact area of the scanning probes.[83, 84, 86]

The mechanical buckling technique has proven useful in determining the tensile modulus of a range of inorganic and organic thin films,[85, 86 88] and even of individual single-walled carbon nanotubes.[89] The method is based on the buckling instability that gives rise to wrinkles in a relatively rigid film on a relatively compliant substrate under compressive strain.[90, 91] The wavelength of the wrinkling pattern, λ_b, can be related to the tensile modulus

of the film, E_f, in terms of the modulus of the substrate, E_s, the thickness of the film, d_f, and the Poisson ratios of the film and substrate, v_f and v_s, in equation 1.[86]

$$E_f = 3E_s\left(\frac{1-v_f^2}{1-v_s^2}\right)\left(\frac{\lambda_b}{2\pi d_f}\right)^3 \quad (1)$$

In practice, plotting λ_b as a function of d_f for a series of samples (or for a single sample bearing a gradient in thickness) and inserting the slope into equation 1 yields the modulus of the film. The modulus scales with the cube of the slope, and this sensitivity thus requires that the measurement be carried out with strict adherence to established procedures.[86] Poor interfacial adhesion[92] and surface defects—such as pre-existing wrinkles, delamination, and cracking—can produce apparent buckling wavelengths that produce measurements that deviate significantly from the intrinsic values of the films. **Table 2.1** is a comprehensive table containing the modulus of every organic electronic material and composite measured by the buckling method.

2.2.1.3. Influence of alkyl side chains on mechanical properties of conjugated polymers

An analysis of the literature reveals that a critical structural determinant of the mechanical properties of solution-processible conjugated polymers is the alkyl side chain.[27, 28, 57] The role of the side chain in a comb-like polymer in determining its stiffness can be understood intuitively: the longer the alkyl chains (*n*), the lower the density of load-bearing bonds in the main chain per cross sectional area.[56] Indeed, the fraction of volume occupied by the main chain (versus the side chain) per molecule are 0.31 for butyl side chains and 0.20 for dodecyl chains.[57] Additionally, in polymers with long alkyl side chains, secondary interactions between adjacent main chains are reduced; Wudl and coworkers

observed similar effects in another class of comb-like polymers, the poly(alkyl isocyanates).[56] **Figure 2.2a** plots the tensile modulus vs. the length of the alkyl side chain for a series of poly(3-alkylthiophenes) (P3ATs).[28] The steepest drop-off in modulus occurs between polymers having between six and seven[76] carbon atoms in the side chain, and corresponds to the point at which the glass transition temperature (T_g) drops below ambient temperature (25 °C) with increasing n.[27] The glass transition refers only to the amorphous domains of the polymer, and is always lower than the melting temperature (T_m) of the crystalline domains. The behavior shown in **Figure 2.2a** suggests the intriguing possibility that P3ATs with $n \geq 7$ might behave as semiconducting thermoplastic elastomers (if the crystallites could be melted without decomposing the polymer). Values of T_g for the most well studied member of this family, P3HT, have been measured to occupy a range of values between 15 to 25 °C.[93, 94] This proximity to "room temperature" might account for measurements of the modulus that are typical (~1 GPa)[28, 32] or substantially lower (~0.1 GPa).[33] Similar to P3HT, the values T_g for other P3ATs are reported as a range, most likely due to differences in molecular weight, polydispersity, thermal history, and method of measurement.[95, 96] The glass transition of the amorphous domains is thus an important predictor of the mechanical properties of a conjugated polymer, but the percent crystallinity and the order within the crystallites also play important roles.[24]

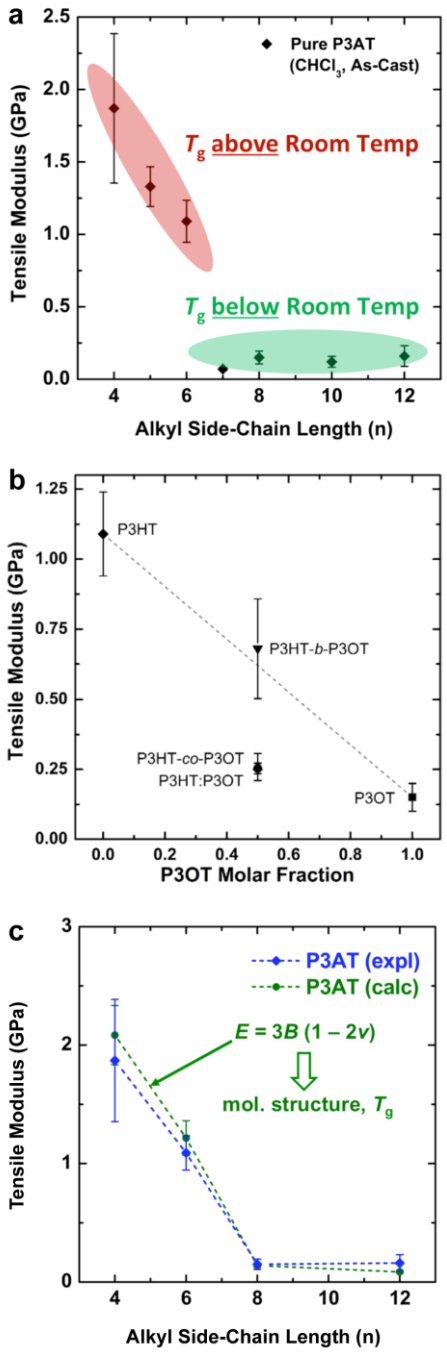

Figure 2.2. Tensile moduli of poly(3-alkylthiophenes) (P3ATs). (a) Tensile modulus vs. the length of the alkyl side chain (*n*). A sharp drop-off occurs with increasing *n* as the glass transition drops below ambient temperature, from *n* = 6 to *n* = 7. (b) Moduli of three "hybrid" materials with equimolar ratios of hexyl and octyl side chains: a block copolymer (P3HT-*b*-P3OT), a statistical copolymer (P3HT-*co*-P3OT), and a physical blend (P3HT:P3OT). Reproduced with permission from ref.[28]. Copyright 2014, American Chemical Society. (c) Overlay of the experimental and theoretical tensile moduli of P3ATs vs. the length of the alkyl side chains. Reproduced with permission from ref.[28] Copyright 2014 Wiley-VCH Verlag GmbH & Co. KGaA.

The interesting mechanical behavior of P3ATs in which $6 \leq n \leq 8$ led us to investigate "hybrid" systems, comprising equal molar fractions of hexyl and octyl side chains (**Figure 2.2b**).[27] These hybrid systems were a physical blend of P3HT and P3OT (P3HT:P3OT), a block copolymer (P3HT-*b*-P3OT), and a statistical copolymer (P3HT-*co*-P3OT). The modulus of the block copolymer sat on a line extrapolated between P3HT and P3OT. This average modulus can be attributed to the covalent connectivity of the relatively stiff P3HT and the relatively plastic P3OT. The modulus of the physical blend, in contrast, sat below the extrapolated modulus, possibly because the P3OT domains—unconstrained by covalent tethering to the P3HT domains—absorbed the strain and thus dominated the mechanical response of the composite material.[27] None of these hybrid materials, however, exhibited as low a tensile modulus as did P3HpT, and the factors governing the combination of high compliance and good photovoltaic properties of this interesting material are still under investigation. It appears, however, that the percent aggregate and the order within the crystalline domains of P3HpT are similar to that of P3HT, while these quantities for P3OT are substantially reduced.

The presence or absence of interdigitation of the side chains of conjugated polymers could be a predictor of the mechanical properties of the solid film.[75] The side chains of the P3ATs generally do not interdigitate,[75] and thus the lamellae within the crystallites should not be as highly registered vertically as in materials in which the side chains do interdigitate (such as PBTTT[33, 66] and PT2T[97]). The decreased number of van der Waals interactions between side chains in non-interdigitated polymers should produce crystallites that are more easily deformable than those in which the side chains are interdigitated. Evidence for interdigitation of the side chains in PBTTT comes by way of a reduction in the (*a*00)

lamellar spacing (measured by GIXD) compared to the spacing predicted by the addition of the lengths of two opposing alkyl side chains in their fully extended conformations.[66] Smaller lamellar spacing thus implies interdigitation. Mechanical measurements of PBTTT by O'Connor et al. are highly correlated with its thermal history and thin-film morphology.[33] As-cast samples of PBTTT, which have small crystallites,[66] exhibited tensile moduli that were half those of annealed films,[33] which exhibited large crystallites (and low amorphous fractions) in an earlier study by AFM.[66] Both the as-cast film and the annealed film were highly brittle, and both cracked at strains <2.5% on PDMS substrates.[33] PT2T (**Figure 2.1**), a structural analogue of P3HT that differs from P3HT on the basis of the regioisomerism and density of attachment of hexyl side chains (which are incorporated in two of every three monomers for PT2T, and in every monomer for P3HT), forms a solid film in which interdigitation is the preferred packing structure.[97] Interestingly, the tensile modulus of PT2T was similar to that of P3HT when cast under similar conditions.[29]

Different crystalline polymorphs of the same material are expected to have substantially different mechanical properties.[75] For example, the crystalline domains of P3ATs have two known packing structures.[76] Form I is the polymorph found under most conditions. It is characterized by side chains that do not interdigitate. Form II occurs in oligomers of 3-hexylthiophene,[75] and for both P3BT and P3HT, conversion from Form I to Form II can occur by exposure to certain solvent vapors (e.g., carbon disulfide).[98, 99] The defining characteristic of Form II is a shortened lamellar spacing, which is attributed to interdigitation of the side chains.[76] Koch et al. made qualitative observations about the mechanical properties as "somewhat brittle in form II while plastic crystalline behavior was observed for form I," but the mechanical properties were not quantified.[75]

2.2.1.4. Effect of rigidity of the main chain

The high modulus of unsubstituted conjugated polymers (e.g., polyacetylene), compared to analogous saturated polymers (e.g., polyethylene), is a consequence of at least two effects: (1) the inherent rigidity of an all-sp^2-hybridized main chain[73] and (2) the high polarizability of π bonds compared to σ bonds, which produces a high dispersive component of the van der Waals force, and strong interactions between the main chains.[100] While the effect of structural rigidity on the mechanical properties of a solid film has not been investigated rigorously, a few observations have been made in the literature. First, direct comparison of the tensile moduli of PDPP2T-TT (0.99 GPa) and PDPP2T-2T (0.74 GPa), of similar molecular weight, suggested that the fused thienothiophene (TT) unit lent greater structural rigidity to the polymer than did the biothiophene unit (2T).[31] A reasonable hypothesis is that an increasing proportion of fused rings in the main chain ("ladder-like" character[101]) correlates with increasing modulus of the solid film. A well known ladder polymer, the electron acceptor BBL,[102, 103] exhibited a high modulus of 7.6 GPa by tensile testing.[81] Another interesting effect of rigidity of the main chain is on the orientation of molecular packing in high-aspect-ratio crystallites. In typical conjugated polymers (e.g., P3HT) that form one-dimensional nanostructures, the axis of π-stacking is parallel to the long axis of the nanostructure.[104] For one-dimensional nanobelts of the ladder polymer BBL, however, the molecular axis is parallel to the long axis of the nanostructure.[105] These observations suggest that the mechanical properties of individual molecules could be engineered to produce packing structures in the solid state that optimize charge transport for a given application.

2.2.1.5. Theoretical predictions of mechanical properties

The mechanical properties of simple conjugated polymers can be predicted with high accuracy using a simple semi-empirical theory first reported by Seitz,[106] and applied to semicrystalline semiconducting polymers for the first time by Tahk et al.[32] Our further application of this technique to conjugated polymers with complex molecular structures has revealed significant deficiencies in this technique,[29] but it is nevertheless remarkable in its ability to predict the tensile moduli of the regioregular P3ATs,[28] and other relatively simple polymers.[106] The accuracy of the technique in obtaining the moduli of some semicrystalline P3ATs is remarkable because it was originally intended to apply to amorphous materials.[106] The technique can be used, at the very least, to screen the structures of materials intended for applications requiring significant mechanical deformation, and to guide the selection of more sophisticated theoretical models.[106] The approach described by Seitz, based on a topological method for correlating molecular structure with bulk properties, is briefly outlined as follows.

The tensile modulus, E_f, of a thin film (or any material under small strains) is related to the bulk modulus (B) and the Poisson ratio (v_f) by equation 2,

$$E_f = 3B(1 - 2v_f) \qquad (\mathbf{2})$$

The bulk modulus is related, through the Lennard-Jones potential, to the cohesive energy (E_{coh}), the van der Waals volume at 0 K (V_0), and the volume at the temperature of interest (V) by equation 3.

$$B \approx 8.23E_{coh}\left[\frac{5V_0^4}{V^5} - \frac{3V_0^2}{V^3}\right] \qquad (\mathbf{3})$$

The cohesive energy can, in turn, be calculated from semi-empirical parameters derived from the bond connectivity indices assigned to each atom in the structure of the monomer, in a method described by Fedors.[107] The bond connectivity indices are parameters that embody the size and the structure of the monomer as well as the conformational freedom of its bonds. The Poisson ratio is related empirically to the cross-sectional area of the monomer (*A*), by equation 4.

$$\nu = 0.513 - 2.37 \times 10^6 \sqrt{A} \qquad (\mathbf{4})$$

The area is determined by equation 5,

$$A = \frac{V_{\mathrm{w}}}{N_{\mathrm{A}} l_{\mathrm{m}}} \qquad (\mathbf{5})$$

where V_{w} is the van der Waals volume and l_{m} is the length of the monomer. Molecular dimensions are also estimated from the connectivity indices. The closeness of the calculated tensile moduli to those of the experimental values for a series of P3ATs is plotted in **Figure 2.2c**.[28]

2.2.1.6. Correlation of microstructure and texture on mechanical properties

The mechanical properties of a polymeric thin film are to a large extent a function of its microstructure.[108] The π-stacking distance, lamellar spacing, crystalline order, molecular orientation, and degree of crystallinity[18] will influence the mechanical properties, and are determined by thermal history,[109] processing conditions,[110, 111] and plastic deformation by strain.[78, 80, 112] Several methods of characterization can be used to correlate microstructure and texture to the mechanical properties for several conjugated polymers and polymer:fullerene blends. These methods are spectroscopic (e.g., the weakly

interacting H-aggregate model),[24] imaging-based (e.g., AFM), and those based on synchrotron radiation (e.g., grazing-incidence X-ray diffraction, GIXD).[113]

2.2.1.7. Spectroscopically determined morphology by the weakly interacting H-aggregate model.

In the seminal paper by Spano and coworkers,[114] the authors showed that the UV-vis spectra of P3HT can be deconvoluted into contributions from the vibronic transitions arising from the aggregated—i.e., crystalline—phase, which are superimposed with the lower-energy, broad absorption of the amorphous phase (**Figure 2.3a**). The ratio of the absorption, after taking into account the unequal absorption coefficients of the crystalline and the amorphous domains, can be used as an approximate measure of the percent aggregate (taken to be a percentage of material in well ordered domains). Awartani et al. found a strong correlation between the spectroscopically determined order in P3HT:PCBM films (the percent aggregate and the inverse of the Gaussian linewidths of the vibronic transitions, $1000/\sigma$), the power conversion efficiencies of these blends, and the tensile modulus (**Figure 2.3b**).[24] The authors found a similar correlation between order and brittleness, as manifested in the crack-onset strain.[24] This observation, along with a similar one that correlated the tensile modulus and brittleness with charge-carrier mobility of P3HT and PBTTT as a function of thermal history,[33] suggests that electronic performance and mechanical compliance are mutually exclusive properties. This is a theme, to which we will return, that represents an opportunity for researchers interested in combining properties—e.g., electrical conductivity and transparency—that seem to be antithetical.[45] Poly(3-heptylthiophene) (P3HpT),[109] whose side chains contain seven carbon atoms, is an

example of a material for which brittleness, crystalline order, and photovoltaic efficiency are not correlated.[27] Measurements of both tensile modulus and photovoltaic efficiency in P3HpT suggest that it exhibits the "best of both worlds." (We note, however, that P3HpT:PCBM composites are nearly as stiff as P3HT:PCBM films, presumably due to the stiffening effect of PCBM on the amorphous domains of P3HpT, but a recent trend in the literature is to replace PCBM with polymeric or other small molecule acceptors, which may not increase the stiffness of bulk heterojunction films to the extent that PCBM does.)

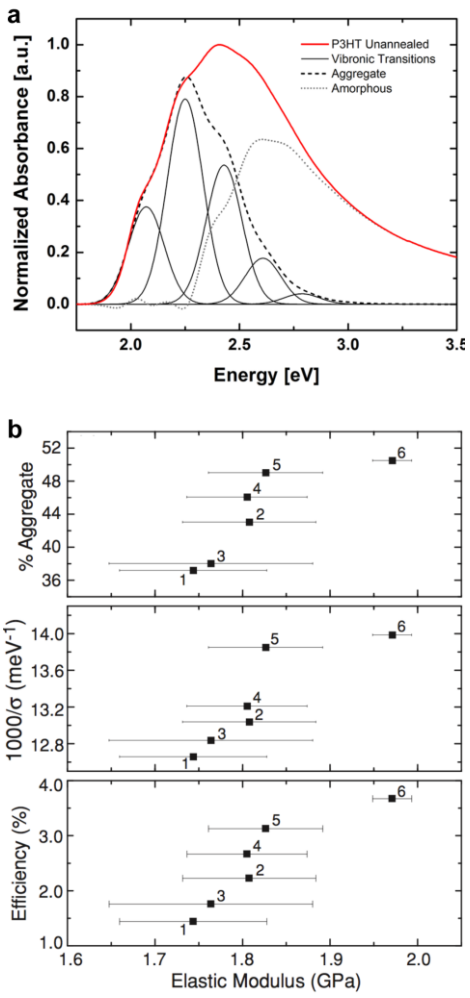

Figure 2.3. Determination of order within P3HT films by the weakly interacting H-aggregate model. (a) Deconvolution of UV-vis absorption spectrum of P3HT into vibronic peaks associated with aggregated—i.e., crystalline—phases and higher energy absorption of the amorphous domains. Reproduced with permission from ref.[24]. Copyright 2013 Wiley-VCH Verlag GmbH & Co. KGaA.

2.2.1.8. Morphology of the surface by atomic force microscopy.

The surface of a polymeric thin film can be readily visualized by AFM.[18] Conclusions about the bulk morphology of such films are often drawn, but the morphology visible at the surface of the film does not necessarily resemble that of the bulk.[18] Furthermore, it is difficult to assign apparent differences in phase contrast to specific domains in the film. The usual caveats about artifacts, specific to AFM, also apply. It is important to use a sharp AFM tip to resolve detail, e.g., the nanowire-like morphology observable in low-MW samples of P3HT.[115] Despite its shortcomings, under favorable circumstances, quantities measurable by AFM images can be used to correlate morphology to mechanical properties. For example, PBTTT undergoes a very drastic transition upon thermal annealing, from semicrystalline with small crystallites to a highly crystalline state, in which the well ordered domains are observable by AFM (**Figure 2.4a**).[66] The annealed, well-ordered state of PBTTT had a substantially increased modulus.[33] For films of P3ATs, roughness is generally correlated to crystallinity, and is thus also loosely correlated to stiffness and ductility (**Figure 2.4b**). We hasten to add that degree of crystallinity is only one parameter that defines the mechanical properties of a conjugated polymer. Wholly amorphous polymers, such as MEH-PPV and PCDTBT,[116] are in the glassy state at room temperature and can be relatively stiff, in the case of PCDTBT.

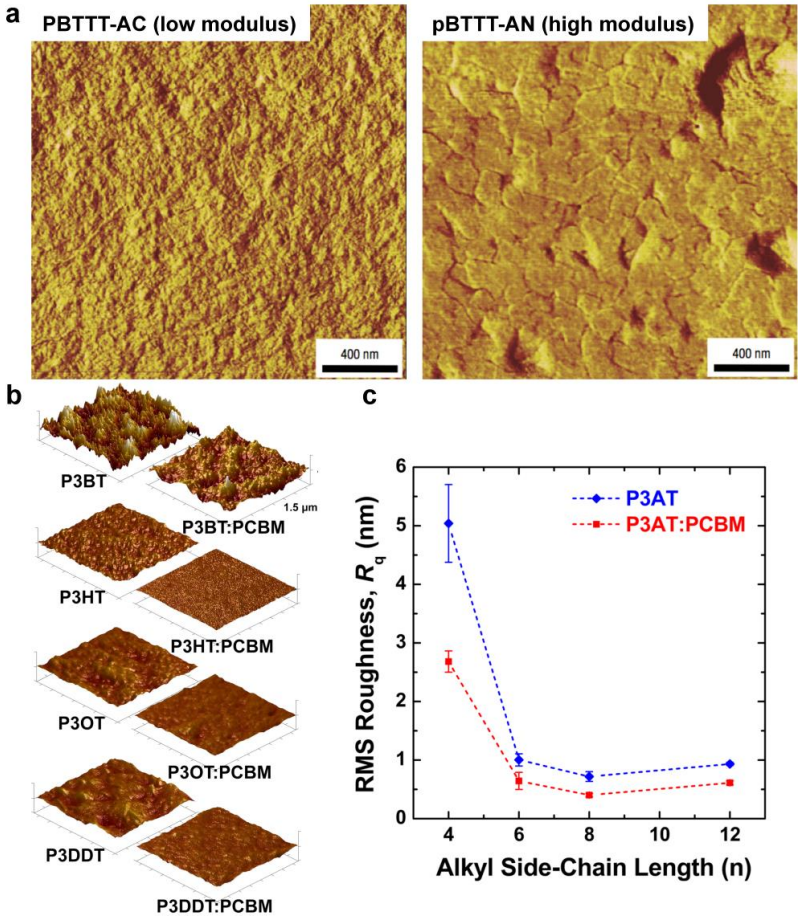

Figure 2.4. Correlation of surface morphology by atomic force microscopy with mechanical properties. (a) PBTTT undergoes a transition upon thermal annealing from an as-cast form with small crystallites, which is relatively compliant, and a highly crystalline annealed form, which is relatively stiff. Reproduced with permission from ref.[66] Copyright 2006, Nature Publishing Group. (b and c) Roughness is loosely correlated to tensile modulus in P3ATs. Reproduced with permission from ref.[28] Copyright 2014 Wiley-VCH Verlag GmbH & Co. KGaA.

2.2.1.9. Synchrotron-based X-ray techniques

The most sophisticated approaches to determining the bulk morphology or texture of polymeric thin films involve synchrotron-based methods of characterization. Grazing-incidence X-ray diffraction (GIXD), near-edge X-ray absorption fine structure (NEXAFS), and other techniques provide a wealth of information about microstructure and texture of films of organic semiconductors[18] that can be correlated to mechanical properties. The

lamellar spacing can be used to quantify the extent of interdigitation of the side chains in pure polymer phases,[97, 113] intercalation of fullerenes between the side chains,[23, 117, 118] relative crystallinity (and absolute crystallinity under favorable circumstances),[113] cumulative and non-cumulative disorder,[119] alignment of chains,[78] and can assign the texture as being either edge-on or face-on.[120] Correlations that have been found include the high tensile modulus of PBTTT because of its interdigitated packing structure and highly crystalline morphology when annealed,[33] and the observation that P3HT in its kinetically favorable Form II structure, in which the side chains interdigitate, is relatively brittle.[75]

2.2.2. Mechanical properties of polymer:fullerene composites

While the mechanical properties of pure polymer films have begun to receive some attention, and conclusions and design rules can be drawn, blending pure polymers with electron acceptors—usually fullerenes—produces effects that can be difficult to predict. The general outcome is that a polymer:PCBM composite is stiffer, more brittle, and has decreased interlayer adhesion than does the pure polymer. The current model that describes the P3HT:PCBM blend comprises (at least) a three-phase system: a crystalline polymer domain, a fullerene-rich domain, and a mixed phase.[19, 121-124] Each phase is expected to contribute to the overall mechanical properties of the film. Processing conditions—e.g., the rate at which the bulk heterojunction forms—affects the order within the crystalline polymer phase, and thus affects the mechanical properties.[24] Intercalation of fullerenes between the side chains of conjugated polymers to form bimolecular crystallites[117, 118] or to prevent crystallization[97] is known to have dramatic effects on the tensile modulus and

fracture behavior of polymer:fullerene blends.[23] Other factors, such as the size and purity of the fullerene samples, also play an important role.[125]

2.2.2.1. Theoretical determination of modulus of composites

Predicting the tensile modulus of polymer:fullerene composites for P3AT:$PC_{61}BM$ is possible using a simple composite theory, which was first applied to these systems by Tahk et al.[32] In this approach, the tensile modulus of the composite is a function of the modulus of the polymer, the Poisson ratio of the film (*v*, either calculated by equation 4,[28] or more commonly taken as 0.35,[32, 33]), the volume fraction of PCBM in the blend (ϕ_{PCBM}), and the maximum packing fraction of PCBM (ϕ_m, taken as 0.7,[32]).

$$\frac{E_{P3AT:PCBM}}{E_{P3AT}} = \frac{1 + AB\phi_{PCBM}}{1 - B\psi\phi_{PCBM}} \qquad (\mathbf{6})$$

$$A = \frac{7 - 5\nu_{P3AT}}{8 - 10\nu_{P3AT}}, B = \frac{\frac{E_{PCBM}}{E_{P3AT}} - 1}{\frac{E_{PCBM}}{E_{P3AT}} + A}, \psi = 1 + \frac{1 - \phi_m}{\phi_m^2}\phi_{PCBM} \qquad (\mathbf{7})$$

The results from this model are plotted in **Figure 2.5** on the same set of axes as the experimental data.[28] These composite theories do not account, however, for the ways in which the presence of the fullerene changes the morphology of the polymer phase. In particular, miscibility[123] and intercalation[118] of the PCBM between the side chains of the polymer, can have profound effects on the mechanical properties of films.[23]

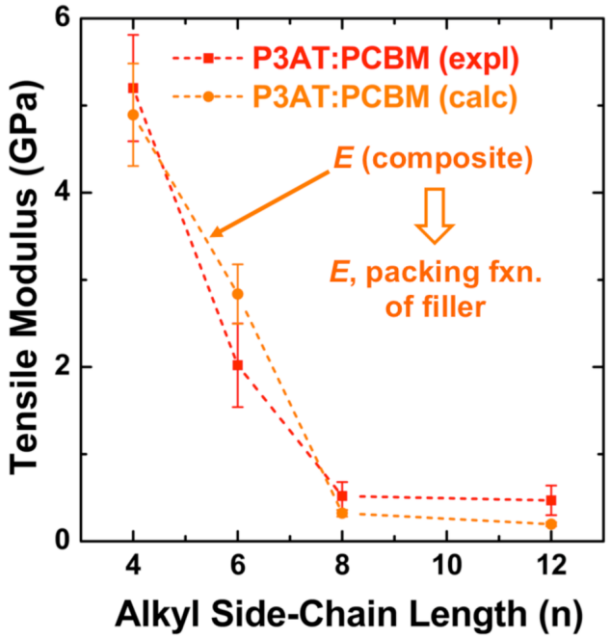

Figure 2.5. Tensile modulus vs. alkyl side chain length for P3AT:PCBM composites in a ratio of 2:1. The composite theory described in Section 2.2.1 nearly overlaps with the experimental values. Reproduced with permission from ref.[28] Copyright 2014, Wiley-VCH Verlag GmbH & Co. KGaA.

2.2.2.2. Intercalation and molecular mixing

The original model of the morphology of the polymer:fullerene bulk heterojunction comprised two, generally bicontinuous domains of pure donor and pure acceptor.[126-128] The current three-phase model has been assigned largely by electron tomography[121] (**Figure 2.6a**) and X-ray analysis.[18, 19, 113, 129] The extent of the mixed phase is governed by the solubility of the fullerene in the amorphous domains of the polymer[122] and by the presence of tie-chains between crystalline domains.[130] The tie chains constrain the expansion of the polymer and thus limit the amount of fullerene that the amorphous domains of the polymer can solubilize.[130] Regiorandom P3HT is completely amorphous and can disperse PCBM at any concentration.[130] The mixing is also dependent on the details of the molecular packing (i.e., the ability of fullerenes to occupy free volume between side chains of the polymer).[118]

For example, PT2T is a type of polythiophene that is derived from a tail-to-tail coupled bithiophene bearing hexyl chains and an unsubstituted thiophene ring (**Figure 2.6c**).[97] The polymer therefore contains a notch (i.e., the absence of an alkyl chain) every third repeat unit. This structural motif encourages the formation of crystalline domains in which the hexyl chains of adjacent polymer chains interdigitate.[97] Favorable positions of the frontier molecular orbitals suggest that blending this material with PCBM would produce an OPV effect that is possibly greater than that of P3HT:PCBM.[97] In the PT2T composite, however, the fullerene molecules sit in the notch, and thus prevent interdigitation of the side chains of adjacent polymer chains.[97] Thermal annealing does not recover the crystalline microstructure of the pure polymer, and the absence of pure polymer and pure fullerene phases have a disastrous effect on the power conversion efficiency of PT2T:PCBM blends.[97] Intercalation of fullerenes between the side chains is also the basis of the high ratio of fullerenes needed to achieve high efficiencies in blends of PBTTT and PCBM,[117] and probably also MDMO-PPV and PCBM;[118] that is, the weight percentage of fullerenes must surpass some threshold value, beyond which the crystalline phase cannot accommodate additional fullerene molecules. Pure or substantially enriched domains of fullerenes are required for high efficiency. Thus, blends of PBTTT and MDMO-PPV and PCBM, for example, are typically optimized with ratios of polymer to fullerene around 1:4.[118]

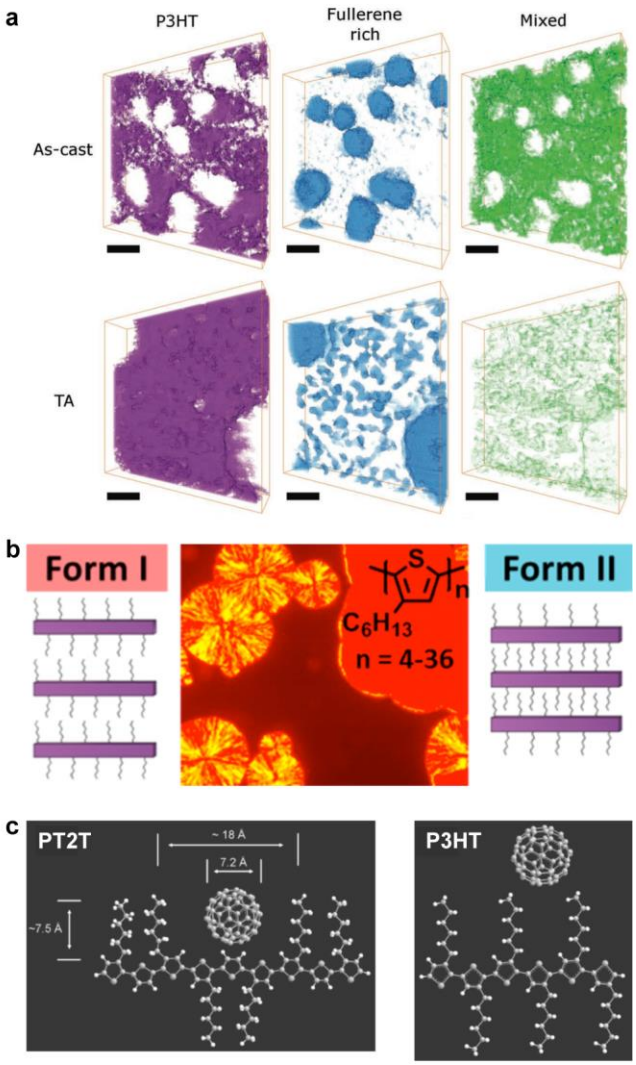

Figure 2.6. Morphology and packing of organic semiconductor films. (a) Electron tomography using endohedral fullerenes reveals a three-phase system comprising polymer- and fullerene- rich phases, and a mixed phase, which is substantially reduced by thermal annealing. Reproduced with permission from ref.[121] Copyright 2013, Wiley-VCH Verlag GmbH & Co. KGaA. (b) Two crystalline polymorphs of P3HT exist, a thermodynamically favored Form I (spherulites), in which the side chains do not interdigitate, and a kinetically favored Form II (solid red phase), in which they do. Form II is expected to have a greater modulus and higher brittleness than does Form I. Reproduced with permission from ref.[75] Copyright 2013, American Chemical Society. (c) Schematic drawings of PT2T and P3HT, and the hypothesized way in which fullerene molecules can fit between the side chains of PT2T, but not P3HT. Reproduced with permission from ref.[97] Copyright 2007, Wiley-VCH Verlag GmbH & Co. KGaA.

The mechanical properties of polymer:fullerene blends were previously reported to be intimately related to the details of molecular mixing.[23] The tensile moduli of most P3AT:fullerene blends are a factor of 3-5 greater than those of the neat polymers.[28, 32] The

typical rationale for the increased modulus of P3AT:PCBM relative to the neat polymer is the stiffness of the fullerene-rich phase.[28, 32] **Figure 2.7a** plots the factor by which selected polymer:fullerene composites are greater than that of the neat polymer both before and after annealing. The salient example is P3HpT:PCBM (factor of 7 greater than neat P3HpT).[131] As discussed in Section 2.1.3, P3HpT is the P3AT that maximizes mechanical compliance and electronic performance. Differential compliance and ductility of the P3ATs is largely a function of the fluidity of the amorphous domains at room temperature.[27] In a P3AT:fullerene composite, however, the current model predicts the absence of pure amorphous domains of P3ATs,[130] and thus we conclude that the presence of fullerenes produce stiffened mixed domains, which dominate the mechanical properties of the blend.

The dominance by the stiffened mixed domains on the mechanical properties of polymer:fullerene blends was observable not only in blends with P3ATs, which do not allow fullerene intercalation, but also in other polythiophenes which do allow fullerene intercalation. **Figure 2.7b** plots the tensile modulus of selected polymer:fullerene blends against the tensile modulus of the neat polymers. Interestingly, for these polythiophenes, there is a linear correlation between the tensile moduli of the neat polymers and the polymer:fullerene blends. This linear correlation suggests that the effects of molecular mixing play a relatively small role in the tensile modulus of polymer:fullerene blends. A striking example is PT2T:PCBM. The neat polymer is relatively highly aggregated due to the interdigitation of the alkyl side chains, though the modulus is similar to that of neat P3HT (~1 GPa, depending on batch-to-batch variability).[28, 29] Blending with PCBM, however, destroys the aggregate microstructure of PT2T. Remarkably, the tensile modulus

of even a 1:1 blend of PT2T:PCBM is similar to that of P3HT:PCBM, despite the completely different microstructures. The mechanical properties of bulk heterojunction composites—due to the complex nature of the blend, which has at least three phases—can vary widely, and offer interesting opportunities for studying nanocomposite materials.

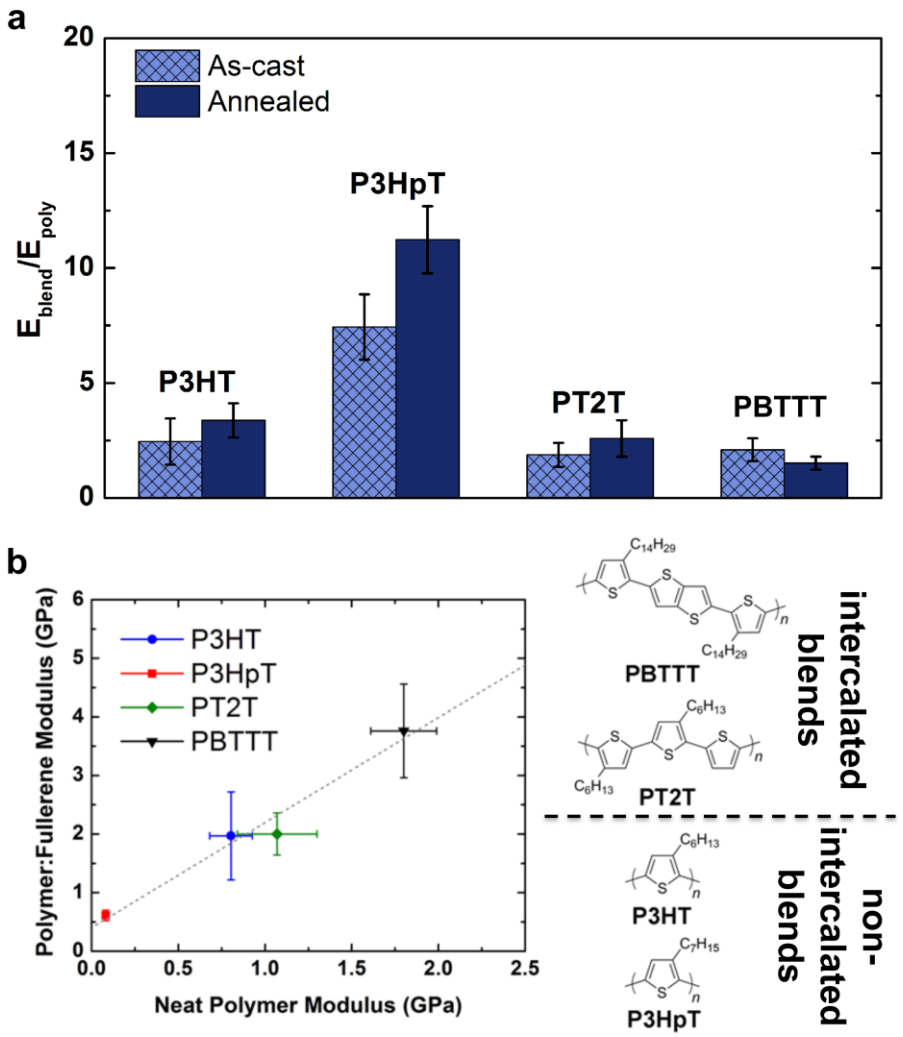

Figure 2.7. Effect of molecular mixing on the stiffness of polythiophenes. (a) A plot of the modulus of a polymer:fullerene blend vs. the modulus of the neat polymer reveals that the presence of fullerenes have a stiffening effect on the neat polymer; the correlation, however, implies that the details of molecular mixing—i.e., whether or not the fullerenes intercalate between the side chains of the polymer—have a relatively small effect, at least for the materials examined in this study. (b) Plot showing the factor by which a 1:1 blend of polymer and PCBM is greater in modulus than is the neat polymer in both annealed an unannealed forms.

2.2.2.3. Purity of fullerene samples

Fullerenes are the most popular electron acceptor in organic photovoltaics because of their high charge-carrier mobilities[132] and their spherical (or quasi-spherical) shapes, which permit them to accept electrons from any direction.[133] There are, however, several disadvantages to fullerenes, including cost,[4] embodied energy,[134] possible environmental degradation,[135] and the potential for toxicity. These drawbacks have motivated researchers to explore alternatives to fullerenes[136] to mitigate environmental concerns, or investigate less pure samples of fullerenes to reduce the cost and embodied energy. We undertook a study to understand the effect of the size and purity of the fullerene on the tensile modulus and crack-onset strain of P3HT:PCBM composites using four different samples of derivatized fullerenes: $PC_{61}BM$ (99%), $PC_{61}BM$ technical grade (90% $PC_{61}BM$, 10% $PC_{71}BM$), $PC_{71}BM$ (99%), and $PC_{71}BM$ technical grade (90% $PC_{71}BM$, 10% $PC_{61}BM$). The purer films were stiffer, but the less pure samples produced devices that were only somewhat—but not catastrophically—less efficient than those made from the purest samples (5% degradation in *PCE* for $PC_{71}BM$, and 19% degradation for $PC_{61}BM$.[125] These effects were attributed to the propensity of the fullerene with higher purity to form larger crystalline domains. A slight increase in order of the polymer phase with increasing purity of the fullerene was also observed through UV-vis spectra as analyzed by the weakly interacting H-aggregate model.[125] This study suggests that the use of lower-purity fullerenes may substantially reduce the cost and production energy of organic solar cells, and also increase the compliance and environmental stability of devices (**Figure 2.8**).[125]

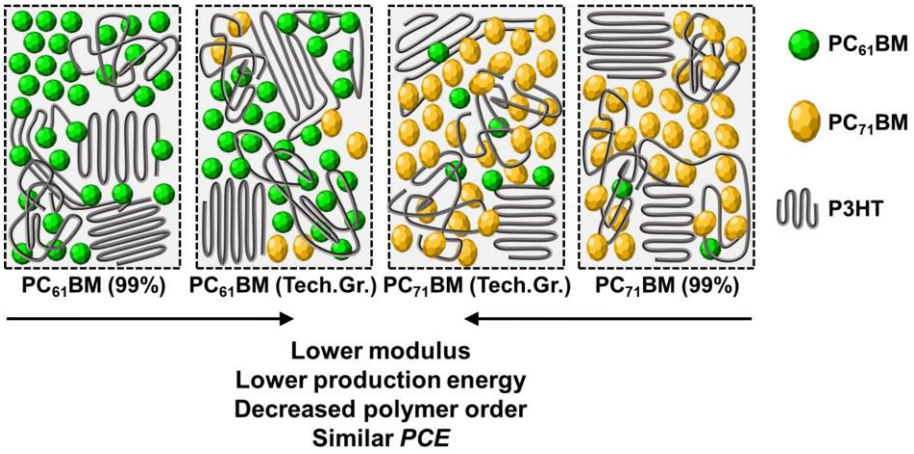

Figure 2.8. Schematic summary of the effect of purity of fullerenes on the stiffness of P3HT:PCBM blends for $PC_{61}BM$ and $PC_{71}BM$. "Purity" refers to the extent of separation of C_{60} and C_{70} derivatives, where technical grade (Tech. Gr.) contains ≤10% fullerenes of the other size. The results suggest that it is possible to increase the compliance of polymer:fullerene blends while decreasing the purity of the fullerenes to decrease the embodied energy (and therefore the cost).

2.2.2.4. Effect of additives and plasticizers

High-boiling additives are often included in bulk heterojunction films to increase the performance of polymer:fullerene blends and PEDOT:PSS films by improving the morphology.[137, 138] Small-molecule additives in polymer engineering often have the effect of plasticizers. Plasticizers increase the free volume within samples of solid polymers, and lower the T_g and the tensile modulus. Common additives, such as 1,8-dithiooctane and 1,8-diiodooctane (DIO),[137, 138] have been used for certain bulk heterojunctions comprising low-bandgap polymers blended with PCBM to improve their performance. Graham et al. found that PDMS, often used as a lubricant in the syringes used to dispense polymer "inks" for spin-coating, is also associated with generating a favorable morphology and increased efficiency in solar cells based on solution-processed small molecules.[139] Using P3HT:PCBM as a model system, we found a plasticizing effect for both DIO (69% decrease in tensile modulus) and PDMS (28% decrease), using concentrations typically used in the literature.[28] It is not yet known whether the decrease in modulus can be

attributed to a typical plasticizing effect (i.e., increasing the free volume) or by a change in microstructure that affects the mechanical properties.

Additives and cosolvents are essentially always used in solution-processed films of PEDOT:PSS,[140, 141] and these adjuncts have effects on the modulus (**Figure 2.9a**) and ductility (**Figure 2.9b**),[71] along with effects on the sheet resistance (**Figure 2.9c**),[140] some of which are already known.[142] High-boiling liquids and polar additives, such as dimethylsulfoxide (DMSO) and sorbitol, are associated with increasing the size of the conductive PEDOT-rich grains, and thus increasing the conductivity of the film.[143, 144] Zonyl fluorosurfactant (now called Capstone by DuPont) is used to enable wetting of aqueous dispersions of PEDOT:PSS on hydrophobic plastic substrates,[140, 145] or on the hydrophobic surface of the bulk heterojunction film in the inverted architecture.[146] Poly(ethyleneimine) (PEI),[147] and other amine-containing polymers and small molecules,[148, 149] is used to lower the work function of PEDOT:PSS to permit its use as the cathode (as well as the anode) in all-organic devices. While the use of a thin-layer of PEI seems to have a stiffening effect, Zonyl, when present in the ink in concentrations up to 10%, has a very strong plasticizing effect.[71] It seems, thus, that additives may serve a dual purpose: as cosolvents for one or more components of the bulk heterojunction, and as plasticizers for increased mechanical stability. Interestingly, the concentration of DMSO in the ink of 5%, which produced the most conductive films when the concentration of Zonyl was kept constant, also produced films of greater stiffness and brittleness.[71] The interconnected morphology that supports good charge transport may thus embrittle the films, but this effect can be mitigated by adding Zonyl (or perhaps another surfactant) without degrading the electronic performance substantially.

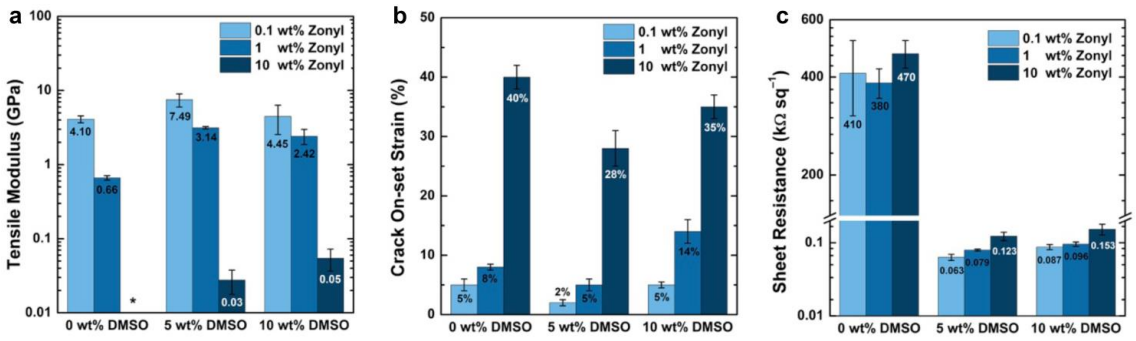

Figure 2.9. Effect of common additives, Zonyl fluorosurfactant and DMSO, on the (a) tensile modulus, (b) crack-onset strain, and (c) sheet resistance of the ubiquitous transparent conductive polymer, PEDOT:PSS.

2.2.2.5. Small molecules and oligomers

Compared to their polymeric counterparts, solution-processed small molecules offer advantages of monodispersity and increased overall purity, a greater tendency to produce highly crystalline microstructures, and low cost and low production energy. The power conversion efficiencies of devices with active layers based on small-molecule:fullerene blends are nearly as high as the typical polymer:fullerene system.[150] It may be, however, that the highly crystalline morphology of π-conjugated small molecule films also renders them stiff and brittle. The transition from polymer to oligomeric to small-molecule can coincide with a transition between polymorphs, which can have different mechanical properties. Koch et al., as mentioned in Section 2.1.3, found that oligo(3-hexylthiophene) (degree of polymerization = 4 – 36) exhibited the kinetically favored crystalline polymorph—"Form II"—in which the side chains interdigitated, and underwent a qualitative increase in stiffness.[75] The forms could be interconverted by appropriate treatments, but Form II was generally favored for the shorter oligomers. There is far less information available on the mechanical properties of small-molecule semiconductors than there is about polymeric ones. Films of evaporated pentacene, in addition to having an

extraordinarily high tensile modulus of 15 GPa, also exhibited substantial cracking when transferred to a PDMS substrate for analysis by the buckling methodology.[32] Preliminary observations by our group on solution-processible, small-molecule semiconductors, TIPS-pentacene, SMDPPEH, and pDTS($FBTTh_2$)$_2$, suggest that these van der Waals solids are characteristically brittle. Attempts to measure the moduli and crack-onset strain on PDMS substrates have thus far been unsuccessful, because of cracking of the films during the process of transferring from passivated glass or silicon to PDMS. In high-modulus materials that were eventually measured successfully, this behavior correlated with high stiffness and brittleness, as in P3BT:PCBM.[28] There is, however, a dearth of literature on the mechanical properties of small-molecule films, and definitive statements about the mechanical stability of devices based on solution-processed small molecules cannot be made.

2.2.2.6. Are mechanical and electronic figures of merit mutually exclusive?

Analyses of several organic conductors, semiconductors, and composites have suggested that good electronic properties—as manifested in conductivity, charge-carrier mobility, and photovoltaic efficiency—and mechanical properties (i.e., elasticity and ductility) are antithetical.[24, 151] Systems in which this competition was observed include P3ATs with side chains having an even number of carbon atoms,[28] P3HT:PCBM films dried at different rates,[24] annealed and unannealed PBTTT,[33] and PEDOT:PSS deposited from inks containing different amounts of DMSO.[71] Recent studies, however, have shown possible routes toward systems that exhibit substantial compliance along with high photovoltaic efficiency. For example, P3HpT has a vibronic structure (as seen in the UV-

vis absorption spectrum) that nearly overlaps with that of P3HT, which indicates a similar percentage of aggregate and a similar level of order within the aggregate. Moreover, P3HpT exhibits photovoltaic parameters in blends with PCBM that are similar to those of the standard (and more brittle) material, P3HT.[27] The amorphous phase in P3HpT is mobile at room temperature, however, while the amorphous phase in P3HT is glassy. The similar electronic performance thus seems to be a manifestation of the degree of crystallinity and the order within the crystalline domains, while the differential mechanical properties are dominated by the amorphous domains. These observations point to a design rule, valid at minimum for semicrystalline materials, for organic semiconductors that are at once high-performance and highly compliant. Another route toward films exhibiting the best of both worlds is plasticization of the active materials by additives—such as DIO and PDMS for semiconductors, and Zonyl for PEDOT:PSS—that are already known to increase the electronic figures of merit.[28] Other approaches, such as covalent incorporation of flexible units (e.g., polyethylene blocks[34] or oligoethylene glycol side chains[152]) may provide further routes toward tailoring the mechanical properties of bulk heterojunctions of high-performance conjugated polymers. Intentional reduction in crystallinity by introducing random units in a polymeric backbone represents another possible method to achieve good photovoltaic performance and high elasticity,[29] as does substitution of fused rings in the main chain of a polymer (e.g., thienothiophene) for isolated rings (e.g., bithiophene),[31] and tailoring the rate at which the bulk heterojunction forms.[24] **Figure 2.10** shows a plot of power conversion efficiency vs. tensile modulus for six samples of polythiophene. Materials occupying the top-left quadrant in such a plot are potential candidates for

mechanically stable solar cells (e.g., P3HpT), or embody rules that will inform the design of high-performance materials in the future.

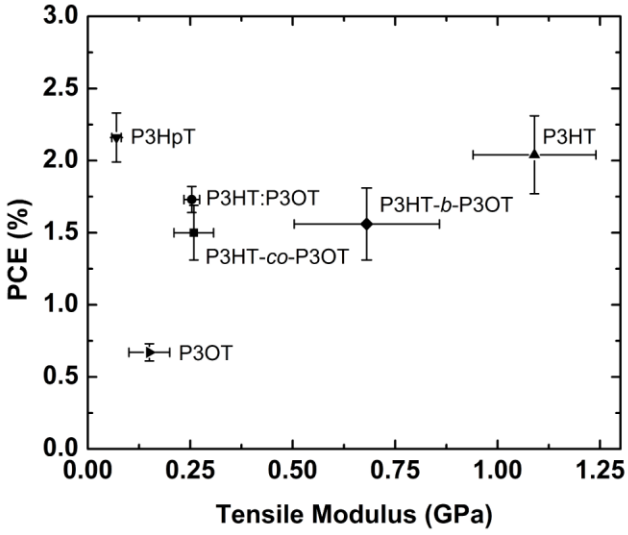

Figure 2.10. Power conversion efficiency (*PCE*) of polymer:fullerene blends vs. tensile modulus of the pure poly(3-alkylthiophenes): P3HT, P3OT, a physical blend of the two (P3HT:P3OT), a block copolymer (P3HT-*b*-P3OT), a random copolymer (P3HT-*co*-P3OT), and P3HpT. Materials occupying the top-left quadrant (e.g., P3HpT) in principle exhibit a favorable combination of mechanical compliance and photovoltaic performance. Reproduced with permission from ref.[27] Copyright 2014 American Chemical Society.

2.3. Behavior of materials and devices under strain

All thin-film technologies are susceptible to damage by environmental forces. If changes in the photovoltaic output of devices upon imposition of mechanical stress are not prevented, they should at least be anticipated, so that their effects can be mitigated downstream. We divide the response to strain into two regimes: (1) pre-catastrophic failure and (2) catastrophic failure. The behavior in the first regime, characterized by small-strains (prior to cracking or delamination that produces substantial loss of function) is in principle affected by elastic or plastic deformation of the active materials and contacts. Deformation of the materials continues throughout the second regime, but the photovoltaic output is dominated instead by cracking of the active materials and contacts, failure of the barrier

films, and short-circuiting of the electrodes. We define catastrophic failure as occurring when the device loses most or all of its photovoltaic efficiency. This section also discusses the factors that control interfacial debonding, cracking, and the molecular and environmental determinants of this type of failure.

2.3.1. Pre-catastrophic failure behavior

This section reviews the evolution in photovoltaic properties in response to strain-evolved microstructures, change in interfacial energies, and the formation of small cracks. The defining characteristic of this regime is that the photovoltaic properties remain generally intact. Many of the strain-evolved changes in microstructure observed in some conjugated polymers—alignment of chains,[78] change in texture from edge-on to face-on,[78, 79] and increased degree of crystallinity[78]—might actually increase the photovoltaic performance of devices under some circumstances.

2.3.1.1. Strain-evolved microstructure of organic semiconductors.

Charge transport in organic semiconductors is intimately linked to solid-state packing structure,[44] which is perturbed when an active material is strained (**Figure 2.11**). It is clear, thus, that even the smallest applied strains will change the photovoltaic response of the active material. Strained microstructures do not always have deleterious consequences on the electronic output. For example, Giri et al. found that crystalline films of TIPS-pentacene could exhibit metastable polymorphs with shortened π-stacking distances and thus increased charge-carrier mobility in field-effect transistors.[153] Some of these polymorphs, which are accessible by changing the speed of solution-shearing, are

applicable to large-area coverage.[154] Furthermore, the direct application of compressive strain has been shown to increase the mobilities in films of pentacene and tetracene, where the photoconductivity of the crystals increased linearly with applied hydrostatic pressure.[155] Zinc octakis(β-decoxyethyl)porphyrin films have also exhibited a strong correlation between the increase in compressive strains and a higher photoconductivity, when pressures using a micro tip were applied.[156] The authors attributed these effects to a compression of the π-stacking axis and better overlap of the molecular orbital wavefunctions.

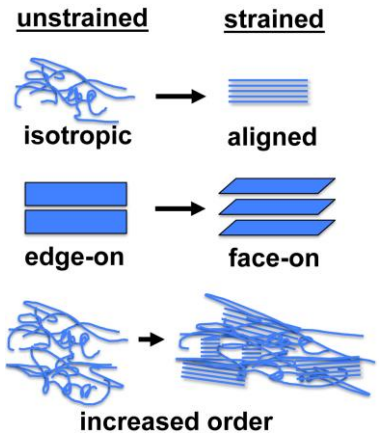

Figure 2.11. Strain-evolved changes in microstructure shown to occur in polythiophenes. (Top) Tensile strain aligns chains, (middle) affects a reorientation in texture from principally edge-on to face-on, and (bottom) increases the overall percent aggregate.

The most well known effect of tensile strain on a conjugated polymer is alignment of the chains along the strained axis. This effect has been known since early work on conjugated polymers, and is responsible for the extraordinarily high tensile strength of uniaxially aligned polyacetylene.[53, 54] Drawn films of P3HT exhibit highly anisotropic hole mobility, which has been noted by Vijay et al.[112] and O'Connor et al.[78] These studies highlight the importance of along-chain transport in the overall ability of a film to transport

charge. This fact was reinforced in a paper by Heeger and coworkers, in which low-bandgap polymers aligned in nanoimprinted grooves exhibited among the highest charge-carrier mobilities reported to date.[157] Aligned films also exhibit polarization-dependent absorption, because of the orientation of the π-π* transition, which is perpendicular to the molecular axis.[158] Awartani et al. has shown substantial birefringence in stretch-aligned bulk heterojunction films, and thus organic solar cells with polarization-dependent absorption and efficiency.[80] The increase in charge-carrier mobility induced by stretch aligning may benefit field-effect transistors, but the anisotropy is in the wrong direction to benefit organic solar cells, in which charges are transported through the thickness of a film.

A secondary effect of strain on the microstructure of conjugated polymer films, as seen in P3HT, is on the texture. O'Connor et al. noted that strain produced realignment of the π system of the molecules from predominantly edge-on (regarded as the preferred orientation for P3ATs and other conjugated polymers) to largely face-on.[78, 79] The latter orientation may be favorable for OSCs. O'Connor, DeLongchamp, and coworkers have observed this effect in P3HT films under both uniaxial[78] and biaxial[79] deformation. The mechanism and fundamental basis for this realignment remains an interesting and important question for further inquiry, and has implications for the photovoltaic output of devices under strain. It suggests that mechanical strain might actually improve power conversion efficiencies of devices under some circumstances.

A third effect of strain, observed by increases in the intensities of the vibronic transitions of P3ATs, is an increase in the percent crystalline aggregate within the film.[78] This strain-evolved microstructural change could, in principle, produce greater photovoltaic performance, as percent aggregate in the polymer phase is correlated with

increased efficiency in P3HT:PCBM devices.[24] While such increases in crystalline order produced by other means—i.e., thermal annealing,[159] solvent-vapor annealing,[160] and slowness of evaporation of the solvent during solution casting[24]—are generally correlated with increases in *PCE*; in a solar cell, tensile strain has possibly detrimental effects on the other components of the device, such as the substrates, interfaces, barrier films, and electrodes, which make it difficult to isolate the effects of strain itself on the overall properties of the device.[31] **Figure 2.12a** and 2.**12b** shows the evolution in photovoltaic properties with tensile strain for two types of devices fabricated on PDMS substrates, one based on P3HT:PCBM, and the other based on PDPP2T-TT:PCBM, from 0 to 20% strain.[31] The apparent increase in V_{OC} with small strains for the brittle P3HT:PCBM was attributed to fracturing of the oxide "skin" that forms on the liquid eutectic gallium-indium (EGaIn) cathode—used because it is stretchable—when extruded in air. The same effect is observed if the EGaIn is extruded in air, placed in the glovebox, and then agitated with a wooden applicator, but the effect disappears when the EGaIn is extruded in a nitrogen atmosphere. The effect is more pronounced for P3HT:PCBM than it is for PDPP2T-TT:PCBM, because the former bulk heterojunction is more brittle, and the opening and closing of cracks in the active layer perturb the top electrode to a greater extent. This experiment highlights the difficulty in isolating the effects of the change in microstructure of the active materials from the detrimental effects on the electrodes and other materials.

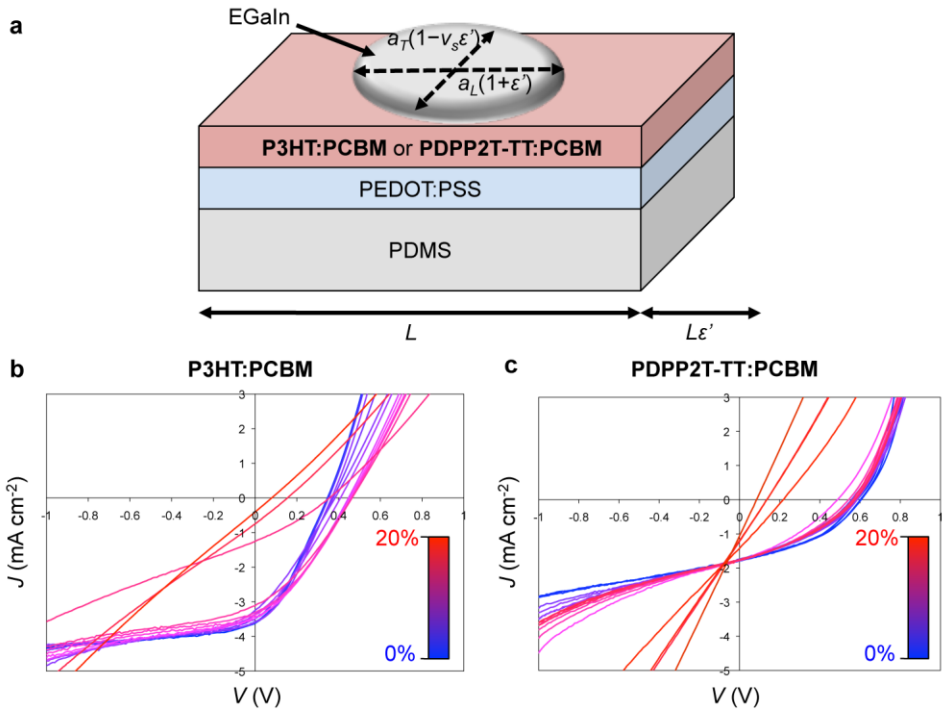

Figure 2.12. Evolution in photovoltaic output with tensile strain, ε. (a) Schematic diagram of a stretchable device. (b) Current density vs. voltage for a P3HT:PCBM device from 0% to 20% strain. (c) A similar plot for a PDPP2T-TT:PCBM device. Current densities were calculated using the area of the footprint of the drop of eutectic gallium indium (EGaIn), which deformed with strain, by the equation $A(\varepsilon') = \pi a_L(1+\varepsilon')a_T(1-v_S\varepsilon')$, where $\varepsilon' = \varepsilon/100\%$, a_L and a_T are the longitudinal and transverse semi-major axes, and v_S is the Poisson ratio of PDMS (and assumed to be constant within the relatively small range of strains, between 0 and 20%.) Reproduced with permission from ref.[31] Copyright 2012, Elsevier.

Global strains, applied to whole devices, can manifest as damage at interfaces. While the effects of pre-catastrophic bending strains on interfaces have not been rigorously determined for organic solar cells, Sokolov et al. has performed relevant studies on field-effect transistors.[161] The authors' principal conclusion was that the strains applied to these transistors changed the alignment of polymer chains and altered the field-effect mobility of the strained devices due to reorientation of the surface dipoles.[161] Poor interfacial adhesion can produce cracks at sites of local delamination that propagate through multiple layers in the device.[30, 142] Adhesion promoters can reduce this effect substantially, as has been observed for PEDOT:PSS,[30, 142] which behaves as a prime coat that increases adhesion

of bulk heterojunction films to hydrophobic substrates. Lu et al. observed a similar effect in films of copper on polyimide substrates, which could be stretched up to 50%, without cracking, if a chromium adhesion layer was used.[162]

2.3.1.2. Pre-catastrophic cracking under tensile strain.

There are scenarios in which lateral cracks that appear on the surface of the active material would not lead to catastrophic failure in a device. One can imagine, for example, that a solar cell that cracks without shorting of the electrodes might behave like many smaller solar cells connected in parallel. In fact, Chortos et al. showed that microcracked organic semiconductors functioned normally while strained in stretchable field-effect transistors.[163] In principle, cracking of an electrode would increase the sheet resistance of the contact, which would manifest in increased series resistance, and would, in turn, reduce the fill factor and short-circuit current. Cracks and thin areas in the active layer could produce shunts and lowered parallel (i.e., shunt) resistance, and ultimately decrease the fill factor and open-circuit voltage. These qualitative features are consistent with the behavior of a device with the architecture PDMS/PEDOT:PSS/PDPPT2T-TT:PCBM/EGaIn (**Figure 2.12c**).[31] As the applied strain approaches 20%, the *J*–*V* curve resembles a short circuit. In contrast to the examples shown in **Figure 2.12**, which show the evolution in photovoltaic output with strain due to cracks that appear in the surface of the film, there have not been any studies in which interfacial debonding or cohesive failure were explicitly identified as the origin of failure. One intriguing possibility is that some organic semiconductors might undergo stimulus-responsive healing or repair after damage. It has become clear, for example, that fullerene molecules are highly mobile within the

amorphous domains of P3AT films, and can diffuse across interfaces of laminated films.[123, 124] Kahn and coworkers have reported lamination of conjugated polymer films by transfer printing, and while the laminated film was reported to be essentially identical to a single film with respect to charge transport, the mechanical properties of the welded interface—in particular, the cohesion—has not been characterized.[164, 165]

2.3.2. Catastrophic fracture

In contrast to Section 2.3.1.1, which dealt largely with the theoretical effects of strain-evolved changes in microstructure on the photovoltaic properties, the effects of cracking are easily seen in plots of current density vs. voltage, and are nearly always deleterious.[31] The detail to which these effects are characterized in the literature is, however, not fine-grained. In general, bending studies are performed to illustrate the superior mechanical flexibility of one material (e.g., the transparent electrode) over a control device that uses a conventional material (e.g., ITO, though the mechanism by which ITO itself degrades under strain is an active area of research[166]).[167] Degradation of function is attributed to cracking within the control device, however, strain is almost never estimated based on the bending radius and thickness of the substrate, and the specific ways in which the damage manifests in the degraded *J*–*V* plots are generally not identified. This section is subdivided on the basis of the relative orientation of the strain to the plane of the device: (1) strain applied parallel to the device plane that generally produces cracking and cracking-induced delamination in one or more layers,[31, 145] and (2) strain applied normal to the device plane, which is associated with cohesive and adhesive failure of the thin films that make up the device.

2.3.2.1. Strain applied parallel to device plane

Strain occurs within the plane of the device when stretched or bent (the strain is tensile on the convex surfaces above the neutral plane, and compressive on the concave surfaces below the neutral plane).[168] Strain also appears during deformation associated with thermal expansion and contraction.[51] Tensile strains can produce cracks in all layers of the device and concomitant delamination if one layer deforms more than another in response to the same stress. Cracks in either the anode or cathode increase the series resistance of the device, and lower the fill factor and short-circuit current; thin areas in the active layers, or any scenario in which the electrodes are brought closer together, decrease the parallel (i.e., shunt) resistance, and also lower the fill factor and tend to decrease the open-circuit voltage. Catastrophic debonding of the electrodes produce open circuits, while cracks in the active layer that permit the electrodes to make physical contact produce short circuits,[28, 30] for which the *J–V* plots resemble resistors in parallel with photovoltaic cells (as in **Figures 2.12b** and 2.**12c**).[31] In another example, Nickel et al. attributed cracking of a composite PEDOT:PSS/silver nanowire electrode as the source of degradation of a device based on a PTB7:$PC_{71}BM$ active layer while strained, but the device lost only 10% of its initial performance even at 14% strain.[169] It thus possible in principle for a solar cell to retain function even if the electrodes and the active materials are cracked all the way through, as long as the pathways leading to the electrodes are not interrupted. Compressive strain can also crack layers, especially of brittle materials, such as films of small molecule semiconductors (as observed by Tahk et al., **Figure 2.13a**).[32] Wrinkling of the surface (**Figure 2.13b**) can also occur under compressive strain if there is a mismatch in elasticity between the device layers and the substrate, or if the layers are poorly adhered.[51]

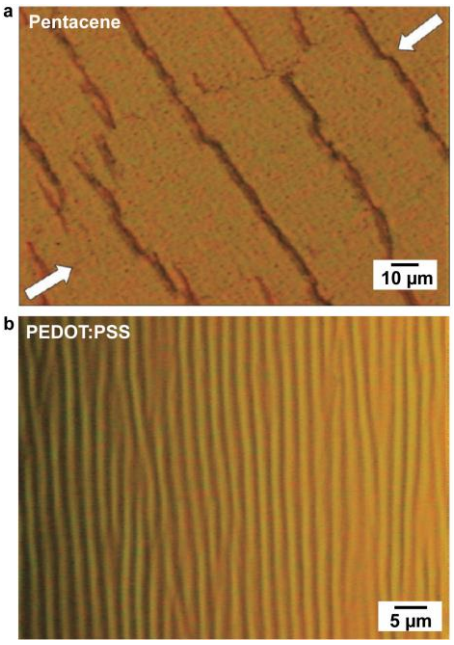

Figure 2.13. Images of cracks and buckles that appear in organic thin-film devices. (a) A cracked film of pentacene evaporated on a PDMS substrate and subjected to a 10% compressive strain. (b) A surface wrinkling pattern characteristic of the deformation that occurs in rigid films under compression due to direct application of mechanical force or because of thermal contraction. Reproduced with permission from ref.[32] Copyright 2009, American Chemical Society.

2.3.2.2. Strain applied normal to device plane

In contrast to the experiments described in this review so far, in which strain was applied in the plane of the device, the failure patterns of some types of devices may be predicted more realistically by experiments in which stress is applied perpendicular to the plane of the device. Stressing a multilayered device in this way can produce cohesive (within-layer) or adhesive (between-layer) failure. The Dauskardt laboratory published a series of studies that related the cohesive or adhesive fracture energy—G_c, the work needed to break or separate polymer films or interfaces—to various molecular parameters and processing conditions (**Figure 2.14**).[23, 50, 52, 68-70] The authors generally used a four-point bending test (**Figure 2.14a**) or double cantilever beam apparatus to apply strain perpendicular to the plane of the device. The setup is intended to mimic modes of

deformation that lead to separation within the device plane. Several important conclusions were drawn from this research that establish important design rules for improved reliability and yield of production of OPV devices.

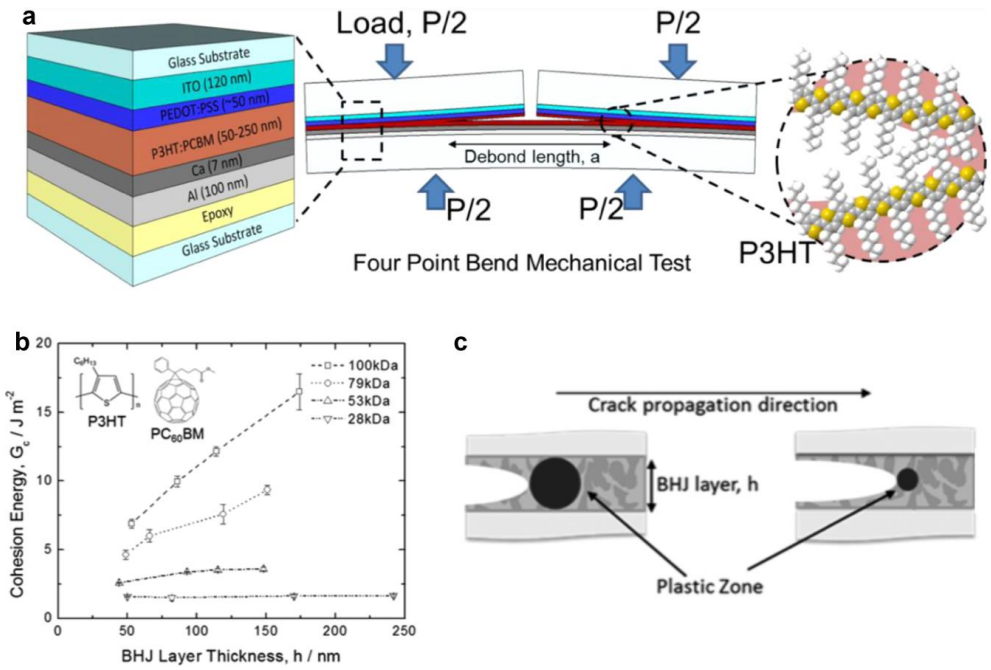

Figure 2.14. Schematic diagrams and data summarizing cohesive and delaminative fracture under different conditions. (a) Schematic diagram of the four bend mechanical test designed to measure the cohesive fracture energy of the P3HT:PCBM active layer in an organic solar cell as a function of molecular weight of the P3HT. (b) Cohesive energy vs. thickness of the BHJ layer with different molecular weights. Extremely high values of cohesion were obtained for thick films of high molecular weight. (c) Schematic illustration of the effect of the size of the plastic zone at the crack tip on the cohesion; brittle materials with small plastic zones exhibit less of a dependence on layer thickness, because the plastic zone is smaller than the distance between plates. Reproduced with permission from ref.[50] Copyright 2014, American Chemical Society.

The range of values of G_c for cohesion of the P3HT:fullerene bulk heterojunction were found to be 1–20 J m^{-2}, although the high end of this range was only measured for P3HT:ICBA[23] and in systems of thick P3HT:PCBM films in which the P3HT had high molecular weight.[50] Typical values of 1–5 J m^{-2} are lower (more unfavorable) than those of other dielectric materials—e.g., crosslinked polymers and oxides—commonly used in

microelectronics.[52] The cohesion was found to be strongly dependent on the composition of the bulk heterojunction. In particular, cohesion decreased with increasing PCBM concentration, from 0.5 J m^{-2} for pure PCBM to a maximum of 2.5 J m^{-2} for BHJs containing 75% P3HT.[52] The cohesive energy was not found to be affected by thickness, at least in the initial report, which the authors noted was different from the behavior of more-ductile polymers.[52] The cohesion, trajectory of the propagation of the crack, and the roughness after cohesive fracture depends on the mechanical properties of the material encountered by the crack during propagation. In examples of polymers exhibiting substantial plasticity (e.g., high-molecular-weight P3HT, **Figure 2.14b**), a plastic zone forms at the crack tip and expands until it is confined by either crystalline domains in the film or by the rigid top and bottom substrate (**Figure 2.14c**)—i.e., glass or epoxy in these experiments.[52] This plastic zone dissipates energy of the deformation, and decreases the cohesion measured in thin films of polymers with high ductility as thickness decreases, in which the volume of the plastic zone is confined by the hard substrate and backing.[50, 52] Dependence of cohesion on thickness is, however, present in high molecular weight P3HT,[50] which is consistent with a lowered degree of crystallinity and a larger plastic zone of the crack tip that is relatively unconstrained by rigid crystallites of samples with lower molecular weight. Formation of bimolecular crystals, in the case of PQT-12 and PBTTT and their mixtures with monofunctionalized PCBM, tends to produce bulk heterojunction films with relatively high cohesion (G_c ~ 2–5 J m^{-2}).[23] While this is an important observation that informs the selection of materials for mechanical robustness, bulk heterojunctions with bimolecular crystals at ratios of polymer:fullerene of 1:1 (i.e., below the concentration at which pure PCBM domains form) are inefficient, and those with ratios

of 1:4 fail cohesively more readily ($G_c \sim 1$ J m^{-2}) because of the fragility of the pure PCBM phase.[23]

In roll-to-roll processed flexible devices with the inverted architecture, adhesive failure was found to occur most commonly between the bulk heterojunction layers and PEDOT:PSS, with values of G_c between 0.1 to 1.6 J m^{-2}.[68] The adhesion decreased with increasing concentration of PCBM, which can be attributed to low interaction volume of fullerenes[100] and relatively weak van der Waals attraction to adjacent layers. We note that the order in which the layers are deposited has an effect on mechanical stability. For cells with the conventional geometry, in which the P3HT:PCBM is coated on top of the PEDOT:PSS, this interface survived, whereas the P3HT:PCBM failed cohesively.[52] The adhesion in the inverted geometry could be increased by increasing the time and temperature of annealing, or by replacing the PEDOT:PSS with another hole-transporting layer, such as vanadium oxide (V_2O_5). Use of V_2O_5, deposited from solution, produced an interface that was dramatically stronger (up to 150 J m^{-2}), but a device that was very inefficient.[68] Increased adhesion was attributed to a 10-nm-thick mixed layer between V_2O_5 and P3HT:PCBM. Depth profiling XPS determined that failure occurred between this mixed layer and the active layer. Reduced mixing and a weaker interface was found when solution processed V_2O_5 was replaced with vapor-deposited molybdenum oxide (MoO_3).[69] A mixed interfacial layer has also been invoked to explain the good adhesion between PEDOT:PSS and the active layer, if the PEDOT:PSS has been deposited first, and is possibly concomitant with the formation of $P3HT^+$:PSS^- species where the polymer chains interact.[69] (The pure PEDOT:PSS phase itself is, however, subject to decohesion that accelerates in the presence of atmospheric moisture, attributed by DuPont et al. to hydrogen

bonds of PSS^- to water which disrupt the existing PSS^----H^+---PSS^- that give the polymer its cohesive strength.[70])

2.4. Possible routes of increasing the mechanical stability of organic solar cells

The experiments described in this review point to several routes that can be explored toward the end goal of increasing the mechanical robustness of organic solar cells. We identify several approaches that have been proposed explicitly or suggested by the results of experiments in the literature, and comment on the probability of success in a large-scale environment.

2.4.1. Buckled or wavy solar cells

The concepts introduced by Whitesides,[90] Rogers,[170] Wagner[171, 172] and others,[173] involving the production of thin-film devices whose active materials are buckled on pre-strained surfaces, and which accommodate strain by local bending and unbending of the buckles, has been exploited by Lipomi et al.[145] and then later by Kaltenbrunner et al.[3] to form unencapsulated stretchable organic solar cells. (Buckles and deep folds were later used as structures to increase light trapping by Loo and coworkers.[174]) This concept would be difficult to apply in a roll-to-roll scheme, because of the requirement that the substrate be under tension and the low probability that a multilayered device could be buckled by compressive strain without introducing substantial interfacial stress. The authors' experience suggests that under compressive strain, metallic electrodes, or solution processed oxides to modify the work function of one or more of the electrodes, would almost certainly crack and have a deleterious effect on the photovoltaic output of the

devices. Furthermore, surface wrinkling requires a substantial mismatch in moduli between the substrate (~1 MPa for PDMS) and the thin films (≥10 MPa). The use of such deformable substrates in roll-to-roll coating apparatuses may not be straightforward.

2.4.2. Use of highly compliant conjugated polymers

A promising strategy to increase the mechanical robustness of OPV devices is to increase the elasticity, plasticity, or both, of the conjugated polymer. The highly compliant nature of P3HpT, a material with well ordered crystalline aggregates, is attributed to the amorphous domains whose glass transition is below room temperature, and suggests one possible way to achieve the "best of both worlds" of electronic and mechanical properties.[27] Another strategy is to take a material with a low bandgap and high mobility (such as a DPP-based material depicted in **Figure 2.1**) and introduce unlike conjugated monomers at random into the backbone, to decrease the degree of crystallinity (which would be effective so long as the material maintained high charge-carrier mobility in the absence of high crystallinity).[29] In general, factors that increase the compliance and ductility (independent of their effects on charge transport) are long alkyl side chains,[57] high molecular weight (at least in P3HT),[50] substitution of fused rings in the polymer backbone to isolated rings,[31] and structural randomness to reduce the degree of crystallinity.[29] All things being equal, highly cohesive and non-brittle conjugated polymers will perform better than brittle ones. The extent to which one component of the active material influences the failure behavior of the entire device, however, is an open question, and requires more testing. It also requires knowledge of the effects of other materials not only in the device stack, but within the active layer itself.

2.4.3. Substitution of PCBM

The ubiquitous acceptor PCBM has many deleterious effects on the mechanical stability of OPV devices. Pure PCBM phases have low cohesive energy,[52] high tensile moduli,[125] low crack-onset strains,[125] and weak interfaces with other layers in the device.[68] They can also substantially stiffen active materials that have low moduli by themselves (e.g., P3HpT).[27] Decreasing the purity of the fullerene might suppress crystallization and therefore reduce the modulus, but this is not a guaranteed strategy.[125] Another potential route would be to find a different acceptor,[136] but our (very) preliminary observations on the mechanical properties of solution-processed small molecule films suggest that they are brittle. Polymer:polymer heterojunctions[59, 175] might represent a way forward, and indeed all-polymer solar cells have achieved high efficiencies in trials by several groups.[176, 177] The mechanical properties of electron-acceptor polymers are relatively unexplored, but we suspect that the design rules for robust donors would be easily translated to acceptors.

2.4.4. Plasticizers

The use of plasticizers represents an approach that is familiar to the engineering plastics community. For example, small molecules that increase the free volume in a polymer sample also tend to reduce its T_g and modulus, and increase its ductility. As discussed in Section 2.2.2.4, our group has found that compounds that are added to bulk heterojunction blends to increase efficiency (for example DIO or PDMS)[28] and to PEDOT:PSS to improve conductivity and wettability (DMSO or Zonyl),[71] can also have plasticizing effects on thin films. Since only a few plasticizers have been thoroughly tested in a laboratory setting, their success leads us to believe other combinations of additives

could play a key role in improving mechanical stability. The effect of these plasticizers on the failure mechanisms of whole devices, however, is an open question; plasticizers may segregate to the surface and change the interfacial adhesive properties.[68] Another question is mechanistic: do these additives increase the compliance and ductility simply by increasing the free volume (if they remain in the film) or by altering the morphology or extent of mixing, or some combination thereof?

2.4.5. Importance of adhesion

Strong interlayer adhesion is an important design characteristic, irrespective of the mechanical properties of the isolated materials. Interlayer adhesion[68] is generally increased if at least one of the interacting partners has a high surface energy, which is typically produced by a high dipolar contribution to the van der Waals coefficient of the material. Specific interactions, such as hydrogen bonding surfaces could also increase the adhesive fracture energy of the interfaces. Adhesion promoters would be beneficial, provided they do not have deleterious effects on charge transport in the device stack. In some cases, materials behave as serendipitous "prime coats," which is the case for PEDOT:PSS,[30] which improves the adhesion of bulk heterojunction films to hydrophobic substrates.[142]

2.4.6. Toward standardization of mechanical testing

As of yet, there is no standardized procedure for characterization of the mechanical stability of organic solar cells. Any international standards must begin with a full description of the dimensions and composition of all layers in the device, and the way in which it was processed. In particular, the order in which layers are processed will influence

which materials or interfaces fail. The temperature and relative humidity must be reported, as the mechanical properties of the materials can be highly sensitive to these parameters. Devices intended for outdoor use must be tested for the effects of thermal cycling, and the effects of thermal expansion and contraction should be isolated from those that occur because of thermal cycling independent of the concomitant mechanical deformation. Bending and tensile tests should be performed in a way that most realistically mimics the deformation expected in the environment. Simply reporting bending radius is insufficient for tests of flexibility; the depth of the active materials within the device stack must be specified, and their proximity to the mechanically neutral plane should be stated so that it is possible to calculate—in most cases by finite-element modeling—the strain on the active materials. Stresses that will produce cracks within or between layers will be highly dependent on the mechanical properties of the substrates and encapsulants. For devices on flexible substrates, torsion should also be tested, and the angle of torsion (e.g., 180° vs 360°) and number of cycles should be reported. Diligence in reporting these parameters will allow for a more thorough understanding of failure mechanisms and streamline the process for developing robust organic electronic devices.

2.5. Outlook and future work

The majority of all work on the stability of organic electronic devices in general—and organic solar cells in particular—has focused on photochemical, thermal, oxidative, morphological, and other thermodynamic modes of degradation.[20, 21] The exclusion of mechanical modes of degradation is somewhat surprising, because both the production and

use of thin-film flexible solar modules requires—often substantial—bending, shear, and tensile deformations and thus requires resistance or at least a predictable response to mechanical strain. This review described the literature on the mechanical response of organic semiconductors and whole devices with the aim of identifying design principles for robust materials and devices to determine avenues of future research on the topic. We find several areas in which very little work has been done. For example, while the mechanical properties of polymers is a mature field, and many of the principles can be applied directly to the properties of semiconducting polymers, the mechanical properties of films of small-molecule semiconductors and their effects on the yield of devices in roll-to-roll production are unexplored.

Much of the work has focused on the mechanical properties of single materials or interfaces. Only one study to our knowledge used a module fabricated in an industrially relevant manner.[68] The study of whole modules will require a close connection between experiments and computational modeling to determine which materials will absorb strain at different depths within the device stack. It might turn out, for example, that the barrier foils, which are often multilayered laminate structures of polymers and ceramic films, will crack first, and thus mechanical deformation may lead to failure by photochemical damage. As the field has not yet "settled" on the ideal barrier technology, attention toward the mechanical properties of barrier materials should be increased.

In the past, thermal stability has implied accelerated degradation by chemical processes, or by phase segregation within the bulk heterojunction. The suspected mechanism by which phase separation degrades the performance of solar cells is that the domains grow to critical dimensions that are larger than the diffusion lengths of excitons.

Phase segregation is not, however, the only potential pathway of degradation initiated by heat. Differential thermal expansion and contraction of the different layers in an outdoor environment will inevitably produce large-scale buckling of support structures in pilot organic photovoltaic installations, just as smaller scale deformations will tend to place shear stress on the layers and could be especially problematic for the interfaces, which are often weak.

While the topics discussed in this review suggest that all deformation leads to fracture and therefore is deleterious to the long-term stability of devices, it is conceivable that strain in the pre-fracture regime may produce changes that are either non-degrading or perhaps even beneficial to the photovoltaic output of devices. Very little is known about the effects of strain on device performance in the pre-fracture regime, but some ideas can be put forth. For example, strain has at least three effects on the morphology of P3HT:PCBM blends (as illustrated in **Figure 2.12**): (1) alignment of polymer chains along the axis of strain, (2) increase in the percentage of crystalline aggregates and order within the aggregated phase, and (3) evolution in texture from one in which the axis of π-stacking is parallel to the substrate (edge-on), to one in which the π-stacking axis is perpendicular to the substrate (face-on). While it is difficult to predict the effect of (1) on the photovoltaic properties, since the direction of charge-transport is orthogonal to the stretch-aligned chains, the effects of (2), and especially (3), would seem to be beneficial in a device whose charge carriers move vertically through the stack.

One intriguing aspect of research on the mechanical stability of organic solar cells is its interdisciplinarity. It requires teams whose members have expertise in organic chemistry, microstructural determination, polymeric science and engineering, device

physics, manufacturing engineering, and solid mechanics. It is our hope that this review served to stimulate interest in the field in an effort to produce low-cost renewable power sources that are both highly efficient and also mechanically stable.

Acknowledgements

This work was supported by the Air Force Office of Scientific Research (AFOSR) Young Investigator Program, Grant FA9550-13-1-0156 and laboratory startup funds from the University of California, San Diego. S.S. acknowledges a fellowship from the National Science Foundation Graduate Research Fellowship Program under Grant DGE-1144086. A.V.Z. acknowledges a fellowship from SoCal Clean Energy Technology Acceleration Program from the von Liebig Center at UCSD sponsored by the U.S. Department of Energy. The authors acknowledge helpful discussions with Prof. Frederik C. Krebs.

Chapter 2, in full, is a reprint of the material as it appears in *Energy & Environmental Science*, 2015, 8, 55-80. Royal Society of Chemistry, 2015. Suchol Savagatrup, Adam D. Printz, Timothy F. O'Connor, Aliaksandr V. Zaretski, Daniel Rodriquez, Eric J. Sawyer, Kirtana M. Rajan, Raziel I. Acosta, Samuel E. Root, and Darren J. Lipomi. The dissertation author was the primary investigator and author of this paper.

References

(1) L. T. Dou, J. B. You, Z. R. Hong, Z. Xu, G. Li, R. A. Street and Y. Yang, *Adv. Mater.*, 2013, **25**, 6642-6671.

(2) C. H. Peters, I. T. Sachs-Quintana, J. P. Kastrop, S. Beaupre, M. Leclerc and M. D. McGehee, *Adv. Energy Mater.*, 2011, **1**, 491-494.

(3) M. Kaltenbrunner, M. S. White, E. D. Glowacki, T. Sekitani, T. Someya, N. S. Sariciftci and S. Bauer, *Nat. Comm.*, 2012, **3**, 770.

(4) N. Espinosa, M. Hosel, D. Angmo and F. C. Krebs, *Energ. Environ. Sci.*, 2012, **5**, 5117-5132.

(5) T. R. Cook, D. K. Dogutan, S. Y. Reece, Y. Surendranath, T. S. Teets and D. G. Nocera, *Chem. Rev.*, 2010, **110**, 6474-6502.

(6) Y. Galagan, E. W. C. Coenen, B. Zimmermann, L. H. Slooff, W. J. H. Verhees, S. C. Veenstra, J. M. Kroon, M. Jorgensen, F. C. Krebs and R. Andriessen, *Adv. Energy Mater.*, 2014, **4**, 1300498.

(7) F. C. Krebs, N. Espinosa, M. Hosel, R. R. Sondergaard and M. Jorgensen, *Adv. Mater.*, 2014, **26**, 29-39.

(8) D. J. Burke and D. J. Lipomi, *Energ. Environ. Sci.*, 2013, **6**, 2053-2066.

(9) T. P. Osedach, T. L. Andrew and V. Bulovic, *Energ. Environ. Sci.*, 2013, **6**, 711-718.

(10) F. C. Krebs, M. Jorgensen, K. Norrman, O. Hagemann, J. Alstrup, T. D. Nielsen, J. Fyenbo, K. Larsen and J. Kristensen, *Sol. Energy Mater. Sol. Cells*, 2009, **93**, 422-441.

(11) F. C. Krebs, *Sol. Energy Mater. Sol. Cells*, 2008, **92**, 715-726.

(12) K.-S. Chen, H. L. Yip, C. W. Schlenker, D. S. Ginger and A. K. Y. Jen, *Org. Electron.*, 2012, **13**, 2870-2878.

(13) I. Burgues-Ceballos, F. Machui, J. Min, T. Ameri, M. M. Voigt, Y. N. Luponosov, S. A. Ponomarenko, P. D. Lacharmoise, M. Campoy-Quiles and C. J. Brabec, *Adv. Funct. Mater.*, 2014, **24**, 1449-1457.

(14) J. E. Carle, M. Helgesen, M. V. Madsen, E. Bundgaard and F. C. Krebs, *J. Mater. Chem. C*, 2014, **2**, 1290-1297.

(15) R. Po, A. Bernardi, A. Calabrese, C. Carbonera, G. Corso and A. Pellegrino, *Energy Environ. Sci.*, 2014, **7**, 925-943.

(16) J. L. Bredas, J. E. Norton, J. Cornil and V. Coropceanu, *Acc. Chem. Res.*, 2009, **42**, 1691-1169.

(17) A. J. Heeger, *Adv. Mater.*, 2014, **26**, 10-28.

(18) A. Salleo, R. J. Kline, D. M. DeLongchamp and M. L. Chabinyc, *Adv. Mater.*, 2010, **22**, 3812-3838.

(19) M. A. Brady, G. M. Su and M. L. Chabinyc, *Soft Matter*, 2011, **7**, 11065-11077.

(20) M. Jorgensen, K. Norrman and F. C. Krebs, *Sol. Energy Mater. Sol. Cells*, 2008, **92**, 686-714.

(21) M. Jorgensen, K. Norrman, S. A. Gevorgyan, T. Tromholt, B. Andreasen and F. C. Krebs, *Adv. Mater.*, 2011, **24**, 580-612.

(22) D. J. Lipomi and Z. N. Bao, *Energ. Environ. Sci.*, 2011, **4**, 3314-3328.

(23) C. Bruner, N. C. Miller, M. D. McGehee and R. H. Dauskardt, *Adv. Funct. Mater.*, 2013, **23**, 2863-2871.

(24) O. Awartani, B. Lemanski, H. W. Ro, L. J. Richter, D. M. DeLongchamp and B. T. O'Connor, *Adv. Energy Mater.*, 2013, **3**, 399-406.

(25) M. Hosel, R. Sondergaard, M. Jorgensen and F. C. Krebs, *Adv. Energy Mater.*, 2014, **4**, 1301625.

(26) F. C. Krebs, T. D. Nielsen, J. Fyenbo, M. Wadstrom and M. S. Pedersen, *Energ. Environ. Sci.*, 2010, **3**, 512-525.

(27) S. Savagatrup, A. D. Printz, D. Rodriquez and D. J. Lipomi, *Macromolecules*, 2014, **47**, 1981-1992.

(28) S. Savagatrup, A. S. Makaram, D. J. Burke and D. J. Lipomi, *Adv. Funct. Mater.*, 2014, **24**, 1169-1181.

(29) A. D. Printz, S. Savagatrup, D. J. Burke, T. Purdy and D. J. Lipomi, *RSC Adv.*, 2014, **4**, 13635-13643.

(30) T. F. O'Connor, A. V. Zaretski, B. A. Shiravi, S. Savagatrup, A. D. Printz, M. I. Diaz and D. J. Lipomi, *Energy Environ. Sci.*, 2014, **7**, 370-378.

(31) D. J. Lipomi, H. Chong, M. Vosgueritchian, J. G. Mei and Z. N. Bao, *Sol. Energy Mater. Sol. Cells*, 2012, **107**, 355-365.

(32) D. Tahk, H. H. Lee and D. Y. Khang, *Macromolecules*, 2009, **42**, 7079-7083.

(33) B. O'Connor, E. P. Chan, C. Chan, B. R. Conrad, L. J. Richter, R. J. Kline, M. Heeney, I. McCulloch, C. L. Soles and D. M. DeLongchamp, *ACS Nano*, 2010, **4**, 7538-7544.

(34) C. Muller, S. Goffri, D. W. Breiby, J. W. Andreasen, H. D. Chanzy, R. A. J. Janssen, M. M. Nielsen, C. P. Radano, H. Sirringhaus, P. Smith and N. Stingelin-Stutzmann, *Adv. Funct. Mater.*, 2007, **17**, 2674-2679.

(35) J. J. Liang, L. Li, X. F. Niu, Z. B. Yu and Q. B. Pei, *Nat. Photonics*, 2013, **7**, 817-824.

(36) Z. B. Yu, Q. W. Zhang, L. Li, Q. Chen, X. F. Niu, J. Liu and Q. B. Pei, *Adv. Mater.*, 2011, **23**, 664-668.

(37) B. Hu, *Workshop on Key Scientific and Technological Issues for Development of Next-Generation Organic Solar Cells*, Arlington, VA, 2012.

(38) F. C. Krebs, M. Biancardo, B. Winther-Jensen, H. Spanggard and J. Alstrup, *Sol. Energy Mater. Sol. Cells*, 2006, **90**, 1058-1067.

(39) A. Anctil, C. W. Babbitt, R. P. Raffaelle and B. J. Landi, *Prog. Photovolt: Res. Appl.*, 2012, **DOI: 10.1002/pip**.

(40) N. S. Lewis and D. G. Nocera, *Proc. Natl. Acad. Sci. USA*, 2007, **104**, 20142-20142.

(41) J. Y. Lee, S. T. Connor, Y. Cui and P. Peumans, *Nano Lett.*, 2010, **10**, 1276.

(42) G. Li, R. Zhu and Y. Yang, *Nat. Photonics*, 2012, **6**, 153-161.

(43) C. M. Amb, M. R. Craig, U. Koldemir, J. Subbiah, K. R. Choudhyry, S. A. Gevorgyan, M. Jorgensen, F. C. Krebs, F. So and J. R. Reynolds, *ACS Appl. Mater. Interfaces*, 2012, **4**, 1847-1853.

(44) V. Coropceanu, J. Cornil, D. A. da Silva, Y. Olivier, R. Silbey and J. L. Bredas, *Chem. Rev.*, 2007, **107**, 926-952.

(45) S. Savagatrup, A. D. Printz, T. F. O'Connor, A. V. Zaretski and D. J. Lipomi, *Chem. Mater.*, 2014, **26**, 3028-3041.

(46) S. Bauer, S. Bauer-Gogonea, I. Graz, M. Kaltenbrunner, C. Keplinger and R. Schwodiauer, *Adv. Mater.*, 2014, **26**, 149-162.

(47) M. Kaltenbrunner, T. Sekitani, J. Reeder, T. Yokota, K. Kuribara, T. Tokuhara, M. Drack, R. Schwodiauer, I. Graz, S. Bauer-Gogonea, S. Bauer and T. Someya, *Nature*, 2013, **499**, 458-463.

(48) D. Ghezzi, M. R. Antognazza, R. Maccarone, S. Bellani, E. Lanzarini, N. Martino, M. Mete, G. Pertile, S. Bisti, G. Lanzani and F. Benfanati, *Nat. Photonics*, 2013, **7**, 400-406.

(49) M. Manceau, E. Bundgaard, J. E. Carle, O. Hagemann, M. Helgesen, R. Sondergaard, M. Jorgensen and F. C. Krebs, *J. Mater. Chem.*, 2011, **21**, 4132-4141.

(50) C. Bruner and R. H. Dauskardt, *Macromolecules*, 2014, **47**, 1117-1121.

(51) V. Brand, K. Levi, M. D. McGehee and R. H. Dauskardt, *Sol. Energy Mater. Sol. Cells*, 2012, **103**, 80-85.

(52) V. Brand, C. Bruner and R. H. Dauskardt, *Sol. Energy Mater. Sol. Cells*, 2012, **99**, 182-189.

(53) Y. Cao, P. A. Smith and A. J. Heeger, *Synthetic Met.*, 1991, **41-43**, 181-184.

(54) Y. Cao, P. Smith and A. J. Heeger, *Polymer*, 1991, **32**, 1210-1218.

(55) S. Tokito, P. Smith and A. J. Heeger, *Synthetic Met.*, 1990, **36**, 183-194.

(56) A. R. Postema, K. Liou, F. Wudl and P. Smith, *Macromolecules*, 1990, **23**, 1842-1845.

(57) J. Moulton and P. Smith, *Polymer*, 1992, **33**, 2340-2347.

(58) G. Yu, J. Gao, J. C. Hummelen, F. Wudl and A. J. Heeger, *Science*, 1995, **270**, 1789-1791.

(59) J. J. M. Halls, C. A. Walsh, N. C. Greenham, E. A. Marseglia, R. H. Friend, S. C. Moratti and A. B. Holmes, *Nature*, 1995, **376**, 498-500.

(60) J. H. Burroughes, D. D. C. Bradley, A. R. Brown, R. N. Marks, K. Mackay, R. H. Friend, P. L. Burns and A. B. Holmes, *Nature*, 1990, **347**, 539-541.

(61) A. Tsumura, H. Koezuka and T. Ando, *Appl. Phys. Lett.*, 1986, **49**, 1210-1212.

(62) Z. N. Bao, A. Dodabalapur and A. J. Lovinger, *Appl. Phys. Lett.*, 1996, **69**, 4108-4110.

(63) A. Facchetti, *Chem. Mater.*, 2011, **23**, 733-758.

(64) J. G. Mei and Z. N. Bao, *Chem. Mater.*, 2014, **26**, 604-615.

(65) H. Bronstein, Z. Y. Chen, R. S. Ashraf, W. M. Zhang, J. P. Du, J. R. Durrant, P. S. Tuladhar, K. Song, S. E. Watkins, Y. Geerts, M. M. Wienk, R. A. J. Janssen, T. Anthopoulos, H. Sirringhaus, M. Heeney and I. McCulloch, *J. Am. Chem. Soc*, 2011, **133**, 3272-3275.

(66) I. McCulloch, M. Heeney, C. Bailey, K. Genevicius, I. MacDonald, M. Shkunov, D. Sparrowe, S. Tierney, R. Wagner, W. M. Zhang, M. L. Chabinyc, R. J. Kline, M. D. McGehee and M. F. Toney, *Nat. Mater.*, 2006, **5**, 328-333.

(67) A. J. Heeger, *Chem. Soc. Rev.*, 2010, **39**, 2354-2371.

(68) S. R. Dupont, M. Oliver, F. C. Krebs and R. H. Dauskardt, *Sol. Energy Mater. Sol. Cells*, 2012, **97**, 171-175.

(69) S. R. Dupont, E. Voroshazi, P. Heremans and R. H. Dauskardt, *Org. Electron.*, 2013, **14**, 1262-1270.

(70) S. R. Dupont, F. Novoa, E. Voroshazi and R. H. Dauskardt, *Adv. Funct. Mater.*, 2013, **24**, 1325-1332.

(71) S. Savagatrup, E. Chan, S. Renteria-Garcia, A. D. Printz, A. V. Zaretski, T. F. O'Connor, D. Rodriquez, E. Valle and D. J. Lipomi, *Adv. Funct. Mater.*, 2014, accepted.

(72) A. J. Heeger, *Angew. Chem., Int. Ed.*, 2001, **40**, 2591-2611.

(73) S. M. Aharoni, *Polymer*, 1981, **22**, 418-419.

(74) R. D. McCullough, *Adv. Mater.*, 1998, **10**, 93-116.

(75) F. P. V. Koch, M. Heeney and P. Smith, *J. Am. Chem. Soc*, 2013, **135**, 13699-13709.

(76) M. Brinkmann, *Polym. Phys.*, 2011, **49**, 1218-1233.

(77) J. Rivnay, M. F. Toney, Y. Zheng, I. V. Kauver, Z. H. Chen, V. Wagner, A. Facchetti and A. Salleo, *Adv. Mater.*, 2010, **22**, 4359-4363.

(78) B. O'Connor, R. J. Kline, B. R. Conrad, L. J. Richter, D. Gundlach, M. F. Toney and D. M. DeLongchamp, *Adv. Funct. Mater.*, 2011, **21**, 3697-3705.

(79) D. Gargi, R. J. Kline, D. M. DeLongchamp, D. A. Fischer, M. F. Toney and B. T. O'Connor, *J. Phys. Chem. C*, 2013, **117**, 17421-17428.

(80) O. Awartani, M. W. Kudenov and B. T. O'Connor, *Appl. Phys. Lett.*, 2014, **104**, 093306.

(81) F. E. Arnold and Vandeuse.Rl, *Macromolecules*, 1969, **2**, 497-&.

(82) M. R. Vanlandingham, J. S. Villarrubia, W. F. Guthrie and G. F. Meyers, *Macromol. Symp.*, 2001, **167**, 15-43.

(83) P. G. Karagiannidis, S. Kassavetis, C. Pitsalidis and S. Logothetidis, *Thin Solid Films*, 2011, **519**, 4105-4109.

(84) C. Koidis, S. Logothetidis, S. Kassavetis, P. G. Kapnopoulos, P. G. Karagiannidis, D. Georgiou and A. Laskarakis, *Sol. Energy Mater. Sol. Cells*, 2013, **112**, 36-46.

(85) J. Y. Chung, A. J. Nolte and C. M. Stafford, *Adv. Mater.*, 2011, **23**, 349-368.

(86) C. M. Stafford, C. Harrison, K. L. Beers, A. Karim, E. J. Amis, M. R. Vanlandingham, H. C. Kim, W. Volksen, R. D. Miller and E. E. Simonyi, *Nat. Mater.*, 2004, **3**, 545-550.

(87) C. M. Stafford, B. D. Vogt, C. Harrison, D. Julthongpiput and R. Huang, *Macromolecules*, 2006, **39**, 5095-5099.

(88) D. Y. Khang, J. A. Rogers and H. H. Lee, *Adv. Funct. Mater.*, 2009, **19**, 1526-1536.

(89) D. Y. Khang, J. L. Xiao, C. Kocabas, S. MacLaren, T. Banks, H. Q. Jiang, Y. Y. G. Huang and J. A. Rogers, *Nano Lett.*, 2008, **8**, 124-130.

(90) N. Bowden, S. Brittain, A. G. Evans, J. W. Hutchinson and G. M. Whitesides, *Nature*, 1998, **393**, 146-149.

(91) N. Bowden, W. T. S. Huck, K. E. Paul and G. M. Whitesides, *Appl. Phys. Lett.*, 1999, **75**, 2557-2559.

(92) J.-B. Lee, S.-S. Yoon and D. Y. Khang, *RSC Adv.*, 2013, **3**, 17364-17372.

(93) J. Y. Kim and C. D. Frisbie, *J. Phys. Chem. C*, 2008, **112**, 17726-17736.

(94) J. Zhao, A. Swinnen, G. V. Assche, J. Manca, D. Vanderzande and B. V. Mele, *J. Phys. Chem. B*, 2009, **113**, 1587-1591.

(95) S. A. Chen and J. M. Ni, *Macromolecules*, 1992, **25**, 6081-6089.

(96) H. K. Reimschuessel, *J. Polym. Sci. A: Polym. Chem.*, 1979, **17**, 2447-2457.

(97) M. Koppe, M. Scharber, C. J. Brabec, W. Duffy, M. Heeney and I. McCulloch, *Adv. Funct. Mater.*, 2007, **17**, 1371-1376.

(98) A. Buono, N. H. Son, G. Raos, L. Gila, A. Cominetti, M. Catellani and S. V. Meille, *Macromolecules*, 2010, **43**, 6772-6781.

(99) J. G. Liu, Y. Sun, X. Gao, R. Xing, L. D. Zheng, S. P. Wu, Y. H. Geng and Y. C. Han, *Langmuir*, 2011, **27**, 4212-4219.

(100) J. N. Israelachvili, *Intermolecular and Surface Forces*, Elsevier, Waltham, MA, 2011.

(101) H. L. Zhong, Z. Li, F. Deledalle, E. Collado Fregoso, M. Shahid, Z. P. Fei, C. B. Nielsen, N. Yaacobi-Gross, S. Rossbauer, T. D. Anthopoulos, J. R. Durrant and M. Heeney, *J. Am. Chem. Soc*, 2013, **135**, 2040.

(102) D. J. Lipomi, R. C. Chiechi, W. F. Reus and G. M. Whitesides, *Adv. Funct. Mater.*, 2008, **18**, 3469-3477.

(103) D. J. Lipomi, R. C. Chiechi, M. D. Dickey and G. M. Whitesides, *Nano Lett.*, 2008, **8**, 2100-2105.

(104) F. S. Kim, G. Q. Ren and S. A. Jenekhe, *Chem. Mater.*, 2011, **23**, 682-732.

(105) A. L. Briseno, S. C. B. Mannsfeld, P. J. Shamberger, F. S. Ohuchi, Z. N. Bao, S. A. Jenekhe and Y. N. Xia, *Chem. Mater.*, 2008, **20**, 4712-4719.

(106) J. T. Seitz, *J. Appl. Polym. Sci.*, 1993, **49**, 1331-1351.

(107) R. F. Fedors, *Polym. Eng. Sci.*, 1974, **14**, 147-154.

(108) B. S. Hsiao, *Nanostructure development in semicrystalline polymers during deformation by synchrotron X-ray scattering and diffraction techniques*, Taylor & Francis, 2005.

(109) S. T. Salammal, E. Mikayelyan, S. Grigorian, U. Pietsch, N. Koenen, U. Scherf, N. Kayunkid and M. Brinkmann, *Macromolecules*, 2012, **45**, 5575-5585.

(110) F. Padinger, R. S. Rittberger and N. S. Sariciftci, *Adv. Funct. Mater.*, 2003, **13**, 85-88.

(111) S. E. Shaheen, C. J. Brabec, N. S. Sariciftci, F. Padinger, T. Fromherz and J. C. Hummelen, *Appl. Phys. Lett.*, 2001, **78**, 841-843.

(112) V. Vijay, A. D. Rao and K. S. Narayan, *J. Appl. Phys.*, 2011, **109**, 084525.

(113) J. Rivnay, S. C. B. Mannsfeld, C. E. Miller, A. Salleo and M. F. Toney, *Chem. Rev.*, 2012, **112**, 5488-5519.

(114) J. Clark, C. Silva, R. H. Friend and F. C. Spano, *Phys. Rev. Lett.*, 2007, **98**, 206406.

(115) R. J. Kline, M. D. McGehee, E. N. Kadnikova, J. S. Liu, J. M. J. Frechet and M. F. Toney, *Macromolecules*, 2005, **38**, 3312-3319.

(116) A. J. Pearson, T. Wang, A. D. F. Dunbar, H. N. Yi, D. C. Watters, D. M. Coles, P. A. Staniec, A. Iraqi, R. A. L. Jones and D. G. Lidzey, *Adv. Funct. Mater.*, 2013, **24**, 659.

(117) N. C. Miller, R. Gysel, Z. Beiley, C. E. Miller, M. F. Toney, M. Heeney, I. McCulloch and M. D. McGehee, *Nano Lett.*, 2009, **9**, 4153-4157.

(118) N. C. Miller, E. K. Cho, R. Gysel, C. Risko, V. Coropceanu, C. E. Miller, S. Sweetnam, A. Sellinger, M. Heeney, I. McCulloch, J. L. Bredas, M. F. Toney and M. D. McGehee, *Adv. Energy Mater.*, 2012, **2**, 1208-1217.

(119) J. Rivnay, R. Noriega, R. J. Kline, A. Salleo and M. F. Toney, *Phys. Rev. B*, 2011, **84**, 045203.

(120) E. Verploegen, R. Mondal, C. J. Bettinger, S. Sok, M. F. Toney and Z. Bao, *Adv. Funct. Mater.*, 2010, **20**, 3519-3529.

(121) J. D. Roehling, K. J. Batenburg, F. B. Swain, A. J. Moule and I. Arslan, *Adv. Funct. Mater.*, 2013, **23**, 2115-2122.

(122) W. Ma, J. R. Tumbleston, M. Wang, E. Gann, F. Huang and H. Ade, *Adv. Energy Mater.*, 2013, **3**, 864-872.

(123) N. D. Treat, A. Varotto, C. J. Takacs, N. Batara, M. Al-Hashimi, M. J. Heeney, A. J. Heeger, F. Wudl, C. J. Hawker and M. L. Chabinyc, *J. Am. Chem. Soc*, 2012, **134**, 15869-15879.

(124) N. D. Treat, M. A. Brady, G. Smith, M. F. Toney, E. J. Kramer, C. J. Hawker and M. L. Chabinyc, *Adv. Energy Mater.*, 2011, **1**, 82-89.

(125) S. Savagatrup, D. Rodriquez, A. D. Printz, A. Sieval, J. C. Hummelen and D. J. Lipomi, *Submitted*, 2014.

(126) L. H. Nguyen, H. Hoppe, T. Erb, S. Gunes, G. Gobsch and N. S. Sariciftci, *Adv. Funct. Mater.*, 2007, **17**, 1071-1078.

(127) H. Hoppe and N. S. Sariciftci, *Journal of Materials Chemistry*, 2006, **16**, 45-61.

(128) H. Hoppe, M. Niggemann, C. Winder, J. Kraut, R. Hiesgen, A. Hinsch, D. Meissner and N. S. Sariciftci, *Adv. Funct. Mater.*, 2004, **14**, 1005-1011.

(129) F. Liu, Y. Gu, X. B. Shen, S. Ferdous, H. W. Wang and T. P. Russell, *Prog. Polym. Sci.*, 2013, **38**, 1990-2052.

(130) H. W. Ro, B. Akgun, B. T. O'Connor, M. Hammond, R. J. Kline, C. R. Snyder, S. K. Satija, A. L. Ayzner, M. F. Toney, C. L. Soles and D. M. DeLongchamp, *Macromolecules*, 2012, **45**, 6587-6599.

(131) A. D. Printz, S. Savagatrup, D. Rodriquez, T. F. O'Connor and D. J. Lipomi, *Sol. Energy Mater. Sol. Cells*, 2014, in press.

(132) H. Y. Li, B. C.-K. Tee, G. Giri, J. W. Chung, S. Y. Lee and Z. N. Bao, *Adv. Mater.*, 2012, **24**, 2588-2591.

(133) T. Liu and A. Troisi, *Adv. Mater.*, 2013, **25**, 1038-1041.

(134) A. Anctil, C. W. Babbitt, R. P. Raffaelle and B. J. Landi, *Environ. Sci. Technol.*, 2011, **45**, 2353-2359.

(135) Y.-S. Zimmermann, A. Schaffer, C. Hugi, K. Fent, P. F.-X. Corvini and M. Lenz, *Environ. Int.*, 2012, **49**, 128-140.

(136) P. Sonar, J. P. F. Lim and K. L. Chan, *Energ. Environ. Sci.*, 2011, **4**, 1558-1574.

(137) J. Peet, A. J. Heeger and G. C. Bazan, *Acc. Chem. Res.*, 2009, **42**, 1700-1708.

(138) J. Peet, J. Y. Kim, N. E. Coates, W. L. Ma, D. Moses, A. J. Heeger and G. C. Bazan, *Nat. Mater.*, 2007, **6**, 497-500.

(139) K. R. Graham, J. G. Mei, R. Stalder, J. W. Shim, H. Cheun, F. Steffy, F. So, B. Kippelen and J. R. Reynolds, *ACS Appl. Mater. Interfaces*, 2011, **3**, 1210-1215.

(140) M. Vosgueritchian, D. J. Lipomi and Z. N. Bao, *Adv. Funct. Mater.*, 2012, **22**, 421-428.

(141) N. Kim, S. Kee, S. H. Lee, B. H. Lee, Y. H. Kahng, Y. R. Jo, B. J. Kim and K. Lee, *Adv. Mater.*, 2014, **26**, 2268-2272.

(142) D. J. Lipomi, J. A. Lee, M. Vosgueritchian, B. C.-K. Tee, J. A. Bolander and Z. N. Bao, *Chem. Mater.*, 2012, **24**, 373-382.

(143) X. Crispin, F. L. E. Jakobsson, A. Crispin, P. C. M. Grim, P. Andersson, A. Volodin, C. van Haesendonck, M. Van der Auweraer, W. R. Salaneck and M. Berggren, *Chem. Mater.*, 2006, **18**, 4354-4360.

(144) D. S. Hecht, L. B. Hu and G. Irvin, *Adv. Mater.*, 2011, **23**, 1482-1513.

(145) D. J. Lipomi, B. C.-K. Tee, M. Vosgueritchian and Z. N. Bao, *Adv. Mater.*, 2011, **23**, 1771-1775.

(146) M. M. Voigt, R. C. I. Mackenzie, C. P. Yau, P. Atienzar, J. Dane, P. E. Keivanidis, D. D. C. Bradley and J. Nelson, *Sol. Energy Mater. Sol. Cells*, 2011, **95**, 731-734.

(147) Y. H. Zhou, C. Fuentes-Hernandez, J. W. Shim, J. Meyer, A. J. Giordano, H. Li, P. Winget, T. Papadopoulos, H. Cheun, J. Kim, M. Fenoll, A. Dindar, W. Haske, E. Najafabadi, T. M. Khan, H. Sojoudi, S. Barlow, S. Graham, J. L. Bredas, S. R. Marder, A. Kahn and B. Kippelen, *Science*, 2012, **336**, 327-332.

(148) L. Lindell, A. Burquel, F. L. E. Jakobsson, V. Lemaur, M. Berggren, R. Lazzaroni, J. Cornil, W. R. Salaneck and X. Crispin, *Chem. Mater.*, 2006, **18**, 4246-4252.

(149) F. L. E. Jakobsson, X. Crispin, L. Lindell, A. Kanciurzewska, M. Fahlman, W. R. Salaneck and M. Berggren, *Chem. Phys. Lett.*, 2006, **433**, 110-114.

(150) J. E. Coughlin, Z. B. Henson, G. C. Welch and G. C. Bazan, *Acc. Chem. Res.*, 2013, **47**, 257-270.

(151) M. Shin, J. H. Song, G. H. Lim, B. Lim, J. J. Park and U. Jeong, *Adv. Mater.*, 2014, **26**, 3706-3711.

(152) Z. B. Yu, X. F. Niu, Z. Liu and Q. B. Pei, *Adv. Mater.*, 2011, **23**, 3989-3994.

(153) G. Giri, E. Verploegen, S. C. B. Mannsfeld, S. Atahan-Evrenk, D. H. Kim, S. Y. Lee, H. A. Becerril, A. Aspuru-Guzik, M. F. Toney and Z. Bao, *Nature*, 2011, **480**, 504-509.

(154) Y. Diao, B. C.-K. Tee, G. Giri, J. Xu, D. H. Kim, H. A. Becerril, R. M. Stoltenberg, T. H. Lee, G. Xue, S. C. B. Mannsfeld and Z. N. Bao, *Nat. Mater.*, 2013, **12**, 665-671.

(155) Z. L. Rang, A. Haraldsson, D. M. Kim, P. P. Ruden, R. J. Chesterfield and C. D. Frisbie, *Appl. Phys. Lett.*, 2001, **79**, 2731-2733.

(156) C.-Y. Liu and A. J. Bard, *Nature*, 2002, **418**, 162-164.

(157) H. R. Tseng, H. Phan, C. Luo, M. Wang, L. A. Perez, S. N. Patel, L. Ying, E. J. Kramer, T. Q. Nguyen, G. C. Bazan and A. J. Heeger, *Adv. Mater.*, 2014, **online**, 10.1002/adma.201305084.

(158) H. C. Wu, S. J. Benight, A. Chortos, W. Y. Lee, J. G. Mei, J. W. F. To, C. Lu, M. Q. He, J. B.-H. Tok, W. C. Chen and Z. N. Bao, *Chem. Mater.*, 2014, dx.doi.org/10.1021/cm502271j.

(159) D. Chirvase, J. Parisi, J. C. Hummelen and V. Dyakonov, *Nanotechnology*, 2004, **15**, 1317-1323.

(160) G. Li, Y. Yao, H. C. Yang, V. Shrotriya, G. W. Yang and Y. Yang, *Adv. Funct. Mater.*, **17**, 1636-1644.

(161) A. N. Sokolov, Y. Cao, O. B. Johnson and Z. N. Bao, *Adv. Funct. Mater.*, 2012, **22**, 175-183.

(162) N. S. Lu, X. Wang, Z. G. Suo and J. Vlassak, *Appl. Phys. Lett.*, 2007, **91**, 221909.

(163) A. Chortos, J. Lim, J. W. F. To, M. Vosgueritchian, T. J. Dusseault, T. H. Kim, S. W. Hwang and Z. N. Bao, *Adv. Mater.*, 2014, **26**, 4253-4259.

(164) A. L. Shu, A. Dai, H. Wang, Y. L. Loo and A. Kahn, *Org. Electron.*, 2013, **14**, 149-155.

(165) A. Dai, Y. H. Zhou, A. L. Shu, S. K. Mohapatra, H. Wang, C. Fuentes-Hernandez, Y. D. Zhang, S. Barlow, Y. L. Loo, S. R. Marder, B. Kippelen and A. Kahn, *Adv. Funct. Mater.*, 2013, **24**, 2197-2204.

(166) G. Lubineau and M. N. Saleh, *Sol. Energy Mater. Sol. Cells*, 2014, **130**, 199-207.

(167) S. K. Hau, H. L. Yip, J. Y. Zou and A. K. Y. Jen, *Org. Electron.*, 2009, **10**, 1401-1407.

(168) D. H. Kim and J. A. Rogers, *Adv. Mater.*, 2008, **20**, 4887-4892.

(169) F. Nickel, T. Haas, E. Wegner, D. Bahro, S. Salehin, O. Kraft, P. A. Gruber and A. Colsmann, *Sol. Energy Mater. Sol. Cells*, 2014, **130**, 317-321.

(170) W. M. Choi, J. Z. Song, D. Y. Khang, H. Q. Jiang, Y. Y. Huang and J. A. Rogers, *Nano Lett.*, 2007, **7**, 1655-1663.

(171) J. Jones, S. P. Lacour, S. Wagner and Z. G. Suo, *J. Vac. Sci. Technol., A*, 2004, **22**, 1723-1725.

(172) S. P. Lacour, S. Wagner, Z. Y. Huang and Z. Suo, *Appl. Phys. Lett.*, 2003, **82**, 2404-2406.

(173) H. S. Wu, S. Kustra, E. M. Gates and C. J. Bettinger, *Org. Electron.*, 2013, **14**, 1636-1642.

(174) J. B. Kim, P. Kim, N. C. Pegard, S. J. Oh, C. R. Kagan, J. W. Fleischer, H. A. Stone and Y. L. Loo, *Nat. Photonics*, 2012, **6**, 327-332.

(175) X. M. He, F. Gao, G. Tu, D. Hasko, S. Huttner, U. Steiner, N. C. Greenham, R. H. Friend and W. T. S. Huck, *Nano Lett.*, 2010, **10**, 1302-1307.

(176) W. W. Li, W. S. C. Roelofs, M. Turbiez, M. M. Wienk and R. A. J. Janssen, *Adv. Mater.*, 2014, **26**, 3304-3309.

(177) Y. Zhou, T. Kurosawa, W. Ma, Y. K. Guo, L. Fang, K. Vandewal, Y. Diao, C. G. Wang, Q. F. Yan, J. Reinspach, J. G. Mei, A. L. Appleton, G. I. Koleilat, Y. L. Gao, S. C. B. Mannsfeld, A. Salleo, H. Ade, D. H. Zhao and Z. N. Bao, *Adv. Mater.*, 2014, **26**, 3767-3772.

Chapter 3

Mechanical properties of conjugated polymers and polymer-fullerene composites as a function of molecular structure

Suchol Savagatrup, Aditya S. Makaram, Daniel J. Burke, and Darren J. Lipomi

Department of NanoEngineering, University of California, San Diego

9500 Gilman Drive, Mail Code 0448, La Jolla, CA 92093-0448

Abstract

Despite the importance of mechanical compliance in essentially all applications of solution-processable conjugated (semiconducting) polymers, the effects of basic structural parameters of these materials on the mechanical properties are typically not considered during the design and evaluation of the new materials. The core of this paper examines the effect of length of the alkyl solubilizing group—from butyl to dodecyl—on the tensile modulus and brittleness for a series of regioregular poly(3-alkylthiophenes) (P3ATs: P3BT, P3HT, P3OT, P3DDT) and their blends with a soluble fullerene derivative, [6,6]-phenyl C_{61} butyric acid methyl ester (PCBM). The tensile modulus decreases with increasing length of the alkyl side-chain, from 1.87 GPa for butyl side chains to 0.16 GPa for dodecyl side chains. A similar trend exists for blends of the P3ATs with PCBM (with a ratio of 2:1), though the moduli of the blended films are greater than those of the polymer alone by factors of 2–4. A model that considers structural characteristics along with the glass transition temperatures of the polymers produces a trend in the effect of alkyl side chain on tensile modulus that follows remarkably closely to the experimental measurements. Tensile modulus correlates with brittleness, as the strain at which cracks appear is 6% for P3BT and >60% for P3OT. Adhesion of the P3AT film to a polydimethylsiloxane (PDMS) substrate is believed to play a role in an apparent increase in brittleness from P3OT to P3DDT. The crack density at a fixed strain follows the same trend as does the crack-onset strain: the stiffest materials exhibit the greatest density of cracks, except for an increased crack density from P3OT to P3DDT, which is also attributed to weakened adhesion to the substrate with longer alkyl side chains. 1,8-Diiodooctane (DIO), a processing additive commonly included to augment the

performance of organic solar cells, reduces the tensile modulus of a P3HT:PCBM (2:1) blend by a factor of 3. These results could inform the process by which researchers select and design organic semiconductors for applications requiring mechanical robustness, extreme flexibility, and stretchability.

3.1 Introduction

One of the most important motivations for research in the field of organic electronics is the promise that organic devices can be processed inexpensively from solution in roll-to-roll manner.[1] A corollary to this driving force is that organic materials can be used in applications that demand mechanical compliance.[2,3] The assumption of mechanical compliance arises from the extremely small bending radii to which organic electronic devices can be subjected without failure of the device.[2] The extent to which a thin (<100 nm) film can be bent without fracture, however, is largely a function of the thickness of the substrate in practical systems.[4] For very thin substrates—*i.e.*, ≤100 μm—the mechanical properties of a film that fractures at 2% tensile strain only come into play if the film and substrate are bent to very small radii, or less than approximately 2.5 mm.[5] Thus an organic photovoltaic device based on poly(3-hexylthiophene):[6,6]-phenyl C_{61} butyric acid methyl ester (P3HT:PCBM) on a 1.4-μm polyethylene terephthalate (PET) substrate is extraordinarily flexible even though the active materials would fracture at very small (~2%) tensile strain.[2] Organic semiconductors exhibit a wide range of tensile moduli, from 30 MPa – 16 GPa,[6] and also exhibit unequal interfacial energies[7,8] and ductilities.[9,10] These disparities suggest that not all films of conjugated polymers can be treated as equally "plastic"—in the sense of deformability. Understanding the structural characteristics that

determine the mechanical properties of semiconducting polymers is critical for large-scale implementation of devices that do not fail as a result of mechanical deformation—*e.g.*, in portable,[11] ultra-thin,[2] and flexible displays,[12] biomedical implants[13] and prostheses,[14] and solar cells that survive the forces of wind, rain, snow, and diurnal and seasonal expansion and contraction.[15] The design of conjugated polymers whose molecular structures permit significant tensile deformation without loss of electronic function, moreover, would permit applications in stretchable electronics that are not accessible by many of the most frequently used organic electronic materials and composites.

While the seminal work of Smith and Heeger characterized many aspects of the mechanical properties of polyacetylene[16] and derivatives of poly(phehylene vinylene)[17] and regiorandom polythiophenes,[18] the research community has shifted toward regioregular, low-bandgap, and structurally complex polymers that give improved performance in thin-film transistors and solar cells.[19] These materials and devices are typically optimized on the basis of their abilities to transport holes and electrons (*i.e.*, on their field-effect mobilities and photovoltaic efficiencies) and, less frequently, on photochemical stability.[15,20] Interest in the mechanical properties of conjugated polymers has given way to the exclusive optimization of electronic performance. The applications for which these materials are most promising solutions, however, are the applications that place the greatest strains on the active materials.[21] Stretchable electronics, and the promise that active materials could be designed whose molecular structures permit substantial deformation, add urgency to reviving the interest in the mechanical properties of modern conjugated polymers and composites. This paper reports the tensile moduli and two measures of brittleness (crack on-set strain and crack density at fixed strain) for a series of

poly(3-alkylthiophenes) (P3ATs) and their blends with a soluble derivative of C_{60} (PCBM) and the effects of the length of the alkyl side-chain, surface energy, and the presence of processing additives on these mechanical properties. We also describe the effect of tensile strains up to 10% on the photovoltaic properties of solar cells based on P3AT:PCBM fabricated on stretchable poly(dimethylsiloxane) (PDMS) substrates. We show that while devices based on the popular P3HT:PCBM are destroyed as a result of the strain, our analysis enables the selection of materials that accommodate the strain easily.

3.2 Background

The field of stretchable electronics is an offshoot of the widely explored field of flexible electronics.[2,21–27] Several research groups, including those of Rogers,[28] Someya,[29] Wagner,[30,31] Bauer,[2,32] Lacour,[33] Suo,[4] and Vlassak[34] have made extraordinary progress toward rendering circuits composed of metals, inorganic semiconductors, and organic semiconductors extremely compliant.[35,36] Most of these approaches, however, rely on directing the strain away from the active components in the circuits. Strategies include intentional fracturing,[31] use of conductive particles dispersed in an elastic matrix,[37] or design of structures that convert global tensile strains to bending and unbending of wavy or serpentine structures.[3,38,39] There still remain, however, significant scientific and technological interest in exploring materials that combine the electronic properties of semiconductors (or metals) with the mechanical properties of plastics that are intrinsic to molecular structure of the materials.[40] To this end, Müller et al. synthesized an extraordinary ductile block copolymer comprising P3HT and polyethylene that accommodated strains of 600% and retained significant charge mobilities with weight

fractions of the insulating component of up to 90%.[40] For many applications (*i.e.*, solar cells and displays) however, it will not be desirable to have such a high weight fraction of insulating, non-absorbing, non-emissive material. Some pure films of conjugated polymers can exhibit substantial ductility. Pei and coworkers, for example, demonstrated that a soluble polyfluorene derivative retained functionality as an emitter of blue light when heated and stretched between electrodes comprising carbon nanotubes.[12] For application requiring one-time bonding to non-planar substrates, plasticity is sufficient. For applications that must accommodate reversible deformation under cyclic loading, however, elasticity is the more important characteristic.

The tensile moduli of organic semiconductors occupy a range that spans nearly three orders of magnitude.[6,9] Using the buckling-based method, Tahk et al. measured the tensile moduli of the transparent conductor poly(3,4-ethylenedioxythiophene):poly(styrenesulfonate) (PEDOT:PSS), poly(3-hexylthiophene) (P3HT), and the molecular semiconductor pentacene; all showed the tensile moduli in the range of GPa (similar to those of cross-linked epoxy resins).[6] Many of the most prominent organic semiconductors and ancillary components of devices (*e.g.*, indium tin oxide) have also been shown to crack at modest strains.[9,10,41] In addition to the intrinsic stiffness of some conjugated materials, the addition of small molecules, such as fullerenes in organic solar cells, often have deleterious effects on the compliance of the active layers and the adhesion of the active layers with other layers in the device.[7] A 1:1 mixture of P3HT and [6,6]-phenyl C_{61} butyric acid methyl ester (PCBM) had a tensile modulus five times greater that than of the pure polymer.[6] O'Connor et al. have observed an apparent competition between electronic performance and mechanical compliance.[9] These authors studied the

differences in mechanical properties between two thiophene-based polymers, P3HT and poly(2,5-bis(3-alkylthiophene-2-yl)thieno[3,2-b]thiophene) (PBTTT), and correlated these differences to differences in hole mobility. The authors concluded that hole mobility and stiffness is directly correlated for the materials tested.[9] In a later study, the authors also showed that the details of processing (in particular, the rate of evaporation of the solvent) that resulted in improved photovoltaic performance of composite films of P3HT and PCBM had the unwanted effect of decreasing the compliance and ductility of the films.[42] The mechanical properties of stretchable organic solar cells comprising of two conjugated polymers, P3HT and a copolymer of diketopyrrolopyrrole, thiophene, and thieno[3,2-*b*]thiophene (DPPT-TT), and their blends with PCBM, have also been investigated.[10] The results showed good agreement with those previously described: the addition of PCBM to P3HT has a stiffening effect, a factor of five (400%) increase in tensile modulus.[10] This significant effect was not generalizable to all conjugated polymer films, however, as the modulus of a 1:1 blend of DPPT-TT and PCBM was only 40% greater than that of pure DPPT-TT.[10] Higher tensile modulus is correlated to the tendency of cracks to form in the thin film: films of a 1:1 mixture of P3HT:PCBM fracture at strains of around 2% on poly(dimethylsiloxane) (PDMS) substrates.[10]

Polythiophenes are a widely studied class of solution-processable organic electronic materials.[43] Pure polythiophenes or thiophene-containing copolymers are ubiquitous materials in the field of organic electronics and are the active materials in some of the highest-performing thin-film transistors and organic solar cells.[44] Processible conjugated polymers have alkyl side chains that permit solubility, as in the regioregular poly(3-alkylthiopehenes) (P3ATs).[45] These alkyl side-chains also affect the long-range

ordering, intra-crystalline ordering, and thermal and charge-transport properties.[46–50] For example, the side chains in P3BT and P3HT are liquid-like and do not interdigitate.[51] Disordered side-chains lead to two-dimensional crystal structures with poor inter-lamellar ("vertical") registry. PBTTT, in contrast, possesses side chains that do interdigitate; interdigitation of side chains improves inter-lamellar registry and form crystallites whose order extends in three dimensions.[9] This ordering has been implicated in the increased tensile modulus of PBTTT as a function of thermal annealing.[9] The side-chains of the P3DDT, in contrast to those of P3HT, have been shown to be solid-like with a well-defined melting temperature.[52] Given these effects, we expected that the length of the alkyl side-chain would play a significant role in the mechanical compliance of the P3AT films.

3.3. Experimental design

3.3.1. Selection of materials

The goals of the experiments were to obtain the fundamental understanding of the parameters controlling the mechanical properties of the P3ATs and their blends with PCBM. Poly(3-butylthiophene) (P3BT), poly(3-hexylthiophene) (P3HT), poly(3-octylthiophene) (P3OT), and poly(3-dodecylthiophene) (P3DDT) were selected to extract the effects of varying alkyl chain length on mechanical properties of the thin films. Researchers have observed several trends in the electronic properties of P3ATs as a function of increasing length of the alkyl chain. For example, field-effect mobility was found to decrease,[53] doped conductivity was found to increase,[54] and photovoltaic efficiency in a series of P3AT:polyfluorene bulk heterojunction devices was maximized when A = hexyl.[55] We selected P3HT and PCBM because they are the standard materials

in the literature for bulk heterojunction OPV devices. We chose to study P3BT, P3OT, and P3DDT to produce a data set in which the materials differed by regular intervals of four methylene units, and to put the values obtained for P3HT in context. The ultimate goal of this research is to develop a model for how structural features of a conjugated polymer can influence its mechanical properties.

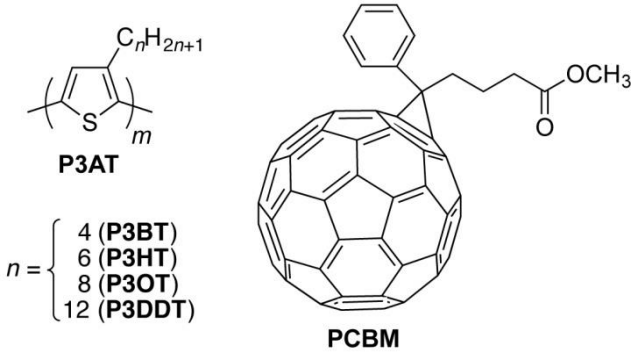

Figure 3.1. Chemical structures of the organic semiconductors used in this paper.

3.3.2. Measurement of mechanical properties

We measured the elastic moduli of thin films of pure P3ATs and their blends with PCBM using the strain-induced elastic buckling instability.[56] A quantitative description of the surface wrinkling pattern of a relatively stiff film on a relatively compliant substrate under compressive strain was described originally by Hutchinson, Whitesides, and coworkers[57,58] and developed into a technique for metrology by Stafford et al.[56] This method has been used to measure the mechanical properties of otherwise difficult-to-measure thin films.[22] For example, the tensile moduli of organic semiconductors,[6,9] nano-fibrillated cellulose,[59] polymer films,[56,60] carbon nanotubes,[61] polyelectrolyte multilayer films,[62] and conjugated polymer films for heterojunction OPV devices.[10] This technique is

ideal for studying a wide range of film types, film thicknesses, and over a wide range of tensile moduli.

In a system comprising a thin and relatively rigid film adhered to a thicker and relatively soft substrate, the buckling instability is a result of the balance between the energy required to bend the rigid upper film and the energy required to deform the soft underlying substrate.[56] The buckling wavelength, λ_b, is related to the thickness of the film, d_f, the tensile moduli of the film and the substrate, E_f and E_s, and the Poisson ratios of the two materials, v_f and v_s by the following equation:

$$E_f = 3E_s\left(\frac{1-v_f^2}{1-v_s^2}\right)\left(\frac{\lambda_b}{2\pi d_f}\right)^3 \qquad (\mathbf{1})$$

We measured the tensile modulus of the substrate, E_s, the buckling wavelength, λ_b, and the film thickness, d_f. The Poisson's ratios were assumed to be 0.5 and 0.35 for PDMS and the conjugated polymer films, respectively;[6] the values of moduli produced from this calculation agree well with those obtained by traditional methods and dynamic mechanical analysis.[40,63,64] The tensile moduli of thin polymer films obtained using this method remain constant for thin films with thicknesses between 20 to 500 nm.[59,65]

3.3.3. Calculation of tensile moduli using a theoretical model

We employed a theoretical model to estimate the tensile moduli of P3ATs and P3AT:PCBMs. Seitz had developed a semi-empirical method to predict mechanical properties of polymers from five basic molecular properties: molecular weight, van der Waals volume, the length and number of rotational bonds in the monomer, and the glass transition temperature (T_g) of the polymer.[66] The method was refined by Tahk et al. and

applied to conjugated polymers with T_g higher than room temperature.[6] We further modified the method to account for behaviors for polymer with T_g lower than room temperature. A full description of the methodology can be found in the Supporting Information. To outline the method briefly, the tensile modulus can be related to the bulk modulus, B, and the Poisson's ratio, v_f, by equation 2,

$$E_f = 3B(1 - 2v_f) \qquad (\mathbf{2})$$

The bulk modulus was estimated from the Lennard-Jones potential with the resulting expression as a function of the cohesive energy, E_{coh}, and the molar volume, V, at room temperature and at 0 K,

$$B \approx 8.23E_{coh}\left[\frac{5V_0^4}{V^5} - \frac{3V_0^2}{V^3}\right] \qquad (\mathbf{3})$$

The cohesive energy can be estimated from the chemical structure of the monomer using the method outlined by Fedors.[67] Values for molar volume were calculated using the empirical correlations depending on the range of the T_g of the polymer of interest. We used three different equations corresponding to the polymer with T_g higher than room temperature (P3BT), T_g close to room temperature (P3HT), and T_g below room temperature (P3OT and P3DDT), (equation **S11**, **S12**, and **S13**, supporting information)**.** The Poisson's ratio was modeled from empirical data relating the Poisson's ratio to the molecular cross-sectional area, A,[66]

$$\nu = 0.513 - 2.37 \times 10^6\sqrt{A} \qquad (\mathbf{4})$$

This cross-sectional area, A, can then be related to the van der Waals volume, V_w, and the length of the monomer in its fully extended conformation, l_m, by,

$$A = \frac{V_{\mathrm{w}}}{N_{\mathrm{A}} l_{\mathrm{m}}} \qquad (\mathbf{5})$$

where N_A is the Avogadro's number. Both V_w and l_m are estimated from the structure of the monomer, Figure **A.5** (supporting information). For the blends of P3AT:PCBM, we employed a composite theory[6] that relates the tensile modulus of the pure film to that of the composite film as a function of Poisson's ratio, volume fraction of the filler (PCBM) and the maximum packing fraction of PCBM (equation **S14**, supporting information).

3.3.4. Selection of processing additives

Common processing additives for organic solar cells, 1,8-diiodooctane (DIO) and low molecular weight PDMS, were added to the P3HT:PCBM films to measure their effects on mechanical properties of the thin films. Lee et al. reported the significantly improvement in the efficiencies of bulk heterojunction solar cells from 3.4% to 5.1% with the addition of 1,8-diiodooctane (DIO).[68] Reynolds and coworkers also have shown that the addition of low-molecular weight PDMS improved the power conversion efficiency of device comprising of a thiophene and isoindigo-containing small molecule and PCBM.[69] Addition of PDMS greatly reduced the roughness of the film and the sizes of the features observable by atomic force microscopy (AFM).[69] We expected that these additives would also affect the mechanical properties of the films.

3.3.5. Fabrication and testing of organic photovoltaic devices under strain

We compared the photovoltaic properties of the standard materials in literature for bulk heterojunction solar cells, P3HT:PCBM, with those of a less common blend,

P3DDT:PCBM, under the strain of 10%. Existing studies have shown that P3HT:PCBM outperforms P3DDT:PCBM.[70] Babel and Jenekhe reported the difference in hole mobilities for different P3ATs, stating that the value for P3HT is orders of magnitude higher than that of P3DDT—0.01 $cm^2\ V^{-1}\ s^{-1}$ for P3HT compared to 2.4 x 10^{-5} $cm^2\ V^{-1}\ s^{-1}$ for P3DDT.[71] Friedel and coworkers demonstrated that in the all-polymer solar cells, P3HT outperformed other P3ATs tested when paired with a polyfluorene copolymer as an acceptor, poly((9,9-dioctylfluorene)-2,7-diyl-alt-[4,7-bis(3-hexylthien-5-yl)-2,1,3-benzothiadiazole]-2',2"-diyl) (F8TBT).[55] Nguyen et al. showed that optimized annealing conditions produced P3HT:PCBM cells that were almost four times more efficient than were P3DDT:PCBM cells.[70] The performance of polymer:PCBM bulk heterojunction devices under strain is highly dependent on the identity of the polymer, however.[10] We expected a significantly different response to applied strain between devices containing P3HT:PCBM and those containing P3DDT:PCBM.

We used a previously described technique for fabricating stretchable devices on PDMS substrates.[10] Briefly, high-conductivity poly(3,4-ethylenedioxythiophene):poly(styrenesulfonate) (PEDOT:PSS) films on PDMS substrates were used as the transparent electrode. PEDOT:PSS—when doped with dimethylsulfoxide (DMSO) and Zonyl (FS-300) fluorosurfactant—has been shown to reversibly stretchable up to 30% strain (though cracks begin to appear at 12% strain).[72] For the stretchable top electrode, we used a liquid metal cathode, eutectic gallium-indium (EGaIn).[73–75] We measured the photovoltaic properties of P3HT:PCBM and P3DDT:PCBM devices under two conditions: as-fabricated (0% strain) and stretched (10% strain).

3.4. Results and discussion

3.4.1. Elastic moduli of pure P3AT thin films

We began by determining the tensile moduli of the pure P3AT films spin-coated from chloroform. For each polymer—P3BT, P3HT, P3OT, and P3DDT—the buckling wavelengths were plotted as a function of the film thickness. **Figure 3.2a** and **3.2b** show an example of the optical micrographs of the buckled films of P3HT and P3HT:PCBM; and **Figure 3.2c** shows the plot of buckling wavelength vs. thickness. We then substituted the slopes of the linear fits, λ_b/d_f, into equation 1 to obtain the tensile moduli of the thin films, E_f. The error in the tensile moduli was calculated from the propagation of standard error of the line fits and the standard deviation of the tensile modulus of the PDMS, E_s. In our experiment, E_s obtained were in the range of 0.8–1.0 MPa depending on the exact mix ratio, curing time, and batch-to-batch variability. The values obtained for the pure P3ATs are shown in **Figure 3.2d** and **Table 3.1**. The tensile modulus of P3HT agrees well with the previously reported values of 1.33 GPa[6] and 0.92 GPa[10] obtained using the same method. The values of the tensile modulus decrease dramatically as the length of the alkyl side-chain increases from 4 to 8 (P3BT to P3HT to P3OT). The moduli of P3OT and P3DDT, however, are similar. Our theoretical calculation of the tensile moduli using the molecular structure of the monomer as well as the T_g of the polymer agreed extremely well with the experimental data, **Figure 3.2e**. The calculated values highlighted the trend of decreasing values of tensile modulus with increasing side-chain length.

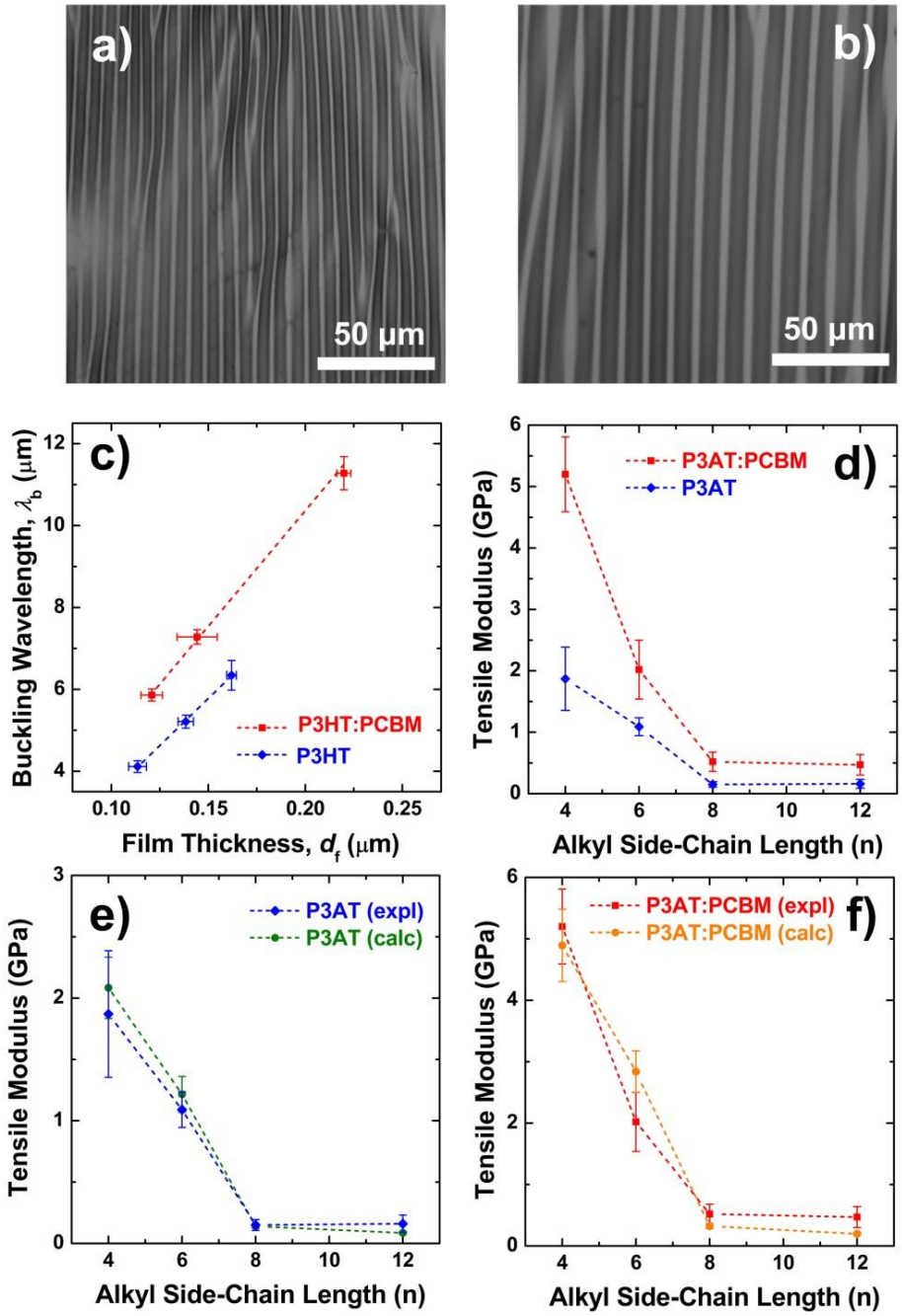

Figure 3.2. Mechanical properties of P3ATs and their blends with PCBM. Optical micrographs of buckled films of (a) P3HT with λ_b = 6.34 μm and d_f = 162 nm and (b) P3HT:PCBM with λ_b = 11.3 μm and d_f = 220 nm; (c) buckling wavelength vs. film thickness, the slope of the linear fit, λ_b/d_f, was used to calculate the tensile modulus; (d) summary of the tensile modulus of the P3ATs and P3AT:PCBMs as a function of alkyl side-chain length; comparison of the experimental and calculated moduli of P3ATs (e) and their blends with PCBM (f).

Table 3.1. Comparison of tensile moduli of P3ATs and their blends with PCBM both from measurement with buckling-based method and theoretical calculations[†]

Materials	Tensile Modulus (GPa)			
	P3AT		P3AT:PCBM	
	(expl)	(calc)	(expl)	(calc)
P3BT	1.87 ± 0.52	2.08 ± 0.25	5.20 ± 0.61	4.89 ± 0.59
P3HT	1.09 ± 0.15	1.22 ± 0.15	2.02 ± 0.48	2.84 ± 0.34
P3OT	0.15 ± 0.05	0.14 ± 0.02	0.52 ± 0.16	0.32 ± 0.04
P3DDT	0.16 ± 0.07	0.09 ± 0.01	0.47 ± 0.17	0.20 ± 0.02

[†]The reported moduli were measured from as-cast films. All P3AT:PCBM weight ratios were 2:1. The errors in the experimental moduli were calculated from the propagation of standard errors of the line fits and the standard deviation of the tensile moduli of the PDMS substrates. The errors in the calculated moduli were the inherent standard deviation associated with the methodology.

The high modulus of P3BT films rendered them somewhat problematic for the buckling technique. We found that 4% compressive strain cracked and delaminated the film and led to inaccurate buckling wavelengths, because compressive strain is accommodated by cracks and areas of the film that are delaminated from the substrate.[6,59] The critical strain that leads to cracking and delamination has been shown to decrease dramatically as the tensile modulus increases.[76] To mitigate this problem, we applied the compressive strain of 2%, rather than 4%, to all P3BT films. The buckling wavelength is not dependent on compressive strains less than approximately 5% because the excess strain energy is manifested as an increase in the wave amplitude.[22] The ease of film cracking and delamination suggested a high degree of brittleness of the P3BT films.

The effect the length of the alkyl side-chain on the tensile modulus can be understood, in part, through the thermal properties of the P3ATs. Crystallization of the P3ATs has been studied with the focus on the effects of the side-chains by Causin et al.[46] (P3BT, P3OT, P3DDT), Ho et al.[52] (P3HT, P3DDT), and Malik and Nandi[47] (P3HT, P3OT, P3DDT). All the studies reported the decrease in melting temperature with longer side-chain length.[46,47,52] Elevated melting temperature typically correlates with an increase in crystallinity and stiffness of the material resulting from strong intermolecular forces.[50] Our

observation of decreasing values of the tensile modulus with increasing length of the alkyl side-chain is consistent with these earlier findings. The relatively high tensile modulus of the P3BT is expected because its T_g is well above the room temperature, a property that is characteristic of brittle and rigid polymers. The T_g of P3BT has been reported from 55 °C to 75 °C.[77] Similar to those of the other P3ATs, the T_g of P3BT are reported in literature as a range, most likely due to the differences in processing and methods of measurement, molecular weight, polydispersity, and thermal history.

The trend in mechanical properties as a function of alkyl side-chain length has been analyzed for other polymeric systems. For example, Moulton and Smith measured the tensile moduli of regiorandom P3AT fibers and have shown that the moduli of the regiorandom P3AT fibers decrease with longer alkyl side-chain length.[18] The authors attributed this effect mainly to the irregularity in the interchain π-π overlap caused by head-to-head and tail-to-tail couplings.[18] However, in regioregular P3ATs, the contributions from defects in regioregularity are dominated by the reduction of volume fraction of the main-chain with increasing length of the side chain. The fractions of cross-sectional area of the main-chain (versus the alkyl side-chain) per macromolecule, based on the crystal lattice dimensions, are 0.31, 0.28, 0.25, and 0.20 for P3BT, P3HT, P3OT, and P3DDT respectively.[18] This dilution of the volume fraction reduces the number of load-bearing covalent bonds and may reduce the secondary interaction between the main-chains that can lead to decreases in the stiffness and strength of the materials, as observed in previous studies involving poly(alkyl isocyanates).[78,79]

3.4.2. Elastic moduli of P3AT:PCBM thin films

Blends of P3HT and PCBM have been shown to be stiffer and more brittle than the pure polymer.[6,10] We expected to observe the same behavior in other P3ATs. The tensile moduli of the P3AT:PCBM films were determined in the same manner as the pure P3AT films. We found that the moduli of P3AT:PCBM (2:1) were 2 to 4 times higher than those of the pure P3AT films, **Figure 3.2d**. These results agrees well with previously reported increase in modulus from pure P3HT to P3HT:PCBM.[6,10] Similar to the trend we observed for the pure polymers, the moduli decreased as the alkyl side chain length increased. The preservation of this trend suggests that the effects on the tensile modulus from the addition of PCBM and the varying length of the alkyl side-chain are decoupled. Again, our calculated values were consistent with the experimental results, **Figure 3.2f**.

While the morphology of the surface a polymer film visible by AFM is not directly related to its bulk crystallinity or mechanical properties, an analysis of images of the four P3ATs and their blends with PCBM nevertheless informed our analysis. Height images for the eight materials are shown in **Figure 3.3** and the rms roughness obtained from the images is plotted in **Figure 3.4**. We identified two trends from the data: a general decrease in roughness with increasing length of the alkyl side chain from P3BT to P3OT that loosely followed the trends measured for tensile modulus and T_g, and a roughened morphology of P3HT:PCBM compared to that of the pure polymer. Verploegen et al. found a correlation between the sizes of crystallites observed by grazing-incidence X-ray diffraction (GIXD) and the roughness measured by AFM for P3HT and P3HT:PCBM films annealed below T_M.[80] It is known that increases in crystallinity can produce dramatic increases in tensile modulus, as is the case for PBTTT.[9] We therefore can attribute part of the increase in

modulus with decreasing length of the alkyl chain to a possible increase in crystallinity in our films.

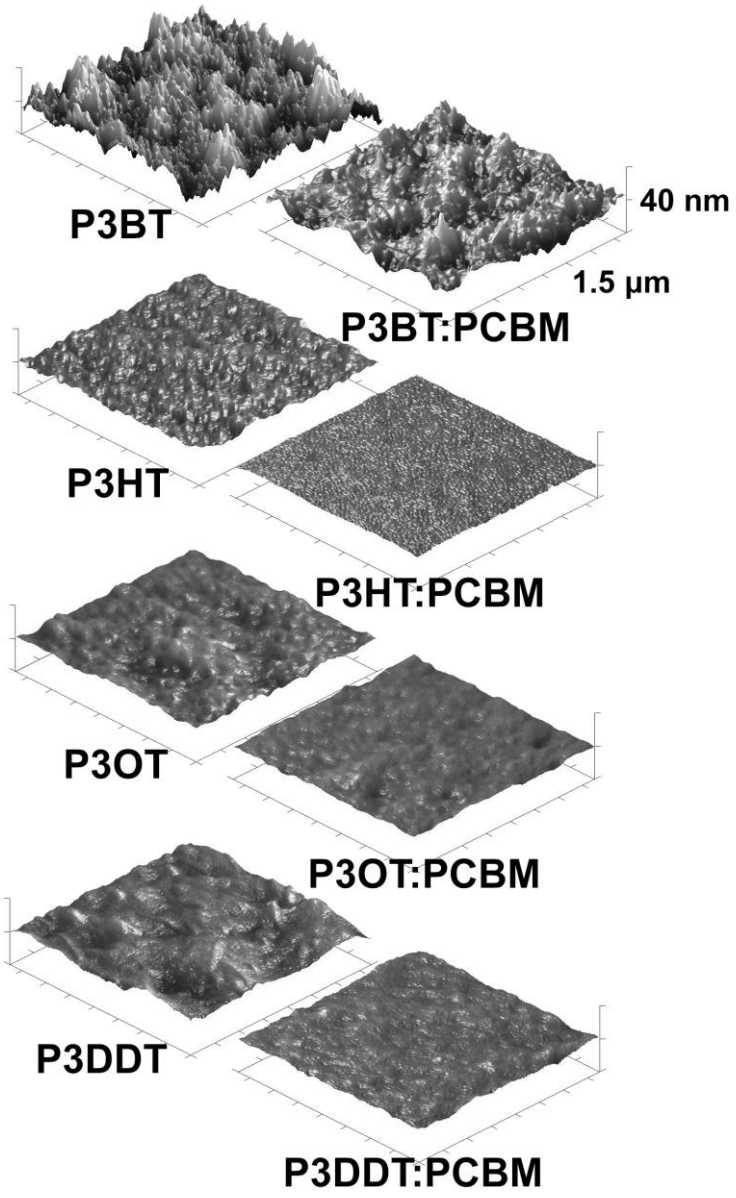

Figure 3.3. Atomic force microscopy height images comparing the pure P3AT films and their blend with PCBM spin-coated on Si wafer with no annealing. The dimensions are 1.5 µm × 1.5 µm × 40 nm.

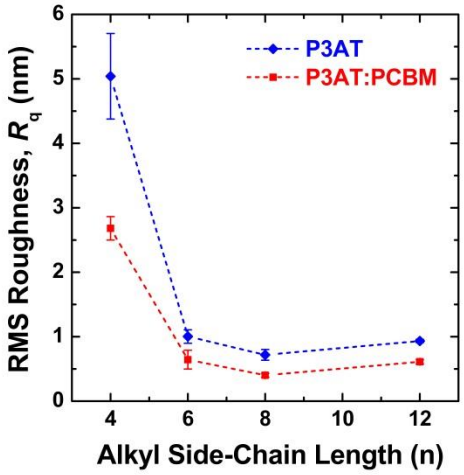

Figure 3.4. Root mean squared roughness (R_q) of the height images of the pure P3AT films and P3AT:PCBM films obtained from tapping mode AFM.

3.4.3. Ductility of thin films

Other studies have found a correlation between tensile modulus and the propensity of conjugated polymer films to crack when stretched on a compliant substrate.[9,10,42] **Figure 3.5a** summarized the strains at which cracks first appear (crack on-set strains) for the conjugated polymer films and shows examples of the optical micrographs of the film at 0% strains and one at 80%. We observed the expected trend in which pure polymer films of P3BT and P3HT crack at much lower applied strains than P3OT and P3DDT. Similarly, the blends of P3BT and P3HT with PCBM cracked at smaller applied strains that did P3OT:PCBM. These trends correlated well with the measured tensile moduli of the films and suggest that tensile modulus—obtained experimentally or calculated—can be used as a proxy for brittleness. Both P3OT:PCBM and P3DDT:PCBM films cracked at similar applied strains; this observation is consistent with the closeness of their respective tensile moduli. Previous studies have shown that the formations of cracks in thin films are

influenced by the mismatch between the tensile modulus of the substrate and that of the film.[81,82] However, this dependency is negligible for material systems with sufficiently small values of E_s/E_f, which allowed us to compare systems comprising different P3ATs.

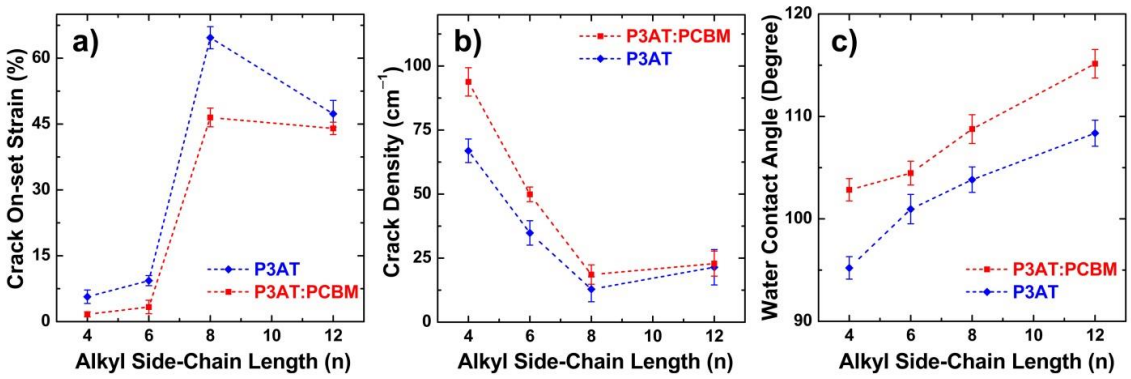

Figure 3.5. Ductility of P3AT and P3AT:PCBM films. (a) Crack on-set strains, (b) crack density at a fixed strain of 80%, and (c) water contact angle measurements of the pure P3AT films and their blends with PCBM.

Table 3.2. Summary of the crack on-set strains and crack densities of P3ATs and their blends with PCBM‡

Materials	P3AT		P3AT:PCBM	
	Crack on-set strain (%)	Crack density (cm^{-1})	Crack on-set strain (%)	Crack density (cm^{-1})
P3BT	6 ± 1.5	67 ± 4.6	2 ± 0.6	94 ± 5.5
P3HT	9 ± 1.2	35 ± 4.8	3 ± 1.5	50 ± 2.9
P3OT	65 ± 2.5	13 ± 4.9	47 ± 2.1	19 ± 3.8
P3DDT	47 ± 3.1	21 ± 6.9	44 ± 1.4	23 ± 4.9

‡ The reported moduli were measured from as-casted films. All P3AT:PCBM weight ratios were 2:1. Crack on-set strains were observed by optical microscope with the increment of 1% strains. Crack densities were measured from the optical micrographs. Errors in both the crack on-set strains and the crack densities were the standard deviations of the sample tested.

A curious feature of **Figure 3.5a** is the large apparent increase in brittleness from P3OT to P3DDT that would not be expected on the basis of the mechanical properties intrinsic to the materials. Optical micrographs also showed that the cracks found in P3OT films are much smaller than those found in P3DDT films. We attributed the apparent increase in brittleness to the weakened adhesion of the P3AT to PDMS with increasing side-chain length. From the water contact angle measurements, we observed that the contact angle increases with the longer side-chain length, as shown in **Figure 3.5c**. The

values for P3OT and P3DDT films are 103° and 109° respectively. We believe that the lower surface energy of P3DDT led to the poor adhesion between the film and the PDMS substrate. It has been observed in other systems that poor adhesion of a film to a substrate under strain produces cracking in regions of local delamination.[83] In such regions, the local strain can greatly exceed the global strain. Indeed, chromium adhesion layers inserted between copper films and Kapton substrates,[83] and PEDOT:PSS films inserted between P3HT:PCBM films and PDMS substrates,[84] reduced the formation of cracks in the upper film substantially. These adhesion-promoting layers distribute strains more uniformly across the upper film and permit substantially more deformation than is possible for poorly adhered films.

We further quantified the formation of cracks by investigating the crack density (number of cracks cm^{-1}) of the thin films at a fixed strain of 80%. **Figure 3.5b** shows a trend that was similar to that observed in the tensile modulus. The high-modulus films containing P3BT exhibited much higher crack densities than P3HT, P3OT, and P3DDT. At 80% strains, we observed the differences in the fracture characteristics between films with T_g higher than room temperature and those with T_g lower than room temperature. From the optical micrographs, P3BT, P3BT:PCBM, and P3HT:PCBM films showed characteristic brittle behaviors while the other films exhibited ductile behaviors. Fractures found in P3BT, P3BT:PCBM, and P3HT:PCBM films showed little apparent plastic deformation. Specifically, the cracks that formed in these brittle films tended to propagate along the entire axis perpendicular to the strained axis. On the other hand, the cracks found in the other films were much shorter and exhibited less of a tendency to propagate. From the data obtained, we again observed higher crack density in P3DDT compared to P3OT

and in P3DDT:PCBM compared to P3OT:PCBM. As in the case of crack-onset strain, we attribute the apparent increase in brittleness from P3OT to P3DDT to weakened adhesion to the PDMS substrate with increasing length of the alkyl side-chain.

3.4.4. Effects of processing additives on mechanical properties of P3HT:PCBM blends

We also measured the tensile moduli of P3HT:PCBM films with processing additives, DIO and low molecular weight PDMS. For this part of the experiment, we used ODCB rather than chloroform to simulate the conditions used in the literature for systems containing processing additives. We expected the resulting films to have different mechanical properties because of the structural differences reported in P3HT:PCBM films processed from different conditions,[42] and also because of possible plasticizing effects of residual additive. Thus to establish a meaningful comparison, P3HT:PCBM with no additive spin-coated from ODCB, with tensile modulus of 1.23 ± 0.43 GPa, served as a control experiment. We observed that the addition of processing additives, that have been shown to improve the photovoltaic performance significantly,[68,69] also improve the mechanical resiliency. The addition of 0.5 mg mL^{-1} PDMS into the solution of 1-EtHx:PCBM showed almost two-fold increase in the device efficiency.[69] In the same manner, the addition of DIO to the solution of PCPDTBT:$PC_{71}BM$ increased the efficiency from 3.35% to 5.12%.[68] We observed that the small concentration of PDMS lowered the tensile modulus of P3HT:PCBM films to 0.88 ± 0.24 GPa; and, the P3HT:PCBM films spin-coated from 98% ODCB and 2% DIO showed a significantly lowered tensile modulus of 0.38 ± 0.03 GPa (~30% of P3HT:PCBM with no additives). Understanding the exact relationship between the improvement in device performance and the mechanical

properties is beyond the scope of this work. We attributed the reduction in the films brittleness with the additives, however, to plasticizing effects of DIO and PDMS, that is, by increasing the free volume.

3.4.5. Photovoltaic properties of OPV devices under strains

We fabricated stretchable OPV devices using solutions of P3HT:PCBM and P3DDT:PCBM with a 1:1 ratio in ODCB. A layer of PEDOT:PSS, spin-coated from a solution containing 7% DMSO and 1% Zonyl fluorosurfactant, served as transparent electrode on a UV/O_3-treated PDMS substrate. The PEDOT:PSS layer was annealed at 100 °C for 10 min and cooled slowly to room temperature. The annealing temperature was chosen to be lower than the temperature ordinarily used for PEDOT:PSS to avoid the generation of wrinkles caused by the thermal expansion and retraction of the PDMS substrate. On top of the PEDOT:PSS layer, we spin-coated the active layer of P3HT:PCBM or P3DDT:PCBM. We did not anneal the active layers. We applied drops of the liquid metal, EGaIn, on top of the active layer to create electrical contact; the areas of the EGaIn drops served as the active area in our measurements. EGaIn has been found to be a mechanically compliant alternative to evaporated aluminum.[39] We measured the photovoltaic properties of each sample at 0% strains and then again at 10% strain.

When the strains of 10% applied, major cracks on the surface of the P3HT:PCBM can be observed without a microscope, **Figure 3.6a**. No cracks were observed for P3DDT:PCBM, **Figure 3.6b**. **Figure 3.6c** and **3.6d** show the *J-V* plots that depict the change in the photovoltaic properties of P3HT:PCBM and P3DDT:PCBM devices at 0% and at 10% applied strain. At 0% strains, the superior performance of P3HT:PCBM is

expected and is consistent with the superior electronic properties of P3HT. Under strain, however, the photovoltaic properties of the devices based on the two different polymers exhibited a striking contrast: the *J-V* curves of P3HT:PCBM devices at 10% resembled that of a solar cell in parallel with a resistor, with slightly non-zero J_{SC}. The device based on P3DDT:PCBM exhibited a slight loss in J_{SC} and an increase in V_{OC} when strained. We attribute the increases V_{OC} to possible disruption of the gallium oxide "skin" of the EGaIn droplets, and possibly better contact of the bulk liquid with the surface of the organic semiconductor.[10] The resiliency of the P3DDT:PCBM films was expected from the measured tensile modulus. We believed that the demonstration of fractures in P3HT:PCBM devices provide a substantial motivation to pursue materials with greater compliance for applications demanding flexibility or stretchability.

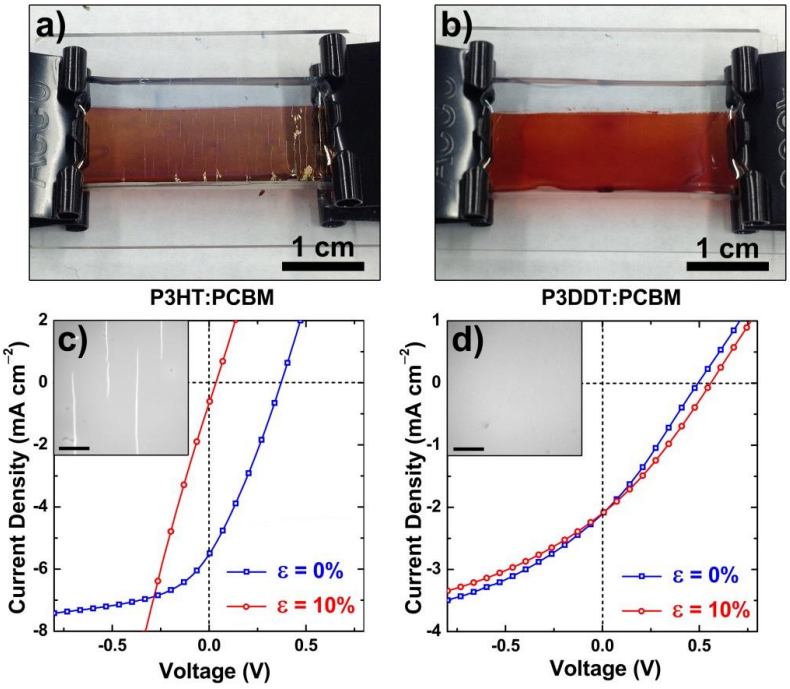

Figure 3.6. Photographs of P3HT:PCBM (a) and P3DDT:PCBM (b) devices under 10% strain; characteristic photovoltaic properties of P3HT:PCBM (c) and P3DDT:PCBM (d) devices; the insets are optical micrographs of the surfaces of the devices, the scale bar is 0.5 cm.

Table 3.3. Figure of merits for OPV devices on PDMS substrates at 0% strains and at 10% strains

Device (% strain)	V_{OC} (V)	J_{SC} (mA cm^{-2})	FF (%)	PCE (%)
P3HT:PCBM (0%)	0.37 ± 0.005	5.52 ± 1.14	28.7 ± 3.02	0.594 ± 0.119
P3HT:PCBM (10%)	0.04 ± 0.003	0.66 ± 0.06	22.1 ± 4.91	0.008 ± 0.011
P3DDT:PCBM (0%)	0.50 ± 0.001	2.10 ± 0.57	27.7 ± 1.55	0.291 ± 0.088
P3DDT:PCBM (10%)	0.58 ± 0.034	1.88 ± 0.47	29.8 ± 3.66	0.381 ± 0.029

3.5. Conclusions

This paper describes the mechanical properties of a series of poly(3-alkylthiophenes) as a function of the length of the alkyl solubilizing group. We found that the tensile modulus and brittleness of P3ATs and their blends with PCBM decreased with increasing length of the alkyl side chain. These trends were predictable using a semi-empirical model that incorporated knowledge of the glass transition temperature and the chemical structure of the polymer. We also found a significant influence of the presence of processing additives and the adhesion of the semiconductor film to the substrate on the mechanical properties of conjugated polymers and polymer-fullerene composites.

It is important to note that the modest strains at which some of the materials described in the text fail—*i.e.*, P3HT:PCBM at 2%—could be reached easily during the lifetime of a device through standard handling and/or installation as well as environmental and temporal changes.[85] Additionally, stretchability and flexibility of the active components are extremely crucial for devices fabricated in a large-scale roll-to-roll manner.[86,87] Fabrication of multi-junction solar cells demands iterative deposition of as many as 12 layers not including backing and encapsulant;[88] all of which can have drastically different mechanical properties. This work shows that the mechanical properties of each layer must be measured and accounted for when designing the manufacturing process such that the most compliant layers can be deposited earliest when possible.

Studying bilayer thin films under strain can also give crucial insight into delamination behavior; understanding of which will be crucial in designing tandem cells that can withstand repeated bending and strain. Future work will also explore the effects of chemical structure on yield strain, interlayer adhesion, and cyclic loading of strain brought about by direct mechanical deformation or thermal cycling to simulate diurnal and seasonal expansion and contraction of multilayer devices.

We believe that our analysis could improve the selection and design of organic semiconductors for applications that require mechanical compliance. Specifically, the apparent competition between charge carrier mobility and other metrics of electronic performance with mechanical properties suggests that materials should be chosen on the basis of the application. That is, there is a strong possibility that a given application could sacrifice state-of-the-art electronic performance for the sake of improved mechanical performance. Alternatively, our analysis may suggest alternative polymers that combine "the best of both worlds." It is possible, for example, that high-performance polymers exhibiting low crystallinity may provide a way toward compliant organic semiconductors that does not put electronic properties and mechanical properties at odds. The abilities of certain additives to improve mechanical and photovoltaic properties simultaneously suggest that these properties need not be mutually exclusive. Selection and design of organic semiconductors on the basis of mechanical compliance (as opposed to on the basis of only electronic performance) represents a different perspective from the way in which organic semiconductors are typically selected and designed. We believe this approach will be necessary to realize the original promise of organic electronics, that is, the combination

of high-performance electronic properties with elasticity, plasticity, and processability that can be predicted by theory and tailored by synthesis.

3.6. Experimental methods

3.6.1. Materials

The P3ATs were obtained from Sigma-Aldrich with the following approximate weight-average molar mass (M_w) of 54k, 97k, 34k, and 60k with regioregularity of 80-90%, 98%, 98.5%, and 98.5% for P3BT, P3HT, P3OT, and P3DDT respectively. P3BT produced poor quality films as received. It was dissolved in chloroform, reprecipitated in methanol, and collected by filtration. Separately, we synthesized a sample of regioregular P3HT using the method described by McCullough[43] and obtained tensile moduli that were identical to those of the commercial material. PCBM was obtained from Sigma-Aldrich with >99% purity. PDMS, Sylgard 184, Dow Corning, was prepared according to the manufacturer's instructions at a ratio of 10:1 (base:crosslinker) and cured at room temperature for 36 to 48 hours when it was used for buckling experiments. We observed better adhesion and transfer of the P3AT films to the PDMS surfaces when the PDMS was cured at room temperature, as opposed to elevated temperature. We cured the PDMS at 60°C for 2 h when it was used as substrates for stretchable solar cells, and for all experiments, used the PDMS surfaces cured at the air interface. 1,8-Diiodooctane (DIO) was obtained from Sigma-Aldrich with 98% purity and low-M_w PDMS was obtained from Gelest with the weight average molar mass of 550. (Tridecafluoro-1,1,2,2-tetrahydrooctyl)-1-trichlorosilane (FOTS) was also obtained from Gelest. PEDOT:PSS (Clevios PH1000) was purchased from Heraeus. The solid content of the PH 1000 solution was 1–1.3% and had a ratio of PEDOT to PSS of

1:2.5 by weight. Chloroform, *ortho*-dichlorobenzene (ODCB), eutectic gallium-indium (EGaIn, ≥99.99%) and Zonyl (FS-300) fluorosurfactant were also purchased from Sigma-Aldrich and used as received. DMSO was purchased from BDH with purity of 99.9% and used as supplied.

3.6.2. Preparation of films

We began by preparing the hydrophobic glass slides as the initial substrate for the P3AT and P3AT:PCBM films. Glass slides were cut into 2.5 cm × 2.5 cm squares and cleaned by bath sonication in detergent, water, acetone, and isopropanol for 15 minutes each and dried under a stream of compressed air. The surface of the glass slides was activated with an air plasma (30 W, 200 mTorr, 3 minutes) before enclosing them in a vacuum desiccator with (tridecafluoro-1,1,2,2-tetrahydrooctyl)-1-trichlorosilane (FOTS). The desiccator was left under dynamic vacuum for at least 12 h. The glass slides were then rinsed with additional isopropanol and dried under stream of compressed air before use. We then spin-coated the polymer solutions directly on the FOTS-treated glass slides. For each polymer or blend, we used the following solvents and concentrations: P3AT (chloroform, 15 mg mL^{-1}); P3AT:PCBM (2:1 mass ratio, chloroform, 22.5 mg mL^{-1} total solid content). We used a mass ratio of 2:1 for the blended films because greater concentrations of PCBM led to weakened adhesion of the film to the PDMS substrate during the buckling experiment, delamination, and buckling wavelengths that were difficult to measure. We used three different spin speeds—0.5, 1, 1.5 krpm—to obtain three different thickness for each polymer samples. For P3HT:PCBM with processing additives, the films were spin-coated from ODCB to closely emulate the conditions most often used

for fabrication of the most efficient devices. The solutions were as followed for P3HT and P3OT: (1) P3AT:PCBM (2:1 mass ratio, 100% ODCB, 40 mg mL^{-1} total solid content); (2) P3AT:PCBM with DIO (2:1 mass ratio, 98% ODCB and 2% DIO *v/v*, 40 mg mL^{-1} total solid content); (3) P3AT:PCBM with DMS (2:1 mass ratio, ODCB with 0.5 mg mL^{-1} of DMS, 40 mg mL^{-1} total solid content). Films made from ODCB were spin-coated at 0.5, 0.75, and 1 krpm.

3.6.3. Buckling-based method

The elastomer poly(dimethylsiloxane) (PDMS) was chosen as the relatively soft substrate for all experiments. The mixed and degassed prepolymer was allowed to cure at room temperature for 36–48 hours before it was used in an experiment. We then cut the PDMS into rectangular pieces (l = 8 cm, w = 1 cm, h = 0.3 cm) and stretched to strains of 4% using a computer-controlled stage, which applied strain to samples using a linear actuator. While the PDMS rectangles were under strain, microscope slides (5 cm × 2.5 cm activated using oxygen plasma and treated with FOTS to later facilitate separation of the PDMS) were clipped onto the back of each rectangle using binder clips to maintain the strain. Transferring the conjugated polymer films to the pre-strained PDMS substrate was performed by initially scoring the films along the edges with a razor and placing the films against the PDMS. After applying a minimum amount of pressure to create a conformal seal between the PDMS and the conjugated polymer film, we separate the glass/stretched PDMS from the glass/conjugated polymer film in one fast motion.[89] In most cases, the areas in which the films were in contact with the PDMS were successfully transferred to the pre-strain PDMS rectangles. We then removed the binder clips and allowed the PDMS

to relax to the equilibrium length. Buckles formed in the conjugated polymer films upon relaxation of the substrate.

3.6.4. Imaging of polymer films

We obtained the buckling wavelength, λ_b, from optical micrographs, for which we divided the length of each images by the number of buckles. We developed a MATLAB code to count the number of buckles in each image using the intensity of each pixel, the Savizky-Golay smoothing filter, and the peak-finder methodology. The buckling wavelengths reported represent the averages from seven different regions of each film. The thicknesses of the conjugated polymer films were measured using a Veeco Dektak stylus profilometer. Each value of the reported thickness represents an average of seven different measurements taken from different locations of the films. We obtained the tensile modulus of each batch of PDMS, E_s, from the slope of the stress-strain curved generated by a commercial pull tester. AFM images were taken using tapping mode from Veeco Scanning Probe Microscope.

3.6.5. Measurements of ductility

We assayed the ductility of the films by measuring two parameters: the crack on-set strains and the crack density at a fixed strain. To measure crack on-set strain, the conjugated polymer films of each P3AT and P3AT:PCBM were prepared as described above. The films were then transferred onto unstrained PDMS rectangles. The rectangles were then stretched from 0% to 80% strain using a linear actuator with a step size of 1% using a computer-controlled stage. At each step, optical microscope images of the films

were taken in order to observe the generation of cracks. The crack on-set strain of each conjugated polymer was defined as the strain at which the first crack was observed. The crack densities were obtained from the optical microscope images of each film at a fixed strain of 80%. The number of cracks was divided by the length of the image to obtain the crack density.

3.6.6. Fabrication and characterization of organic solar cells under stains

The PDMS used as the substrate of the OPV were cured at 60 °C for 2 h. We then activated the surfaces of the substrate by UV/O_3 (Novascan 4-inch UV/O_3 cleaner operating at 20 mW cm^{-2}) for 1 h. We spin-coated PEDOT:PSS films from solutions containing 7% DMSO and 1% Zonyl on the substrate at 0.5 krpm for 4 min and 2 krpm for 1 min. Glass slides were used as support for the PDMS substrates for the whole process to avoid applying unwanted strains to the elastomeric substrate during manipulations. The PEDOT:PSS films were then thermally annealed at 100 °C for 10 minutes on a hotplate. The hotplate was turned off and the substrates were allowed to cool slowly to room temperature. We prepared P3AT:PCBM films from a 1:1 (*w*/*w*) solution of 40 mg mL^{-1} total in ODCB. The active layers were spin-coated on top of the PEDOT:PSS layer using the same conditions as those described for pure P3AT films. After spin-coating, the films were placed in the antechamber of the glovebox under dynamic vacuum for 15 min to completely evaporate residual solvents and to reduce adsorbed water and oxygen. EGaIn drops and copper wires were placed to create electrical contacts; and, the photovoltaic properties, at 0% strains, were measured using a solar simulator operated at AM 1.5G conditions inside a glovebox filled with nitrogen. The devices were then removed from the

glovebox, peeled from the glass supports and placed on the computer-controlled stage to apply 10% strain. The stretched devices were then clipped back onto the glass supports using binder clips to maintain the applied strain. The photovoltaic properties at 10% strains were measured under the same conditions.

Acknowledgments

This work was supported by the Air Force Office of Scientific Research (AFOSR) Young Investigator Program, grant number FA9550-13-1-0156. Additional support was provided by the National Science Foundation Graduate Research Fellowship under Grant No. DGE-1144086, awarded to S. S., and by laboratory startup funds from the University of California, San Diego.

Chapter 3, in full, is a reprint of the material as it appears in *Advanced Functional Materials*, 2014, 24, 1169 – 1181. Wiley-VCH Verlag GmbH & Co. KGaA, 2014. Suchol Savagatrup, Aditya S. Makaram, Daniel J. Burke, and Darren J. Lipomi. The dissertation author was the primary investigator and author of this paper.

References

(1) Krebs, F.; Gevorgyan, S.; Alstrup, J. A Roll-to-Roll Process to Flexible Polymer Solar Cells: Model Studies, Manufacture and Operational Stability Studies. *J. Mater. Chem.* **2009**, *19*, 5442.

(2) Kaltenbrunner, M.; White, M. S.; Głowacki, E. D.; Sekitani, T.; Someya, T.; Sariciftci, N. S.; Bauer, S. Ultrathin and Lightweight Organic Solar Cells with High Flexibility. *Nat. Commun.* **2012**, *3*, 770.

(3) Rogers, J. A.; Someya, T.; Huang, Y. Materials and Mechanics for Stretchable Electronics. *Science.* **2010**, *327*, 1603.

(4) Gleskova, H.; Cheng, I.-C.; Wagner, S.; Sturm, J. C.; Suo, Z. Mechanics of Thin-

Film Transistors and Solar Cells on Flexible Substrates. *Sol. Energy* **2006**, *80*, 687.

(5) Suo, Z.; Ma, E.; Gleskova, H.; Wagner, S. Mechanics of Rollable and Foldable Film-on-Foil Electronics. *Appl. Phys. Lett.* **1999**, *74*, 1177.

(6) Tahk, D.; Lee, H. H.; Khang, D.-Y. Elastic Moduli of Organic Electronic Materials by the Buckling Method. *Macromolecules* **2009**, *42*, 7079–7083.

(7) Dupont, S. R.; Oliver, M.; Krebs, F. C.; Dauskardt, R. H. Interlayer Adhesion in Roll-to-Roll Processed Flexible Inverted Polymer Solar Cells. *Sol. Energ. Mat. Sol. Cells* **2012**, *97*, 171–175.

(8) Brand, V.; Bruner, C.; Dauskardt, R. H. Cohesion and Device Reliability in Organic Bulk Heterojunction Photovoltaic Cells. *Sol. Energ. Mat. Sol. Cells* **2012**, *99*, 182.

(9) O'Connor, B.; Chan, E. P.; Chan, C.; Conrad, B. R.; Richter, L. J.; Kline, R. J.; Heeney, M.; McCulloch, I.; Soles, C. L.; DeLongchamp, D. M. Correlations between Mechanical and Electrical Properties of Polythiophenes. *ACS Nano* **2010**, *4*, 7538–7544.

(10) Lipomi, D. J.; Chong, H.; Vosgueritchian, M.; Mei, J.; Bao, Z. Toward Mechanically Robust and Intrinsically Stretchable Organic Solar Cells : Evolution of Photovoltaic Properties with Tensile Strain. *Sol. Energy Mater. Sol. Cells* **2012**, *107*, 355–365.

(11) Krebs, F. C.; Nielsen, T. D.; Fyenbo, J.; Wadstrøm, M.; Pedersen, M. S. Manufacture, Integration and Demonstration of Polymer Solar Cells in a Lamp for the "Lighting Africa" Initiative. *Energy Environ. Sci.* **2010**, *3*, 512.

(12) Yu, Z.; Niu, X.; Liu, Z.; Pei, Q. Intrinsically Stretchable Polymer Light-Emitting Devices Using Carbon Nanotube-Polymer Composite Electrodes. *Adv. Mater.* **2011**, *23*, 3989.

(13) Ghezzi, D.; Antognazza, M. R.; Maccarone, R.; Bellani, S.; Lanzarini, E.; Martino, N.; Mete, M.; Perile, G.; Bisti, S.; Lanzani, G.; *et al.* A Polymer Optoelectronic Interface Restores Light Sensitivity in Blind Rat Retinas. *Nat. Photon.* **2013**, *7*, 400.

(14) Sekitani, T.; Someya, T. Stretchable, Large-Area Organic Electronics. *Adv. Mater.* **2010**, *22*, 2228–2246.

(15) Jørgensen, M.; Norrman, K.; Gevorgyan, S. A.; Tromholt, T.; Andreasen, B.; Krebs, F. C. Stability of Polymer Solar Cells. *Adv. Mater.* **2012**, *24*, 580.

(16) Cao, Y.; Smith, P.; Heeger, A. Mechanical and Electrical Properties of Highly Oriented Polyacetylene Films. *Synth. Met.* **1991**, *43*, 181–184.

(17) Tokito, S.; Smith, P.; Heeger, A. Highly Conductive and Stiff Fibres of Poly (2, 5-Dimethoxy- P-Phenylenevinylene) Prepared from Soluble Precursor Polymer. *Polymer (Guildf).* **1991**, *32*, 464–470.

(18) Moulton, J.; Smith, P. Electrical and Mechanical Properties of Oriented Poly (3-Alkylthiophenes): 2. Effect of Side-Chain Length. *Polymer (Guildf).* **1992**, *33*, 2340.

(19) Facchetti, A. π-Conjugated Polymers for Organic Electronics and Photovoltaic Cell Applications †. *Chem. Mater.* **2011**, *23*, 733–758.

(20) Peters, C. H.; Sachs-Quintana, I. T.; Kastrop, J. P.; Beaupré, S.; Leclerc, M.; McGehee, M. D. High Efficiency Polymer Solar Cells with Long Operating Lifetimes. *Adv. Energy Mater.* **2011**, *1*, 491–494.

(21) Lipomi, D. J.; Bao, Z. Stretchable, Elastic Materials and Devices for Solar Energy Conversion. *Energy Environ. Sci.* **2011**, *4*, 3314.

(22) Khang, D.-Y.; Rogers, J. a.; Lee, H. H. Mechanical Buckling: Mechanics, Metrology, and Stretchable Electronics. *Adv. Funct. Mater.* **2009**, *19*, 1526.

(23) Yang, S.; Lu, N. Gauge Factor and Stretchability of Silicon-on-Polymer Strain Gauges. *Sensors* **2013**, *13*, 8577–8594.

(24) Kettlgruber, G.; Kaltenbrunner, M.; Siket, C. M.; Moser, R.; Graz, I. M.; Schwödiauer, R.; Bauer, S. Intrinsically Stretchable and Rechargeable Batteries for Self-Powered Stretchable Electronics. *J. Mater. Chem. A* **2013**, *1*, 5505.

(25) Graudejus, O.; Morrison, B.; Goletiani, C.; Yu, Z.; Wagner, S. Encapsulating Elastically Stretchable Neural Interfaces: Yield, Resolution, and Recording/Stimulation of Neural Activity. *Adv. Funct. Mater.* **2012**, *22*, 640–651.

(26) Pharr, M.; Sun, J.; Suo, Z. Rupture of a Highly Stretchable Acrylic Dielectric Elastomer. *J. Appl. Phys.* **2012**, *111*, 104114.

(27) Graz, I. M.; Cotton, D. P. J.; Robinson, A.; Lacour, S. P. Silicone Substrate with in Situ Strain Relief for Stretchable Thin-Film Transistors. *Appl. Phys. Lett.* **2011**, *98*, 124101.

(28) Kim, D.-H.; Xiao, J.; Song, J.; Huang, Y.; Rogers, J. a. Stretchable, Curvilinear Electronics Based on Inorganic Materials. *Adv. Mater.* **2010**, *22*, 2108–2124.

(29) Someya, T.; Kato, Y.; Sekitani, T.; Iba, S.; Noguchi, Y.; Murase, Y.; Kawaguchi, H.; Sakurai, T. Conformable, Flexible, Large-Area Networks of Pressure and Thermal Sensors with Organic Transistor Active Matrixes. *Proc. Natl. Acad. Sci. USA* **2005**, *102*, 12321.

(30) Lacour, S. P.; Jones, J.; Wagner, S. Stretchable Interconnects for Elastic Electronic Surfaces. *Proc. IEEE* **2005**, *93*, 1459.

(31) Lacour, S. P.; Chan, D.; Wagner, S.; Li, T.; Suo, Z. Mechanisms of Reversible Stretchability of Thin Metal Films on Elastomeric Substrates. *Appl. Phys. Lett.* **2006**, *88*, 204103.

(32) Kaltenbrunner, M.; Kettlgruber, G.; Siket, C.; Schwödiauer, R.; Bauer, S. Arrays of Ultracompliant Electrochemical Dry Gel Cells for Stretchable Electronics. *Adv. Mater.* **2010**, *22*, 2065.

(33) Graz, I. M.; Cotton, D. P. J.; Lacour, S. P. Extended Cyclic Uniaxial Loading of Stretchable Gold Thin-Films on Elastomeric Substrates. *Appl. Phys. Lett.* **2009**, *94*, 071902.

(34) Lu, N.; Wang, X.; Suo, Z.; Vlassak, J. Failure by Simultaneous Grain Growth, Strain Localization, and Interface Debonding in Metal Films on Polymer Substrates. *J. Mater. Res.* **2009**, *24*, 379–385.

(35) Ko, H. C.; Stoykovich, M. P.; Song, J.; Malyarchuk, V.; Choi, W. M.; Yu, C.-J.; Geddes, J. B.; Xiao, J.; Wang, S.; Huang, Y.; *et al.* A Hemispherical Electronic Eye Camera Based on Compressible Silicon Optoelectronics. *Nature* **2008**, *454*, 748–753.

(36) Rogers, J. a; Lagally, M. G.; Nuzzo, R. G. Synthesis, Assembly and Applications of Semiconductor Nanomembranes. *Nature* **2011**, *477*, 45–53.

(37) Sekitani, T.; Noguchi, Y.; Hata, K.; Fukushima, T.; Aida, T.; Someya, T. A Rubberlike Stretchable Active Matrix Using Elastic Conductors. *Science (80-.).* **2008**, *321*, 1468–1472.

(38) Wu, H.; Kustra, S.; Gates, E. M.; Bettinger, C. J. Topographic Substrates as Strain Relief Features in Stretchable Organic Thin Film Transistors. *Org. Electron.* **2013**, *14*, 1636.

(39) Lipomi, D. J.; Tee, B. C.-K.; Vosgueritchian, M.; Bao, Z. Stretchable Organic Solar Cells. *Adv. Mater.* **2011**, *23*, 1771.

(40) Müller, C.; Goffri, S.; Breiby, D. W.; Andreasen, J. W.; Chanzy, H. D.; Janssen, R. a. J.; Nielsen, M. M.; Radano, C. P.; Sirringhaus, H.; Smith, P.; *et al.* Tough, Semiconducting Polyethylene-poly(3-Hexylthiophene) Diblock Copolymers. *Adv. Funct. Mater.* **2007**, *17*, 2674–2679.

(41) Hau, S. K.; Yip, H.-L.; Zou, J.; Jen, A. K.-Y. Indium Tin Oxide-Free Semi-Transparent Inverted Polymer Solar Cells Using Conducting Polymer as Both Bottom and Top Electrodes. *Org. Electron.* **2009**, *10*, 1401–1407.

(42) Awartani, O.; Lemanski, B. I.; Ro, H. W.; Richter, L. J.; DeLongchamp, D. M.; O'Connor, B. T. Correlating Stiffness, Ductility, and Morphology of Polymer:Fullerene Films for Solar Cell Applications. *Adv. Energy. Mater.* **2013**, *3*, 399–406.

(43) McCullough, R. D. The Chemistry of Conducting Polythiophenes. *Adv. Mater.* **1998**, *10*, 93–116.

(44) Li, G.; Zhu, R.; Yang, Y. Polymer Solar Cells. *Nat. Photon.* **2012**, *6*, 153–161.

(45) Loewe, R. S.; Khersonsky, S. M.; McCullough, R. D. A Simple Method to Prepare Head-to-Tail Coupled, Regioregular Poly(3-Alkylthiophenes) Using Grignard Metathesis. *Adv. Mater.* **1999**, *11*, 250–253.

(46) Causin, V.; Marega, C.; Marigo, A. Crystallization and Melting Behavior of Poly (3-Butylthiophene), Poly (3-Octylthiophene), and Poly (3-Dodecylthiophene). *Macromolecules* **2005**, *38*, 409–415.

(47) Malik, S.; Nandi, A. Crystallization Mechanism of Regioregular Poly (3-• alkyl Thiophene)s. *J. Polym. Sci., Part B Polym. Phys.* **2002**, *40*, 2073–2085.

(48) Liu, S.; Chung, T. Crystallization and Melting Behavior of Regioregular Poly (3-Dodecylthiophene). *Polymer (Guildf).* **2000**, *41*, 2781–2793.

(49) Park, K. C.; Levon, K. Order−Disorder Transition in the Electroactive Polymer Poly(3-Dodecylthiophene). *Macromolecules* **1997**, *30*, 3175–3183.

(50) Clark, E.; Hoffman, J. Regime III Crystallization in Polypropylene. *Macromolecules* **1984**, *17*, 878–885.

(51) Gurau, M.; Delongchamp, D.; Vogel, B. Measuring Molecular Order in Poly (3-Alkylthiophene) Thin Films with Polarizing Spectroscopies. *Langmuir* **2007**, *23*, 834–842.

(52) Ho, V.; Boudouris, B. W.; Segalman, R. A. Tuning Polythiophene Crystallization through Systematic Side Chain Functionalization. *Macromolecules* **2010**, *43*, 7895–7899.

(53) Park, Y.; Kim, D.; Jang, Y.; Cho, J.; Hwang, M. Effect of Side Chain Length on Molecular Ordering and Field-Effect Mobility in Poly (3-Alkylthiophene) Transistors. *Org. Electron.* **2006**, *7*, 514–520.

(54) McCullough, R. D.; Tristram-Nagle, S.; Williams, S. P.; Lowe, R. D.; Jayaraman, M. Self-Orienting Head-to-Tail poly(3-Alkylthiophenes): New Insights on Structure-Property Relationships in Conducting Polymers. *J. Am. Chem. Soc.* **1993**, *115*, 4910–4911.

(55) Friedel, B.; McNeill, C.; Greenham, N. Influence of Alkyl Side-Chain Length on the Performance of Poly (3-alkylthiophene)/Polyfluorene All-Polymer Solar Cells. *Chem. Mater.* **2010**, *22*, 3389.

(56) Stafford, C. M.; Harrison, C.; Beers, K. L.; Karim, A.; Amis, E. J.; VanLandingham, M. R.; Kim, H.-C.; Volksen, W.; Miller, R. D.; Simonyi, E. E. A Buckling-Based Metrology for Measuring the Elastic Moduli of Polymeric Thin Films. *Nat. Mater.* **2004**, *3*, 545–550.

(57) Bowden, N.; Brittain, S.; Evans, A. G.; Hutchinson, J. W.; Whitesides, G. M.

Spontaneous Formation of Ordered Structures in Thin Films of Metals Supported on an Elastomeric Polymer. *Nature* **1998**, *393*, 146.

(58) Bowden, N.; Huck, W. T. S.; Paul, K. E.; Whitesides, G. M. The Controlled Formation of Ordered, Sinusoidal Structures by Plasma Oxidation of an Elastomeric Polymer. *Appl. Phys. Lett.* **1999**, *75*, 2557.

(59) Cranston, E. D.; Eita, M.; Johansson, E.; Netrval, J.; Salajkova, M.; Arwin, H.; Wagberg, L. Determination of Young's Modulus for Nanofibrillated Cellulose Multilayer Thin Films Using Buckling Mechanics. *Biomacromolecules* **2011**, *12*, 961–969.

(60) Chung, J. Y.; Nolte, A. J.; Stafford, C. M. Surface Wrinkling: A Versatile Platform for Measuring Thin-Film Properties. *Adv. Mater.* **2011**, *23*, 349–368.

(61) Khang, D.-Y.; Xiao, J.; Kocabas, C.; MacLaren, S.; Banks, T.; Jiang, H.; Huang, Y. Y.; Rogers, J. a. Molecular Scale Buckling Mechanics in Individual Aligned Single-Wall Carbon Nanotubes on Elastomeric Substrates. *Nano Lett.* **2008**, *8*, 124.

(62) Nolte, A. J.; Treat, N. D.; Cohen, R. E.; Rubner, M. F. Effect of Relative Humidity on the Young's Modulus of Polyelectrolyte Multilayer Films and Related Nonionic Polymers. *Macromolecules* **2008**, *41*, 5793–5798.

(63) Kuila, B. K.; Nandi, A. K. Structural Hierarchy in Melt-Processed poly(3-Hexyl Thiophene)-Montmorillonite Clay Nanocomposites: Novel Physical, Mechanical, Optical, and Conductivity Properties. *J. Phys. Chem. B* **2006**, *110*, 1621–1631.

(64) Kuila, B. K.; Nandi, A. K. Physical , Mechanical , and Conductivity Properties of Poly (3-Hexylthiophene) -Montmorillonite Clay Nanocomposites Produced by the Solvent Casting Method. *Macromolecules* **2004**, *37*, 8577–8584.

(65) Huang, H.; Chung, J. Y.; Nolte, A. J.; Stafford, C. M. Characterizing Polymer Brushes via Surface Wrinkling. *Chem. Mater.* **2007**, *19*, 6555–6560.

(66) Seitz, J. The Estimation of Mechanical Properties of Polymers from Molecular Structure. *J. Appl. Polym. Sci.* **1993**, *49*, 1331–1351.

(67) Fedors, R. F. A Method for Estimating Both the Solubility Parameters and Molar Volumes of Liquids. Supplement. *Polym. Eng. Sci.* **1974**, *14*, 472–472.

(68) Lee, J. K.; Ma, W. L.; Brabec, C. J.; Yuen, J.; Moon, J. S.; Kim, J. Y.; Lee, K.; Bazan, G. C.; Heeger, A. J. Processing Additives for Improved Efficiency from Bulk Heterojunction Solar Cells. *J. Am. Chem. Soc.* **2008**, *130*, 3619–3623.

(69) Graham, K. R.; Mei, J.; Stalder, R.; Shim, J. W.; Cheun, H.; Steffy, F.; So, F.; Kippelen, B.; Reynolds, J. R. Polydimethylsiloxane as a Macromolecular Additive for Enhanced Performance of Molecular Bulk Heterojunction Organic Solar Cells. *ACS Appl. Mater. Interfaces* **2011**, *3*, 1210–1215.

(70) Nguyen, L. H.; Hoppe, H.; Erb, T.; Günes, S.; Gobsch, G.; Sariciftci, N. S. Effects of Annealing on the Nanomorphology and Performance of Poly(alkylthiophene):Fullerene Bulk-Heterojunction Solar Cells. *Adv. Funct. Mater.* **2007**, *17*, 1071–1078.

(71) Babel, A.; Jenekhe, S. Alkyl Chain Length Dependence of the Field-Effect Carrier Mobility in Regioregular poly(3-Alkylthiophene)s. *Synth. Met.* **2005**, *148*, 169–173.

(72) Vosgueritchian, M.; Lipomi, D. J.; Bao, Z. Highly Conductive and Transparent PEDOT:PSS Films with a Fluorosurfactant for Stretchable and Flexible Transparent Electrodes. *Adv. Funct. Mater.* **2012**, *22*, 421.

(73) Pasquier, A. Du; Miller, S.; Chhowalla, M. On the Use of Ga–In Eutectic and Halogen Light Source for Testing P3HT–PCBM Organic Solar Cells. *Sol. Energ. Mat. Sol. Cells* **2006**, *90*, 1828.

(74) Chiechi, R. C.; Weiss, E. A.; Dickey, M. D.; Whitesides, G. M. Eutectic Gallium-Indium (EGaIn): A Moldable Liquid Metal for Electrical Characterization of Self-Assembled Monolayers. *Angew. Chem. Int. Ed.* **2008**, *47*, 142–144.

(75) Dickey, M. D.; Chiechi, R. C.; Larsen, R. J.; Weiss, E. A.; Weitz, D. A.; Whitesides, G. M. Eutectic Gallium-Indium (EGaIn): A Liquid Metal Alloy for the Formation of Stable Structures in Microchannels at Room Temperature. *Adv. Funct. Mater.* **2008**, *18*, 1097–1104.

(76) Wilder, E. A.; Guo, S.; Lin-Gibson, S.; Fasolka, M. J.; Stafford, C. M. Measuring the Modulus of Soft Polymer Networks via a Buckling-Based Metrology. *Macromolecules* **2006**, *39*, 4138.

(77) Chen, S.; Ni, J.-M. Structure/Properties of Conjugated Conductive Polymers. 1. Neutral Poly(3-Alkyl Thiophene)s. *Macromolecules* **1992**, *25*, 6081.

(78) Aharoni, S. Rigid Backbone Polymers XXI: Stress-Strain Behaviour of Uncrosslinked and of Crosslinked Rodlike Polyisocyanates. *Polymer (Guildf).* **1981**, *22*, 418–419.

(79) Postema, A.; Liou, K.; Wudl, F.; Smith, P. Highly Oriented Low-Modulus Materials from Liquid-Crystalline Polymers: The Ultimate Penalty for Solubilizing Alkyl Side Chains. *Macromolecules* **1990**, *23*, 1842.

(80) Verploegen, E.; Mondal, R.; Bettinger, C. J.; Sok, S.; Toney, M. F.; Bao, Z. Effects of Thermal Annealing Upon the Morphology of Polymer-Fullerene Blends. *Adv. Funct. Mater* **2010**, *20*, 3519.

(81) Waller, J. H.; Lalande, L.; Leterrier, Y.; Månson, J. -a. E. Modelling the Effect of Temperature on Crack Onset Strain of Brittle Coatings on Polymer Substrates. *Thin Solid Films* **2011**, *519*, 4249–4255.

(82) Douville, N. J.; Li, Z.; Takayama, S.; Thouless, M. D. Fracture of Metal Coated Elastomers. *Soft Matter* **2011**, *7*, 6493.

(83) Lu, N.; Wang, X.; Suo, Z.; Vlassak, J. Metal Films on Polymer Substrates Stretched beyond 50%. *Appl. Phys. Lett.* **2007**, *91*, 221909.

(84) Lipomi, D. J.; Lee, J. A.; Vosgueritchian, M.; Tee, B. C.-K.; Bolander, J. A.; Bao, Z. Electronic Properties of Transparent Conductive Films of PEDOT: PSS on Stretchable Substrates. *Chem. Mater.* **2012**, *24*, 373.

(85) Krebs, F. C.; Hösel, M.; Corazza, M.; Roth, B.; Madsen, M. V.; Gevorgyan, S. a.; Søndergaard, R. R.; Karg, D.; Jørgensen, M. Freely Available OPV-The Fast Way to Progress. *Energy Technol.* **2013**, *1*, 378–381.

(86) Sommer-Larsen, P.; Jørgensen, M.; Søndergaard, R. R.; Hösel, M.; Krebs, F. C. It Is All in the Pattern-High-Efficiency Power Extraction from Polymer Solar Cells through High-Voltage Serial Connection. *Energy Technol.* **2013**, *1*, 15–19.

(87) Hösel, M.; Søndergaard, R. R.; Jørgensen, M.; Krebs, F. C. Fast Inline Roll-to-Roll Printing for Indium-Tin-Oxide-Free Polymer Solar Cells Using Automatic Registration. *Energy Technol.* **2013**, *1*, 102–107.

(88) Andersen, T. R.; Dam, H. F.; Andreasen, B.; Hösel, M.; Madsen, M. V.; Gevorgyan, S. a.; Søndergaard, R. R.; Jørgensen, M.; Krebs, F. C. A Rational Method for Developing and Testing Stable Flexible Indium- and Vacuum-Free Multilayer Tandem Polymer Solar Cells Comprising up to Twelve Roll Processed Layers. *Sol. Energ. Mat. Sol. Cells* **2013**, 1–9.

(89) Meitl, M. A.; Zhu, Z.-T.; Kumar, V.; Lee, K. J.; Feng, X.; Huang, Y. Y.; Adesida, I.; Nuzzo, R. G.; Rogers, J. A. Transfer Printing by Kinetic Control of Adhesion to an Elastomeric Stamp. *Nat. Mater.* **2005**, *5*, 33–38.

Chapter 4

Best of both worlds: conjugated polymers exhibiting good photovoltaic behavior and high tensile elasticity

Suchol Savagatrup, [†] Adam D. Printz, [†] Daniel Rodriquez, and Darren J. Lipomi

([†] Equal contribution)

Department of NanoEngineering, University of California, San Diego

9500 Gilman Drive, Mail Code 0448, La Jolla, CA 92093-0448

Abstract

This paper examines a series of poly(3-alkylthiophene)s (P3ATs), a class of materials for which mechanical compliance and electronic performance have been observed to be in competition. P3ATs with longer alkyl side chains ($n \geq 8$) have high elasticity and ductility, but poor electronic performance (as manifested in photovoltaic efficiency in blends with fullerenes); P3ATs with shorter chains ($n \leq 6$) exhibit the opposite characteristics. A series of four polymer films in which the average length of the side chain is $n = 7$ is tested using mechanical, spectroscopic, microscopic, and photovoltaic device-based measurements to determine whether or not it is possible, in principle, to maximize both mechanical and electronic performance in a single organic semiconductor (the "best of both worlds"). The four polymer samples are (1) a physical blend of equal parts P3HT and P3OT (P3HT:P3OT, $n = 6$ and $n = 8$); (2) a block copolymer (P3HT-*b*-P3OT); (3) a random copolymer (P3HT-*co*-P3OT); and (4) poly(3-heptylthiophene) (P3HpT, $n = 7$). The tensile moduli obtained by mechanical buckling correlate well with spectroscopic evidence (using the weakly interacting H-aggregate model) of a well-ordered microstructure of the polymers. The block copolymer was the stiffest of the hybrid samples (680 ± 180 MPa), while P3HpT exhibited maximum compliance (70 ± 10 MPa) and power conversion efficiency in a 1:1 blend with the fullerene $PC_{61}BM$ using stretchable electrodes ($PCE = 2.16 \pm 0.17\%$) that was similar to that of P3HT:$PC_{61}BM$. These analyses may permit the design of organic semiconductors with improved mechanical and electronic properties for mechanically robust and stretchable applications.

4.1 Introduction and background

There is an apparent competition between electronic performance and mechanical compliance in semiconducting polymers.[1–4] We previously observed the increase in elasticity in a series of regioregular poly(3-alkylthiophene)s (P3ATs) with increasing side-chain length (from n = 4 to 12, **Figures 4.1 and 4.2**).[1,2] Various groups have reported the decrease in electronic and photovoltaic properties with increasing side-chain length, including field-effect mobilities[5,6] and power conversion efficiency (*PCE*) in bulk heterojunctions (BHJs) when paired with a polyfluorene copolymer[7] and fullerene.[8] O'Connor and coworkers had reported a similar trend in competition between field-effect mobilities and tensile moduli of various conjugated polymers.[3] This competition has been attributed to the rigid, π-conjugated main chains and the three-dimensionally ordered crystallites generally regarded as beneficial for charge transport.[1–4] These crystallites, however, are correlated with high stiffness and low ductility of the highest-performing pure polymers and—for organic solar cells (OSCs)—polymer:fullerene composites.[1–4] The competing attributes of compliance and performance have significant consequences for the environmental stability of ultra-thin OSCs[9] and devices based on organic thin-film transistors (OTFTs).[10] Beyond the near-term goal of rendering devices already known in the literature more mechanically stable, intrinsically elastic and ductile ("stretchable") semiconductors could find applications in new types of systems, such as wearable and implantable biomedical sensors[11] and in soft robotics.[12] This paper represents an attempt to find the "best of both worlds"—i.e., to co-engineer the mechanical compliance and photovoltaic efficiencies—in a series of regioregular poly(3-alkylthiophene)s (P3ATs), the most-studied class of materials in the field of organic electronics.[13] The lengths of the

alkyl side-chains in P3ATs have very large effects on virtually all mechanical and electronic properties of the materials.[1,5,14] The largest increase in mechanical compliance occurs in a series of P3ATs having between six and eight carbon atoms—poly(3-hexylthiophene) (P3HT) and poly(3-octylthiophene) (P3OT). We thus sought to determine the effect of the length of alkyl side-chain in the "sweet spot" on the elasticity and photovoltaic performance and to attempt to maximize the two parameters. Toward this goal, we obtained or synthesized a series of four materials exhibiting an average side-chain length of n = 7: (1) a physical blend (P3HT:P3OT); (2) a block copolymer (P3HT-*b*-P3OT); (3) a random copolymer (P3HT-*co*-P3OT); and (4) poly(3-heptylthiophene) (P3HpT), whose side chain contains exactly seven carbon atoms (**Figure 4.1**) and its field effect mobility had been reported between those of P3HT and P3OT.[6]

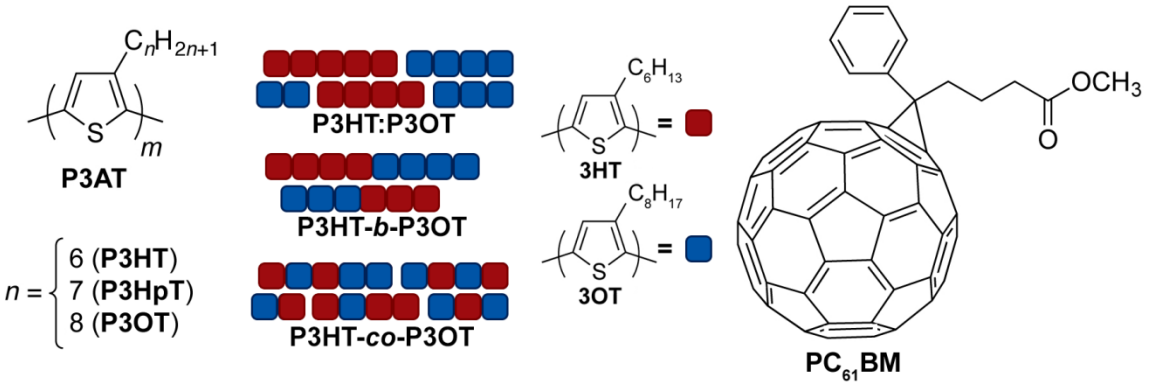

Figure 4.1. Chemical structures and schematic diagrams of the organic semiconductors examined in this paper.

Plastic electronics. The vision of organic electronics has always been to fabricate traditional semiconductor devices using inexpensive materials that can be processed from solution in a roll-to-roll manner.[15–17] The thinness of the active layers (≤200 nm) required to realize applications such as OSCs, OTFTs, and organic light-emitting devices

(OLEDs) permits extremely small bending radii and substantial overall flexibility, as long as the device is fabricated on a sufficiently thin substrate (OSCs with a total thickness of 2 μm have been demonstrated).[16] The strains imposed on materials under bending are rarely >2%, however, and for a material to accommodate substantial tensile strain for integration with ultra-thin substrates,[18] textiles,[19] the moving parts of machines and portable devices,[20] medical prostheses and implants,[11] robotics,[21] and three-dimensional surfaces other than cones and cylinders,[2] significantly more mechanical robustness is required of these nominally plastic semiconductors.[22] The best-performing organic semiconductors—including pentacene, poly[2,5-bis(3-tetradecylthiophen-2-yl)thieno[3,2-*b*]thiophene] (PBTTT), and P3HT:PCBM blends—are stiff (elastic moduli >1 GPa) and brittle (crack-onset strain on elastomeric substrates <2%)[3,23,24]

Electronic properties for organic electronic materials and devices have surpassed or are approaching those of their inorganic counterparts.[25–27] Semiconducting polymers now exhibit ambipolar field-effect mobilities greater than those of amorphous silicon,[25] and organic solar cells have reached efficiencies over ten percent.[28] Studies on roll-to-roll manufacturing suggest that modules can be made at low-cost.[29] While some of the most impressive demonstrations have used high-mobility, low-bandgap polymers,[30] regioregular P3HT is still the archetypal conjugated polymer and serves as a reference point for comparing the properties of new materials.[13] Even though the photovoltaic properties of structurally complex, donor-acceptor copolymers have surpassed those of P3HT (though perhaps not by much[31]), P3HT has significant advantages including synthetic accessibility[32] and low embodied energy,[33] facile functionalization by side-

chain engineering,[14] amenability to block copolymerization,[34] and a band gap that is complementary to modern donor-acceptor copolymers for tandem cells.[26]

While the power conversion efficiency (*PCE*) is frequently the focal point for studies of organic solar cells, the mechanical resiliency is often overlooked. Despite its good photovoltaic performance under ideal conditions,[31] P3HT—especially when combined with $PC_{61}BM$—has been shown to fracture at relatively low applied strains.[1,4,23,24] Our laboratory has shown that small changes in the structure of a conjugated polymer,[35] such as varying the length of the alkyl side chains, can significantly alter the electronic and mechanical properties of the poly(3-alkylthiophene)s (P3ATs).[1,2] For example, increasing the length of the side chain of P3AT from butyl to hexyl decreases the tensile modulus from 1.87 GPa to 1.09 GPa; increasing it further to octyl decreases the modulus to 150 MPa **(Figure 4.2)**.[1] The extreme compliance of P3OT—even in a blend with PCBM[1]—permits it to be strained to conform to hemispherical objects without wrinkling.[2] The elasticity and ductility of P3OT, however, come at a cost of significantly degraded field-effect mobility and photovoltaic efficiency compared to P3HT.[2,5]

Elasticity and ductility are regarded as antithetical to electronic performance; several studies are consistent with this perception. O'Connor et al. noted a correlation between stiffness and charge-carrier mobility in two types of polythiophenes, P3HT and PBTTT.[3] Intercalation of the side-chains in the case of PBTTT led to good vertical registration and a highly crystalline morphology.[3] This ordered microstructure was correlated with good charge transport properties (although high crystallinity is not always a prerequisite for good photovoltaic performance[36]). Poor vertical registration in the case

of P3HT, whose side chains are liquid-like at room temperature, produces a semicrystalline film that is relatively stretchable but has a field-effect mobility that is no longer considered state-of-the art.[3] In another system, Awartani et al. showed that slow evaporation of the solvent during casting of P3HT:$PC_{61}BM$ blends led to greater order of the polymer (as determined by applying the weakly interacting H-aggregate model to UV-vis spectra of the solid films)[37] and greater photovoltaic performance, but also greater stiffness and brittleness.[4] This paper explores the range in side-chain length between n = 6 and n = 8 (**Figure 4.2**) within which we postulated the existence of a "sweet spot" that maximizes mechanical resilience and photovoltaic performance. In particular, we compared the tensile moduli, structure as deduced by ultraviolet-visible (UV-vis) spectroscopy and atomic force microscopy (AFM), and photovoltaic properties (when blended with $PC_{61}BM$) of the six polymeric samples shown in **Figure 4.1**.

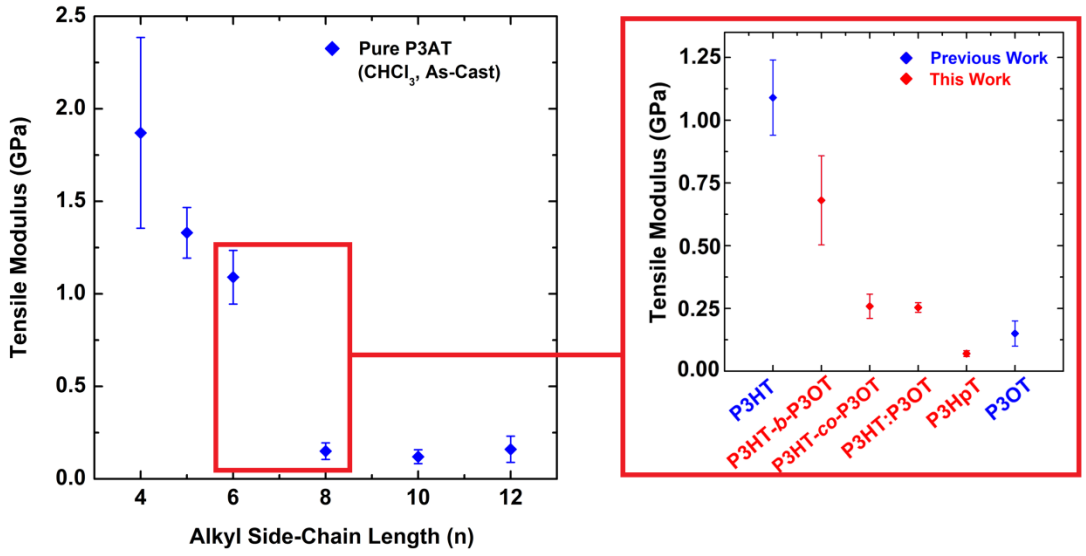

Figure 4.2. Plot of tensile modulus vs. alkyl side-chain length. Tensile moduli of the pure polymer thin films spin-coated from chloroform were measured via buckling methodology. Materials examined for the first time are indicated in red. The "sweet spot" between n = 6–8 is highlighted.

4.2 Experimental design

4.2.1 Selection of materials

P3HT, P3OT, and P3HpT. We chose P3HT because it is the most studied conjugated polymer for organic solar cells.[13,26] The photovoltaic performance of P3HT:$PC_{61}BM$ was used as the benchmark for the performance of all other tested organic photovoltaic devices. P3OT was selected for its low tensile modulus,[1] which is a necessary characteristic for polymers that are to be used in stretchable and flexible electronics. P3HpT was selected because the number of carbons in its alkyl side-chain (seven) is the average of the number of carbons in the alkyl side-chains of P3HT and P3OT. Our initial hypothesis was that the properties of P3HpT would be intermediate between those of P3HT and P3OT.[6]

Block and random copolymers. We also synthesized block and random copolymers having both hexyl and octyl side chains. Jenekhe and coworkers have measured differences in photovoltaic properties between physical blends of P3BT and P3OT and the covalently bonded block and random copolymers.[38,39] The authors found that the copolymers outperformed not only the physical blend, but also the homopolymers.[38,39] We expected that comparison of the properties of a physical blend, and block and random copolymers of P3HT and P3OT would provide insights into the relationship between molecular structure, morphology, and mechanical properties.

4.2.2 Mechanical characterization

Buckling-based metrology. We measured two parameters—the tensile modulus and the crack on-set strain—that permitted comparison of the elasticity and ductility of

each thin film. The tensile moduli were measured using the mechanical buckling technique originally described by Stafford et al.[40] This method provides rapid quantitative measurements and is well suited for analyzing the mechanical properties for various thin-film systems including conjugated polymer films.[1,4,23,24] The technique relates the tensile modulus of the film to the quantitative description of the surface buckling pattern of the film under compressive strains on a relatively compliant substrate—as described originally by Hutchinson, Whitesides, and coworkers.[41,42] The advantages of using the buckling technique are twofold: (1) conventional mechanical testing devices typically lack the sensitivity to measure the forces involved in straining a thin film;[40] and (2) techniques with adequate sensitivity such as nanoindentation do not provide accurate measurement for polymeric materials with viscoelastic behavior.[43] Briefly, the conjugated polymers were spin-coated onto passivated glass slides, then transferred to poly(dimethylsiloxane) (PDMS) substrates each bearing small pre-strain. After transfer, the PDMS substrates were relaxed; this action created a compressive strain that forced the conjugated polymer film to adopt sinusoidal buckles. The buckling wavelength, λ_b, and the thickness of the film, d_f, can be related to the tensile moduli of the film and the substrate, E_f and E_s, and the Poisson ratios of the two materials, v_f and v_s by the following equation:

$$E_f = 3E_s\left(\frac{1-v_f^2}{1-v_s^2}\right)\left(\frac{\lambda_b}{2\pi d_f}\right)^3 \qquad (\mathbf{1})$$

We measured the tensile modulus of the substrate, E_s (using a commercial pull tester), the buckling wavelength, λ_b (by optical microscopy), and the film thickness, d_f (by stylus profilometry). The slope of a plot of λ_b vs. d_f for three different film thicknesses was

inserted into Equation 1. The Poisson's ratios were taken as 0.5 and 0.35 for PDMS and the conjugated polymers films.[1,23] The experimental method is described in detail elsewhere.[1]

Ductility. Crack on-set strains have been shown to provide qualitative measure of the ductility of the thin polymer films,[1,3,4] with the caveat that poor adhesion of the P3AT to PDMS for long alkyl side chains ($n > 8$) leads to increased apparent brittleness.[1] The propensity of the conjugated polymer films to form cracks when stretched on a compliant substrate was measured by transferring the film to the PDMS substrate bearing no pre-strain, which was then stretched uniformly using a computer-controlled actuator. Optical micrographs of each film subjected to the strain of 1% to 80%, with a step size of 1%, were examined for the first sign of crack formation.

4.2.3 Theoretical determination of tensile modulus

We attempted to compare the tensile moduli obtained experimentally to those calculated by a semi-empirical theory that takes into account the chemical structure and thermal properties of the polymers. This approach was originally described by Seitz,[44] applied to conjugated polymers by Tahk et al,[23] and then modified to account for differential glass transition temperatures between polymers.[1] The model successfully predicts the tensile moduli of pure polythiophenes and, in conjunction with composite theory, blends of conjugated polymers with fullerene derivatives.[1,23] However, the simple theory does not account for the sequence of monomers within copolymers, and predicts, for example, the same tensile modulus for both block and random copolymers. A more

sophisticated approach is necessary to describe these copolymers and is being pursued by us in a separate project.

4.2.4 Fabrication of devices

We compared the photovoltaic properties of the various conjugated polymers using $PC_{61}BM$ as the electron acceptor. All conjugated polymer samples—P3HT, P3HpT, P3OT, physical blend (P3HT:P3OT), block copolymer (P3HT-*b*-P3OT), and random copolymer (P3HT-*co*-P3OT)—were mixed with $PC_{61}BM$ in a 1:1 ratio. We deposited a layer of PEDOT:PSS containing 7% DMSO and 0.1% Zonyl fluorosurfactant as the transparent anode.[45] For the top contact, we used a liquid metal cathode, eutectic gallium-indium (EGaIn), extruded manually from a syringe. The use of EGaIn (work function 4.1–4.2 eV) has been reported in the literature to give similar results to those of devices comprising evaporated aluminum.[46–48] We chose EGaIn because it facilitated rapid characterization of our devices and because of our overarching interest in stretchable materials and devices, in which EGaIn is a ubiquitous stretchable conductor.[49]

4.2.5 Weakly interacting H-aggregate model

Order in films of semiconducting polymers is associated with both greater electronic performance and increased stiffness.[3] The extent of order, as determined by UV-vis spectroscopy, has been correlated to increased tensile moduli in P3HT:PCBM films.[4] Spano et al. and others have shown that aggregates of P3HT in solid films can be considered as weakly interacting H-aggregates, due to cofacial π-π stacking and weak excitonic coupling.[4,37,50–53] We used this model to compare trends in conjugation length

from the UV-vis absorption spectra of the polymers, in an attempt to correlate these values with the mechanical stiffness and device performance. The model works as follows. Upon absorption of a photon, an electron is excited from the ground electronic state to an excited electronic state. In H-aggregates, these electronic excitations are coupled with nuclear vibrations.[37] This coupling can be understood by a semi-classical picture, in which the nuclei of the polymer aggregates can be thought of as existing in potential wells with quantized vibrational levels, analogous to an electron trapped in a potential well.[54] At lower vibrational levels, the potential wells can be approximated as harmonic oscillators; in this approximation, the vibrational energy levels are equally spaced.[37,54] In conjugated molecules, such as P3ATs, the vibrational levels arise from the symmetric stretching and ring breathing of the C = C bonds.[4,37,51,53] When an electron is excited, the position of the nuclear potential well in the excited state is shifted from the ground state and the electron and vibrational modes are therefore coupled.[37]

In the aggregated state (i.e., crystallites in solid films), these coupled electron-vibrational (vibronic) transitions determine the adsorption of weakly interactive H-aggregates and can be modeled as Gaussian fits by:[4,37,50,51,53]

$$A(E) \propto \sum_{m=0} \left(\frac{S^m}{m!}\right) \times \left(1 - \frac{We^{-S}}{2E_\mathrm{p}} \sum_{n \neq m} \frac{S^n}{n!\,(n-m)}\right)^2 \times exp\left(\frac{-\left(E - E_{00} - mE_\mathrm{p} - \frac{1}{2}WS^m e^{-S}\right)^2}{2\sigma^2}\right) \quad (\mathbf{2})$$

In the above equation, A is the absorption by an aggregate as a function of the photon energy (E). E_{00} is the energy of the 0→0 vibronic transition, which is allowed assuming some disorder in the aggregates.[37] S is the Huang-Rhys factor, which quantifies the nuclear potential well shift upon vibronic transition from the ground state to the excited state.[37] It is calculated from absorption and emission spectra, and is set to 1 for

P3ATs.[37,51] E_p is the intermolecular vibration energy, which (in the case where $S = 1$) is the difference in energy between the vibrational levels in the excited state. It is set to 0.179 eV as determined by Raman spectroscopy.[55] W is the free exciton bandwidth, which is related to the nearest neighbor interchain excitonic coupling. Upon coupling, a dispersion of the energies occurs, the width of which is equal to W (which is four times the nearest neighbor coupling).[37] W is also inversely related to conjugation length; a lower W indicates better ordering of the aggregates.[50] The terms m and n are the ground- and excited state vibrational levels and σ is the Gaussian linewidth.

4.3. Results and discussion

4.3.1 Characterization of the polymers

After synthesizing P3HT-*b*-P3OT and P3HT-*co*-P3OT, we examined the ^{1}H NMR spectra to estimate the ratios of 3HT and 3OT in the polymers. Because the signals arising from the terminal methyl groups of the hexyl and octyl side-chains were partially overlapped, we estimated the ratio of 3HT and 3OT monomers was the same as the molar ratios of the starting materials, approximately 1:1. The percent regioregularity for each sample was as follows: P3HT, 88%; P3HT-*b*-P3OT, 90%; P3HT-*co*-P3OT, 89%; P3HpT, 92%; P3OT, 82%. While the mechanical properties of most polymeric materials exhibit dependency on the molecular weight, this effect tends to saturate at a sufficiently high molecular weight.[56] Our laboratory has shown that the difference in tensile moduli between the commercial sample of P3HT (M_w = 29,000 g mol^{-1}, PDI = 2.0) and the sample synthesized in-house by the Grignard Metathesis polymerization[57] (M_w = 7500 g mol^{-1}, PDI = 1.2) was minimal: 1.09 ± 0.15 GPa for the commercial sample and 1.05 ±

0.35 GPa for the sample synthesized in-house.[2] Dauskardt and coworkers also reported the dependency of the mechanical properties on molecular weight, and found similar storage and loss moduli for samples with M_w ranging from 28,000 to 100,000 g mol^{-1} (samples with M_w < 28,000 g mol^{-1} were not tested).[58] These data suggest that in the elastic regime, M_w does not significantly affect the tensile moduli for the values of M_w of P3AT samples typically reported in the literature. We assumed covalent connectivity of the blocks in P3HT-*b*-P3OT by following the same synthetic protocol as used in several previous studies on P3AT block copolymers.[38,59–62]

4.3.2 Mechanical properties of pure polymer films

We began the characterization of the mechanical properties of each conjugated polymer by measuring the tensile modulus of the pure polymer film spin-coated from chloroform. In a previous report from our group, we measured decreasing moduli with increasing length of the alkyl side-chain in a series of P3ATs where A = butyl, hexyl, octyl, and dodecyl.[1] **Figure 4.2** and **Table 4.1** show the values obtained for the hybrid polymers on the same set of axes as those obtained in our previous study (we have since added pentyl and decyl to the plot for the purposes of this paper). The tensile moduli of the three individual polymer films containing both hexyl and octyl side-chains—the block and random copolymer and the physical blend—lie in between those of the P3HT and P3OT, as expected; however, the tensile modulus of block (680 ± 180 MPa) was determined to be almost three times those of random (260 ± 50 MPa) and physical blend (250 ± 20 MPa), which were nearly identical. For all three samples, the molar concentration of the 3HT and 3OT were approximately 1:1. We thus attributed the

differences in moduli to unequal microstructures of the three samples in the solid state rather than solely from the ratio of total hexyl and octyl side chains in the samples. Previous work on polymer-polymer blends that exhibit some extent of mutual solubility suggested that the tensile modulus of the blend is the synergistic modulus (weighted average) of the two homopolymers. For example, in the blend of poly(ether ether ketone) (PEEK) and poly(aryl ether sulfone) (PES),[63] and a blend of poly(ether imide) (PEI) and poly(trimethylene terephthalate) (PTT),[64] the authors demonstrated that the tensile moduli of each blend can be plotted against the molar concentration of one of the components to yield a linear relationship. Interestingly, we observed that the modulus of the block copolymer (P3HT-*b*-P3OT) was close to the synergistic modulus, while the moduli of the random copolymer and physical blend lied below (**Figure 4.3a**). To determine if the differences in moduli were attributable to variations in surface morphology, we examined thin films of these polymers by AFM; the results for these experiments are discussed in **section 4.3.5**.

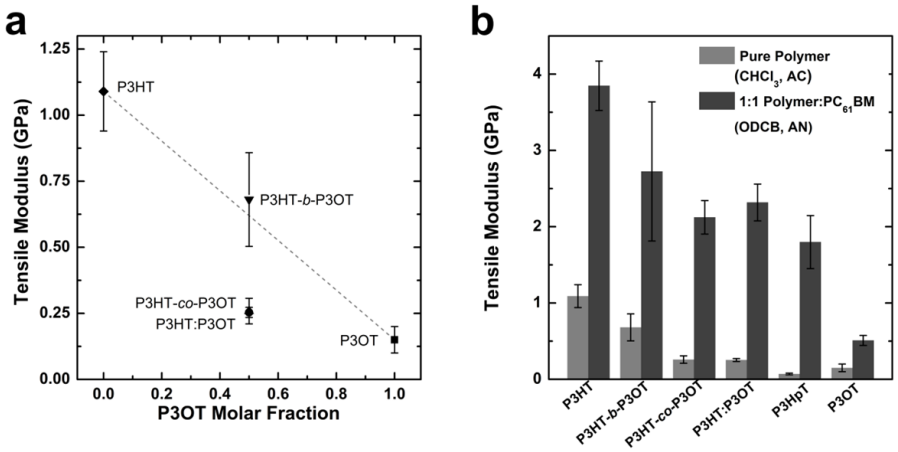

Figure 4.3. Tensile moduli of the polymers and polymer:fullerene blends in this work. **(**a) Tensile moduli of polymer films containing both hexyl and octyl side-chains along with the pure polymers. The dashed line shows the weighted average of the pure polymers. (b) Comparison between the pure polymer films spin-coated from chloroform (as-cast, AC) and the films comprising 1:1 polymer:$PC_{61}BM$ blends spin-coated from ODCB and thermally annealed at 100°C (AN).

Table 4.1. Tensile moduli of pure polymers spin-coated from $CHCl_3$ as-cast and their blends with $PC_{61}BM$ spin-coated from ODCB and thermally annealed at 100°C. *Values taken from ref. 1.

Polymer	**Tensile Modulus (GPa)**	
	Pure polymer ($CHCl_3$, As-Cast)	**1:1 Polymer:$PC_{61}BM$ (ODCB, Annealed)**
P3HT	1.09 ± 0.15 *	3.85 ± 0.32
P3HT-*b*-P3OT	0.68 ± 0.18	2.72 ± 0.91
P3HT-*co*-P3OT	0.26 ± 0.05	2.12 ± 0.22
P3HT:P3OT	0.25 ± 0.02	2.32 ± 0.24
P3HpT	0.07 ± 0.01	1.79 ± 0.35
P3OT	0.15 ± 0.05*	0.51 ± 0.07

Block copolymer. We attributed the higher value of tensile modulus of the block copolymer to the covalent bonds between the P3HT and P3OT segments that promote the formation of connected crystalline domains comprising both P3HT and P3OT. Jenekhe and coworkers observed two distinct interchain (lamellar) spacings by grazing incidence X-ray diffraction (GIXD) in a block copolymer of P3BT (n = 4) and P3OT of equal composition of monomers.[38] These two distinct signals corresponded to the lamellar spacings of the blocks of P3BT and P3OT.[38] We expected that P3HT-*b*-P3OT would behave similarly and form two distinct crystalline domains. Because the domains are covalently linked through the conjugated main chain, the more compliant P3OT phase is bound to the more rigid P3HT phase and thus the block copolymer is less able to accommodate strain than is the physical blend, P3HT:P3OT, discussed in the next paragraph.

Random copolymer. Unlike P3HT-*b*-P3OT, P3HT-*co*-P3OT, which has statistically incorporated monomers, is not likely to form two distinct crystalline domains. In films of a similar copolymer, P3BT-*co*-P3OT, Jenekhe and coworkers observed a single type of crystalline domain whose lamellar spacing correlated with the

ratio of the monomers.[39] The standard model for packing within P3HT crystallites assumes no interdigitation of side chains;[65] although interdigitation has been observed in the oligomer of 3HT with repeat units ≤ 20.[66] The randomness in packing of side chains in the interlamellar regions, along with decreased registration between the lamellae, could contribute to the tensile modulus that was lower for P3HT-*co*-P3OT than for P3HT-*b*-P3OT.

Physical blend. Our next task was to understand the mechanical behavior of the physical blend of P3HT and P3OT (P3HT:P3OT). A tensile modulus for P3HT:P3OT that was lower than the synergistic modulus would be consistent with a blend in which the phases were at least partially separated. In phase-separated blends, the more compliant P3OT phase may accommodate the strain, thus rendering the modulus of the blend closer to that of P3OT. This behavior is in contrast to that of P3HT-*b*-P3OT, in which the covalent connectivity of the domains resists deformation of the film. We note that co-crystallization has been observed in P3HT:P3OT blends by Nandi and coworkers by observation of a single lamellar spacing by X-ray diffraction.[67] The authors found, however, that the tendency to co-crystallize was extremely sensitive to differences in both the ratio of the components and regioregularity between the two isolated polymers.[67]

Poly(3-heptylthiophene). The P3ATs are a class of comb-like polymers[68] whose properties represent a compromise between the rigid main chain and the paraffinic side chains. For many systems, a monotonic decrease in T_g accompanies increasing side-chain length, n, up to a critical side-chain length, n_c. The trend exhibits a discontinuity at n_c, and for $n > n_c$, T_g changes little or even increases.[69] If one defines the critical alkyl side chain length in terms of the tensile modulus, then it appears that $n_c = 7$ for P3ATs, even

though T_g continues to decrease up to at least $n = 12$.[70] The observed modulus of P3HpT (70 ± 10 MPa) is within the same order of magnitude as that of P3OT and P3DDT (**Figure 4.2**).[1] Unlike the copolymers and the physical blend, the compliance of P3HpT cannot be a consequence of the interaction between monomers with different side chains. Our measurement of the modulus of poly(3-pentylthiophene) (P3PT, $n = 5$) (1.33 ± 0.14 GPa) and its placement on the line connecting P3BT and P3HT suggest that the conspicuously low modulus of P3HpT is also not a manifestation of the odd number of carbon atoms in the side chain. While the overall reduction in modulus with increasing n is expected on the basis of a corresponding reduction in T_g and the dilution of volume fraction of the main-chain with increasing length of the alkyl side-chains,[1] the sharp drop in modulus from $n = 6$ to $n = 7$ is nonetheless conspicuous. This drop in modulus is consistent with the fact that P3HpT is the P3AT with the shortest side chains whose T_g is extrapolated to be significantly below room temperature (T_g for P3HT has been measured in the range of 12–25 °C for P3HT and –14 °C for P3OT).[4,71] Our theoretical calculation of the tensile moduli using the molecular structure of the monomers[1,23,35,44] predicted a value for P3HpT (130 ± 20 MPa) that was close to the experimental value (70 ± 10 MPa). This simple model, however, was unable to simulate the moduli for the hybrid polymer samples. We believe that its failure arises from its inability to incorporate the interaction between different polymer chains within the films and the distribution of the monomers in the backbones (in both block and random copolymers).

Ductility. While the theoretical model failed to predict the tensile moduli of the copolymers and the physical blend, the trend in the apparent brittleness agrees well with the experimental values. Our group and others have found that the tensile modulus of

P3AT correlates with brittleness when stretched on a compliant substrate.[1,3,4,24] We measured the strain at which the first crack appeared on the surface of the film (crack on-set strain) of pure polymer films, spin-coated from chloroform without annealing (as-cast, AC). We observed that thin films of P3HT-*b*-P3OT crack at much lower applied strains (8%) than those of P3HT:P3OT and P3HT-*co*-P3OT, whose crack on-set strains are similar (30% and 32% respectively). In addition, P3HpT was observed to have a high crack on-set strain (58%), which was similar to those of P3OT and P3DDT.[1]

4.3.3 Mechanical properties of polymer:$PC_{61}BM$ composites

The presence of fillers has a strong influence on the mechanical properties of composite materials.[1,24] For bulk heterojunction solar cells, polymers are usually blended with fullerene derivatives ($PC_{61}BM$ or $PC_{71}BM$) at a ratio by weight of 1:1 to 1:4 (polymer:fullerene).[26,28] We measured the moduli of polymer:$PC_{61}BM$ films in a 1:1 ratio, which were spin-coated from ODCB and thermally annealed. All samples were annealed at the same temperature (100 °C) for consistency and to decouple the effect of temperature on the mechanical and electronic properties. Various studies have demonstrated that the addition of fullerenes to conjugated polymers produces composites that are stiffer and more brittle than are the pure polymers.[1–3,23,24] We have also previously shown that the moduli of 2:1 blends of P3AT:$PC_{61}BM$ (including P3BT, P3HT, P3OT, and P3DDT) are 2–3 times that of pure P3ATs.[1] The exact factor by which the blend is stiffer than the pure polymer, however, depends strongly on the identity of the polymer[24] and the processing conditions (e.g., as in fast-dried and slow-dried films).[4] A previous report showed that the increase in modulus of a P3HT:$PC_{61}BM$ film over that

of the pure polymer was a factor of approximately five, whereas the increase in modulus of DPPT-TT:$PC_{61}BM$ over the pure polymer was only 40 percent.[24] This behavior suggests that interaction between the polymer and the $PC_{61}BM$ additive depends heavily on the morphologies of the blend, including miscibility of the polymer and the fullerene,[72] intercalation of the fullerene molecules between the side chain of the polymer,[73] and possible formation of bimolecular crystallites.[74] Each of these effects would strongly influence the mechanical properties of the blended films, and we are investigating these effects separately. **Figure 4.3b** and **Table 4.1** show the values of the tensile moduli of polymer blends with $PC_{61}BM$. The P3AT:$PC_{61}BM$ composites are observed to have higher tensile moduli than the pure polymers for all cases. The value of P3HT:$PC_{61}BM$ reported here is similar to those reported previously in literature.[23,24]

4.3.4 Photovoltaic properties

We fabricated photovoltaic devices by mixing the polymers in a 1:1 ratio with $PC_{61}BM$. PEDOT:PSS was used as the transparent anode and eutectic gallium-indium (EGaIn) as the cathode.[46] **Figure 4.4a** shows the current density vs. voltage (*J*–*V*) plots for the devices based on P3AT homopolymers. The P3HT:$PC_{61}BM$ (*PCE* = 2.04 ± 0.27, *N* = 8) and P3OT:$PC_{61}BM$ (*PCE* = 0.67 ± 0.06, *N* = 7) devices performed as expected relative to each other and the results agree with previously published results.[8] The P3OT:$PC_{61}BM$ devices performed poorly due to the low short-circuit current (J_{sc}), 2.71 ± 0.32 mA cm^{-2}, and fill factor (*FF*), 43.7 ± 1.0%. Surprisingly, the performance of P3HpT:$PC_{61}BM$ (*PCE* = 2.16 ± 0.17, *N* = 8) did not fall between these values. Compared to P3HT:$PC_{61}BM$, these devices had a similar J_{sc} (6.95 ± 0.91 for P3HT:$PC_{61}BM$ vs. 6.27

± 0.48 mA cm^{-2} for P3HpT:$PC_{61}BM$), open circuit voltage (V_{oc}) (568 ± 9 vs. 598 ± 5 mV), and *FF* (51.7 ± 1.9 vs. 57.5 ± 1.8 %).

The *J*-*V* plots for the blended and copolymer devices are shown in **Figure 4.4b**. Among these polymers, the physical blend P3HT:P3OT:$PC_{61}BM$ (*PCE* = 1.24 ± 0.21, *N* = 7) performed the poorest, while P3HT-*b*-P3OT:$PC_{61}BM$ (*PCE* = 1.56 ± 0.25, *N* = 8) and P3HT-*co*-P3OT:$PC_{61}BM$ (*PCE* = 1.50 ± 0.19, *N* = 7) performed similarly. The poor performance by the physical blend devices is likely due to its much lower J_{sc} (3.67 ± 0.56 mA cm^{-2}) compared to P3HT-*b*-P3OT:$PC_{61}BM$ (5.80 ± 0.58 mA cm^{-2}) and P3HT-*co*-P3OT:$PC_{61}BM$ (5.19 ± 0.76 mA cm^{-2}). The reduced J_{sc} in the physical blend devices is attributed to the incorporation of P3OT phases, which have a low J_{sc} as shown in the homopolymers devices. The photovoltaic properties for all devices tested are summarized in **Table 4.2**.

Table 4.2. Summary of the averaged J_{sc} (short-circuit current), V_{oc} (open-circuit voltage), *FF* (fill factor), and *PCE* (power conversion efficiency) for the solar cells fabricated in this work ($N \geq 7$). The solar device architecture was PEDOT:PSS/Polymer/$PC_{61}BM$/EGaIn. The active layer was spin-coated from a solution of 1:1 Polymer:$PC_{61}BM$ in ODCB (40 mg mL^{-1}). To ensure the preparation of solar devices was consistent with the preparation of samples for mechanical testing, all devices were annealed at 100 °C in an inert atmosphere.

Polymer	J_{sc} (mA cm^{-2})	V_{oc} (mV)	*FF* (%)	*PCE* (%)
P3HT	6.95 ± 0.91	568 ± 9	51.7 ± 1.9	2.04 ± 0.27
P3HpT	6.27 ± 0.48	598 ± 5	57.5 ± 1.8	2.16 ± 0.17
P3OT	2.71 ± 0.32	570 ± 14	43.7 ± 1.0	0.67 ± 0.06
P3HT:P3OT	3.67 ± 0.56	592 ± 11	57.0 ± 1.6	1.24 ± 0.21
P3HT-*b*-P3OT	5.19 ± 0.76	607 ± 5	49.4 ± 0.5	1.56 ± 0.25
P3HT-*co*-P3OT	5.80 ± 0.58	549 ± 9	47.0 ± 1.6	1.50 ± 0.19

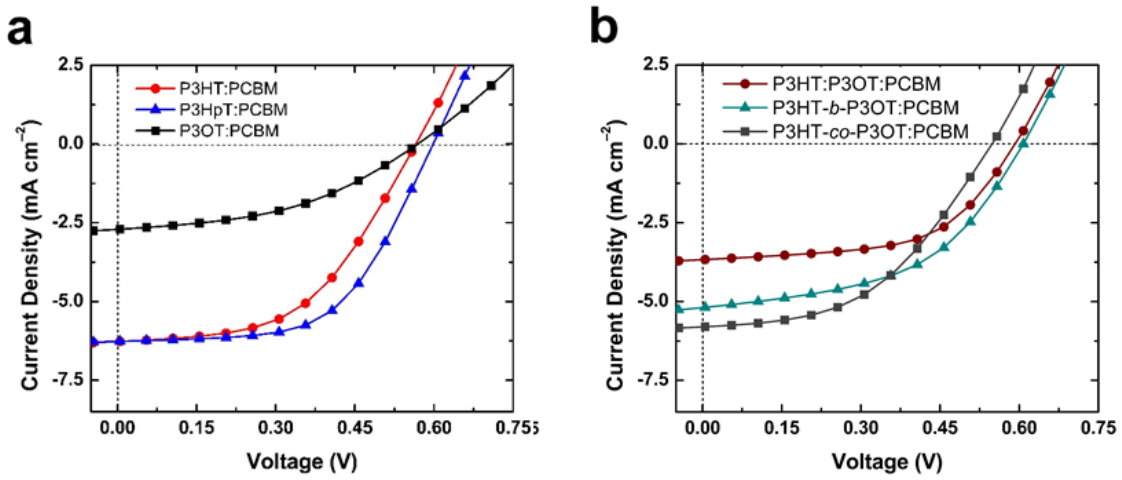

Figure 4.4. *J-V* curves of average devices ($N \geq 7$) with an active layer of 1:1 blend of polymer and $PC_{61}BM$. The architecture of the devices was PEDOT:PSS/polymer:$PC_{61}BM$/EGaIn.

4.3.5 Microstructural characterization of the polymer films

AFM analysis. To determine if the mechanical and photovoltaic properties were due to differences in the morphologies of the films, films of the pure polymers were characterized by atomic force microscopy (AFM). We characterized both as-cast films and films annealed at 100 °C. **Figure 4.5** shows the phase images obtained by AFM for these films. Fibril structures were observed in all as-cast films except for P3OT. Upon annealing, there was an increase in the phase contrast, which is indicative of an increase in order,[75] for all of the polymers except for P3HT-*b*-P3OT and P3HT-*co*-P3OT. The increase in order demonstrated by pure polymers and the physical blend was expected, but the apparent lack of further ordering in the P3HT-*b*-P3OT and P3HT-*co*-P3OT films was surprising. The covalent connectivity of the copolymers might suppress a change in microstructure that is too small to be visible by AFM. For a finer-grained analysis of the evolution in microstructure with annealing, we turned to UV-vis spectrophotometry.

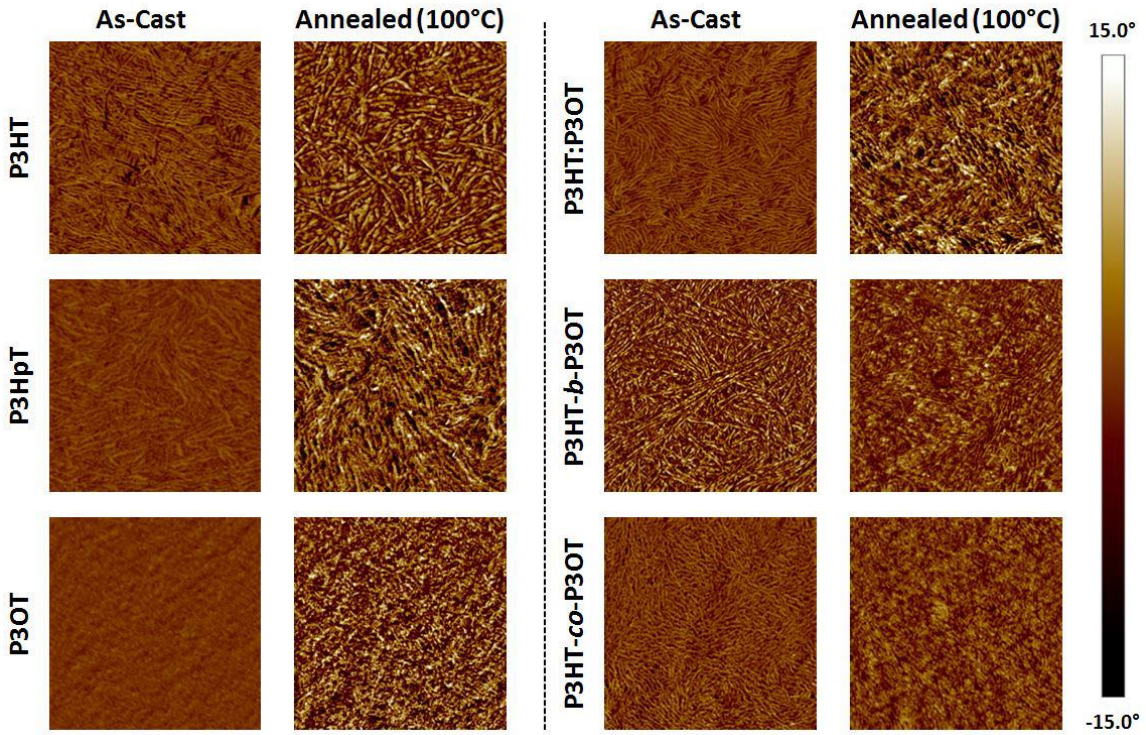

Figure 4.5. Phase images of pure polymers spin-coated from ODCB both as-cast and annealed. The dimensions are 1.5 μm x 1.5 μm.

UV-vis spectrophotometry. To extract information about the relative conjugation lengths of the pure polymers, we characterized them by UV-vis spectrophotometry. The polymers were spin-coated onto glass out of $CHCl_3$ and the absorption of the films was measured over the range 1.46–4.13 eV (λ = 850–300 nm). The UV-vis spectra of the homopolymers are shown in **Figures 4.6a** and **4.6b** and those of the polymer blend and copolymers are shown in **Figures 4.6c** and **4.6d**. The polymers represented in **Figures 4.6a** and **4.6c** were unannealed, while those represented in **Figures 4.6b** and **4.6d** are after annealing at 100 °C in an inert atmosphere. Two observations can be made from visual inspection of these absorption spectra. First, all of the curves for the annealed polymer films have better defined shoulders than their unannealed counterparts. The increase in definition of the shoulders indicates an increase

in order in the polymer films upon annealing.[4,37,50–53] Second, after annealing, P3HT and P3HpT have very similar absorption spectra, which implies similar electronic structures and order in the solid film. The absorption spectrum of P3OT suggests less ordering. The annealed P3HT-*b*-P3OT and P3HT:P3OT samples also have very similar absorption spectra which are consistent with similarly ordered crystallites in the films. Jenehke and coworkers have previously shown that block copolymers of P3BT and P3OT form distinct domains of each polymer.[76] From our analysis, we believe that our samples of P3HT-*b*-P3OT and P3HT:P3OT likely form distinct crystallites of P3HT and P3OT, as these materials have UV-vis spectra that essentially overlap with the superposition of the pure P3HT and P3OT films.

To explore further the effects of annealing on the polymer films, we utilized the weakly interacting H-aggregate model. The absorption spectrum of P3HT, and by extension other P3ATs, can be envisioned as a superposition of the absorption by polymer crystallites and the absorption by the regions of amorphous polymer. The absorption by crystallites dominates the lower energy region, while the absorption at higher energies occurs predominantly by the amorphous polymer.[4] The weakly interacting H-aggregate model was used to deconvolute the absorption spectra and determine the absorption by the polymer aggregates. From this model, we attempted to correlate the conjugation length (from the exciton bandwidth) to mechanical stiffness and device performance. With the Huang-Rhys factor, *S*, set to 1, the exciton bandwidth, *W*, can be calculated from the approximated expression:[50]

$$\frac{A_{0-0}}{A_{0-1}} \approx \left(\frac{1 - 0.24W/E_p}{1 + 0.073W/E_p}\right)^2 \qquad (\mathbf{3})$$

where A_{0-0} and A_{0-1} are the absorption intensities of photons with the energies of the 0→0 and 0→1 vibronic transitions, respectively. Qualitatively, a decrease in the ratio of A_{0-0} to A_{0-1} is related to an increase in local order.[4,37,50] More specifically, W is inversely related to conjugation length and order; a lower W is indicative of a longer conjugation length and better order.[50]

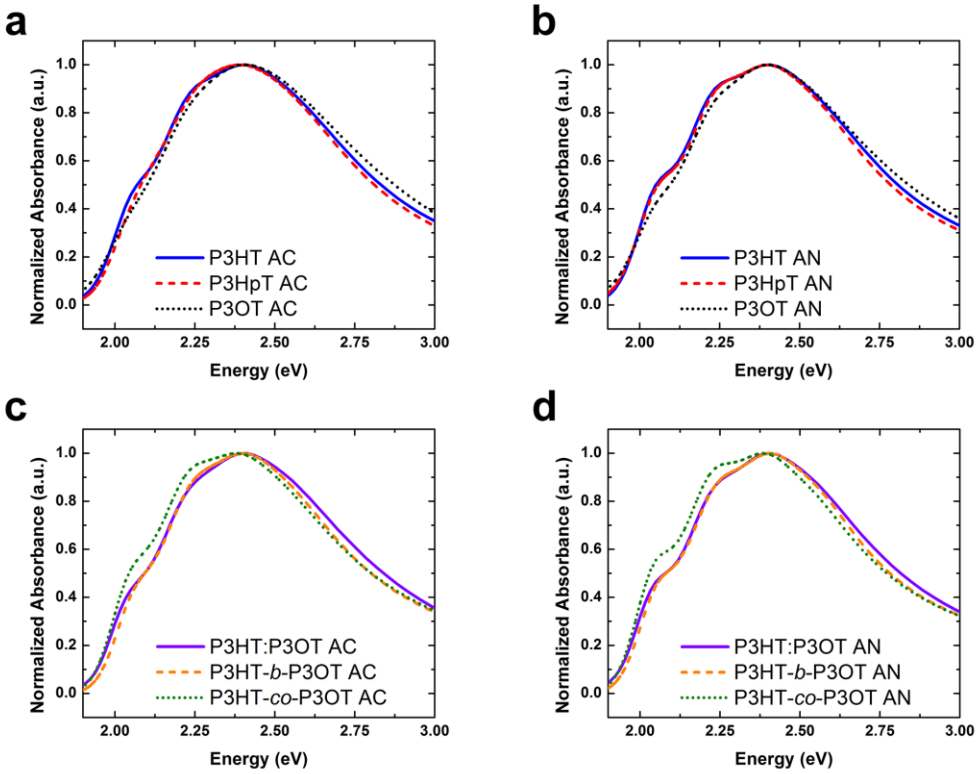

Figure 4.6. Absorption of polymer thin films cast from $CHCl_3$. (a) Homopolymers as-cast (AC). (b) Homopolymers annealed at 100 °C in an inert atmosphere (AN). (c) Blend and copolymers as-cast (AC). (d) Blend and copolymers annealed at 100 °C in an inert atmosphere (AN).

The energy of the 0→0 vibronic transition, E_{00}, was found by calculating the second derivative of the absorption curves using a Matlab program. The same procedure was repeated to find the energy of the 0→1 vibronic transition. The absorption at these energies was then used to calculate the exciton bandwidth, W from Equation 3. The

Gaussian linewidth, σ, and the scaling factor for the calculated absorption were then found by a least squares fit to the experimental absorption in the region of 1.93 to 2.25 eV.[4,53,77] This region was selected because the absorption is dominated by the polymer aggregates. Above 2.30 eV, the amorphous polymer dominates absorption.[51,77] The results are summarized in **Table 4.3**.

Table 4.3. Summary of the weakly interacting H-aggregate model parameters for the polymers in this work. All materials were cast from $CHCl_3$ and then annealed at 100 °C in an inert atmosphere.

Polymer	W (eV)	$1/W$ (eV^{-1})	σ (eV)	E_{00} (eV)	λ_{E00} (nm)
P3HT	0.160	6.250	0.079	2.043	607
P3HpT	0.158	6.335	0.081	2.050	605
P3OT	0.189	5.278	0.091	2.039	608
P3HT:P3OT	0.174	5.762	0.079	2.036	609
P3HT-*b*-P3OT	0.169	5.922	0.079	2.050	605
P3HT-*co*-P3OT	0.145	6.889	0.077	2.039	608

Among the homopolymers cast from chloroform after annealing, we found that the inverse of W, and thus conjugation length, of P3HT is similar to P3HpT and greater than P3OT. These values agree with our observations of the materials in our photovoltaic measurements and suggest that a contributing factor for poor device performance in P3OT is a shorter conjugation length than P3HT (and P3HpT). The conjugation length also appears to fit the trend (but not as strongly) of the tensile moduli of the materials. O'Connor and coworkers first noted the correlation of order derived from UV-vis data with tensile moduli.[4]

4.3.6 Correlations between tensile modulus and photovoltaic performance

We began our investigation motivated by our observations and those of others that mechanical compliance and electronic performance of organic semiconductors were

apparently in competition. Our analysis of four conjugated polymer samples with characteristics that represented different methods of hybridizing P3HT (stiff but good electronic properties) and P3OT (compliant but poor electronic properties) revealed P3HpT as the material that best combined both mechanical compliance and photovoltaic performance. In particular, the similarities of the photovoltaic properties and the order as measured by UV-vis spectroscopy and the H-aggregate model are largely manifestations of the crystalline regions in a polymer film, which were of similar extent in both P3HT and P3HpT. The mechanical properties for a material operating above its T_g, however, are largely manifestations of the amorphous regions of a polymer. The relatively long side chains of P3HpT and P3OT tend to suppress T_g well below room temperature, and provide increased elasticity and ductility compared to P3HT. The effect of blending $PC_{61}BM$ into polymers to form bulk heterojunctions is to increase the modulus of the polymer:fullerene composite relative to that of the pure polymer. Because the fullerenes exist in fullerene-rich and mixed phases (they do not intercalate into the crystalline phases of P3ATs), the increase in modulus is most likely dependent on the solubility of the fullerene in the amorphous regions of the polymer, which in turn depends at minimum on the length of the alkyl side chain. While the field has recently achieved an impressive model of the morphology of the bulk heterojunction,[78–80] additional work will be required to develop a composite theory that predicts accurately the mechanical properties of these types of blends. **Figure 4.7** presents our best evidence that combining mechanical compliance and electronic performance in the same material is possible in principle. That is, P3HpT lies in the extreme corner of the quadrant that combines favorable mechanical and electronic properties, as manifested in good photovoltaic

properties in blends with fullerenes. While the P3HpT:$PC_{61}BM$ blend is considerably stiffer than is the pure polymer, $PC_{61}BM$ is not the only acceptor that can be used in organic solar cells; it is likely that blending P3ATs with other acceptors will produce composites with mechanical properties that are far different from polymer:fullerene blends.

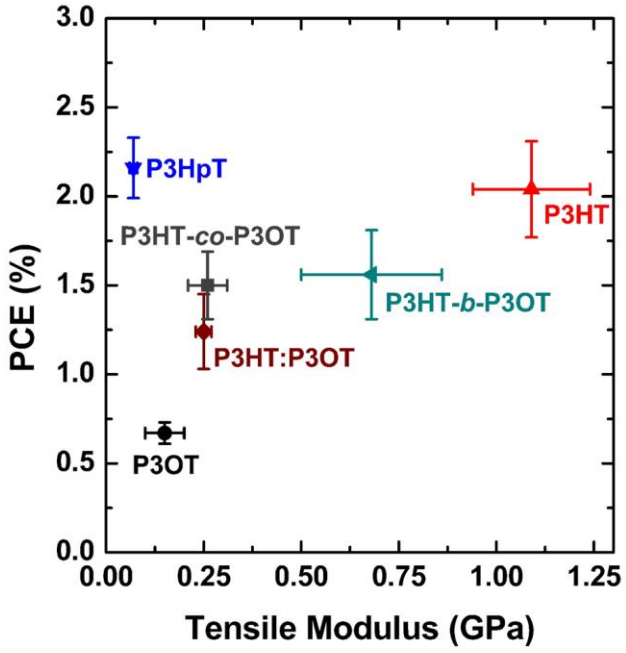

Figure 4.7. Plot of tensile moduli of the pure polymers vs. power conversion efficiency of the polymers in a 1:1 blend with $PC_{61}BM$. The position of P3HpT well above and to the left of the line connecting P3HT and P3OT suggest that in principle it is possible to co-engineer mechanical and photovoltaic properties in a single material.

4.4. Conclusion

This paper described our efforts to synthesize or discover a conjugated polymer that exhibited high values of mechanical compliance and electronic performance manifested in good photovoltaic properties using P3ATs as the model organic semiconductor. We discovered a very large effect of the alkyl side chain (between six and eight carbon atoms) in determining the mechanical and electronic properties. In

particular, we found that polythiophene with side chains containing seven carbon atoms, P3HpT, exhibited the optimal combination of mechanical compliance and photovoltaic efficiency. Examination of the mechanical and photovoltaic properties of the block and random copolymers and a physical blend of P3HT and P3OT revealed that the block copolymer exhibited the synergistic (average) modulus, while the random copolymer and physical blend did not.

Our findings may provide insights toward the design and synthesis of organic semiconductors that combine state-of-the-art electronic properties with extreme softness. It also highlights the critical role played by small changes (from six to seven carbon atoms in the alkyl side chain) in determining the bulk and electronic properties of these materials. Our work on copolymers exposed the shortcoming in a common semi-empirical approach to predicting the moduli of semiconducting polymers in its inability to differentiate the spatial distribution of unlike monomers (block vs. random copolymers with identical mole fractions of the components). Understanding of the role of chemical structure on the mechanical properties of organic semiconductors could lead the way toward truly multifunctional materials with tunable properties.

4.5. Experimental methods

4.5.1 Materials

Poly(3-pentylthiophene), Poly(3-heptylthiophene), and Poly(3-decylthiophene) were purchased from Rieke Metals, Inc. and used as received. Poly(3-hexylthiophene) and poly(3-octylthiophene) were purchased from Sigma-Aldrich and used as received. 3-Hexylthiophene and 3-octylthiophene were purchased from TCI and used as received.

Dichlorobistriphenylphosphinopropane nickel(II) was purchased from Strem. [6,6]-phenyl C_{61} butyric acid methyl ester ($PC_{61}BM$) was obtained from Sigma-Aldrich with >99% purity. PDMS, Sylgard 184 (Dow Corning), was prepared according to the manufacturer's instructions at a ratio of 10:1 (base:crosslinker) and cured at room temperature for 36 to 48 h before it was used for mechanical testing. (Tridecafluoro-1,1,2,2-tetrahydrooctyl)-1-trichlorosilane (FOTS) was obtained from Gelest. PEDOT:PSS (Clevios PH1000) was purchased from Heraeus. DMSO was purchased from BDH with purity of 99.9% and Zonyl (FS-300) fluorosurfactant were purchased from Sigma-Aldrich. All reagents were obtained from commercial suppliers and used without purification. Chloroform ($CHCl_3$), ortho-dichlorobenzene (ODCB), acetone, isopropyl alcohol (IPA), methanol, hexanes, and tetrahydrofuran (THF) were obtained from Sigma-Aldrich and used as received.

4.5.2 Synthesis of block and random copolymers

P3HT-*b*-P3OT. Poly(3-octylthiophene)-block-poly(3-hexylthiophene) (P3OT-*b*-P3HT, "block"). In the first round-bottom flask (flask A), a solution of 2,5-dibromo-3-octylthiophene (2.00 g, 5.65 mmol) was prepared in THF (60 mL) at ambient temperature. To this solution was added isopropyl magnesium chloride (4.5 mL of a 1.3 M solution in THF, 5.65 mmol). A suspension of $Ni(dppp)Cl_2$ (61 mg, 0.113 mmol, in 10 mL THF) was added by syringe in one portion. The polymerization proceeded to produce a dark red solution that fluoresced red-orange when illuminated with a long-wave ultraviolet lamp. This reaction was allowed to proceed for 10 min. Meanwhile, in a separate round-bottom flask (flask B), a solution of 2,5-dibromo-3-hexylthiophene (1.84

g, 5.65 mmol) was prepared in THF (60 mL). This solution was treated with isopropyl magnesium chloride (4.5 mL of a 1.3 M solution in THF, 5.65 mmol). After the 10 min reaction time in flask A, the contents of flask B were added to flask A by syringe. The combined solution was allowed to stir for 3 h. The reaction mixture was quenched by pouring into 400 mL of methanol. The quenched mixture was poured into centrifuge tubes, spun at 2.5 krpm, and decanted. The pellets were combined, placed on filter paper, and inserted into a Soxhlet extractor. The material was washed with methanol and hexanes, and extracted with chloroform. The chloroform fraction was concentrated in vacuo to give 562 mg (16% yield) of a red solid. ^{1}H NMR (300 MHz, $CDCl_3$): δ (ppm) = 7 (s, 1H), 2.92-2.45 (br, 2H), 1.82-1.63 (br, 2H), 1.54-1.23 (br ovlp, 8H), 0.94 (t ovlp, approx. 1.5H), 0.91 (t ovlp, approx. 1.5H).

P3HT-*co*-P3OT. Poly(3-octylthiophene)-co-poly(3-hexylthiophene) (P3OT-*co*-P3HT, "random"). In a round-bottom flask, a solution of 2,5-dibromo-3-octylthiophene (2.00 g, 5.65 mmol) and 2,5-dibromo-3-hexylthiophene (1.84 g, 5.65 mmol) was prepared in THF (120 mL) at ambient temperature. To this solution was added isopropyl magnesium chloride (9.0 mL of a 1.3 M solution in THF, 11.3 mmol). A suspension of Ni(dppp)Cl_2 (122 mg, 0.113 mmol, in 10 mL THF) was added by syringe in one portion. The reaction was allowed to stir for 3 h, then quenched and purified in the manner described for the block copolymer. The chloroform fraction was concentrated in vacuo to give 693 mg (18% yield) of a red solid. ^{1}H NMR (300 MHz, $CDCl_3$): δ (ppm) = 7 (s, 1H), 2.92-2.45 (br, 2H), 1.82-1.63 (br, 2H), 1.54-1.23 (br ovlp, 8H), 0.94 (t ovlp, approx. 1.5H), 0.91 (t ovlp, approx. 1.5H).

4.5.3 Preparation of substrates

Glass slides used as substrates for solar devices were cut into 1-in squares with a diamond-tipped scribe. They were then subsequently cleaned with Alconox solution (2 mg mL^{-1}), deionized water, acetone, and then isopropyl alcohol (IPA) in an ultrasonic bath for 10 min each and then rinsed and dried with compressed air. Next, the glass was plasma treated at ~30 W for 3 min at a base pressure of 200 mtorr ambient air to remove residual organic material and activate the surface.

Glass slides used as substrates for thin films for UV/vis spectrophotometry measurements were cut into 1-in squares with a diamond-tipped scribe. The slides were then rinsed with water and ultrasonicated in IPA for 20 min. The slides were then rinsed with IPA and dried by compressed air. Next the glass was plasma treated as described above. Blanks used to subtract the absorption of the glass were cleaned in the same manner.

Silicon substrates used for AFM measurements were cut into 1-cm^2 pieces. To remove debris from the surfaces, the silicon substrates were ultrasonicated in acetone for 10 min, followed by IPA for 10 min and subsequently rinsed with IPA and then dried with compressed air. The wafers were then plasma treated as described above.

4.5.4 Preparation of polymer solutions

Solutions of P3HT, P3HpT, P3OT, and hybrid materials of P3HT and P3OT (physical blend, random copolymer, and block copolymer) in $CHCl_3$ (15 mg ml^{-1}) were prepared for the buckling technique and UV-vis. Solutions of the polymers in ODCB (20 mg ml^{-1}) were prepared for AFM, and 1:1 polymer:$PC_{61}BM$ solutions in ODCB (40 mg

ml^{-1}) were prepared for solar cells. All solutions were allowed to stir overnight and filtered with a 1-μm glass microfiber (GMF) syringe filter immediately before being spin-coated onto glass or silicon substrates.

4.5.5 Fabrication of solar cells

We deposited a layer of PEDOT:PSS from an aqueous solution containing 92.9 wt% Clevios PH 1000 (~0.9-1.2 wt% PEDOT:PSS), 7.0 wt% DMSO, and 0.1 wt% Zonyl fluorosurfactant as the transparent anode. The solution was filtered with a 1-μm glass microfiber syringe filter and then spin-coated at a speed of 500 rpm (250 rpm s^{-1} ramp) for 60 s, followed by 2000 rpm (750 rpm s^{-1} ramp) for 60 s. The samples were subsequently dried at 150 °C for 30 minutes. The photoactive layer was then spin-coated onto the electrode layer at a speed of 500 rpm (250 rpm s^{-1} ramp) for 240 s, followed by 2000 rpm (750 rpm s^{-1} ramp) for 60 s. A thin strip of the PEDOT:PSS electrode was exposed by wiping away some of the photoactive layer with chloroform so that electrical contact could be made. The samples were then immediately placed in a nitrogen-filled glovebox and annealed at 100 °C for 30 min. The substrates were then allowed to cool slowly to room temperature. EGaIn (extruded by hand from a syringe) was used as the top contact. The photovoltaic properties were measured in a nitrogen-filled glovebox using a solar simulator with a 100 mW cm^{-2} flux that approximated the solar spectrum under AM 1.5G conditions (ABET Technologies 11016-U up-facing unit calibrated with a reference cell with a KG5 filter). The current density versus voltage was measured for both dark and under illumination using a Keithley 2400 SourceMeter.

4.5.6 Characterization of materials

The absorbance of the materials was measured using a PerkinElmer Lambda 1050 UV-vis-NIR spectrophotometer. The wavelength range measured was 850–300 nm with a step size of 1 nm. The polymer solutions were spin-coated onto the glass slides at a spin speed of 500 rpm (250 rpm s^{-1} ramp) for 240 s followed by 2000 rpm (750 rpm s^{-1} ramp) for 60 s. For each solution, two films were prepared. The first film was left as-cast and the second film was immediately placed in a nitrogen-filled glove box and annealed at 100 °C for 30 min under a Pyrex petri dish covered in aluminum foil. After 30 min, the samples were allowed to slowly cool back down to room temperature.

Atomic Force Microscopy (AFM) micrographs were taken using a Veeco Scanning Probe Microscope in tapping mode. Data was analyzed with NanoScope Analysis v1.40 software (Bruker Corp.). The samples were prepared in the same manner as the samples for UV-vis, except the substrates used were Si pieces.

All compounds were characterized by ^{1}H NMR (300 MHz, Varian) using $CDCl_3$ as the solvent. The residual chloroform peak at 7.26 ppm was used to calibrate the chemical shifts.

Acknowledgements

This work was supported by the Air Force Office of Scientific Research (AFOSR) Young Investigator Program, grant number FA9550–13–1–0156. Additional support was provided by the National Science Foundation Graduate Research Fellowship under Grant No. DGE-1144086, awarded to S.S., by Initiative for Maximizing Student Development awarded to D.R., and by laboratory startup funds from the University of California, San

Diego. The authors thank Prof. Brendan O'Connor, Prof. Frank Spano, and Prof. Paul Smith for helpful discussions.

Chapter 4, in full, is a reprint of the material as it appears in *Macromolecules*, 2014, 47, 1981. American Chemical Society, 2014. Suchol Savagatrup,[†] Adam D. Printz,[†] Daniel Rodriquez, and Darren J. Lipomi. ([†] Equal contribution). The dissertation author was the primary investigator and author of this paper.

References

(1) Savagatrup, S.; Makaram, A. S.; Burke, D. J.; Lipomi, D. J. Mechanical Properties of Conjugated Polymers and Polymer-Fullerene Composites as a Function of Molecular Structure. *Adv. Funct. Mater.* **2014**, *24*, 1169–1181.

(2) O'Connor, T. F.; Zaretski, A. V.; Shiravi, B. A.; Savagatrup, S.; Printz, A. D.; Diaz, M. I.; Lipomi, D. J. Stretching and Conformal Bonding of Organic Solar Cells to Hemispherical Surfaces. *Energy Environ. Sci.* **2014**, *7*, 370–378.

(3) O'Connor, B.; Chan, E. P.; Chan, C.; Conrad, B. R.; Richter, L. J.; Kline, R. J.; Heeney, M.; McCulloch, I.; Soles, C. L.; DeLongchamp, D. M. Correlations between Mechanical and Electrical Properties of Polythiophenes. *ACS Nano* **2010**, *4*, 7538–7544.

(4) Awartani, O.; Lemanski, B. I.; Ro, H. W.; Richter, L. J.; DeLongchamp, D. M.; O'Connor, B. T. Correlating Stiffness, Ductility, and Morphology of Polymer:Fullerene Films for Solar Cell Applications. *Adv. Energy Mater.* **2013**, *3*, 399–406.

(5) Babel, A.; Jenekhe, S. A. Alkyl Chain Length Dependence of the Field-Effect Carrier Mobility in Regioregular poly(3-Alkylthiophene)s. *Synth. Met.* **2005**, *148*, 169–173.

(6) Salammal, S.; Mikayelyan, E.; Grigorian, S.; Pietsch, U.; Koenen, N.; Scherf, U.; Brinkmann, M.; Kayunkid, N. Impact of Thermal Annealing on the Semicrystalline Nanomorphology of Spin-Coated Thin Films of Regioregular Poly (3-Alkylthiophene) S as Observed by High-Resolution Transmission Electron Microscopy and Grazing Incidence X-Ray Diffraction. *Macromolecules* **2012**, *45*, 5575–5585.

(7) Friedel, B.; McNeill, C.; Greenham, N. Influence of Alkyl Side-Chain Length on the Performance of Poly (3-alkylthiophene)/Polyfluorene All-Polymer Solar Cells. *Chem. Mater.* **2010**, *22*, 3389–3398.

(8) Nguyen, L. H.; Hoppe, H.; Erb, T.; Günes, S.; Gobsch, G.; Sariciftci, N. S. Effects of Annealing on the Nanomorphology and Performance of Poly(alkylthiophene):Fullerene Bulk-Heterojunction Solar Cells. *Adv. Funct. Mater.* **2007**, *17*, 1071–1078.

(9) Dupont, S. R.; Voroshazi, E.; Heremans, P.; Dauskardt, R. H. Adhesion Properties of Inverted Polymer Solarcells: Processing and Film Structure Parameters. *Org. Electron.* **2013**, *14*, 1262–1270.

(10) Sokolov, A. N.; Cao, Y.; Johnson, O. B.; Bao, Z. Mechanistic Considerations of Bending-Strain Effects within Organic Semiconductors on Polymer Dielectrics. *Adv. Funct. Mater.* **2012**, *22*, 175–183.

(11) Ghezzi, D.; Antognazza, M. R.; Maccarone, R.; Bellani, S.; Lanzarini, E.; Martino, N.; Mete, M.; Perile, G.; Bisti, S.; Lanzani, G.; Benfenati, F. A Polymer Optoelectronic Interface Restores Light Sensitivity in Blind Rat Retinas. *Nat. Photonics* **2013**, *7*, 400–406.

(12) Ilievski, F.; Mazzeo, A. Soft Robotics for Chemists. *Angew. Chem. Int. Ed.* **2011**, *50*, 1890–1895.

(13) Brinkmann, M. Structure and Morphology Control in Thin Films of Regioregular poly(3-Hexylthiophene). *J. Polym. Sci. Part B Polym. Phys.* **2011**, *49*, 1218–1233.

(14) Mei, J.; Bao, Z. Side Chain Engineering in Solution-Processable Conjugated Polymers. *Chem. Mater.* **2014**, *26*, 604–615.

(15) Krebs, F.; Gevorgyan, S.; Alstrup, J. A Roll-to-Roll Process to Flexible Polymer Solar Cells: Model Studies, Manufacture and Operational Stability Studies. *J. Mater. Chem.* **2009**, *19*, 5442.

(16) Kaltenbrunner, M.; White, M. S.; Głowacki, E. D.; Sekitani, T.; Someya, T.; Sariciftci, N. S.; Bauer, S. Ultrathin and Lightweight Organic Solar Cells with High Flexibility. *Nat. Commun.* **2012**, *3*, 770.

(17) Rogers, J. A.; Someya, T.; Huang, Y. Materials and Mechanics for Stretchable Electronics. **2010**, *327*, 1603–1607.

(18) Kaltenbrunner, M.; Sekitani, T.; Reeder, J.; Yokota, T.; Kuribara, K.; Tokuhara, T.; Drack, M.; Schwödiauer, R.; Graz, I.; Bauer-Gogonea, S.; Bauer, S.; Someya,

T. An Ultra-Lightweight Design for Imperceptible Plastic Electronics. *Nature* **2013**, *499*, 458–463.

(19) Krebs, F.; Tromholt, T.; Jørgensen, M. Upscaling of Polymer Solar Cell Fabrication Using Full Roll-to-Roll Processing. *Nanoscale* **2010**, *2*, 873–886.

(20) Lipomi, D. J.; Bao, Z. Stretchable, Elastic Materials and Devices for Solar Energy Conversion. *Energy Environ. Sci.* **2011**, *4*, 3314–3328.

(21) Martinez, R. V; Branch, J. L.; Fish, C. R.; Jin, L.; Shepherd, R. F.; Nunes, R. M. D.; Suo, Z.; Whitesides, G. M. Robotic Tentacles with Three-Dimensional Mobility Based on Flexible Elastomers. *Adv. Mater.* **2013**, *25*, 205–212.

(22) Suo, Z.; Ma, E.; Gleskova, H.; Wagner, S. Mechanics of Rollable and Foldable Film-on-Foil Electronics. *Appl. Phys. Lett.* **1999**, *74*, 1177.

(23) Tahk, D.; Lee, H. H.; Khang, D.-Y. Elastic Moduli of Organic Electronic Materials by the Buckling Method. *Macromolecules* **2009**, *42*, 7079–7083.

(24) Lipomi, D. J.; Chong, H.; Vosgueritchian, M.; Mei, J.; Bao, Z. Toward Mechanically Robust and Intrinsically Stretchable Organic Solar Cells: Evolution of Photovoltaic Properties with Tensile Strain. *Sol. Energy Mater. Sol. Cells* **2012**, *107*, 355–365.

(25) Chen, Z.; Lee, M. J.; Shahid Ashraf, R.; Gu, Y.; Albert-Seifried, S.; Meedom Nielsen, M.; Schroeder, B.; Anthopoulos, T. D.; Heeney, M.; McCulloch, I.; Sirringhaus, H. High-Performance Ambipolar Diketopyrrolopyrrole-thieno[3,2-B]thiophene Copolymer Field-Effect Transistors with Balanced Hole and Electron Mobilities. *Adv. Mater.* **2012**, *24*, 647–652.

(26) Dou, L.; You, J.; Hong, Z.; Xu, Z.; Li, G.; Street, R. A.; Yang, Y. 25Th Anniversary Article: A Decade of Organic/Polymeric Photovoltaic Research. *Adv. Mater.* **2013**, *25*, 6642–6671.

(27) McCulloch, I.; Heeney, M.; Bailey, C.; Genevicius, K.; Macdonald, I.; Shkunov, M.; Sparrowe, D.; Tierney, S.; Wagner, R.; Zhang, W.; Chabinyc, M. L.; Kline, R. J.; McGehee, M. D.; Toney, M. F. Liquid-Crystalline Semiconducting Polymers with High Charge-Carrier Mobility. *Nat. Mater.* **2006**, *5*, 328–333.

(28) Li, G.; Zhu, R.; Yang, Y. Polymer Solar Cells. *Nat. Photonics* **2012**, *6*, 153–161.

(29) Sommer-Larsen, P.; Jørgensen, M.; Søndergaard, R. R.; Hösel, M.; Krebs, F. C. Fast Inline Roll-to-Roll Printing for Indium-Tin-Oxide-Free Polymer Solar Cells Using Automatic Registration. *Energy Technol.* **2013**, *1*, 102–107.

(30) Facchetti, A. Π-Conjugated Polymers for Organic Electronics and Photovoltaic Cell Applications †. *Chem. Mater.* **2011**, *23*, 733–758.

(31) Liao, S.-H.; Li, Y.-L.; Jen, T.-H.; Cheng, Y.-S.; Chen, S.-A. Multiple Functionalities of Polyfluorene Grafted with Metal Ion-Intercalated Crown Ether as an Electron Transport Layer for Bulk-Heterojunction Polymer Solar Cells: Optical Interference, Hole Blocking, Interfacial Dipole, and Electron Conduction. *J. Am. Chem. Soc.* **2012**, *134*, 14271–14274.

(32) Osedach, T. P.; Andrew, T. L.; Bulović, V. Effect of Synthetic Accessibility on the Commercial Viability of Organic Photovoltaics. *Energy Environ. Sci.* **2013**, *6*, 711–718.

(33) Anctil, A.; Babbitt, C. W.; Raffaelle, R. P.; Landi, B. J. Cumulative Energy Demand for Small Molecule and Polymer Photovoltaics. *Prog. Photovolt Res. Appl.* **2013**, *21*, 1541–1554.

(34) Scherf, U.; Gutacker, A.; Koenen, N. All-Conjugated Block Copolymers. *Acc. Chem. Res.* **2008**, *41*, 1086–1097.

(35) Printz, A. D.; Savagatrup, S.; Burke, D. J.; Purdy, T. N.; Lipomi, D. J. Increased Elasticity of a Low-Bandgap Conjugated Copolymer by Random Segmentation for Mechanically Robust Solar Cells. *RSC Adv.* **2014**, *4*, 13635–13643.

(36) Pearson, A. J.; Wang, T.; Dunbar, A. D. F.; Yi, H.; Watters, D. C.; Coles, D. M.; Staniec, P. A.; Iraqi, A.; Jones, R. A. L.; Lidzey, D. G. Morphology Development in Amorphous Polymer:Fullerene Photovoltaic Blend Films During Solution Casting. *Adv. Funct. Mater.* **2014**, *24*, 659–667.

(37) Spano, F. C. Modeling Disorder in Polymer Aggregates: The Optical Spectroscopy of Regioregular poly(3-Hexylthiophene) Thin Films. *J. Chem. Phys.* **2005**, *122*, 234701.

(38) Ren, G.; Wu, P.-T.; Jenekhe, S. a. Enhanced Performance of Bulk Heterojunction Solar Cells Using Block Copoly(3-Alkylthiophene)s. *Chem. Mater.* **2010**, *22*, 2020–2026.

(39) Wu, P.-T.; Ren, G.; Jenekhe, S. a. Crystalline Random Conjugated Copolymers with Multiple Side Chains: Tunable Intermolecular Interactions and Enhanced Charge Transport and Photovoltaic Properties. *Macromolecules* **2010**, *43*, 3306–3313.

(40) Stafford, C. M.; Harrison, C.; Beers, K. L.; Karim, A.; Amis, E. J.; VanLandingham, M. R.; Kim, H.-C.; Volksen, W.; Miller, R. D.; Simonyi, E. E. A

Buckling-Based Metrology for Measuring the Elastic Moduli of Polymeric Thin Films. *Nat. Mater.* **2004**, *3*, 545–550.

(41) Bowden, N.; Brittain, S.; Evans, A. G.; Hutchinson, J. W.; Whitesides, G. M. Spontaneous Formation of Ordered Structures in Thin Films of Metals Supported on an Elastomeric Polymer. *Nature* **1998**, *393*, 146–149.

(42) Bowden, N.; Huck, W. T. S.; Paul, K. E.; Whitesides, G. M. The Controlled Formation of Ordered, Sinusoidal Structures by Plasma Oxidation of an Elastomeric Polymer. *Appl. Phys. Lett.* **1999**, *75*, 2557–2559.

(43) VanLandingham, M. R.; Villarrubia, J. S.; Guthrie, W. F.; Meyers, G. F. Nanoindentation of Polymers: An Overview. *Macromol. Symp.* **2001**, *167*, 15–43.

(44) Seitz, J. The Estimation of Mechanical Properties of Polymers from Molecular Structure. *J. Appl. Polym. Sci.* **1993**, *49*, 1331–1351.

(45) Vosgueritchian, M.; Lipomi, D. J.; Bao, Z. Highly Conductive and Transparent PEDOT:PSS Films with a Fluorosurfactant for Stretchable and Flexible Transparent Electrodes. *Adv. Funct. Mater.* **2012**, *22*, 421–428.

(46) Pasquier, A. Du; Miller, S.; Chhowalla, M. On the Use of Ga–In Eutectic and Halogen Light Source for Testing P3HT–PCBM Organic Solar Cells. *Sol. Energy Mater. Sol. Cells* **2006**, *90*, 1828–1839.

(47) Chiechi, R. C.; Weiss, E. A.; Dickey, M. D.; Whitesides, G. M. Eutectic Gallium-Indium (EGaIn): A Moldable Liquid Metal for Electrical Characterization of Self-Assembled Monolayers. *Angew. Chem. Int. Ed. Engl.* **2008**, *47*, 142–144.

(48) Dickey, M. D.; Chiechi, R. C.; Larsen, R. J.; Weiss, E. A.; Weitz, D. A.; Whitesides, G. M. Eutectic Gallium-Indium (EGaIn): A Liquid Metal Alloy for the Formation of Stable Structures in Microchannels at Room Temperature. *Adv. Funct. Mater.* **2008**, *18*, 1097–1104.

(49) Palleau, E.; Reece, S.; Desai, S. C.; Smith, M. E.; Dickey, M. D. Self-Healing Stretchable Wires for Reconfigurable Circuit Wiring and 3D Microfluidics. *Adv. Mater.* **2013**, *25*, 1589–1592.

(50) Clark, J.; Chang, J.-F.; Spano, F. C.; Friend, R. H.; Silva, C. Determining Exciton Bandwidth and Film Microstructure in Polythiophene Films Using Linear Absorption Spectroscopy. *Appl. Phys. Lett.* **2009**, *94*, 163306.

(51) Clark, J.; Silva, C.; Friend, R.; Spano, F. Role of Intermolecular Coupling in the Photophysics of Disordered Organic Semiconductors: Aggregate Emission in Regioregular Polythiophene. *Phys. Rev. Lett.* **2007**, *98*, 206406.

(52) Spano, F. C.; Clark, J.; Silva, C.; Friend, R. H. Determining Exciton Coherence from the Photoluminescence Spectral Line Shape in poly(3-Hexylthiophene) Thin Films. *J. Chem. Phys.* **2009**, *130*, 074904.

(53) Turner, S. T.; Pingel, P.; Steyrleuthner, R.; Crossland, E. J. W.; Ludwigs, S.; Neher, D. Quantitative Analysis of Bulk Heterojunction Films Using Linear Absorption Spectroscopy and Solar Cell Performance. *Adv. Funct. Mater.* **2011**, *21*, 4640–4652.

(54) Turro, N. J. *Modern Molecular Photochemistry*; 1st ed.; University Science Books: Sausalito, CA, 1991.

(55) Louarn, G.; Trznadel, M. Raman Spectroscopic Studies of Regioregular Poly (3-Alkylthiophenes). *J. Phys. Chem.* **1996**, *3654*, 12532–12539.

(56) Nielsen, L. E.; Landel, R. F. *Mechanical Properties of Polymers and Composites*; CRC Press; Rev and Expanded edition, 1993.

(57) McCullough, R. D. The Chemistry of Conducting Polythiophenes. *Adv. Mater.* **1998**, *10*, 93–116.

(58) Bruner, C.; Dauskardt, R. Role of Molecular Weight on the Mechanical Device Properties of Organic Polymer Solar Cells. *Macromolecules* **2014**, *47*, 1117–1121.

(59) Verswyvel, M.; Monnaie, F.; Koeckelberghs, G. AB Block Copoly(3-Alkylthiophenes): Synthesis and Chiroptical Behavior. *Macromolecules* **2011**, *44*, 9489–9498.

(60) Ge, J.; He, M.; Qiu, F.; Yang, Y. Synthesis, Cocrystallization, and Microphase Separation of All-Conjugated Diblock Copoly(3-Alkylthiophene)s. *Macromolecules* **2010**, *43*, 6422–6428.

(61) Ge, J.; He, M.; Yang, X.; Ye, Z.; Liu, X.; Qiu, F. Microphase Separation-Promoted Crystallization in All-Conjugated poly(3-Alkylthiophene) Diblock Copolymers with High Crystallinity and Carrier Mobility. *J. Mater. Chem.* **2012**, *22*, 19213–19221.

(62) He, M.; Zhao, L.; Wang, J.; Han, W.; Yang, Y.; Qiu, F.; Lin, Z. Self-Assembly of All-Conjugated Poly(3-Alkylthiophene) Diblock Copolymer Nanostructures from Mixed Selective Solvents. *ACS Nano* **2010**, *4*, 3241–3247.

(63) Nandan, B.; Kandpal, L. D.; Mathur, G. N. Poly(ether Ether ketone)/Poly(aryl Ether Sulfone) Blends: Relationships between Morphology and Mechanical Properties. *J. Appl. Polym. Sci.* **2003**, *90*, 2887–2905.

(64) Ramiro, J.; Equiazabal, J. I.; Nazabal, J. Synergistic Mechanical Behaviour and Improved Processability of Poly(ether Imide) by Blending with Poly(trimethylene Terephthalate). *Polym. Advan. Technol.* **2003**, *14*, 129–136.

(65) Chen, T.; Wu, X.; Rieke, R. Regiocontrolled Synthesis of Poly (3-Alkylthiophenes) Mediated by Rieke Zinc: Their Characterization and Solid-State Properties. *J. Am. Chem. Soc.* **1995**, *117*, 233–244.

(66) Koch, F. P. V.; Heeney, M.; Smith, P. Thermal and Structural Characteristics of Oligo (3-Hexylthiophene) S (3HT) N, N= 4–36. *J. Am. Chem. Soc.* **2013**, *135*, 13699–13709.

(67) Pal, S.; Nandi, A. K. Cocrystallization Behavior of Poly(3-Alkylthiophenes): Influence of Alkyl Chain Length and Head to Tail Regioregularity. *Macromolecules* **2003**, *36*, 8426–8432.

(68) Plate, N. A.; Shibaev, V. P. Comblike Polymers. Structure and Properties. *J. Polym. Sci. Macromol. Rev.* **1974**, *8*, 117–253.

(69) Reimschuessel, H. K. On the Glass Transition Temperature of Comblike Polymers: Effects of Side Chain Length and Backbone Chain Structure. *J. Polym. Sci. Polym. Chem. Ed.* **1979**, *17*, 2447–2457.

(70) Chen, S.; Ni, J.-M. Structure/Properties of Conjugated Conductive Polymers. 1. Neutral Poly(3-Alkyl Thiophene)s. *Macromolecules* **1992**, *25*, 6081–6089.

(71) Kim, J. Y.; Frisbie, C. D. Correlation of Phase Behavior and Charge Transport in Conjugated Polymer/Fullerene Blends. *J. Phys. Chem. C* **2008**, *112*, 17726–17736.

(72) Treat, N.; Mates, T.; Hawker, C. Temperature Dependence of the Diffusion Coefficient of PCBM in Poly (3-Hexylthiophene). *Macromolecules* **2013**, *46*, 1002–1007.

(73) Koppe, M.; Scharber, M.; Brabec, C.; Duffy, W.; Heeney, M.; McCulloch, I. Polyterthiophenes as Donors for Polymer Solar Cells. *Adv. Funct. Mater.* **2007**, *17*, 1371–1376.

(74) Kline, R. J.; McGehee, M. D.; Kadnikova, E. N.; Liu, J.; Frechet, J. M. J.; Toney, M. F. Dependence of Regioregular Poly (3-Hexylthiophene) Film Morphology and Field-Effect Mobility on Molecular Weight. *Macromolecules* **2005**, *38*, 3312–3319.

(75) Brinkmann, M.; Wittmann, J.-C. Orientation of Regioregular Poly(3-Hexylthiophene) by Directional Solidification: A Simple Method to Reveal the

Semicrystalline Structure of a Conjugated Polymer. *Adv. Mater.* **2006**, *18*, 860–863.

(76) Wu, P.-T.; Xin, H.; Kim, F. S.; Ren, G.; Jenekhe, S. A. Regioregular Poly(3-Pentylthiophene): Synthesis, Self-Assembly of Nanowires, High-Mobility Field-Effect Transistors, and Efficient Photovoltaic Cells. *Macromolecules* **2009**, *42*, 8817–8826.

(77) Pingel, P.; Zen, A. Temperature Resolved Local and Macroscopic Charge Carrier Transport in Thin P3HT Layers. *Adv. Funct. Mater.* **2010**, *20*, 2286–2295.

(78) Roehling, J. D.; Batenburg, K. J.; Swain, F. B.; Moulé, A. J.; Arslan, I. Three-Dimensional Concentration Mapping of Organic Blends. *Adv. Funct. Mater.* **2013**, *23*, 2115–2122.

(79) Liu, F.; Gu, Y.; Shen, X.; Ferdous, S.; Wang, H.-W.; Russell, T. P. Characterization of the Morphology of Solution-Processed Bulk Heterojunction Organic Photovoltaics. *Prog. Polym. Sci.* **2013**, *38*, 1990–2052.

(80) Brady, M. A.; Su, G. M.; Chabinyc, M. L. Recent Progress in the Morphology of Bulk Heterojunction Photovoltaics. *Soft Matter* **2011**, *7*, 11065–11077.

Chapter 5

Viability of stretchable poly(3-heptylthiophene) (P3HpT) for organic solar cells and field-effect transistors

Suchol Savagatrup,[†a] Adam D. Printz,[†a] Haosheng Wu,[b] Kirtana M. Rajan,[a] Eric J. Sawyer,[a] Aliaksandr V. Zaretski,[a] Christopher J. Bettinger,[b] and Darren J. Lipomi[a]

([†] Equal contribution)

[a] *Department of NanoEngineering, University of California, San Diego, 9500 Gilman Drive Mail Code 0448, La Jolla, CA 92093-0448.*

[b] *Department of Materials Science and Engineering, Carnegie Mellon University, 5000 Forbes Hall, Pittsburgh, PA, 15213-3890.*

Abstract

Mechanical compliance is a critical attribute for organic semiconductors in flexible, stretchable, mechanically robust, and biologically integrated electronics. This paper substantially develops the observation that a small change in the length of the alkyl side chain of regioregular poly(3-alkylthiophene)s has a dramatic effect on the interplay between their mechanical and charge-transport properties. Specifically, the thermal, mechanical, and charge-transport properties of poly(3-heptylthiophene) (P3HpT, n = 7), which we found to be an unusual example of a stretchable semiconducting thermoplastic, are described in comparison to those of poly(3-hexylthiophene) (P3HT, n = 6) and poly(3-octylthiophene) (P3OT, n = 8). Neat P3HpT was found to have mechanical properties similar to that of P3OT, and when mixed in 1:1 blends with the fullerene [6,6]-phenyl C_{61} butyric acid methyl ester (PCBM), exhibited electronic properties comparable to P3HT. However, the charge-carrier mobility of neat P3HpT is substantially inferior to that of P3HT; the good performance of P3HpT-based solar cells is the result of improved mobility in P3HpT:PCBM blends compared to the neat material. While P3HpT may be a favorable alternative to P3HT in ultra-flexible, stretchable, and mechanically robust organic solar cells, P3HpT would only make a good field-effect transistor in situations in which mechanical compliance was more important than high mobility.

5.1 Introduction

Given the vast literature devoted to the regioregular poly(3-alkylthiophenes) (P3ATs), it may seem that every aspect of the chemical, physical, and optoelectronic properties of this class of materials have been characterized exhaustively. This paper

shows that a small change in the length of the alkyl side chain—in the range of $6 \leq n \leq 8$—nevertheless has profound effects on these properties, in particular the flexibility, stretchability, and resistance to mechanical failure of devices. The mechanical properties of organic semiconductors are highly variable and sensitive to small molecular and microstructural changes.[1–4] Moreover, there is substantial evidence that suggests that good charge-transport and mechanical compliance are mutually exclusive properties.[5,6] We recently reported the tensile moduli of a series of P3AT homopolymers and copolymers and their power conversion efficiencies (*PCEs*) when combined in 1:1 blends with [6,6]-phenyl C_{61} butyric acid methyl ester (PCBM) in organic solar cells (OSCs).[2] We found that the tensile moduli of the thin films (E_f) exhibited a drop-off of more than one order of magnitude when the length of the side chain was increased from six carbon atoms—as in poly(3-hexylthiophene) (P3HT, E_f = 1.0 GPa) the workhorse of organic electronics—to seven carbon atoms, as in poly(3-heptylthiophene) (P3HpT, E_f = 0.07 GPa).[2] Spectroscopic evidence using the weakly interacting H-aggregate model showed similarities in the level of order between P3HT and P3HpT, and both materials exhibited similar photovoltaic performance. The good performance of P3HpT, especially in the context of OSCs, suggested to us that P3HpT could be useful in applications that demand mechanical flexibility, stretchability, and robustness (that is, some applications of organic semiconductors that currently use P3HT). The purpose of this paper is to develop substantially our previous finding by characterizing the thermal, mechanical, photovoltaic, and charge-transport properties of P3HpT in comparison to P3HT and poly(3-octylthiophene) (P3OT) for pure films (*i.e.*, for thin-film transistors) and when blended with PCBM (*i.e.*, for solar cells, **Figure 5.1a**). Our measurements point to

seemingly minor changes in the chemical structure of polymers that can have dramatic effects on their physical properties. We found that P3HpT is in fact an unusual example of a stretchable semiconducting thermoplastic. While we believe P3HpT is an excellent candidate to replace P3HT in OSCs, its high mobility in this context seems to be the result of blending with fullerenes. In pure form, as required for organic thin-film transistors, the material is more elastic and ductile than P3HT, but the charge-carrier mobility of P3HpT is inferior to that of P3HT.

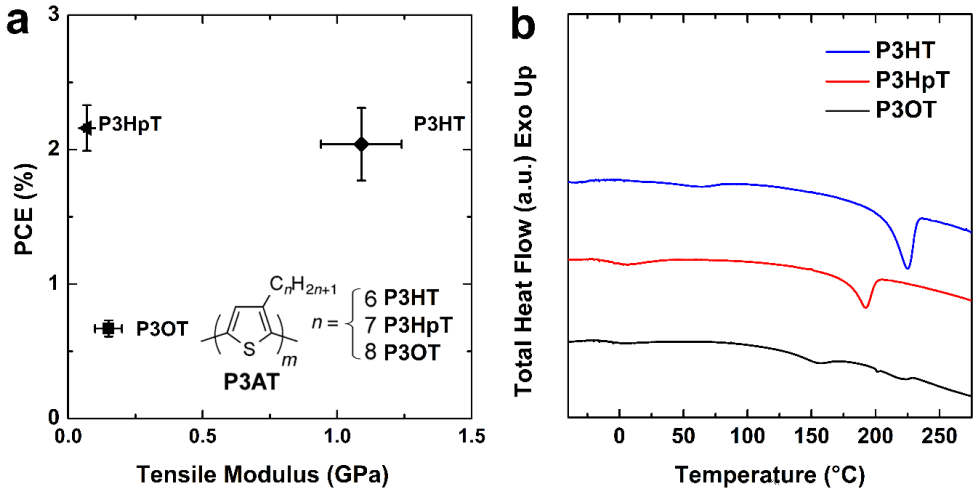

Figure 5.1. Mechanical, electronic, and thermal properties of the P3ATs in this work. (a) Plot of power conversion efficiency of the P3ATs in a 1:1 blend with $PC_{61}BM$ vs. tensile moduli of the pure polymers. The position of P3HpT well above and to the left of the line connecting P3HT and P3OT suggests the possibility of co-optimization of photovoltaic and mechanical properties (data reproduced from ref. 2) (b) DSC thermograms of representative P3HT, P3HpT, and P3OT samples at a heating rate of 10 °C min^{-1}. The chemical structures are inset in the figure. T_g values of 11 to 13 °C were determined for P3HT, –5 to –4 °C for P3HpT, and –10 to –8 °C for P3OT. T_m values were observed at 225, 192, and 155 °C for P3HT, P3HpT, and P3OT respectively.

5.2 Results and discussion

5.2.1 Characterization of the polymers

P3HT, P3HpT, and P3OT were examined for regioregularity and purity using ^1H NMR spectra. The percent regioregularity for each sample was as follows: P3HT, 88%;

P3HpT, 92%; and P3OT, 82%. We observed no additional peaks beside those expected (**Figure B.1,** Supporting Information). From size-exclusion chromatography, we determined that the molecular weights of the polymers are as follows: P3HT, M_n = 44 kDa, PDI = 2.0; P3HpT, M_n = 35 kDa, PDI = 1.5; and P3OT, M_n = 34 kDa, PDI = 2.5.

5.2.2 Thermal properties

The intuitive rationale for the increase in elasticity and ductility measured as a function of increasing length of the side chain P3AT (a comb-like polymer) is a reduction in the density of load-bearing carbon-carbon bonds along the main chain per cross sectional area.[1,7] The glass transition temperature (T_g) for comb-like polymers also decreases with increasing length of the side chain until a critical value, after which T_g remains roughly constant or even increases.[8] Long side chains installed for solubility on otherwise rigid backbone structures thus have deleterious consequences for polymers intended for structural applications.[9] For flexible and stretchable organic devices, however, high compliance (low tensile modulus) is desirable. Values of T_g in the literature occupy a wide range of values for P3HT, but it seems that the consensus value is equal to or slightly less than room temperature (*i.e.*, 15–25 °C, though our experience is that research laboratories are often kept at temperatures significantly below 25 °C).[5] The value for P3OT is unequivocally below room temperature,[10] and we have used the ductility of P3OT:PCBM composites at ambient temperature to stretch, conform, and bond whole OSCs to hemispherical surfaces without generating cracks or wrinkles.[11]

We used differential scanning calorimetry (DSC, **Figure 5.1b**) to measure the T_g and melting temperature (T_m) of P3HpT (red curve) and compared it to those of P3HT

(blue curve) and P3OT (black curve). From the analysis of the total heat flow for the heating of the pure polymer samples, we found values of T_g between 11 and 13 °C for P3HT, –5 and –4 °C for P3HpT, and –10 and –8 °C for P3OT. These data are consistent with decreasing T_g with increasing length of the side chain, and that T_g is substantially below room temperature for P3HpT and P3OT. The melting temperatures, T_m, also decreased with increasing length of the side chain, which agreed with previously reported results.[12] We note that the values of T_g found in literature can vary significantly due to the different heating rates employed and the thermal history of the sample. The relationship of T_g for P3HpT and P3OT to ambient temperature suggests that these materials can be treated as stretchable semiconducting thermoplastics. Our experience with OSCs based on either P3HpT or P3OT, however, suggest that the two polymers have significantly different semiconducting performance.

The addition of fullerene to P3HT has previously been reported to produce a greater T_g in the blend compared to that of the neat polymer.[13] We reasoned that this increase in T_g would occur in all P3ATs, and that the good photovoltaic performance of P3HpT:PCBM might be produced concomitantly with anti-plasticization of P3HpT by PCBM. To determine if the T_g of the P3ATs increased significantly with the addition of PCBM, we analysed the total heat flow for the P3AT:PCBM samples. We found the T_g of P3HT:PCBM increased to the range between 37 and 40 °C, which agrees with previously reported results,[14] and the T_g of P3OT:PCBM increased to the range between –5 and 0 °C. Interestingly, the T_g of P3HpT:PCBM increased to the range between 33 and 35 °C, which is close to that of P3HT:PCBM. The similarity in T_g between P3HT:PCBM and P3HpT:PCBM is consistent with their similar photovoltaic properties.[2]

5.2.3 Band structure

Increasing the length of the side chain in P3ATs has a very small effect on the bandgap, however, with a side chain longer than n = 6, the absolute positions of the frontier molecular orbitals decrease in energy (become more negative relative to the vacuum level).[15] To verify this trend previously identified in the literature for P3ATs with an even number of carbon atoms in the side chains,[15] we measured the positions of the HOMOs for the three P3ATs by cyclic voltammetry. The onset of oxidation for P3HT, P3HpT, and P3OT can be seen in **Figure 5.2a**, which reveals a linear dependence on ionization potential with the length of the side chain. To determine the LUMO, we added the optical band gap, $E_{g,opt}$, and 0.3 eV to the HOMO. The 0.3 eV is added because it is the typical difference between the optical and electrochemical band gaps, previously attributed to the exciton binding energy.[16] The absorption spectra of the solid films, shown in **Figure 5.2b**, reveal similar onsets of absorption, 1.92–1.94 eV (639–646 nm). The spectra also show better order in P3HT and P3HpT compared to P3OT. The optical and electrochemical properties of the P3ATs are summarized in **Table 5.1**. We initially hypothesized that similar order when n = 6 or 7 would produce similar charge-carrier mobilities, though the effect of unequal T_g between P3HT and P3HpT could also have an effect.

Table 5.1. Optical and electrochemical properties of the P3ATs.

Polymer	E_{ox} **(V)**	**HOMO** [a] **(eV)**	$E_{g,opt}$ **(eV)**	**LUMO** [b] **(eV)**
P3HT	0.54	–5.25	1.94	–3.01
P3HpT	0.68	–5.39	1.92	–3.17
P3OT	0.75	–5.46	1.92	–3.24

[a] HOMO = –e(E_{ox} + 4.71) (eV) [b] LUMO = $E_{g,opt}$ + 0.3 + HOMO (eV)

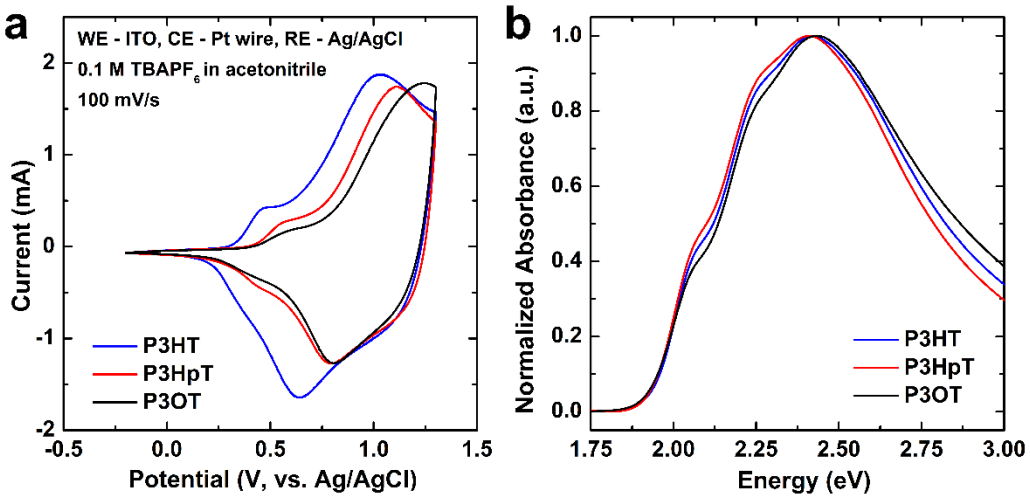

Figure 5.2. Determination of the HOMO and LUMO for P3HT, P3HpT, and P3OT. (a) Cyclic voltammetry oxidation curves measured at a scan rate of 100 mV/s. (b) Absorption spectra of the polymer thin films on ITO and annealed at 100 °C for 30 min.

5.2.4 Charge transport properties

The good charge-transport properties of P3ATs are generally attributed to the semicrystalline morphology in which well ordered aggregates (observed spectroscopically or by X-ray diffraction) have been correlated with high hole mobilities in organic thin-film transistors (OTFTs) and good efficiencies in OSCs.[5,17] To compare directly the field-effect hole mobility, μ_h, for P3HT, P3HpT, and P3OT, we fabricated bottom-gate, bottom-contact thin-film transistors with the dimensions of 500 µm (width) and 10 µm (length). **Figures 5.3a, 5.3b,** and **5.3c** show the output plots and **Figure 5.3d** shows the transfer plots for P3HT, P3HpT, and P3OT. The field effect mobilities, μ_h, were extracted from the slopes of the linear fits in the saturation regime on the plots of $(-I_{DS})^{1/2}$ vs. V_{GS} (**Figure 5.3d**), and the threshold voltages, V_T, were extracted from the interception of the linear fits and the x-axis using the following equation,[18,19]

$$\sqrt{I_{DS}} = \sqrt{\mu_h C_d \frac{W}{2L}} (V_{GS} - V_T) \quad (1)$$

where C_d = 1.38 × 10^{-8} F cm^{-2}, W = 500 µm, and L = 10 µm. The mobilities, threshold voltage, and on-off ratios extracted from the current-voltage characteristics for the three materials are listed in **Table 5.2**.

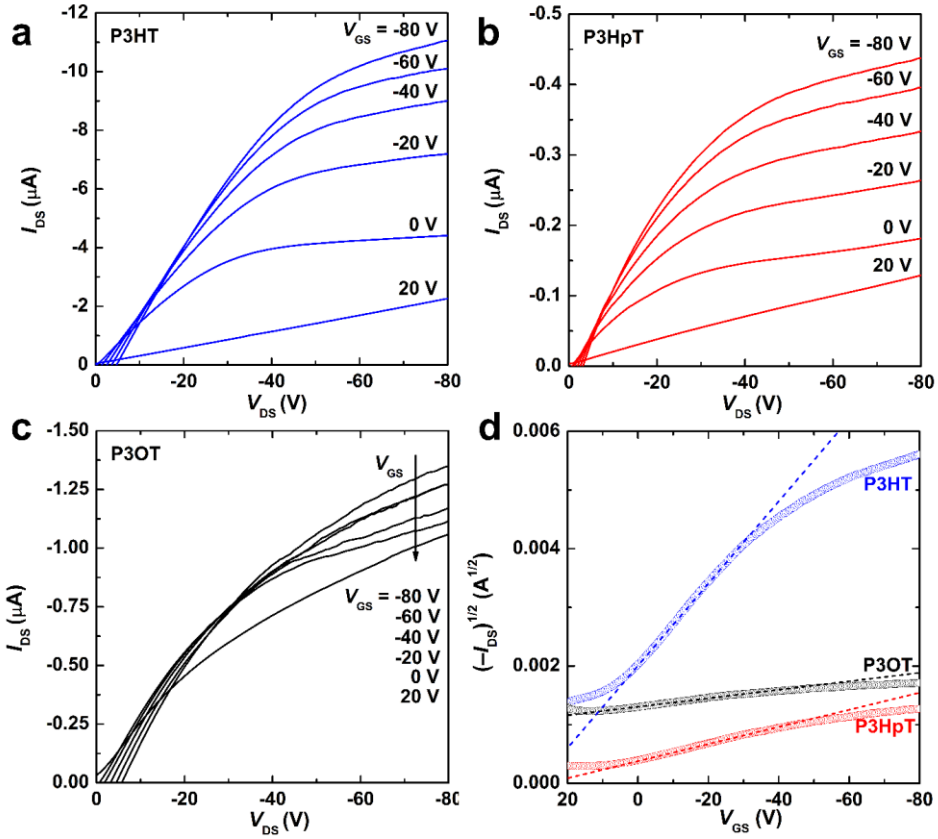

Figure 5.3. Electrical characteristics of P3AT organic thin films transistors (OTFTs): current-voltage output characteristics of a 10 µm (length) by 500 µm (width) channel for (a) P3HT, (b) P3HpT, and (c) P3OT. (d) Transfer characteristics $(-I_{DS})^{1/2}$ vs. V_{GS} at V_{DS} = –80V with respect to alkyl side chain length. Dashed lines represent the linear fit in the saturation regime.

As expected, P3HT exhibited the greatest mobility, 0.01 cm^2 V^{-1} s^{-1}, while P3OT exhibited the lowest, 0.0001 cm^2 V^{-1} s^{-1}. The mobility of P3HpT was intermediate, 0.0006 cm^2 V^{-1} s^{-1}, but closer to that of P3OT than to that of P3HT. Although P3HT, P3HpT, and P3OT have different HOMO values (**Table 5.1**), the injection barriers at

Au/P3AT interfaces are sufficiently small (work function of Au $\Phi_M \approx 5.1 \sim 5.3$ eV)[20,21] and should only result in minimal differences among three different P3AT samples in contact resistance values, which are largely dominated by the polymer nano-morphologies at the Au/channel contact edges in bottom-contact OTFT configuration.[22] The disparity in hole mobilities could be a manifestation of the thermal properties, where the amorphous domains are less mobile for P3HT than they are for P3HpT or P3OT. The relative rigidity of the amorphous domains of P3HT could be conducive to greater charge mobility than P3HpT, despite the similarity in aggregation apparent in the UV-vis spectra of the solid films (**Figure 5.2b**).

Table 5.2. Average mobility values obtained from the transfer curve of the P3HT, P3HpT, and P3OT OTFTs.

Materials	**Mobility, μ_h ($\times 10^{-3}$) (cm^2 / V s)**	**Threshold Voltage, V_T (V)**	**On-off ratio†**
P3HT	11 ± 1.8	34.5 ± 3.63	13.8 ± 3.00
P3HpT	0.55 ± 0.082	36.4 ± 4.25	10.2 ± 2.44
P3OT	0.14 ± 0.032	180 ± 32.0	1.68 ± 0.21
P3HT:PCBM	10 ± 3.3	12.8 ± 5.63	375 ± 231
P3HpT:PCBM	4.0 ± 1.0	23.5 ± 4.47	165 ± 86.8
P3OT:PCBM	1.2 ± 0.66	45.0 ± 18.1	48.8 ± 33.2

† On-off ratios were calculated through I (v_{gs} = –80 V) / I (v_{gs} = +20 V)

The low hole mobility of P3HpT should be deleterious to photovoltaic performance, yet we found that P3HpT:PCBM devices performed as well as P3HT:PCBM devices.[16] It has been reported by others that blending MDMO-PPV with PCBM can improve the hole mobility of the polymer by orders of magnitude.[23,24] The exact mechanism that produces the improvement in mobility is unknown, but it has been speculated that the presence of the fullerene improves ordering in the polymer.[25] We therefore tested this hypothesis for the three P3AT:PCBM composites. The hole mobility of P3HT, 0.01 cm^2 V^{-1} s^{-1}, remained similar to that of the neat polymer, however, the

mobilities of P3HpT and P3OT increased by an order of magnitude to 0.004 $cm^2\ V^{-1}\ s^{-1}$ and 0.001 $cm^2\ V^{-1}\ s^{-1}$, respectively. Such a large increase in μ_h for P3HpT and P3OT with the addition of fullerene correlates with the increase in T_g. These results support the hypothesis that immobilization of polymer chains with the incorporation of an anti-plasticizer may increase the mobility and thus the photovoltaic performance.

5.2.5 Combined mechanical and photovoltaic properties

Given that the charge-transport properties of P3HpT compare favourably to those of P3HT, we believed that P3HpT might be useful as a stretchable and mechanically robust semiconductor for flexible solar cells and wearable devices. **Figure 5.4a** compares the representative *J*-*V* curves of the three P3AT:PCBM devices and the figures of merit are summarized in **Table 5.3**. P3HT:PCBM and P3HpT:PCBM exhibited similar power conversion efficiencies, while P3OT:PCBM performed considerably poorer.

Table 5.3. Characteristics of P3HpT:PCBM films as a function of weight percentage of PCBM. All films were spin-coated from ODCB and thermally annealed at 100 °C.

Wt% PCBM[a]	***PCE*** [b] **(%)**	E_f [c] **(GPa)**	***CoS*** [d] **(%)**	***W*** [e] **(eV)**	**Agg. Fraction**[f]
0%	–	0.19 ± 0.05	54 ± 2	0.181	0.547
10%	0.014 ± 0.002	0.33 ± 0.07	40 ± 2	0.165	0.552
16.7%	0.12 ± 0.01	0.82 ± 0.28	26 ± 2	0.168	0.555
25%	0.59 ± 0.03	1.01 ± 0.22	16 ± 2	0.169	0.550
33.3%	1.24 ± 0.09	1.75 ± 0.35	12 ± 2	0.169	0.547
40%	1.58 ± 0.06	1.84 ± 0.28	6 ± 1	0.172	0.518
50%	2.16 ± 0.17	1.92 ± 0.22	4 ± 1	0.179	0.464

[a]The weight percentage of PCBM in the solution prepared in ODCB. [b]The architecture of the OSC devices was PEDOT:PSS/P3HpT:PCBM/EGain. The thickness of the active layer for each sample was ~150 nm. The power conversion efficiencies were averages of $N \geq 8$ devices. [c]Tensile modulus of each sample was determined by the buckling-based methodology. [d]Crack-onset strain was determined by transferring the film of each sample (~150 nm) onto an unstrained PDMS substrate and incrementally increasing the induced strain. Optical micrographs were taken to observe the formation of cracks. [e]The exciton bandwidth, *W*, which is inversely correlated to aggregate order, and [f]the Aggregate Fraction were calculated from a least-squares fit of the weakly interacting H-aggregate model to the absorption spectra.

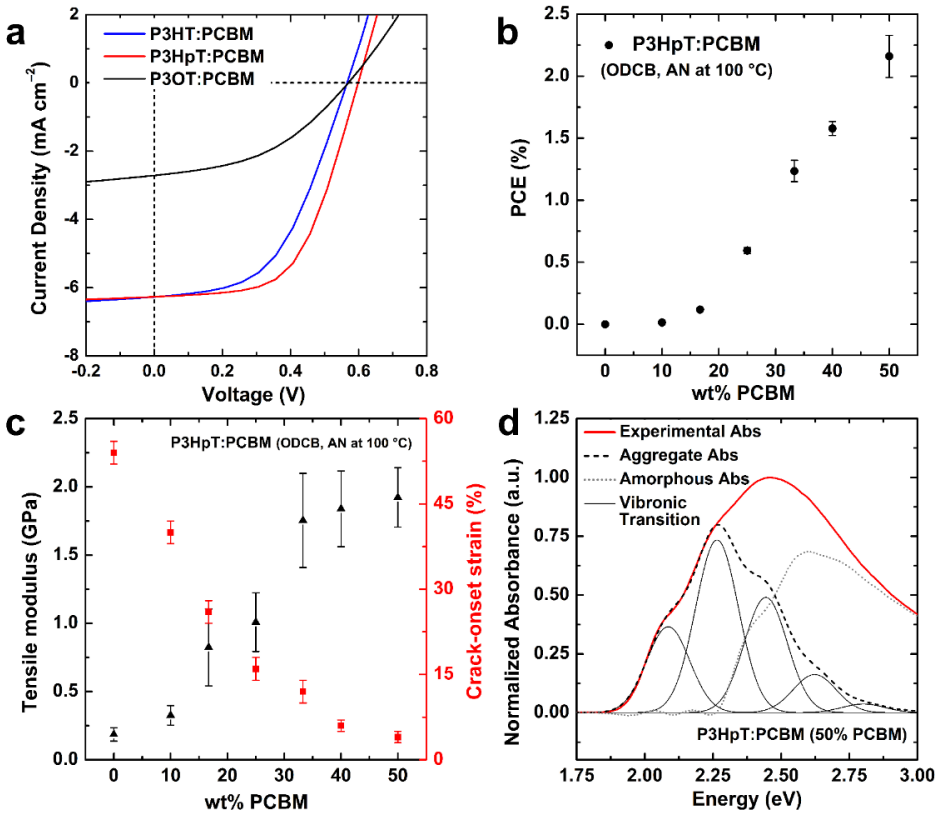

Figure 5.4. Optoelectronic and mechanical properties of P3AT:fullerene blends. (a) *J-V* curves of average devices ($N \geq 7$) with an active layer of 1:1 blend of P3AT and $PC_{61}BM$. The architecture of the devices was PEDOT:PSS/P3AT:PCBM/EGaIn. The data were reproduced from ref. [2]. (b) Power conversion efficiency of average devices ($N \geq 7$) comprising P3HpT and PCBM as a function of weight fraction of PCBM. (c) Values of tensile modulus and crack-onset strain of P3HpT:PCBM as a function of weight fraction of PCBM. All films were fabricated by spin-coating from solutions of ODCB and thermally annealed at 100 °C. (d) Example of deconvolution of the absorption spectra into vibronic transitions of ordered P3HpT and amorphous absorption using the weakly interacting H-aggregate model.

The necessity to add fullerenes (*e.g.*, PCBM) to conjugated polymers to make a bulk heterojunction has the unwanted effect of increasing the stiffness and brittleness of the composite film.[1,2,26] We hypothesized that there may be a concentration of PCBM that maximized both compliance and power conversion efficiency (*PCE*) of solar cells with the architecture glass/PEDOT:PSS/P3HpT:PCBM/eutectic gallium-indium (EGaIn). **Figure 5.4b** plots the *PCE* of P3HpT:PCBM blend as a function of the weight fraction of PCBM in the blend. The tensile modulus (E_f, left vertical axis) and the crack-onset strain (*CoS*, right vertical axis) as a function of PCBM concentration are plotted in **Figure 5.4c**.

We observed that the three quantities were highly correlated. This apparent trade-off between stiffness and electronic performance has been observed before in polythiophenes exhibiting different levels of crystalline order, specifically P3HT:PCBM blends with different order in the polymer phase produced by different rates of drying during solution casting,[5] and in the conductive polyelectrolyte complex PEDOT:PSS, when spin-coated from inks containing different concentrations of dimethylsulfoxide (DMSO).[27]

We also examined the effect of PCBM concentration on the extent of ordering in the polymer component, as measured by UV-vis spectroscopy and analysed by the weakly interacting H-aggregate model (**Figure 5.4d**). The UV-vis spectra can be de-convoluted into contributions from the aggregated material (the lower-energy shoulders in the spectra) and from the amorphous material. The percent aggregate has been correlated to increased stiffness and crack-onset strain in P3HT:PCBM blends.[5] Interestingly, small concentrations of PCBM appear to have an ordering effect on the polymer, however this effect disappears with larger loading of PCBM. Both the *W* value, which is inversely related to the aggregate order, and the aggregate fraction suggests that a decrease in ordering begins with a loading of PCBM above 33.3%. At lower loadings, the PCBM is likely to be dispersed in the amorphous domains of the polymer;[28] at higher loadings, larger PCBM-rich domains form that serve as electron-conducting regions required for efficient solar cells, but are also hard inclusions in the film that stiffen and embrittle the film and are deleterious to polymer ordering. Of note, these results suggest that the increase in hole mobility we measured in 1:1 P3AT:PCBM blends is not due to increased polymer ordering, and thus, further studies are required to fully understand the mechanism responsible.

We note that molecular weight affects the mechanical properties of the P3ATs in ways that have not yet been fully characterized. For example, Dauskardt and coworkers found that cohesive fracture energy of P3HT increases with molecular weight (M_w) in a range of 28 to 100 kDa,[29] while the entanglement molecular weight has been estimated to be 10–20 kDa for P3HT.[28] Koch et al. observed that monodisperse samples of P3HT with exceptionally low degrees of polymerization (dp = 12) can exhibit structures in which the side chains intercalate that have been described qualitatively as brittle.[30] We have previously found that the tensile modulus was similar within experimental error for P3HT with M_n between 7 and 44 kDa.[2,11] We thus did not attribute differences in mechanical properties to differences in the molecular weight (M_n) of the samples used in this study (P3HT 44 kDa, P3HpT 35 kDa, P3OT 34 kDa).

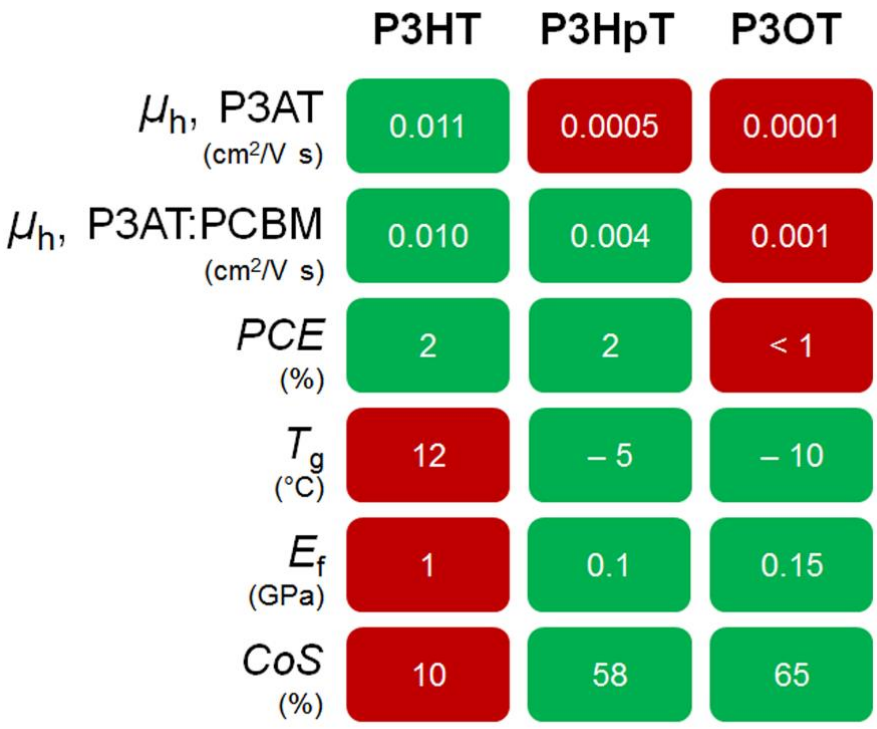

Figure 5.5. A summary of the electronic and mechanical properties of the polymers and polymer:fullerene blends studied in this work. Favourable properties are highlighted in green, while unfavourable properties are highlighted in red.

A summary of the electronic and mechanical properties of P3HT, P3HpT, and P3OT is presented in **Figure 5.5**. While P3HT has a favourable μ_h and *PCE,* it exhibits poor compliance and ductility. P3OT, on the other hand, has high compliance and ductility, but poor μ_h and *PCE*. In contrast, P3HpT is a chimera; in neat films, it has a similar compliance and ductility to P3OT, and when blended with fullerene, its electronic performance becomes closer to or equal to that of P3HT. While P3HpT is stiffened by PCBM, the blend is still less stiff than P3HT:PCBM by a factor of approximately two: E_f = 1.46 ± 0.16 GPa for P3HpT:PCBM compared to 2.75 ± 0.59 GPa for P3HT:PCBM.[31]

5.3 Conclusion

Poly(3-heptylthiophene) is an interesting example of a stretchable semiconducting thermoplastic. While P3OT could also be described as an STE, the semiconducting performance of P3HpT is better, especially when blended with PCBM. The mechanical compliance of P3HpT arises from the fact that its glass transition is the first in the series of P3ATs that is well below ambient temperature. When compared to P3HT and P3OT, the *PCE* of an organic solar cell with an active layer comprising P3HpT:PCBM is comparable to that of P3HT:PCBM, while the hole mobility of P3HpT is poor—closer to P3OT than P3HT—it is increased by nearly an order of magnitude with the addition of PCBM. P3HpT is thus attractive as a potential replacement for P3HT in flexible, stretchable, wearable, and mechanically robust solar cells, though it would not make an especially good transistor. More generally, the behaviour observed in these relatively simple conjugated polymer systems should provide insight into designing highly elastic

and high performing organic electronic devices in outdoor, portable, and wearable applications that require mechanical robustness

Acknowledgments

This work was supported by the Air Force Office of Scientific Research (AFOSR) Young Investigator Program, Grant Number FA9550-13-1-0156. Additional support was provided by the National Science Foundation Graduate Research Fellowship, awarded to both S.S. and A.Z., and by laboratory startup funds from the University of California, San Diego. The authors thank Prof. Joseph Wang and Amay Bandodkar for helpful discussions and use of their equipment to perform cyclic voltammetry experiments.

Chapter 5, in full, is a reprint of the material as it appears in *Synthetic Metals*, 2015, 203, 208. Elsevier B.V., 2015. Suchol Savagatrup,[†] Adam D. Printz,[†] Haosheng Wu, Kirtana Rajan, Eric J. Sawyer, Aliaksandr V. Zaretski, Christopher J. Bettinger, and Darren J. Lipomi ([†] Equal contribution). The dissertation author was the primary investigator and author of this paper.

References

(1) Savagatrup, S.; Makaram, A. S.; Burke, D. J.; Lipomi, D. J. Mechanical Properties of Conjugated Polymers and Polymer-Fullerene Composites as a Function of Molecular Structure. *Adv. Funct. Mater.* **2014**, *24*, 1169–1181.

(2) Savagatrup, S.; Printz, A. D.; Rodriquez, D.; Lipomi, D. J. Best of Both Worlds: Conjugated Polymers Exhibiting Good Photovoltaic Behavior and High Tensile Elasticity. *Macromolecules* **2014**, *47*, 1981–1992.

(3) Printz, A. D.; Savagatrup, S.; Burke, D. J.; Purdy, T. N.; Lipomi, D. J. Increased Elasticity of a Low-Bandgap Conjugated Copolymer by Random Segmentation for Mechanically Robust Solar Cells. *RSC Adv.* **2014**, *4*, 13635–13643.

(4) Tahk, D.; Lee, H. H.; Khang, D.-Y. Elastic Moduli of Organic Electronic Materials by the Buckling Method. *Macromolecules* **2009**, *42*, 7079–7083.

(5) Awartani, O.; Lemanski, B. I.; Ro, H. W.; Richter, L. J.; DeLongchamp, D. M.; O'Connor, B. T. Correlating Stiffness, Ductility, and Morphology of Polymer:Fullerene Films for Solar Cell Applications. *Adv. Energy Mater.* **2013**, *3*, 399–406.

(6) O'Connor, B.; Chan, E. P.; Chan, C.; Conrad, B. R.; Richter, L. J.; Kline, R. J.; Heeney, M.; McCulloch, I.; Soles, C. L.; DeLongchamp, D. M. Correlations between Mechanical and Electrical Properties of Polythiophenes. *ACS Nano* **2010**, *4*, 7538–7544.

(7) Moulton, J.; Smith, P. Electrical and Mechanical Properties of Oriented Poly (3-Alkylthiophenes): 2. Effect of Side-Chain Length. *Polymer (Guildf).* **1992**, *33*, 2340–2347.

(8) Reimschuessel, H. K.; Chemical, A. On the Glass Transition Temperature of Comblike Polymers : Effects of Side Chain Length and Backbone Chain Structure. **1979**, *17*, 2447–2457.

(9) Postema, A. R.; Liou, K.; Wudl, F.; Smith, P. Highly Oriented, Low-Modulus Materials from Liquid Crystalline Polymers: The Ultimate Penalty for Solubilizing Alkyl Side Chains. *Macromolecules* **1990**, *23*, 1842–1845.

(10) Kim, J. Y.; Frisbie, C. D. Correlation of Phase Behavior and Charge Transport in Conjugated Polymer/Fullerene Blends. *J. Phys. Chem. C* **2008**, *112*, 17726–17736.

(11) O'Connor, T. F.; Zaretski, A. V.; Shiravi, B. A.; Savagatrup, S.; Printz, A. D.; Diaz, M. I.; Lipomi, D. J. Stretching and Conformal Bonding of Organic Solar Cells to Hemispherical Surfaces. *Energy Environ. Sci.* **2014**, *7*, 370–378.

(12) Salammal, S.; Mikayelyan, E.; Grigorian, S.; Pietsch, U.; Koenen, N.; Scherf, U.; Brinkmann, M.; Kayunkid, N. Impact of Thermal Annealing on the Semicrystalline Nanomorphology of Spin-Coated Thin Films of Regioregular Poly (3-Alkylthiophene) S as Observed by High-Resolution Transmission Electron Microscopy and Grazing Incidence X-Ray Diffraction. *Macromolecules* **2012**, *45*, 5575–5585.

(13) Zhao, J.; Swinnen, A.; Van Assche, G.; Manca, J.; Vanderzande, D.; Van Mele, B. Phase Diagram of P3HT/PCBM Blends and Its Implication for the Stability of Morphology. *J. Phys. Chem. B* **2009**, *113*, 1587–1591.

(14) Bruner, C.; Novoa, F.; Dupont, S.; Dauskardt, R. Decohesion Kinetics in Polymer Organic Solar Cells. *ACS Appl. Mater. Interfaces* **2014**, *6*, 21474–21483.

(15) Friedel, B.; McNeill, C.; Greenham, N. Influence of Alkyl Side-Chain Length on the Performance of Poly (3-alkylthiophene)/Polyfluorene All-Polymer Solar Cells. *Chem. Mater.* **2010**, *22*, 3389–3398.

(16) Heeney, M.; Zhang, W.; Crouch, D. J.; Chabinyc, M. L.; Gordeyev, S.; Hamilton, R.; Higgins, S. J.; McCulloch, I.; Skabara, P. J.; Sparrowe, D.; Tierney, S. Regioregular Poly(3-hexyl)selenophene: A Low Band Gap Organic Hole Transporting Polymer. *Chem. Commun. (Camb).* **2007**, 5061–5063.

(17) Pingel, P.; Zen, A.; Abellón, R. D.; Grozema, F. C.; Siebbeles, L. D. A.; Neher, D. Temperature-Resolved Local and Macroscopic Charge Carrier Transport in Thin P3HT Layers. *Adv. Funct. Mater.* **2010**, *20*, 2286–2295.

(18) Giri, G.; Verploegen, E.; Mannsfeld, S. C. B.; Atahan-Evrenk, S.; Kim, D. H.; Lee, S. Y.; Becerril, H. A.; Aspuru-Guzik, A.; Toney, M. F.; Bao, Z. Tuning Charge Transport in Solution-Sheared Organic Semiconductors Using Lattice Strain. *Nature* **2011**, *480*, 504–508.

(19) Bettinger, C. J.; Bao, Z. Organic Thin-Film Transistors Fabricated on Resorbable Biomaterial Substrates. *Adv. Mater.* **2010**, *22*, 651–655.

(20) Singh, K. A.; Young, T.; McCullough, R. D.; Kowaiewski, T.; Porter, L. M. Planarization of Polymeric Field-Effect Transistors: Improvement of Nanomorphology and Enhancement of Electrical Performance. *Adv. Funct. Mater.* **2010**, *20*, 2216–2221.

(21) Sachtler, W. M. H.; Dorgelo, G. J. H.; Holscher, A. A. The Work Function of Gold. *Surf. Sci.* **1966**, *5*, 221–229.

(22) Park, Y.; Kim, D.; Jang, Y.; Cho, J.; Hwang, M. Effect of Side Chain Length on Molecular Ordering and Field-Effect Mobility in Poly (3-Alkylthiophene) Transistors. *Org. Electron.* **2006**, *7*, 514–520.

(23) Choulis, S. a.; Nelson, J.; Kim, Y.; Poplavskyy, D.; Kreouzis, T.; Durrant, J. R.; Bradley, D. D. C. Investigation of Transport Properties in Polymer/fullerene Blends Using Time-of-Flight Photocurrent Measurements. *Appl. Phys. Lett.* **2003**, *83*, 3812–3814.

(24) Melzer, C.; Koop, E. J.; Mihailetchi, V. D.; Blom, P. W. M. Hole Transport in Poly(phenylene vinylene)/Methanofullerene Bulk-Heterojunction Solar Cells. *Adv. Funct. Mater.* **2004**, *14*, 865–870.

(25) Beaujuge, P. M.; Fréchet, J. M. J. Molecular Design and Ordering Effects in Π-Functional Materials for Transistor and Solar Cell Applications. *J. Am. Chem. Soc.* **2011**, *133*, 20009–20029.

(26) Lipomi, D. J.; Chong, H.; Vosgueritchian, M.; Mei, J.; Bao, Z. Toward Mechanically Robust and Intrinsically Stretchable Organic Solar Cells: Evolution of Photovoltaic Properties with Tensile Strain. *Sol. Energy Mater. Sol. Cells* **2012**, *107*, 355–365.

(27) Savagatrup, S.; Chan, E.; Renteria-Garcia, S. M.; Printz, A. D.; Zaretski, A. V.; O'Connor, T. F.; Rodriquez, D.; Valle, E.; Lipomi, D. J. Plasticization of PEDOT:PSS by Common Additives for Mechanically Robust Organic Solar Cells and Wearable Sensors. *Adv. Funct. Mater.* **2015**, *25*, 427–436.

(28) Treat, N. D.; Chabinyc, M. L. Phase Separation in Bulk Heterojunctions of Semiconducting Polymers and Fullerenes for Photovoltaics. *Annu. Rev. Phys. Chem.* **2014**, *65*, 59–81.

(29) Bruner, C.; Dauskardt, R. Role of Molecular Weight on the Mechanical Device Properties of Organic Polymer Solar Cells. *Macromolecules* **2014**, *47*, 1117–1121.

(30) Koch, F. P. V.; Heeney, M.; Smith, P. Thermal and Structural Characteristics of Oligo (3-Hexylthiophene) S (3HT) N, N= 4–36. *J. Am. Chem. Soc.* **2013**, *135*, 13699–13709.

(31) Printz, A. D.; Savagatrup, S.; Rodriquez, D.; Lipomi, D. J. Role of Molecular Mixing on the Stiffness of Polymer:fullerene Bulk Heterojunction Films. *Sol. Energy Mater. Sol. Cells* **2015**, *134*, 64–72.

Chapter 6

[70]PCBM and incompletely separated grades of methanofullerenes produce bulk heterojunctions with increased robustness for ultra-flexible and stretchable electronics

Suchol Savagatrup,[a] Daniel Rodriquez,[a] Adam D. Printz,[a] Alexander B. Sieval,[b] Jan C. Hummelen,[b,c] and Darren J. Lipomi[a]

[a] *Department of NanoEngineering, University of California, San Diego, 9500 Gilman Drive Mail Code 0448, La Jolla, CA 92093-0448.*

[b] *Solenne BV, Zernikepark 6-8, 9747 AN Groningen, Netherlands*

[c] *Stratingh Institute for Chemistry and Zernike Institute for Advanced Materials, University of Groningen, Nijenborgh 4, 9747 AG Groningen, Netherlands*

Abstract

An organic solar cell based on a bulk heterojunction (BHJ) of a polymer and a methanofullerene ([60]PCBM or [70]PCBM) exhibits a complex morphology that controls both its photovoltaic and mechanical compliance (robustness, flexibility, and stretchability). Methanofullerenes are excellent electron acceptors, however they have relatively high cost and production energy (in the purest samples) compared to other small-molecule semiconductors. Moreover, [60]PCBM and [70]PCBM—typical of van der Waals solids—can be stiff and brittle. Stiffness and brittleness may lower the yield of working modules in roll-to-roll manufacturing, shorten the lifetime against mechanical failure in outdoor conditions, and jeopardize wearable and portable applications that demand stretchability or extreme flexibility. This paper tests the hypothesis that "technical grade" PCBM (incompletely separated but otherwise pure blends containing ≥90% [60]PCBM or [70]PCBM) could lower the cost of manufacturing organic solar cells while simultaneously increasing their mechanical stability. Measurements of tensile modulus of five methanofullerene samples, "technical grades" and 99% grades of both [60]PCBM and [70]PCBM, and a 1:1 mixture [60]PCBM and [70]PCBM, along with their blends with regioregular poly(3-hexylthiophene) (P3HT), lead to two important conclusions: (1) Films of pure [70]PCBM are approximately five times more compliant than films of pure [60]PCBM; BHJ films with [70]PCBM are also more compliant than those with [60]PCBM. (2) Bulk heterojunction films comprising technical grades of [60]PCBM and [70]PCBM are approximately two to four times more compliant than are films made using 99% grades. Tensile modulus is found to be an excellent predictor of brittleness: BHJs produced with technical grade methanofullerene accommodate strains 1.4 to 2.2 times

greater than those produced with 99% grades. The smallest range of stretchability was found for BHJs with 99% [60]PCBM (fracture at 3.5% strain), while the greatest is found for technical grade [70]PCBM (11.5% strain). Mechanical properties are correlated to the microstructures of the blended films informed from analyses of UV-vis spectra using the weakly interacting H-aggregate model. Photovoltaic measurements show that solar cells made with technical grade [70]PCBM have similar efficiencies to those made with higher-grade material, but with decreased cost, and increased mechanical robustness.

6.1 Introduction and Background

6.1.1 Methanofullerenes in organic solar cells

Increasing the mechanical compliance of organic semiconductors in a way that does not sacrifice electronic performance will accomplish two goals. The first goal is to improve the lifetime against mechanical failure for printed, flexible devices.[1] The second goal is to enable a new class of ultra-flexible and intrinsically stretchable devices for portable, lightweight power sources,[2] wearable and implantable health monitors,[3] and fracture-proof consumer electronics.[4] One important application of organic semiconductors is the organic solar cell, in which fullerenes and their derivatives are present in all of the most efficient devices produced to date.[5] The high electron mobilities of fullerenes,[6] the solubility of methanofullerenes (e.g., [60]PCBM and [70]PCBM, **Figure 6.1**), high rates of charge transfer,[7] and their spherical (or quasi-spherical) shape, which permits transfer of an electron from any direction, suggest that fullerenes will continue to be the material of choice for a variety of applications. These materials, however, have high embodied energy in their purest form,[8,9] and polymer:methanofullerene bulk heterojunction films are stiffer,

more brittle, and have lower cohesive energy in comparison to films of the pure polymer.[10–12] Additionally, the high energies of production (because of the resources needed to separate them by chromatography) are correlated with the high cost of methanofullerenes (compared to conjugated polymers and small molecules, such as copper phthalocyanine).[9] We hypothesized that disorder introduced into BHJ films in the form of isomers or mixed sizes within the PCBM phases would affect the mechanical properties of polymer:methanofullerene bulk heterojunction blends, which will influence the yield of working devices during roll-to-roll coating[13] and the lifetime against mechanical failure in outdoor or portable environments, or in stretchable and ultra-flexible applications.[1,14] Using "technical grades" of PCBM,[15–17] in which the C_{60} and C_{70} derivatives are incompletely separated but otherwise pure, it might be possible to address two problems at the same time: reducing the cost and production energy of organic solar cells, and simultaneously increasing the mechanical resilience. While our group and others have examined the role of the polymer in determining the deformability of the active components in ultra-compliant systems, the role of small molecule semiconductors—of which methanofullerenes may be the most prominent class—has not been explored.

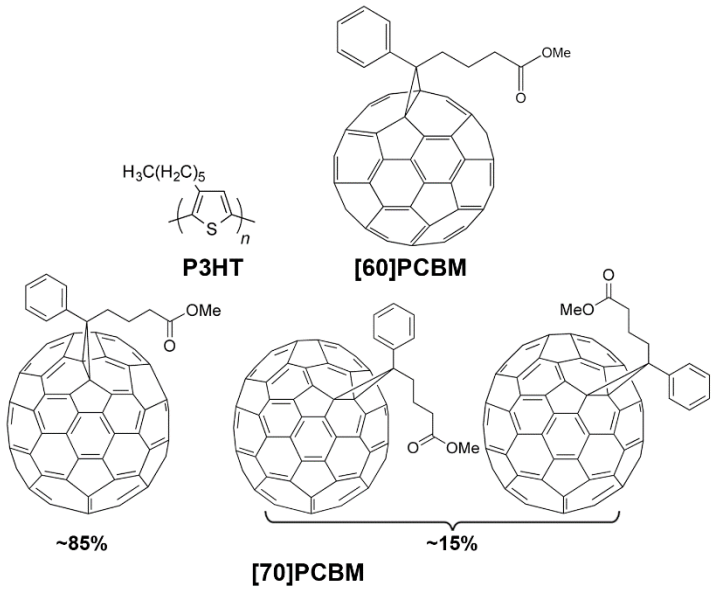

Figure 6.1. Chemical structures of P3HT and the methanofullerenes studied. Isomers of [70]PCBM depicting the structures of the chiral α-type isomer (left) and the two possible β-type isomers (right). The α-type isomer is present in 85% and the two β-type isomers are present in approximately equal amounts. More isomers exists in theory (not in figure), but at most in very small amounts (from HPLC and ^{1}H NMR) (see also ref. [18]).

6.1.2 Embodied energy of methanofullerenes

Fullerenes have high energies of production, in part, because they need to be separated from the carbon soot produced by the two common methods of production: pyrolysis (of toluene or tetralin) or arc plasma with graphite as a feedstock.[9] According to the analysis by Anctil et al., pyrolysis requires 146 kg tetralin to produce 1 kg of C_{60} and 0.78 kg of C_{70}.[9] C_{70} has a greater production energy than does C_{60} largely because C_{70} is more difficult to separate from higher-order fullerenes than is C_{60}; the purification steps (from 95% to 99.9% purity) increase the embodied energy of C_{60} by a factor of two and of C_{70} by a factor of three.[9] The net result is that the embodied energies of [60]PCBM and [70]PCBM (after functionalization of the fullerene core) at 99.9% purity are 65 GJ kg^{-1} and 90 GJ kg^{-1}, respectively.[9] (While these values are nearly an order of magnitude higher than those of polysilicon,[19] methanofullerenes are present in much smaller absolute

amounts in organic solar cells than polysilicon is present in conventional cells.) The contribution of methanofullerenes to the cumulative energy demand of an entire module, however, is substantial: from 19% to 31%, depending on the choices of other materials in devices in which the electron donor is a polymer.[20] Substantial savings in embodied energy (which correlates well with cost for manufactured products)[9] are thus possible if one can use mixtures of methanofullerenes. The use of these mixed methanofullerene derivatives (technical grades) will produce different morphologies in bulk heterojunction films than will highly purified samples. For example, Andersson et al. showed a drastic change in the morphology of a polymer:[60]PCBM blend with the addition of <10% [70]PCBM to the methanofullerene component.[15] One expects these different morphologies to affect not only the electronic performance of the blend, but also its compliance and mechanical stability,[15,21] through the effect of increased free volume in mixtures of molecules of different sizes or isomers.

6.1.3 Mechanical properties and morphology of the bulk heterojunction

Organic semiconductors exhibit a wide range of tensile moduli, ranging from 30 MPa to 16 GPa,[11] and propensity to fracture, from <2.5% strain to greater than 150% strain on elastic substrates.[22] This disparity suggests that modules composed of different organic semiconductors may have unequal yields during mechanically rigorous roll-to-roll manufacturing processes, unequal lifetimes in the environment, and unequal amenabilities to stretchable and ultra-flexible applications.[23] One key determinant of the variation in mechanical properties in the active layer of an organic solar cell is the morphology of the donor-acceptor bulk heterojunction. Morphology refers to the details of molecular mixing,

the texture and degree of crystallinity of the phases, and the extent of phase separation.[24] These key parameters have a large influence on the power conversion efficiencies of organic solar cells, given materials with good charge-transport properties, complementary absorption, and favorable relative positions of their frontier molecular orbitals. It has been shown that the mechanical properties of bulk heterojunction systems comprising conjugated polymers and small molecules are influenced by many aspects of the chemical structure (e.g., the presence of the fused or isolated rings in the main chain,[25,26] length and the composition of pendant groups,[10,27] size and intermolecular forces within crystallites)[22] and microstructural order (e.g., the addition of methanofullerene,[10,11,21,25–27] intercalation of methanofullerenes between side chains of polymers,[28,29] effect of processing conditions,[21] presence of plasticizing additives).[10,30] One aspect of the makeup of the bulk heterojunction whose effects on the mechanical properties have not been explored is the makeup (i.e., size and purity) of the methanofullerene phase.

We thus investigated two methanofullerene derivatives—[60]PCBM and [70]PCBM—at two different grades—99% grade, and technical grades (≥90% either [60]PCBM or [70]PCBM, and the remainder the other) along with their blends with regioregular poly(3-hexylthiophene) (P3HT). The hypothesis that guided our experiments was that the use of methanofullerene samples with technical grades of [60]PCBM and [70]PCBM (i.e., incomplete separation of C_{60} and C_{70} derivatives) would form BHJ films with greater compliance than films in which the methanofullerene sample was of 99% grade. We measured two mechanical properties, the tensile modulus and the ductility (as manifested in the crack on-set strain), of P3HT:methanofullerene films before thermal annealing (as-cast, AC) and after thermal annealing (annealed, AN), as well as pure

methanofullerene films. The tensile moduli were measured using the mechanical buckling technique.[31,32] The crack on-set strains were used to measure the ductility of the film on a stretchable substrate. We observed trends in the mechanical properties that were correlated with the microstructures of the blended films informed from analyses of UV-vis spectra using the weakly interacting H-aggregate model. Our results led us to conclude that it is possible to increase the mechanical compliance of a bulk heterojunction film by using technical grade methanofullerenes (thereby lowering the cost and embodied energy), which produce statistically similar photovoltaic efficiencies.

6.2 Results and discussion

6.2.1 Mechanical properties of pure methanofullerene and bulk heterojunction films

We measured the tensile moduli of films using the buckling technique.[11,31] Briefly, the film of interest was spin-coated onto passivated glass slide, then transferred to an elastomeric substrate bearing a small tensile pre-strain. The pre-strain was then released, and the resulting compression forced the film to adopt buckles. For the bulk heterojunction films, the tensile modulus of each film, E_f, was calculated from the measured buckling wavelength, λ_b, the thickness of the film, d_f, the tensile modulus of the substrate, E_s, and the Poisson's ratios of the film and the substrate, v_f and v_s, using equation 1:

$$E_f = 3E_s\left(\frac{1-v_f^2}{1-v_s^2}\right)\left(\frac{\lambda_b}{2\pi d_f}\right)^3 \quad (\mathbf{1})$$

However, the high stiffness and brittleness of the pure methanofullerenes caused the films to fracture when the pre-strain was released; this damage precluded accurate measurements.[10,33] To avoid this problem, we performed the measurement on a bilayer

system comprising a PEDOT:PSS film and the pure methanofullerene film. We chose the layer of PEDOT:PSS as the second layer to behave as a substrate with favorable surface energy and allow for a uniform film of pure methanofullerene. Studies on the interface mixing of PEDOT:PSS and the layer of P3HT:PCBM by Huang et al.[34] and Dupont et al.[35] have shown that very little methanofullerene diffuses into PEDOT:PSS at room temperature, and thus we assumed the presence of a distinct interface. We then used equation 2 to calculate the modulus of the methanofullerene film ($E_{f,2}$) (**Figure 6.2a**, dark grey bars) from the effective modulus of the bilayer (E_{eff}) and the modulus of the PEDOT:PSS film ($E_{f,1}$);[32] both E_{eff} and $E_{f,1}$ are obtained separately via the typical buckling method. (A detailed explanation of the calculation is provided in the Supporting Information.)

$$E_{\text{eff}} = \frac{1 + m^2n^4 + 2mn(2n^2 + 3n + 2)}{(1+n)^3(1+mn)} E_{\text{f},1};\ \text{where } m = \frac{E_{\text{f},2}}{E_{\text{f},1}},\ n = \frac{d_{\text{f},2}}{d_{\text{f},1}} \qquad (\mathbf{2})$$

From the results summarized in **Figure 6.2a** and **Table 6.1**, the moduli of the pure [60]PCBM films were higher than the pure [70]PCBM films for both technical grade (Tech. Gr.) and 99% samples. We attributed this observation to the greater tendency of [60]PCBM to pack efficiently and to crystallize.[36,37] The difference in behavior is consistent with the presence of isomers in [70]PCBM, which hinder efficient packing. Importantly, we observed that technical grade [60]PCBM had a lower modulus than 99% [60]PCBM. The average value for technical grade [70]PCBM was somewhat lower than for 99% [70]PCBM, but within experimental error. In addition, we observed that value of the 1:1 mixture of [60]PCBM and [70]PCBM sat between the values of the technical grades of [60]PCBM and [70]PCBM.

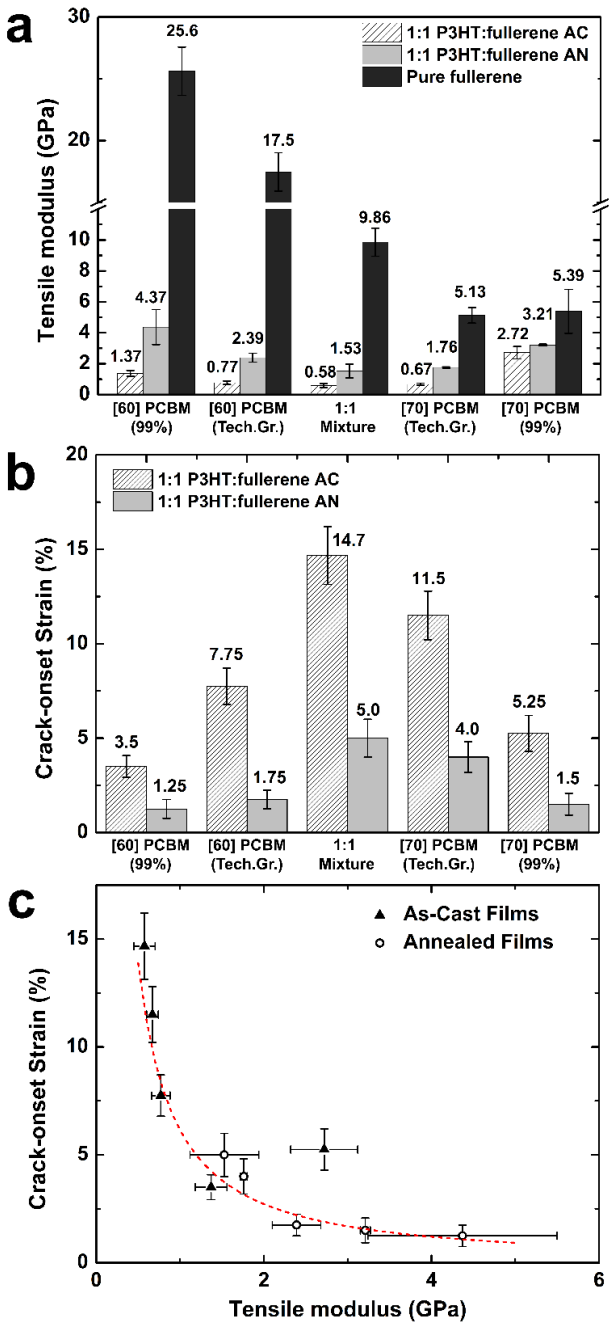

Figure 6.2. Mechanical properties of the bulk heterojunction and pure methanofullerene films, arranged from left to right in order of increasing content of [70]PCBM. (a) Tensile moduli of films tested in this work. The dark gray bars represent the tensile moduli of pure methanofullerene films as obtained from the bilayer method. The bilayer systems consisted of PEDOT:PSS/methanofullerene. The light gray bars and gray bars represent the moduli of blends of P3HT:methanofullerene (1:1 ratio) spin-coated from chloroform solution for both as-cast and annealed films. The value of the tensile modulus of the pure P3HT film measured in parallel to these experiments was 0.55 ± 0.09 GPa. (b) Uniaxial crack-onset strains of the thin films transferred onto PDMS substrate. All pure methanofullerene films cracked at strains below 0.5%. (c) Plot of the correlation between crack-onset strains and tensile moduli of all the films tested.

Table 6.1. Summary of tensile moduli of the methanofullerene films tested in this work from measurement with the buckling-based method and the bilayer technique.[†] The value of the pure as-cast P3HT used in this experiment, obtained in parallel, was 0.55 ± 0.09 GPa.

Materials	Tensile modulus (GPa)				
	[60]PCBM (99%)	[60]PCBM (Tech. Gr.)	1:1 Mixture	[70]PCBM (Tech. Gr.)	[70]PCBM (99%)
Pure methanofullerene[§]	25.6 ± 1.95	17.5 ± 1.55	9.86 ± 0.91	5.13 ± 0.50	5.39 ± 1.42
P3HT:methanofullerene (1:1, As-cast) [‡]	1.37 ± 0.19	0.77 ± 0.11	0.58 ± 0.13	0.67 ± 0.07	2.72 ± 0.40
P3HT:methanofullerene (1:1, Annealed) [‡]	4.37 ± 1.13	2.39 ± 0.29	1.53 ± 0.44	1.76 ± 0.04	3.21 ± 0.06

[†] The bilayer technique uses the buckling-based method to obtain the effective modulus of the bilayer system comprising a layer of PEDOT:PSS film (modulus obtained separately) and pure methanofullerene film, and then backs out the modulus of the pure methanofullerene film. [§] Obtained from the modified bilayer technique. [‡] Obtained from conventional buckling-based method.

Table 6.2. Summary of crack-onset strains of the thin films when transferred onto PDMS substrate.

Materials	Crack-onset strain (%)				
	[60]PCBM (99%)	[60]PCBM (Tech.Gr.)	1:1 Mixture	[70]PCBM (Tech. Gr.)	[70]PCBM (99%)
Pure methanofullerene	< 0.5	< 0.5	< 0.5	< 0.5	< 0.5
P3HT:methanofullerene (1:1, As-cast)	3.5 ± 0.58	7.75 ± 0.98	14.7 ± 1.53	11.5 ± 1.29	5.25 ± 0.96
P3HT:methanofullerene (1:1, Annealed)	1.25 ± 0.5	1.75 ± 0.5	5.0 ± 1.0	4.0 ± 0.82	1.5 ± 0.58

We then characterized the mechanical properties of the P3HT:methanofullerene blends. We used a single polymer (regioregular P3HT) to isolate the effects of the methanofullerene. We selected regioregular P3HT because it is the most widely studied material in the literature for bulk heterojunction OPV devices.[38] While it has not produced state-of-the-art values of *PCE* in several years[39] (though some recent reports have been favorable),[40] it seems to be especially amenable to scale-up by roll-to-roll coating[41] because it works well in relatively thick films, and it has a low cost due to its short synthetic route.[8,42] Moreoever, the morphology of P3HT when mixed with [60]PCBM is the basis for many studies in the field,[38] and the mechanical properties of pure P3HT and P3HT:[60]PCBM films have been well characterized.[10,11,21,25] In previous publications by our group, we reported the tensile modulus of pure P3HT to be 1.09 ± 0.15 GPa.[10] This

value was in the range of those reported by various groups, or 0.22 to 1.33 GPa.[11,21,25] The modulus of the batch of pure P3HT used in this study was 0.55 ± 0.09 GPa, approximately half the value we obtained in our previous study.[10] We attribute the differences in moduli commonly obtained for P3HT (and generally not other materials) primarily to the closeness of its glass transition temperature (T_g = 12–25 °C)[43,44] to ambient temperature, and possibly to the sensitivity of its T_g to batch-to-batch variability. Our principal concern, however, was not with the absolute values of the tensile moduli, but with the effects of the methanofullerene component.

Figure 6.2a shows the tensile modulus of the BHJ films, and **Table 6.1** summarizes the tensile moduli of the films tested in this work. The crack-onset strains (**Figure 6.2b**) correlate well with the measured tensile moduli: films with higher modulus are more brittle (**Figure 6.2c**). While we note that the crack-onset strains provide a measurement of the apparent brittleness of the active layer films, the mechanical properties of complete solar cell devices will be dependent not only on the P3HT:methanofullerene actively layer, but also on all other components of the device (e.g. the substrate and the electrode). However, in the case that the substrate and the electrode are more compliant than the active layer,[30] the active layer will be the limiting factor in the mechanical compliance and robustness of solar cell devices. In stretchable devices for wearable or biologically integrated applications, all components must accommodate tensile strain in a specified range.

The data in **Figure 6.2** reveal four salient features: (1) all BHJ films were stiffer than films of the pure polymer (consistent with previous results[10,11,21,25]); (2) thermal annealing increased the stiffness of all BHJ films;[22,27] (3) technical grade methanofullerenes and 1:1 mixture of [60]PCBM and [70]PCBM produced lower moduli

in the BHJ films; (4) films containing principally [70]PCBM were more compliant than films containing principally [60]PCBM given the same thermal history in three of four cases. The following discussion attempts to explain these key observations using spectroscopic and photovoltaic measurements, and arguments from the literature.

6.2.2 Stiffening effect of methanofullerenes on the pure polymers

The current model of the bulk heterojunction, which has been derived principally from blends of poly(3-alkylthiophene) (P3AT) and [60]PCBM, comprises a three-phase system: an aggregated polymer-rich phase, a methanofullerene-rich phase, and a well-mixed amorphous phase.[38] The mixed phase forms as a consequence of the miscibility of methanofullerene molecules within the amorphous domains of the polymer,[45,46] and thus the current model predicts the absence of pure amorphous polymer domains in P3HT:PCBM films. In a compelling visualization of the evolution in morphology of the BHJ, Roehling et al. used electron-tomographic three-dimensional reconstructions of a blend before and after annealing (using an endohedral methanofullerene for phase contrast), and showed a clear reduction of the fraction of the mixed phase.[47] The ratio of phases within the ternary system went from (P3HT:methanofullerene:mixed) 28:28:44 (as-cast) to 50:37:13 (annealed), or "mostly mixed" to "mostly crystalline P3HT."[47]

The crystalline phases of methanofullerenes have been characterized in detail.[48] In particular, Zheng et al. observed a striking evolution in crystalline morphology in pure [60]PCBM films from needle-like, to axialite, to faceted crystalline slices.[49] A similar transformation was observed in crystallites grown in the interface between a solvent and a non-solvent.[50] In blended films of P3HT:[60]PCBM, Verploegen et al. used grazing

incidence X-ray scattering (GIXS) to measure the evolution in crystallization of the two components during thermal annealing, and observed diffraction peaks consistent with crystalline [60]PCBM.[36] Indeed [60]PCBM is known to form crystals upon extended annealing that are large enough to be visible by optical microscopy.[51] Thus, the current model predicts that the [60]PCBM-enriched phase in the bulk heterojunction is at least partially crystalline.[38] Due to the presence of isomers in [70]PCBM, however, has not been observed to crystallize in neat films or in blends. The disorder in [70]PCBM was the basis of our hypothesis that the larger methanofullerene might produce films with reduced stiffness.

In every instance in which the moduli of pure conjugated polymers and their blends with fullerenes are reported in the same paper, the blends are stiffer than the pure polymer.[10,11,21] The mechanical properties of pure P3ATs are influenced, among other factors, by the degree of crystallinity and the T_g of the amorphous domains relative to ambient temperature. The proximity of T_g to ambient temperature suggests that the temperature at which experiments are carried out is near the high end of the range in which P3HT is in the glassy state. While the ordered domains of P3HT are generally unaffected by the presence of methanofullerenes in BHJ films,[52] the pure amorphous phase of the polymer is consumed by methanofullerene to form the mixed phase. Methanofullerene molecules not dispersed in the mixed phase form a third, methanofullerene-enriched phase that is either amorphous or partially ordered (in the case of [60]PCBM, which can pack efficiently because it is a single isomer). Differences in mechanical properties between the pure polymer and the BHJ can thus be attributed to the effects of the mixed phase and the methanofullerene-enriched phase. Because the pure methanofullerene films are stiffer than

either pure P3HT or the corresponding BHJ, we predicted that the methanofullerene-enriched domains behave as stiff inclusions within the BHJ film. We also suspect that the mixed phase in a BHJ film is stiffer than the amorphous phase in pure P3HT. This behavior is consistent with the observation by Hopkinson et al., and confirmed by us, that the addition of [60]PCBM increases T_g of P3HT—i.e., [60]PCBM is an anti-plasticizer.[53] The high modulus of the P3HT:[60]PCBM blend relative to the pure polymer is also predicted on the basis of the composite theory applied to BHJ films by Tahk et al.,[11] but the agreement may be serendipitous because it does not take into account the presence of pure, unmixed phases. In a separate study, our group has shown that the ratio of the polymer to methanofullerene also strongly influenced the mechanical properties of the resulting BHJ films; the tensile modulus increased when the weight percentage of methanofullerene was increased from 0% to 50%.[54]

6.2.3 Stiffening effect of thermal annealing

A trade-off between electronic and mechanical properties has been observed in the context of thermal history of organic semiconductors.[21] Generally, post-processing treatment such as thermal annealing increases the crystallinity of the materials, which usually improves the electrical properties while in some cases increases the stiffness. For example, films of PBTTT doubled in tensile modulus after thermal annealing,[22] while pure P3HT films exhibited a minimal change in modulus.[21,25] The effect of thermal annealing of pure polymer films on the mechanical properties is thus not generalizable. Polymer:methanofullerene blends, however, have been consistently shown to increase in tensile modulus with thermal treatment.[27] The origin of the increase in modulus is the

thermally evolved microstructure of the ternary blend. As-cast P3HT:PCBM films are characterized by low order and a large percentage of mixed phase.

An increasing volume fraction of ordered polymer and methanofullerene-enriched phases should be correlated with an increase in modulus of the blended film. Order in P3HT can be determined using a widely practiced method, based on the work of Spano and coworkers, who showed that the UV-vis spectra of the polymer can be deconvoluted into contributions from the aggregated (i.e., ordered) and amorphous phases utilizing the weakly interacting H-aggregate model.[55] The ratio of these contributions, after taking into account the unequal absorption coefficients of the ordered and the amorphous domains, can be used to determine the percent aggregated polymer. To analyze the order of different P3HT:methanofullerene blends, we first obtained the UV-vis spectra of the blend and then subtracted the absorption of the pure methanofullerene. **Figures 6.3a** and 6.**3b** show the evolution in the ultraviolet-visible (UV-vis) spectra of the P3HT component of the P3HT:methanofullerene blends. The absorption due to the methanofullerenes was approximated as the absorption of thin films of the methanofullerenes (prepared in the same manner as the blends) and subtracted from the spectra of the blends.[21,56] (Before subtraction, the methanofullerene absorption spectra were normalized to the peaks at 335 nm for [60]PCBM and 379 nm for [70]PCBM.) Though this method of subtraction overestimates the methanofullerene contribution to the absorption spectra, it has a minimal effect on the strongly absorbing regions of P3HT. (While we note that [70]PCBM is more strongly absorbing in the visible region than [60]PCBM, the absorbance is still dominated by the P3HT component of the blend in the visible region.) The absence of vibronic peaks (longer-wavelength shoulders) in the as-cast films suggests the absence of ordered

aggregates of pure polymer. A clear increase in order upon thermal annealing is observed from the differences in the UV-vis spectra. To obtain the percent of the polymer in the aggregated phase of the annealed films, we used a MATLAB program to perform a least-squares fit of the weakly interacting H-aggregate model to the experimental data. This method was introduced by Clark et al. and later used by Awartani et al. to correlate microstructure to mechanical properties,[21,57] and produces consistent fits that are relatively insensitive to the range of bounds for the fit (as long as it is performed in the strongly absorbing region for aggregated polymer).[56] The morphology as assayed by UV-vis was not dependent on the substrate: spin-coating the BHJ films on glass treated with oxygen plasma, passivated with a fluorinated silane monolayer, or on glass bearing a film of PEDOT:PSS produced indistinguishable UV-vis spectra (**Figure C.1**, Supporting Information).

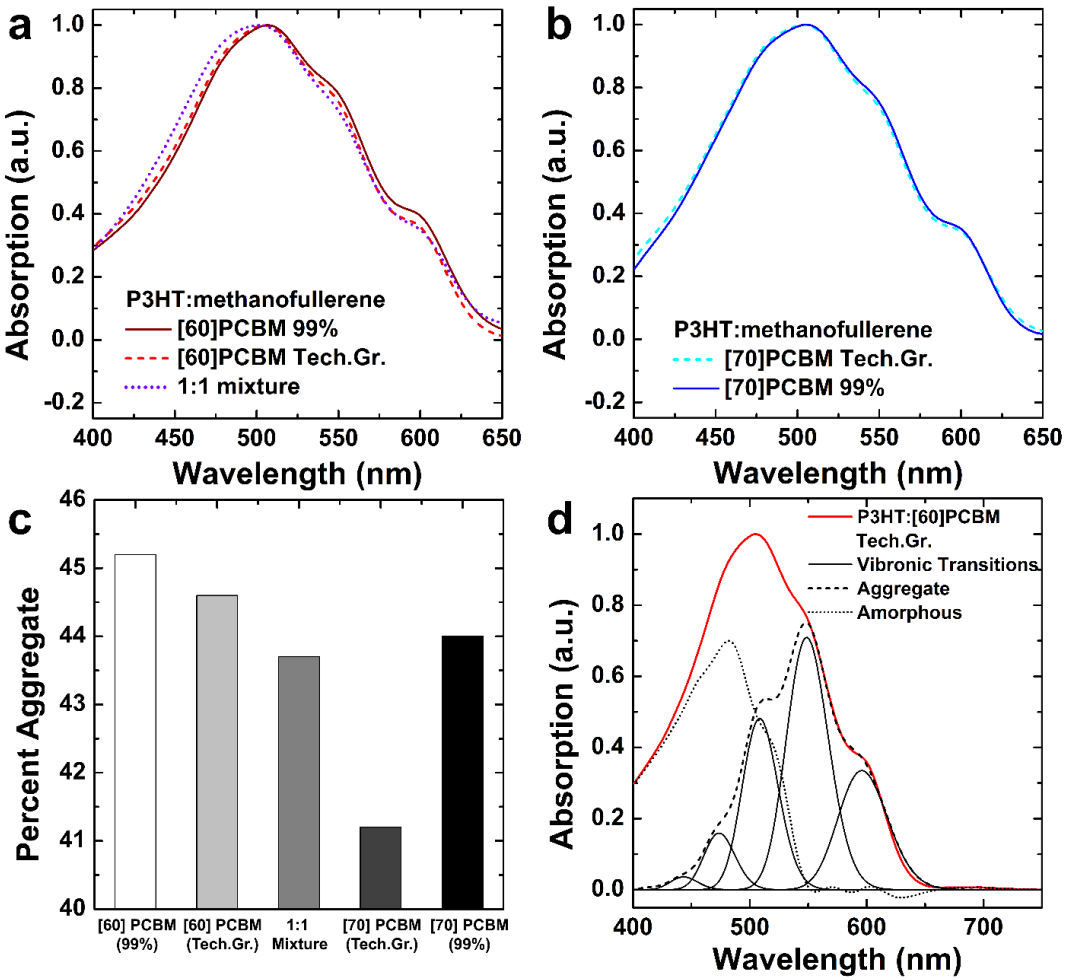

Figure 6.3. Absorption of P3HT:methanofullerene thin films after annealing treatment with the methanofullerene signal subtracted. (a) P3HT with [60]PCBM for 99% grade and technical grade (Tech. Gr.) along with the 1:1 mixture of [60]PCBM and [70]PCBM. (b) P3HT with [70]PCBM for technical grade (Tech. Gr.) and 99% grade. (c) Percent aggregate of the P3HT:methanofullerene films as calculated via the weakly interacting H-aggregate analysis. (d) Example of deconvolution of the absorption spectra using the weakly interacting H-aggregate analysis.

6.2.4 Effect of incomplete separation of [60]PCBM and [70]PCBM in technical grades

Enrichment of [60]PCBM and [70]PCBM from technical grade to 99% increased the tensile modulus of the resulting films. We attributed this effect to two factors. The first factor is that neat films of the technical grade methanofullerenes had lower tensile moduli (though the moduli of neat films of technical grade [70]PCBM and 99% [70]PCBM were within error, those of the corresponding BHJ films were not). If the packing structures of

the methanofullerene-enriched phases in the BHJ films resemble those of the neat methanofullerene films, then it stands to reason that the stiffening effect of the methanofullerene-rich inclusions would be reduced for technical grade samples in the BHJ films. One possible reason for decreased stiffness of the technical grade samples may be a consequence of less efficient packing of methanofullerenes in the presence of molecules of the "wrong" size. There may be a differential stiffening effect between [60]PCBM and [70]PCBM on the mixed phase of the BHJ, which may account for the fact that the moduli of the BHJ comprising technical grade [70]PCBM were less stiff than the one comprising 99% [70]PCBM, even though the moduli of the neat [70]PCBM films of both grades were similar. We admit to some uncertainty in rationalizing the greater modulus (though also greater ductility) of the as-cast P3HT:methanofullerene blend comprising 99% [70]PCBM compared to that of the as-cast blend comprising 99% [60]PCBM, especially in light of the significantly lower modulus of unblended 99% [70]PCBM compared to 99% [60]PCBM. We note however, that the mechanical properties will not necessarily be proportional to the modulus of the pure methanofullerene component, because differences observed between blended films comprising [60] and [70]PCBM are dependent on at least four factors: (1) unequal miscibility of [60]PCBM and [70]PCBM in amorphous P3HT; (2) unequal anti-plasticization even given the same miscibility; (3) unequal influence on the aggregation behavior of the polymer; and (4) packing structures—and thus mechanical properties—within the methanofullerene-enriched phases that do not necessarily resemble those in the neat methanofullerene films. Ultimately, the expected behavior was recovered upon annealing. That is, the annealed blend comprising 99% [70]PCBM had a lower modulus and greater ductility than the annealed blend comprising 99% [60]PCBM.

Another factor that may account for increased modulus of the BHJ film for 99% grade methanofullerenes is the increase in the order within the polymer phase induced by the higher-grade methanofullerene. Analysis of the spectra shown in **Figures 6.3a** and **6.3b** by the weakly interacting H-aggregate model[21,27,55] reveal that the percent aggregate of the polymer increases from 44.6% to 45.2% (for technical grade [60]PCBM to 99% [60]PCBM) and from 41.2% to 44.0% (for [70]PCBM technical grade to [70]PCBM 99%) (**Figure 6.3c**). The reason that the ordered polymer phase increased with increasing purity of the methanofullerene is not immediately clear. We tentatively assigned this effect, nevertheless, to the expectation that efficient packing of methanofullerene-enriched phases might remove methanofullerenes from the mixed phase, and thus permit additional polymer chains to form aggregates, which are correlated with stiffer films.

6.2.5 Effect of methanofullerene size and isomerism

Increasing the size of the fullerene core, from [60]PCBM to [70]PCBM, decreased the tensile moduli of the resulting blended films. While holding the grade and the post-treatment of the film constant, the moduli of the P3HT:methanofullerene films were lower in [70]PCBM samples compared to [60]PCBM samples (with one exception out of four pairs, the as-cast BHJ film made with 99% grade [60]PCBM was more compliant than the as-cast BHJ film made with 99% grade [70]PCBM, though the relationship was reversed after annealing). We attributed the lower compliance of BHJs comprising [70]PCBM compared to [60]PCBM principally to the presence of isomers of [70]PCBM, which impede crystallization. As shown in **Figure 6.1**, [70]PCBM exists as isomers because C_{70} has D5 symmetry.

6.2.6 Photovoltaic properties

We then measured the photovoltaic properties of the four BHJ blends for which we obtained mechanical data. We fabricated the devices by mixing the methanofullerenes in a 1:1 ratio with P3HT, using *o*-dichlorobenzene (ODCB) as the solvent. Given our ultimate interest in systems in which every component is stretchable, we chose PEDOT:PSS, doped with DMSO and Zonyl,[27] as the transparent anode, and eutectic gallium-indium (EGaIn) as the cathode. **Figure 6.4a** shows the current density vs. voltage (*J*-*V*) plots and **Table 6.3** summarizes the figures of merit. We observed increases in the short-circuit current (J_{sc}) in devices comprising [70]PCBM when compared to those with [60]PCBM. The observation agreed well with previously published results.[15–17] The effect of purity on J_{sc} and V_{oc} between the same methanofullerene size were minimal—similar values were obtained from [60]PCBM with technical grade and 99% grade as well as [70]PCBM with technical grade and 99% grade. However, in this study, the 99% [60]PCBM produced an increase in the fill factor (*FF*) and therefore the power conversion efficiency (*PCE*), compared to technical grade [60]PCBM. The difference in performance between technical grade [70]PCBM and 99% [70]PCBM was within experimental error. The only methanofullerene sample of the four measured with statistically lower *PCE* than the other three was technical grade [60]PCBM.

External quantum efficiency (*EQE*) of the devices are shown in **Figure 6.4b**. The effect of the size of the methanofullerenes were observed to be similar to that on the J_{sc}. High *EQE* values were observed in devices prepared from both technical grade and 99% [70]PCBM, suggesting that the photon-electron conversion processes are efficient. The purity of the methanofullerene increased the *EQE* values slightly, however the trend in the

EQE values generally corresponded with the *PCE* values obtained in the solar cells. We calculated the expected short-circuit current ($J_{SC,Calc}$), shown in **Table 6.3**, using the following equation:

$$J_{SC,Calc} = \int e\, EQE(\lambda)\, N_p(\lambda)\, d\lambda \qquad (\mathbf{3})$$

Where e is the elemental charge, λ is the wavelength, $EQE(\lambda)$ is external quantum efficiency, and $N_p(\lambda)$ is the total number of incident photons per second per square centimeter, obtained from the reference solar spectral irradiance AM 1.5G. The differences in the calculated J_{SC} between technical grade and higher purity samples were small, 8% for [60]PCBM and 5% for [70]PCBM. We also observed that our measured J_{SC} are lower than the calculated values, though within the 20% error margins outlined by Zimmermann et al.[58]

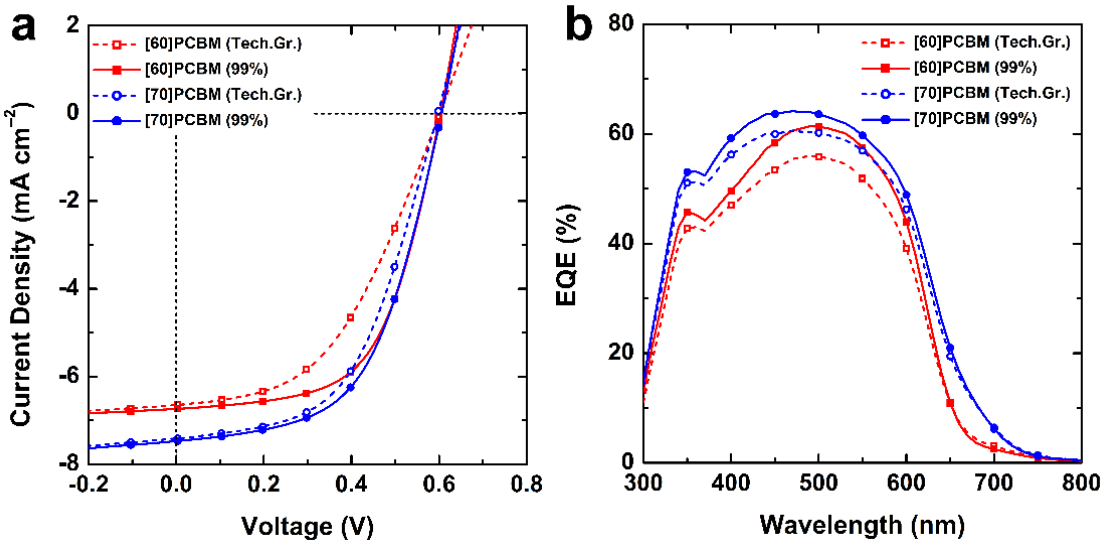

Figure 6.4. (a) Photovoltaic characteristic of averaged devices (N ≥ 8) with an active layer of 1:1 blend of P3HT and respective methanofullerenes. The architecture of the devices was PEDOT:PSS/P3HT:methanofullerene/EGaIn. (b) External quantum efficiencies of the devices with the same composition.

Table 6.3. Summary of the photovoltaic figures of merit for P3HT:methanofullerene solar cells fabricated in this work ($N \geq 8$) [†]

Device	V_{OC} (mV)	J_{SC} (mA cm^{-2})	*FF* (%)	*PCE* (%)	J_{SC}, calc from *EQE* (mA cm^{-2})
P3HT:[60]PCBM (99%)	602 ± 5.5	6.74 ± 0.2	59 ± 3.0	2.36 ± 0.2	8.27
P3HT:[60]PCBM (Tech.Gr.)	602 ± 3.7	6.60 ± 0.4	48 ± 4.8	1.89 ± 0.2	7.58
P3HT:[70]PCBM (Tech.Gr.)	598 ± 11.2	7.41 ± 0.3	53 ± 1.7	2.35 ± 0.1	8.92
P3HT:[70]PCBM (99%)	606 ± 7.5	7.47 ± 0.4	55 ± 1.3	2.48 ± 0.1	9.40

[†]The solar cell device architecture was PEDOT:PSS/P3HT:methanofullerene/EGaIn. PEDOT:PSS, doped with 7% DMSO and 0.1% Zonyl, was spin-coated to create a layer of ~150 nm thick. The active layer was spin-coated from a solution of 1:1 P3HT:methanofullerene in ODCB (40 mg mL^{-1}) and thermally annealed at 125 °C in an inert atmosphere. EGaIn droplets were extruded to create the active area of ~0.02 cm^{-2}.

6.3 Conclusion

Organic solar cells are in principal capable of producing substantial amounts of renewable energy at low cost, but only if they can be made in high yield using techniques for high-speed (e.g., roll-to-roll) manufacturing. Furthermore, organic solar cells have the potential to occupy niches in ultra-flexible, stretchable, wearable, collapsible, and portable applications, which would not be amenable to conventional—or even other thin-film—technologies. Mechanical compliance is often assumed for organic optoelectronic devices because of the ability to bend thin films to small radii of curvature. The mechanical properties, however, are not favorable for every organic semiconductor; it is important to understand these properties to mitigate potential routes of mechanical failure during fabrication and use in the outdoor environment (due to the forces of thermal expansion, wind, and precipitation, for example) and to enable stretchable and ultra-flexible applications. All applications demanding moderate to extreme mechanical deformation, however, require elucidation of the interplay between molecular structure and microstructure, and their influence on the mechanical properties of organic semiconductors.

This paper explored the effect of the size and the extent of mixing of two ubiquitous methanofullerene materials on the mechanical properties of organic solar cells. Our analysis, summarized in **Figure 6.5**, illustrates the effect of the extent of mixing on the mechanical properties of polymer:methanofullerene bulk heterojunction blends. In particular, use of technical grade [70]PCBM instead of 99% [60]PCBM increased the stretchability by a factor of three (from a crack-onset strain of 3.5% to 11.5%). This increase in compliance would, for example, substantially increase the range of tensile strains available in a wearable or portable device. The influence on flexibility is also significant: the less compliant film on the surface of a substrate with a thickness of 200 μm could be wrapped around a cylinder with a diameter of approximately 6 mm without fracture, while the more compliant film could be wrapped around a cylinder with a diameter of approximately 2 mm. Increased deformability should also increase the lifetime against damage during repeated loading.

While an earlier study found no statistically significant influence of the ratio between [60]PCBM and [70]PCBM of several methanofullerene derivatives on the power conversion efficiency of the P3HT:methanofullerene OPV devices,[15–17] the photovoltaic measurements in this study suggest that devices made using [70]PCBM of lower grade may be slightly but not substantially less efficient than those made using materials of higher grade. We note however, in contrast to earlier studies, that we used ITO-free anodes and EGaIn cathodes because of our underlying interest in stretchable and ultra-flexible applications. These substitutions could in principle lead to small differences observed between this study and earlier ones. Lowered efficiency could be tolerated if

counterbalanced by decreased cost and increased yield and lifetime, as appears to be possible in principle, based on our observations.

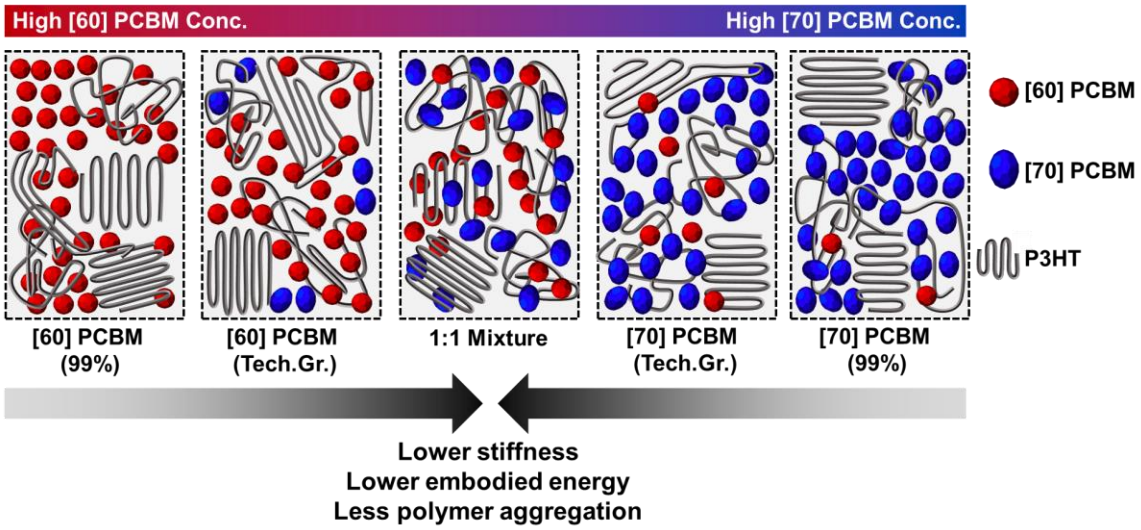

Figure 6.5. Schematic summary of the effect of mixed grades of methanofullerenes on the mechanical properties of P3HT:methanofullerene blends.

6.4. Experimental methods

6.4.1 Materials

Methanofullerene derivatives were synthesized by Solenne BV, Groningen, The Netherlands. We conducted our experiments using four different methanofullerene samples: [60]PCBM (99% and technical grade, which was 90% [60]PCBM with the remainder [70]PCBM), and [70]PCBM (99% and technical grade, which was 93.5% [70]PCBM with the remainder [60]PCBM). Mixtures with a 1:1 ratio were prepared by mixing 99% grades of [60]PCBM and [70]PCBM by weight. Regioregular poly(3-hexylthiophene) (P3HT, M_n = 44 kDa, PDI = 2.0) was purchased from Sigma-Aldrich and used as received. PDMS, Sylgard 184, Dow Corning, was prepared according to the manufacturer's instruction at a ratio of 10:1 (base:crosslinker) and cured at room temperature for 36 to 48 h when it was used for buckling experiments. (Tridecafluoro-

1,1,2,2-tetrahydrooctyl)-1-trichlorosilane (FOTS) was obtained from Gelest. PEDOT:PSS (Clevios PH1000) was purchased from Heraeus. DMSO was purchased from BDH with purity of 99.9%. Zonyl (FS-300) fluorosurfactant, chloroform, ODCB, acetone, isopropanol, and eutectic gallium-indium (EGaIn) were purchased from Alfa Aesar.

6.4.2 Preparation of films

For the buckling-based method and crack-onset experiments, hydrophobic glass slides were prepared as the initial substrate for the thin films. Glass slides (2.5 cm × 2.5 cm) were cleaned by bath sonication in detergent, deionized water, acetone, and isopropanol for 15 min each and dried under a stream of compressed air. The surface was then activated with an air plasma (30 W, 200 mTorr, 3 min) before enclosing in a vacuum desiccator with FOTS. The desiccator was left under dynamic vacuum for 12 h. The glass slides were rinsed with deionized water and isopropanol and dried under a stream of compressed air before use. For buckling-based method, P3HT:methanofullerene films were spin-coated onto FOTS treated glass slides using three different spin speeds to achieve three thicknesses. For the crack-onset experiments, all films were spin-coated at the parameters to obtain similar thicknesses. The as-cast (AC) films were then placed under vacuum for 1 h to remove any residual solvent. The annealed (AN) films were placed on the hot plate under inert atmosphere at 125 °C for 30 min before use. The films were spin-coated on plasma cleaned glass slides for UV-vis absorption experiments. We observed minimal differences in the UV-vis absorption when the films were spin-coated onto plasma-treated, FOTS-treated, and PEDOT:PSS glass slides (**Figure C.1,** Supporting Information).

6.4.3 Buckling-based methodology and crack-onset experiment

The elastomer poly(dimethylsiloxane) (PDMS) was chosen as the substrate for all mechanical measurements. The mixed and degassed prepolymer was allowed to cure at room temperature for 36 to 48 h before it was used in an experiment. The PDMS was then cut into rectangular pieces (l = 8 cm, w = 1 cm, h = 0.3 cm) and stretched to strains of 2% using a computer-controlled stage, which applied strain to samples using a linear actuator. While the PDMS rectangles were under strain, microscope slides (5 cm × 2.5 cm activated using oxygen plasma and treated with FOTS to later facilitate separation of the PDMS) were clipped onto the back of each rectangle using binder clips to maintain the strain. Transferring the P3HT:methanofullerene films to the pre-strained PDMS substrate was performed by initially scoring the films along the edges with a razor and placing the films against the PDMS. After applying a minimum amount of pressure to create a conformal seal between the PDMS and the P3HT:methanofullerene films, we separated the glass/stretched PDMS from the glass/conjugated polymer film in one fast motion. In most cases, the areas in which the films were in contact with the PDMS were successfully transferred to the pre-strained PDMS rectangles. The binder clips were then removed and the PDMS allowed to relax to the equilibrium length. Buckles formed in the P3HT:methanofullerene films upon relaxation of the PDMS. Buckling wavelengths were obtained from the optical micrographs. Due to the inherent brittleness of the pure methanofullerene films, we employed the bilayer technique to obtain the tensile moduli. In these sets of experiments, a layer of PEDOT:PSS film of known tensile modulus is used as interfacial layer. The PEDOT:PSS films were spin-coated onto the FOTS glass slides before spin-coating the desirable layers of the pure methanofullerene films. The

PEDOT:PSS layer assisted in modifying the surface energy such that the methanofullerene solutions can be easily deposited and facilitate the buckling-based experiment by lowering the effective modulus of the bilayer system. From the known modulus of the PEDOT:PSS and the measured thickness ratio between the PEDOT:PSS and the methanofullerene layer, the modulus of the methanofullerene layers were calculated using equation 2.

For crack-onset experiments, the PDMS substrates were cut into rectangular pieces (l = 8 cm, w = 1 cm, h = 0.15 cm). The P3HT:methanofullerene films were transferred onto the PDMS substrates baring no pre-strain in the same manner as described above. The P3HT:methanofullerene films/PDMS was then subjected to incremental increase in uniaxial strain with a step size of 0.5%. At each step, an optical micrograph was taken and the strain at which the first crack formed was recorded.

6.4.4 Fabrication of organic solar cells

We deposited a layer of PEDOT:PSS from an aqueous solution containing 92.9 wt % Clevios PH 1000 (~0.9−1.2 wt % PEDOT:PSS), 7.0 wt % DMSO, and 0.1 wt % Zonyl fluorosurfactant on plasma treated glass slides as the transparent anode. The solution was filtered and spin-coated at a speed of 500 rpm for 120 s, followed by 2000 rpm for 30 s. The films were then dried at 150 °C for 30 min. The photoactive layers were subsequently spin-coated on the PEDOT:PSS layer at a speed of 500 rpm for 240 s, followed by 2000 rpm for 60 s. A thin strip of the PEDOT:PSS anode was exposed by wiping away a section of the photoactive layer with chloroform for electrical contact. The samples were then immediately placed in a nitrogen-filled glovebox and annealed at 125 °C for 30 min. EGaIn was used as the top contact.

6.4.5 Characterization of films

The photovoltaic properties were measured in a nitrogen-filled glovebox using a solar simulator with a 100 mW cm^{-2} flux under AM 1.5G condition (ABET Technologies 11016-U up-facing using calibrated with a reference cell with a KG5 filter). The current density versus voltage was measured using a Keithley 2400 SourceMeter. The absorbance of the materials was measured using a PerkinElmer Lambda 1050 UV-vis-NIR spectrophotometer. The wavelength range measured was 300-850 nm with a step size of 1 nm. The films were prepared in the same manner as described in the above section of preparation of films. *EQE* measurement were measured in air. The photocurrent as a function of wavelength were recorded by a multifunction optical power meter (Newport Model 2936-R) using 300 W xenon lamp and Cornerstone monochromator (Newport Model 74004) illumination.

6.4.6 Weakly interacting H-aggregate model

In the aggregated state (i.e., crystallites in solid films), the coupled electron-vibrational (vibronic) transitions determine the absorption of weakly interactive H-aggregates and can be modeled as Gaussian fits by:[21,55–57]

$$A(E) \propto \sum_{m=0} \left(\frac{S^m}{m!}\right) \times \left(1 - \frac{We^{-S}}{2E_{\mathrm{p}}} \sum_{n \neq m} \frac{S^n}{n!\,(n-m)}\right)^2 \times exp\left(\frac{-\left(E - E_{00} - mE_{\mathrm{p}} - \frac{1}{2}WS^m e^{-S}\right)^2}{2\,\sigma^{\,2}}\right) \quad (\mathbf{4})$$

In the above equation, *A* is the absorption by an aggregate as a function of the photon energy (*E*). E_{00} is the energy of the 0→0 vibronic transition, which is allowed assuming some disorder in the aggregates.[55] *S* is the Huang-Rhys factor, which is calculated from

absorption and emission spectra, and is set to 1 for P3HTs.[55,57] E_p is the intermolecular vibration energy, which (in the case where $S = 1$) is set to 0.179 eV as determined by Raman spectroscopy.[59] W is the free exciton bandwidth, which is related to the nearest neighbor interchain excitonic coupling. Upon coupling, a dispersion of the energies occurs, the width of which is equal to W (which is four times the nearest neighbor coupling). The terms m and n are the ground- and excited state vibrational levels and σ is the Gaussian linewidth. The Gaussian linewidth, σ, E_p, W, and the scaling factor for the calculated absorption were found by a least squares fit to the experimental absorption in the region of 1.93 to 2.25 eV.[21,56,60] This region was selected because the absorption is dominated by the polymer aggregates. Above 2.30 eV, the amorphous polymer dominates absorption.[57,60]

Acknowledgements

This work was supported by the Air Force Office of Scientific Research (AFOSR) Young Investigator Program, grant number FA9550-13-1-0156. Additional support was provided by the laboratory startup funds from the University of California, San Diego. S.S. acknowledges support provided by the National Science Foundation Graduate Research Fellowship under Grant No. DGE-1144086. D. R. acknowledges support from the Initiative for Maximizing Student Development at UCSD.

Chapter 6, in full, is a reprint of the material as it appears in *Chemistry of Materials*, 2015, 27, 3902-3911. American Chemical Society, 2015. Suchol Savagatrup, Daniel Rodriquez, Adam D. Printz, Alexander B. Sieval, Jan C. Hummelen, and Darren J. Lipomi. The dissertation author was the primary investigator and author of this paper.

References

(1) Savagatrup, S.; Printz, A. D.; O'Connor, T. F.; Zaretski, A. V.; Rodriquez, D.; Sawyer, E. J.; Rajan, K. M.; Acosta, R. I.; Root, S. E.; Lipomi, D. J. Mechanical Degradation and Stability of Organic Solar Cells: Molecular and Microstructural Determinants. *Energy Environ. Sci.* **2015**, *8*, 55–80.

(2) Kaltenbrunner, M.; White, M. S.; Głowacki, E. D.; Sekitani, T.; Someya, T.; Sariciftci, N. S.; Bauer, S. Ultrathin and Lightweight Organic Solar Cells with High Flexibility. *Nat. Commun.* **2012**, *3*, 770.

(3) O'Connor, T. F.; Rajan, K. M.; Printz, A. D.; Lipomi, D. J. Toward Organic Electronics with Properties Inspired by Biological Tissue. *J. Mater. Chem. B* **2015**, *3*, 4947.

(4) Savagatrup, S.; Printz, A. D.; O'Connor, T. F.; Zaretski, A. V.; Lipomi, D. J. Molecularly Stretchable Electronics. *Chem. Mater.* **2014**, *26*, 3028–3041.

(5) Dou, L.; You, J.; Hong, Z.; Xu, Z.; Li, G.; Street, R. A.; Yang, Y. 25th Anniversary Article: A Decade of Organic/Polymeric Photovoltaic Research. *Adv. Mater.* **2013**, *25*, 6642.

(6) Li, H.; Tee, B. C.-K.; Giri, G.; Chung, J. W.; Lee, S. Y.; Bao, Z. High-Performance Transistors and Complementary Inverters Based on Solution-Grown Aligned Organic Single-Crystals. *Adv. Mater.* **2012**, *24*, 2588.

(7) Liu, T.; Troisi, A. What Makes Fullerene Acceptors Special as Electron Acceptors in Organic Solar Cells and How to Replace Them. *Adv. Mater.* **2013**, *25*, 1038.

(8) Burke, D. J.; Lipomi, D. J. Green Chemistry for Organic Solar Cells. *Energy Environ. Sci.* **2013**, *6*, 2053–2066.

(9) Anctil, A.; Babbitt, C. W.; Raffaelle, R. P.; Landi, B. J. Material and Energy Intensity of Fullerene Production. *Environ. Sci. Technol.* **2011**, *45*, 2353.

(10) Savagatrup, S.; Makaram, A. S.; Burke, D. J.; Lipomi, D. J. Mechanical Properties of Conjugated Polymers and Polymer-Fullerene Composites as a Function of Molecular Structure. *Adv. Funct. Mater.* **2014**, *24*, 1169–1181.

(11) Tahk, D.; Lee, H. H.; Khang, D.-Y. Elastic Moduli of Organic Electronic Materials by the Buckling Method. *Macromolecules* **2009**, *42*, 7079–7083.

(12) Brand, V.; Bruner, C.; Dauskardt, R. H. Cohesion and Device Reliability in Organic Bulk Heterojunction Photovoltaic Cells. *Sol. Energ. Mat. Sol. Cells* **2012**, *99*, 182.

(13) Dupont, S. R.; Voroshazi, E.; Heremans, P.; Dauskardt, R. H. Adhesion Properties of Inverted Polymer Solarcells: Processing and Film Structure Parameters. *Org.*

Electron. **2013**, *14*, 1262.

(14) Jørgensen, M.; Norrman, K.; Gevorgyan, S. A.; Tromholt, T.; Andreasen, B.; Krebs, F. C. Stability of Polymer Solar Cells. *Adv. Mater.* **2012**, *24*, 580.

(15) Andersson, L. M.; Hsu, Y.-T.; Vandewal, K.; Sieval, A. B.; Andersson, M. R.; Inganäs, O. Mixed C60/C70 Based Fullerene Acceptors in Polymer Bulk-Heterojunction Solar Cells. *Org. Electron.* **2012**, *13*, 2856.

(16) Popescu, L. M. Fullerene Based Organic Solar Cells, University of Groningen, 2008.

(17) Kronholm, D. F.; Hummelen, J. C.; Sieval, A. B.; Van't Hof, P. Patent US2013/8435716, 2013.

(18) Wienk, M. M.; Kroon, J. M.; Verhees, W. J. H.; Knol, J.; Hummelen, J. C.; van Hal, P. A.; Janssen, R. A. J. Efficient Methano[70]fullerene/MDMO-PPV Bulk Heterojunction Photovoltaic Cells. *Angew. Chem.* **2003**, *115*, 3493.

(19) Williams, E. D.; Ayres, R. U.; Heller, M. The 1.7 Kilogram Microchip: Energy and Material Use in the Production of Semiconductor Devices. *Environ. Sci. Technol.* **2002**, *36*, 5504.

(20) Anctil, A.; Babbitt, C. W.; Raffaelle, R. P.; Landi, B. J. Cumulative Energy Demand for Small Molecule and Polymer Photovoltaics. *Prog. Photovolt Res. Appl.* **2013**, *21*, 1541.

(21) Awartani, O.; Lemanski, B. I.; Ro, H. W.; Richter, L. J.; DeLongchamp, D. M.; O'Connor, B. T. Correlating Stiffness, Ductility, and Morphology of Polymer:Fullerene Films for Solar Cell Applications. *Adv. Energy. Mater.* **2013**, *3*, 399–406.

(22) O'Connor, B.; Chan, E. P.; Chan, C.; Conrad, B. R.; Richter, L. J.; Kline, R. J.; Heeney, M.; McCulloch, I.; Soles, C. L.; DeLongchamp, D. M. Correlations between Mechanical and Electrical Properties of Polythiophenes. *ACS Nano* **2010**, *4*, 7538–7544.

(23) Dupont, S. R.; Oliver, M.; Krebs, F. C.; Dauskardt, R. H. Interlayer Adhesion in Roll-to-Roll Processed Flexible Inverted Polymer Solar Cells. *Sol. Energ. Mat. Sol. Cells* **2012**, *97*, 171–175.

(24) Liu, F.; Gu, Y.; Jung, J. W.; Jo, W. H.; Russell, T. P. On the Morphology of Polymer-Based Photovoltaics. *J. Polym. Sci. Part B Polym. Phys.* **2012**, *50*, 1018.

(25) Lipomi, D.; Chong, H.; Vosgueritchian, M.; Mei, J.; Bao, Z. Toward Mechanically Robust and Intrinsically Stretchable Organic Solar Cells: Evolution of Photovoltaic Properties with Tensile Strain. *Sol. Energ. Mat. Sol. Cells* **2012**, *107*, 355–365.

(26) Printz, A.; Savagatrup, S.; Burke, D.; Purdy, T.; Lipomi, D. Increased Elasticity of a Low-Bandgap Conjugated Copolymer by Random Segmentation for Mechanically Robust Solar Cells. *RSC Adv.* **2014**, *4*, 13635–13643.

(27) Savagatrup, S.; Printz, A. D.; Rodriquez, D.; Lipomi, D. J. Best of Both Worlds: Conjugated Polymers Exhibiting Good Photovoltaic Behavior and High Tensile Elasticity. *Macromolecules* **2014**, *47*, 1981.

(28) Printz, A. D.; Savagatrup, S.; Rodriquez, D.; Lipomi, D. J. Role of Molecular Mixing on the Stiffness of Polymer:fullerene Bulk Heterojunction Films. *Sol. Energy Mater. Sol. Cells* **2015**, *134*, 64–72.

(29) Brand, V.; Levi, K.; McGehee, M. D.; Dauskardt, R. H. Film Stresses and Electrode Buckling in Organic Solar Cells. *Sol. Energ. Mat. Sol. Cells* **2012**, *103*, 80.

(30) Savagatrup, S.; Chan, E.; Renteria-Garcia, S. M.; Printz, A. D.; Zaretski, A. V.; O'Connor, T. F.; Rodriquez, D.; Valle, E.; Lipomi, D. J. Plasticization of PEDOT:PSS by Common Additives for Mechanically Robust Organic Solar Cells and Wearable Sensors. *Adv. Funct. Mater.* **2015**, *25*, 427.

(31) Stafford, C. M.; Harrison, C.; Beers, K. L.; Karim, A.; Amis, E. J.; VanLandingham, M. R.; Kim, H.-C.; Volksen, W.; Miller, R. D.; Simonyi, E. E. A Buckling-Based Metrology for Measuring the Elastic Moduli of Polymeric Thin Films. *Nat. Mater.* **2004**, *3*, 545–550.

(32) Stafford, C. M.; Guo, S.; Harrison, C.; Chiang, M. Y. M. Combinatorial and High-Throughput Measurements of the Modulus of Thin Polymer Films. *Rev. Sci. Instrum.* **2005**, *76*, 062207.

(33) Wilder, E. A.; Guo, S.; Lin-Gibson, S.; Fasolka, M. J.; Stafford, C. M. Measuring the Modulus of Soft Polymer Networks via a Buckling-Based Metrology. *Macromolecules* **2006**, *39*, 4138.

(34) Huang, D. M.; Mauger, S. A.; Friedrich, S.; George, S. J.; Dumitriu-LaGrange, D.; Yoon, S.; Moule, A. J. The Consequences of Interface Mixing on Organic Photovoltaic Device Characteristics. *Adv. Funct. Mater.* **2011**, *21*, 1657.

(35) Dupont, S. R.; Voroshazi, E.; Nordlund, D.; Vandewal, K.; Dauskardt, R. H. Controlling Interdiffusion, Interfacial Composition, and Adhesion in Polymer Solar Cells. *Adv. Mater. Interfaces* **2014**, 1400135.

(36) Verploegen, E.; Mondal, R.; Bettinger, C. J.; Sok, S.; Toney, M. F.; Bao, Z. Effects of Thermal Annealing Upon the Morphology of Polymer-Fullerene Blends. *Adv. Funct. Mater* **2010**, *20*, 3519.

(37) Miller, N. C.; Gysel, R.; Miller, C. E.; Verploegen, E.; Beiley, Z.; Heeney, M.; McCulloch, I.; Bao, Z.; Toney, M. F.; McGehee, M. D. The Phase Behavior of a

Polymer-Fullerene Bulk Heterojunction System That Contains Bimolecular Crystals. *J. Polym. Sci. Part B Polym. Phys.* **2011**, *49*, 499.

(38) Brady, M. M. A.; Su, G. G. M.; Chabinyc, M. M. L. Recent Progress in the Morphology of Bulk Heterojunction Photovoltaics. *Soft Matter* **2011**, *7*, 11065.

(39) Dang, M. T.; Hirsch, L.; Wantz, G. P3HT:PCBM, Best Seller in Polymer Photovoltaic Research. *Adv. Mater.* **2011**, *23*, 3597–3602.

(40) Liao, S.-H.; Li, Y.-L.; Jen, T.-H.; Cheng, Y.-S.; Chen, S.-A. Multiple Functionalities of Polyfluorene Grafted with Metal Ion-Intercalated Crown Ether as an Electron Transport Layer for Bulk-Heterojunction Polymer Solar Cells: Optical Interference, Hole Blocking, Interfacial Dipole, and Electron Conduction. *J. Am. Chem. Soc.* **2012**, *134*, 14271.

(41) Krebs, F. C.; Espinosa, N.; Hösel, M.; Søndergaard, R. R.; Jørgensen, M. 25th Anniversary Article : Rise to Power – OPV-Based Solar Parks. *Adv. Mater.* **2014**, *26*, 29–39.

(42) Osedach, T. P.; Andrew, T. L.; Bulović, V. Effect of Synthetic Accessibility on the Commercial Viability of Organic Photovoltaics. *Energy Environ. Sci.* **2013**, *6*, 711.

(43) Kim, J. Y.; Frisbie, C. D. Correlation of Phase Behavior and Charge Transport in Conjugated Polymer/Fullerene Blends. *J. Phys. Chem. C* **2008**, *112*, 17726.

(44) Zhao, J.; Swinnen, A.; Van Assche, G.; Manca, J.; Vanderzande, D.; Van Mele, B. Phase Diagram of P3HT/PCBM Blends and Its Implication for the Stability of Morphology. *J. Phys. Chem. B* **2009**, *113*, 1587.

(45) Treat, N. D.; Brady, M. A.; Smith, G.; Toney, M. F.; Kramer, E. J.; Hawker, C. J.; Chabinyc, M. L. Interdiffusion of PCBM and P3HT Reveals Miscibility in a Photovoltaically Active Blend. *Adv. Energy Mater.* **2011**, *1*, 82.

(46) Treat, N. D.; Varotto, A.; Takacs, C. J.; Batara, N.; Al-Hashimi, M.; Heeney, M. J.; Heeger, A. J.; Wudl, F.; Hawker, C. J.; Chabinyc, M. L. Polymer-Fullerene Miscibility: A Metric for Screening New Materials for High-Performance Organic Solar Cells. *J. Am. Chem. Soc.* **2012**, *134*, 15869.

(47) Roehling, J. D.; Batenburg, K. J.; Swain, F. B.; Moulé, A. J.; Arslan, I. Three-Dimensional Concentration Mapping of Organic Blends. *Adv. Funct. Mater.* **2013**, *23*, 2115.

(48) Choi, S. H.; Liman, C. D.; Krämer, S.; Chabinyc, M. L.; Kramer, E. J. Crystalline Polymorphs of [6,6]-Phenyl-C61-Butyric Acid N -Butyl Ester (PCBNB). *J. Phys. Chem. B* **2012**, *116*, 13568.

(49) Zheng, L.; Liu, J.; Ding, Y.; Han, Y. Morphology Evolution and Structural

Transformation of Solution-Processed Methanofullerene Thin Film under Thermal Annealing. *J. Phys. Chem. B* **2011**, *115*, 8071.

(50) Zheng, L.; Han, Y. Solvated Crystals Based on [6,6]-Phenyl-C61-Butyric Acid Methyl Ester (PCBM) with the Hexagonal Structure and Their Phase Transformation. *J. Phys. Chem. B* **2012**, *116*, 1598.

(51) Müller, C.; Ferenczi, T. a. M.; Campoy-Quiles, M.; Frost, J. M.; Bradley, D. D. C.; Smith, P.; Stingelin-Stutzmann, N.; Nelson, J. Binary Organic Photovoltaic Blends: A Simple Rationale for Optimum Compositions. *Adv. Mater.* **2008**, *20*, 3510.

(52) Treat, N. D.; Chabinyc, M. L. Phase Separation in Bulk Heterojunctions of Semiconducting Polymers and Fullerenes for Photovoltaics. *Annu. Rev. Phys. Chem.* **2014**, *65*, 59.

(53) Hopkinson, P. E.; Staniec, P. A.; Pearson, A. J.; Dunbar, A. D. F.; Wang, T.; Ryan, A. J.; Jones, R. A. L.; Lidzey, D. G.; Donald, A. M. A Phase Diagram of the P3HT: PCBM Organic Photovoltaic System: Implications for Device Processing and Performance. *Macromolecules* **2011**, *44*, 2908.

(54) Savagatrup, S.; Printz, A. D.; Wu, H.; Rajan, K. M.; Sawyer, E. J.; Zaretski, A. V.; Bettinger, C. J.; Lipomi, D. J. Viability of Stretchable poly(3-Heptylthiophene) (P3HpT) for Organic Solar Cells and Field-Effect Transistors. *Synth. Met.* **2015**, *203*, 208.

(55) Spano, F. C. Modeling Disorder in Polymer Aggregates: The Optical Spectroscopy of Regioregular poly(3-Hexylthiophene) Thin Films. *J. Chem. Phys.* **2005**, *122*, 234701.

(56) Turner, S. T.; Pingel, P.; Steyrleuthner, R.; Crossland, E. J. W.; Ludwigs, S.; Neher, D. Quantitative Analysis of Bulk Heterojunction Films Using Linear Absorption Spectroscopy and Solar Cell Performance. *Adv. Funct. Mater.* **2011**, *21*, 4640.

(57) Clark, J.; Chang, J.-F.; Spano, F. C.; Friend, R. H.; Silva, C. Determining Exciton Bandwidth and Film Microstructure in Polythiophene Films Using Linear Absorption Spectroscopy. *Appl. Phys. Lett.* **2009**, *94*, 163306.

(58) Zimmermann, E.; Ehrenreich, P.; Pfadler, T.; Dorman, J. A.; Weickert, J.; Schmidt-Mende, L. Erroneous Efficiency Reports Harm Organic Solar Cell Research. *Nat. Photonics* **2014**, *8*, 669.

(59) Louarn, G.; Trznadel, M. Raman Spectroscopic Studies of Regioregular Poly (3-Alkylthiophenes). *J. Phys. Chem.* **1996**, *3654*, 12532.

(60) Pingel, P.; Zen, A.; Abellon, R. D.; Grozema, F. C.; Siebbeles, L. D. A.; Neher, D. Temperature Resolved Local and Macroscopic Charge Carrier Transport in Thin

P3HT Layers. *Adv. Funct. Mater.* **2010**, *20*, 2286.

Chapter 7

Plasticization of PEDOT:PSS by common additives for mechanically robust organic solar cells and wearable sensors

S Suchol Savagatrup, Esther Chan, Sandro M. Renteria-Garcia, Adam D. Printz, Aliaksandr V. Zaretski, Timothy F. O'Connor, Daniel Rodriquez, Eduardo Valle, and Darren J. Lipomi

Department of NanoEngineering, University of California, San Diego

9500 Gilman Drive, Mail Code 0448, La Jolla, CA 92093-0448

Abstract

Despite the ubiquity of poly(3,4-ethylenedioxythiophene):poly(styrenesulfonate) (PEDOT:PSS) in applications demanding mechanical flexibility, the effect on the mechanical properties of common additives—i.e., dimethylsulfoxide (DMSO), Zonyl fluorosurfactant (Zonyl), and poly(ethyleneimine) (PEI)—has not been reported. This paper describes these effects and uses plasticized films in solar cells and mechanical sensors for the detection of human motion. The tensile moduli of films spin-coated from solutions containing 0%, 5%, and 10% DMSO and 0.1%, 1%, and 10% Zonyl (nine samples total) are measured using the buckling technique, and the ductility is inferred from measurements of the strain at which cracks form on elastic substrates. Elasticity and ductility are maximized in films deposited from solutions containing 5% DMSO and 10% Zonyl, but the conductivity is greatest for samples containing 0.1% Zonyl. These experiments reveal enlargement of presumably PEDOT-rich grains, visible by atomic force microscopy, when the amount of DMSO is increased from 0% to 5%. PEI—which is used to lower the work function of PEDOT:PSS—has a detrimental effect on the mechanical properties of the PEDOT:PSS/PEI bilayer films. Wearable electronic sensors employing PEDOT:PSS films containing 5% DMSO and 10% Zonyl are fabricated, which exhibit detectable responses at 20% strain and high mechanical robustness through elastic deformation.

7.1 Introduction

Poly(3,4-ethylenedioxythiophene):poly(styrenesulfonate) (PEDOT:PSS, **Figure 7.1**) is a polyelectrolyte complex used ubiquitously as an electrode in organic electronic and

optoelectronic devices.[1] Its high conductivity[2] and transparency,[3] low sheet resistance,[4] and versatility of processing from aqueous solution[5] make it an attractive choice for transparent anodes in organic solar cells,[6] and light-emitting devices,[7] and as electrodes in organic bioelectronics.[8,9] It can be used either alone[6] or in concert with indium tin oxide (ITO) or transparent conductors based percolated networks of conductive nanoparticles.[10,11] General methods of lowering the work function of PEDOT:PSS—e.g., using thin layers of amine-containing small molecules[7,12] and polymers[13]—enable its use as the cathode for organic solar cells in all-organic devices.[14] The use of transparent electrodes as both the top and bottom contacts enable semitransparent solar cells and displays.[7] The use of polymeric top and bottom contacts, in particular, enables all-solution-processing[6] and could pave the way toward ultra-compliant—i.e., stretchable and extremely flexible—devices.[15–18] The use of PEDOT:PSS in flexible and stretchable electronics,[5] however, demands a rigorous characterization of its mechanical properties. While the tensile modulus of the most common formulation of PEDOT:PSS can be quite high (≥ 2 GPa),[19] it has also demonstrated potential value as a stretchable transparent conductor for mechanically robust, portable devices for energy[20] and biomedical applications.[9] Additives, such as co-solvents,[21] surfactants,[4] and other polymers[13] designed to improve the processability or work function of PEDOT:PSS for a given application are also likely to change drastically the mechanical properties of the pure material.[22] Despite the necessity of additives in essentially all applications to PEDOT:PSS in flexible electronics,[14] quantification of the substantial effects of these additives on the mechanical properties has received relatively little attention,[15–18] though previous reports have described the mechanical properties as a function of relative humidity under strain applied parallel[23] and perpendicular to the

films.[24] This paper describes the effect of dimethylsulfoxide (DMSO, added to PEDOT:PSS to increase its conductivity[14]) a flurosurfactant (Zonyl, added to increase its wettability on hydrophobic substrates[21]), and polyethyleneimine (PEI, laminated to PEDOT:PSS to alter its work function[13]) on the tensile modulus and ductility of PEDOT:PSS. We then used these highly plasticized films to produce (1) organic solar cells using the plasticized formulation of PEDOT:PSS and (2) wearable electronic sensors exhibiting detectable responses at 20% strain and high mechanical robustness through elastic deformation.

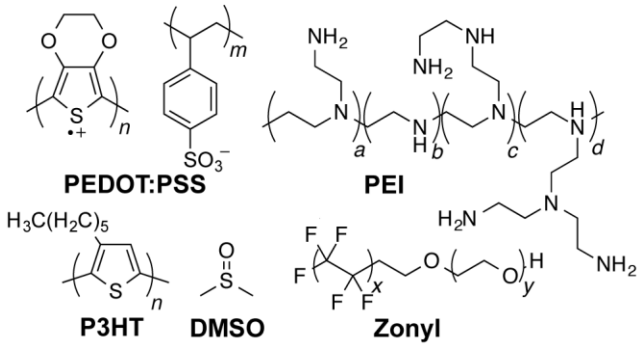

Figure 7.1. Chemical structure of PEDOT:PSS, PEI, P3HT, DMSO, and Zonyl

Stretchable (i.e., elastic or ductile) electronic devices based on organic semiconductors could have applications in a wide range of fields, from energy[25] to medicine.[26,27] The most successful approaches to the realization of stretchable organic electronic devices have relied on directing strain away from the active components by using stretchable interconnects or buckled, wavy layouts to convert global tensile strains into local bending strain to minimize deformation.[28,29] Another approach is to use fractured films of organic materials that nevertheless maintain percolated pathways to the

electrodes.[30] Materials that accommodate strain by virtue of their molecular or solid-state packing structures—intrinsic stretchability—could simplify processing and fabrication, and lead to better performing devices than those that rely on topographic patterns or fractured thin films.[31] Our group and others are attempting to understand the molecular and microstructural parameters that influence the mechanical properties of organic semiconductors.[32,33] We believe that a complete understanding of these properties will not only facilitate processing of devices for near-term applications, but could also further the development of a new form of stretchable electronics in which every component of the device accommodates the strain due to its molecular or microstructural characteristics.[31]

PEDOT:PSS is a polyelectrolyte complex prepared by the oxidative polymerization of EDOT in the presence of PSS.[1] In solution, it exists as relatively high-MW chains of PSS decorated by relatively shorter oligomers of PEDOT.[19] It is perhaps the most technologically ubiquitous conductive polymer, and is used commonly as an antistatic coating on photographic film.[34] In research laboratories, it is a component of essentially all organic solar cells and light-emitting diodes. Commercially available formulations differ primarily on the basis of the ratio of PEDOT and PSS. The formulation Clevios PH1000, manufactured by Hereaus, has a weight ratio of 1:2.5. It has achieved bulk conductivities of ~500 S cm^{-1} when 5–7% dimethylsulfoxide (DMSO) is added as a secondary dopant.[35]

PEDOT:PSS is generally cast into films from aqueous suspension by spin-coating for laboratory-scale devices;[4] recent work has shown its amenability to spray-coating,[5] gravure printing,[21] and slot-die coating.[36] The surface tension of pure water renders as-received formulations incompatible with hydrophobic substrates.[21] Co-solvents (e.g., isopropanol[5]) or surfactants (e.g., Zonyl fluorosurfactant,[21] now called Capstone by

DuPont) are generally required to coat plastic foils or organic active layers as is required in "inverted" solar cells. [21] The dramatic effects of these additives on the morphology and intermolecular forces of PEDOT:PSS—as manifested in the surface energy—suggests that the effect on the mechanical properties might be equally dramatic. These effects have not, however, been described.

The mechanical properties of pure films of PEDOT:PSS have been measured by several research groups. Measured by tensile testing of relatively thick (≥10 μm) films and fibers at 50% relative humidity, PEDOT:PSS exhibited moduli of 1.1–2.2 GPa.[23] Tahk et al. used the method based on the mechanical buckling of thin films of PEDOT:PSS films on PDMS substrates and found a similar modulus of 2.2 GPa.[19] Interestingly, the modulus was relatively insensitive to the ratio of PEDOT to PSS in the film.[19] The authors attributed this effect to the fact that the PSS component had a significantly greater molecular weight and dominated the mechanical response of the composite material.[19] Dupont and coworkers have noted that thin films of PEDOT:PSS exhibit moisture-assisted decohesion.[24] Other PEDOT-containing composites have achieved impressive combinations of elasticity and conductivity. For example, EDOT electropolymerized in a solution containing *para*-toluenesulfonate and polyurethane can form a conductive composite that can be stretched reversibly up to 50%, while maintaining a conductivity of up to 100 S cm^{-1} when stretched up to 100% strain.[37] A PEDOT:PSS-polyionic liquid blend achieved strains of 350% with an decrease in conductivity of only a factor of two at the maximum strain (but from a low initial conductivity of 10^{-3} S cm^{-1}).[38] The commercial formulation of PEDOT:PSS can also accommodate strains of up to 30% reversibly, on stretchable substrates, though smaller strains of about 10% cause the film to deform plastically; repeated strains above the onset

of plastic deformation are thus accommodated by topographic buckles, as opposed to the intrinsic elasticity of the material.[22]

In addition to its role as an electrode, PEDOT:PSS has a serendipitous role as an adhesion promoter between compliant substrates and organic semiconductors. For example, our laboratory observed that the presence of the PEDOT:PSS—which has good adhesion to both UV/ozone-activated PDMS and polymer:fullerene films—significantly suppressed the formation of cracks in devices under biaxial tensile strain.[39] The importance of adhesion on suppressing the formation of cracks in compliant thin-film devices has been observed before in copper films on polyimide substrates, in which systems employing a chromium adhesion layer can accommodate strains up to 50% without cracking the copper film.[40] For film-substrate systems exhibiting poor adhesion, global strains localize in the film to delaminated regions and cause premature cracking.[41] Moreover, cracks propagate through layers, and thus the strain at which an organic electronic device fails may therefore depend entirely on the mechanical properties of the PEDOT:PSS, regardless of the elasticity or ductility of the active materials. In situations that impose stresses at the interface between layers in a device, it is often the interface between PEDOT:PSS and the active material that fractures. Fracture energies in the range of 0.1 – 1.6 J m^{-2}, depending on the ratio of P3HT to PCBM in the active layer, have been reported by Dupont et al. for organic solar cells.[42] Factors known to weaken the adhesion of PEDOT:PSS with other layers include relative humidity, temperature, mechanical stress, and the percent incorporation of PCBM in P3HT:PCBM bulk heterojunctions.[43] Our experiments were designed to isolate other parameters and test only the effect of DMSO, Zonyl, and PEI on

the elasticity and ductility of PEDOT:PSS for devices in which each component was highly stretchable.

Dimethylsulfoxide (DMSO) is added to aqueous inks containing PEDOT:PSS in weight percentages of 5%–10% in essentially all applications. The role of polar "secondary dopants" such as DMSO, ethylene glycol, and sorbitol is to increase the conductivity significantly, from a native conductivity of <1 S cm^{-1} to conductivities approaching 10^3 S cm^{-1}.[4] The effect of these secondary dopants is attributed to the enlargement and coalescence of conductive grains of PEDOT in the solid film upon drying at elevated temperature, which produces large regions of uninterrupted pathways for charge carriers to traverse the film.[44] While it is not believed that DMSO persists in films after drying (e.g., on a hotplate), and thus cannot behave as a plasticizer, differences in microstructure produced by different processing conditions could easily lead to large differences in the mechanical properties of thin polymeric films.[45]

Zonyl is a fluorosurfactant comprising a poly(tetrafluoroethylene) segment and a poly(ethylene oxide) segment (**Figure 7.1**). When added to commercial formulations of PEDOT:PSS in concentrations as low as 0.01–0.1%, Zonyl permits wetting of hydrophobic substrates. It is widely used to improve the wetting behavior in roll-to-roll production, especially given the inability of unmodified PEDOT:PSS formulations to wet organic active layers in organic solar cells with the inverted architecture.[21] Zonyl was also found to have the additional advantage of improving the conductivity of PEDOT:PSS beyond what is possible with DMSO alone—i.e., as a "tertiary dopant."[4] The rationale for this improvement was similar to that of the improvement brought about by DMSO, namely a coalescing of conductive grains of PEDOT within an insulating, continuous phase of PSS,

as supported by atomic force microscope (AFM) images.[4] The conductivity was maximized for films cast from solutions containing 5% DMSO and 0.01–0.1% Zonyl. In addition to improved wetting behavior and conductivity, an incidental observation noted in an earlier publication suggests that Zonyl may also behave as a plasticizer.[22] In particular, for PEDOT:PSS on PDMS substrates treated with oxygen plasma, the increase in electrical resistance of films cast from solutions containing 1% Zonyl was an order of magnitude less than that of films prepared without Zonyl, when both types of films were strained by 50%.[22] Direct measurements of tensile modulus and ductility as a function of the concentration of the additive, however, were not performed.

Polyethyleneimine (PEI) was introduced by Zhou et al. as a universal method of altering the work function of electrode materials for thin-film applications.[13] In particular, a thin film of PEI changes the work function of PEDOT:PSS from 5.1 eV to 4.3 eV.[13] This addition of PEI enables the modified PEDOT:PSS to behave as the cathode and the unmodified PEDOT:PSS to behave as an anode when used together in a single cell. Our group has applied this approach to fabricate biaxially stretchable, all-polymer solar cells in order to bond them to hemispherical surfaces, but we did not examine the influence of the thin (~20 nm) PEI layer and its solvent on the mechanical properties of the PEDOT:PSS.[39] In addition, the solvent used to deposit PEI, 2-methoxyethanol (MOE), could potentially have an effect on the mechanical properties of the PEDOT:PSS films.

We measured two parameters of mechanical properties, tensile modulus and the crack on-set strain, of PEDOT:PSS films comprising different composition of DMSO and Zonyl as well as PEDOT:PSS films with a PEI layer laminated on top at constant room temperature of 23 °C and relative humidity of 50%. The tensile moduli were measured

using the mechanical buckling technique originally described by Stafford et al.[46] The PEDOT:PSS films were first spin-coated on a passivated glass substrate then transferred to a PDMS substrate bearing a small pre-strain (2–4%). Release of the pre-strain produced buckling in the PEDOT:PSS films. The slope of a plot of buckling wavelength vs. the thickness of the film was used to determine the tensile modulus of the film. The crack on-set strain can be used to measure the effective ductility of a film/substrate system. We measured the electrical conductivity of the films using a two-terminal measurement with silver paint as electrodes. The absence of significant contact resistance was verified using four-terminal measurements for randomly selected samples.

7.2. Results and discussion

The results of the mechanical measurements are shown in **Figure 7.2**. Zonyl has a dramatic plasticizing effect on PEDOT:PSS, as seen in the decrease in tensile modulus (**Figure 7.2a**) and increase in crack-onset strain (**Figure 7.2b**). In each triad on the plots in which the concentration of DMSO in the ink was kept constant at 0, 5, or 10 wt.%, the concentration of Zonyl dramatically increased the ductility of the film, as manifested by an increase in the crack-onset strain from ≤5% strain for all samples with 0.1% Zonyl, to up 25 – 40% strain for all samples coated from inks containing 10% Zonyl. These values are a factor of three greater than previous highest ductility reported in PEDOT:PSS films, which cracked at strains of 12%.[22] Ductility was highly correlated with tensile modulus (**Figure 7.2b**). An increase in Zonyl from 0.1 wt.% to 1 wt.% produced a decrease in the tensile moduli by a factor of two for samples with 5% and 10% DMSO, and by a factor of eight for samples with 0% DMSO. Due to the high vapor pressure of Zonyl, we expected

that a significant fraction remained in the PEDOT:PSS film, and that it functioned as a typical plasticizer, i.e., by increasing the free volume in the film and weakening intermolecular forces between the polymer chains. We note that obtaining the tensile moduli of films containing 10% Zonyl by the buckling method was difficult, because the buckling technique requires that the modulus of the film be at least two orders of magnitude greater than that of the PDMS substrate.[46] We did not observe buckles for the sample spin-coated from a solution with 0% DMSO and 10% Zonyl. We believe this film simply compressed along with the PDMS substrate after release of the pre-strain, rather than formed buckles.

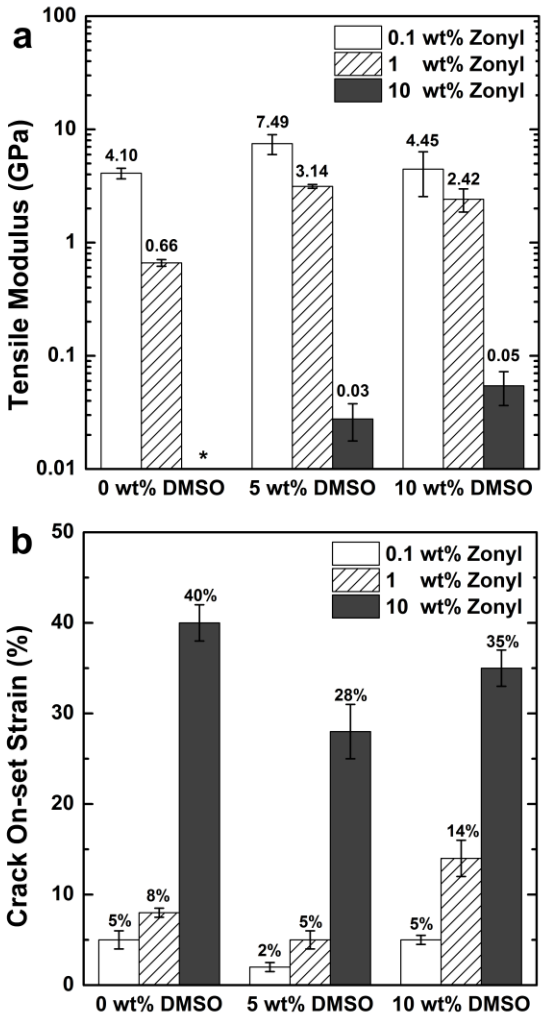

Figure 7.2. Mechanical properties of PEDOT:PSS films as a function of DMSO and Zonyl concentration in the ink. (a) Tensile moduli obtained via the buckling methodology. The asterisk (*) refers to the absence of data from the sample coated from ink containing 0 wt% DMSO and 10 wt.% Zonyl, which was too soft to measure. (b) Crack-onset strains of the thin films transferred onto PDMS substrates.

The data shown in **Figures 7.2a** and **7.2b** also revealed a dependence of the mechanical properties of PEDOT:PSS on the amount of DMSO present in the ink. Films deposited from solutions containing 5% DMSO were the stiffest and least ductile, though the effect was not nearly as strong as for Zonyl. Unlike Zonyl, significant amounts of DMSO were not likely to remain in the film after drying at 100 °C on a hotplate, and thus effects produced by DMSO were attributed to changes in the microstructure of the film.

The relative stiffness and brittleness of the films containing 5% DMSO mirrored the effects of DMSO on the conductivity (a topic to which we will return), which suggest that the interconnectedness of the PEDOT-rich domains in the film that are associated with the greatest conductivity also produced the greatest stiffness.

While the substantial increase in ductility of the PEDOT:PSS films could be optimized by varying the concentration of DMSO and Zonyl, we note that the mechanical properties of the solar cell devices will be dependent on all of the components and not solely on the properties of PEDOT:PSS films. Other components of the devices—the active component layer, the electrode, the substrate, and the encapsulation—may generate cracks that lead to the device failure prior to the crack-onset strain of the PEDOT:PSS films. However, in the case which the active layer and the top electrode are more mechanically compliant than the PEDOT:PSS films, the PEDOT:PSS films had a deleterious effect on the effective ductility of the devices.[39] Further work in determining the final architecture and components of the solar cell will be required before the crack-onset strain experiment on the full solar cell could be executed. We also attempted to correlate the mechanical data to the conductivity as a function of both the concentrations of DMSO and Zonyl present in the aqueous solution. **Figure 7.3a** shows the measured sheet resistance of the PEDOT:PSS films with constant thickness of 150 nm. While the effect of DMSO on the conductivity of PEDOT:PSS has been studied exhaustively,[14] the effect of Zonyl has only been examined one other time, and with only one concentration of DMSO.[4] Our results are largely consistent with those previously reported: the sheet resistance of the films coated without DMSO were too high for most device applications (>100 kΩ sq^{-1}). Similar values of sheet resistance were obtained for inks containing both 5% and 10% DMSO, with 5% producing

somewhat more conductive films (other reports suggest 7% may be the optimum value).[35] The lowest sheet resistance of 63 Ω sq^{-1} was achieved using 5% DMSO and 0.1% Zonyl. While small concentrations of Zonyl increased the conductivity (lowered the sheet resistance) of PEDOT:PSS compared to samples without Zonyl, concentration in excess of 0.1% increased the sheet resistance of the samples spin-coated from solutions containing either 5% or 10% DMSO. This result agreed well with the previous findings by Vosgueritchian et al. where Zonyl at the concentration of 0.01% and 0.1% lowered the sheet resistance of PEDOT:PSS films containing 5% DMSO when compared to PEDOT:PSS films containing 5% DMSO and no Zonyl; however, when the concentration of Zonyl increased to 1% and 10%, higher sheet resistances were obtained.[4] The conventional rationale for the improvement in conductivity with either DMSO or Zonyl is the apparent enlargement of PEDOT-rich grains within a PSS matrix; which are generally assigned on the basis of AFM; however, morphology at the surface is not necessarily representative of the microstructure of the bulk.[14]

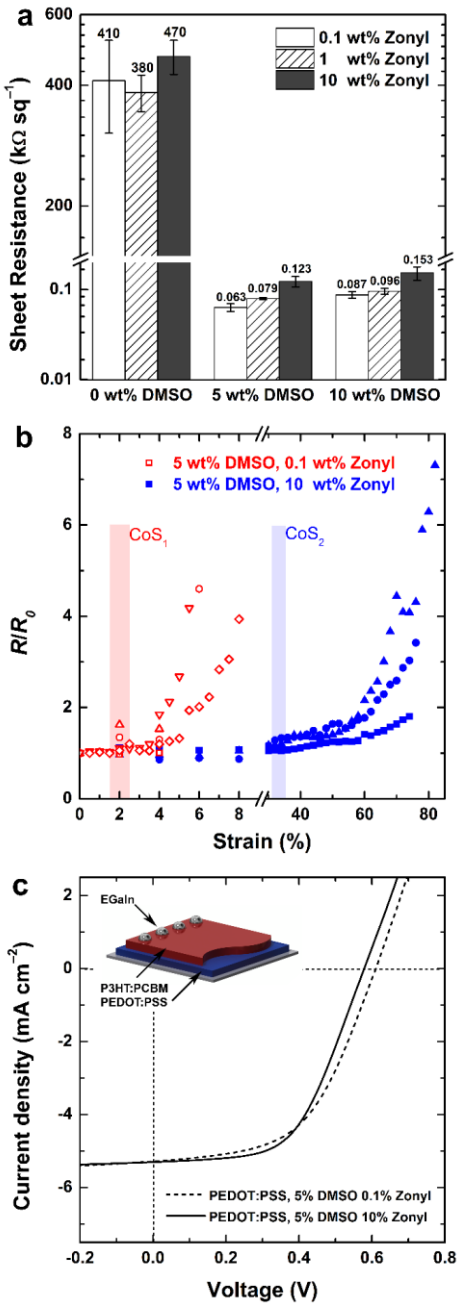

Figure 7.3. Resistance measurements of PEDOT:PSS films studied in this work. (a) Sheet resistance as a function of both DMSO and Zonyl concentration in the ink. (b) Plot of normalized resistance (R/R_0) vs. strain for PEDOT:PSS films spun from 0.1% and 10% Zonyl (with constant 5% DMSO) transferred onto PDMS substrates. Shaded areas represent the crack-onset strains (CoS) of the respective films. The widths of the shaded areas are two times the standard deviations for the measurements of crack-onset strain. The different marker symbols (squares, triangles, etc.) refer to different films coated from the same solution. (c) Typical (dashed red) and modified (solid blue) photovoltaic properties of bulk heterojunction devices with the architecture PEDOT:PSS/P3HT:PCBM/EGaIn. Each curve represents the average of 8 devices.

We examined the evolution of resistance as a function of strain for PEDOT:PSS films coated from solutions containing 0.1% Zonyl and 10% Zonyl (with a constant 5% DMSO), **Figure 7.3b**. The PEDOT:PSS films were spin-coated on passivated glass then transferred to unstrained PDMS substrate. Electrical contact was made using eutectic gallium-indium (EGaIn). The resistances of the films were then measured as a function of the linear strain applied by a computer-controlled linear actuator. As expected from the values of the respective crack-onset strain, the relative resistance (R/R_0) of the films spun using 0.1% Zonyl increased rapidly at relatively low strain compared to those of the films spun using 10% Zonyl. For the films containing 0.1% Zonyl, the increase in relative resistance occurred at the strain slightly greater that the crack-onset strain of 2%, and after 8% strain, the resistance of the films were greater than the sensitivity limit of our electrometer. We attributed the initial increase in resistance to the generation of minor cracks on the films and the result of increase in the particle separation when the films are stretched. The large increase in resistance thereafter to major cracks that led to the catastrophic failure of the films. We observed a much smaller increase in the relative resistance for the films with 10% Zonyl for up to ~40% strain and catastrophic failure at ~80% strain. We note that the observed relative resistance had a wider spread between samples after the films were stretched beyond the crack-onset strain. We attributed this effect to the idiosyncratic nature of the formation and propagation of cracks between samples prepared similarly. For example, a sample with a crack spanning nearly the entire width of the sample will have a much higher resistance than one with two disconnected cracks, which permit substantial conductance.

We fabricated bulk heterojunction organic photovoltaic (OPV) devices to evaluate whether the increase in the sheet resistance of the PEDOT:PSS films spun using 10% Zonyl will have a deleterious effect on the device performance when compared to films spun using 0.1% Zonyl. The sheet resistance of the transparent electrodes plays an important role in the performance of the OPV devices. High values of sheet resistance directly influence the value of series resistance within an OPV device; high series resistance lowers the fill factor (*FF*) and the overall power conversion efficiency (*PCE*). We compared OPV devices based on P3HT:PCBM with cell architecture of PEDOT:PSS/P3HT:PCBM/EGaIn using two different PEDOT:PSS solutions: (1) 5% DMSO, 10% Zonyl and (2) 5% DMSO, 0.1% Zonyl. We chose the solution containing 5% DMSO and 10% Zonyl because we found the composition of the films spun from this ink to be the most mechanically compliant while retaining adequate conductivity. The solution containing 5% DMSO and 0.1% Zonyl was chosen to isolate the possible effect arising from the concentration of DMSO; and, the solution with 0.1% Zonyl was used previously by our group to optimize *PCE* in OPV devices comprising P3AT:PCBM.[33] **Figure 7.3c** shows that the *J*-*V* curves of devices using two different compositions of the PEDOT:PSS solutions were relatively similar. The photovoltaic performances for the two configurations were constant, within experimental error, exhibiting *FF* of 54% to 56% and *PCE* of 1.7%, which agrees well with results reported earlier in literature with similar cell architecture.[4] These results suggested that the higher sheet resistance of the solution containing 5% DMSO and 10% Zonyl had minor effects on the performance of the solar cells and could be employed in highly stretchable devices.

To attempt to correlate the microstructure of the films as apparent on the surface to the conductivity (sheet resistance), we obtained AFM phase images of samples spun from inks with all nine combinations of concentrations of DMSO and Zonyl (**Figure 7.4**). Samples deposited from solutions containing either 0% or 5% DMSO and 0.1% or 1% Zonyl (the top-left four images) exhibited a qualitative increase in size of the PEDOT-rich domains as visible in the phase-contrast images (from 0% to 5% DMSO). Increasing the concentration of DMSO further to 10%—again ignoring the right-hand column—decreased the sizes of these grains (which is particularly clear in the transition from 5% DMSO/1% Zonyl to 10% DMSO/1% Zonyl); this reduction in size is correlated to a decrease in conductivity, as we expected due to precedent in the literature.[14] All samples containing 10% Zonyl exhibited high-aspect-ratio fibrils at the surface whose size showed no correlation with conductivity at any concentration of DMSO; these samples did however exhibit the greatest compliance and ductility. The morphology of the surface, however, may not have been representative of the microstructure of the bulk, given the likelihood that Zonyl segregated to the surface.

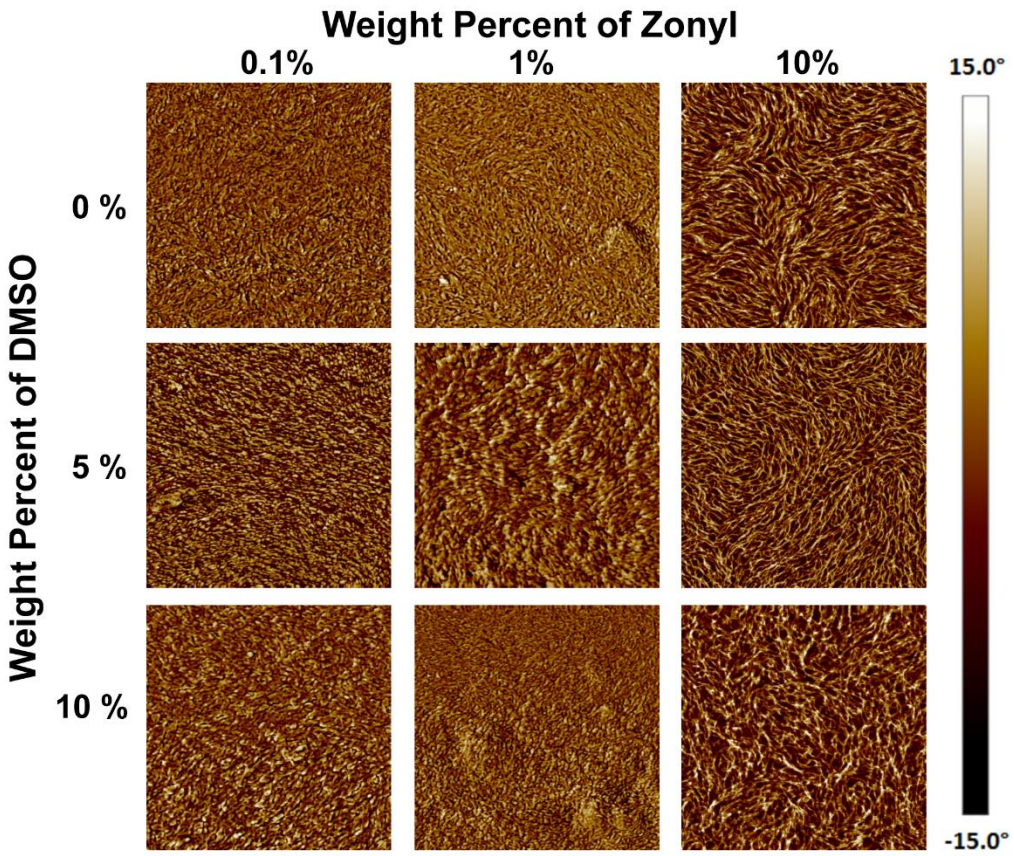

Figure 7.4. AFM phase images of PEDOT:PSS films as a function of the content of DMSO and Zonyl additives in the solution used for deposition. The dimensions of each AFM image are 1.5 μm × 1.5 μm.

Additives such as poly(ethyleneimine) (PEI) have been used to lower the work function of PEDOT:PSS.[13] Such materials are necessary to produce asymmetry in the work functions in devices in which PEDOT:PSS serves as both the anode and cathode, such that the electrons and holes drift in the proper direction. The effect of treating PEDOT:PSS with PEI on the mechanical properties has not been characterized. **Figure 7.5a** compares the crack-onset strains of three pure PEDOT:PSS films (i, ii, and v) and two PEDOT:PSS/PEI bilayer films (iii and iv) prepared using 5% DMSO and 10% Zonyl and stretched on PDMS substrates. Sample (i) represents the PEDOT:PSS films that were spin-coated on passivated glass and transferred to PDMS substrates; the value is duplicated from **Figure 7.2**; sample

(ii) represents the films that were spin-coated directly onto PDMS substrates. The minor increase in crack-onset strain, or the apparent ductility, of films that were spin-coated directly from the films that were transferred is attributed to increased adhesion between the PEDOT:PSS films and the PDMS substrates when spin-coated directly on the PDMS. In samples represented by (iii) and (iv), a layer of PEI was deposited on the PEDOT:PSS films by spin-coating from a dilute solution of PEI in 2-methoxyethanol (MOE) after the initial annealing of the PEDOT:PSS films. We observed significant decreases in the crack-onset strain with the addition of PEI layer for both transferred and directly spin-coated samples, sample (iii) and (iv) respectively. We investigated this increase in apparent brittleness by conducting a control experiment in which we treated the PEDOT:PSS films with the solution of pure MOE via the same spin-coating parameters. The further decrease in the crack-onset strain exhibited by sample (v) suggested that the MOE significantly embrittled the PEDOT:PSS films, perhaps by extracting some of the Zonyl from the films. **Figure 7.5b** shows the evolution of relative resistance as a function of tensile strain. The results correlated well with the crack-onset strains in which the films that were treated with MOE, the most brittle films, experienced a rapid increase in R/R_0 values at low strains, ~8%. Films with a thin layer of PEI showed relatively constant R/R_0 values up to 16% strain, at which point the resistance increased over the detection limit. We observed a very different trend in the sample spin-coated with PEI when compared to the other samples where the relative resistance remained relatively constant through the crack-onset strain and suddenly increased beyond the detection limit. We attributed this effect to the sudden development of large cracks in the bilayer films rather the generation of minor cracks found in the other samples. The major cracks that spanned the whole length of the films led to the

sudden failure of the devices rather than the gradual increase in the relative resistance. The increase in apparent brittleness in PEDOT:PSS films laminated with PEI or exposed to MOE solvent was an unfortunate yet important observation that should be taken into account when designing organic electronic systems requiring mechanical robustness or substantial deformation.

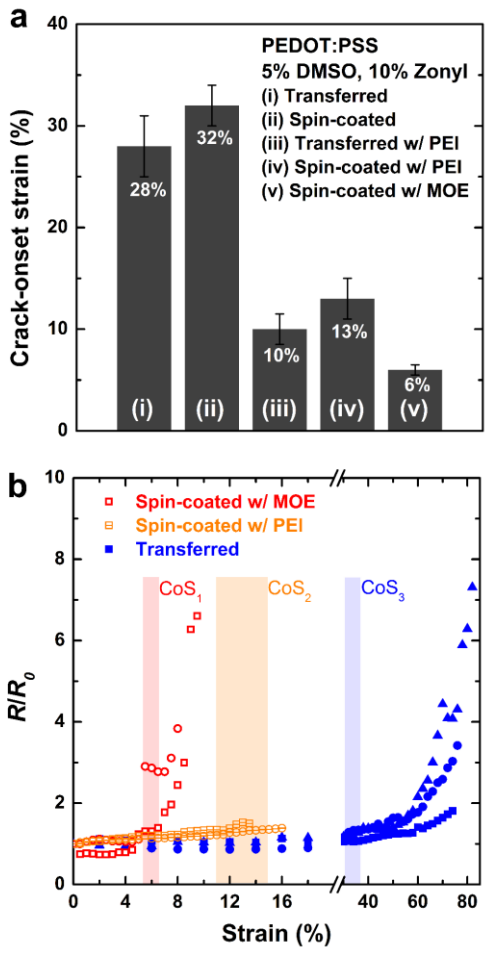

Figure 7.5. (a) Comparison of the crack-onset strains of the PEDOT:PSS films spun using 5% DMSO and 10% Zonyl with five different treatments: neat PEDOT:PSS films (both transferred from passivated glass, (i), and directly spin-coated onto PDMS substrate, (ii), films with a layer of PEI (both transferred, (iii), and directly spin-coated, (iv), and films treated after deposition by spin-coating with neat 2-methoxyethanol, (v). (b) Evolution of relative resistance as a function of strain. Shaded areas refer to the crack-onset strains of respective samples. The widths of the shaded areas correspond to two times the standard deviation of the measurements of crack-onset strain.

To demonstrate the utility of these plasticized films of PEDOT:PSS in devices, we fabricated wearable electronic sensors in which we measured the change in resistance as a function of bending strain (i.e., to indicate the motion of a joint). A piezoresistive effect—i.e., a change in electrical resistivity upon the application of mechanical strain—has been described for PEDOT:PSS by Lang and coworkers.[47] The authors patterned PEDOT:PSS films on polyimide membranes using standard photolithography of photoresist and lift-off procedure and fabricated resistors with dimensions of 4 × 4 mm.[47,48] We reasoned that films of PEDOT:PSS, when plasticized by common additives (i.e., cast from inks containing 5% DMSO and 10% Zonyl), might behave as piezoresistive strain gauges for applications requiring extreme mechanical deformation (as would be required for medical prostheses and soft robotics). Unlike capacitive sensors, resistive modalities are much simpler to implement, as they are relatively unaffected by electric fields or by nearby conductors. The skin-like resistive strain sensors comprised PEDOT:PSS films that were transferred onto thin PDMS substrates and adhered to a nitrile glove using copper tape, **Figure 7.6a**. We selected materials for this experiment based on a finite-element analysis whose goal was to predict the maximum strain associated with the bending and unbending of the fingers, **Figure 7.6b**. The computational simulation accounted for the dimension of the PEDOT:PSS films and PDMS substrate and subjected them to the bending onto a 5 mm radius of curvature, approximately the radius of curvature of the second knuckle. As expected, the maximum strain occurred at the apex of the curvature with the strain of ~20%. Our analysis suggested that PEDOT:PSS films with 10% Zonyl would survive the repeated deformation of 20% strain and that the change in resistance would be measurable.

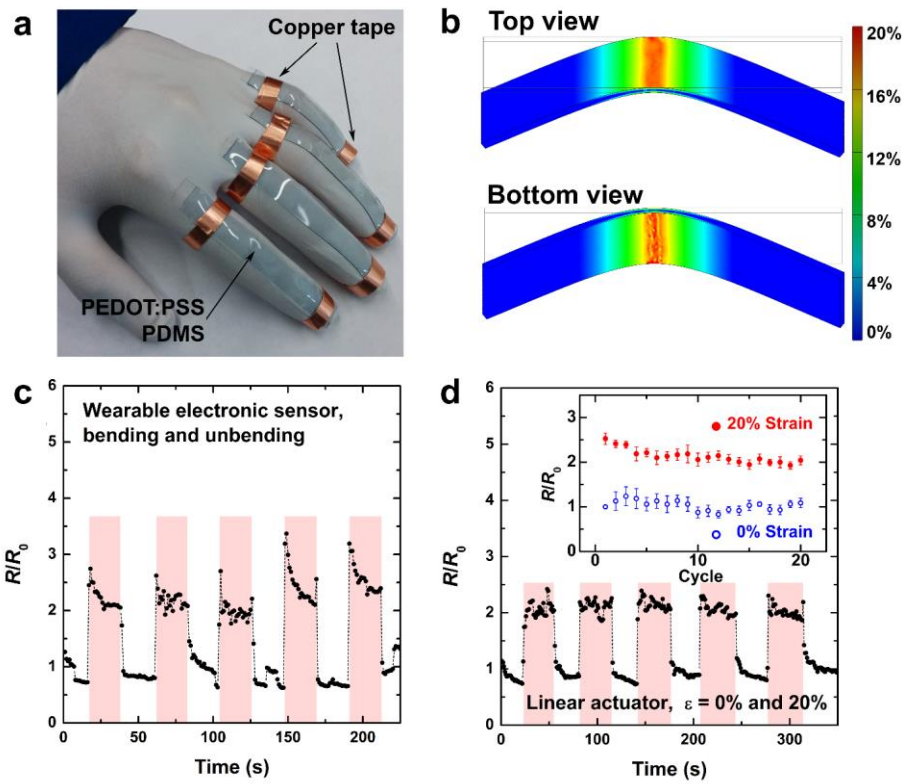

Figure 7.6. Images showing the characteristics of the skin-like resistive strain sensors. (a) Photograph of the devices comprising PEDOT:PSS films with 5% DMSO and 10% Zonyl transferred onto thin PDMS substrates (1 mm thick) and adhered to a nitrile glove using conductive copper tape. (b) Computational analysis of strain produced in the thin films when subjected to bending with the radius curvature of 5 mm, approximately the radius of curvature of the second knuckle. The peak strain occurred at the location of the second knuckle with an equivalent strain of ~20%. (c) Plot of relative resistance (R/R_0) as a function of time for the devices placed on the human hand. The shaded areas refer to when strains are applied by bending of the fingers. (d) R/R_0 vs. time of the devices on the linear actuator cycling between 0% and 20% strains. The inset shows the average R/R_0 at both positions as a function of the number of cycle.

Figure 7.6c shows the representative result obtained from the resistive sensor placed on the nitrile glove. The measured relative resistance increased by a factor of 2–3 when the strains were applied (fingers bent). The resistance returned to the original value when the strains were removed. This behavior was sustained during cyclic loading; we tested 20 cycles. We observed instantaneous increases in R/R_0 when the strains were applied, and relatively slower decays to constant values over the period of applied strains; however, the signal to noise ratios remained relatively high throughout the experiment. We

attributed the different increase in R/R_0 values among different cycles to the inability of the human hand to apply consistent strains. We note that the use of four-terminal probe will likely decrease the hysteresis in the measurement; however, the average increase in relative resistance due to the bending motion would likely remain unchanged. To control for the inconsistency of human motion, we subjected the sensors to the cycling of 0% and 20% tensile strains using a computer-controlled linear actuator (**Figure 7.6d**). Unlike the wearable sensor shown in **Figures 7.6a** and **7.6c**, the electrodes used for the experiment shown in **Figure 7.6d** were droplets of EGaIn rather than copper tape. Given the similarity in results obtained between four-terminal measurements with brass contacts, and two-terminal measurements using EGaIn and copper tape, we suggest an absence of substantial contact resistance. We observed a substantial reduction in noise, however, the non-instantaneous decays to the original resistance values upon relaxation remained. Such delays could be attributed to the viscoelasticity of the PDMS (the elastic regime of PDMS is approximately 10%) and the inherent properties of PEDOT:PSS. Measurement performed at the strain below the elastic limit of PDMS provided measurable change in the relative resistance; however, as shown in Figure 3b, the increase in relative resistance in that region are not sufficiently pronounced to isolate the origin of the time dependence. The inset of **Figure 7.6d** shows the cyclability of the mechanical sensor. After 20 cycles, the relative resistance of the stretched state remained constant: approximately double its value in the relaxed state.

7.3. Conclusions

This paper described the mechanical and electrical properties PEDOT:PSS thin films as a function of concentration of the common additives in the solution used to deposit the films. We discovered that the addition of Zonyl significantly improved the mechanical compliance, while good electrical properties (i.e., sheet resistance) were retained. The effect of the concentration of DMSO on the mechanical properties was relatively small. Our findings may provide insights toward the design of mechanically robust, highly flexible, or stretchable displays and solar cells, and resistive strain sensors for medical and robotic applications. Our experiments also highlighted a deleterious effect of incorporating PEI into all-rubber electronics; examination of the additional layer of PEI or exposure to its common solvent, MOE, revealed embrittlement of the PEDOT:PSS films. Using highly plasticized PEDOT:PSS films as resistive strain sensors could be valuable in providing electronic feedback for soft actuators in robotic applications. Understanding the role of common additives on not only the electrical properties—but also the mechanical ones—will be necessary for virtually all applications of organic semiconductors destined for stretchable, ultra-flexible, and mechanically stable applications in energy, consumer electronics, and biomedicine.

7.4. Experimental methods

7.4.1. Materials

PEDOT:PSS (Clevios PH1000) was purchased from Heraeus. The solid content of the PH 1000 solution was 1–1.3% and had a ratio of PEDOT to PSS of 1:2.5 by weight. Dimethyl sulfoxide (DMSO) was purchased from BDH with purity of 99.9% and used as

supplied. Zonyl FS-300 (Zonyl), ortho-dichlorobenzene (ODCB), poly(3-hexylthiophene) (P3HT), [6,6]-phenyl C_{61} butyric acid methyl ester (PCBM, >99%), eutectic gallium-indium (EGaIn, ≥99.99%) were purchased from Sigma-Aldrich and used as received. Polyethylenimine (PEI) was also purchased from Sigma-Aldrich and was dissolved in 2-methoxyethanol (Sigma-Aldrich) with the concentration of 1 mg mL^{-1} prior to usage. (Tridecafluoro-1,1,2,2-tetrahydrooctyl)-1-trichlorosilane (FOTS) was obtained from Gelest. PDMS (Sylgard 184, Dow Corning) was prepared according to the manufacturer's instructions at a ratio of 10:1 (base:crosslinker) and cured at room temperature for 36 to 48 hours. The dimensions of the PDMS substrates are 8 cm × 1 cm; the thickness varied depending on the experiment: 3 mm for buckling; 1.5 mm for crack-onset strain; and 1 mm for resistive strain sensors.

7.4.2. Preparation of PEDOT:PSS solutions and films

PEDOT:PSS solutions with different concentrations of DMSO and Zonyl were prepared in solution phase. The PEDOT:PSS films were prepared on FOTS-passivated glass slides as the initial substrate for all experiments. Glass slides, 2.5 cm × 2.5 cm, were cleaned by bath sonication in Alconox solution, pure deionized water, acetone, and isopropanol for 10 min each. The glass slides were then treated in a plasma cleaner (30 W, 200 mtorr ambient air, 3 min) before enclosing them in a vacuum desiccator with a vial containing ca. 100 μL FOTS. The desiccator was left under dynamic vacuum for at least 12 h. The FOTS-treated glass slides were rinsed with isopropanol and dried under a stream of compressed air before use. PEDOT:PSS solutions were spin-coated directly onto FOTS-treated glass slides with spin speeds determined by the desired thicknesses. The

PEDOT:PSS films were then dried on the hot plate at 100 °C for 30 min and cooled to room temperature before further testing.

7.4.3. Characterization of PEDOT:PSS films

The tensile moduli of the films were measured using the buckling-based method. The PDMS substrates were prepared according to the manufacturer's instruction and cured in air at room temperature for 36-48 hours before use. We then cut the PDMS into rectangular pieces (l = 8 cm, w = 1 cm, h = 0.3 cm) and stretched to strains of 4% using a computer-controlled actuator (Newmark model ET-100-11). While the PDMS substrates were under strain, clean glass slides (5 cm × 2.5 cm, treated with FOTS to later facilitate separation of PDMS) were clipped onto the back of each PDMS substrate to maintain the strain. For each PEDOT:PSS solution, films with three different thicknesses were prepared by varying the spin speed onto separate FOTS glass slides. Transferring the PEDOT:PSS films to the pre-strained PDMS substrate was performed by initially scoring the films along the edges with a razor and placing the films against the PDMS. After applying a minimum amount of pressure to create a conformal seal between the PDMS and the PEDOT:PSS films, we separate the glass/stretched PDMS from the glass/PEDOT:PSS film in one fast motion. We used the surface of the PDMS that was cured at the air interface. We then removed the clips and allowed the PDMS to relax to the equilibrium length. Buckles formed in the PEDOT:PSS films upon relaxation of the substrates. We plotted the buckling wavelengths, λ_b, as a function of film thicknesses, d_f, then substituted the slopes of the linear fits, λ_b/d_f, and the moduli of the PDMS substrates, E_s, into **Equation 1** to calculate the moduli of the PEDOT:PSS films, E_f. The Poisson's ratios of the films and the substrate,

v_f and v_s, were assumed to be 0.35 and 0.5 respectively. In our experiment, E_s obtained were in the range of 0.6 to 0.8 MPa depending on the exact mixing ratio of base to hardener, curing time, and batch-to-batch variability.

$$E_f = 3E_S\left(\frac{1-\nu_f^2}{1-\nu_s^2}\right)\left(\frac{\lambda_b}{2\pi d_f}\right)^3 \qquad (1)$$

We measured the crack-onset strain of each film by transferring PEDOT:PSS films onto unstrained PDMS substrates with thickness of 1.5 mm and stretching the substrates from 0% to 50% strains with a step size of 1% using a computer-controlled linear actuator. The thickness of all PEDOT:PSS films were kept relatively constant at ~150 nm. At each step, optical micrographs were taken to observe the film surfaces. The crack-onset strains were defined by the strain at which the first crack was observed by optical microscopy.

The sheet resistance and conductivity of the films were measured by two-terminal measurements as previously described.[49] PEDOT:PSS films were prepared on FOTS-treated glass as described above; films thickness were kept constant at ~150 nm. The absence of significant contact resistance was verified by four-terminal measurements for some samples, with good agreement in the resistance values between the two methods. AFM images were taken using tapping mode (Veeco Scanning Probe Microscope). The images were taking with the dimensions 1.5 μm × 1.5 μm. Samples used to measure the relative resistance as a function of strain were prepared in the same manner as those used to measure the crack-onset strains. The films and substrates were then mounted on the computer controlled linear actuator; electrical contacts were made using EGaIn. We measured resistance from 0% to 80% strains with a step size of 0.5% strains.

7.4.4. Fabrication and characterization of OPV devices

OPV devices were fabricated on FOTS-treated glass slides, prepared in the same manner described above. PEDOT:PSS solutions were then spin-coated onto the glass slides at 500 rpm for 4 min then 2k rpm for 60 s. The slides were then dried on a hot plate in ambient air for 30 min; slides with PEDOT:PSS with 7% DMSO and 0.1% Zonyl were annealed at 150 °C, and slides with PEDOT:PSS with 5% DMSO and 10% Zonyl were annealed at 100 °C to avoid the formation of surface buckling. The active layer solution was prepared with a 1:1 solution of P3HT:PCBM in ODCB and stirred overnight at room temperature (40 mg mL^{-1} total solid concentration). The solution was spin-coated directly onto the PEDOT:PSS films at 500 rpm for 4 min and 2 krpm for 60 s. The films were then annealed in inert atmosphere at 125 °C for 30 min. EGaIn droplets were then applied as the top electrodes. Photovoltaic properties were measured using a solar simulator operated at AM 1.5G conditions inside a glovebox filled with nitrogen.

Acknowledgements

This work was supported by the Air Force Office of Scientific Research (AFOSR) Young Investigator Program, grant number FA9550-13-1-0156. Additional support was provided by the laboratory startup funds from the University of California, San Diego. S.S. acknowledges support provided by the National Science Foundation Graduate Research Fellowship under Grant No. DGE-1144086. A. Z. acknowledges a fellowship from SoCal Clean Energy Technology Acceleration Program from the von Liebig Center at UCSD sponsored by the US Department of Energy. E.V acknowledges support provided by the

Ronald McNair Program. S. M. R.-G. acknowledges the Bridge to Engineering Success program from Tufts University.

Chapter 7, in full, is a reprint of the material as it appears in *Advanced Functional Materials*, 2015, 25, 427 – 436. Wiley-VCH Verlag GmbH & Co. KGaA, 2015. Suchol Savagatrup, Esther Chan, Sandro M. Renteria-Garcia, Adam D. Printz, Aliaksandr V. Zaretski, Timothy F. O'Connor, Daniel Rodriquez, Eduardo Valle, and Darren J. Lipomi. The dissertation author was the primary investigator and author of this paper.

References

(1) Elschner, A.; Kirchmeyer, S.; Lovenich, W.; Merker, U.; Reuter, K. *PEDOT: Principles and Applications of an Intrinsically Conductive Polymer*; CRC Press: New York, 2011.

(2) Kim, N.; Kee, S.; Lee, S. H.; Lee, B. H.; Kahng, Y. H.; Jo, Y.-R.; Kim, B.-J.; Lee, K. Highly Conductive PEDOT:PSS Nanofibrils Induced by Solution-Processed Crystallization. *Adv. Mater.* **2014**, *26*, 2268–2272.

(3) Kim, Y. H.; Sachse, C.; MacHala, M. L.; May, C.; M??ller-Meskamp, L.; Leo, K. Highly Conductive PEDOT:PSS Electrode with Optimized Solvent and Thermal Post-Treatment for ITO-Free Organic Solar Cells. *Adv. Funct. Mater.* **2011**, *21*, 1076–1081.

(4) Vosgueritchian, M.; Lipomi, D. J.; Bao, Z. Highly Conductive and Transparent PEDOT:PSS Films with a Fluorosurfactant for Stretchable and Flexible Transparent Electrodes. *Adv. Funct. Mater.* **2012**, *22*, 421.

(5) Tait, J. G.; Worfolk, B. J.; Maloney, S. a.; Hauger, T. C.; Elias, A. L.; Buriak, J. M.; Harris, K. D. Spray Coated High-Conductivity PEDOT:PSS Transparent Electrodes for Stretchable and Mechanically-Robust Organic Solar Cells. *Sol. Energy Mater. Sol. Cells* **2013**, *110*, 98–106.

(6) Galagan, Y.; Coenen, E. W. C.; Zimmermann, B.; Slooff, L. H.; Verhees, W. J. H.; Veenstra, S. C.; Kroon, J. M.; J??rgensen, M.; Krebs, F. C.; Andriessen, R. Scaling up ITO-Free Solar Cells. *Adv. Energy Mater.* **2014**, *4*, 1300498.

(7) Jakobsson, F. L. E.; Crispin, X.; Lindell, L.; Kanciurzewska, A.; Fahlman, M.; Salaneck, W. R.; Berggren, M. Towards All-Plastic Flexible Light Emitting Diodes. *Chem. Phys. Lett.* **2006**, *433*, 110–114.

(8) Rivnay, J.; Owens, R. M.; Malliaras, G. G. The Rise of Organic Bioelectronics. *Chem. Mater.* **2014**, *26*, 679–685.

(9) Leleux, P.; Badier, J. M.; Rivnay, J.; B??nar, C.; Herv??, T.; Chauvel, P.; Malliaras, G. G. Conducting Polymer Electrodes for Electroencephalography. *Adv. Healthc. Mater.* **2014**, *3*, 490–493.

(10) Gaynor, W.; Lee, J.-Y.; Peumans, P. Fully Solution-Processed Inverted Polymer Solar Cells with Laminated Nanowire Electrodes. *ACS Nano* **2010**, *4*, 30–34.

(11) Wu, J.; Becerril, H. A.; Bao, Z.; Liu, Z.; Chen, Y.; Peumans, P. Organic Solar Cells with Solution-Processed Graphene Transparent Electrodes. *Appl. Phys. Lett.* **2008**, *92*, 263302.

(12) Lindell, L.; Burquel, A.; Jakobsson, F. L. E.; Lemaur, V.; Berggren, M.; Lazzaroni, R.; Cornil, J.; Salaneck, W. R.; Crispin, X. Transparent, Plastic, Low-Work-Function Poly(3,4-Ethylenedioxythiophene) Electrodes. *Chem. Mater.* **2006**, *18*, 4246–4252.

(13) Zhou, Y.; Fuentes-Hernandez, C.; Shim, J.; Meyer, J.; Giordano, A. J.; Li, H.; Winget, P.; Papadopoulos, T.; Cheun, H.; Kim, J.; *et al.* A Universal Method to Produce Low-Work Function Electrodes for Organic Electronics. *Science (80-.).* **2012**, *336*, 327–332.

(14) Po, R.; Carbonera, C.; Bernardi, A.; Tinti, F.; Camaioni, N. Polymer- and Carbon-Based Electrodes for Polymer Solar Cells: Toward Low-Cost, Continuous Fabrication over Large Area. *Sol. Energy Mater. Sol. Cells* **2012**, *100*, 97–114.

(15) Lipomi, D. J.; Tee, B. C.-K.; Vosgueritchian, M.; Bao, Z. Stretchable Organic Solar Cells. *Adv. Mater.* **2011**, *23*, 1771.

(16) Li, Y.; Masuda, Y.; Iriyama, Y.; Okuzaki, H. Stretchable and Highly Conductive Polymer Films. *Trans. Mater. Res. Soc. Japan* **2012**, *37*, 303–306.

(17) Li, Y.; Tanigawa, R.; Okuzaki, H. Soft and Flexible PEDOT/PSS Films for Applications to Soft Actuators. *Smart Mater. Struct.* **2014**, *23*, 074010.

(18) Chen, C.; Torrents, A.; Kulinsky, L.; Nelson, R. D.; Madou, M. J.; Valdevit, L.; LaRue, J. C. Mechanical Characterizations of Cast Poly(3,4-ethylenedioxythiophene):Poly(styrenesulfonate)/Polyvinyl Alcohol Thin Films. *Synth. Met.* **2011**, *161*, 2259–2267.

(19) Tahk, D.; Lee, H. H.; Khang, D.-Y. Elastic Moduli of Organic Electronic Materials by the Buckling Method. *Macromolecules* **2009**, *42*, 7079–7083.

(20) Krebs, F. C.; Nielsen, T. D.; Fyenbo, J.; Wadstrøm, M.; Pedersen, M. S. Manufacture, Integration and Demonstration of Polymer Solar Cells in a Lamp for the "Lighting Africa" Initiative. *Energy Environ. Sci.* **2010**, *3*, 512.

(21) Voigt, M. M.; MacKenzie, R. C. I.; Yau, C. P.; Atienzar, P.; Dane, J.; Keivanidis, P. E.; Bradley, D. D. C.; Nelson, J. Gravure Printing for Three Subsequent Solar Cell Layers of Inverted Structures on Flexible Substrates. *Sol. Energy Mater. Sol. Cells* **2011**, *95*, 731–734.

(22) Lipomi, D. J.; Lee, J. A.; Vosgueritchian, M.; Tee, B. C.-K.; Bolander, J. A.; Bao, Z. Electronic Properties of Transparent Conductive Films of PEDOT: PSS on Stretchable Substrates. *Chem. Mater.* **2012**, *24*, 373.

(23) Lang, U.; Naujoks, N.; Dual, J. Mechanical Characterization of PEDOT:PSS Thin Films. *Synth. Met.* **2009**, *159*, 473–479.

(24) Dupont, S. R.; Novoa, F.; Voroshazi, E.; Dauskardt, R. H. Decohesion Kinetics of PEDOT : PSS Conducting Polymer Films. *Adv. Funct. Mater.* **2014**, *24*, 1325–1332.

(25) Lee, J.; Wu, J.; Shi, M.; Yoon, J.; Park, S. Il; Li, M.; Liu, Z.; Huang, Y.; Rogers, J. A. Stretchable GaAs Photovoltaics with Designs That Enable High Areal Coverage. *Adv. Mater.* **2011**, *23*, 986.

(26) Kim, D.-H.; Lu, N.; Ma, R.; Kim, Y.-S.; Kim, R.-H.; Wang, S.; Wu, J.; Won, S. M.; Tao, H.; Islam, A.; *et al.* Epidermal Electronics. *Science* **2011**, *333*, 838.

(27) Bauer, S.; Bauer-Gogonea, S.; Graz, I.; Kaltenbrunner, M.; Keplinger, C.; Schw??diauer, R. 25th Anniversary Article: A Soft Future: From Robots and Sensor Skin to Energy Harvesters. *Adv. Mater.* **2014**, *26*, 149–162.

(28) Fan, J. a; Yeo, W.-H.; Su, Y.; Hattori, Y.; Lee, W.; Jung, S.-Y.; Zhang, Y.; Liu, Z.; Cheng, H.; Falgout, L.; *et al.* Fractal Design Concepts for Stretchable Electronics. *Nat. Commun.* **2014**, *5*, 3266.

(29) Kaltenbrunner, M.; Sekitani, T.; Reeder, J.; Yokota, T.; Kuribara, K.; Tokuhara, T.; Drack, M.; Schwödiauer, R.; Graz, I.; Bauer-Gogonea, S.; *et al.* An Ultra-Lightweight Design for Imperceptible Plastic Electronics. *Nature* **2013**, *499*, 458.

(30) Chortos, A.; Lim, J.; To, J. W. F.; Vosgueritchian, M.; Dusseault, T. J.; Kim, T.-H.; Hwang, S.; Bao, Z. Highly Stretchable Transistors Using a Microcracked Organic Semiconductor. *Adv. Mater.* **2014**, *26*, 4253–4259.

(31) Savagatrup, S.; Printz, A. D.; O'Connor, T. F.; Zaretski, A. V.; Lipomi, D. J. Molecularly Stretchable Electronics. *Chem. Mater.* **2014**, *26*, 3028–3041.

(32) Savagatrup, S.; Makaram, A. S.; Burke, D. J.; Lipomi, D. J. Mechanical Properties of Conjugated Polymers and Polymer-Fullerene Composites as a Function of Molecular Structure. *Adv. Funct. Mater.* **2014**, *24*, 1169–1181.

(33) Savagatrup, S.; Printz, A. D.; Rodriquez, D.; Lipomi, D. J. Best of Both Worlds: Conjugated Polymers Exhibiting Good Photovoltaic Behavior and High Tensile Elasticity. *Macromolecules* **2014**, *47*, 1981.

(34) Chiechi, R. C.; Hummelen, J. C. Polymer Electronics, Quo Vadis? *ACS Macro Lett.* **2012**, *1*, 1180–1183.

(35) Na, S.-I.; Wang, G.; Kim, S.-S.; Kim, T.-W.; Oh, S.-H.; Yu, B.-K.; Lee, T.; Kim, D.-Y. Evolution of Nanomorphology and Anisotropic Conductivity in Solvent-Modified PEDOT:PSS Films for Polymeric Anodes of Polymer Solar Cells. *J. Mater. Chem.* **2009**, *19*, 9045.

(36) Espinosa, N.; Hösel, M.; Angmo, D.; Krebs, F. C. Solar Cells with One-Day Energy Payback for the Factories of the Future. *Energy Environ. Sci.* **2012**, *5*, 5117.

(37) Hansen, T. S.; West, K.; Hassager, O.; Larsen, N. B. Highly Stretchable and Conductive Polymer Material Made from Poly(3,4-Ethylenedioxythiophene) and Polyurethane Elastomers. *Adv. Funct. Mater.* **2007**, *17*, 3069–3073.

(38) Kwon, S. J.; Kim, T. Y.; Lee, B. S.; Lee, T. H.; Kim, J. E.; Suh, K. S. Elastomeric Conducting Polymer Nano-Composites Derived from Ionic Liquid Polymer Stabilized-poly(3,4-Ethylenedioxythiophene). *Synth. Met.* **2010**, *160*, 1092–1096.

(39) O'Connor, T. F.; Zaretski, A. V.; Shiravi, B. A.; Savagatrup, S.; Printz, A. D.; Diaz, M. I.; Lipomi, D. J. Stretching and Conformal Bonding of Organic Solar Cells to Hemispherical Surfaces. *Energy Environ. Sci.* **2014**, *7*, 370.

(40) Lu, N.; Wang, X.; Suo, Z.; Vlassak, J. Metal Films on Polymer Substrates Stretched beyond 50%. *Appl. Phys. Lett.* **2007**, *91*, 221909.

(41) Lipomi, D. J.; Chong, H.; Vosgueritchian, M.; Mei, J.; Bao, Z. Toward Mechanically Robust and Intrinsically Stretchable Organic Solar Cells : Evolution of Photovoltaic Properties with Tensile Strain. *Sol. Energy Mater. Sol. Cells* **2012**, *107*, 355–365.

(42) Dupont, S. R.; Oliver, M.; Krebs, F. C.; Dauskardt, R. H. Interlayer Adhesion in Roll-to-Roll Processed Flexible Inverted Polymer Solar Cells. *Sol. Energ. Mat. Sol. Cells* **2012**, *97*, 171–175.

(43) Brand, V.; Bruner, C.; Dauskardt, R. H. Cohesion and Device Reliability in Organic Bulk Heterojunction Photovoltaic Cells. *Sol. Energ. Mat. Sol. Cells* **2012**, *99*, 182.

(44) Crispin, X.; Jakobsson, F. L. E.; Crispin, A.; Grim, P. C. M.; Andersson, P.; Volodin, A.; van Haesendonck, C.; Van der Auweraer, M.; Salaneck, W. R.; Berggren, M. The Origin of the High Conductivity of poly(3,4-Ethylenedioxythiophene)-Poly(styrenesulfonate) (PEDOT- PSS) Plastic Electrodes. *Chem. Mater.* **2006**, *18*, 4354–4360.

(45) Awartani, O.; Lemanski, B. I.; Ro, H. W.; Richter, L. J.; DeLongchamp, D. M.; O'Connor, B. T. Correlating Stiffness, Ductility, and Morphology of Polymer:Fullerene Films for Solar Cell Applications. *Adv. Energy. Mater.* **2013**, *3*, 399–406.

(46) Stafford, C. M.; Harrison, C.; Beers, K. L.; Karim, A.; Amis, E. J.; VanLandingham, M. R.; Kim, H.-C.; Volksen, W.; Miller, R. D.; Simonyi, E. E. A Buckling-Based Metrology for Measuring the Elastic Moduli of Polymeric Thin Films. *Nat. Mater.* **2004**, *3*, 545–550.

(47) Lang, U.; Rust, P.; Dual, J. Towards Fully Polymeric MEMS: Fabrication and Testing of PEDOT/PSS Strain Gauges. *Microelectron. Eng.* **2008**, *85*, 1050.

(48) Lang, U.; Rust, P.; Schoberle, B.; Dual, J. Piezoresistive Properties of PEDOT:PSS. *Microelectron. Eng.* **2009**, *86*, 330–334.

(49) Printz, A. D.; Chan, E.; Liong, C.; Martinez, R. S.; Lipomi, D. J. Photoresist-Free Patterning by Mechanical Abrasion of Water-Soluble Lift-off Resists and Bare Substrates: Toward Green Fabrication of Transparent Electrodes. *PLoS One* **2013**, *8*, e83939.

Chapter 8

Increased elasticity of a low-bandgap conjugated copolymer by random segmentation for mechanically robust solar cells

Suchol Savagatrup,[†] Adam D. Printz,[†] Daniel J. Burke, Trevor N. Purdy, and Darren J. Lipomi

([†] Equal contribution)

Department of NanoEngineering, University of California, San Diego

9500 Gilman Drive, Mail Code 0448, La Jolla, CA 92093-0448

Abstract

Despite the necessity of organic electronic materials to undergo large deformations in flexible, ultra-thin, and stretchable applications, many high-performance organic semiconductors are mechanically fragile. This paper describes an approach to increase the elasticity of low-bandgap conjugated polymers by statistical incorporation of unlike monomers. The material under study is PDPP2FT, an alternating copolymer. Synthesized by the Stille polymerization, it comprises an *N*-alkylated diketopyrrolopyrrole (DPP) unit flanked by two furan rings (2F) alternating with thiophene (T). In the modified ("segmented") polymer, PDPP2FT-seg-2T, the DPP is exchanged for a tail-to-tail coupled unit of two 3-hexylthiophene rings (bithiophene, 2T) in an average of one of approximately five repeat units. ^{1}H NMR spectroscopy, ultraviolet-visible spectroscopy, and gel-permeation chromatography confirm the presence and covalent incorporation of the 2T units within the conjugated backbone of the segmented polymer. The tensile modulus of the segmented polymer, 0.93 ± 0.16 GPa, is lower than that of the homopolymer, 2.17 ± 0.35 GPa. When blended with $PC_{61}BM$, the segmented material produces devices with power conversion efficiencies of 2.82 ± 0.28%, which is similar to that of PDPP2FT, 2.52 ± 0.34%. These results suggest that it is possible to increase the mechanical resiliency of semiconducting polymers for solar cells without having a deleterious effect on the photovoltaic properties.

8.1 Introduction

Mechanical compliance of organic electronic devices is typically regarded as a solved—or never extant—problem, and thus the mechanical properties of modern (*i.e.*,

low-bandgap, high mobility, and high photovoltaic efficiency) conjugated polymers are generally unreported.[1] Typical thicknesses of active materials (~100 nm) and substrates (~100 μm and recently ~1 μm) can accommodate small bending radii without imposing significant tensile deformations to the active materials.[2] Reports of ultra-flexible devices have enabled "imperceptible" electronics and skin-like devices on thin plastic foils and demonstrations of ultrathin organic solar cells with the highest power-to-mass ratio of any photovoltaic technology.[3] Implementation of this technology for large-area applications and full exploitation of the benefit provided by thinness[2] (including possible reductions in balance of systems costs) requires that the active materials accommodate at least modest tensile strains reversibly. Mechanical robustness is prerequisite for thinness because small environmental forces will produce large strains on ultra-thin substrates.[4,5] The mechanical properties of organic semiconductors, however, exhibit a range of tensile moduli and propensity to fracture.[1,6–8] Establishing not only the structural parameters that control the mechanical properties but simple methods to tune the elasticity without adversely affecting the electronic properties would be a significant benefit to the field of organic electronics.[9] The establishment of such knowledge might enable truly "rubber" semiconductors, which could have a range of applications in devices for energy and biomedicine.[10–12]

Our laboratory has studied the mechanical properties of regioregular poly(3-alkylthiophene) (P3AT) as a function of the length of the alkyl solubilizing group.[1] Our observations led us to conclude that this structural element had a drastic effect on both the mechanical and photovoltaic properties.[1] In particular, we concluded that the length of the side chain was inversely correlated with photovoltaic efficiency for P3AT:$PC_{61}BM$, from A = hexyl to A = dodecyl, but that the length of the side chain was directly correlated with

compliance.[1] The tensile modulus of P3HT was nearly an order of magnitude greater (1.09 GPa) than that of P3OT (0.15 GPa), but the photovoltaic efficiency of P3HT-based devices was noted by us and others to be significantly greater than that of P3OT-based devices.[13] There is a notion that electronic and mechanical properties tend to be in competition (if one places value on elasticity and ductility). Notably, Awartani et al. have shown that increasing order in the pure P3HT phases in P3HT:$PC_{61}BM$ blends with decreasing rate of evaporation of solvent during spin coating produces efficient—but stiff and brittle—photovoltaic active layers.[6]

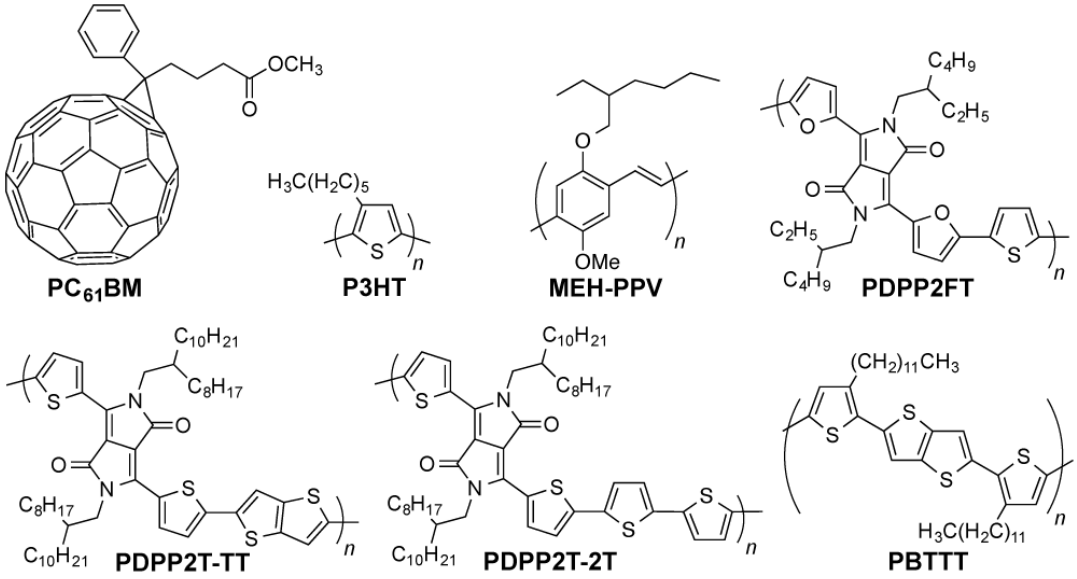

Figure 8.1. Chemical structures of materials discussed in the text.

While the regioregular P3ATs represent an important class of materials for fundamental studies of mechanical properties, it seems likely that a low-bandgap, donor-acceptor copolymer will emerge as the preferred "p-type" material,[14] with a fullerene or another polymer as the "n-type" material, provided both materials can be manufactured at scale with low cost and with low environmental impact.[15] To this end, a previous report measured the tensile moduli of PDPP2T-TT and PDPP2T-2T and attributed the slightly

lower tensile modulus of PDPP2T-2T (0.74 GPa) to that of PDPP2T-TT (0.99 GPa) to the relative stiffness[7] of the fused thienothiophene (TT) unit to that of the separated bithiophene (2T) unit (**Figure 8.1**).[16] These values of modulus, however, are very close, and it does not seem that replacement of fused rings for isolated rings will be the most effective strategy to provide improvements in mechanical properties. Within classes of similar materials, the mechanical compliance is inversely correlated to the crystallinity.[7] This effect has been noted in both P3ATs with different side chain lengths[1] and P3ATs compared to highly crystalline annealed films of PBTTT.[7,17] While it has previously been believed that high crystallinity was necessary for high charge transport, PDPP2T-TT exhibits balanced electron and hole mobilities for field-effect transistors that are among the highest of any material yet reported,[18,19] but it is significantly less crystalline than are annealed films of PBTTT.[20] Indeed, while the power conversion efficiencies (*PCE*s) of blends of MEH-PPV and MDMO-PPV[21] with $PC_{61}BM$ are no longer state-of-the-art, the efficiencies are not drastically lower than that of the typical P3HT:$PC_{61}BM$ cell[22] (~2 times lower), even though P3HT is semicrystalline and MEH-PPV and MDMO-PPV are amorphous.[23] PCDTBT is another example of a predominantly amorphous polymer[24] that has achieved values of *PCE* in blends with $PC_{71}BM$ greater than typical values for P3HT:$PC_{61}BM$.[25,26] Thus an effective strategy to combine mechanical compliance and photovoltaic efficiency might include the use of a conjugated polymer with good transport along the molecular axis but with a disrupted ability to form large crystallites in the solid state[27] which may stiffen the film.[7]

Block copolymers prepared by controlled living radical polymerization offer opportunities to combine advantageous properties of their component blocks,[28] but the

method is not amenable to the preparation of low-bandgap conjugated polymers. Recently, segmented, or "blocky" copolymers have been prepared by metal mediated olefin polymerization[29] and also by polycondensation reactions.[30] This work has demonstrated that segmented polymers can separate into domains rich in their component segments; segmentation thus provides a route to tailor the properties in a way that is analogous to block copolymerization, specifically for improved mechanical properties and processing behavior. All-conjugated block copolymers, such as analogues of regioregular polythiophenes, are generally synthesized by chain-growth mechanism. Alternating copolymerization, which is necessary to produce low-bandgap materials, follows step-growth kinetics and is not easily adapted to the production of block copolymers.[31] Ku et al., however, recently demonstrated a hybrid strategy in which a low-bandgap copolymer was appended to a polythiophene segment bearing a reactive chain end.[32] Our goal was thus to apply the strategy of segmented polymerization to a wholly low-bandgap conjugated polymer.

We focused our efforts on PDPP2FT and derivatives thereof. PDPP2FT, first reported by Woo et al., is a furan-containing donor-acceptor copolymer that is promising for photovoltaic applications.[33] It is synthesized by a metal-mediated polycondensation reaction of two monomers: the DPP unit flanked by two furan rings terminated in bromides and a unit of distannylated thiophene.[33] Superior solubility of polymers containing the furan moiety permits the use of ethylhexyl solubilizing groups whereas an analogous material in which the furans are substituted with thiophenes requires the much longer octyldodecyl side chains to afford useful solubility.[33] Solar cells based on PDPP2FT:$PC_{71}BM$ blends spin-coated from chlorobenzene with a chloronapthalene

additive exhibited photovoltaic efficiencies of 5.0%.[33] Using PDPP2FT as a starting point, we tested a simple method for increasing the elasticity of the material through random segmentation—that is, random incorporation of an alkylated conjugated units throughout the backbone (**Figure 8.2**). We believed this approach would have two effects: (1) disruption of the regular order in the main chain of the polymer and (2) alteration of the distribution of side chains. We predicted that both effects could lower the tensile modulus without significantly affecting the photovoltaic response of these materials in blends with fullerenes.

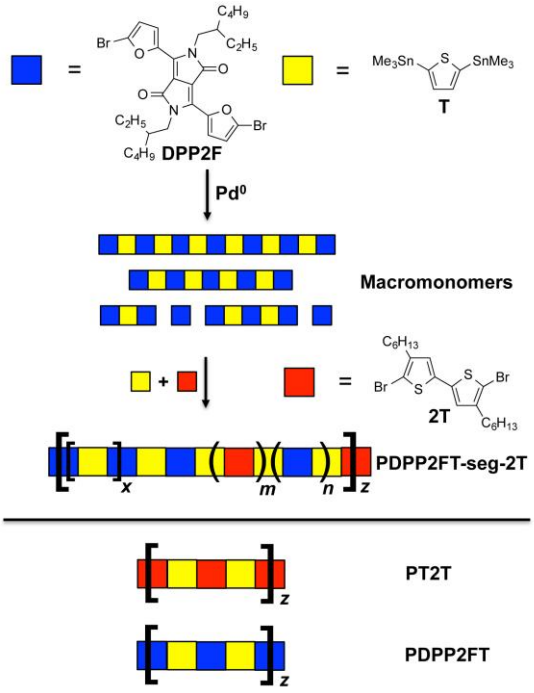

Figure 8.2. Summary of the synthetic strategy used to generate segmented copolymers. Two monomers, the dibromide (DPP2F) and the distannane (T), are reacted in the presence of Pd^0. Shortly after initialization of the reaction (when "macromonomers" began to form), additional T and dibrominated bithiophene (2T) were added to the reaction mixture to form the segmented polymer, PDPP2FT-seg-2T. Separately, the homopolymers PT2T and PDPP2FT were also prepared.

8.2 Experimental Section

8.2.1 Materials

A soluble fullerene derivative, [6,6]-phenyl C_{61} butyric acid methyl ester ($PC_{61}BM$) was obtained from Sigma-Aldrich with >99% purity. PDMS, Sylgard 184 (Dow Corning), was prepared according to the manufacturer's instructions at a ratio of 10:1 (base:crosslinker) and cured at room temperature for 36 to 48 hours before it was used for mechanical testing. (Tridecafluoro-1,1,2,2-tetrahydrooctyl)-1-trichlorosilane (FOTS) was obtained from Gelest. PEDOT:PSS (Clevios PH1000) was purchased from Heraeus. DMSO was purchased from BDH with purity of 99.9% and Zonyl (FS-300) fluorosurfactant was purchased from Sigma-Aldrich.

8.2.2 General

All reagents were obtained from commercial suppliers and used without purification. Chloroform ($CHCl_3$), ortho-dichlorobenzene (ODCB), dimethylformamide (DMF) and tetrahydrofuran (THF) were obtained from Sigma-Aldrich. All compounds were characterized by ^{1}H NMR and ^{13}C NMR (300 MHz, Varian) using $CDCl_3$ as the solvent. The residual chloroform peak at 7.26 ppm was used to calibrate the chemical shifts for ^{1}H NMR. Gel-permeation chromatography (GPC) was performed in chloroform ($CHCl_3$) on a Waters 2690 Separation Module equipped with a Waters 2414 Refractive Index Detector and a Waters 2996 Photodiode Array Detector. Molecular weights were calculated relative to linear PS standards. Atomic force microscope (AFM) images were obtained with a Veeco Scanning Probe Microscope in tapping mode. AFM data was analyzed with NanoScope Analysis v1.40 software (Bruker Corp.). Ultraviolet-visible

(UV-vis) spectra were obtained of the polymers in chroloform and in the solid state, as-cast from 4:1 $CHCl_3$:ODCB (by volume, 5 mg ml^{-1}) using a Perkin Elmer Lambda 1050 UV-vis-NIR spectrophotometer. We synthesized the two known polymers, PDPP2FT[33] and PT2T (formerly called C_6-TT),[34,35] according to previously established procedures.

8.2.3 Synthesis of PDPP2FT-seg-2T

We synthesized this material using a method related to that of PDPP2FT, except that after allowing the **DPP2F** and **T** (**Figure 8.2**) to react for a short time, we added brominated bithiophene monomer (**2T**) and additional stannylated thiophene (**T**), as follows. In a 12-mL reaction tube, **DPP2F** (234 mg, 0.360 mmol), 2,5-bis(trimethylstannyl)-thiophene (**T**, 147 mg, 0.360 mmol), $Pd_2(dba)_3$ (2 mol %) and P(o-tol)$_3$ (8 mol %) were dissolved in 4 mL chlorobenzene and degassed by bubbling argon through the mixture for 20 min. In a separate identical reaction tube, 2,5-bis(trimethylstannyl)-thiophene (**T**, 49 mg, 0.120 mmol) and brominated bithiophene (**2T**, 59 mg, 0.120 mmol) were dissolved in 2 mL chlorobenzene and degassed in the same manner. The first reaction tube was heated in an oil bath to 110 °C for 15 min, and a color change was observed from red monomer to green/blue oligomeric species. The first tube was removed from the oil bath and allowed to cool, and then the contents of the second reaction tube were added by cannula. The reaction was again heated to 110 °C for 6 h and then was allowed to cool to room temperature and was diluted with chloroform to reduce viscosity, and was precipitated into cold methanol. The solid was collected on filter paper, which was loaded into a Soxhlet and extracted with methanol and hexanes before the segmented polymer was collected by extraction with chloroform. Concentration under

reduced pressure yielded 235 mg of a dark solid. GPC analysis provided values of M_w = 55 kDa and PDI = 2.5. ^{1}H NMR (300 MHz, $CDCl_3$): δ (ppm) = 8.70-8.30 (br, 2H), 7.22-6.33 (br, 4H), 4.65-3.3 (br, 4H), 2.88-2.38 (br, 0.91H inferred, signal due to randomly incorporated **2T**), 2.03-1.76 (br, 2H), 1.74-1.63 (br ovlp, 0.91H inferred), 1.60-1.06 (br, 16H), 1.04-0.70 (br ovlp, 13.36H inferred).

8.2.4 Mechanical characterization

We measured the tensile modulus of each material using the mechanical buckling technique originally described by Stafford et al.[36] This method has been used in various thin film systems including conjugated polymer films for heterojunction OPV devices.[1,6,8,16] In brief, the films were spin-coated on passivated glass slides and transferred to poly(dimethylsiloxane) (PDMS) substrates bearing a small pre-strain. After transfer, the PDMS substrates were relaxed and the conjugated polymer film adopted sinusoidal buckles. The buckling wavelength, λ_b, is related to the thickness of the film, d_f, the tensile moduli of the film and the substrate, E_f and E_s, and the Poisson's ratios of the two materials, v_f and v_s by the following equation:

$$E_f = 3E_s\left(\frac{1-v_f^2}{1-v_s^2}\right)\left(\frac{\lambda_b}{2\pi d_f}\right)^3 \qquad (\mathbf{1})$$

We measured the tensile modulus of the substrate, E_s (using a commercial pull tester), the buckling wavelength, λ_b (by optical microscopy), and the film thickness, d_f (by stylus profilometry). The slope of a plot of λ_b vs. d_f for three different film thicknesses was inserted into Equation 1. The Poisson's ratios were taken as 0.5 and 0.35 for PDMS and

the conjugated polymers films, which agree well with the previously reported values and our theoretical predictions.[1,8]

We also computed the values for the tensile moduli of the conjugated polymer using a theoretical model originally described by Seitz,[37] applied to conjugated polymers by Tahk,[8] and further refined by our group to account for differential glass transition temperature between various conjugated polymers.[1] The model incorporated the knowledge of the chemical structure of the polymer—*i.e.* molecular weight, van der Waals volume, the length and the number of rotational bonds in the monomer—and the glass transition temperature (T_g).

8.2.5 Fabrication and testing of photovoltaic devices

The conjugated polymer:fullerene bulk heterojunction (BHJ) films were spin-coated onto glass slides pre-coated with a PEDOT:PSS films. Prior to spin-coating the PEDOT:PSS, the glass slides were cleaned with Alconox solution (2 mg mL^{-1}), deionized water, acetone, and then isopropyl alcohol (IPA) in an ultrasonic bath for 10 min each, followed by a plasma treatment at ~30 W for 3 min at a base pressure of 200 mTorr in ambient air. The PEDOT:PSS layer was deposited from an aqueous solution containing 93 wt% Clevios PH 1000 (~0.9–1.2 wt% PEDOT:PSS), 6.9 wt% DMSO, and 0.1 wt% Zonyl.[38] The solution was filtered with a 1-μm glass microfiber (GMF) syringe filter and then spin coated at a speed of 500 rpm (100 rpm s^{-1} ramp) for 60 s, followed by 2000 rpm (750 rpm s^{-1} ramp) for 60 s, which produced in a layer 200 nm thick. The samples were subsequently dried at 150 °C for 30 min before the deposition of the polymer:fullerene BHJ films. The BHJ films were deposited from solutions of 1:2 by weight polymer and

$PC_{61}BM$ in 4:1 $CHCl_3$:ODCB (2.5 mg mL^{-1}), which were stirred overnight and filtered with 0.20 μm poly(tetrafluoroethylene) (PTFE) syringe filters. The solutions were then spin coated onto the electrode layer at a speed of 300 rpm (100 rpm s^{-1} ramp) for 240 s, followed by 2000 rpm (750 rpm s^{-1} ramp) for 60 s. For each device, a thin strip of the PEDOT:PSS electrode was exposed by wiping away some of the polymer:$PC_{61}BM$ film with chloroform so that electrical contact could be made. To minimize exposure to ambient air by transferring devices into and out of an evaporator in a different building, EGaIn (extruded by hand from a syringe) was used as the top contact.[39] The photovoltaic properties were measured in a nitrogen-filled glovebox using a solar simulator with a 100 mW cm^{-2} flux that approximated the solar spectrum under AM 1.5G conditions (ABET Technologies 11016-U up-facing unit calibrated with a reference cell with a KG5 filter). The current density versus voltage was measured for both dark and under illumination using a Keithley 2400 SourceMeter.

8.3 Results and Discussion

8.3.1 ^1H NMR

Our first task was to verify the incorporation of the 2T units in the PDPP2FT-seg-2T polymer. **Figure 8.3** compares the ^1H NMR spectra for PDPP2FT, PDPP2FT-seg-2T and PT2T; the inset highlights the signal from 3.0 to 1.5 ppm. Because the PDPP2FT and PDPP2FT-seg-2T are compositionally similar, differences in spectra were expected to be quite minor. The spectrum for PDPP2FT-seg-2T is largely similar to that of PDPP2FT, except that PDPP2FT-seg-2T exhibited a signal at 2.88-2.38 ppm and a partially overlapping signal at 1.74-1.63 ppm, which we attribute to the methylene protons located

α and β to the aromatic rings of the bithiophene unit as shown in the inset of **Figure 8.3**. From integration of the signals, we estimated that there was one 2T unit incorporated per 4.4 DPP2F units in the segmented polymer. While the ^{1}H NMR experiments provided evidence for 2T units in our samples, further investigation was necessary to conclude that they were covalently incorporated into the main polymer chain. ^{13}C NMR spectra of the polymer samples are shown in **Figure D.1** but were inconclusive owing to a low signal to noise ratio for PDPP2FT and PDPP2FT-seg-2T, which we attribute to a low effective concentration of magnetically distinct carbon atoms even at the limit of solubility (*ca*. 50 mg mL^{-1}) and with data collection times of 9 h.

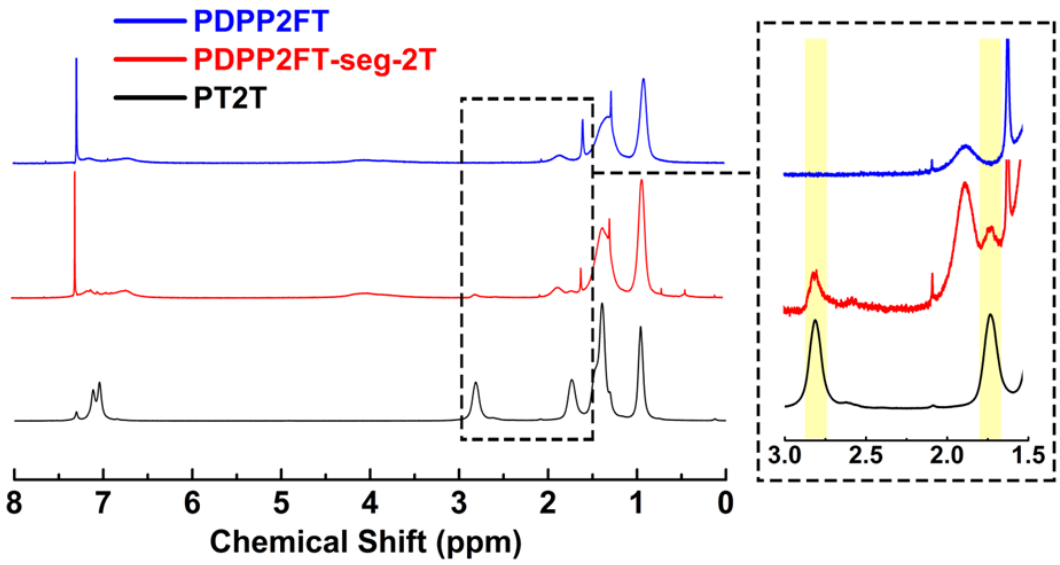

Figure 8.3. ^{1}H NMR spectra of PDPP2FT, PDPP2FT-seg-2T, and PT2T. Peaks associated with the bithiophene are highlighted in the inset at δ = 2.88-2.38 ppm and 1.74-1.63 ppm.

8.3.2 UV-Visible absorption

We compared the ultraviolet-visible absorption spectra of the three materials. **Figure 8.4** shows the absorption spectrum. The band gaps were determined from the onset

of absorption for thin films of the pure polymers (**Figure 8.4a**). PT2T exhibited an onset of optical absorption at around 660 nm (band gap = 1.88 eV), with a maximum absorption around 540 nm, while the pure PDPP2FT exhibited an onset of optical absorption at around 930 nm (band gap = 1.33 eV), with a maximum at 800 nm. PDPP2FT-seg-2T, which contains segments of PDPP2FT interspersed by statistical incorporation of monomers (PDPP2FT-seg-2T) exhibits features similar to PDPP2FT. However, the peaks in PDPP2FT-seg-2T are broader and less defined, which could suggest decreased order than what is observed in the homopolymer, PDPP2FT. The details of the vibronic structure have been used to correlate the extent of π-stacked, ordered structures (H-aggregates) in P3HT:$PC_{61}BM$ blends to their tensile moduli and ductility, with samples that exhibited significant H-aggregates also exhibited increased stiffness and ductility.[6] Further work would be required to correlate order as measured spectroscopically to mechanical properties for this class of low-bandgap materials.

To determine if the ^{1}H NMR and the above UV-vis results were due to PT2T contamination in the PDPP2FT-seg-2T sample as opposed to covalently bound segments, we performed two additional UV-vis experiments. We first measured the extinction coefficients of the pure polymers from their absorption in $CHCl_3$ (1×10^{-5} M) and used these values to calculate the absorption spectra of physical blends of PDPP2FT:PT2T (**Figure 8.4b**). Because the samples were dilute and did not form aggregates, our calculated absorptions were superpositions of the pure polymers in various ratios. We calculated the minimum ratio of PDPP2FT:PT2T before a noticeable onset of absorption in the PT2T absorbing region to be approximately 100:1. The normalized absorption spectra of the pure polymers and the calculated 100:1 physical blend absorption spectra, as well as the ratio of

DPP2F:2T in PDPP2FT-seg-2T (4.4:1) are plotted in **Figure D.2**. We then determined the absorption of a thin film of a 100:1 physical blend of PDPP2FT:PT2T (**Figure D.3**). The absorption spectrum of the physical blend was approximately that of the pure PDPP2FT, with more well defined peaks than those of PDPP2FT-seg-2T.

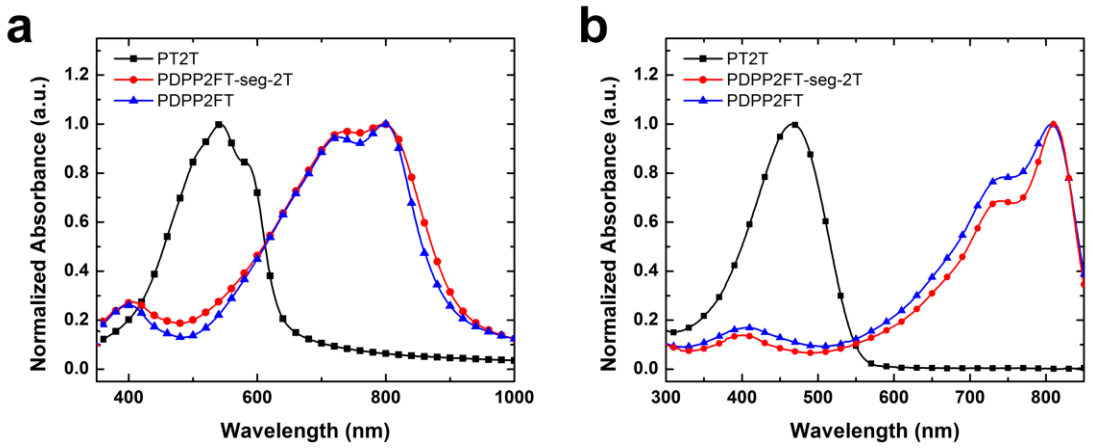

Figure 8.4. Absorption spectra of the three polymers synthesized in this work. (a) Thin films of the pure polymers spin cast from 4:1 $CHCl_3$:ODCB and (b) the pure polymers in $CHCl_3$ at a concentration of 1×10^{-5} M.

8.3.3 Gel-permeation chromatography

From the ^{1}H NMR spectra, we demonstrated that both PDPP2FT and 2T units are present in the product. The next essential step was to confirm the purity—*i.e.*, the absence of homopolymers—within the segmented product. Gel permeation chromatography provided evidence of covalent connectivity of the bithiophene units within the segmented polymer. **Figure 8.5** shows the GPC traces (intensity vs. retention time) and contour plots (wavelength vs. retention time) of all three conjugated polymer samples. For PDPP2FT (**Figure 8.5a**), the main absorbance peak occurred at 550-800 nm from 10 to 14 min with a much smaller peak at 350-450 nm. Minor tailing was observed in the GPC traces; these tails probably correspond to lower molecular weight polymers. A relatively polydisperse

sample was expected from a step-growth mechanism. The GPC trace for the segmented polymer (PDPP2FT-seg-2T) also showed similar tailing and a broad shoulder. This shoulder may originate from either lower molecular weight segmented polymer or from the presence of residual homopolymers. We addressed this concern using the contour plot based on a photodiode UV detector as described by Hawker and coworkers for an all-conjugated block copolymer.[32] The contour plot for the segmented polymer (PDPP2FT-seg-2T, **Figure 8.5b**) shows two absorbance peaks at 350-550 and 550-800 nm centered on a single retention time of 11-14 min. The plot for PT2T (**Figure 8.5c**) also suggests the absence of major impurities; it shows a dominant absorbance peak from 350-500 nm at 13 min. This analysis strongly suggests that the product in PDPP2FT-seg-2T contains no contamination of either homopolymers and the low molecular weight tail contains both PDPP2FT and 2T segments. If homopolymers contamination were to occur, two distinct absorption regions with different retention times would be observed. The closeness in retention time of PDPP2FT and PDPP2FT-seg-2T suggests a minimal difference in molecular weights; thus we neglect the effects of molecular weight on the mechanical properties and photovoltaic properties of the two materials (**Table 8.1**).

Table 8.1. Molecular weights and PDIs for the conjugated polymer samples as determined by GPC versus polystyrene standards.

Polymer	M_n **(g mol^{-1})**	M_w **(g mol^{-1})**	**PDI**
PDPP2FT	26 400	69 600	2.64
PDPP2FT-seg-2T	22 300	55 300	2.47
PT2T	14 800	19 400	1.31

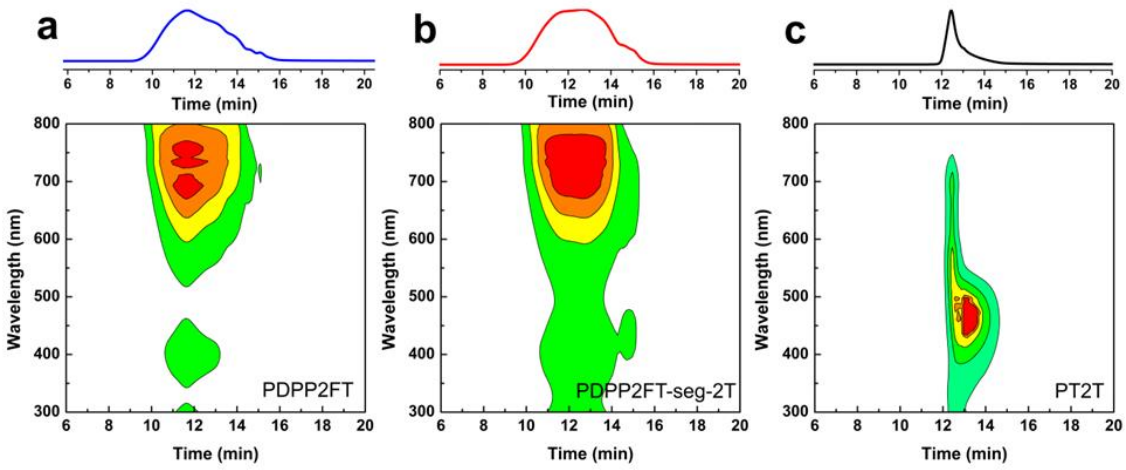

Figure 8.5. GPC traces and contour plots for (a) PDPP2FT, (b) PDPP2FT-seg-2T, and (c) PT2T based on a UV detector.

8.3.4 Tensile moduli of conjugated polymer thin films

We determined the tensile moduli of the pure polymer thin films spin-coated from chloroform. For each film, the buckling wavelengths were plotted as a function of the film thickness. The slopes of the linear fits were then substituted into Equation 1 to obtain the tensile moduli of the thin films. The tensile modulus of PT2T, whose structure is closely related to P3HT,[35] was determined to be 1.11 ± 0.19 GPa. This value agrees well with the values of P3HT reported previously by our group[1] and literature values[8,16] obtained using the same method. The obtained value for PDPP2FT, 2.17 ± 0.35 GPa, was twice that of PT2T. This value was greater than that previous reported for PDPP2T-TT (0.99 GPa),[16] though we note that PDPP2T-TT contains octyldodecyl side chains and PDPP2FT contains ethylhexyl side chains. Long alkyl side chains tend to reduce the tensile modulus and increase the ductility of a conjugated polymer significantly.[1]

We then measured the tensile modulus of the segmented polymer, PDPP2FT-seg-2T. The incorporation of the 2T units, as determined from ^{1}H NMR spectra, produced a

significantly reduced stiffness (modulus = 0.93 ± 0.16 GPa) compared to PDPP2FT. The reduction in modulus by segmentation is possibly attributable to three effects. The first effect is that random incorporation tends to disrupt the ability of a conjugated polymer to form crystallites, and highly crystalline films tend to be stiffer than amorphous ones with similar chemical structures.[7] The second effect is that in the segmented sample, approximately one of every five DPP2F units is substituted for a 2T unit. Substitution of fused rings for isolated rings have been correlated to decreased stiffness of the film in both polythiophene[7] and DPP-based systems.[16] The third effect is that statistical incorporation of alkylated bithiophene units significantly altered the distribution of side chains compared to that of the homopolymer. While predicting the effect of this change in the distribution of side chains on the mechanical properties would be difficult to accomplish, small changes in the lengths of the side-chains have significant effects on the thermal, electrical, and mechanical properties of P3ATs.[1,40] As a control experiment, we also measured the tensile modulus of the 100:1 physical blend between PDPP2FT and PT2T (**Figure D.4** and **Table D.1**). We found that, within experimental error, the physical blend had a comparable tensile modulus to PDPP2FT.

Our theoretical calculations of the tensile moduli that uses the molecular structure of the monomer as well as the T_g of the polymer[1,8,37] agreed extremely well with experimental values for the homopolymers, PT2T and PDPP2FT. The calculated values were 1.13 ± 0.14 (PT2T) and 2.47 ± 0.30 (PDPP2FT), using the T_g values of 14 °C and 50 °C. This simple theoretical model, however, failed to predict the reduction in modulus of PDPP2FT-seg-2T relative to that of the homopolymer, PDPP2FT. We attribute its failure primarily to its inability to incorporate the effects of randomness in the polymer chain.

8.3.5 Photovoltaic characteristics

To determine the applicability of these materials in organic solar cells, we fabricated devices by mixing the polymers in a 1:2 ratio with $PC_{61}BM$. We used PEDOT:PSS as the transparent anode and eutectic gallium-indium (EGaIn) as the cathode.[39] **Figure 8.6** shows the current density vs. voltage (*J–V*) plots for representative devices. (**Figure D.5** and **Table D.2** include devices fabricated with a 100:1 PDPP2FT:PT2T physical blend, which performed similarly to, but slightly poorer than the PDPP2FT devices). The poor behavior we observed for the PT2T sample is consistent with similarly poor performance reported by Koppe et al.,[35] who attributed the inefficiency of PT2T:$PC_{61}BM$ compared to P3HT:$PC_{61}BM$ (despite favorable offsets of the frontier molecular orbitals) to intercalation of $PC_{61}BM$ within the large gap between side chains in PT2T and suppression of the ability of the polymer to crystallize.[35] The power conversion efficiency (*PCE*) of PDPP2FT:$PC_{61}BM$ (*PCE* = 2.52 ± 0.34%, *N* = 7) and PDPP2FT-seg-2T:$PC_{61}BM$ (*PCE* = 2.82 ± 0.28%, *N* = 6), however, were similar. The data for all devices tested are summarized in **Table 8.2**. The short circuit current (J_{sc}), open circuit voltage (V_{oc}), fill factor (*FF*), series resistance (R_{series}), and *PCE* are all very similar for PDPP2FT and PDPP2FT-seg-2T. The similarity in figures of merit suggests that the charge-transport properties are preserved despite the incorporation of 2T units. Interestingly, even though the incorporation of the 2T units increased the mechanical compliance of PDPP2FT-seg-2T, it did not appear to have a deleterious effect on the photovoltaic properties.

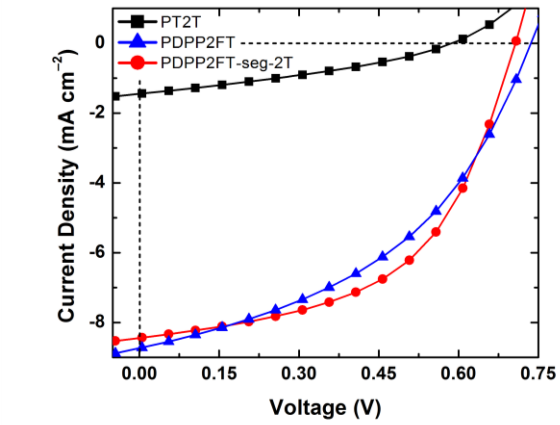

Figure 8.6. Photovoltaic characteristics of representative samples of polymer-fullerene blends. All active layers comprised 1:2 polymer:$PC_{61}BM$.

Table 8.2. Summary of the figures of merit for the solar cells fabricated in this work.

Polymer	***n***	J_{sc} **[mA cm^{-2}]**	V_{oc} **[mV]**	***FF*** **[%]**	η_e **[%]**
PT2T	3	1.5 ± 0.1	579 ± 21	32.9 ± 1.1	0.28 ± 0.01
PDPP2FT-seg-2T	6	8.4 ± 0.5	699 ± 23	48.2 ± 3.3	2.82 ± 0.28
PDPP2FT	7	8.3 ± 0.5	715 ± 25	42.5 ± 3.6	2.52 ± 0.34

8.3.6 Atomic force microscopy

To determine if the difference in tensile modulus between the PDPP2FT and the PDPP2FT-seg-2T could be attributed to a significant change in the morphology of the films, we examined spin-coated films by AFM. Previous studies have suggested that roughness observable by AFM correlates with crystalline order, as determined by grazing-incidence X-ray diffraction, in conjugated polymer films annealed below T_m.[41] A similar effect was noted in a series of P3ATs from A = butyl to A = dodecyl, where the shortest alkyl chains had the greatest roughness (presumably due to greater crystallinity) and stiffness.[1] **Figure 8.7** shows AFM micrographs of the heights of the PDPP2FT and the PDPP2FT-seg-2T films. We observed that PDPP2FT had a root mean square (rms) roughness of 1.13 ± 0.09 nm and PDPP2FT-seg-2T had an rms roughness of 1.25 ± 0.08

nm. The similarity of these values suggests that the correlation between roughness (as a manifestation of crystallinity) and tensile modulus—as observed in other systems—is not general.

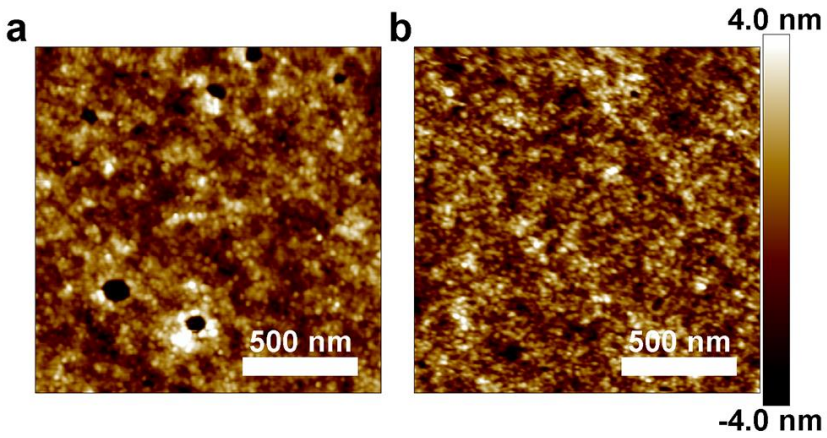

Figure 8.7. Height images from atomic force micrographs of unannealed polymer thin films. (a) PDPP2FT and (b) PDPP2FT-seg-2T.

8.3.7 Competition between photovoltaic performance and stiffness

Within groups of structurally related conjugated polymers, charge transport and photovoltaic efficiency are regarded as antithetical to mechanical compliance.{Merging Citations} Along with the tensile moduli of the pure polymers, we measured the moduli of the 1:2 polymer:$PC_{61}BM$ blends spin-coated from 4:1 chloroform:ODCB. **Figure 8.8a** compares the tensile moduli of the pure polymer films and the blended films. For all three polymers, we observed increased in the tensile moduli with the addition of $PC_{61}BM$. Various studies have reported the same trend in system comprising conjugated polymer and fullerene composites.[1,7,8,13,16] In **Figure 8.8b**, we plotted the power conversion efficiencies (*PCE*) of the polymer:$PC_{61}BM$ BHJ films as a function of tensile modulus. For materials in which these figures of merit are strongly correlated, such as in P3HT:$PC_{61}BM$ exhibiting increasing order, the data points would sit (very roughly) on a diagonal

extending from low tensile modulus and low *PCE* to high values of both parameters. Interestingly, the sample PDPP2FT-seg-2T:$PC_{61}BM$ shows a similar *PCE* to that of PDPP2FT:$PC_{61}BM$, but the PDPP2FT-seg-2T is a factor of two more elastic than PDPP2FT. While polymer:$PC_{61}BM$ blends are always measured to be stiffer than the pure polymers, the factor by which the tensile modulus of the blend is greater than that of the pure polymer tends to be similar within similar classes of materials.[1,16] The segmented copolymer, PDPP2FT-seg-2T appears to exhibit photovoltaic properties resembling PDPP2FT, but mechanical properties resembling those of PT2T. It is possible that the "random" segments interspersed between PDPP2FT segments have a softening effect on the material. The all-conjugated nature of the "random" segments may provide advantages over block copolymers in which the plasticizing block is insulating.[42]

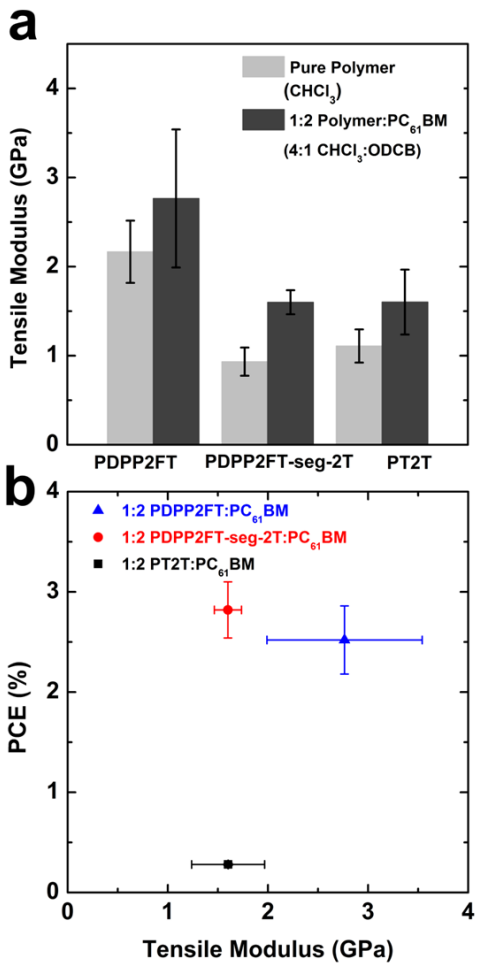

Figure 8.8. Mechanical and electronic properties of the polymer and polymer:fullerene blends in this work. (a) Comparison between the tensile moduli of pure polymer films spin-coated from chloroform and the films comprising 1:2 polymer:$PC_{61}BM$ blends spin-coated from 4:1 chloroform:ODCB. (b) Plot of power conversion efficiency of the polymers in a 1:2 blend with $PC_{61}BM$ spin-coated from 4:1 chloroform:ODCB. The architecture of the devices was PEDOT:PSS/polymer:$PC_{61}BM$/EGaIn. The vertical error bars for 1:2 PT2T:$PC_{61}BM$ sample overlap with the marker.

8.4 Conclusion

We have demonstrated that segmentation could be an effective strategy to increase the mechanical compliance of low-bandgap conjugated polymers without deleteriously affecting their optoelectronic properties. The method does not add significant complexity to the synthetic protocol—a third monomer is simply added to the reaction mixture after a

predetermined length of time. The polymerization strategy described here suggests the possibility of fully segmented polymer comprising "macromonomers" of polymers with different band structures. Such materials could be analogous to block copolymers except that block copolymers are synthesized by living, chain-growth processes. In contrast, polymers in which both components are synthesized by step-growth processes (*i.e.*, the Stille polymerization) are not amenable to the synthesis of block copolymers. Segmented polymerization may therefore be a route to synthesizing single-component organic semiconductors with tailored thermal and mechanical properties (*i.e.*, semiconducting thermoplastic elastomers). Our analysis also exposed deficiencies in the ways in which standard semi-empirical theories predict mechanical properties in semicrystalline polymers. Future work will attempt to incorporate the effects of randomness in the polymer backbones as well as address the behavior of these softened polymers in real-world conditions.

Acknowledgements

This work was supported by the Air Force Office of Scientific Research (AFOSR) Young Investigator Program, grant number FA9550-13-1-0156. Additional support was provided by the NSF Graduate Research Fellowship under grant number DGE-1144086, awarded to S. S., and by laboratory startup funds from the University of California, San Diego.

Chapter 8, in full, is a reprint of the material as it appears in *RSC Advances*, 2014, 4, 13635. The Royal Society of Chemistry, 2014. Adam D. Printz,[†] Suchol Savagatrup,[†]

Daniel J. Burke, Trevor N. Purdy, and Darren J. Lipomi. († Equal contribution). The dissertation author was the primary investigator and author of this paper.

References

(1) Savagatrup, S.; Makaram, A. S.; Burke, D. J.; Lipomi, D. J. Mechanical Properties of Conjugated Polymers and Polymer-Fullerene Composites as a Function of Molecular Structure. *Adv. Funct. Mater.* **2014**, *24*, 1169–1181.

(2) Kaltenbrunner, M.; White, M. S.; Głowacki, E. D.; Sekitani, T.; Someya, T.; Sariciftci, N. S.; Bauer, S. Ultrathin and Lightweight Organic Solar Cells with High Flexibility. *Nat. Commun.* **2012**, *3*, 770.

(3) Kaltenbrunner, M.; Sekitani, T.; Reeder, J.; Yokota, T.; Kuribara, K.; Tokuhara, T.; Drack, M.; Schwödiauer, R.; Graz, I.; Bauer-Gogonea, S.; Bauer, S.; Someya, T. An Ultra-Lightweight Design for Imperceptible Plastic Electronics. *Nature* **2013**, *499*, 458–463.

(4) Dupont, S. R.; Oliver, M.; Krebs, F. C.; Dauskardt, R. H. Interlayer Adhesion in Roll-to-Roll Processed Flexible Inverted Polymer Solar Cells. *Sol. Energy Mater. Sol. Cells* **2012**, *97*, 171–175.

(5) Brand, V.; Bruner, C.; Dauskardt, R. H. Cohesion and Device Reliability in Organic Bulk Heterojunction Photovoltaic Cells. *Sol. Energy Mater. Sol. Cells* **2012**, *99*, 182–189.

(6) Awartani, O.; Lemanski, B. I.; Ro, H. W.; Richter, L. J.; DeLongchamp, D. M.; O'Connor, B. T. Correlating Stiffness, Ductility, and Morphology of Polymer:Fullerene Films for Solar Cell Applications. *Adv. Energy Mater.* **2013**, *3*, 399–406.

(7) O'Connor, B.; Chan, E. P.; Chan, C.; Conrad, B. R.; Richter, L. J.; Kline, R. J.; Heeney, M.; McCulloch, I.; Soles, C. L.; DeLongchamp, D. M. Correlations between Mechanical and Electrical Properties of Polythiophenes. *ACS Nano* **2010**, *4*, 7538–7544.

(8) Tahk, D.; Lee, H. H.; Khang, D.-Y. Elastic Moduli of Organic Electronic Materials by the Buckling Method. *Macromolecules* **2009**, *42*, 7079–7083.

(9) Lipomi, D. J.; Bao, Z. Stretchable, Elastic Materials and Devices for Solar Energy Conversion. *Energy Environ. Sci.* **2011**, *4*, 3314–3328.

(10) Sekitani, T.; Someya, T. Stretchable Organic Integrated Circuits for Large-Area Electronic Skin Surfaces. *Mrs Bull.* **2012**, *37*, 236–245.

(11) Rogers, J. A.; Someya, T.; Huang, Y. Materials and Mechanics for Stretchable Electronics. **2010**, *327*, 1603–1607.

(12) Kim, D.-H.; Lu, N.; Ma, R.; Kim, Y.-S.; Kim, R.-H.; Wang, S.; Wu, J.; Won, S. M.; Tao, H.; Islam, A.; Yu, K. J.; Kim, T.; Chowdhury, R.; Ying, M.; Xu, L.; Li, M.; Chung, H.-J.; Keum, H.; McCormick, M.; Liu, P.; Zhang, Y.-W.; Omenetto, F. G.; Huang, Y.; Coleman, T.; Rogers, J. A. Epidermal Electronics. *Science* **2011**, *333*, 838–843.

(13) O'Connor, T. F.; Zaretski, A. V.; Shiravi, B. A.; Savagatrup, S.; Printz, A. D.; Diaz, M. I.; Lipomi, D. J. Stretching and Conformal Bonding of Organic Solar Cells to Hemispherical Surfaces. *Energy Environ. Sci.* **2014**, *7*, 370–378.

(14) Dou, L.; You, J.; Hong, Z.; Xu, Z.; Li, G.; Street, R. A.; Yang, Y. 25Th Anniversary Article: A Decade of Organic/Polymeric Photovoltaic Research. *Adv. Mater.* **2013**, *25*, 6642–6671.

(15) Burke, D. J.; Lipomi, D. J. Green Chemistry for Organic Solar Cells. *Energy Environ. Sci.* **2013**, *6*, 2053–2066.

(16) Lipomi, D. J.; Chong, H.; Vosgueritchian, M.; Mei, J.; Bao, Z. Toward Mechanically Robust and Intrinsically Stretchable Organic Solar Cells: Evolution of Photovoltaic Properties with Tensile Strain. *Sol. Energy Mater. Sol. Cells* **2012**, *107*, 355–365.

(17) McCulloch, I.; Heeney, M.; Bailey, C.; Genevicius, K.; Macdonald, I.; Shkunov, M.; Sparrowe, D.; Tierney, S.; Wagner, R.; Zhang, W.; Chabinyc, M. L.; Kline, R. J.; McGehee, M. D.; Toney, M. F. Liquid-Crystalline Semiconducting Polymers with High Charge-Carrier Mobility. *Nat. Mater.* **2006**, *5*, 328–333.

(18) Chen, Z.; Lee, M. J.; Shahid Ashraf, R.; Gu, Y.; Albert-Seifried, S.; Meedom Nielsen, M.; Schroeder, B.; Anthopoulos, T. D.; Heeney, M.; McCulloch, I.; Sirringhaus, H. High-Performance Ambipolar Diketopyrrolopyrrole-thieno[3,2-B]thiophene Copolymer Field-Effect Transistors with Balanced Hole and Electron Mobilities. *Adv. Mater.* **2012**, *24*, 647–652.

(19) Bronstein, H.; Chen, Z.; Ashraf, R. S.; Zhang, W.; Du, J.; Durrant, J. R.; Tuladhar, P. S.; Song, K.; Watkins, S. E.; Geerts, Y.; Wienk, M. M.; Janssen, R. A.; Anthopoulos, T.; Sirringhaus, H.; Heeney, M.; McCulloch, I. Thieno[3,2-B]thiophene-Diketopyrrolopyrrole-Containing Polymers for High-Performance Organic Field-Effect Transistors and Organic Photovoltaic Devices. *J. Am. Chem. Soc.* **2011**, *133*, 3272–3275.

(20) Zhang, X.; Richter, L. J.; Delongchamp, D. M.; Kline, R. J.; Hammond, M. R.; McCulloch, I.; Heeney, M.; Ashraf, R. S.; Smith, J. N.; Anthopoulos, T. D.; Schroeder, B.; Geerts, Y. H.; Fischer, D. A.; Toney, M. F. Molecular Packing of High-Mobility Diketo Pyrrolo-Pyrrole Polymer Semiconductors with Branched Alkyl Side Chains. *J. Am. Chem. Soc.* **2011**, *133*, 15073–15084.

(21) Shaheen, S. E.; Brabec, C. J.; Sariciftci, N. S.; Padinger, F.; Fromherz, T.; Hummelen, J. C. 2.5% Efficient Organic Plastic Solar Cells. *Appl. Phys. Lett.* **2001**, *78*, 841–843.

(22) Jørgensen, M.; Carlé, J. E.; Søndergaard, R. R.; Lauritzen, M.; Dagnæs-Hansen, N. A.; Byskov, S. L.; Andersen, T. R.; Larsen-Olsen, T. T.; Böttiger, A. P. L.; Andreasen, B.; Fu, L.; Zuo, L.; Liu, Y.; Bundgaard, E.; Zhen, X.; Chen, H.; Krebs, F. C. The State of Organic Solar cells—A Meta Analysis. *Sol. Energy Mater. Sol. Cells* **2013**, *119*, 84–93.

(23) Qin, T.; Troisi, A. Relation between Structure and Electronic Properties of Amorphous MEH-PPV Polymers. *J. Am. Chem. Soc.* **2013**, *135*, 11247–11256.

(24) Pearson, A. J.; Wang, T.; Dunbar, A. D. F.; Yi, H.; Watters, D. C.; Coles, D. M.; Staniec, P. A.; Iraqi, A.; Jones, R. A. L.; Lidzey, D. G. Morphology Development in Amorphous Polymer:Fullerene Photovoltaic Blend Films During Solution Casting. *Adv. Funct. Mater.* **2014**, *24*, 659–667.

(25) Seo, J. H.; Gutacker, A.; Sun, Y.; Wu, H.; Huang, F.; Cao, Y.; Scherf, U.; Heeger, A. J.; Bazan, G. C. Improved High-Efficiency Organic Solar Cells via Incorporation of a Conjugated Polyelectrolyte Interlayer. *J. Am. Chem. Soc.* **2011**, *133*, 8416–8419.

(26) Osedach, T. P.; Andrew, T. L.; Bulović, V. Effect of Synthetic Accessibility on the Commercial Viability of Organic Photovoltaics. *Energy Environ. Sci.* **2013**, *6*, 711–718.

(27) Rivnay, J.; Toney, M. F.; Zheng, Y.; Kauvar, I. V.; Chen, Z.; Wagner, V.; Facchetti, A.; Salleo, A. Unconventional Face-on Texture and Exceptional in-Plane Order of a High Mobility N-Type Polymer. *Adv. Mater.* **2010**, *22*, 4359–4363.

(28) Hawker, C. J.; Russell, T. P. Block Copolymer Lithography: Merging "Bottom-Up" with "Top-Down" Processes. *MRS Bull.* **2005**, *30*, 952–966.

(29) Arriola, D. J.; Carnahan, E. M.; Hustad, P. D.; Kuhlman, R. L.; Wenzel, T. T. Catalytic Production of. *Science (80-.).* **2006**, *312*, 714–719.

(30) Zhang, M.; Moore, R. B.; Long, T. E. Melt Transesterification and Characterization of Segmented Block Copolyesters Containing 2,2,4,4-Tetramethyl-1,3-Cyclobutanediol. *J. Polym. Sci. Part A Polym. Chem.* **2012**, *50*, 3710–3718.

(31) Scherf, U.; Gutacker, A.; Koenen, N. All-Conjugated Block Copolymers. *Acc. Chem. Res.* **2008**, *41*, 1086–1097.

(32) Ku, S.-Y.; Brady, M. a; Treat, N. D.; Cochran, J. E.; Robb, M. J.; Kramer, E. J.; Chabinyc, M. L.; Hawker, C. J. A Modular Strategy for Fully Conjugated Donor-Acceptor Block Copolymers. *J. Am. Chem. Soc.* **2012**, *134*, 16040–16046.

(33) Woo, C. H.; Beaujuge, P. M.; Holcombe, T. W.; Lee, O. P.; Fréchet, J. M. J. Incorporation of Furan into Low Band-Gap Polymers for Efficient Solar Cells. *J. Am. Chem. Soc.* **2010**, *132*, 15547–15549.

(34) Tierney, S.; Heeney, M.; McCulloch, I. Microwave-Assisted Synthesis of Polythiophenes via the Stille Coupling. *Synth. Met.* **2005**, *148*, 195–198.

(35) Koppe, M.; Scharber, M.; Brabec, C.; Duffy, W.; Heeney, M.; McCulloch, I. Polyterthiophenes as Donors for Polymer Solar Cells. *Adv. Funct. Mater.* **2007**, *17*, 1371–1376.

(36) Stafford, C. M.; Harrison, C.; Beers, K. L.; Karim, A.; Amis, E. J.; VanLandingham, M. R.; Kim, H.-C.; Volksen, W.; Miller, R. D.; Simonyi, E. E. A Buckling-Based Metrology for Measuring the Elastic Moduli of Polymeric Thin Films. *Nat. Mater.* **2004**, *3*, 545–550.

(37) Seitz, J. T. The Estimation of Mechanical Properties of Polymers from Molecular Structure. *J. Appl. Polym. Sci.* **1993**, *49*, 1331–1351.

(38) Vosgueritchian, M.; Lipomi, D. J.; Bao, Z. Highly Conductive and Transparent PEDOT:PSS Films with a Fluorosurfactant for Stretchable and Flexible Transparent Electrodes. *Adv. Funct. Mater.* **2012**, *22*, 421–428.

(39) Pasquier, A. Du; Miller, S.; Chhowalla, M. On the Use of Ga–In Eutectic and Halogen Light Source for Testing P3HT–PCBM Organic Solar Cells. *Sol. Energy Mater. Sol. Cells* **2006**, *90*, 1828–1839.

(40) Babel, A.; Jenekhe, S. A. Alkyl Chain Length Dependence of the Field-Effect Carrier Mobility in Regioregular poly(3-Alkylthiophene)s. *Synth. Met.* **2005**, *148*, 169–173.

(41) Verploegen, E.; Mondal, R.; Bettinger, C. J.; Sok, S.; Toney, M. F.; Bao, Z. Effects of Thermal Annealing Upon the Morphology of Polymer-Fullerene Blends. *Adv. Funct. Mater.* **2010**, *20*, 3519–3529.

(42) Müller, C.; Goffri, S.; Breiby, D. W.; Andreasen, J. W.; Chanzy, H. D.; Janssen, R. A. J.; Nielsen, M. M.; Radano, C. P.; Sirringhaus, H.; Smith, P.; Stingelin-Stutzmann, N. Tough, Semiconducting Polyethylene-poly(3-Hexylthiophene) Diblock Copolymers. *Adv. Funct. Mater.* **2007**, *17*, 2674–2679.

Chapter 9

Mechanical properties of a library of low-bandgap polymers

Suchol Savagatrup,[†a] Bérenger Roth,[†b] Nathaniel De Los Santos,[a] Ole Hagemann,[b] Jon E. Carlé,[b] Martin Helgesen,[b] Francesco Livi,[b] Eva Bundgaard,[b] Roar R. Søndergaard,[b] Frederik C. Krebs,[b] and Darren J. Lipomi[a]

([†] Equal contribution)

[a] *Department of NanoEngineering, University of California, San Diego, 9500 Gilman Drive Mail Code 0448, La Jolla, CA 92093-0448.*

[b] *Department of Energy Conversion and Storage, Technical University of Denmark, Frederiksborgvej 399, DK-4000 Roskilde, Denmark.*

Abstract

The mechanical properties of low-bandgap polymers are important for the long-term survivability of roll-to-roll processed organic electronic devices. Such devices—e.g., solar cells, displays, and thin-film transistors—must survive the rigors of roll-to-roll coating and also thermal and mechanical forces in the outdoor environment and in stretchable and ultra-flexible form factors. This paper measures the stiffness (tensile modulus), ductility (crack-onset strain), or both, of a combinatorial library of 51 low-bandgap polymers. The purpose of this study is to systematically screen a library of low-bandgap polymers to better understand the connection between molecular structures and mechanical properties, in order to design conjugated polymers that permit mechanical robustness and even extreme deformability. While one of the principal conclusions of these experiments is that the structure of an isolated molecule only partially determines the mechanical properties—another important co-determinant is the packing structure—some general trends can be identified. (1) Fused rings tend to increase the modulus and decrease the ductility. (2) Branched side chains have the opposite effect. Despite the rigidity of the molecular structure, the most deformable films can be surprisingly compliant (modulus $\geq$ 150 MPa) and ductile (crack-onset strain $\leq$ 68%). This paper concludes by proposing a new composite merit factor that combines the power conversion efficiency in a fully solution processed device obtained via roll and roll-to-roll coating and printing (as measured in an earlier paper) and the mechanical deformability toward the goal of producing modules that are both efficient and mechanically stable.

9.1. Introduction

The conventional rationale for research on organic photovoltaic (OPV) materials and devices is the promise of inexpensive, lightweight, flexible solar modules that can be fabricated by roll-to-roll (R2R) processing in ambient atmosphere on flexible substrates.[1] These defining advantages are thus contingent on stability against bending and other thermomechanical modes of deformation.[2] The work of Dauskardt *et al.* has shown, however, that the cohesive and adhesive fracture energies encountered within and between layers in organic solar cells occupy a typical range of 1–5 J m^{-2}, which is significantly lower than the values that characterize devices based on conventional semiconducting materials (though these values are dependent on thickness of the active layer, polymer:fullerene blend, processing conditions, composition, molecular weight, and relative humidity).[3] Despite an increase in interest in the mechanical properties of nominally flexible electronic materials,[4,5] almost all previous work has focused on the properties of poly(3-alkylthiophenes) (P3ATs, for which we have previously shown that structural features such as the length of the alkyl side chain play critical roles in determining the stiffness, yield point, and ductility of conjugated polymers[2,6]). While the P3ATs (particularly where A = hexyl) have been a useful model system[7]—and also appears to have significant advantages in R2R production[8]—the best power conversion efficiencies are achieved with low-bandgap polymers comprising an alternating arrangement of donor and acceptor (D-A) units.[9]

This paper describes a large-scale investigation of the mechanical properties of D-A polymers by measuring the tensile modulus, cracking behavior, or both, of a combinatorial library of 51 compounds, which represent combinations of acceptors A1–10

and A12–14 and donors D1–D3 and D5–D9, shown in **Figure 9.1**. The purpose of this study was to take the first steps toward developing guidelines for the rational design of conjugated polymers for increased mechanical stability and deformability. Combined with an earlier report from Bundgaard *et al.*[8] on the photovoltaic performance of a library of which the materials studied here is a subset, the ultimate goal of this work is thus to permit the co-optimization of electronic and mechanical performance. A favorable outcome would not only improve the stability of R2R processed organic solar modules, but would also allow the integration of OPVs—or any organic electronic devices—in many form factors inaccessible by conventional devices, such as in clothing, portable electronics, biomedical applications, and extremely flexible and stretchable devices.[2]

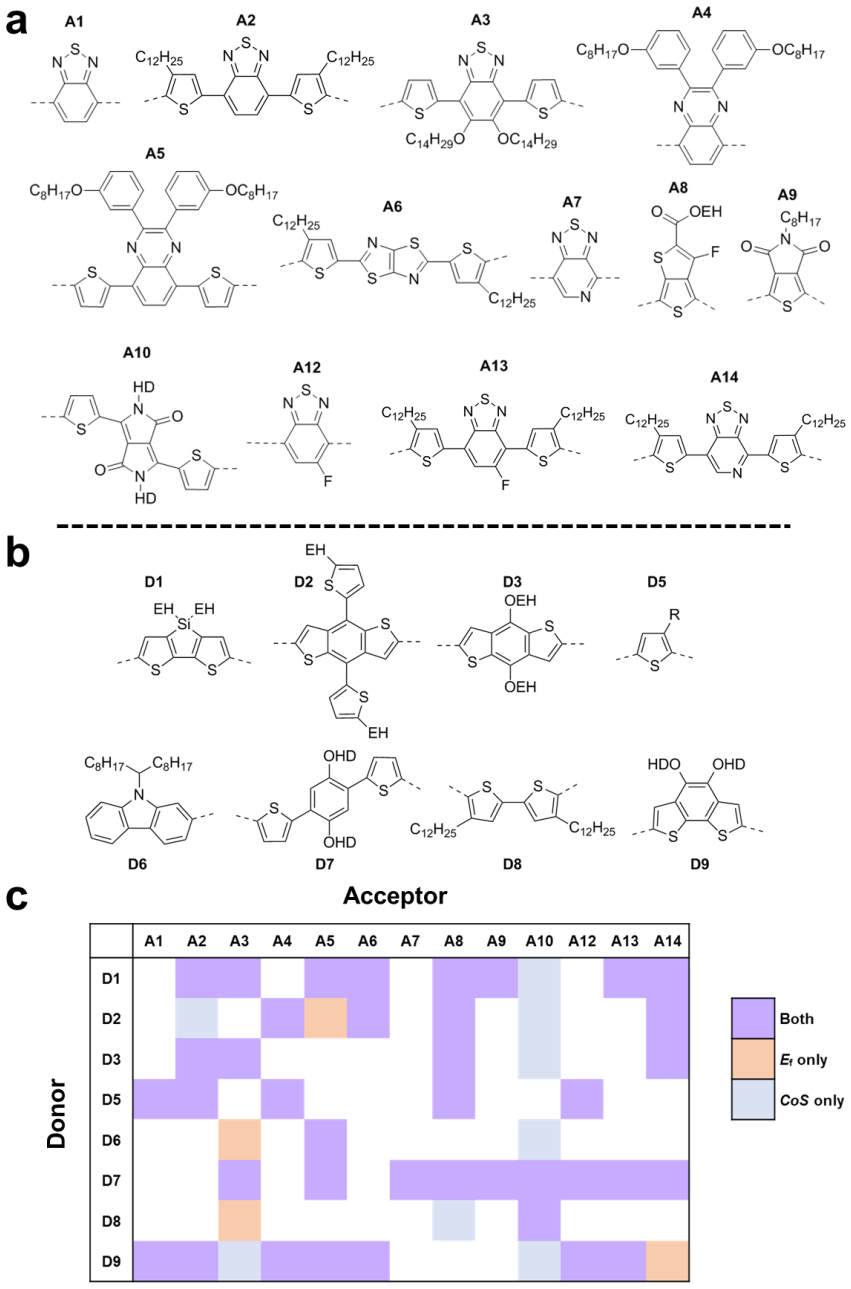

Figure 9.1. Chemical structures of the thirteen acceptor monomers (a) and eight donor monomers (b) as synthesized and described in a previous paper.[8] (c) Table of the combination of D-A polymers measured in this work. The tensile moduli (E_f) were measured for a total of 43 polymers, the crack-onset strains (CoS) were measured for 47 polymers, and both quantities were measured for 39 polymers. The "missing" combinations are the result of failure to obtain the material by synthesis, failure to create devices via roll-coating, or insufficient material available after the initial studies performed in ref. [8].For D5, R is H for A2 and A4 and $C_{12}H_{25}$ for A1, A8, and A12. The abbreviation EH stands for 2-ethylhexyl, and HD stands for 2-hexyldecyl.

9.2 Background

Mechanical stability of conjugated polymers, specifically D-A polymers, has until now received little attention in the literature. The absence of emphasis on this topic has been due to the focus on improving the power conversion efficiency (*PCE*) on small scale laboratory device on glass where thermomechanical properties rarely present a limitation to observations of device performance. However, for flexible devices that require flexibility during manufacturing, in the actual application/integration, and in the operation of the device, the thermomechanical properties become a dominant boundary condition that if not met will prevent success (regardless of device *PCE*).[1] Recently, laboratory-scale *PCE* for D-A polymers has reached well over 10% on optimized architectures on devices with small active areas.[10] However, these devices were prepared on rigid substrates—i.e., glass coated with indium tin oxide (ITO)—that are not compatible with R2R manufacturing.[1] Moreover, rigid substrates mask the potential fragility of the D-A polymers and polymer:fullerene composites that could lead to mechanical failure in flexible modules.[2] The recent effort by Bundgaard *et al.* to screen 104 different combinations of D-A polymers has revealed that 13 out of 104 polymers outperformed P3HT on a merit factor that is weighted toward the suitability of the materials for R2R processing.[8] This merit factor accounted for not only the electrical performance but also the chemical stability and simplicity of the synthesis,[8] but did not account for the predicted stability against thermomechanical degradation.

While most earlier work by us and others on the mechanical properties of organic semiconductors has focused on P3ATs,[2] a few studies have suggested some ways in which the molecular structures of the D-A polymers influence their mechanical properties. An

earlier paper examined the mechanical properties of PDPP-2TTT (a D-A polymer whose repeating units comprise diketopyrrolopyrrole (DPP), thiophene (T), thienothiophene (TT), and thiophene in the backbone) and PDPP-4T (a close structural analog in which the fused thienothiophene structure was substituted with bithiophene, which comprises two isolated thiophene rings).[11] The results of this work suggested (though not rigorously confirmed) that the polymer with the fused ring system produced a tensile modulus that was higher (0.99 GPa for PDPP-2TTT) than that of the polymer bearing the isolated rings (0.74 GPa for PDPP-4T).[11] In a separate study, we found that random incorporation of bithiophene units into the structure of PDPP-2FT (where F = furan) decreased the tensile modulus from 2.17 ± 0.35 GPa to 0.93 ± 0.16 GPa.[12] The brittleness of polymers comprising rigid large fused rings in the backbone was also suggested by the results of Wu *et al*., who observed significant cracking in highly crystalline organic thin film transistors fabricated from a DPP-based polymer with four fused thiophene rings.[13] Additionally, Kim *et al.* have also investigated the mechanical properties of D-A polymers, namely that of PBDTTTPD (same structure as A9D2, however we did not have this material available for this study).[14] They found that the tensile modulus of the composite of PBDTTTPD and a non-fullerene electron acceptor (at 1:1 ratio) was 0.43 GPa, which is much lower than when combined with PCBM at 1.76 GPa (at 1:1.5 ratio), and were able to make a solar cell with good efficiency and high intrinsic deformability.[14] These experimental results have recently been complemented with computational tools designed to study the effects of molecular structures of conjugated polymers on mesoscale (~10 – 100 nm) conformational structures, and thus may also accelerate the understanding of the connection between molecular structure and mechanical properties.[15]

Despite the efforts noted above, mechanical data for D-A polymers is sparsely reported. We thus sought to lay the groundwork for a rigorous understanding of the structural determinants of the mechanical properties of D-A polymers by reporting the properties of a sufficiently large library comprising several popular donors and acceptors. We admit at the outset several limitations of this approach. First, the mechanical properties of polymers are determined not only by the molecular structure, but by the microstructure in the solid state. The microstructure/morphology is difficult to predict by computation[15] (though eventually it should be possible to do so) and moreover the microstructure/morphology was not within our means to measure for the entire library. Second, the microstructure/morphology that forms is a strong function of the solvent, film-casting method, drying, and post-processing steps,[9,16] which it was not practical to optimize for every material. Third, the molecular weight and dispersity ($Đ$) for step-growth polymerizations are notoriously difficult to control, though it is possible that the stiffness of D-A polymers precludes a highly entangled microstructure, even at high molecular weights.[17] Fourth, the mechanical properties of bulk heterojunction films are significantly affected by the electron-transporting phase.[2] For polythiophenes, we found that the tensile moduli of polythiophene:[60]PCBM blends was linearly correlated to the tensile moduli of the pure polymers,[18] though this behavior cannot be assumed for all polymers, nor can it be assumed that methanofullerenes will be used in all organic solar cells in the future, and thus we measured the properties of the pure polymers only. Despite these limitations, we found that several rules of thumb did emerge for increased deformability of D-A polymers. Moreover, we expect that the mechanical characteristics of the library of polymers reported

here will stimulate computational and microstructural studies designed to connect molecular structure not only to electronic performance, but also to mechanical behavior.

9.3 Experimental Design

9.3.1 Selection of materials.

We selected the combination of eight different donor monomers and thirteen different acceptor monomers in order to test a library of D-A polymers with diversity in chemical structures (**Figure 9.1a** and **9.1b)**. The library is a subset of that used in a recent paper by Bundgaard *et al.* on the viability of these materials for R2R fabrication.[8] The chemical structures were selected on the basis of polymers from the current literature that produced highly efficient solar cells, including polymers containing the subunits benzothiadiazole (BT), quinoxaline (as seen in TQ1), benzodithiophene (BDT), diketopyrrolopyrrole (DPP), carbozole, thiophene, and bithiophene. Our initial hypothesis was that two prominent features of the chemical structures—(1) fused vs. isolated rings and (2) branched vs. linear side chains—would affect the mechanical properties of the films bearing them. The monomers containing fused rings are A6, A10, D1, D2, D3, D6, and D9. We made the distinction between structures with fused rings aligned along the backbone such as those found in diketopyrrolopyrrole (DPP) and fused rings not in the direction of the backbone such as benzothiadiazole (BT). The solubilizing side chains on the structures range from relatively short alkyl side chains of eight carbons (C_8H_{17}) to long alkyl side chains of fourteen carbons ($C_{14}H_{29}$) as well as branching side chains of 2-ethylhexyl (EH) and 2-hexyldecyl (HD). We also examined the effects of molecular weight and dispersity on the mechanical properties of the polymers.

9.3.2 Measurement of mechanical properties

We measured the mechanical properties of the D-A polymers using two specific values: tensile modulus and the crack-onset strain. Both measurements are performed using the film-on-elastomer techniques. In particular, the tensile moduli were measured using the buckling instability as developed by Stafford *et al*.[19] and expanded to conjugated polymers by Tahk *et al*.,[20] and used extensively by us and others.[2,4,11,21] Low tensile modulus is regarded as "good" from the standpoint of mechanical stability, because films that require a low energy density to elongate in the elastic regime will minimize interfacial stresses with other layers in the device stack that would otherwise lead to delamination.[2,22] For polythiophenes, low tensile modulus is also highly correlated to high crack-onset strain. Crack-onset strains of films on elastomers are often interpreted as analogous to the elongation at fracture of bulk samples or free-standing films of the polymers, though these quantities are not exactly equivalent because poor adhesion of a film to a substrate—and unequal adhesion among different polymers—localizes strain to cracks and defects and causes premature cracking.[4,23] The polymer films were transferred to elastomeric substrates and stretched, and we recorded the crack onset strain by obtaining micrographs at each level of strain. We also took note of the qualitative nature of the cracks, *i.e.* either brittle cracks (which propagated the entire length of the film perpendicular to the stretched axis) or ductile cracks (whose propagation was limited). We note that previous studies by Stafford and coworkers[19,24,25] and O'Connor et al.[4] have shown that the tensile modulus of a thin film is a relatively weak function of its thickness, when the film is above ~40 nm and below 500 nm. We judiciously prepared our thin films to be within this range. We also observed no significant deviation from the averaged value of the crack-onset strain for any

polymer sample. Furthermore, we chose this range of film thicknesses to better correlate with the result from Bundgaard et al., in which the thicknesses of all the devices were between 300 to 500 nm.[8]

9.4 Results and Discussion

9.4.1 Tensile moduli of low bandgap D-A polymers

We began by measuring the tensile modulus of each D-A polymer using the buckling-based method. **Figure 9.2a** shows a comprehensive overview of all the tensile moduli collected for the available polymers. The standard deviation of each value was calculated from the propagation of standard errors of the line fits (buckling wavelength vs. film thickness) and the standard deviation of the tensile moduli of the PDMS substrates; the values are provided in **Table 9.1**. We discarded the values of the modulus from the samples in which the standard errors of the line fits were too high ($R^2 < 0.95$) or the characteristic buckling wavelengths could not be obtained. The reasons for the failure to obtain good linear fits or a consistent buckling wavelength arose from the difficulty in handling some thin films. In some cases, the films adhered too well to the glass substrates; strong adhesion to the glass substrate led to either partial transfer onto the PDMS substrate or damage to the films. For other cases, the strain induced by handling the transferred film on PDMS or the compressive strain induced to generate buckles resulted in delamination or cracking of the films, or both. These defects in the films resulted in the misrepresentation of the buckling wavelengths because the compressive strain was accommodated by delamination and cracking, as opposed to by buckling.[26] Polymers with a high tendency to crack under the minute strains produced by transfer were treated as having effective crack-

onset strains of 0%. Measurements of the crack-onset strain, described in the next section, were performed to further test the dependency of ductility on molecular structure.

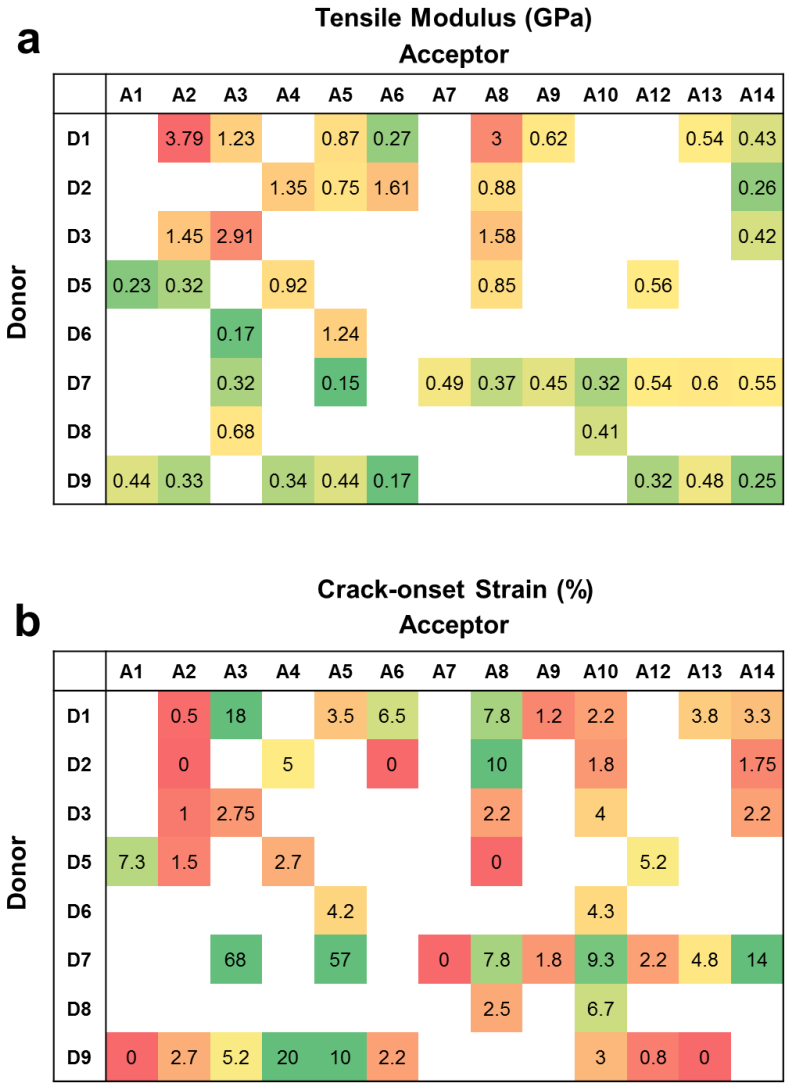

Figure 9.2. Summary of the mechanical properties measured in this paper. (a) Tensile moduli of the examined polymers in GPa. The indicated colors correspond to the ranking of the lowest value of the modulus (green) to the highest value of the modulus (red). (b) Crack-onset strain of the polymers. The colors correspond to the ranking from the highest value (green) to the lowest value (red). Standard deviations are omitted in this figure for the sake of clarity and provided in **Table 9.1**. No values were plotted for the polymers for which the measurements were not obtained.

The values of the tensile modulus occupied a range between 200 MPa to 4 GPa, which corresponded well with the range of the previously reported moduli for other D-A

conjugated polymers using the same method of measurement.[2] The highest value of tensile modulus measured was that of A2D1 at 3.79 ± 0.80 GPa. The first qualitative trend we observed was the relatively high stiffness (larger values of tensile moduli) of polymers comprising donor units with fused rings in the backbone. The polymers with donor units with fused rings (D1, D2, and D3) were found to have an average tensile modulus on the order of 1 GPa, while polymers with isolated rings such as D5, D7, and D8 had moduli on the order of 500 MPa. This qualitative trend agrees well with the previously reported increase in stiffness when the polymer backbone comprises fused rings rather than isolated rings.[27] We note here that D6 and D9 also comprise fused rings in their backbone; however, the resulting polymers from these two donor units were found to have much lower average modulus, which was similar to values obtained for polymers with isolated rings. We attributed this lower than expected moduli to the presence of long and branched solubilizing side-chains found on both D6 and D9.

The effect of the length of the solubilizing side-chains on the tensile modulus of P3AT was studied by us in a previous publication.[23] We found that with an increase in length of the alkyl side chain from 4 to 8 (P3BT to P3OT) dramatically reduced the tensile modulus by approximately an order of magnitude. This effect was attributed to the decrease in glass transition temperature with longer side chains and the reduction of the volume fraction of the load-bearing main chain.[23] The presence of the long and branching side chains have been known to affect the microstructure and therefore electronic properties of the polymers in many aspects, for example by increasing the separation between main chains.[16] This reduction in the intermolecular packing of the polymer chains could explain the large reduction in tensile moduli found in polymers comprising D6 and D9.

Table 9.1. Tensile moduli and crack-onset strain of all the polymers measured by film-on-elastomer technique in this study. The number averaged molecular weights and the values of dispersity are reproduced from ref. [8]. Polymers are separated by the designated number of the acceptor (**Figure 9.1**) for readability.

Polymer	Mn (Da)	*Đ*	Tensile Modulus (GPa)	Crack-onset Strain (%)	Crack Behavior
A1D5	9 300	2.2	0.24 ± 0.08	7.3 ± 2	Ductile
A1D9	6 900	1.4	0.44 ± 0.18	0 †	Brittle
A2D1	9 500	2.0	3.79 ± 0.80	0.5 ‡	Brittle
A2D2	12 400	11.4	NA*	0 †	Brittle
A2D3	90 000	4.5	1.45 ± 0.47	1 ‡	Brittle
A2D5	540 000	4.2	0.32 ± 0.02	1.5 ‡	Brittle
A2D9	9 400	1.8	0.33 ± 0.12	2.7 ± 1.5	Brittle
A3D1	50 000	10.8	1.23 ± 0.52	18 ± 5	Ductile
A3D3	16 000	3.5	2.91 ± 1.30	2.75 ‡	Brittle
A3D6	3 800	3.1	0.17 ± 0.02	NA*	NA
A3D7	24 000	2.7	0.32 ± 0.03	68 ± 14	Ductile
A3D8	2 200	3.1	0.68 ± 0.14	NA*	NA
A3D9	19 000	2.1	NA*	5.2 ± 2	Ductile
A4D2	22 000	9.1	1.35 ± 0.76	5.0 ± 1.3	Brittle
A4D5	29 000	9.2	0.92 ± 0.19	2.7 ± 0.6	Brittle
A4D9	7 000	1.5	0.34 ± 0.18	19.7 ± 1.5	Ductile
A5D1	18 000	3.0	0.87 ± 0.11	3.5 ± 0.5	Brittle
A5D2	100 700	3.1	0.75 ± 0.23	NA*	NA
A5D6	11 000	26.7	1.24 ± 0.29	4.2 ± 1.3	Brittle
A5D7	34 000	3.4	0.15 ± 0.04	56.8 ± 9.9	Ductile
A5D9	138 000	8.0	0.44 ± 0.15	10 ± 3.6	Ductile
A6D1	9 600	2.0	0.27 ± 0.02	6.5 ± 2.0	Brittle
A6D2	11 000	2.2	1.61 ± 0.51	0 †	Brittle
A6D9	21 600	2.7	0.17 ± 0.05	2.2 ± 0.8	Brittle
A7D7	1 200	3.3	0.49 ± 0.18	0 †	Brittle
A8D1	16 000	2.0	3.00 ± 0.56	7.8 ± 0.8	Brittle
A8D2	14 000	2.4	0.88 ± 0.40	10 ± 2	Ductile
A8D3	14 000	2.2	1.58 ± 0.64	2.2 ± 0.8	Brittle
A8D5	5 000	1.4	0.85 ± 0.21	0 †	Brittle
A8D7	6 100	2.6	0.37 ± 0.10	7.8 ± 1.6	Ductile
A8D8	3 700	2.2	NA*	2.5 ± 1.5	Brittle
A9D1	9 500	2.8	0.62 ± 0.20	1.2 ± 0.6	Brittle
A9D7	7 200	1.7	0.45 ± 0.17	1.8 ± 0.3	Brittle
A10D1	21 000	2.5	NA*	2.2 ± 0.8	Brittle
A10D2	103 000	3.3	NA*	1.8 ± 0.6	Brittle
A10D3	68 000	3.3	NA*	4 ± 1	Brittle
A10D6	6 700	3.5	NA*	4.3 ± 1.3	Brittle
A10D7	34 000	4.2	0.32 ± 0.06	9.3 ± 1.5	Ductile
A10D8	1 200	2.8	0.41 ± 0.22	6.7 ± 0.8	Ductile
A10D9	2 300	5.4	NA*	3 ± 1.7	Brittle
A12D5	13 000	3.1	0.56 ± 0.25	5.2 ± 2.4	Brittle
A12D7	5 600	2.1	0.54 ± 0.24	2.2 ± 0.8	Brittle
A12D9	37 000	2.3	0.32 ± 0.05	0.8 ± 0.6	Brittle
A13D1	12 000	7.5	0.54 ± 0.25	3.8 ± 2.4	Brittle
A13D7	10 000	2.1	0.60 ± 0.16	4.8 ± 0.3	Brittle
A13D9	12 000	76.7	0.48 ± 0.13	0 †	Brittle
A14D1	9 800	1.7	0.43 ± 0.26	3.3 ± 0.8	Brittle

Table 9.1., Cont. Tensile moduli and crack-onset strain of all the polymers measured by film-on-elastomer technique in this study. The number averaged molecular weights and the values of dispersity are reproduced from ref. [8]. Polymers are separated by the designated number of the acceptor (**Figure 9.1**) for readability.

Polymer	Mn (Da)	*Đ*	Tensile Modulus (GPa)	Crack-onset Strain (%)	Crack Behavior
A14D2	4 600	4.1	0.26 ± 0.05	1.75 ‡	Brittle
A14D3	-	-	0.42 ± 0.14	2.2 ± 1.0	Brittle
A14D7	19 000	2.6	0.55 ± 0.09	13.7 ± 1.5	Ductile
A14D9	1 600	1.9	0.25 ± 0.12	NA*	NA

*The values obtained from so-designated polymer samples were omitted or removed due to (1) insufficient material available, (2) failure to obtain smooth films, or (3) too large of propagated error. †The polymer samples cracked upon the start of the test under the strain of less than the minimum step of 0.5% strain. ‡The polymer samples exhibited inconsistent cracking behaviors and the values of the crack-onset strains reported are the lowest measured crack-onset strains.

9.4.2 Ductility of D-A polymers

We measured the ductility of the D-A polymers as manifested in the crack-onset strain.[4,11,23] **Figure 9.2b** shows the average values of the crack-onset strains. The standard deviations, reported in **Table 9.1**, were taken from the statistics from measurements of different samples ($N > 3$). Six polymers cracked upon the preparation of the film—transferring onto an elastomer substrate and mounting the film-on-elastomer onto the linear actuator—and their values are reported as 0% strains in **Figure 9.2b** and **Table 9.1**. However, it is important to note that despite the effort to minimize the applied strain during preparation of the samples, some finite tensile strains were induced during the preparation stages. We estimated this value to be lower than 0.5%.

We found that the majority of D-A polymers has relatively low crack-onset strains when compared to other conjugated polymers such as P3ATs. Most of the D-A polymer films experienced catastrophic cracking at tensile strains lower than 5% (**Figure 9.2b**). The cracking behavior of each film is also summarized in **Table 9.1**. We observed that the films with crack-onset strains below 5% cracked in a brittle mode. Specifically, the cracks that

formed in these films tended to propagate rapidly along the entire axis perpendicular to the strained axis. In contrast, a few polymers comprising the combination of monomers A3, A8, D1, D5, D7, and D9 were found to have higher crack-onset strains (highlighted in green in **Figure 9.2b**). The increased crack-onset strains for these polymer films could potentially be explained by the nature of the ductile fracture found in these films. Cracks found in these polymer films, labeled "ductile" in **Table 9.1**, appeared as pinholes and exhibited less of a tendency to propagate with increased in strain (qualitatively equivalent to greater fracture toughness). The example of the visual contrast between the two cracking behaviors is shown in **Figure 9.3**. While both brittle and ductile fractures are deleterious to the films and possibly to the performance of a fully fabricated OPV, the ductile films would have a lower tendency to propagate cracks and to cause failure: i.e., short circuits in devices with vertical charge transport (solar cells) and open circuits in devices requiring horizontal charge transport (thin-film transistors).

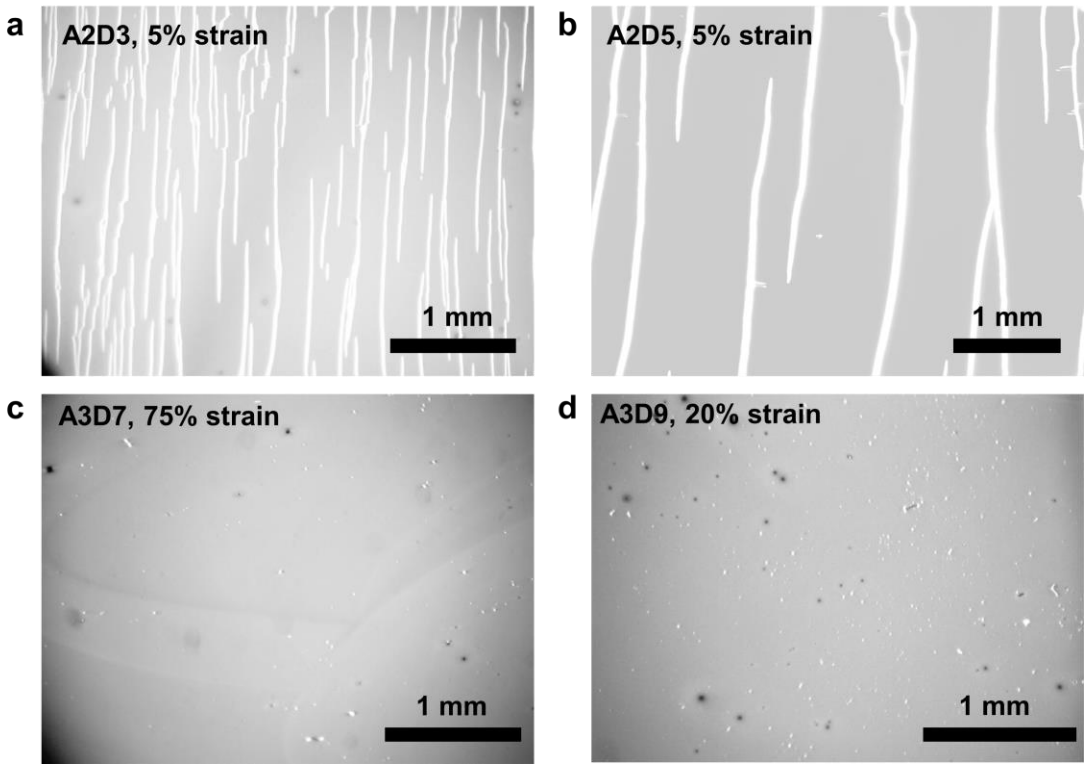

Figure 9.3. Optical micrographs of the two different natures of cracking behavior: brittle fracture (a, b) and ductile fracture (c, d).

Previous studies on conjugated polymers have found a correlation between tensile modulus and the propensity of the polymer films to crack upon the applied tensile strains; i.e., films with higher moduli tend to crack at lower applied strains. However, these studies are usually performed on P3ATs.[21,23] The same correlation was not found when comparing the D-A polymers of vastly different structures. **Figure 9.4** shows the crack-onset strain as a function of tensile modulus of 39 polymers (the subset of the library for which we were able to measure both tensile modulus and crack-onset strain). As described earlier, most of the samples with higher crack-onset strain exhibited ductile fractures (blue) and those with lower values exhibited brittle fractures (red). For many polymers, despite the low values of stiffness, the films did not appear to be ductile as previously predicted for P3ATs. From the 47 polymers in which the crack-onset strains were measured, only 16 polymers

withstood at least 5% tensile strains before fracture. The brittleness of D-A polymers has also been reported in mixtures with either [60] PCBM or non-PCBM electron acceptor. Kim *et al.* measured the mechanical properties via the pseudo free-standing tensile test for composite of PBDTTTPD (A9D2) and PCBM or P(NDI2HD-T), a non-PCBM electron acceptor, by obtaining a pull test of the film supported on the surface of water.[14] The authors reported that the mixtures with PCBM cracked well before 0.30% strain and the mixture with P(NDI2HD-T) cracked around 7% strain.[14] This apparent brittleness was further elucidated in the comparison between P3HT and PTDPPTFT4 (a DPP-based polymer with a ladder-like unit in the backbone comprising four fused thiophene rings) by Wu *et al.*;[13] P3HT films fabricated in the same manner as the D-A polymer could withstand over 100% tensile stains in contrast to <5% for the D-A polymer. Despite the lack of the inverse correlation between the stiffness and ductility of the D-A polymers, both quantities will be important for the implementation of a full working device designed for R2R fabrication.

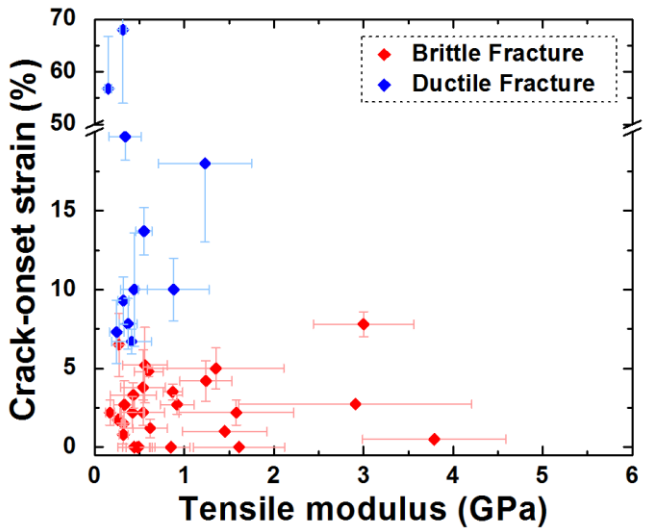

Figure 9.4. Plot of crack-onset strains vs. tensile moduli of the polymers tested in this study. Data points are distinguished in color by the nature of the fracture: red (brittle) and blue (ductile).

9.4.3 Toward rational design for mechanical deformability

We sought to identify the molecular structural determinants that influence the mechanical properties of D-A polymers in an effort to co-optimize the mechanical and electrical performance, and scalability. We found qualitative rules that collaborated with the general trends. However, exceptions to the rules were also identified. These exceptions could potentially arise from the indirect comparison between the combinations of donor and acceptor, the differences in molecular weight, dispersity, and possibly effects of certain combinations of donor and acceptor monomers that are otherwise difficult to predict. Critically, predictive trends in mechanical properties require understanding both the molecular structure and the solid-state microstructure, or the way that the former produces the latter.[2] Solid-state packing structures[4] have been shown to greatly influence the mechanical properties and certain combinations of monomers may lead to vastly different packing structures than those with similar donor or acceptor monomers.[12] For example, Mei *et al.* studied the effect of the addition of aliphatic conjugation-break spacers into the conjugated backbone of DPP-based polymers.[28] While the lamella spacing as measured from grazing incidence X-ray diffraction (GIXRD) decreased monotonically with higher concentration of the aliphatic conjugation-break spacers, the order of the crystalline domains, manifested as the lamella peak full width at half-maximum (FWHM), followed a non-linear progression.[28] This result illustrated the competition between multiple effects of the molecular structures of the polymer: while the addition of conjugation-break spacers increased the flexibility of the backbone, it also increased the tendency of interdigitation of the alkyl side chains.[28] We outlined these trends in molecular structures below along with the identified exceptions.

9.4.3.1 Presence of fused rings in the backbone

We found that the polymers with fused rings in the backbone structures (namely the polymers with D1, D2, and D3) had average tensile moduli on the order of 1 GPa. This value is of the same order as that of regioregular P3HT.[20,23] We attributed the increase in tensile moduli for these polymers to the fact that a fused ring reduces the flexibility while increasing the length of conjugation of the backbone. Polymers with donors comprising isolated rings (D5, D7, and D8) also showed the averaged tensile modulus of 0.58, 0.42, and 0.55 GPa with the highest values coming from A4D5 (0.92 ± 0.19). There are, however, exceptions to this general trend. Namely, the polymers comprising the donor unit D9 were found to have much lower tensile moduli, on the order of 500 MPa. This reduction in modulus for the D9 monomer was likely the effect of long and branching solubilizing side chains (2-hexyldecyl), which is further discussed in the next section. We found small effects on the tensile modulus from acceptors with fused-ring structures (A6 and A10). In addition, the polymer A6D1 that contained fused ring structures in both the donor and acceptor monomers has a tensile modulus of only 0.27 ± 0.02 GPa.

The effects of fused rings on ductility were found to be less obvious. The values of the crack-onset strains of polymers containing D3 were found to be low (<5% crack-onset strain) and were consistent with the trend, in which the fused ring in the backbone produced brittle polymer films. However, for polymers comprising D1 and D2, some combinations with certain acceptor monomers were found to produce ductile films. Namely A3D1 and A8D2 exhibited ductile fractures with crack-onset strain higher than 10%. Again, we believed the abnormality in the trend was the product of the side chains on the acceptors, which will also be discussed in the next section. The polymers containing the fused DPP

monomer (A10) when combined with donor monomer with fused rings (D1, D2, D3, D6, and D9) also produced brittle films (i.e., low crack-onset strain). Interestingly, the combination of A10 and the non-fused donor monomers (D7 and D8) produced ductile films with higher values of crack-onset strain than the other combinations. We attributed this effect to a possible change in solid-state morphologies and packing when the DPP (A10) acceptors were combined with dialkoxybenzene (D7) and bithiophene (D8).

9.4.3.2 Influence of long and branching solubilizing side-chains

As mentioned earlier in the previous section, the effects of long and branching solubilizing side-chains can dominate the mechanical properties of a polymer film. The tensile moduli of the films containing donor units with branching side-chains, 2-hexyldecyl, (D6, D7, and D9) were found to be lower than donor units with linear side chains. We also observed an improvement in ductility of the films with either 2-hexyldecyl or 2-ethylhexyl side-chains; namely, fourteen out of sixteen polymers in which the crack-onset strain exceeded 5% were found to be in this category. Interestingly, three of the most ductile polymers found in this study comprised the donor D7: A3D7 (crack-onset strain of 68%), A5D7 (57%), and A14D7 (14%). Significant differences between the acceptors A2 and A3, whose similar structures comprise of benzothiadiazole with two flanking thiophenes, were attributed to the locations of the alkyl side chains. For A2, the alkyl side chains ($C_{12}H_{25}$) are located on the two flanking thiophenes; whereas for A3, the alkyl side chains ($C_{14}H_{29}$) are connected to the benzothiadiazole via ether linkages. With the exception of A3D3, whose stiffness and ductility are on the same order as polymers with A2 in the backbone structure, all polymers comprising A3 are less stiff and more ductile

than the A2 counterparts. Notably, A3D1 and A3D7 were found to withstand large tensile strains (~18% and ~68% respectively).

The correlation between the structures of the side chains and the mechanical properties of the polymers could be explained in part from the solid-state molecular packing.[29] While the mechanical properties and the molecular packing or crystalline quality are not necessarily related in a straightforward manner, we can draw some qualitative insights from the effects of the side chains. For example, Yiu et al. demonstrated that branched side chains on a DPP-based polymer led to more steric hindrance between neighboring polymer chains and lower crystalline coherence length when compared to linear side chains.[30] Segalman and coworkers have shown that replacing the hexyl side chains on P3HT to 2-ethylhexyl side chains (P3EHT) reduced the melting temperature and the crystallization kinetics of the polymer.[31] Furthermore, the backbone of the adjacent P3EHT chains have been shown to be significantly tilted, resulting in the larger spacing between the chains and lower intermolecular coupling.[32] These results suggest that the reduction in packing efficiency and lower crystallinity when branched side chains are introduced; these effects could potentially lead to increased deformability.

9.4.3.3 Notes and unresolved questions

As mentioned in the previous section, the ability to predict the mechanical responses of the D-A polymers will require not only knowledge of the molecular parameters (fused-ring and side chains) but also from the propensity to form crystallites,[4] degree of crystallinity, and the rigidity (i.e., glassy behavior) of the amorphous domains.[12] We noticed this limitation of the predictive nature of focusing on one aspect of the

molecular structures as depicted in **Figure 9.5a–9.5d**. **Figures 9.5a** and **9.5b** rank the D-A polymers by the tensile moduli and the crack-onset strains while separating them into three groups: (1) fused-rings in both donor and acceptor, (2) fused-rings in the donor or in the acceptor, and (3) all isolated rings. **Figures 9.5c** and **9.5d** separate the polymers by the nature of the solubilizing side chains: (1) only linear chains, (2) branching chains in either the donor or the acceptor, and (3) all branching side chains. Our initial hypotheses would suggest that the polymers with all isolated rings and with all branching chains would be the most mechanically robust. While the general trends we described hold relatively well, we observed that the polymers in each group sample occupied a large range of both values of the mechanical properties, and substantial overlap. We note that further studies are required to fully isolate the complicated interplay between the nature of the polymer backbone and the nature of the side chains and their effects on the mechanical properties. For example, poly(3-dodecylthiophene) has linear alkyl side chains and has been reported by us to have high crack-onset strains.[23] However, for D-A polymers with relatively higher rigidity in the backbone, the linear side chains are less likely to lead to high crack-onset strains. Furthermore, some polymers comprising both isolated rings and branching side chains performed poorly mechanically. We attributed such outliers to the unknown stiffness of the chains and the solid state packing structures of the polymers.

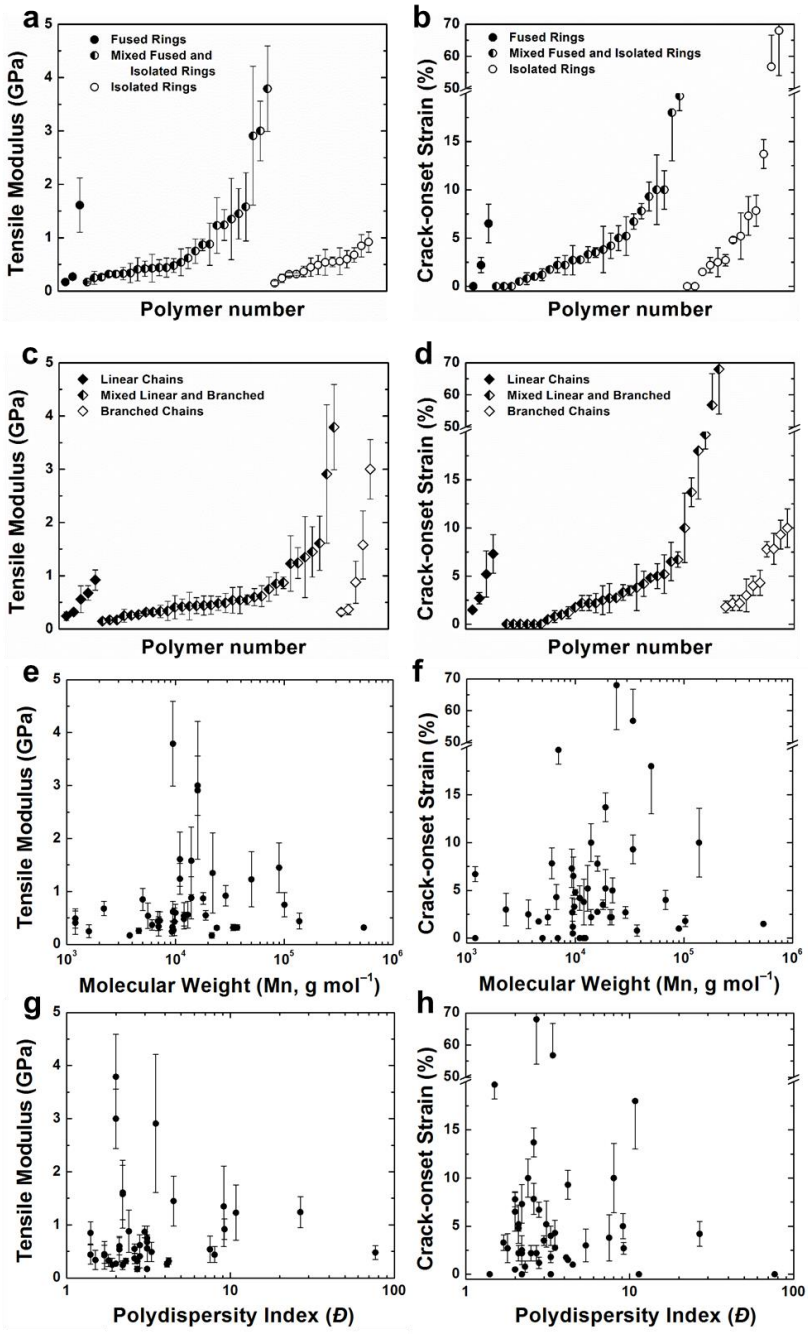

Figure 9.5. Illustration of the range of tensile modulus and crack-onset strains from all the polymer samples. (a, b) Ranking of the polymer samples separated by the presence of fused rings in both donor and acceptor (filled circles), either fused ring in donor or acceptor (half-filled circles), and all isolated rings (open circles). (c, d) Plot in which the polymer samples are separated by the nature of the solubilizing side chains: all linear chains (filled diamonds), branched chain on either the donor or acceptor monomers (half-filled diamonds), and all branched side chains (open diamonds). Plots of tensile moduli and crack-onset strains as a function of number average molecular weight (e and f) and Đ (g and h); values of Mn and Đ are reproduced from ref. [8].

In addition, the dispersity and molecular weight of the D-A polymers must also be taken into account when predicting the mechanical properties. For P3ATs, the dependencies of the solid state packing structure on molecular weight and regioregularity have been previously reported.[33–36] Furthermore, Kim *et al.* have reported significant changes in mechanical and optoelectrical properties of P3HT as a function of regioregularity.[5] These rigorously controlled experiments in which the molecular weight, dispersity, and regioregularity were isolated required carefully controlled synthesis that is only possible for very few polymers, such as P3ATs, which are produced by a quasi-living process.[5,37] For most D-A polymers that require a Stille polycondensation reaction, the control over the molecular weight and the dispersity of the product is typically not high.[37,38] Moreover, the size-exclusion chromatography (SEC) system used to measure the values of $Đ$ operates at low temperatures and employs chloroform as the solvent. In these conditions, aggregation of some polymers could lead to unrealistic $Đ$ values. **Figures 9.5e – 9.5h** plot the mechanical properties of the D-A polymers to the number average molecular weight and the $Đ$. We observed few correlations between the mechanical properties of the different D-A polymers and their molecular weight and $Đ$ (though the usual caveats apply of obtaining molecular weight for conjugated polymers by size-exclusion chromatography when no similarly rigid standards are available). It is noteworthy to point out that while comparing the effect of molecular weight and $Đ$ for a single polymer could potentially provide a meaningful trend, the molecular weight and dispersity of the polymer alone do not explain the measured differences in mechanical properties.

9.4.3.4 Introduction of an electronic-mechanical merit factor

We measured the mechanical properties of D-A polymers in hope of identifying the design rules for optimizing the mechanical robustness and electrical properties for R2R fabrication. We observed that many of the D-A polymers tested exhibited brittle properties despite the low stiffness. This result suggests that it will be a significant challenge to incorporate some D-A polymers in applications demanding significant deformation as well as in R2R fabrication. However, we identified several promising candidates with favorable electronic and mechanical properties. We have combined the power conversion efficiency as reported for the roll-fabricated solar cell reported in ref. [8] and the tensile modulus and crack-onset strain into a new merit factor (ψ) defined as

$$\Psi = PCE \times \frac{1}{E_f} \times CoS \quad (1)$$

$$\Psi_{rel} = \Psi/\Psi_{P3HT} \quad (2)$$

Where E_f is the tensile modulus and the *CoS* is the crack-onset strain. **Figure 9.6** depicts the relative merit factor (Ψ_{rel}) of the polymers tested in this experiment when compared to the properties of P3HT. The blank cells represent the missing data (where at least one quantity was missing). Using this merit factor, we identified nine promising polymers (highlighted in green); four of which comprise the donor D7. We note that the mechanical properties of the composites of the electron-donating polymer and an electron acceptor will be different than those of the pure polymers. The addition of fullerene-based electron acceptors (namely [60] PCBM) has been reported by us and others to lower the mechanical robustness of the composites when compared to the pure polymers.[20,23] However, with the recent advancement in non-fullerene electron acceptors, this deleterious effect can

potentially be avoided.[14] Furthermore, we admit to some shortcomings arising from the simplicity of the proposed figure of merit—namely, the equal contributions from power conversion efficiency, tensile modulus, and crack-onset strain. In order to characterize the electronic and mechanical properties fully, a more in-depth study of the effects of the addition of the electron acceptor, the film thickness, and the processing conditions on the electronic and mechanical properties of the whole modules will be required.

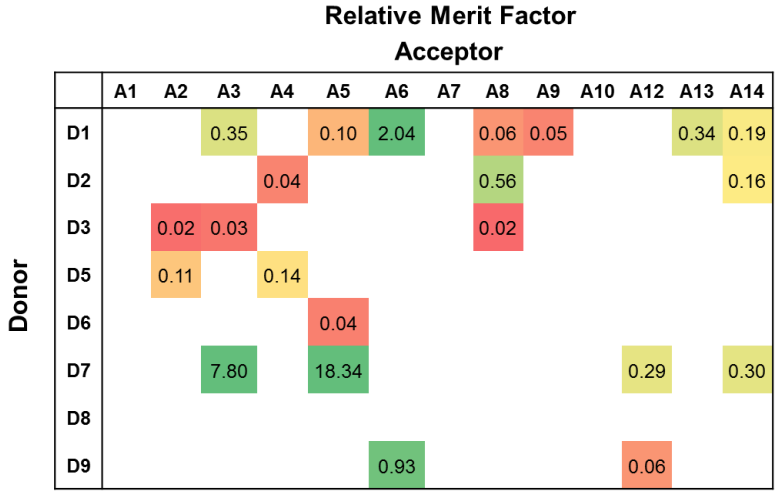

Figure 9.6. The relative merit factor incorporating the power conversion efficiency (PCE) as reported for the R2R fabricated solar cells (from ref. [8]), the tensile modulus, and crack-onset strains in relationship to those of P3HT. Blank cells indicate missing information where at least one quantity was missing. The tensile modulus of P3HT and crack-onset strain, reproduced from ref. [23], were 1.09 ± 0.15 GPa and 9 ± 1.2 % respectively.

9.5 Conclusion

This paper described the mechanical properties of a library of D-A polymers with significant diversity in molecular structure. We identified some trends from the measured values of tensile modulus and crack-onset strain as well as plausible reasons for the exceptions. We found that the stiffness of most D-A polymers was on the same order of magnitude as P3HT or lower (occupying the range between 200 MPa to 1 GPa; however, most were brittle and tended to fracture at low strains, <5%). The polymers comprising the

donors with fused rings tended to have higher stiffness and higher tendency to fracture. In addition, the polymers with branching solubilizing side chains were found to have high deformability. These trends are useful for general guidelines while designing highly mechanically robust materials for R2R fabrication. It is important to note the importance of co-optimization of electronic and mechanical properties for designing materials for both R2R fabrication and flexible or stretchable applications. From the library of D-A polymers, we identified potential candidates whose merit factors (weighted values comprising power conversion efficiency and mechanical properties) are better than those of P3HT. However, we also identified that the molecular structures of the D-A polymers do not completely govern the mechanical properties; further analysis of the solid state packing structure from computation, microstructural analysis, and a complete theory thereof are required to fully understand the interplay between mechanical and electronic behaviors of this class of materials.

9.6 Experimental methods

9.6.1 Materials

Low band gap donor-acceptor polymers used for this work were described in a previous study by Bundgaard *et al.* .[8] Briefly, thirteen acceptor and eight donor units (**Figure 9.1a** and **9.1b**) were selected and all the combinations were synthesized, yielding 104 polymers. Several combinations were omitted in the mechanical studies due to difficulties in synthesis. After chemical and optoelectronic characterization of these materials, 75 polymers were initially available for mechanical characterizations. All the polymers properties and synthesis procedures are reproduced from Ref. [8] in supplemental

info. Polydimethylsiloxane (PDMS) (Sylgard 184) was purchased from Dow Corning. Chloroform and P3HT were purchased from Sigma-Aldrich and used as received.

9.6.2 Sample preparation

The glass substrates (2.5 cm × 2.5 cm) were cleaned by bath sonication of Alconox solution, deionized water, acetone, and isopropanol for 10 min each and dried under compressed air before they were plasma-treated for 3 min (30 W, 200 mtorr ambient air). All polymer solutions were prepared by dissolution in chloroform at a 20 mg mL^{-1} concentration. The solution was then stirred on a hotplate using a magnetic stirrer at 50 ^{o}C for 2 h before cooling to room temperature and filtering through a 1 μm glass microfiber filter. For each polymer, three different thicknesses were prepared by spin coating the solution on top of the plasma treated glass substrates at 500, 1000, and 2000 rpm for 2.5 min.

9.6.3 Tensile moduli and crack-onset strains

Polydimethylsiloxane (PDMS) substrates were prepared according to the manufacturer's instruction at a ratio of 10:1 (base:crosslinker) and cured at room temperature for 36–48 h. PDMS strips (1 cm × 8 cm × 0.3 cm) were then cut out using a razor blade and stretched to strains of 4% using a computer-controlled stage (Newmark model ET-100-11) and clipped onto a glass substrate with binder clips. To transfer the polymer film onto the PDMS strip: the previously spin coated polymer film was then pressed onto the pre-stretched PDMS strip. The sample was then dipped into DI water for a time ranging from 30 s up to 20 min depending of the polymer. The sample was removed

from the water with tweezers and the glass substrate bearing the polymer was stripped of the PDMS leaving the polymer layer on top of the PDMS. The sample was dried in a desiccator under dynamic vacuum for 30 min. Finally the prestrained PDMS was released to form buckles. The buckled polymer films were observed with an optical microscope. Optical micrographs of the buckles were acquired and analyzed via an in-house MATLAB code. The tensile modulus of the PDMS was measured for each batch with a conventional pull-tester and the thickness of the each polymer film was measured using a Veeco Dektak stylus profilometer. The tensile modulus of the polymers was calculated using equation (3).

$$E_f = 3E_s \left(\frac{1-v_f^2}{1-v_s^2}\right)\left(\frac{\lambda_b}{2\pi d_f}\right)^3 \quad (3)$$

Briefly, the buckling wavelength λ_b was plotted as a function of the film thickness d_f. The slope λ_b/d_f obtained by linear fit was then substituted in Equation (3) where E_s is the PDMS substrate modulus, the Poisson ratios of the film (v_f) and the PDMS substrate (v_s) were assumed to be 0.35 and 0.5 respectively.[20] We prepared our films to be within the range of ~40 nm to 500 nm.[4,19,24,25] To minimize the change of experimental error, we also used the slope of the linear fit (λ_b/d_f) between the three data points. Ductility of the films as manifested in a form of the crack-onset strains were measured using the same film-on-elastomer method as described in previous work.[23] The polymer films transferred onto unstrained PDMS were then stretched using a computer-controlled linear actuator with a step size of 0.5% strain. Each step was imaged through an optical microscope to observe the generation of cracks. The crack-onset strain of each film was defined as the strain at which the first crack was observed.

Acknowledgements

This work was supported by the Eurotech Universities Alliance project "Interface science for photovoltaics (ISPV)" and by the Air Force Office of Scientific Research (AFOSR) Young Investigator Program, grant number FA9550-13-1-0156, awarded to D.J.L. This work was supported by the Villum Foundation's Young Investigator Programme (2nd round, project: Materials for Energy Production) awarded to E. B. Additional support was provided by the National Science foundation graduate Research Fellowship under Grant No. DGE-1144086 and the Kaplan Dissertation Year Fellowship, awarded to S.S., and by laboratory startup funds from the University of California, San Diego.

Chapter 9, in full, is a reprint of the material as it appears in *Chemistry of Materials*, 2016, 28, 2363. American Chemical Society, 2016. Bérenger Roth,† Suchol Savagatrup,† Nathaniel De Los Santos, Ole Hagemann, Jon E. Carlé, Martin Helgesen, Francesco Livi, Eva Bundgaard, Roar R. Søndergaard, Frederik C. Krebs, and Darren J. Lipomi († Equal contribution). The dissertation author was the primary investigator and author of this paper.

References

(1) Krebs, F. C.; Espinosa, N.; Hösel, M.; Søndergaard, R. R.; Jørgensen, M. 25th Anniversary Article : Rise to Power – OPV-Based Solar Parks. *Adv. Mater.* **2014**, *26*, 29–39.

(2) Savagatrup, S.; Printz, A. D.; O'Connor, T. F.; Zaretski, A. V.; Rodriquez, D.; Sawyer, E. J.; Rajan, K. M.; Acosta, R. I.; Root, S. E.; Lipomi, D. J. Mechanical Degradation and Stability of Organic Solar Cells: Molecular and Microstructural Determinants. *Energy Environ. Sci.* **2015**, *8*, 55–80.

(3) Bruner, C.; Miller, N. C.; McGehee, M. D.; Dauskardt, R. H. Molecular Intercalation and Cohesion of Organic Bulk Heterojunction Photovoltaic Devices. *Adv. Funct. Mater.* **2013**, *23*, 2863–2871.

(4) O'Connor, B.; Chan, E. P.; Chan, C.; Conrad, B. R.; Richter, L. J.; Kline, R. J.; Heeney, M.; McCulloch, I.; Soles, C. L.; DeLongchamp, D. M. Correlations between Mechanical and Electrical Properties of Polythiophenes. *ACS Nano* **2010**, *4*, 7538–7544.

(5) Kim, J.-S.; Kim, J.-H.; Lee, W.; Yu, H.; Kim, H. J.; Song, I.; Shin, M.; Oh, J. H.; Jeong, U.; Kim, T.-S.; *et al.* Tuning Mechanical and Optoelectrical Properties of Poly(3-Hexylthiophene) through Systematic Regioregularity Control. *Macromolecules* **2015**, *48*, 4339–4346.

(6) Printz, A. D.; Zaretski, A. V.; Savagatrup, S.; Chiang, A. S.-C.; Lipomi, D. J. Yield Point of Semiconducting Polymer Films on Stretchable Substrates Determined by Onset of Buckling. *ACS Appl. Mater. Interfaces* **2015**, *7*, 23257–23264.

(7) Dang, M. T.; Hirsch, L.; Wantz, G. P3HT:PCBM, Best Seller in Polymer Photovoltaic Research. *Adv. Mater.* **2011**, *23*, 3597–3602.

(8) Bundgaard, E.; Livi, F.; Hagemann, O.; Carlé, J. E.; Helgesen, M.; Heckler, I. M.; Zawacka, N. K.; Angmo, D.; Larsen-Olsen, T. T.; dos Reis Benatto, G. A.; *et al.* Matrix Organization and Merit Factor Evaluation as a Method to Address the Challenge of Finding a Polymer Material for Roll Coated Polymer Solar Cells. *Adv. Energy Mater.* **2015**, *5*, 1402186.

(9) Guo, X.; Baumgarten, M.; Müllen, K. Designing π-Conjugated Polymers for Organic Electronics. *Prog. Polym. Sci.* **2013**, *38*, 1832–1908.

(10) Liu, Y.; Zhao, J.; Li, Z.; Mu, C.; Ma, W.; Hu, H.; Jiang, K.; Lin, H.; Ade, H.; Yan, H. Aggregation and Morphology Control Enables Multiple Cases of High-Efficiency Polymer Solar Cells. *Nat. Commun.* **2014**, *5*, 5293.

(11) Lipomi, D. J.; Chong, H.; Vosgueritchian, M.; Mei, J.; Bao, Z. Toward Mechanically Robust and Intrinsically Stretchable Organic Solar Cells : Evolution of Photovoltaic Properties with Tensile Strain. *Sol. Energy Mater. Sol. Cells* **2012**, *107*, 355–365.

(12) Printz, A.; Savagatrup, S.; Burke, D.; Purdy, T.; Lipomi, D. Increased Elasticity of a Low-Bandgap Conjugated Copolymer by Random Segmentation for Mechanically Robust Solar Cells. *RSC Adv.* **2014**, *4*, 13635–13643.

(13) Wu, H.-C.; Benight, S. J.; Chortos, A.; Lee, W.-Y.; Mei, J.; To, J. W. F.; Lu, C.; He, M.; Tok, J. B.-H.; Chen, W.-C.; *et al.* A Rapid and Facile Soft Contact Lamination Method: Evaluation of Polymer Semiconductors for Stretchable Transistors. *Chem. Mater.* **2014**, *26*, 4544–4551.

(14) Kim, T.; Kim, J.-H.; Kang, T. E.; Lee, C.; Kang, H.; Shin, M.; Wang, C.; Ma, B.; Jeong, U.; Kim, T.-S.; *et al.* Flexible, Highly Efficient All-Polymer Solar Cells. *Nat. Commun.* **2015**, *6*, 8547.

(15) Jackson, N. E.; Kohlstedt, K. L.; Savoie, B. M.; Olvera de la Cruz, M.; Schatz, G. C.; Chen, L. X.; Ratner, M. A. Conformational Order in Aggregates of Conjugated Polymers. *J. Am. Chem. Soc.* **2015**, *137*, 6254–6262.

(16) Duan, C.; Huang, F.; Cao, Y. Recent Development of Push–pull Conjugated Polymers for Bulk-Heterojunction Photovoltaics: Rational Design and Fine Tailoring of Molecular Structures. *J. Mater. Chem.* **2012**, *22*, 10416–10434.

(17) Takacs, C. J.; Brady, M. A.; Treat, N. D.; Kramer, E. J.; Chabinyc, M. L. Quadrites and Crossed-Chain Crystal Structures in Polymer Semiconductors. *Nano Lett.* **2014**, *14*, 3096–3101.

(18) Printz, A. D.; Savagatrup, S.; Rodriquez, D.; Lipomi, D. J. Role of Molecular Mixing on the Stiffness of Polymer:fullerene Bulk Heterojunction Films. *Sol. Energy Mater. Sol. Cells* **2015**, *134*, 64–72.

(19) Stafford, C. M.; Harrison, C.; Beers, K. L.; Karim, A.; Amis, E. J.; VanLandingham, M. R.; Kim, H.-C.; Volksen, W.; Miller, R. D.; Simonyi, E. E. A Buckling-Based Metrology for Measuring the Elastic Moduli of Polymeric Thin Films. *Nat. Mater.* **2004**, *3*, 545–550.

(20) Tahk, D.; Lee, H. H.; Khang, D.-Y. Elastic Moduli of Organic Electronic Materials by the Buckling Method. *Macromolecules* **2009**, *42*, 7079–7083.

(21) Awartani, O.; Lemanski, B. I.; Ro, H. W.; Richter, L. J.; DeLongchamp, D. M.; O'Connor, B. T. Correlating Stiffness, Ductility, and Morphology of Polymer:Fullerene Films for Solar Cell Applications. *Adv. Energy. Mater.* **2013**, *3*, 399–406.

(22) Dupont, S. R.; Oliver, M.; Krebs, F. C.; Dauskardt, R. H. Interlayer Adhesion in Roll-to-Roll Processed Flexible Inverted Polymer Solar Cells. *Sol. Energ. Mat. Sol. Cells* **2012**, *97*, 171–175.

(23) Savagatrup, S.; Makaram, A. S.; Burke, D. J.; Lipomi, D. J. Mechanical Properties of Conjugated Polymers and Polymer-Fullerene Composites as a Function of Molecular Structure. *Adv. Funct. Mater.* **2014**, *24*, 1169–1181.

(24) Huang, H.; Chung, J. Y.; Nolte, A. J.; Stafford, C. M. Characterizing Polymer Brushes via Surface Wrinkling. *Chem. Mater.* **2007**, *19*, 6555–6560.

(25) Stafford, C. M.; Vogt, B. D.; Harrison, C.; Julthongpiput, D.; Huang, R. Elastic Moduli of Ultrathin Amorphous Polymer Films. *Macromolecules* **2006**, *39*, 5095–5099.

(26) Lee, J.-B.; Yoon, S.-S.; Khang, D.-Y. The Importance of Interfacial Adhesion in the Buckling-Based Mechanical Characterization of Materials. *RSC Adv.* **2013**, *3*, 17364–17372.

(27) Lipomi, D.; Chong, H.; Vosgueritchian, M.; Mei, J.; Bao, Z. Toward Mechanically Robust and Intrinsically Stretchable Organic Solar Cells: Evolution of Photovoltaic Properties with Tensile Strain. *Sol. Energ. Mat. Sol. Cells* **2012**, *107*, 355–365.

(28) Zhao, Y.; Zhao, X.; Zang, Y.; Di, C.; Diao, Y.; Mei, J. Conjugation-Break Spacers in Semiconducting Polymers: Impact on Polymer Processability and Charge Transport Properties. *Macromolecules* **2015**, *48*, 2048–2053.

(29) Mei, J.; Bao, Z. Side Chain Engineering in Solution-Processable Conjugated Polymers. *Chem. Mater.* **2014**, *26*, 604–615.

(30) Yiu, A. T.; Beaujuge, P. M.; Lee, O. P.; Woo, C. H.; Toney, M. F.; Fréchet, J. M. J. Side-Chain Tunability of Furan-Containing Low-Band-Gap Polymers Provides Control of Structural Order in Efficient Solar Cells. *J. Am. Chem. Soc.* **2012**, *134*, 2180–2185.

(31) Ho, V.; Boudouris, B. W.; Segalman, R. A. Tuning Polythiophene Crystallization through Systematic Side Chain Functionalization. *Macromolecules* **2010**, *43*, 7895–7899.

(32) Himmelberger, S.; Duong, D. T.; Northrup, J. E.; Rivnay, J.; Koch, F. P. V.; Beckingham, B. S.; Stingelin, N.; Segalman, R. a.; Mannsfeld, S. C. B.; Salleo, A. Role of Side-Chain Branching on Thin-Film Structure and Electronic Properties of Polythiophenes. *Adv. Funct. Mater.* **2015**, *25*, 2616–2624.

(33) Meille, S. V.; Romita, V.; Caronna, T.; Lovinger, A. J.; Catellani, M.; Belobrzeckaja, L. Influence of Molecular Weight and Regioregularity on the Polymorphic Behavior of Poly (3-Decylthiophenes). *Macromolecules* **1997**, *30*, 7898–7905.

(34) Goh, C.; Kline, R. J.; McGehee, M. D.; Kadnikova, E. N.; Fréchet, J. M. J. Molecular-Weight-Dependent Mobilities in Regioregular poly(3-Hexyl-Thiophene) Diodes. *Appl. Phys. Lett.* **2005**, *86*, 122110.

(35) Wu, Z.; Petzold, A.; Henze, T.; Thurn-Albrecht, T.; Lohwasser, R. H.; Sommer, M.; Thelakkat, M. Temperature and Molecular Weight Dependent Hierarchical Equilibrium Structures in Semiconducting Poly(3-Hexylthiophene). *Macromolecules* **2010**, *43*, 4646–4653.

(36) Kline, R. J.; McGehee, M. D.; Kadnikova, E. N.; Liu, J.; Frechet, J. M. J.; Toney, M. F. Dependence of Regioregular Poly (3-Hexylthiophene) Film Morphology and Field-Effect Mobility on Molecular Weight. *Macromolecules* **2005**, *38*, 3312–3319.

(37) Burke, D. J.; Lipomi, D. J. Green Chemistry for Organic Solar Cells. *Energy Environ. Sci.* **2013**, *6*, 2053–2066.

(38) Brouwer, F.; Alma, J.; Valkenier, H.; Voortman, T. P.; Hillebrand, J.; Chiechi, R.

C.; Hummelen, J. C. Using Bis(pinacolato)diboron to Improve the Quality of Regioregular Conjugated Co-Polymers. *J. Mater. Chem.* **2011**, *21*, 1582–1592.

Chapter 10

Mechanical and photovoltaic properties of semiconducting polymers with flexible conjugation-break spacers

Suchol Savagatrup,[†a] Xikang Zhao,[†b] Esther Chan,[a] Jianguo Mei,[b] and Darren J. Lipomi[a]

([†] Equal contribution)

[a] *Department of NanoEngineering, University of California, San Diego, 9500 Gilman Drive Mail Code 0448, La Jolla, CA 92093-0448.*

[b] *Department of Chemistry, Purdue University, 560 Oval Drive, West Lafayette, IN 47907.*

Abstract

This paper examines the effect of conjugation break spacers—aliphatic units along the backbone of a semiconducting polymer that interrupt its π-conjugation—on the mechanical and photovoltaic properties of low-bandgap polymers. These materials, based on N-alkylated diketopyrrolopyrrole flanked by bithiophene units on either side, contain repeat units bearing from 0% (DPP-0) up to 100% (DPP-100) of the flexible moiety, in this case three methylene groups. This series of polymers, which also includes DPP-30, DPP-50, and DPP-70, were originally designed to exhibit processability from the melt to form thin-film transistors, in which the log of the hole mobility was linearly related to the fraction of the monomer bearing the flexible moiety. The current paper shows that the mechanical properties—tensile modulus and crack-onset strain—are not related to the fraction of flexible units in a straightforward way. Rather, the mechanical properties are a strong function of the order present in the film. In particular, the modulus increases with decreasing full width at half maximum of the lamellar stacking peak measured from grazing-incidence X-ray diffraction. The photovoltaic power conversion efficiencies of these devices when mixed with [60]PCBM and casted between stretchable PEDOT:PSS (anode) and eutectic gallium-indium (cathode) decrease with increasing fraction of the aliphatic group. These studies highlight the difficulty in predicting the mechanical properties of a conjugated polymer solely by considering its molecular structure—even one bearing a large fraction of flexible groups along its backbone—as opposed to the way in which its molecular structure influences its packing structure in the solid state.

10.1 Introduction

A recurring challenge in materials engineering is overcoming apparent mutual incompatibilities of useful physical properties. For example, conductivity and transparency,[1] elasticity and impermeability,[2] and mechanical deformability and charge transport[3] are pairs of physical properties that derive their mutual exclusivity either from fundamental physical rules or simply from practical inconveniences. In the field of organic electronics, solubility of π-conjugated polymers necessitates alkyl side chains that in some cases reduce the charge-transport properties and in all cases limit the mechanical strength.[4,5] For flexible and stretchable applications of these materials, where supplying mechanical strength is relegated to the substrate, the semiconductors should at least have a high elasticity (low modulus), elastic limit, strain at fracture, and toughness.[6,7] The Mei group has recently introduced low-bandgap conjugated polymers bearing conjugation-break spacers (CBSs, **Figure 10.1**, aliphatic units in the main chain with three or more methylene units), which offer increased solubility and the opportunity to process the materials from the melt.[8] While the charge-carrier mobility (as measured in thin-film transistors) decreased with increasing fraction of the CBS units, the mobility was nonetheless sufficient for some applications (0.3 $cm^2 V^{-1}$ with up to 70% of the monomers bearing a CBS unit).[8] Given the interest of the Lipomi group in molecularly stretchable electronics[9]—electronic materials that accommodate mechanical deformation in their bulk structures as opposed to in wrinkled structures—we sought to test the hypothesis that the flexibility of CBS units might provide a route to materials that maximized both charge-transport and mechanical deformability for stable and stretchable electronics. In particular, this paper describes the mechanical and photovoltaic properties of these materials, and

correlates these results to recent measurements of the mobility and solid-state microstructure.

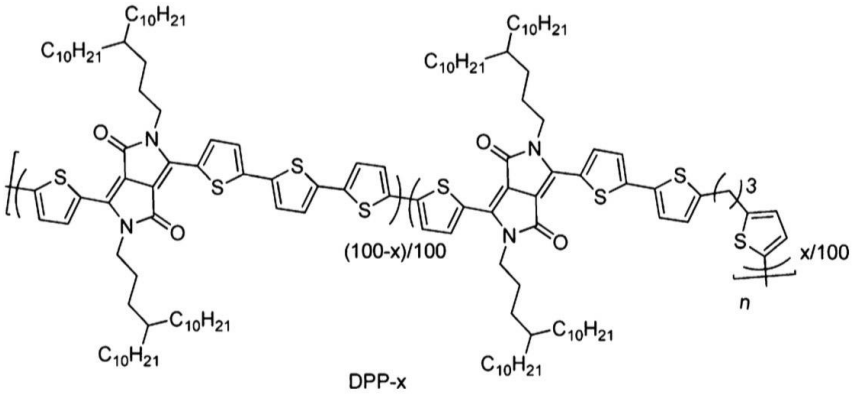

Figure 10.1. Chemical structure of the polymers bearing conjugation-break spacers (CBSs) under study. In particular, this paper examines a series of five materials, where x = 100 (fully flexible), 70, 50, 30, and 0 (fully conjugated).

The ability to accommodate mechanical deformation without fracture is a prerequisite for using organic electronic devices in flexible, stretchable, and portable applications, in the outdoor environment (where they are subjected to a range of thermomechanical stresses) and even for fabricating them by roll-to-roll processing.[10] Despite the interest in using these materials for applications demanding mechanical deformability, the mechanical properties of low-bandgap polymers are generally unreported,[7] and the molecular characteristics that determine these properties are not straightforward to predict.[7,11] For poly(3-alkylthiophene)s (P3ATs), the compliance, yield point, and crack-onset strain all increase with increasing length of the alkyl side chain and with similar molecular weight, with A = heptyl (P3HpT) seeming to embody the best of both worlds in mechanical deformability and electronic performance (in solar cells).[12–14] The microstructure also plays a role, with increasing order being correlated to increased

stiffness and brittleness.[15,16] The effect of main-chain rigidity is to increase the stiffness of the films, with fused rings in the main chain being stiffer than isolated rings, at least in preliminary observations.[11,17–19] The effect of aliphatic groups in the main chain—however deleterious this modification is expected to be on the charge-transport properties—on the mechanical properties has not been investigated.

The Mei group has introduced CBS-containing polymers based on the donor-acceptor architecture comprising diketopyrrolopyrrole flanked by two thiophene rings as the electron-deficient monomer alternating with bithiophene as the electron-rich subunit[8] (the polymer was originally called DPPT-2T by Janssen and coworkers).[20] The CBS unit was introduced by substituting the bithiophene unit with an aliphatic propyl group with a thiophene ring at either end. Introduction of either the bithiophene unit or the unit with broken conjugation into the polymerization at various ratios produced materials with differing overall flexibility in the main chain (**Figure 10.1**): from DPP-100 (completely flexible) to DPP-0 (completely rigid). The goal of this work was to improve processability in two ways: increase solubility and introduce the ability to process conjugated polymers from the melt.[8] While the increase in flexibility was correlated with a decrease in field-effect mobility (the log of the hole mobility was linearly correlated with the ratio of the monomer bearing the aliphatic spacer), materials containing up to 70 wt% of the flexible monomer retained mobilities of ≥ 0.1 cm^2 V^{-1} s^{-1}. Moreover, the flexible polymers exhibited solubility of 50 mg mL^{-1} and could be processed from the melt to form thin-film transistors. In a later paper, the authors also found that addition of as little as 1 wt% of DPP-100 to a solution of DPP-0 increased the field effect mobility by two orders of magnitude, even though the majority fraction contained broken conjugation in every repeat

unit.[21] This finding was explained by the tie chain model, which predicts that the rigid DPP-0 chains—though present in a small weight fraction—provide bridges of uninterrupted conjugation between crystallites of DPP-100, which can permit charge transport through the π-stacking axis.[21]

Given the increased flexibility in the polymer backbone of an isolated chain bearing aliphatic groups compared to that of an all-conjugated chain, it stood to reason that a film comprising the more flexible polymer would have the greatest compliance and ductility. The mechanical properties of a film, however, are not dependent only on molecular structure, but also on how the molecules pack in the solid state.[7,22,23] Interdigitation of side chains in the lamellar axis in particular is known to produce a stiff morphology in films of PBTTT.[15] In the series from DPP-x where x = 0, 30, 50, 70, 100, Zhao et al. found that the lamellar stacking distance decreased monotonically, possibly because the greater average distance between side chains more easily accommodated side chains from opposing main chains within the crystallites.[8] (Within this sequence, the band gap increased while the field-effect mobility decreased.) The full-width-at-half-maximum (FWHM) of the lamellar stacking peak—a measure of crystalline order determined by grazing-incidence X-ray diffraction (smaller FWHM correlates with greater order)—exhibited a non-linear trend in which the DPP-0 had the greatest FWHM (least order), DPP-100 had the smallest FWHM (greatest order), and the FWHM increased in the series from DPP-30, DPP-50, and DPP-70 (decreasing order). The rationale for this finding is that DPP-0 has the least order because it permits the least interdigitation, while the opposite is true for DPP-100. In the series of polymers with increasing main-chain flexibility (x = 30, 50, 70), the order is intermediate but decreases somewhat within this series (the reason for this decrease is not

yet clear). Thus the predicted mechanical behavior could be consistent with one of two competing hypotheses, or a combination thereof. (1) The flexibility of the main chain determines the compliance and ductility of the film. (2) The order in the film determines these mechanical properties, with greater order producing greater stiffness and brittleness. The prediction regarding the photovoltaic properties could be stated somewhat more confidently, namely that the efficiency would mirror the field-effect mobility, and decrease from x = 0 to x = 100 (increased main-chain flexibility, poorer photovoltaic performance).

10.2 Experimental design

We measured two mechanical properties using the film-on-elastomer methods: tensile modulus and crack-onset strain. The tensile modulus is the slope of the stress-strain curve in the elastic regime. It represents the force needed to deform a material elastically per unit area normal to the load. The total energy stored by the material per unit volume prior to plastic yield is termed the resilience. For deformable applications, it is thought that lower moduli would produce more stable devices because a highly elastically deformable film would minimize interfacial stresses between the active material and the substrate or the electrodes, which would typically be of a greater modulus. Moreover, for conjugated polymers, which generally have a molecular weight and low density of entanglements compared to polyolefins (because of their small degrees of polymerization and long persistence length), low tensile modulus is well correlated with high ductility. The tensile modulus was measured by the well-known buckling technique, where a film is deposited on an elastic substrate.[24] Upon compression, the rigid film adopts a sinusoidal wrinkling pattern that can be related to the tensile modulus of the film. The ductility is measured by

the strain at which cracks first appear when the film is stretched while supported by an elastomeric substrate. This quantity—crack-onset strain—can be used as a proxy for the strain at which a device is likely to fail (though devices requiring lateral transport can sometimes survive even in the presence of cracks).[25]

Photovoltaic properties were measured by mixing the DPP-x series of polymers with [60]PCBM in a 1:2 ratio. Given our ultimate interest in deformable electronics, we used only stretchable electrodes, or PEDOT:PSS as the anode, and eutectic gallium-indium (EGaIn) as the reflective cathode.[17] While the use of these electrode materials generally produces devices that are less efficient than those made using typical electrodes—i.e., indium-tin oxide as the anode and evaporated aluminum as the cathode—the performance of the devices is reproducible.[17] Moreover, for our purposes, uncovering trends in the figures of merit was more important than producing the greatest absolute values.

10.3 Results and discussion

The results of our mechanical measurements are summarized in **Table 10.1**. The tensile moduli of the five polymers occupied a range of nearly an order of magnitude, between 0.103 ± 0.05 GPa (DPP-70) and 0.931 ± 0.26 GPa (DPP-30). The modulus of the stiffest material (DPP-30) was typical of the ~1 GPa measured by our laboratory for P3HT and low-bandgap polymers.[11,26] We observed that the crack-onset strains for the DPP-0 and DPP-100 were similar and lower than those of the DPP-30, 50, and 70. The lower values in the apparent ductility could be a manifestation of the lack of statistical randomness in the polymers.[27] The lack of statistical randomness in the molecular structures could potentially explain the reduction in the π-π stacking distance of DPP-0 and DPP-100 when

compared to DPP-30, 50, and 70.[8] Despite our first hypothesis that the DPP-100, with fully flexible backbone, would be the most ductile, we observed brittle fracture exclusively from the DPP-100 films. Furthermore, the most striking characteristic of the data is that the stiffness of the films are not correlated with the stiffness of the polymer chains. For example, the modulus actually increases from DPP-0 to DPP-30, indicating that not only were the mechanical properties of the film determined by the molecular structure, but also strongly dependent on the solid-state packing structure. **Figure 10.2** plots the mechanical properties and the FWHM as reported by Zhao et al. The trends are partial inverses, with the stiffness and ductility highly correlated with the order (low FWHM). DPP-100 was observed to be the exception to the trend, where the low stiffness does not correlate with high ductility.

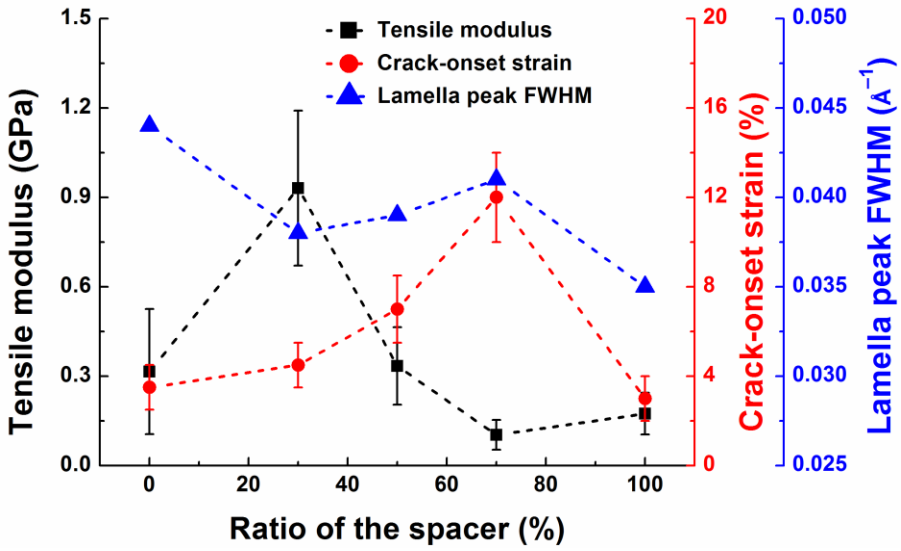

Figure 10.2. Comparison of mechanical properties and microstructural data of the DPP-x polymers.

Table 10.1. Summary of the mechanical properties and the lamella peak FWHM of the polymers studied. The values of the lamella peak FWHM were reproduced from Ref. [8].

Polymer	Tensile modulus (GPa)	Crack-onset strain (%)	Lamella peak FWHM ($Å^{-1}$)
DPP-0	0.315 ± 0.21	3.5 ± 1.0 (pinholes)	0.044
DPP-30	0.931 ± 0.26	4.5 ± 1.0 (pinholes)	0.038
DPP-50	0.334 ± 0.13	7.0 ± 1.5 (pinholes)	0.039
DPP-70	0.103 ± 0.05	12 ± 2.0 (pinholes)	0.041
DPP-100	0.174 ± 0.07	3.0 ± 1.0 (brittle)	0.035

The photovoltaic properties are illustrated in **Figure 10.3a** and the figures of merit are summarized in **Table 10.2**. The overall trend is for decreasing performance with increasing fraction of the CBS unit. Despite vastly different values between DPP-0 and DPP-30 of open-circuit voltage (V_{oc}), short-circuit current density (J_{sc}), and fill factor (*FF*), the two polymers actually have the same overall power conversion efficiency (*PCE*, **Table 10.2**) when combined with [60]PCBM.

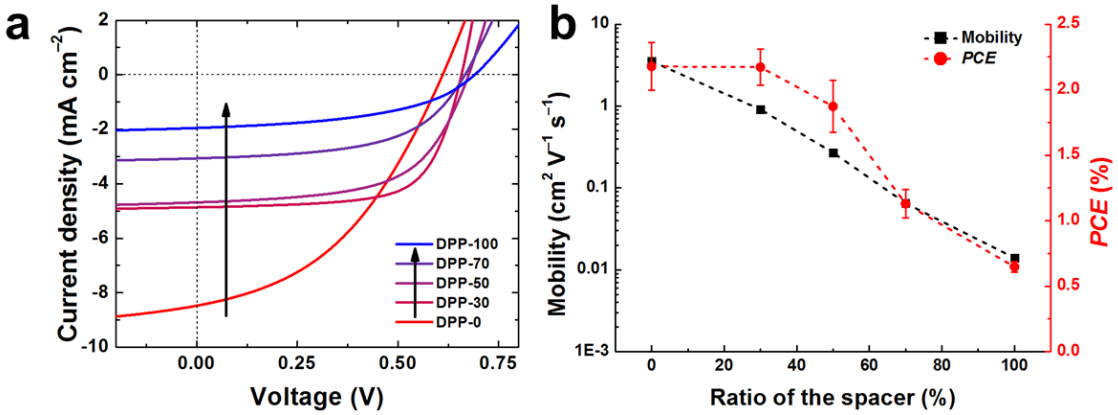

Figure 10.3. Photovoltaic properties and mobility of the DPP-x polymers. (a) Current density vs. voltage curves for DPP-x polymers when fabricated into photovoltaic cells with the architecture PEDOT:PSS/active layer/EGaIn. The active layers were spin-coated from a mixture 1:2 polymer:[60]PCBM at the concentration of 10 mg mL^{-1} in 1:4 ODCB:$CHCl_3$. (b) Comparison between mobility and power conversion efficiency of the the DPP-x polymers.

Table 10.2. Summary of photovoltaic properties of the 1:2 DPP-x:[60]PCBM fabricated in this study. $N \geq 12$. The values of the mobility of the spin-coated films were reproduced from Ref. [8].

Polymer	V_{OC} (mV)	J_{SC} (mA cm^{-2})	*FF* (%)	*PCE* (%)	Mobility (cm^2 V^{-1} s^{-1})
DPP-0	610 ± 5.1	8.46 ± 0.35	42 ± 2.7	2.18 ± 0.18	3.52
DPP-30	664 ± 4.6	4.98 ± 0.31	66 ± 1.2	2.17 ± 0.14	0.91
DPP-50	675 ± 4.4	4.68 ± 0.56	59 ± 2.2	1.87 ± 0.20	0.27
DPP-70	666 ± 4.0	3.07 ± 0.21	55 ± 1.5	1.13 ± 0.11	0.065
DPP-100	690 ± 3.7	1.95 ± 0.08	48 ± 1.1	0.65 ± 0.04	0.014

The *PCE* for these solar cells is compared to the field-effect mobilities for films cast spin-coating in **Figure 10.3b**. While the overall trend is that both mobility and *PCE* decrease with increasing ratio of the CBS, addition of 30 wt% of the monomer bearing the CBS has a large deleterious impact on the mobility of the polymer, but almost no effect on *PCE*. This observation is consistent with those observed in MEH-PPV and also poly(3-heptylthiophene), where acceptable photovoltaic performance is not predicted by poor field-effect mobility.[13]

Finally, we explored Zhao et al.'s interesting observation that the blend of 1 wt% of DPP-0 in DPP-100 had a greater mobility than pure DPP-100 by a factor of nearly 100 (nearly as high as that of pure DPP-0).[21] The rationale was that the presence of rigid, high-mobility tie chains of DPP-100 bridged the crystalline domains of DPP-100. We thus tested the hypothesis that the large weight fraction of the flexible DPP-100 in a 99:1 blend of DPP-100:DPP-0 would produce solar cells when combined with [60]PCBM with both high efficiency and mechanical compliance. Unfortunately, this experiment produced the "worst of both worlds": the *PCE* was as low as the value obtained for pure DPP-100 and the polymer blend films were significantly stiffer (0.50 GPa) than DPP-100 alone (0.17 GPa). It appears thus that the effect of the tie chains of DPP-0 is negated by the presence of the [60]PCBM in the bulk heterojunction film, and that the tie chains of rigid DPP-0 not only

bridge the crystallites of DPP-100 electronically, but mechanically as well (i.e., the tie chains have a substantial stiffening effect). This result suggests another way in which mobility in thin-film transistors is not directly predictive of efficiency in bulk heterojunction solar cells, and also the intricacies of the way in which microstructure, along with the presence of impurities even in in small weight fractions, affects mechanical properties.

10.4 Conclusion

This paper showed that the mechanical properties of conjugated polymers containing large fractions of subunits bearing flexible aliphatic groups cannot be predicted based only on the flexibility of the isolated molecules. Rather, the molecular structure must be combined with knowledge of its packing arrangement in the solid state. This work is also the first to show the effect of adding flexible groups along the conjugated backbone on the mechanical properties. Comparison with other work on the effect of the length of side chains, it is likely that side-chain engineering is more likely to be a successful strategy in producing conjugated polymers with increased flexibility, stretchability, and robustness than is main-chain engineering because of the effects of the main chain on microstructure which can be difficult to predict.

10.5 Experimental methods

10.5.1 Materials

DPP-x polymers used for this work were described in a previous study by Zhao et al.,[8] where synthesis method and characterization via NMR, TGA, DSC, AFM, GIXRD

and OFET device characterization are reported in details. Chloroform, *ortho*-dichlorobenzene (ODCB), acetone, isopropyl alcohol (IPA), Zonyl (FS-300), eutectic gallium-indium (EGaIn), and [60]PCBM were obtained from Sigma-Aldrich and used as received. DMSO was purchased from BDH with purity of 99.9%. PEDLOT:PSS (Clevios PH1000) was purchased from Heraeus. PDMS, Sylgard 184, Dow Corning, was prepared according to the manufacturer's instructions at a ratio of 10:1 (base:crosslinker) and cured at room temperature for 36 hours. For buckling-based experiments, the PDMS were cut into rectangular pieces (l = 8 cm, w = 1 cm, h = 0.3 cm); for crack-onset strain experiments, the rectangular pieces had the dimensions l = 8 cm, w = 1 cm, h = 0.15 cm.

10.5.2 Tensile moduli and crack-onset strains

For the measurements of the mechanical properties, the polymer films were prepared on glass substrates (2.5 cm × 2.5 cm) by spin-coating. The glass substrates were cleaned by bath sonication of Alconox solution, deionized water, acetone, and isopropanol for 10 min each and dried under compressed air before they were plasma treated for 3 min (30 W, 200 mTorr ambient air). All polymer solutions were prepared by dissolution in chloroform at 15 mg mL^{-1} concentration. The solution was stirred at room temperature for 24 h before filtered through a 1 μm glass microfiber filter. For the measurement of the tensile modulus, three different thicknesses of each polymer sample were prepared by varying the spin speed. The thickness range was controlled to be between 100 nm and 300 nm. For the crack-onset strain, all films are prepared to have similar thicknesses, between 150 nm to 200 nm. The polymer films transferred onto unstrained PDMS were then stretched using a computer-controlled linear actuator with a step size of 0.5% strain. Each

step was imaged through an optical microscope to observe the generation of cracks. The crack-onset strain of each film was defined as the strain at which the first crack was observed.

10.5.3 Photovoltaic properties

The photovoltaic devices were fabricated with the following architecture: PEDOT:PSS/polymer:PCBM/EGaIn. We first deposited a layer of PEDOT:PSS from an aqueous solution containing 92.9 wt% Clevios PH 1000 (~0.9–1.2 wt% PEDOT:PSS), 7 wt% DMSO, and 0.1 wt% Zonyl fluorosurfactant as the transparent anode. The solution was filtered with a 1 μm glass microfiber syringe filter and then spin-coated at a speed of 500 rpm for 4 min, followed by 2000 rpm for 30 s. The films were subsequently dried at 150 °C for 30 min, resulting in the thickness of ~150 nm. The photoactive layers were deposited from spin-coating at a speed of 500 rpm for 4 min, followed by 2000 rpm for 30 s from mixtures of 1:2 polymer:[60]PCBM (by mass) dissolved in 1:4 chloroform:ODCB at the concentration of 15 mg mL^{-1}. The samples were then immediately placed in a nitrogen-filled glovebox. The electrical contacts were made by depositing EGaIn droplets (extruded by hand from a syringe) as the top contacts. The photovoltaic properties were measured in a nitrogen-filled glovebox using a solar simulator with a 100 mW cm^{-2} flux that approximated the solar spectrum under AM 1.5G conditions (ABET Technologies 11016-U up-facing unit calibrated with a reference cell with a KG5 filter). The current density versus voltage was measured for both dark and under illumination using a Keithley 2400 SourceMeter.

Acknowledgements

This work was supported by the Air Force Office of Scientific Research (AFOSR) Young Investigator Program, grant number FA9550-13-1-0156, awarded to D.J.L. Additional support was provided by the National Science Foundation Graduate Research Fellowship under grant number DGE-1144086 and the Kaplan Dissertation Year Fellowship, awarded to S.S., and by laboratory startup funds from the University of California, San Diego.

Chapter 10, in part is currently being prepared for submission for publication of the material by Suchol Savagatrup, Xikang Zhao, Esther Chan, Jianguo Mei, and Darren J. Lipomi. The dissertation author was the primary investigator and author of this materials.

References

(1) Ellmer, K. Past Achievements and Future Challenges in the Development of Optically Transparent Electrodes. *Nat. Photonics* **2012**, *6*, 808–816.

(2) Ahmad, J.; Bazaka, K.; Anderson, L. J.; White, R. D.; Jacob, M. V. Materials and Methods for Encapsulation of OPV: A Review. *Renew. Sustain. Energy Rev.* **2013**, *27*, 104–117.

(3) Printz, A. D.; Lipomi, D. J. Competition between Deformability and Charge Transport in Semiconducting Polymers for Flexible and Stretchable Electronics. *Appl. Phys. Rev.* **2016**.

(4) Mei, J.; Bao, Z. Side Chain Engineering in Solution-Processable Conjugated Polymers. *Chem. Mater.* **2014**, *26*, 604–615.

(5) Moulton, J.; Smith, P. Electrical and Mechanical Properties of Oriented Poly (3-Alkylthiophenes): 2. Effect of Side-Chain Length. *Polymer (Guildf).* **1992**, *33*, 2340.

(6) Cheng, P.; Zhan, X. Stability of Organic Solar Cells: Challenges and Strategies. *Chem. Soc. Rev.* **2016**.

(7) Savagatrup, S.; Printz, A. D.; O'Connor, T. F.; Zaretski, A. V.; Rodriquez, D.; Sawyer, E. J.; Rajan, K. M.; Acosta, R. I.; Root, S. E.; Lipomi, D. J. Mechanical

Degradation and Stability of Organic Solar Cells: Molecular and Microstructural Determinants. *Energy Environ. Sci.* **2015**, *8*, 55–80.

(8) Zhao, Y.; Zhao, X.; Zang, Y.; Di, C.; Diao, Y.; Mei, J. Conjugation-Break Spacers in Semiconducting Polymers: Impact on Polymer Processability and Charge Transport Properties. *Macromolecules* **2015**, *48*, 2048–2053.

(9) Savagatrup, S.; Printz, A. D.; O'Connor, T. F.; Zaretski, A. V.; Lipomi, D. J. Molecularly Stretchable Electronics. *Chem. Mater.* **2014**, *26*, 3028–3041.

(10) Krebs, F. C.; Espinosa, N.; Hösel, M.; Søndergaard, R. R.; Jørgensen, M. 25th Anniversary Article : Rise to Power – OPV-Based Solar Parks. *Adv. Mater.* **2014**, *26*, 29–39.

(11) Roth, B.; Savagatrup, S.; De Los Santos, N.; Hagemann, O.; Carle, J. E.; Helgesen, M.; Livi, F.; Bundgaard, E.; Søndergaard, R. R.; Krebs, F. C.; *et al.* Mechanical Properties of a Library of Low-Bandgap Polymers. *Chem. Mater.* **2016**, acs.chemmater.6b00525.

(12) Savagatrup, S.; Printz, A. D.; Rodriquez, D.; Lipomi, D. J. Best of Both Worlds: Conjugated Polymers Exhibiting Good Photovoltaic Behavior and High Tensile Elasticity. *Macromolecules* **2014**, *47*, 1981–1992.

(13) Savagatrup, S.; Printz, A. D.; Wu, H.; Rajan, K. M.; Sawyer, E. J.; Zaretski, A. V.; Bettinger, C. J.; Lipomi, D. J. Viability of Stretchable poly(3-Heptylthiophene) (P3HpT) for Organic Solar Cells and Field-Effect Transistors. *Synth. Met.* **2015**, *203*, 208.

(14) Printz, A. D.; Zaretski, A. V.; Savagatrup, S.; Chiang, A. S.-C.; Lipomi, D. J. Yield Point of Semiconducting Polymer Films on Stretchable Substrates Determined by Onset of Buckling. *ACS Appl. Mater. Interfaces* **2015**, *7*, 23257–23264.

(15) O'Connor, B.; Chan, E. P.; Chan, C.; Conrad, B. R.; Richter, L. J.; Kline, R. J.; Heeney, M.; McCulloch, I.; Soles, C. L.; DeLongchamp, D. M. Correlations between Mechanical and Electrical Properties of Polythiophenes. *ACS Nano* **2010**, *4*, 7538–7544.

(16) Awartani, O.; Lemanski, B. I.; Ro, H. W.; Richter, L. J.; DeLongchamp, D. M.; O'Connor, B. T. Correlating Stiffness, Ductility, and Morphology of Polymer:Fullerene Films for Solar Cell Applications. *Adv. Energy. Mater.* **2013**, *3*, 399–406.

(17) Lipomi, D. J.; Chong, H.; Vosgueritchian, M.; Mei, J.; Bao, Z. Toward Mechanically Robust and Intrinsically Stretchable Organic Solar Cells : Evolution of Photovoltaic Properties with Tensile Strain. *Sol. Energy Mater. Sol. Cells* **2012**, *107*, 355–365.

(18) Wu, H.-C.; Benight, S. J.; Chortos, A.; Lee, W.-Y.; Mei, J.; To, J. W. F.; Lu, C.; He,

M.; Tok, J. B.-H.; Chen, W.-C.; *et al.* A Rapid and Facile Soft Contact Lamination Method: Evaluation of Polymer Semiconductors for Stretchable Transistors. *Chem. Mater.* **2014**, *26*, 4544–4551.

(19) Kim, T.; Kim, J.-H.; Kang, T. E.; Lee, C.; Kang, H.; Shin, M.; Wang, C.; Ma, B.; Jeong, U.; Kim, T.-S.; *et al.* Flexible, Highly Efficient All-Polymer Solar Cells. *Nat. Commun.* **2015**, *6*, 8547.

(20) Zhang, X.; Richter, L. J.; DeLongchamp, D. M.; Kline, R. J.; Hammond, M. R.; McCulloch, I.; Heeney, M.; Ashraf, R. S.; Smith, J. N.; Anthopoulos, T. D.; *et al.* Molecular Packing of High-Mobility Diketo Pyrrolo-Pyrrole Polymer Semiconductors with Branched Alkyl Side Chains. *J. Am. Chem. Soc.* **2011**, *133*, 15073–15084.

(21) Zhao, Y.; Zhao, X.; Roders, M.; Qu, G.; Diao, Y.; Ayzner, A. L.; Mei, J. Complementary Semiconducting Polymer Blends for Efficient Charge Transport. *Chem. Mater.* **2015**, *27*, 7164–7170.

(22) Guo, X.; Baumgarten, M.; Müllen, K. Designing π-Conjugated Polymers for Organic Electronics. *Prog. Polym. Sci.* **2013**, *38*, 1832–1908.

(23) Duan, C.; Huang, F.; Cao, Y. Recent Development of Push–pull Conjugated Polymers for Bulk-Heterojunction Photovoltaics: Rational Design and Fine Tailoring of Molecular Structures. *J. Mater. Chem.* **2012**, *22*, 10416–10434.

(24) Stafford, C. M.; Harrison, C.; Beers, K. L.; Karim, A.; Amis, E. J.; VanLandingham, M. R.; Kim, H.-C.; Volksen, W.; Miller, R. D.; Simonyi, E. E. A Buckling-Based Metrology for Measuring the Elastic Moduli of Polymeric Thin Films. *Nat. Mater.* **2004**, *3*, 545–550.

(25) Chortos, A.; Lim, J.; To, J. W. F.; Vosgueritchian, M.; Dusseault, T. J.; Kim, T.-H.; Hwang, S.; Bao, Z. Highly Stretchable Transistors Using a Microcracked Organic Semiconductor. *Adv. Mater.* **2014**, *26*, 4253–4259.

(26) Savagatrup, S.; Makaram, A. S.; Burke, D. J.; Lipomi, D. J. Mechanical Properties of Conjugated Polymers and Polymer-Fullerene Composites as a Function of Molecular Structure. *Adv. Funct. Mater.* **2014**, *24*, 1169–1181.

(27) Printz, A.; Savagatrup, S.; Burke, D.; Purdy, T.; Lipomi, D. Increased Elasticity of a Low-Bandgap Conjugated Copolymer by Random Segmentation for Mechanically Robust Solar Cells. *RSC Adv.* **2014**, *4*, 13635–13643.

Chapter 11

Iterative mapping of photovoltaic properties in organic solar cells comprising one- and two-dimensional gradients in processing parameters using non-damaging electrodes

Suchol Savagatrup, Adam D. Printz, Timothy F. O'Connor, Insik Kim, and Darren J. Lipomi

Department of NanoEngineering, University of California, San Diego, 9500 Gilman Drive Mail Code 0448, La Jolla, CA 92093-0448.

Abstract

This paper describes a novel technique for measuring the photovoltaic properties of organic solar cells based on iterative mapping of one- and two-dimensional gradients in processing parameters using non-damaging liquid top electrode. Photovoltaic mapping, PVMAP, provides a tool for research to understand the effects of processing parameters on the photovoltaic properties without evaporating electrodes, enabling subsequent characterizations of the same substrates and significantly reducing the consumption of scarce compounds. We present facile techniques to obtain spatially resolved measurements of photovoltaic properties for gradients in processing parameters, *e.g.*, annealing temperature and thickness of the active layer. Gradients in annealing temperature and restricted-flow spin-coating technique are employed to generate varying parameters onto a single substrate. A unique device architecture comprising a liquid metal—eutectic gallium indium—as the top electrode on a movable probe permits the repeatable and non-damaging measurement of photovoltaic properties and further investigations, *i.e.*, UV-vis absorption spectroscopy. To validate the approach, we employ PVMAP on regioregular poly(3-hexylthiophene) (P3HT) and a soluble fullerene derivative (PCBM). We extend the applications of PVMAP to demonstration its capability by investigating the new system comprising a low-bandgap polymer synthesized previously by our group. The combination of non-damaging electrode and the use of gradients provides a significant reduction in the amount of materials and time required to understand the effects of processing parameters on the performance of organic solar cells.

11.1 Introduction

In recent years, advances in the field include development of highly efficient low-bandgap π-conjugated polymers,[1–3] new conditions for processing of thin films and fabrication of devices,[4] structures of solid-state morphology,[5] long-term stability of devices, photochemical degradation[6] and mechanical stress.[7] Organic solar cells based on π-conjugated polymers and small molecules require an order of magnitude less active material than other "thin-film" photovoltaic technologies. In addition, the extreme thinness of these devices confers mechanical compliance (e.g., flexibility and even stretchability),[7–9] along with the ability to manufacture devices in a roll-to-roll manner.[10] The photovoltaic properties of organic solar cells are, however, notoriously sensitive to the morphology (*e.g.*, size and orientation of crystallites), the composition of the active materials (*e.g.*, ratio of electron donor to electron acceptor), and to external effects such as mechanical or photochemical degradation. While there has been some effort to standardize conditions of fabrication in order to compare results between laboratories,[11,12] one area that has not been changed fundamentally is the serial nature of the experimental methodology by which photovoltaic properties are measured.

Solar cells comprising novel materials require a considerable amount of effort to optimize for various processing parameters. Current experimental methods, in which several devices must be fabricated in series to test the effect of a single variable potentially introduced variability, which paints an incomplete picture of the parameters that determine the photovoltaic properties. This method also consumes copious amounts of precious, non-commercial π-conjugated polymers and other materials.[13] Therefore, only a small number

of variables for a new system of materials can be optimized. These limitations gave rise to either an uneconomical optimization or an incomplete understanding of the system.

This paper describes a novel technique for measuring the photovoltaic properties of organic solar cells based on iterative mapping of one- and two-dimensional gradients in processing parameters using non-damaging liquid top electrode. Photovoltaic mapping, PVMAP, provides a tool for research to understand the effects of processing parameters on the photovoltaic properties without evaporating electrodes, enabling subsequent characterizations of the same substrates and reducing the consumption of scarce compounds. A non-wetting, liquid metal probe (eutectic gallium-indium, EGaIn[14]) was used to scan the surface of the semiconducting film, point-by-point. Each coordinate was treated as a single device with the active area correlated to the foot-print of the EGaIn droplet. The devices were then reused to obtain morphological information via UV-vis absorption spectra. The purpose of this study was to demonstrate the capability and generality of the technique to pinpoint the optimal processing conditions. Our results demonstrated that the technique is capable of (1) providing a convenient method to understand structure-property relationship in ultrathin organic films, (2) improving the quality and reproducibility of data by ensuring that photovoltaic and morphological data are collected on a single substrate, (3) reducing the waste in scarce materials and time associated with conventional, serial approaches in optimization, and (4) allowing for the systematic optimization of photovoltaic devices by mapping multiple gradients on a single substrate.

11.2 Experimental design

11.2.1 Selection of materials

The goals of the experiments were to develop the rapid optimization technique using gradients in parameters. We selected two systems of organic solar cells to validate our findings. The blend of poly(3-hexylethiohene) and [6,6]-phenyl C_{61} butyric acid methyl ester (P3HT:PCBM) was selected because it is the standard materials in the literature with decent performance and commercial possibility.[15,16] To show the generalization of the technique, we also selected a novel system of PCBM and a low-bandgap polymer based on N-alkylated diketopyrrolopyrrole, PDPP2FT-seg-2T, that was previously synthesized by our group but the parameters of fabrication for the solar cells have never been optimized.[17] The purpose of the experiment is to demonstrate the usefulness of the technique to arrive at the two optimal parameters—film thickness and annealing temperature—with minimal materials and sample numbers.

11.2.2 Selection of gradients in parameters

The two gradients in parameters were chosen because (1) both film thickness and annealing temperature can be precisely measured at every location and (2) both parameters significantly affect the performance of the organic solar cells. Thermal annealing temperature has been shown to significantly affect the morphology of the bulk heterojunctions and the photovoltaic performance. Verploegen et al. demonstrated the effects of thermal annealing temperature on the pure P3HT films and its blend with PCBM via grazing incident X-ray scattering (GIXS), showing the re-orientation of P3HT lamella parallel to the substrate and slight crystallization of PCBM.[18] Similarly, Zheng et al.

investigated the film morphology and nanostructure of PCBM films when subjected to varying annealing temperatures.[19] These changes in the morphology of the BHJ directly translate directly into the performance of the devices.[20] Furthermore, the optimal annealing temperature differs for each system even for systems depending on the identity, the composition, and the initial morphology of the bulk heterojunction. For example, Friedel et al. discovered that the optimal annealing temperatures for different poly(3-alkylthiophenes) changes significantly depending on the length of the alkyl side chains.[21] Similarly, the thickness of the active layer have been shown to strongly impact the electrical and optical properties of the photovoltaic devices.[22–24] Predicting the optimal film thickness for a novel system is challenging due to the differences in the absorption coefficients, charge transport properties, and thin-film interference.[23] The architecture of the device, the refractive indices, and the extinction coefficients of the layers (substrate, transparent electrode, and active layer) contributed to the absorption profiles of the device that is not a trivial function of the layer thicknesses.[22,25] Understanding the effects of these two parameters for every novel system is extremely time- and material-consuming and could potentially lead to an incomplete characterization. Specifically, at least four separate device substrates must be fabricated to evaluate the photovoltaic performance for each annealing temperature or film thickness; for typical 1 in × 1 in substrates, at least 1 mL of solution will be consumed to validate the effect of a single parameter.

11.2.3 PVMAP and device fabrication

The architecture of the solar cells for this study was chosen to facilitate the removable and non-permanent top electrode. We started by depositing a layer of

PEDOT:PSS containing 7% DMSO and 0.1% Zonyl fluorosurfactant (by weight) as the transparent electrode.[26] The active layers were deposited by spin-coating from a solution of 1:1 P3HT:PCBM or 1:2 PDPP2FT-seg-2T:PCBM. The detailed experimental procedures are outlined in the experimental method section. Eutectic gallium indium (EGaIn) suspended on a movable probe was used as the top electrode to complete the circuit. A micromanipulator with degrees of freedom along thw x, y, and z axes was used to position the top electrode to obtain spatially resolved photovoltaic figures of merits—short circuit current density (J_{SC}), open circuit voltage (V_{OC}), fill factor (*FF*), and power conversion efficiency (*PCE*)—of the OSCs. Photographs, taken from below the samples, were used to determine the contact areas between the EGaIn probe and the sample surface. This contact area was then used as the active area of each devices. The solar cell architecture of PEDOT:PSS/active layer/EGaIn has been demonstrated as an alternative to the common architecture with comparable efficiency in some systems.[27] We chose EGaIn because it facilitated the rapid characterization of our device and in an inert atmosphere, e.g. Nitrogen-filled glovebox, it can be placed and displaced without fouling of the device surface, **Figure 11.1**. EGaIn is a non-volatile, non-toxic alternative to mercury that does not permanently wet hydrophobic surfaces with which it comes into contact.[28]

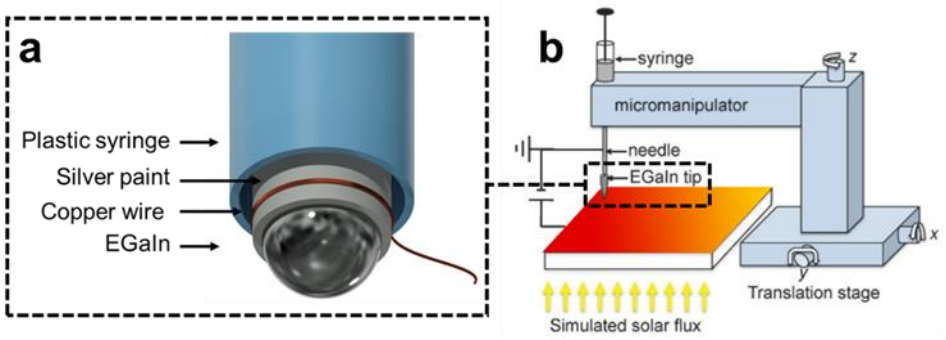

Figure 11.1. Schematic diagram of the architecture of the organic solar cells studied in this work. (a) Movable probe with liquid metal, eutectic gallium indium (EGaIn), was used as the removable and non-permanent top electrode. (b) Micromanipulator with XYZ motions was used to position the top electrode to obtain spatially resolved photovoltaic measurements of the OSCs. The architecture of the OSCs are PEDOT:PSS/active layer/EGaIn.

11.3 Results and discussion

11.3.1 Temperature gradients for thermal annealing

Figure 11.2a shows the schematic diagram of the generation of temperature gradients for thermal annealing, and the detailed experimental procedures are outlined in the experimental methods. Briefly, the photoactive layer was uniformly spin-coated onto a layer of PEDOT:PSS on a glass substrate (3 in × 1 in). The sample was then placed on an aluminum fin and placed perpendicular on the hot plate to create a thermal fin. By setting the nominal temperature of the hot plate at either 150°C or 250°C, we obtained two different temperature gradient profiles with the temperature ranges of 120°C to 175°C and 45°C to 105°C, as shown in **Figure 11.2b**. The temperature at each location on the samples was measured using a digital thermometer. The surface temperature profiles were fitted by modeling the aluminum substrate as a one-dimensional fin with the boundary conditions of a fixed temperature at the hot plate end and a convective heat flux at the tip.

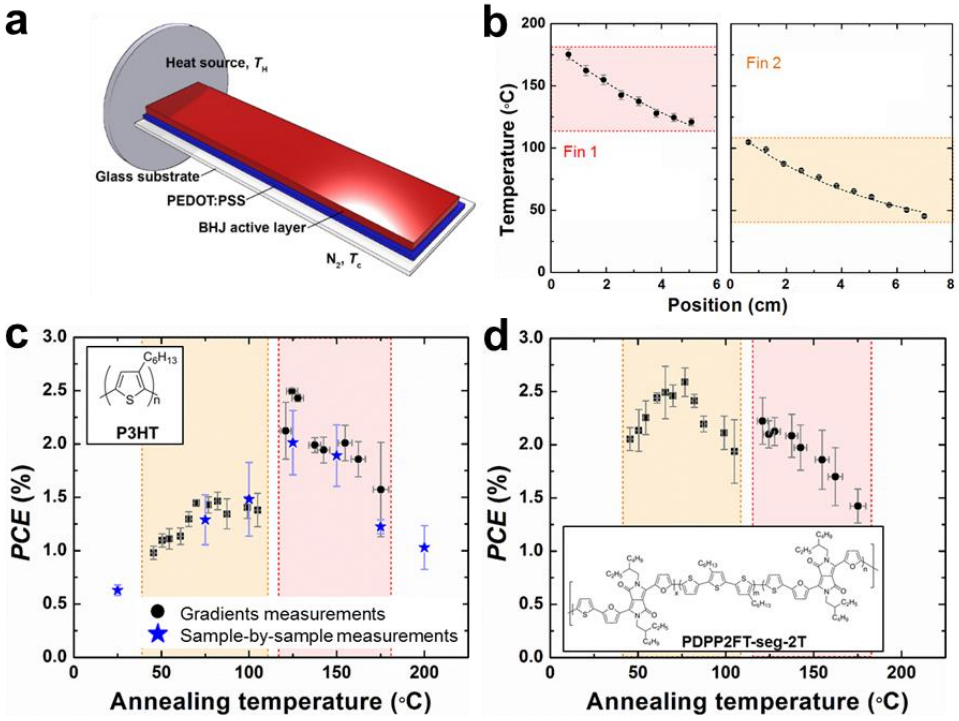

Figure 11.2. Temperature gradients for thermal annealing of organic solar cells. (a) Schematic diagram of the one-dimensional fin used for generating temperature gradients. (b) Temperature profiles of two separate fins with different hot plate temperature, T_H. (c) Power conversion efficiency of P3HT:PCBM (1:1 mass ratio) as a function of annealing temperature using the two temperature gradient profiles (black circles and squares) and the values obtained from sample-by-sample measurements (blue stars). (d) Power conversion efficiency of PDPP2FT-seg-2T:PCBM (1:2 mass ratio) as a function of annealing temperature on temperature gradient profiles.

To validate our method, we fabricated solar cell devices based on the blend of P3HT:PCBM and annealed them using the temperature gradient. Using PVMAP, we obtained the photovoltaic properties as a function of the annealing temperature. The device architecture of PEDOT:PSS/active layer/EGaIn have been shown to be a viable alternative to the typical architecture of ITO/PEDOT:PSS/active layer/Ca/Al.[27] More importantly, the use of liquid metal electrode, EGaIn, allowed us to generate spatially resolved map of the photovoltaic properties through the organic thin films without permanently depositing metal on or fouling the surface of the devices. Using this method, the contact area of the EGaIn droplet, as measured by analyzing the photograph obtained at the time of each

measurement, was used as the active area for the effective solar cell devices. The typical contact area of the EGaIn droplets were measured to be on the order of 3 mm^2. The locally measured photovoltaic properties—short circuit current density (J_{SC}), open circuit voltage (V_{OC}), fill factor (*FF*), and power conversion efficiency (*PCE*)—were averaged over four samples. As shown in **Figure 11.2c**, the *PCE* of the P3HT:PCBM devices annealed using the two temperature gradients was plotted as a function of annealing temperature. We observed the maximum *PCE* of P3HT:PCBM devices at the annealing temperature of 125°C of 2.5 ± 0.03 %, which agreed well with the commonly found optimal annealing temperature in literature for the same device architecture (PEDOT:PSS/active layer/EGaIn)[29] and typical architecture (ITO/PEDOT:PSS/active layer/Ca/Al).[30] To further validate our method, we fabricated individual solar cells of P3HT:PCBM and annealed them separately at the temperature of 75, 100, 125, 150, 175, and 200°C. The average values ($N \geq 4$) of the *PCE* of these reference devices, along with the as-cast devices, shown in **Figure 11.2c** (stars) exhibited the same trends as the sample with thermal gradients. We applied the same experimental procedure to a novel low-bandgap polymer, PDPP2FT-seg-2T, to determine the optimal annealing temperature. **Figure 11.2d** shows the *PCE* of the 1:2 PDPP2FT-seg-2T:PCBM devices as a function of annealing temperature. Similar to the P3HT:PCBM, we observed a single maximum value of *PCE* at approximately 75°C.

11.3.2 Thickness gradients of the active layer

We fabricated solar cell devices comprising thickness gradients for both the polymer blends, P3HT:PCBM and PDPP2FT-seg-2T:PCBM using the modified flow-restricted spin-coating parameter, **Figure 11.3a**. Briefly, before the photoactive layer was

deposited onto the glass substrate (3 in × 1 in) with a PEDOT:PSS layer spin-coated uniformly, a PDMS rectangle was placed across the width of the substrate to create an effective area of 2 in × 1 in. The substrate with the PDMS rectangle was then placed onto the spin-coater off-center such that the center of rotation is placed at the edge of the PDMS rectangle, inset of **Figure 11.3b**. The PDMS rectangles provide a low-energy surface that push the solution away from the center of rotation and restricted the flow of the solution in order one direction. Off-centered spin-coating has been used previously in literature to study the effect of drying rate on the morphology of BHJ;[31–33] however, the technique has never been used to generate significant film thickness gradients. The characteristic thickness gradient is shown in **Figure 11.3b**, where the film of P3HT:PCBM (40 mg mL^{-1}) was spin-coated using this modified method is compared to the film thickness if the sample were spin-coated without the PDMS rectangle. The active layer thickness varied from 40 nm to 200 nm over the span of 5 cm, for P3HT:PCBM devices using the spin-speed of 1000 rpm. We investigated the effect of varying the spin speed using the spin rate of 500, 1000, and 1500 rpm; as shown in **Figure 11.3c**, the thickness profile of the P3HT:PCBM on a single device depended heavily on the spin-speed.[34] As expected from standard spin-coating, the faster spin rate resulted in a thinner gradient profiles. In addition, the effect of the low-energy surface of PDMS was more pronounced when coupled with higher spin-speed. We observed a sudden increase in film thickness near the location of the PDMS rectangle. These initial slopes are less pronounced at slower spin rate. Similarly, the properties of the solution also had significant effects on the generated thickness profile. **Figure 11.3d** demonstrates the differences in the thickness profile of P3HT:PCBM and PDPP2FT-seg-2T:PCBM films. The higher concentration and the slower rate of

evaporation of the P3HT:PCBM solution (1:1, 40 mg mL^{-1}, ODCB) when compared to the solution of PDPP2FT-seg-2T:PCBM (1:2, 10 mg mL^{-1}, 1:4 ODCB:$CHCl_3$) led to the gradients with thicker films at the each position.

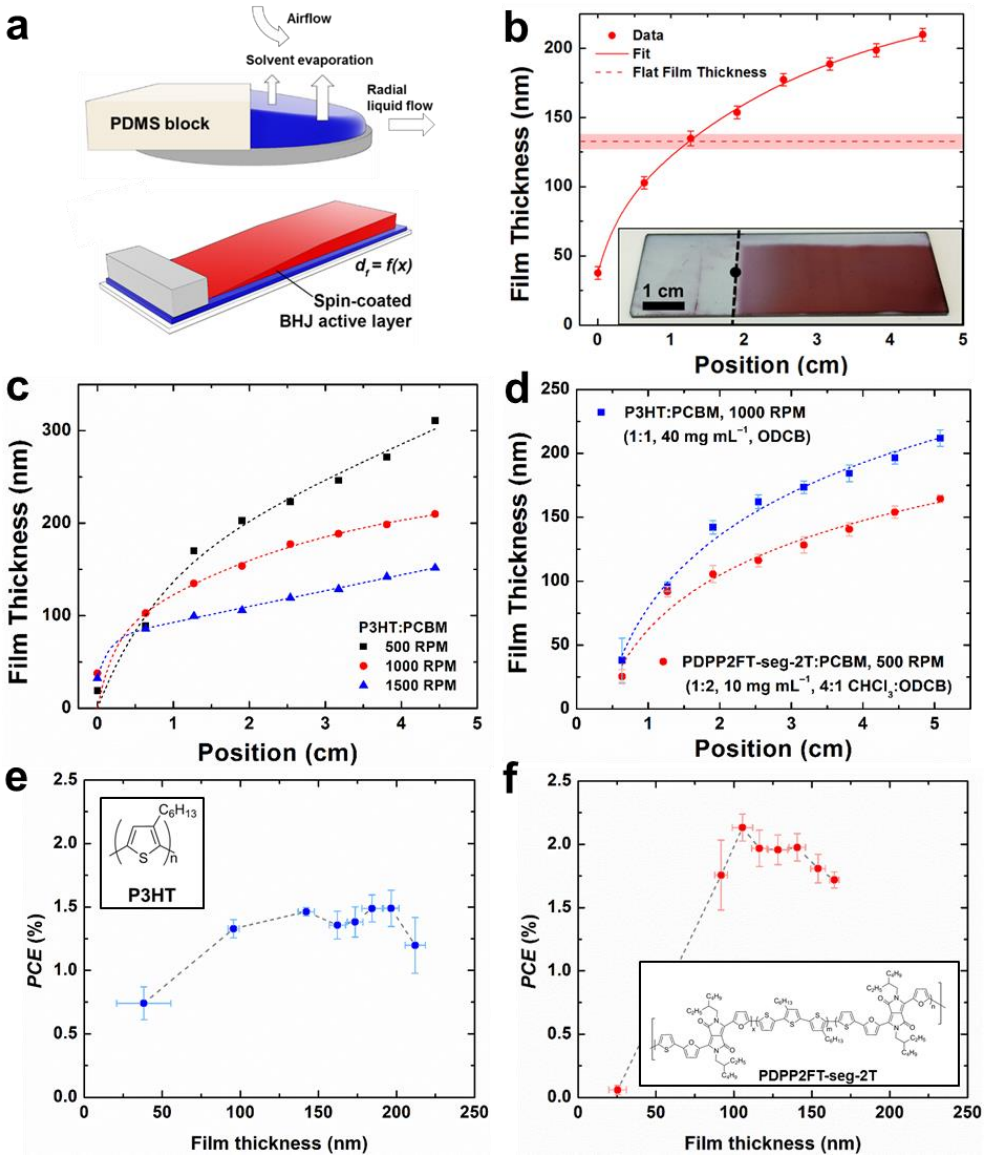

Figure 11.3. Thickness gradients of the active layer for organic solar cell. (a) Schematic diagram depicting the modified process of restricted-flow spin-coating to generate the thickness gradient profile. (b) Comparison between the film thickness profiles generated from typical spin-coating and restricted-flow spin coating at 1000 RPM of the solution of P3HT:PCBM (40 mg mL^{-1}, ODCB). The inset shows the photograph of the same sample. The thickness gradient profiles are heavily dependent on the spin-speed (c) and the properties of the solution (d). Power conversion efficiency as a function of active layer thickness for P3HT:PCBM (e) and PDPP2FT-seg-2T (f).

Using the generated thickness gradients for both polymer solutions, we measured the spatially resolved photovoltaic properties as a function of the film thickness. As shown in **Figure 11.3e**, we observed a clear optimal thickness at 200 nm and a secondary optimal point near 100 nm for P3HT:PCBM, which agreed well with previously reported values.[23,35] Similarly, the trend of the thickness dependent *PCE* correlated well with the previous studies.[22,23] For the PDPP2FT-seg-2T:PCBM devices, we observed an optimal thickness at approximately 100 nm, which is similar to the reported optimized thickness for system comprising PDPP2FT.[36]

11.3.3 Two-dimensional gradients and UV-vis measurements

In order to extend our application of PVMAP, we fabricated samples of P3HT:PCBM comprising both thickness and annealing temperature onto the same substrates. **Figure 11.4a** shows the sample with thickness gradient along the horizontal axis and the annealing temperature gradient along the vertical axis. The fabrication process of thickness gradient was kept the same except the size of the glass substrates, which were 3 in × 2 in. The PDMS rectangles were placed to create an effective area of 2 in × 2 in. The rows—A, B, C, and D—represent the different annealing temperature (**Figure 11.4b** top); and the columns—1, 2, 3, and 4—represent the different film thickness (**Figure 11.4b** bottom).

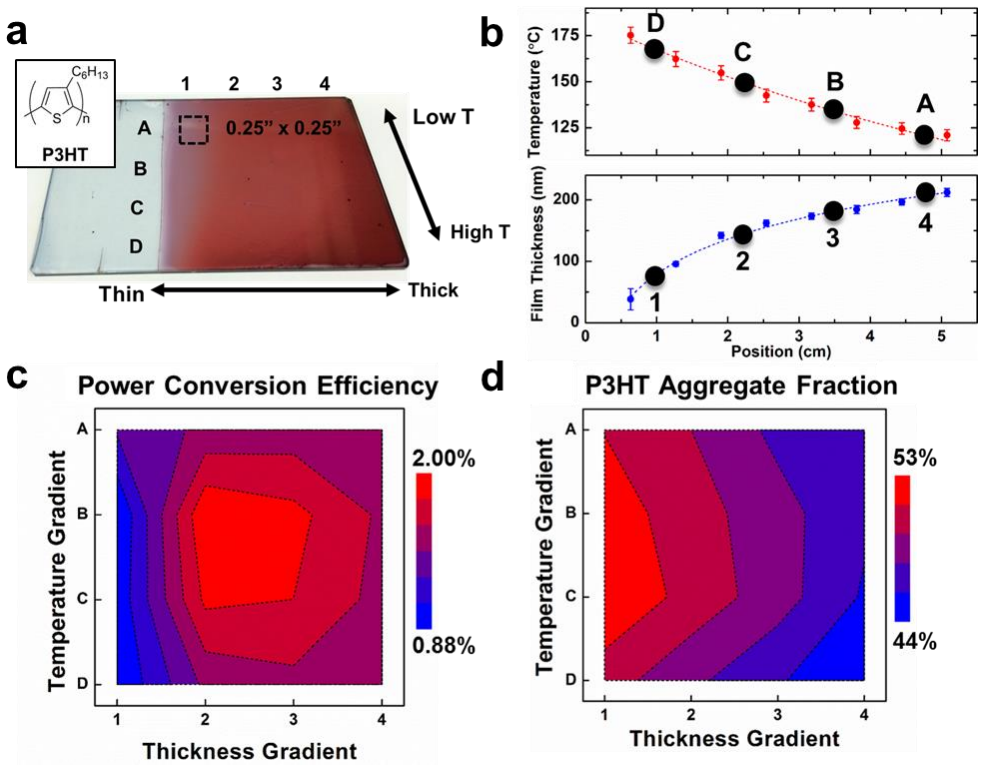

Figure 11.4. Two-dimensional gradient comprising both thermal annealing and thickness gradients on a single substrate. (a) Photograph of a two-dimensional gradients of P3HT:PCBM solar cell device. The positions A, B, C, and D represent the different annealing temperature (b, top) and the positions 1, 2, 3, and 4 represent the different film thickness (b, bottom). Photovoltaic measurements were taken at 16 positions, corresponding to the different thicknesses and annealing temperatures. (c) Contour plot of the power conversion efficiency for the 16 positions. (d) Contour plot for the fraction of P3HT aggregate measured from applying the weakly H-aggregate model to the UV-vis absorption spectra obtained from the 16 locations after the photovoltaic properties were taken.

We obtained the photovoltaic measurement at 16 positions, the cross combination of the four rows and four columns. The *PCE* at each positions are plotted on a contour plot in **Figure 11.4c**. Each value shown was an average of four samples. The optimal combination of annealing temperature and film thickness were found to be at the position B2 and B3, corresponding to the interpolated annealing temperature of 130 °C and the film thickness of between 150 and 180 nm. The results agreed qualitatively with the thermal annealing and thickness gradients measured in the previous sections. The slight inconsistencies may have arisen from the small sample collection size; only 16 locations

were samples, 4 for each gradient. After the photovoltaic measurements, the same samples were then used to obtain the UV-vis absorption spectra at the 16 locations to collaborate the microstructural data with the photovoltaic performance. Order in P3HT can be determined using a widely practiced method based on the work of Spano and coworkers, who showed that the UV-vis spectra can be deconvoluted into contributions from the aggregated and amorphous phases using the weakly interacting H-aggregate model.[37] The contribution of the PCBM were subtracted out from the UV-vis spectra obtained from the P3HT:PCBM films before the analysis. The ratio of these contributions, after taking into account the unequal absorption coefficients of the aggregate and the amorphous domains, can be used to determine the percent aggregated polymer. Using this method, we obtained the aggregate fractions of the P3HT as a function of both thermal annealing temperature and the film thickness, **Figure 11.4d**. Analysis of the spectra revealed that the range of polymer aggregate fraction ranged from 44% to 53%. The higher aggregate fractions were found at the locations B1 and C1, approximately corresponding to the annealing temperature of 130°C and 155°C and film thicknesses of 95 nm. Previously for samples of the same thicknesses, higher polymer aggregate fractions have been shown to produce more efficient solar cells.[38] However, we observed the optimal *PCE* at the position with a lower percent aggregate. We attributed this finding to the higher total light absorption at the locations with higher film thicknesses. The possibility of co-dependent parameters could be a limitation to this technique; however, with finer resolution of sampling size, this limitation could be mitigated.

11.4 Conclusion

This paper described a new technique for measuring the photovoltaic properties of organic solar cells and rapidly optimize the processing parameter, PVMAP, which provided insights on the effects of annealing temperature and film thickness for novel systems. We applied both gradients in annealing temperature and film thickness on a well-known system of P3HT:PCBM as well as a novel system of PDPP2FT-seg-2T:PCBM; in addition, samples comprising both gradients on the same substrates were fabricated using P3HT:PCBM as the photoactive layer. Experimental results for P3HT:PCBM agreed well with previously reported optimal annealing temperature and film thickness measured via sample-by-sample measurements. We obtained the optimal processing condition for the new polymer synthesized in house, PDPP2FT-seg-2T. Results from two-dimensional gradient experiments suggested the generality and practicality of the method to rapidly and economically screen the two processing parameters. Our findings may be useful for fast screening of new materials without the concern of wasting materials and overlooking potentially viable polymers.

11.5 Experimental methods

11.5.1 Materials

Regioregular poly(3-hexylthiophene) (P3HT) and [6,6]-phenyl C_{61} butyric acid methyl ester (PCBM) were obtained from Sigma-Aldrich and used as received. PEDOT:PSS (Clevios PH1000) was purchased from Heraeus. DMSO was purchased from BDH with purity of 99.9%, and Zonyl (FS-300) fluorosurfactant was purchased from Sigma-Aldrich. All reagents were obtained from commercial suppliers and used without

purification. Chloroform ($CHCl_3$), ortho-dichlorobenzene (ODCB), acetone, isopropyl alcohol (IPA) were obtained from Sigma-Aldrich. Eutectic gallium indium was obtained from Alfa Aesar. Conductive silver paint was obtained from Ted Pella Inc. PDMS, Sylgard 184 (Dow Corning), was prepared according to the manufacturer's instructions at a ratio of 10:1 (base:cross-linker) and cured at room temperature for 36 h before it was used. PDPP2FT-seg-2T was synthesized and fully characterized by our group previously.[17]

11.5.2 Preparation of solutions and glass substrates

The solution of P3HT:PCBM was prepared by dissolving a 1:1 mixture by weight of P3HT and PCBM in ODCB at the concentration of 40 mg mL^{-1}. The solution of PDPP2FT-seg-2T:PCBM was prepared at a 1:2 ratio of polymer:PCBM at 10 mg mL^{-1} in 1:4 ODCB:chloroform. The solutions were stirred using a magnetic stirrer for 36 h and filtered through a 1 μm glass microfiber filter. The glass substrates were cleaned by bath sonication of Alconox solution, deionized water, acetone, and isopropanol for 10 min each and dried under compressed air before they were plasma treated for 3 min (30 W, 200 mTorr ambient air).

11.5.3 Thermal annealing gradients

In the thermal gradient studies, the devices are fabricated as followed. A layer of PEDOT:PSS was spin-coated onto clean glass substrates (7.62 cm × 2.54 cm, 3 in × 1 in) at 500 rpm for 240 s, followed by 2000 rpm for 30 s. The films were then dried at 150 °C for 30 min. The photoactive layers were subsequently spin-coated on the PEDOT:PSS layer. For P3HT:PCBM, the spin parameters were 500 rpm for 240 s, followed by 2000

rpm for 30 s. Films of PDPP2FT-seg-2T:PCBM were spin-coated at 1000 rpm for 240 s and 2000 rpm for 30 s. To create the gradient in annealing temperature, the samples were placed on a aluminum fin (*length = 15.24* cm, *width* = 3.175 cm, *depth* = 0.1588 cm) and then placed perpendicular on a hotplate to create a heating fin with an effective length of 15.24 cm. The nominal surface temperature was set at either 150 °C or 250 °C; the ambient temperature in the N_2 filled glovebox was assumed to be constant at 23.2 °C. The samples were annealed for 30 min on the aluminum fin and cooled to room temperature for 20 min. Surface temperatures of the samples were measured at specific points using a digital thermometer. The surface temperature profiles were fitted by modeling the aluminum substrate as a one-dimensional fin with the boundary conditions of a fixed temperature at the hot plate end and a convective heat flux at the tip. The heat conductivity of aluminum was set at a constant value of 250 W m^{-1} K^{-1}. The heat transfer coefficient *h* was fitted using a least-squares method.

11.5.4 Film thickness gradients

For samples with film thickness gradients, the PEDOT:PSS layers were prepared using the same conditions as the samples with thermal annealing gradient on clean glass substrates with dimensions of 7.62 cm × 2.54 cm (3 in × 1 in). Before spin-coating of the photoactive layer, a PDMS rectangle (*l* = 3 cm, *w* = 1 cm, *d* = 3 mm) was placed on top of the PEDOT:PSS film perpendicular to the length of the glass substrate to create an effective area of 2 in × 1 in, the inset of **Figure 11.3b**. The substrate with the PDMS rectangle was then placed on the spin-coater with the center of rotation on the edge of the PDMS rectangle as shown in the inset of **Figure 11.3b**. For P3HT:PCBM, the parameters were 1000 rpm

for 4 min and 2000 rpm for 30 s, and for PDPP2FT-seg-2T, 500 rpm for 4 min and 2000 rpm for 30 s. The film thickness at each position was measured using a stylus profilometry. P3HT:PCBM substrates were annealed uniformly at 125°C; PDPP2FT-seg-2T:PCBM substrates were not annealed.

11.5.5 Generation of samples comprising two-dimensional gradients

Samples comprising 2D gradients were fabricated on glass substrates with the dimensions of 7.62 cm × 5.08 cm (3 in × 2 in). The PEDOT:PSS layer was spin-coated over the whole glass substrate using the same parameters as above. Before depositing the photoactive layer, a PDMS rectangle (l = 6 cm, w = 1 cm, d = 3 mm) was placed to create an effective area of 2 in × 2 in, **Figure 11.4a**. The active layers were then spin-coated at 1000 rpm for 240 s and 2000 rpm for 30 s to generate the thickness gradient. The samples were then placed on an aluminum fin (*length = 15.24* cm, *width* = 6.350 cm, *depth* = 0.1588 cm) and placed perpendicular on top of the hot plate. The samples were placed on the aluminum fin such that the thickness gradient is perpendicular to the thermal annealing gradient, **Figure 11.4a**. The nominal temperature of the hot plate was set at 250°C; the samples were annealed for 30 min and cooled to room temperature for 20 min.

11.5.6 Measurement of photovoltaic properties using PVMAP

The photovoltaic properties were measured in a nitrogen-filled glovebox using a solar simulator with 100 mW cm^{-2} flux under AM 1.5G condition (ABET Technologies 11016-U up-facing calibrated using a reference cell with a KG5 filter. The current density versus voltage was measured using a Keithley 2400 SourceMeter. The movable probes

were fabricated by mounting 3 mL Luer-Lock syringes onto the XYZ micropositioner. The tips of the syringes were made conductive by multiple coatings of conductive silver paint. Copper wires were used to complete the circuit. EGaIn was then extruded slowly from the syringe to create a stable suspension. The syringe with the EGaIn tip was then lowered onto the surface of the sample, via a micropositioner with degrees of freedom in x, y, and z axes, to create an electrical contact. Photographs taken from below, above the light source, of the contact between EGaIn and the samples were used to determine the active area of the solar cells. After each measurement, the syringe was raised slowly and moved to a new location of measurement.

11.5.7 UV-vis absorption spectroscopy and weakly interacting H-aggregate model

The absorbance of the materials was measured using an Agilent 8453 UV-vis spectrophotometer. The wavelength range measured was 300–850 nm with a step size of 1 nm. A film of PEDOT:PSS on glass substrate was used as a baseline for the absorption to account for the contribution to the absorption spectra. The weakly interacting H-aggregate model was then used to perform a least squares fit to the absorption spectra between 550 and 620 nm (2.25 and 2.00 eV) using a Matlab program. The initial spectra of P3HT:PCBM were initially normalized by setting the lowest point between 670 and 750 nm to zero and then normalizing to the peak between 480 and 560 nm. The contributions from PCBM were subtracted out using the absorption spectra of the pure PCBM annealed at corresponding temperature. The window for each of the measurement were 0.635 cm × 0.635 cm.

Acknowledgements

This work was supported by the National Science Foundation, grant number EEC-1341973. Additional support was provided by the National Science Foundation Graduate Research Fellowship under grant number DGE-1144086 and the Kaplan Dissertation Year Fellowship, awarded to S.S., and by laboratory startup funds from the University of California, San Diego.

Chapter 11, in part is currently being prepared for submission for publication of the material by Suchol Savagatrup, Adam D. Printz, Timothy F. O'Connor, Insik Kim, and Darren J. Lipomi. The dissertation author was the primary investigator and author of this materials.

References

(1) Facchetti, A. π-Conjugated Polymers for Organic Electronics and Photovoltaic Cell Applications †. *Chem. Mater.* **2011**, *23*, 733–758.

(2) He, Z.; Xiao, B.; Liu, F.; Wu, H.; Yang, Y.; Xiao, S.; Wang, C.; Russell, T. P.; Cao, Y. Single-Junction Polymer Solar Cells with High Efficiency and Photovoltage. *Nat. Photonics* **2015**, 1–6.

(3) Yang, Y. (Michael); Chen, W.; Dou, L.; Chang, W.-H.; Duan, H.-S.; Bob, B.; Li, G.; Yang, Y. High-Performance Multiple-Donor Bulk Heterojunction Solar Cells. *Nat. Photonics* **2015**, 1–9.

(4) Peet, J.; Heeger, A. J.; Bazan, G. C. "Plastic" solar Cells: Self-Assembly of Bulk Heterojunction Nanomaterials by Spontaneous Phase Separation. *Acc. Chem. Res.* **2009**, *42*, 1700–1708.

(5) Salleo, A.; Kline, R. J.; DeLongchamp, D. M.; Chabinyc, M. L. Microstructural Characterization and Charge Transport in Thin Films of Conjugated Polymers. *Adv. Mater.* **2010**, *22*, 3812–3838.

(6) Peters, C. H.; Sachs-Quintana, I. T.; Kastrop, J. P.; Beaupré, S.; Leclerc, M.; McGehee, M. D. High Efficiency Polymer Solar Cells with Long Operating Lifetimes. *Adv. Energy Mater.* **2011**, *1*, 491–494.

(7) Savagatrup, S.; Printz, A. D.; O'Connor, T. F.; Zaretski, A. V.; Rodriquez, D.; Sawyer, E. J.; Rajan, K. M.; Acosta, R. I.; Root, S. E.; Lipomi, D. J. Mechanical Degradation and Stability of Organic Solar Cells: Molecular and Microstructural Determinants. *Energy Environ. Sci.* **2015**, *8*, 55–80.

(8) Lipomi, D. J.; Chong, H.; Vosgueritchian, M.; Mei, J.; Bao, Z. Toward Mechanically Robust and Intrinsically Stretchable Organic Solar Cells : Evolution of Photovoltaic Properties with Tensile Strain. *Sol. Energy Mater. Sol. Cells* **2012**, *107*, 355–365.

(9) Savagatrup, S.; Printz, A. D.; O'Connor, T. F.; Zaretski, A. V.; Lipomi, D. J. Molecularly Stretchable Electronics. *Chem. Mater.* **2014**, *26*, 3028–3041.

(10) Manceau, M.; Angmo, D.; Jørgensen, M.; Krebs, F. C. ITO-Free Flexible Polymer Solar Cells: From Small Model Devices to Roll-to-Roll Processed Large Modules. *Org. Electron. physics, Mater. Appl.* **2011**, *12*, 566.

(11) Zimmermann, E.; Ehrenreich, P.; Pfadler, T.; Dorman, J. A.; Weickert, J.; Schmidt-Mende, L. Erroneous Efficiency Reports Harm Organic Solar Cell Research. *Nat. Photonics* **2014**, *8*, 669.

(12) Reese, M. O.; Gevorgyan, S. a.; Jørgensen, M.; Bundgaard, E.; Kurtz, S. R.; Ginley, D. S.; Olson, D. C.; Lloyd, M. T.; Morvillo, P.; Katz, E. a.; *et al.* Consensus Stability Testing Protocols for Organic Photovoltaic Materials and Devices. *Sol. Energy Mater. Sol. Cells* **2011**, *95*, 1253.

(13) Bettinger, C. J.; Becerril, H. a; Kim, D. H.; Lee, B.-L.; Lee, S.; Bao, Z. Microfluidic Arrays for Rapid Characterization of Organic Thin-Film Transistor Performance. *Adv. Mater.* **2011**, *23*, 1257.

(14) Chiechi, R. C.; Weiss, E. A.; Dickey, M. D.; Whitesides, G. M. Eutectic Gallium-Indium (EGaIn): A Moldable Liquid Metal for Electrical Characterization of Self-Assembled Monolayers. *Angew. Chem. Int. Ed.* **2008**, *47*, 142–144.

(15) Po, R.; Bianchi, G.; Carbonera, C.; Pellegrino, A. "All That Glisters Is Not Gold": An Analysis of the Synthetic Complexity of Efficient Polymer Donors for Polymer Solar Cells. *Macromolecules* **2015**, 150112143351004.

(16) Krebs, F. C.; Espinosa, N.; Hösel, M.; Søndergaard, R. R.; Jørgensen, M. 25th Anniversary Article : Rise to Power – OPV-Based Solar Parks. *Adv. Mater.* **2014**, *26*, 29–39.

(17) Printz, A.; Savagatrup, S.; Burke, D.; Purdy, T.; Lipomi, D. Increased Elasticity of a Low-Bandgap Conjugated Copolymer by Random Segmentation for Mechanically Robust Solar Cells. *RSC Adv.* **2014**, *4*, 13635–13643.

(18) Verploegen, E.; Mondal, R.; Bettinger, C. J.; Sok, S.; Toney, M. F.; Bao, Z. Effects of Thermal Annealing Upon the Morphology of Polymer-Fullerene Blends. *Adv.*

Funct. Mater **2010**, *20*, 3519.

(19) Zheng, L.; Liu, J.; Ding, Y.; Han, Y. Morphology Evolution and Structural Transformation of Solution-Processed Methanofullerene Thin Film under Thermal Annealing. *J. Phys. Chem. B* **2011**, *115*, 8071.

(20) Khlyabich, P. P.; Burkhart, B.; Rudenko, A. E.; Thompson, B. C. Optimization and Simplification of Polymer–fullerene Solar Cells through Polymer and Active Layer Design. *Polymer (Guildf).* **2013**, *54*, 5267–5298.

(21) Friedel, B.; McNeill, C.; Greenham, N. Influence of Alkyl Side-Chain Length on the Performance of Poly (3-alkylthiophene)/Polyfluorene All-Polymer Solar Cells. *Chem. Mater.* **2010**, *22*, 3389.

(22) Moulé, A. J.; Bonekamp, J. B.; Meerholz, K. The Effect of Active Layer Thickness and Composition on the Performance of Bulk-Heterojunction Solar Cells. *J. Appl. Phys.* **2006**, *100*, 094503.

(23) Nickel, F.; Sprau, C.; Klein, M. F. G.; Kapetana, P.; Christ, N.; Liu, X.; Klinkhammer, S.; Lemmer, U.; Colsmann, A. Spatial Mapping of Photocurrents in Organic Solar Cells Comprising Wedge-Shaped Absorber Layers for an Efficient Material Screening. *Sol. Energ. Mat. Sol. Cells* **2012**, *104*, 18.

(24) Brabec, C. J.; Gowrisanker, S.; Halls, J. J. M.; Laird, D.; Jia, S.; Williams, S. P. Polymer-Fullerene Bulk-Heterojunction Solar Cells. *Adv. Mater.* **2010**, *22*, 3839–3856.

(25) Hoppe, H.; Arnold, N.; Sariciftci, N. S.; Meissner, D. Modeling the Optical Absorption within Conjugated Polymer/fullerene-Based Bulk-Heterojunction Organic Solar Cells. *Sol. Energy Mater. Sol. Cells* **2003**, *80*, 105–113.

(26) Vosgueritchian, M.; Lipomi, D. J.; Bao, Z. Highly Conductive and Transparent PEDOT:PSS Films with a Fluorosurfactant for Stretchable and Flexible Transparent Electrodes. *Adv. Funct. Mater.* **2012**, *22*, 421.

(27) Lipomi, D.; Chong, H.; Vosgueritchian, M.; Mei, J.; Bao, Z. Toward Mechanically Robust and Intrinsically Stretchable Organic Solar Cells: Evolution of Photovoltaic Properties with Tensile Strain. *Sol. Energ. Mat. Sol. Cells* **2012**, *107*, 355–365.

(28) Dickey, M. D.; Chiechi, R. C.; Larsen, R. J.; Weiss, E. A.; Weitz, D. A.; Whitesides, G. M. Eutectic Gallium-Indium (EGaIn): A Liquid Metal Alloy for the Formation of Stable Structures in Microchannels at Room Temperature. *Adv. Funct. Mater.* **2008**, *18*, 1097–1104.

(29) Savagatrup, S.; Printz, A. D.; Rodriquez, D.; Lipomi, D. J. Best of Both Worlds: Conjugated Polymers Exhibiting Good Photovoltaic Behavior and High Tensile Elasticity. *Macromolecules* **2014**, *47*, 1981–1992.

(30) Dang, M. T.; Hirsch, L.; Wantz, G. P3HT:PCBM, Best Seller in Polymer Photovoltaic Research. *Adv. Mater.* **2011**, *23*, 3597–3602.

(31) Huang, J.; Carpenter, J. H.; Li, C.-Z.; Yu, J.-S.; Ade, H.; Jen, A. K.-Y. Highly Efficient Organic Solar Cells with Improved Vertical Donor-Acceptor Compositional Gradient Via an Inverted Off-Center Spinning Method. *Adv. Mater.* **2015**, *28*, 967–974.

(32) Hou, L.; Wang, E.; Bergqvist, J.; Andersson, B. V.; Wang, Z.; Müller, C.; Campoy-Quiles, M.; Andersson, M. R.; Zhang, F.; Inganäs, O. Lateral Phase Separation Gradients in Spin-Coated Thin Films of High-Performance Polymer:Fullerene Photovoltaic Blends. *Adv. Funct. Mater.* **2011**, *21*, 3169.

(33) Kim, N.; Jang, S.; Pace, G.; Caironi, M.; Park, T.; Khim, D.; Kim, J.; Kim, D.; Noh, Y. High-Performance Organic Field-Effect Transistors with Directionally Aligned Conjugated Polymer Film Deposited from Pre-Aggregated Solution High-Performance Organic Field-Effect Transistors with Directionally Aligned Conjugated Polymer Film Deposited from. *Chem. Mater.* **2015**, *27*, 8345–8353.

(34) Norrman, K.; Ghanbari-Siahkali, A.; Larsen, N. B. 6 Studies of Spin-Coated Polymer Films. *Annu. Rep. Prog. Chem., Sect. C* **2005**, *101*, 174.

(35) Li, G.; Shrotriya, V.; Yao, Y.; Yang, Y. Investigation of Annealing Effects and Film Thickness Dependence of Polymer Solar Cells Based on poly(3-Hexylthiophene). *J. Appl. Phys.* **2005**, *98*, 3–8.

(36) Woo, C. H.; Beaujuge, P. M.; Holcombe, T. W.; Lee, O. P.; Fréchet, J. M. J. Incorporation of Furan into Low Band-Gap Polymers for Efficient Solar Cells. *J. Am. Chem. Soc.* **2010**, *132*, 15547.

(37) Spano, F. The Spectral Signatures of Frenkel Polarons in H-and J-Aggregates. *Acc. Chem. Res.* **2009**, *43*, 429–439.

(38) Awartani, O.; Lemanski, B. I.; Ro, H. W.; Richter, L. J.; DeLongchamp, D. M.; O'Connor, B. T. Correlating Stiffness, Ductility, and Morphology of Polymer:Fullerene Films for Solar Cell Applications. *Adv. Energy. Mater.* **2013**, *3*, 399–406.

Appendix A

Supporting information for Chapter 3

Mechanical properties of conjugated polymers and polymer-fullerene composites as a function of molecular structure

Suchol Savagatrup, Aditya S. Makaram, Daniel J. Burke, and Darren J. Lipomi

Department of NanoEngineering, University of California, San Diego

9500 Gilman Drive, Mail Code 0448, La Jolla, CA 92093-0448

A.1 Experimental data for tensile moduli of P3AT films and P3AT:PCBM films

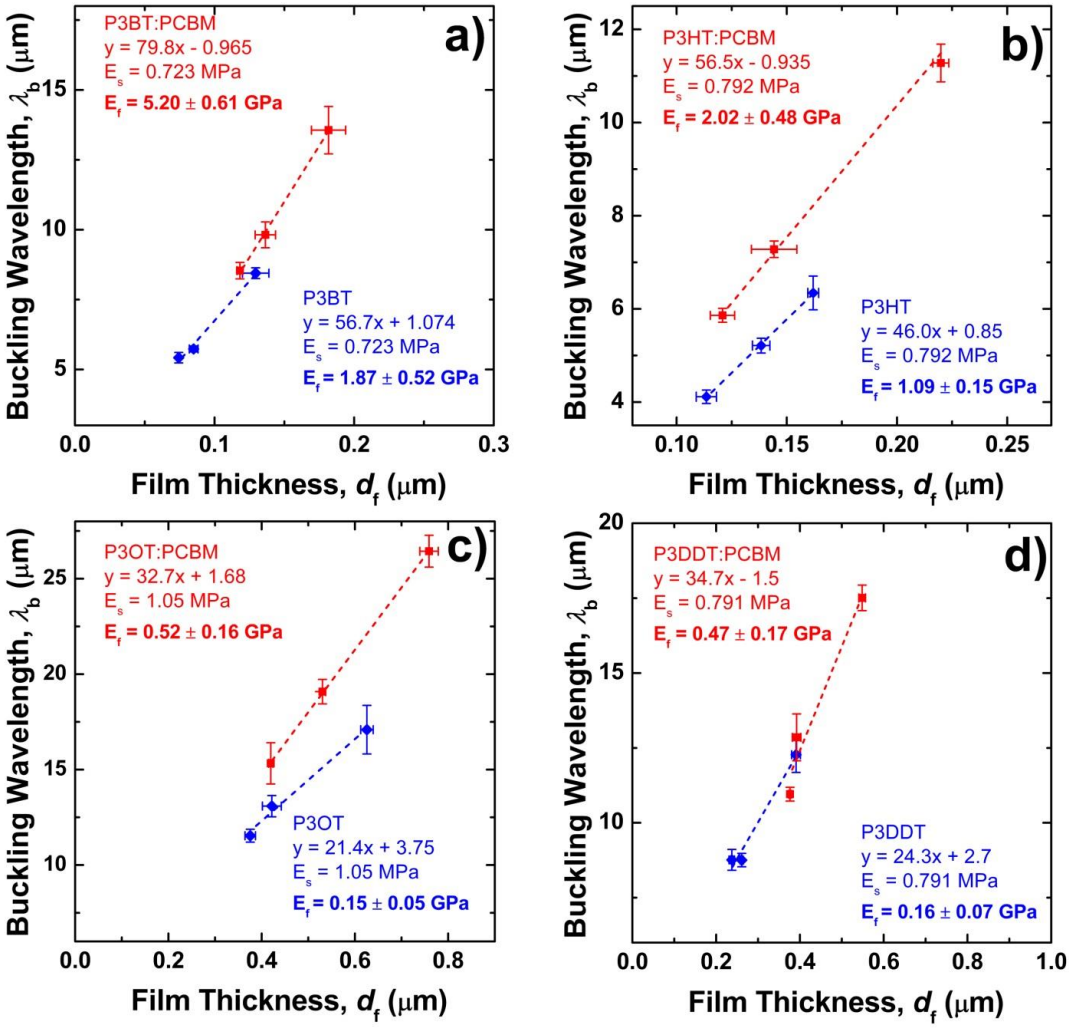

Figure A.1. Buckling wavelength vs. film thickness for P3AT and P3AT:PCBM films. (a) P3BT and P3BT:PCBM, (b) P3HT and P3HT:PCBM, (c) P3OT and P3OT:PCBM, and (d) P3DDT and P3DDT:PCBM. The ratio between P3ATs and PCBM was 2:1 (w/w).

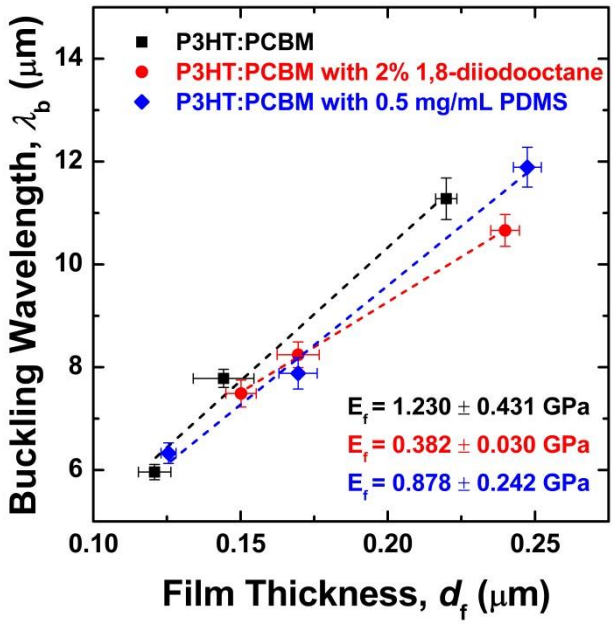

Figure A.2. Buckling wavelength vs. film thickness of P3HT:PCBM spin-coated from ODCB with and without processing additives: (a) no additive, (b) 2% 1,8-diiodooctane, (c) 0.5 mg/mL PDMS. The ratio between P3HT and PCBM was 2:1 (w/w).

A.2 AFM images of P3AT films and P3AT:PCBM films

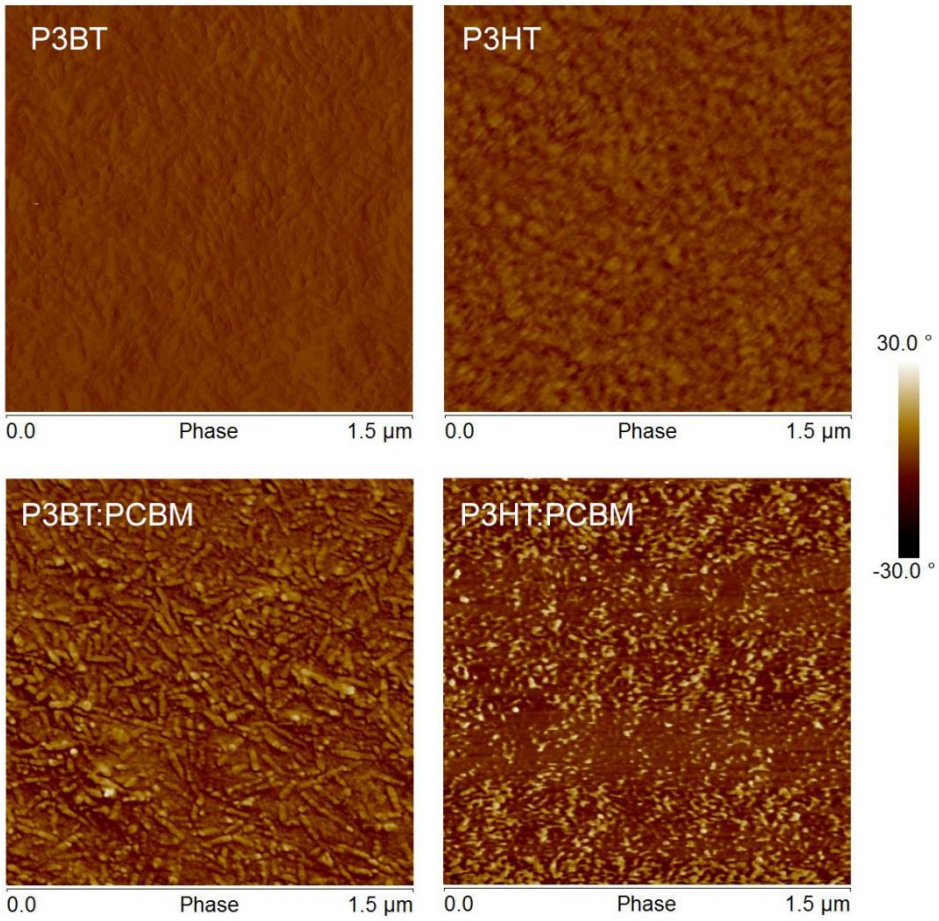

Figure A.3. Atomic force microscopy phase images of P3BT, P3BT:PCBM, P3HT, and P3HT:PCBM films spin-coated on Si wafer with no annealing. The ratio between the P3AT and PCBM was 2:1 (w/w).

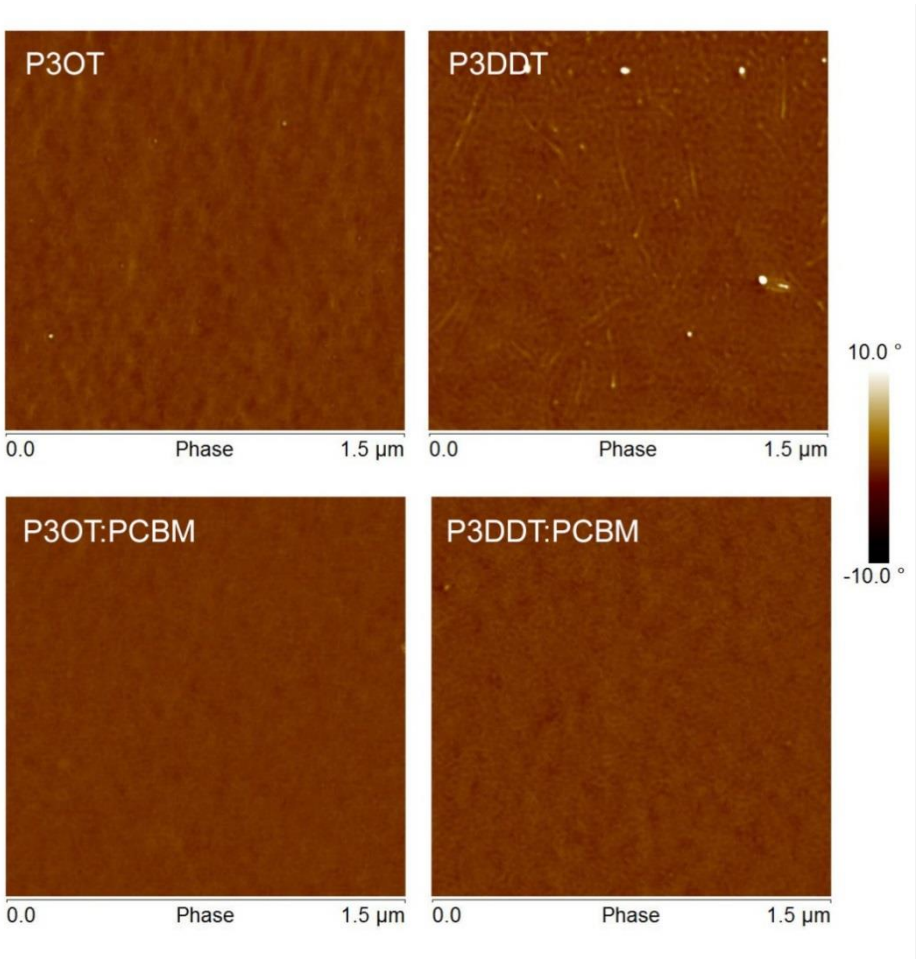

Figure A.4. Atomic force microscopy phase images of P3OT, P3OT:PCBM, P3DDT, and P3DDT:PCBM films spin-coated on Si wafer with no annealing. The ratio between the P3AT and PCBM was 2:1 (w/w).

A.3 Theoretical calculation of the tensile modulus for pure P3AT films

Our method of calculation was developed from Seitz[1] and Tahk et al.[2] The tensile modulus was calculated as a function of the bulk modulus, *B*, and the Poisson's ratio, *v*, as given by equation 2,

$$E = 3B(1 - 2v) \qquad (\mathbf{2})$$

The Poisson's ratio is a function of van der Waals volume and the molecular structure of the monomer. The bulk modulus is a function of cohesive energy and molar volume at room temperature and at 0 K. We divided the calculation into these two sections.

A.3.1 Poisson's ratio, van der Waals volume

The Poisson's ratio was modeled from the empirical data relating the ratio to the polymer molecular cross-sectional area, *A*,[1]

$$\nu = 0.513 - 2.37 \times 10^6 \sqrt{A} \qquad (\mathbf{5})$$

This cross-sectional area, *A*, can then be related to the van der Waals volume, V_w, and the length of the main chain of the monomers, l_m, by

$$A = \frac{V_w}{N_A l_m} \qquad (\mathbf{6})$$

where N_A is Avogadro's number. Both V_w and l_m are estimated from the structure of the monomer. Figure **S5** shows the definition of l_m for each P3AT; because l_m is the length of the main chain only (and not dependent on the side chain), we used the same values for all P3ATs, 0.434 nm.[2]

We used the same topological method presented by Tahk et al.[2] to evaluate the van der Waals volume, V_w,

$$V_w \approx 3.861803\ {}^{0}\chi + 13.748435\ {}^{1}\chi^{v} \qquad (\boldsymbol{S1})$$

where ${}^{0}\chi$ and ${}^{1}\chi^{v}$ are the zeroth-order atomic and first-order bond connectivity indices:

$${}^{0}\chi = \sum_{vertices} \left(\frac{1}{\sqrt{\delta}}\right) \ , \ {}^{1}\chi^{v} = \sum_{edges} \left(\frac{1}{\sqrt{\beta^{v}}}\right) \qquad (\boldsymbol{S2}, \boldsymbol{S3})$$

β^{v} is the product of two values of δ^{v} for a given edge as shown by equation **S4**.

$$\beta^{v} = \delta^{v} \times \delta^{v} \qquad (\boldsymbol{S4})$$

The values of δ and δ^{v} are given in Figure **S5**. δ is the number of non-hydrogen atoms to which a given non-hydrogen atom is bonded. δ^{v} is the valence connectivity index as calculated by equation **S5**.

$$\delta^{v} = \frac{(Z^{v} - N_H)}{(Z - Z^{v} - 1)} \qquad (\boldsymbol{S5})$$

Where Z^{v} and Z are the number of valance electron of an atom and its atomic number, respectively. N_H is the number of hydrogen attached to the atom.

Table A.1. Values used to calculate the Poisson's ratio of the pure P3ATs

	L_m (nm)	${}^{0}\chi$	${}^{1}\chi^{v}$	V_w (cm^3/mole)	ν
P3BT	0.434	6.27	4.11	80.74	0.381272
P3HT	0.434	7.68	5.11	99.95	0.366437
P3OT	0.434	9.10	6.11	119.16	0.352972
P3DDT	0.434	11.92	8.11	157.58	0.328974

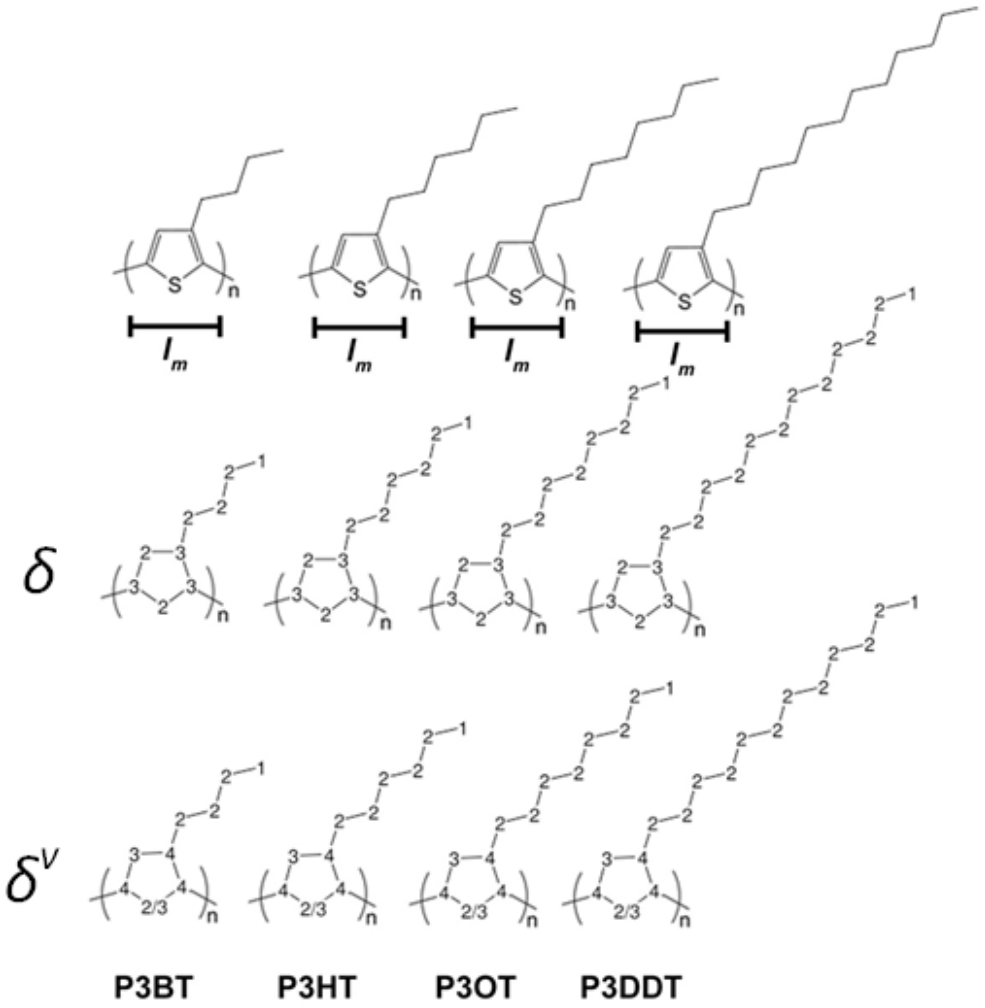

Figure A.5. Schematic for the calculation of l_m, δ, and δ^v for P3BT, P3HT, P3OT, and P3DDT.

A.3.2 Bulk modulus, cohesive energy, and molar volume

The bulk modulus was estimated from the Lennard-Jones potential. The bulk modulus can be defined as,

$$B = V\frac{\partial^2 U}{\partial V^2} \qquad (\boldsymbol{S6})$$

Where, V is the molar volume and U is the internal energy. We can express the Lennard-Jones potential in terms of the molar volume,

$$U = U_0\left[\left(\frac{V_0}{V}\right)^4 - \left(\frac{V_0}{V}\right)^2\right] \qquad (\boldsymbol{S7})$$

From substituting the relationship between the molar volume and the molar radius (equation **S8**) into the model of the Lennard-Jones potential (equation **S9)**,

$$\frac{V_0}{V} = \left(\frac{r_0}{r}\right)^3 \qquad (\boldsymbol{S8})$$

$$U = U_0\left[\left(\frac{r_0}{r}\right)^{12} - \left(\frac{r_0}{r}\right)^6\right] \qquad (\boldsymbol{S9})$$

We used the same empirical relationship between U_0 and E_{coh1} to give the resulting expression of the bulk modulus,

$$B(T) \approx 8.23333E_{coh1}\left[\frac{5V_0^4}{V(T)^5} - \frac{3V_0^2}{V(T)^3}\right] \qquad (\mathbf{3})$$

The cohesive energy was estimated using the method outline by Fedor.[3] The method relies on predicting the solubility of the polymer using the molecular structure of the monomer. Ultimately, the cohesive energy can be expressed as a function of the first-order bond connectivity indices with the correction factor, specifically calculated for P3ATs.[3]

$$E_{coh1} \approx 9882.5\,{}^1\chi^v + 5021.8 \qquad (\boldsymbol{S10})$$

Values for molar volume were calculated using the empirical correlations depending on the range of the T_g of the polymer of interest. We used three different equations corresponding to the polymer with T_g higher than room temperature (P3BT), T_g close to room temperature (P3HT), and T_g below room temperature (P3OT and P3DDT),[1]

$$V_{P3BT} = V_w\left(0.15\frac{T}{T_g} + 1.42\right) \qquad (\boldsymbol{S11})$$

$$V_{P3HT} = V_w\left(0.225\frac{T}{T_g} + 1.57\right) \qquad (\boldsymbol{S12})$$

$$V_{P3OT,P3DDT} = V_w\left(0.30\frac{T}{T_g} + 1.27\right) \qquad (\boldsymbol{S13})$$

Table A.2. Values used to calculate the bulk moduli and tensile moduli of the pure P3ATs

	T_g (K)[4]	V (cm^3/mole)	V_0 (cm^3/mole)	E_{coh1} (J/mole)	B (GPa)	E (GPa)
P3BT	331.85	125.5325	114.6564	45663.08	2.925996	2.084391
P3HT	287.15	180.2668	156.9274	55545.58	1.517079	1.215752
P3OT	258.95	192.4779	151.3378	65428.08	0.157497	0.138939
P3DDT	251.05	256.2469	200.1308	85193.08	0.083258	0.085436

A.4 Theoretical calculation of the tensile modulus for P3AT:PCBM films

For the blends of P3AT:PCBM, we employed a composite theory[2] that relates the tensile modulus of the pure film to that of the composite film as a function of Poisson's ratio, volume fraction of the filler (PCBM) and the maximum packing fraction of PCBM. The methodology was detailed by Tahk et al.[2]

$$\frac{E_{P3AT:PCBM}}{E_{P3AT}} = \frac{1 + AB\phi_{PCBM}}{1 - B\psi\phi_{PCBM}} \qquad (\boldsymbol{S14})$$

$$A = \frac{7 - 5\nu_{P3AT}}{8 - 10\nu_{P3AT}}, B = \frac{\frac{E_{PCBM}}{E_{P3AT}} - 1}{\frac{E_{PCBM}}{E_{P3AT}} + A}, \psi = 1 + \frac{1 - \phi_m}{\phi_m^2}\phi_{PCBM} \qquad (\boldsymbol{S15})$$

Where E_i's are the tensile moduli of either pure P3ATs, P3AT:PCBMs, or PCBM, ν is the Poisson's ratio calculated in Section 3, ϕ_{PCBM} is the fraction of PCBM in the blend, and ϕ_m is the maximum packing fraction of PCBM. The maximum packing fraction of PCBM was taken as 0.7.[2] For a 2:1 weight ratio blends used in this experiment, the packing fraction of PCBM was 1/3. Because the value of the tensile modulus of PCBM is much greater than those of the pure P3AT,[2] the values of *B* for all the blends can be taken as 1.

Table A.3. Values used to calculate the tensile moduli of the P3AT:PCBM films

	E, P3AT (GPa)	*A*	*E, P3AT:PCBM (GPa)*
P3BT	2.084391	1.216455	4.893731
P3HT	1.215752	1.191941	2.837747
P3OT	0.138939	1.171099	0.322692
P3DDT	0.085436	1.136907	0.196802

References

(1) Seitz, J. The Estimation of Mechanical Properties of Polymers from Molecular Structure. *J. Appl. Polym. Sci.* **1993**, *49*, 1331–1351.

(2) Tahk, D.; Lee, H. H.; Khang, D.-Y. Elastic Moduli of Organic Electronic Materials by the Buckling Method. *Macromolecules* **2009**, *42*, 7079–7083.

(3) Fedors, R. F. A Method for Estimating Both the Solubility Parameters and Molar Volumes of Liquids. Supplement. *Polym. Eng. Sci.* **1974**, *14*, 472–472.

(4) Chen, S.; Ni, J.-M. Structure/Properties of Conjugated Conductive Polymers. 1. Neutral Poly(3-Alkyl Thiophene)s. *Macromolecules* **1992**, *25*, 6081.

Appendix B

Supporting information for Chapter 5

Viability of stretchable poly(3-heptylthiophene) (P3HpT) for organic solar cells and field-effect transistors

Suchol Savagatrup,[†a] Adam D. Printz,[†a] Haosheng Wu,[b] Kirtana M. Rajan,[a] Eric J. Sawyer,[a] Aliaksandr V. Zaretski,[a] Christopher J. Bettinger,[b] and Darren J. Lipomi[a]

([†] Equal contribution)

[a] *Department of NanoEngineering, University of California, San Diego, 9500 Gilman Drive Mail Code 0448, La Jolla, CA 92093-0448.*

[b] *Department of Materials Science and Engineering, Carnegie Mellon University, 5000 Forbes Hall, Pittsburgh, PA, 15213-3890.*

B.1 Experimental methods

B.1.1 Materials

Poly(3-heptylthiophene) (P3HpT, M_n = 35 kDa, PDI = 1.5) was purchased from Rieke Metals, Inc. and used as received. Poly(3-hexylthiophene) (P3HT, M_n = 44 kDa, PDI = 2.0) and poly(3-octylthiophene) (P3OT, M_n = 34 kDa, PDI = 2.5) were purchased from Sigma-Aldrich and used as received. PDMS, Sylgard 184 (Dow Corning), was prepared according to the manufacturer's instructions at a ratio of 10:1 (base:crosslinker) and cured at room temperature for 36 to 48 h before it was used for mechanical testing. (Tridecafluoro-1,1,2,2-tetrahydrooctyl)-1-trichlorosilane (FOTS) was obtained from Gelest. PEDOT:PSS (Clevios PH1000) was purchased from Heraeus. DMSO was purchased from BDH with purity of 99.9% and Zonyl (FS-300) fluorosurfactant were purchased from Sigma-Aldrich. Chloroform ($CHCl_3$), ortho-dichlorobenzene (ODCB), acetone, isopropyl alcohol (IPA), and ITO-coated glass slides were obtained from Sigma-Aldrich and used as received.

B.1.2 Preparation of substrates

Glass slides used as substrates for solar cells were cut into squares (2.5 cm × 2.5 cm) with a diamond-tipped scribe. They were then subsequently cleaned with Alconox solution (2 mg mL^{-1}), deionized water, acetone, and then isopropyl alcohol (IPA) in an ultrasonic bath for 10 min each and then rinsed and dried with compressed air. Next, the glass was plasma treated at ~30 W for 3 min at a base pressure of 200 mtorr ambient air to remove residual organic material and activate the surface. ITO-coated slides for cyclic voltammetry and UV–vis spectrophotometry were cleaned in the same manner. Glass

slides used as substrates for thin films to be transferred to PDMS for mechanical testing by the buckling methodology were prepared in the same manner as above, and then subsequently placed in a vacuum desiccator with a glass vial containing ~100 µL of FOTS and put under house vacuum for a minimum of 3 h to passivate the surface.

B.1.3 Preparation of polymer solutions

Solutions of P3HT, P3HpT, and P3OT in $CHCl_3$ (15 mg mL^{-1}) were prepared for cyclic voltammetry and UV-vis. Solutions of the different ratios of P3HpT:$PC_{61}BM$ in ODCB (at a constant concentration of 40 mg mL^{-1}) were prepared for solar cells, crack-onset strain (*CoS*), and H-aggregate analysis. All solutions were allowed to stir overnight and filtered with a 1-µm glass microfiber (GMF) syringe filter immediately before being spin-coated onto glass or silicon substrates.

B.1.4 Thermal analysis

DSC was performed using a Perkin Elmer Diamond differential scanning calorimeter. Indium was used to calibrate the cell capacitance. Samples were prepared from drop-casting thin films of pure polymer and BHJ films onto aluminum pans. The mass of each sample was approximately 10 to 15 mg. Nitrogen was used as a purge gas with flow rate of 50 mL min^{-1}. The samples were held at –50 °C for 10 min and then ramped up to the upper limit of 300°C with the heating rate of 10°C min^{-1}. The samples were held at 30 °C for 1 min before cooling down to –50 °C at the same heating rate. The second heating curves were used for analysis.

B.1.5 Cyclic voltammetry (CV)

Cyclic voltammograms of P3HT, P3HpT and P3OT deposited onto ITO glass were measured relative to ferrocene at room temperature. The electrolyte used was a 0.1 M solution of $TBAPF_6$ in acetonitrile. The data was acquired using a μAutolab III potentiostat at scan rates of 10, 50 and 100 mV s^{-1} using an electrochemical cell consisting of the polymer acting as the working electrode, a platinum counter electrode, and an Ag/AgCl reference electrode.

B.1.6 UV-vis spectroscopy and analysis

The absorbance of the materials was measured using a PerkinElmer Lambda 1050 UV-vis-NIR spectrophotometer. The wavelength range measured was 850–300 nm with a step size of 1 nm. The polymer solutions were spin-coated onto the ITO-coated glass slides at a spin speed of 500 rpm (250 rpm s^{-1} ramp) for 240 s followed by 2000 rpm (750 rpm s^{-1} ramp) for 60 s. The films were immediately placed in a nitrogen-filled glove box and annealed at 100 °C for 30 min under a Pyrex petri dish covered in aluminum foil. After 30 min, the samples were allowed to cool slowly to room temperature.

Order in films of semiconducting polymers is associated with both greater electronic performance and increased stiffness. The extent of order, as determined by UV-vis spectroscopy, has been correlated to increased tensile moduli in P3HT:PCBM films. Spano et al. and others have shown that aggregates of P3HT in solid films can be considered as weakly interacting H aggregates, due to cofacial π-π stacking and weak excitonic coupling.[1–5] We used this model to compare trends in aggregation and

aggregate order from the UV-vis absorption spectra of the polymers, in an attempt to correlate these values with the mechanical stiffness.

In the aggregated state (i.e., crystallites and other aggregates in solid films), coupled electron-vibrational (vibronic) transitions determine the absorption of weakly interacting H aggregates and can be modeled as Gaussian fits by:

$$A(E) \propto \sum_{m=0} \left(\frac{S^m}{m!}\right) \times \left(1 - \frac{We^{-S}}{2E_\mathrm{p}} \sum_{n \neq m} \frac{S^n}{n!\,(n-m)}\right)^2 \times exp\left(\frac{-\left(E - E_{00} - mE_\mathrm{p} - \frac{1}{2}WS^m e^{-S}\right)^2}{2\,\sigma^{\,2}}\right) \quad (\mathbf{1})$$

In the above equation, *A* is the absorption by an aggregate as a function of the photon energy (*E*). E_{00} is the energy of the 0→0 vibronic transition, which is allowed assuming some disorder in the aggregates. *S* is the Huang-Rhys factor, which quantifies the nuclear potential well shift upon vibronic transition from the ground state to the excited state. It is calculated from absorption and emission spectra, and is set to 1 for P3ATs. E_p is the intermolecular vibration energy, which (in the case where $S = 1$) is the difference in energy between the vibrational levels in the excited state. It is set to 0.179 eV as determined by Raman spectroscopy. *W* is the free exciton bandwidth, which is related to the nearest neighbor interchain excitonic coupling. Upon coupling, a dispersion of the energies occurs, the width of which is equal to *W* (which is four times the nearest neighbor coupling). *W* is also inversely related to conjugation length; a lower *W* indicates better ordering of the aggregates. The terms *m* and *n* are the ground- and excited state vibrational levels and σ is the Gaussian linewidth.

The parameters E_{00}, *W*, σ, and a scaling factor were found by using Matlab to perform a least squares fit to the experimental absorption data in the region of 1.93 to

2.25 eV. This region was selected because the absorption is dominated by the polymer aggregates. Above 2.30 eV, the amorphous polymer dominates absorption.[6]

B.1.7 Buckling-based metrology

The tensile moduli of the materials with the buckling method as described elsewhere. Briefly, the elastomer PDMS was chosen as the substrate for all tests. The PDMS was prepared as described above and then cut into rectangular strips (l = 8 cm, w = 1 cm, h = 0.3 cm) before being stretched 4% using a computer-controlled linear actuator. While still under strain, FOTS treated glass slides (5 cm × 2.5 cm) were clipped onto the back of each strip using binder clips. To transfer the polymer or polymer:fullerene films to PDMS, the films were first spin-coated onto FOTS treated glass slides (2.5 cm × 2.5 cm) and then scored to facilitate transfer. The films were then placed against the PDMS, and after applying minimal pressure to achieve a conformal seal, the PDMS and glass slide with film were separated in one fast motion, leaving behind the film on the PDMS. After transfer, the PDMS substrates were relaxed; this action created a compressive strain that forced the conjugated polymer film to adopt sinusoidal buckles. The buckling wavelength, λ_b, and the thickness of the film, d_f, can be related to the tensile moduli of the film and the substrate, E_f and E_s, and the Poisson ratios of the two materials, v_f and v_s by the following equation:

$$E_f = 3E_s\left(\frac{1-v_f^2}{1-v_s^2}\right)\left(\frac{\lambda_b}{2\pi d_f}\right)^3 \qquad (\mathbf{2})$$

We measured the tensile modulus of the substrate, E_s (using a commercial pull tester), the buckling wavelength, λ_b (by optical microscopy), and the film thickness, d_f

(by stylus profilometry). The slope of a plot of λ_b vs. d_f for three different film thicknesses was inserted into eq S2. The Poisson's ratios were taken as 0.5 and 0.35 for PDMS and the conjugated polymers films. The experimental method is described in detail elsewhere.[7]

B.1.8 Fabrication of OTFT devices

The P3HT OTFTs were fabricated in a bottom gate, bottom contact configuration. Heavily n++ doped silicon wafers were used as the common gate with 250 nm of SiO_2 on top acting as the dielectric layer. The source/drain electrodes (2 nm Ti/20 nm Au) were photolithographically patterned on the SiO_2 surfaces with a channel length and width of L = 10 mm and W = 500 mm, respectively. The patterned substrates were cleaned with acetone, IPA, and DI water, and dried under an N_2 flow and placed in a UV-Ozone cleaner for 5 min. The substrates were then chemically modified by submerging in a 3 mM solution of octadecyltrichlorosilane (OTS) in trichloroethylene overnight. After the OTS modification, the substrates were cleaned with acetone, IPA, and DI water in an ultrasonic bath for 5 min each and dried under an N_2 flow.

In a N_2 filled glove box, solutions of P3HT (P3HT:PCBM), P3HPT (P3HpT:PCBM), and P3OT (P3OT:PCBM) in anhydrous chloroform at a concentration of 1 mg mL^{-1} (2 mg mL^{-1}) were completely dissolved on a hotplate at 37 °C. The solutions were cooled down to room temperature before being filtered through a 200 mm PTFE filter. The OTS modified substrates were placed in the center of a glass petri dish and 250 μL of chloroform was added to create a solvent saturated environment. Next, 10 mL of the polymer or polymer:fullerene solution was drop-cast to completely cover the

substrate surfaces (4 mm × 7 mm). After drop-casting the solution, the substrates were immediately covered by the petri dish. The solutions took about 15 min to dry and form a film. After the formation of the semiconducting layers, the devices were taken out of the glove box and kept in a high vacuum chamber (~10^{-6} Torr) for 16 h to completely remove the residual solvent in the films before testing. The devices were characterized in a probe station with continuous Ar flow on the device surfaces.

B.1.9 Fabrication of solar cells

We deposited a layer of PEDOT:PSS from an aqueous solution containing 92.9 wt% Clevios PH 1000 (~0.9-1.2 wt% PEDOT:PSS), 7.0 wt% DMSO, and 0.1 wt% Zonyl fluorosurfactant as the transparent anode. The solution was filtered with a 1-μm glass microfiber syringe filter and then spin-coated at a speed of 500 rpm (250 rpm s^{-1} ramp) for 60 s, followed by 2000 rpm (750 rpm s^{-1} ramp) for 60 s. The samples were subsequently dried at 150 °C for 30 minutes. The photoactive layer was then spin-coated onto the electrode layer at a speed of 500 rpm (250 rpm s^{-1} ramp) for 240 s, followed by 2000 rpm (750 rpm s^{-1} ramp) for 60 s. A thin strip of the PEDOT:PSS electrode was exposed by wiping away some of the photoactive layer with chloroform so that electrical contact could be made. The samples were then immediately placed in a nitrogen-filled glovebox and annealed at 100 °C for 30 min. The substrates were then allowed to cool slowly to room temperature. EGaIn (extruded by hand from a syringe) was used as the top contact. The photovoltaic properties were measured in a nitrogen-filled glovebox using a solar simulator with a 100 mW cm^{-2} flux that approximated the solar spectrum under AM 1.5G conditions (ABET Technologies 11016-U up-facing unit calibrated with

a reference cell with a KG5 filter). The current density versus voltage was measured for both dark and under illumination using a Keithley 2400 SourceMeter.

B.2 UV-vis absorption of P3HpT:PCBM with different PCBM loading

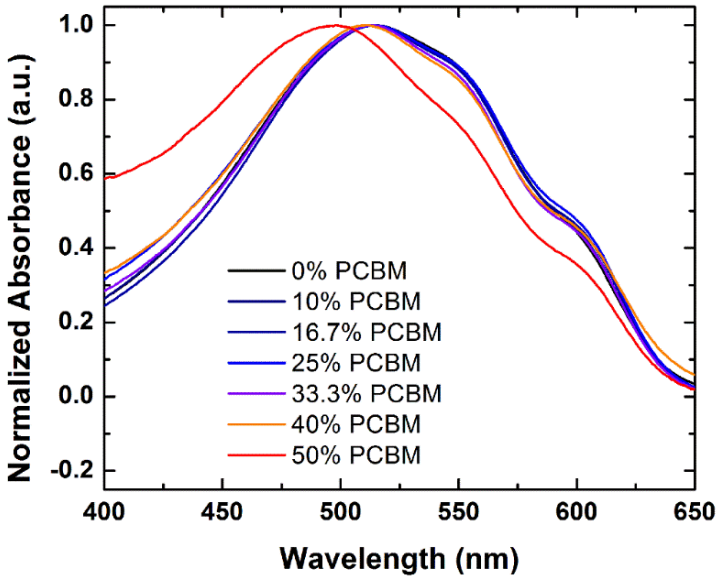

Figure B.1. Normalized UV-Vis spectra of blends of P3HpT:PCBM with different weight concentrations of PCBM after subtracting out the PCBM contribution. Most of the spectra overlap well, but there is a decrease in order above 33.3% PCBM loading, and a distinct blue shift in the absorption at 50% PCBM loading.

B.3 Differential scanning calorimetry (DSC) for P3AT:PCBMs

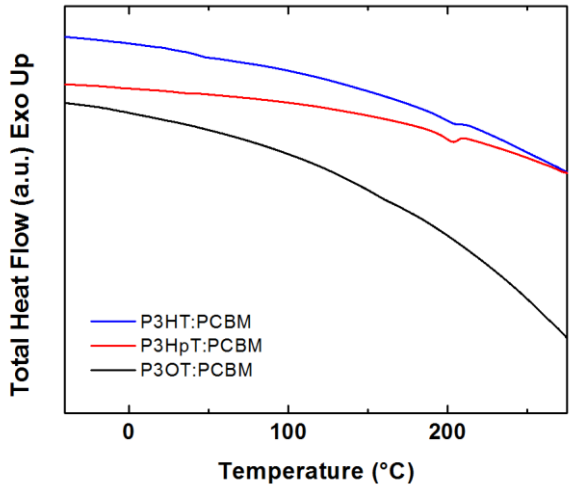

Figure B.2. DSC thermograms of P3AT:PCBMs. The T_g for P3HT:PCBM was detected between 37 and 40 °C. The T_g of P3HpT:PCBM was detected between 33 and 35 °C. The T_g for P3OT:PCBM increased slight from that of P3OT to the range between -5 and 0 °C.

B.4 Approximation of the onset of oxidation from cyclic voltammetry

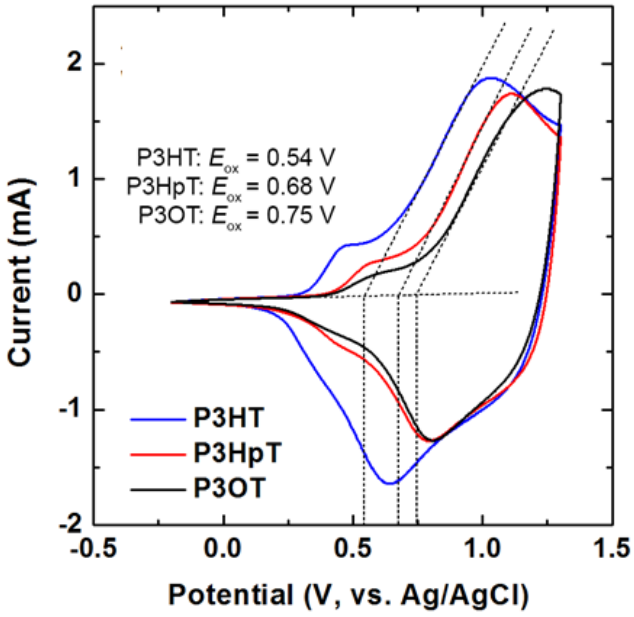

Figure B.3. The oxidation onsets of the P3ATs were determined by the intersection of the extrapolation of the slope of the oxidation curve and the baseline.

B.5 Charge transport properties of P3AT:PCBMs

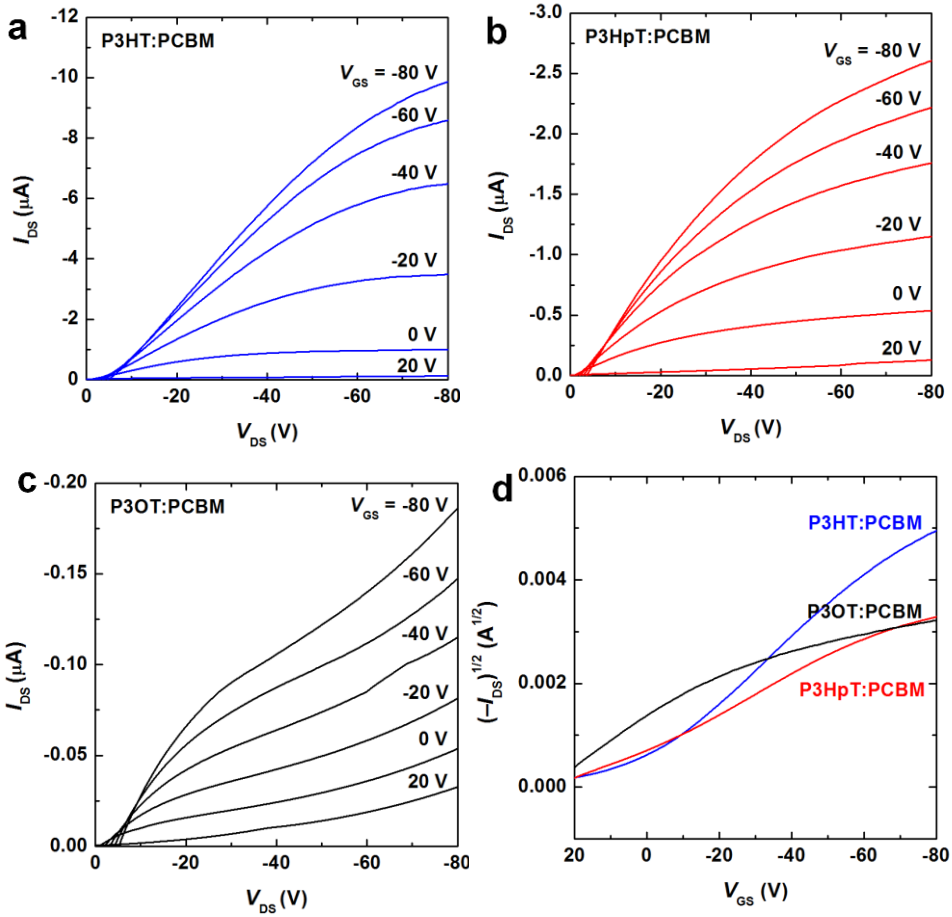

Figure B.4. Electrical characteristics of P3AT organic thin films transistors (OTFTs): current-voltage output characteristics of a 10 μm (length) by 500 μm (width) channel for (a) P3HT:PCBM, (b) P3HpT:PCBM, and (c) P3OT:PCBM. (d) Transfer characteristics $(-I_{DS})^{1/2}$ vs. V_{GS} at V_{DS} = –80 V with respect to alkyl side chain length.

References

(1) Spano, F. C. Modeling Disorder in Polymer Aggregates: The Optical Spectroscopy of Regioregular poly(3-Hexylthiophene) Thin Films. *J. Chem. Phys.* **2005**, *122*, 234701.

(2) Awartani, O.; Lemanski, B. I.; Ro, H. W.; Richter, L. J.; DeLongchamp, D. M.; O'Connor, B. T. Correlating Stiffness, Ductility, and Morphology of Polymer:Fullerene Films for Solar Cell Applications. *Adv. Energy Mater.* **2013**, *3*, 399–406.

(3) Clark, J.; Chang, J.-F.; Spano, F. C.; Friend, R. H.; Silva, C. Determining Exciton Bandwidth and Film Microstructure in Polythiophene Films Using Linear Absorption Spectroscopy. *Appl. Phys. Lett.* **2009**, *94*, 163306.

(4) Spano, F. C.; Clark, J.; Silva, C.; Friend, R. H. Determining Exciton Coherence from the Photoluminescence Spectral Line Shape in poly(3-Hexylthiophene) Thin Films. *J. Chem. Phys.* **2009**, *130*, 074904.

(5) Turner, S. T.; Pingel, P.; Steyrleuthner, R.; Crossland, E. J. W.; Ludwigs, S.; Neher, D. Quantitative Analysis of Bulk Heterojunction Films Using Linear Absorption Spectroscopy and Solar Cell Performance. *Adv. Funct. Mater.* **2011**, *21*, 4640–4652.

(6) Pingel, P.; Zen, A.; Abellón, R. D.; Grozema, F. C.; Siebbeles, L. D. A.; Neher, D. Temperature-Resolved Local and Macroscopic Charge Carrier Transport in Thin P3HT Layers. *Adv. Funct. Mater.* **2010**, *20*, 2286–2295.

(7) Savagatrup, S.; Makaram, A. S.; Burke, D. J.; Lipomi, D. J. Mechanical Properties of Conjugated Polymers and Polymer-Fullerene Composites as a Function of Molecular Structure. *Adv. Funct. Mater.* **2014**, *24*, 1169–1181.

Appendix C

Supporting information for Chapter 6

[70]PCBM and incompletely separated grades of methanofullerenes produce bulk heterojunctions with increased robustness for ultra-flexible and stretchable electronics

Suchol Savagatrup,[a] Daniel Rodriquez,[a] Adam D. Printz,[a] Alexander B. Sieval,[b] Jan C. Hummelen,[b,c] and Darren J. Lipomi[a]

[a] *Department of NanoEngineering, University of California, San Diego, 9500 Gilman Drive Mail Code 0448, La Jolla, CA 92093-0448.*

[b] *Solenne BV, Zernikepark 6-8, 9747 AN Groningen, Netherlands*

[c] *Stratingh Institute for Chemistry and Zernike Institute for Advanced Materials, University of Groningen, Nijenborgh 4, 9747 AG Groningen, Netherlands*

C.1. UV-Vis absorption of P3HT:methanofullerene films on different substrates

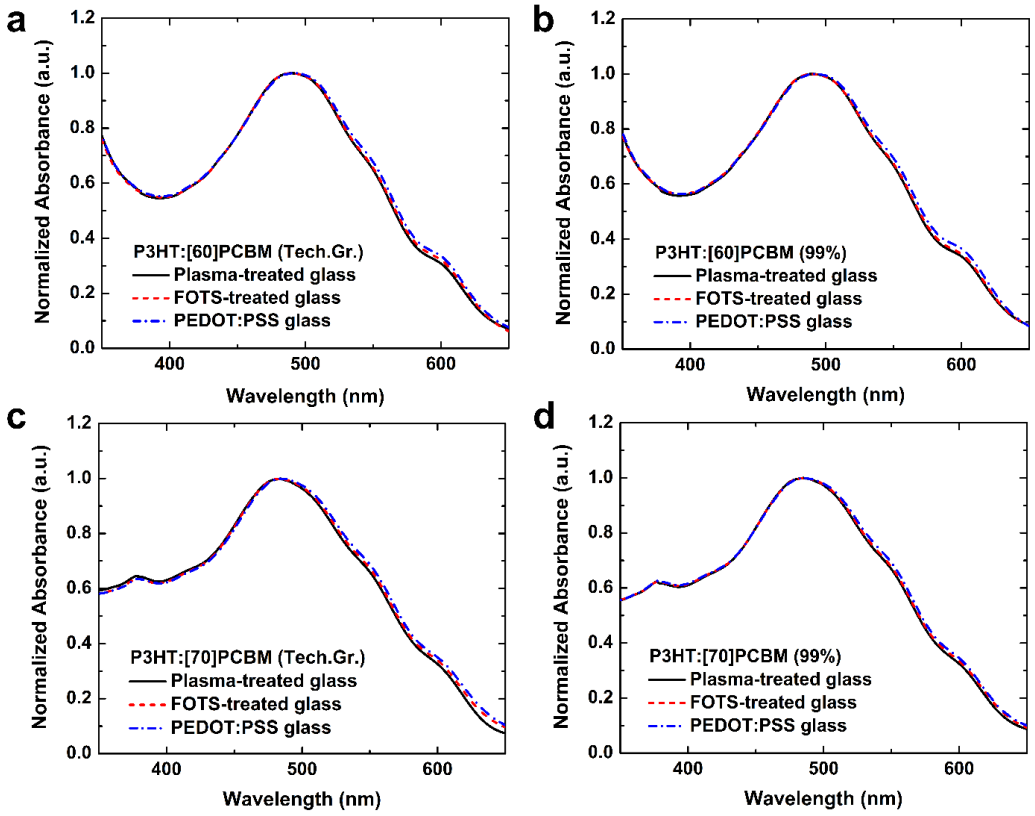

Figure C.1. UV-vis absorption of P3HT:methanofullerene thin films (~150 nm) on plasma-treated glass, FOTS-treated glass, and PEDOT:PSS films. The spin-coating parameters and solution concentration were kept constant through-out all samples. The complete overlaps observed in the normalized absorbance suggest that the differences in the microstructure resulted in these films are minimal.

C.2. Photovoltaic characteristic of P3HT:methanofullerenes with 1:1 mixture of [60]PCBM and [70]PCBM

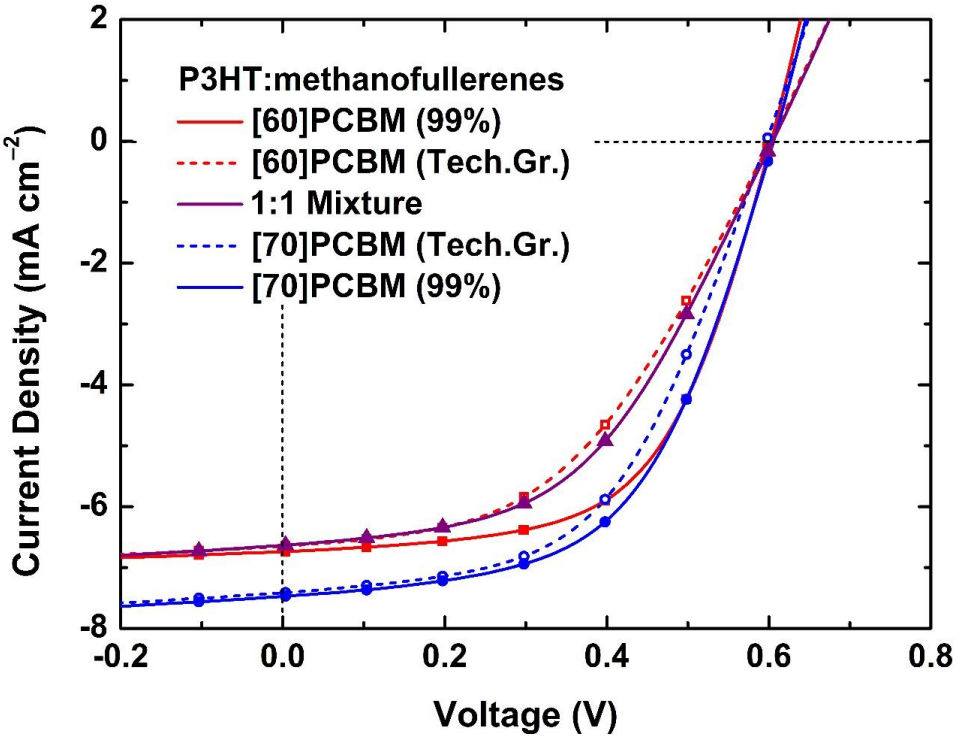

Figure C.2. Photovoltaic characteristic of averaged devices (N ≥ 8) with an active layer of 1:1 blend of P3HT and respective methanofullerenes. The architecture of the devices was PEDOT:PSS/P3HT:methanofullerene/EGaIn.

Table C.1. Summary of the photovoltaic figures of merit for P3HT:methanofullerene solar cells fabricated in this work (N ≥ 8) [†]

Device	V_{OC} (mV)	J_{SC} (mA cm^{-2})	*FF* (%)	*PCE* (%)
P3HT:[60]PCBM (99%)	602 ± 5.5	6.74 ± 0.2	59 ± 3.0	2.36 ± 0.2
P3HT:[60]PCBM (Tech.Gr.)	602 ± 3.7	6.60 ± 0.4	48 ± 4.8	1.89 ± 0.2
P3HT: 1:1 Mixture	605 ± 1.6	6.63 ± 0.5	50 ± 3.4	1.98 ± 0.1
P3HT:[70]PCBM (Tech.Gr.)	598 ± 11.2	7.41 ± 0.3	53 ± 1.7	2.35 ± 0.1
P3HT:[70]PCBM (99%)	606 ± 7.5	7.47 ± 0.4	55 ± 1.3	2.48 ± 0.1

[†]The solar cell device architecture was PEDOT:PSS/P3HT:methanofullerene/EGaIn. PEDOT:PSS, doped with 7% DMSO and 0.1% Zonyl, was spin-coated to create a layer of ~150 nm thick. The active layer was spin-coated from a solution of 1:1 P3HT:methanofullerene in ODCB (40 mg mL^{-1}) and thermally annealed at 125 °C in an inert atmosphere. EGaIn droplets were extruded to create the active area of ~0.02 cm^{-2}.

C.3. Buckling Methodology

To measure the tensile moduli of the pure fullerene films, we tested the bilayer systems comprising a layer of PEDOT:PSS with known tensile modulus and a layer of pure fullerene film with unknown modulus. We obtained the characteristic buckling wavelengths for different thicknesses of the bilayer systems, while keeping the thickness ratio of the PEDOT:PSS and the fullerene film constant. The examples of the optical micrograph of the buckles are shown in Figure S3. The buckling wavelengths were then plotted against the overall thickness of the bilayer system as shown in figure S4. The effective modulus of the bilayer (E_{eff}) was then calculated using equation 1:

$$E_{\text{eff}} = 3E_{\text{s}}\left(\frac{1-v_{\text{f}}^2}{1-v_{\text{s}}^2}\right)\left(\frac{\lambda_{\text{b}}}{2\pi d_{\text{f}}}\right)^3 \quad (\mathbf{1})$$

Where the fitted slope from figure S4 is used as the ratio between buckling wavelength, λ_{b}, and the thickness of the film, d_{f}; E_{s} is the tensile modulus of the PDMS substrate; the Poisson's ratios of the bilayer and the substrate, v_{f} and v_{s}, were 0.35 and 0.5, respectively.

From the known modulus of the PEDOT:PSS films ($E_{\text{f,1}}$) and the effective modulus of the bilayer (E_{eff}), we used equation 2 to calculated the modulus of the pure fullerene film ($E_{\text{f,2}}$). In all of our experiment, the ratio between the thickness of the PEDOT:PSS and the pure fullerene films were kept constant at 1. The examples of the curve of equation 2 are shown in Figure S5. The output, the modulus of the pure fullerene film, are plotted against the modulus of the bilayer system for different values of the PEDOT:PSS. In our experiment, the modulus of the PEDOT:PSS was kept constant at 3 GPa.

$$E_{\text{eff}} = \frac{1+m^2n^4+2mn(2n^2+3n+2)}{(1+n)^3(1+mn)}E_{\text{f,1}};\ \text{where}\ m=\frac{E_{\text{f,2}}}{E_{\text{f,1}}},\ n=\frac{d_{\text{f,2}}}{d_{\text{f,1}}} \quad (\mathbf{2})$$

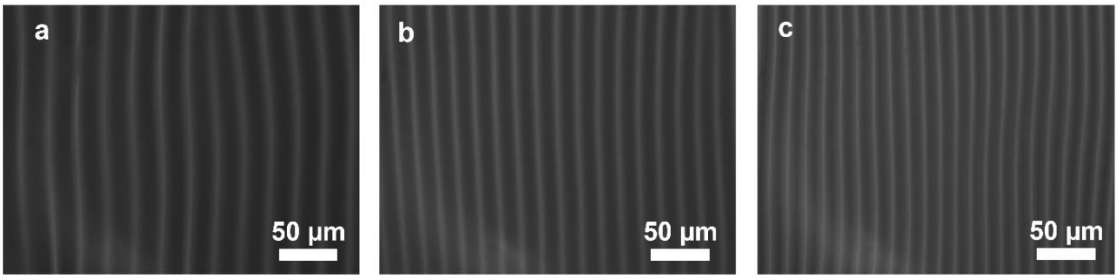

Figure C.3. Examples of the optical micrograph of the buckles obtained from the bilayer systems comprising PEDOT:PSS and pure fullerene films at different thicknesses.

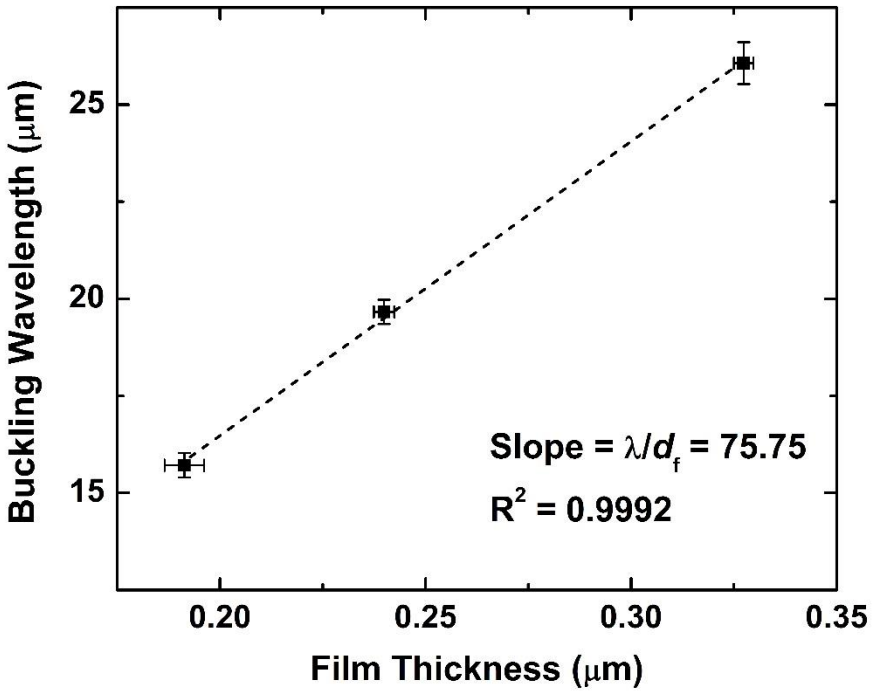

Figure C.4. An example of buckling wavelength vs. film thickness plot for a bilayer system. The slope of the fitted linear line was used as the ratio of the buckling wavelength and film thickness in equation 1.

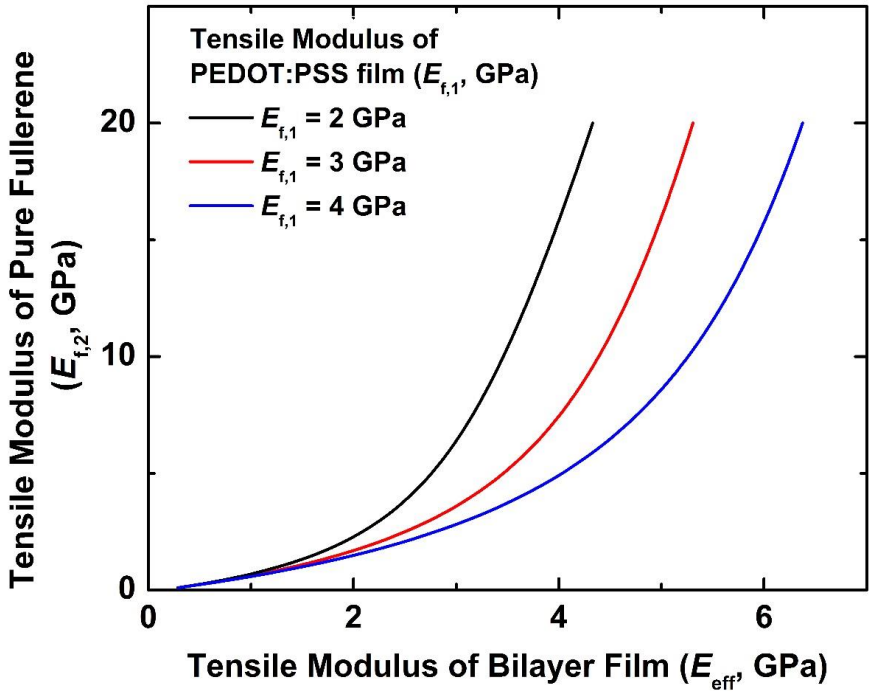

Figure C.5. Plot of the output tensile modulus of the pure fullerene films vs. the obtained tensile modulus of the bilayer films (PEDOT:PSS and pure fullerene) when the ratio of the thickness of the PEDOT:PSS and the pure fullerene film is kept constant at 1.

Appendix D

Supporting information for Chapter 8

Increased elasticity of a low-bandgap conjugated copolymer by random segmentation for mechanically robust solar cells

Suchol Savagatrup,[†] Adam D. Printz,[†] Daniel J. Burke, Trevor N. Purdy, and Darren J. Lipomi

([†] Equal contribution)

Department of NanoEngineering, University of California, San Diego, 9500 Gilman Drive Mail Code 0448, La Jolla, CA 92093-0448.

D.1 ^{13}C NMR

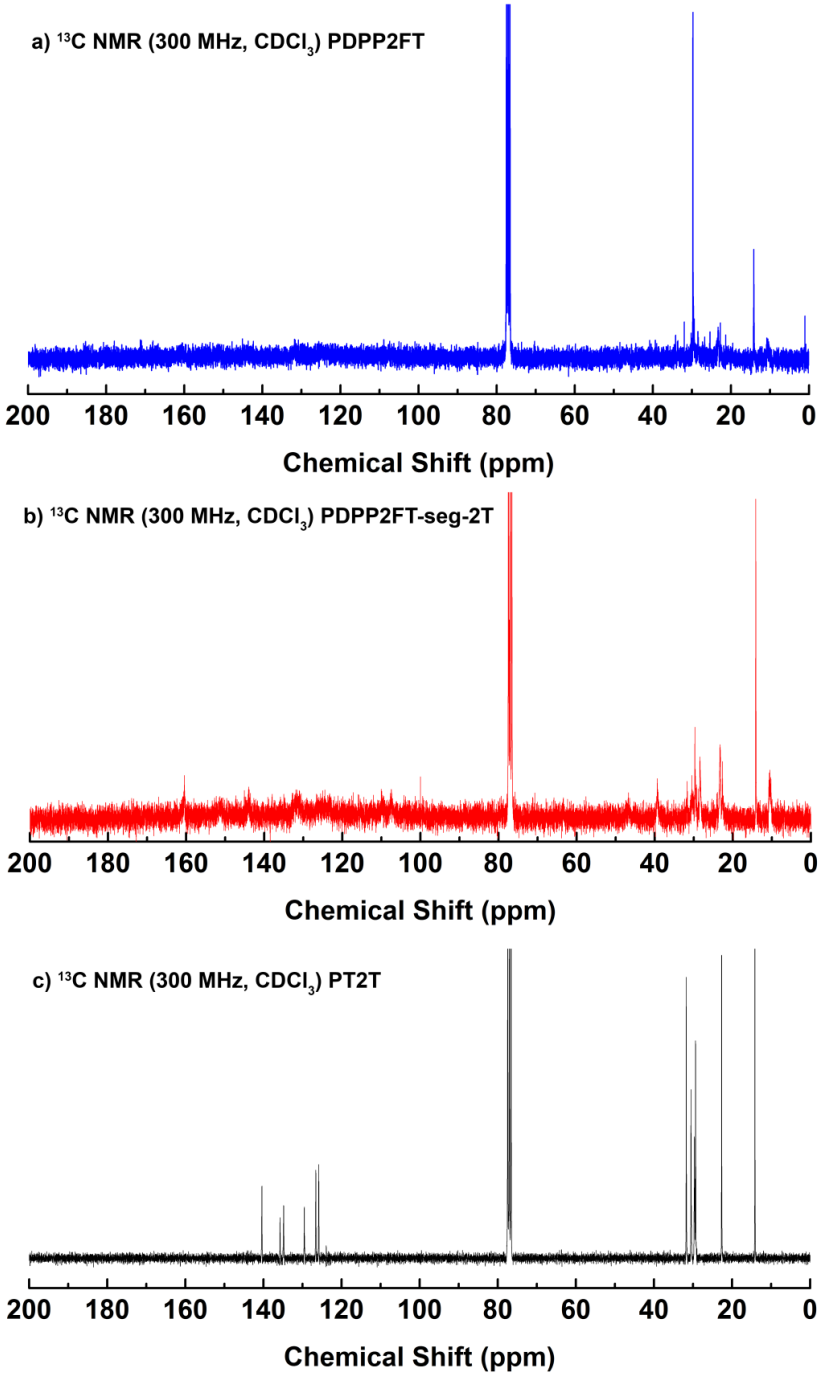

Figure D.1. ^{13}C NMR of (a) PDPP2FT, (b) PDPP2FT-seg-2T, and (c) PT2T.

D.2. UV-vis absorption of polymers (including 100:1 PDPP2FT:PT2T physical blend)

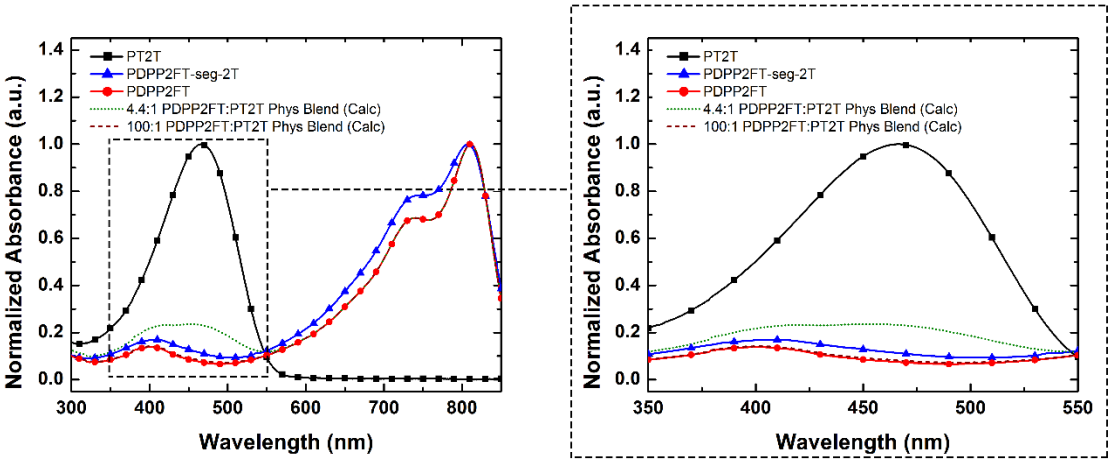

Figure D.2. Normalized absorption spectra of solutions of the pure polymers discussed in this paper. Measurements were made at a concentration of 1×10^{-5} M. Calculated absorption spectra of 4.4:1 and 100:1 physical blends of PDPP2FT:PT2T were superimposed onto the graph. The physical blend absorption spectra were calculated from the extinction coefficients of the pure polymers. The region from 350–550 nm is expanded to show the effect of PT2T contamination in PDPP2FT. The increase in absorption by a blend with a ratio of 100:1 PDPP2FT:PT2T over pure PDPP2FT is imperceptible in the absorbing region of PT2T. However, when the ratio of PDPP2FT:PT2T is decreased to 4.4:1 (the ratio in PDPP2FT-seg-2T as determined by NMR), there is a noticeable increase in absorption. The absence of this increased absorption in the PDPP2FT-seg-2T suggests that the segments are covalently bound and not simply a physical blend of the two components.

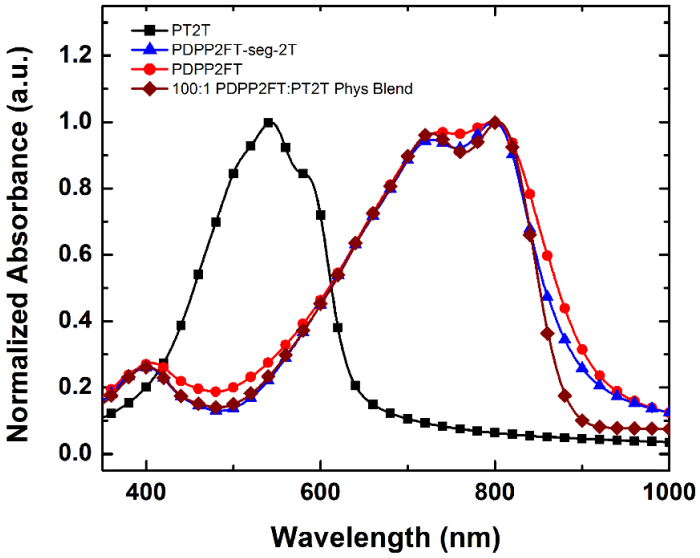

Figure D.3. Normalized absorption of thin films discussed in this paper with a 100:1 physical blend of PDPP2FT:PT2T superimposed on top. The physical blend matches the absorption of the pure PDPP2FT thin film well, which suggests that minor contamination of PT2T in PDPP2FT does not greatly affect the absorption in the solid state.

D.3. *PCE* vs. E_f of polymers (including 100:1 PDPP2FT:PT2T physical blend)

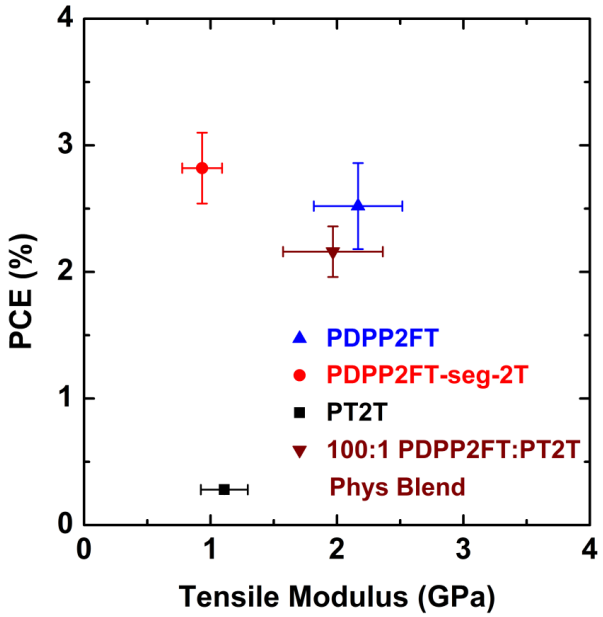

Figure D.4. Plot of the power conversion efficiency of 1:2 blends of the polymer:$PC_{61}BM$ as a function of the tensile modulus of the pure polymer. The PCE of the physical blend is 2.16 ± 0.2 % and the tensile modulus is 1.97 ± 0.39 GPa.

Table D.1. Tensile moduli of pure polymer films spin-coated from chloroform and 1:2 polymer:$PC_{61}BM$ films spin-coated from 4:1 $CHCl_3$:ODCB. The tensile modulus of the physical blend is within error of the pure PDPP2FT.

	Tensile Modulus (GPa)	
Polymer	**Pure polymer ($CHCl_3$)**	**1:2 Polymer:$PC_{61}BM$ (4:1 $CHCl_3$:ODCB)**
PDPP2FT	2.17 ± 0.35	2.76 ± 0.77
PDPP2FT-seg-2T	0.93 ± 0.16	1.60 ± 0.14
PT2T	1.11 ± 0.19	1.60 ± 0.36
100:1 PDPP2FT:PT2T physical blend	1.97 ± 0.39	—

D.4. Photovoltaic characteristics of 1:2 polymer:$PC_{61}BM$ devices (including 100:1 PDPP2FT:PT2T physical blend)

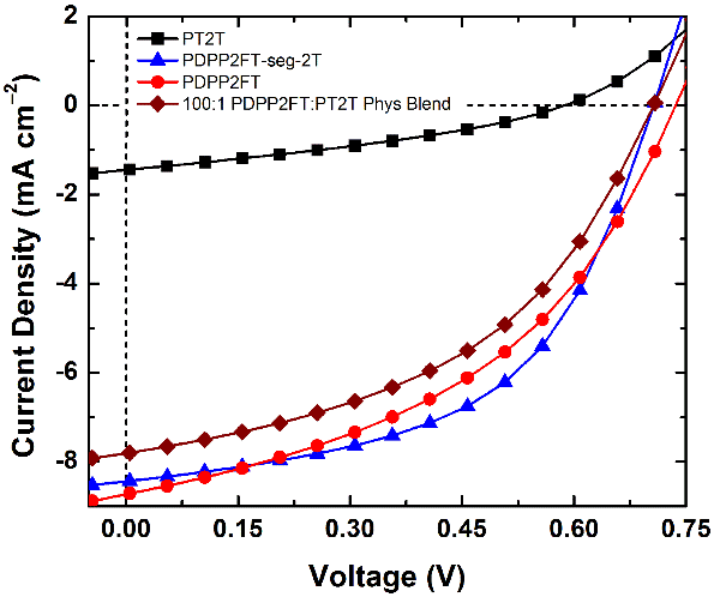

Figure D.5. Photovoltaic characteristics of representative samples of polymer-fullerene blends including a device fabricated with an active layer of 100:1 PDPP2FT:PT2T (and fullerene) physical blend. The *J-V* curve of the physical blend is most similar to the curve of pure PDPP2FT:$PC_{61}BM$.

Table D.2. Summary of the figures of merit for the solar cells fabricated in this work. The photoactive layers comprised a 1:2 polymer:$PC_{61}BM$ blend. In addition to the devices shown in **Table 8.2** of the manuscript, we have also included the figures of merit for solar cells fabricated with an active layer of 100:1 PDPP2FT:PT2T (and fullerene) physical blend. The J_{sc} and η_{ε} are lower than the PDPP2FT:$PC_{61}BM$, although the V_{oc} and *FF* are comparable.

Polymer	***n***	J_{sc} **[mA cm^{-2}]**	V_{oc} **[mV]**	***FF*** **[%]**	η_{ε} **[%]**
PT2T	3	1.5 ± 0.1	579 ± 21	32.9 ± 1.1	0.28 ± 0.01
PDPP2FT-seg-2T	6	8.4 ± 0.5	699 ± 23	48.2 ± 3.3	2.82 ± 0.28
PDPP2FT	7	8.3 ± 0.5	715 ± 25	42.5 ± 3.6	2.52 ± 0.34
100:1 PDPP2FT:PT2T Phys Blend	7	6.8 ± 0.5	710 ± 4	44.6 ± 1.5	2.16 ± 0.20

Appendix E

Supporting information for Chapter 9

Mechanical properties of a library of low-bandgap polymers

Suchol Savagatrup,[†a] Bérenger Roth,[†b] Nathaniel De Los Santos,[a] Ole Hagemann,[b] Jon E. Carlé,[b] Martin Helgesen,[b] Francesco Livi,[b] Eva Bundgaard,[b] Roar R. Søndergaard,[b] Frederik C. Krebs,[b] and Darren J. Lipomi[a]

([†] Equal contribution)

[a] *Department of NanoEngineering, University of California, San Diego, 9500 Gilman Drive Mail Code 0448, La Jolla, CA 92093-0448.*

[b] *Department of Energy Conversion and Storage, Technical University of Denmark, Frederiksborgvej 399, DK-4000 Roskilde, Denmark.*

E.1 Film thicknesses for the calculation of tensile moduli

Table E.1. Values of film thickness used in the calculation of tensile moduli reported in this work. The solutions for all polymers were made by dissolving 10 mg mL^{-1} in $CHCl_3$. The spin speeds were set at 500, 1000, and 200 RPM. The variations in thicknesses among different polymer were the result of differing viscosities. The slopes and the R^2 values of the linear fits are also given for each polymer.

	500 RPM		1000 RPM		2000 RPM		Slope of linear fit	R^2
Polymer	Film thickness (nm)	Buckling wavelength (um)	Film thickness (nm)	Buckling wavelength (um)	Film thickness (nm)	Buckling wavelength (um)		
A1D5	409	17.18	215	11.40	165	8.94	32.65	0.99
A1D9	289	11.17	215	8.75	178	6.78	38.37	0.98
A2D1	231	15.78	210	12.41	153	8.93	81.65	0.96
A2D2	-	-	-	-	-	-	-	-
A2D3	262	10.76	209	7.28	169	5.49	57.38	0.99
A2D5	263	11.26	209	9.12	176	7.74	40.29	1.00
A2D9	299	9.40	242	6.95	174	4.97	35.46	0.99
A3D1	318	15.77	285	13.30	258	12.13	61.62	0.98
A3D3	130	8.06	108	6.69	93	5.09	78.50	0.98
A3D6	501	17.95	345	13.65	268	11.34	28.34	1.00
A3D7	129	5.08	98	3.87	80	3.28	36.83	1.00
A3D8	170	7.67	143	6.22	121	5.16	51.43	1.00
A3D9	-	-	-	-	-	-	-	-
A4D2	216	11.86	197	9.83	145	7.13	63.65	0.97
A4D5	300	14.75	214	9.92	178	8.04	55.50	1.00
A4D9	227	9.44	156	7.12	136	5.81	38.28	0.98
A5D1	233	11.50	166	7.37	129	5.46	58.72	1.00
A5D2	88	5.02	77	4.24	47	2.86	51.51	0.99
A5D6	354	20.26	303	15.52	222	12.20	59.15	0.95
A5D7	511	16.07	392	12.97	306	9.98	29.46	0.99
A5D9	538	18.17	397	12.66	342	9.85	41.73	1.00
A6D1	264	9.92	194	7.48	162	6.28	35.42	1.00
A6D2	334	15.66	271	11.07	215	8.23	62.84	0.99
A6D9	254	10.02	192	7.81	141	6.54	30.90	0.99
A7D7	194	9.79	133	7.71	113	6.57	38.46	0.99
A8D1	239	17.24	217	14.56	154	8.65	99.26	1.00
A8D2	229	14.67	211	12.69	154	9.46	65.96	0.98
A8D3	226	13.92	174	9.52	134	7.39	71.68	0.99
A8D5	254	10.68	221	8.61	179	6.66	52.95	0.99
A8D7	246	10.16	216	8.65	148	6.15	40.06	0.99
A8D8	-	-	-	-	-	-	-	-
A9D1	367	12.61	272	8.19	220	6.61	41.58	0.99
A9D7	259	9.83	205	7.15	170	6.09	42.64	0.98

Table E.1., Cont. Values of film thickness used in the calculation of tensile moduli reported in this work. The solutions for all polymers were made by dissolving 10 mg mL^{-1} in $CHCl_3$. The spin speeds were set at 500, 1000, and 200 RPM. The variations in thicknesses among different polymer were the result of differing viscosities. The slopes and the R^2 values of the linear fits are also given for each polymer.

	500 RPM		1000 RPM		2000 RPM		Slope of linear fit	R^2
Polymer	Film thickness (nm)	Buckling wavelength (um)	Film thickness (nm)	Buckling wavelength (um)	Film thickness (nm)	Buckling wavelength (um)		
A10D1	-	-	-	-	-	-	-	-
A10D2	-	-	-	-	-	-	-	-
A10D3	-	-	-	-	-	-	-	-
A10D6	-	-	-	-	-	-	-	-
A10D7	392	11.10	309	8.31	250	6.70	31.14	1.00
A10D8	265	8.43	241	6.86	180	4.96	38.73	0.96
A10D9	-	-	-	-	-	-	-	-
A12D5	115	6.36	100	5.47	79	4.76	44.24	0.98
A12D7	212	8.31	185	6.62	149	5.24	47.77	0.98
A12D9	141	6.15	110	5.15	84	4.20	33.99	1.00
A13D1	238	9.81	146	6.27	119	4.27	44.62	0.98
A13D7	331	11.82	289	10.09	256	9.12	36.04	0.99
A13D9	211	7.24	184	6.44	170	5.86	33.41	0.99
A14D1	154	6.83	104	5.38	92	4.51	34.72	0.96
A14D2	186	7.99	156	6.69	116	5.31	38.34	1.00
A14D3	116	4.72	88	3.70	71	2.82	40.80	0.99
A14D7	165	9.05	139	7.61	88	5.32	48.11	1.00
A14D9	322	9.53	288	7.84	222	6.42	29.78	0.95

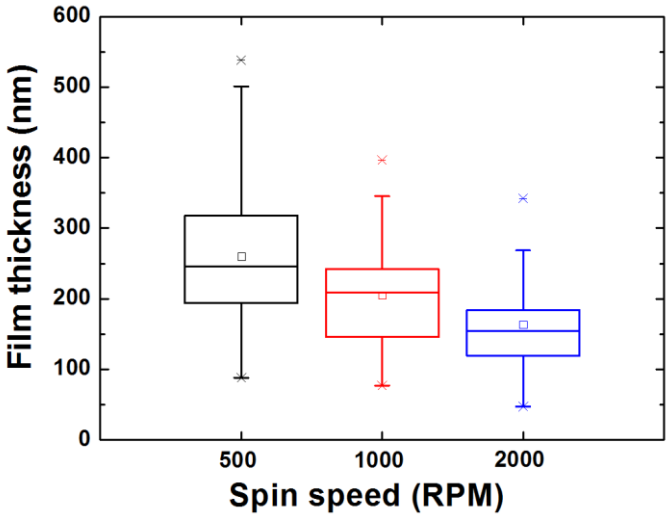

Figure E.1. Box diagram of the film thickness used in the measurement of the tensile moduli separated by the spin speed.

E.2. Film thicknesses for crack-onset strain measurements

Table E.2. Averaged film thicknesses and standard deviations of all the polymer films for the measurement of crack-onset strain.

Polymer	Averaged thickness (nm)	Standard Deviation (nm)	Polymer	Averaged thickness (nm)	Standard Deviation (nm)
A1D5	117.3	3.5	A8D1	374.3	14.6
A1D9	358.7	21.5	A8D2	143.8	1.5
A2D1	168.4	21.0	A8D3	160.3	23.0
A2D2	190.0	9.7	A8D5	290.5	29.0
A2D3	394.6	4.3	A8D7	209.7	12.6
A2D5	148.9	2.8	A8D8	266.7	15.0
A2D9	317.9	3.8	A9D1	242.8	8.0
A3D1	96.8	2.1	A9D7	310.1	26.0
A3D3	368.5	32.5	A10D1	186.4	17.3
A3D6	-	-	A10D2	107.9	0.8
A3D7	206.0	5.6	A10D3	179.9	3.9
A3D8	-	-	A10D6	152.5	4.3
A3D9	150.7	2.5	A10D7	315.6	6.4
A4D2	316.1	6.3	A10D8	221.8	13.5
A4D5	111.8	4.1	A10D9	280.2	11.2
A4D9	137.2	9.2	A12D5	274.5	10.5
A5D1	163.4	3.1	A12D7	249.1	40.0
A5D2	-	-	A12D9	268.7	37.5
A5D6	236.2	19.0	A13D1	109.7	2.6
A5D7	138.9	5.3	A13D7	226.7	5.3
A5D9	260.6	15.8	A13D9	331.3	22.6
A6D1	185.1	7.4	A14D1	271.4	6.0
A6D2	327.7	31.0	A14D2	216.8	5.1
A6D9	165.2	8.0	A14D3	147.4	0.7
A7D7	167.9	5.0	A14D7	198.3	6.5
			A14D9	-	-

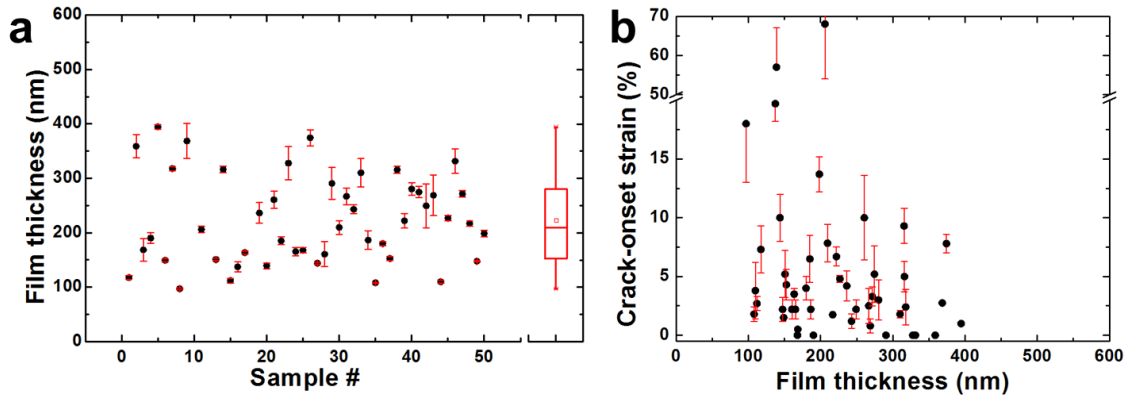

Figure E.2. (a) Film thicknesses for all the polymer samples used in the measurement of the crack-onset strains. (b) Crack-onset strain as a function of film thickness. We found no correlation between the crack-onset and the film thickness for this range of thicknesses.